A CLOSER LOOK AT MEMBRANE PROTEINS

By

Dragana Robajac, Miloš Šunderić, Nikola Gligorijević, Olgica Nedić, Mark Tingey, Steven J. Schnell, Yichen Li, Samuel Junod, Wenlan Yu, Weidong Yang, Nilay K. Roy, Oliver Beckstein, Fiona Naughton, Min Lu, Katherine Si-Jia Lu, Manjusha Lekshmi, Nicholas Wenzel, Sanath H. Kumar, Manuel F. Varela, Raymond J. Turner, Irshad Ahmad, Pikyee Ma, David J. Sharples, Peter J. F. Henderson, Simon G. Patching

CONTRIBUTORS

(Alphabetical order)

Irshad Ahmad	University of Leeds, UK
Oliver Beckstein	Arizona State University, USA
Nikola Gligorijević	University of Belgrade, Serbia
Peter J. F. Henderson	University of Leeds, UK
Samuel Junod	Temple University, USA
Sanath H. Kumar	ICAR-Central Institute of Fisheries Education, India
Manjusha Lekshmi	ICAR-Central Institute of Fisheries Education, India
Yichen Li	Temple University, USA
Katherine Si-Jia Lu	Rosalind Franklin University of Medicine & Science, USA
Min Lu	Rosalind Franklin University of Medicine & Science, USA
Pikyee Ma	University of Leeds, UK
Fiona Naughton	Arizona State University, USA
Olgica Nedić	University of Belgrade, Serbia
Simon G. Patching	University of Leeds, UK
Dragana Robajac	University of Belgrade, Serbia
Nilay K. Roy	Northeastern University, USA
Steven J. Schnell	Temple University, USA
David J. Sharples	University of Leeds, UK
Miloš Šunderić	University of Belgrade, Serbia
Mark Tingey	Temple University, USA
Raymond J. Turner	University of Calgary, Canada
Manuel F. Varela	Eastern New Mexico University, USA
Nicholas Wenzel	Eastern New Mexico University, USA
Weidong Yang	Temple University, USA
Wenlan Yu	Temple University, USA

CONTENTS

PREFACE

Membrane proteins are coded by up to 30% of the open reading frames in know genomes. They have pivotal roles in many biological processes including: transport of ions and molecules, control of transmembrane potential, generation and transduction of energy, signal recognition and transduction, cell-cell communication, enzymatic activity, structural roles. Mutations in membrane proteins are linked with various human diseases including: Alzheimer's disease, Brugada syndrome, cancer, cystic fibrosis, heart disease, hypothyroidism, lysosomal storage disease, nephrogenic diabetes insipidus, retinitis pigmentosa. Membrane proteins are the molecular targets for around 50-60% of validated drugs and they remain a principal target for new drug discovery. Despite all this, the number of structures of membrane proteins is less than 1% of total protein structures in the Protein Data Bank due to various challenges associated with applying the main biophysical techniques for high-resolution protein structure determination: X-ray crystallography, electron microscopy, NMR spectroscopy. There is an infinite amount of information and understanding yet to be obtained about the structure, function and molecular mechanism of membrane proteins and their ligands.

This book "A Closer Look at Membrane Proteins" brings together recent developments in the structures, molecular mechanisms and roles of some different types of membrane proteins using various computational and experimental methods, and also views on the challenges around expression and purification of membrane proteins and a successful demonstration of how these challenges can be overcome.

Chapter One considers insulin-like growth factor receptors and their roles in initiating mitogenic and metabolic pathways involved in cell growth and proliferation and energy metabolism, and also their roles in cell apoptosis. Information on the receptors is related to normal and abnormal tissue growth and development, using placental and colorectal tissues as examples. ***Chapter Two*** demonstrates how transmembrane protein transport across the nuclear envelope can be imaged at high-resolution using dynamic single-molecule microscopy; especially how the technique can be used to interrogate different proposed models for the mechanism of membrane protein transport: diffusion-retention, ATP-dependent, nuclear localization signal–mediated, sorting motif–mediated.

Computer simulation provides a way to study the structure and function of membrane proteins, alternative to using laboratory techniques, and this is the subject of ***Chapter Three***. The focus is on large scale molecular dynamics (MD) simulations with special emphasis on scalable parallel methods, and how correctly relating molecular structures to the physiological properties of proteins is a major challenge in the field. ***Chapter Four*** consolidates general principles of secondary active transporter function, which catalyse transport of ions and small molecules across cell membranes against electrochemical gradients. It considers thermodynamics and molecular mechanism and how these transporters cycle between inward- and outward-facing conformations. Also how experimental structural data and MD simulations indicate that transporters can be understood as gated pores. A unified picture emerges in which symporter, antiporter and uniporter function are extremes in a continuum of functionality.

Following recent high-resolution X-ray crystal structures of substrate-bound proteins, ***Chapter Five*** reviews emerging structural insights about multidrug recognition and extrusion by MATE (Multidrug and Toxic Compound Extrusion) and MFS (Major Facilitator Superfamily) secondary active transporters, which provide a mechanism of resistance to therapeutic drugs. In addition to providing a better understanding about the underlying mechanism of multidrug extrusion, this chapter engenders new ideas about how to curtail efflux-mediated multidrug resistance. A myriad of membrane proteins in the pathogenic bacterium *Vibrio cholerae* are described in ***Chapter Six*** that contribute to its physiology, virulence and antimicrobial resistance. These include outer membrane proteins and efflux pumps of the RND (Resistance-Nodulation-Division) family and MFS. The chapter emphasises how inhibition of efflux pumps can reduce virulence of *V. cholerae* and restore susceptibility to conventional antibiotics, and demonstrates how a complex network involving quorum sensing, efflux pumps and virulence gene expression regulates physiology and virulence.

The challenges around expression and purification of integral membrane proteins and performing laboratory experiments to study their structure and function are well recognised. In this respect, ***Chapter Seven*** gives a personal view on “The commandments of studying integral membrane proteins”. These commandments consider integral membrane protein expression and purification, biochemistry, functionality studies and high-resolution structures. It is possible to overcome the challenges for expression and purification of integral membrane proteins, especially by those who are suitably experienced and have longevity of success. This is demonstrated in ***Chapter Eight*** by the amplified expression, functional characterisation and purification of a cytosine transporter of the NCS1 (Nucleobase Cation Symporter-1) family from the bacterium *Vibrio*

parahaemolyticus. The gene was cloned into plasmid pTTQ18 along with a sequence for introducing a C-terminal hexahistidine-tag to aid purification and amplified expression achieved in *Escherichia coli* BL21(DE3). The secondary structure and stability of the purified protein was analysed by circular dichroism spectroscopy and the protein was confirmed as a cytosine transporter by radiolabelled transport measurements in whole cells.

NOTE TO THE READER

In the interest of advancement in scientific research, the publisher has made this book Open Access so that it reaches the widest readership without barriers and so that no individual(s) or organization(s) receive direct financial profit. All individual chapters in this book were separately subjected to single-blinded peer review.

ABBREVIATIONS

7TMIR	7-TM inverted repeat
ABC	ATP–binding cassette (transporter)
AbgT	p-Aminobenzoyl-glutamate transporter
ADP	Adenosine diphosphate
AMBER	Assisted model building with energy refinement
aMD	Accelerated molecular dynamics
AMP	Antimicrobial peptide
APC	Amino acid-polyamine-organocation (transporter)
AQP	Aquaporin
ARM	Armadillo repeat motif
ATP	Adenosine triphosphate
BAF	Barrier-to-autointegration factor
BCA	Bicinchoninic acid
BCCT	Betaine-choline-carnitine-transporter
BD	Brownian dynamics
BHK	Baby hamster kidney
cAMP	Cyclic adenosine monophosphate
CCCP	Carbonyl cyanide *m*-chlorophenyl hydrazone
CD	Circular dichroism (spectroscopy)
CDG	Congenital disorders of glycosylation
CGMD	Coarse grained molecular dynamics
CHARMM	Chemistry at Harvard Macromolecular Mechanics
CMC	Critical micellar concentration
CMT	Critical micellular concentration
CMM-CG	Center for Molecular Modeling Coarse-Grained
Co-IP	Co-immunoprecipitation
CT	Cholera toxin
DAPI	4′,6-Diamidino-2-phenylindole
DDM	*n*-Dodecyl β-*D*-maltoside
DEER	Double electron-electron resonance (spectroscopy)
DHA1	Drug/H^+ antiporter-1
DinF	DNA damage-inducible protein F
DM	Diabetes mellitus
DMPC	Dimyristoylphosphatidylcholine

DMT	Drug/metabolite transporter
DMSO	Dimethyl sulphoxide
DNA	Deoxyribonucleic acid
DPPC	Dipalmitoylphosphatidylcholine
DSSP	Define secondary structure of proteins
DXC	Deoxycholate
EC	Extracellular
ECM	Extracellular matrix
EDTA	Ethylenediaminetetraacetic acid
EFPA	Enhancing functional protein accumulation
EGF	Epidermal growth factor
EM	Electron microscopy
EMT	Epithelial–tesenchymal transition
ER	Endoplasmic reticulum
EVB	Empirical valence bond
FOXO	Forkhead family box O (transcription factors)
FRAP	Fluorescence recovery after photobleaching (microscopy)
FRB	FKBP12/rapamycin-binding
FRET	Förster resonance energy transfer
FSM	Flexible surface model
GCMC	Grand canonical Monte Carlo
GDM	Gestational diabetes mellitus
GFP	Green fluorescent protein
GH	Growth hormone
GLUT	Glucose transporter
gp210	Glycoprotein-210 (antibody)
GPCR	G–Protein coupled receptor
Grb2	Growth factor–bound protein 2
GROMOS	GROningen MOlecular Simulation
GSK3 β	Glycogen synthase kinase 3β
HILO	Highly inclined and laminated optical sheet (microscopy)
HIV	Human immunodeficiency virus
HLB	Hydrophile-lipophile balance
HPr	Heat-stable protein
HyR	Hybrid receptor
IC	Intracellular

IF	Inward facing (conformation)
IGF	Insulin-like growth factor
IGFBP	Insulin-like growth factor binding protein
IMAC	Immobilised metal affinity chromatography
IMP	Integral membrane protein
IPTG	Isopropyl β-*D*-1-thiogalactopyranoside
INM	Inner nuclear membrane
INM-SM	Inner nuclear membrane sorting motif
IR	Insulin receptor
IRS	Insulin receptor substrate
IUGR	Intrauterine growth restriction
KEGG	Kyoto Encyclopedia of Genes and Genomes
KASH	Klarsicht, ANC-1, syne homology
LB	Luria-Bertani
LBR	Lamin B receptor
LDAO	Lauryldimethylamine oxide
LEM	Lamin-associated protein [LAP]2, emerin, MAN1
MATE	Multidrug and toxic compound extrusion
MD	Molecular dynamics
MDR1	Multidrug resistance protein 1
MES	2-(*N*-Morpholino)ethanesulfonic acid
MFS	Major facilitator superfamily
MMP	Matrix metalloproteinase
MRE	Mean residue ellipiticity
MS-CG	Multiscale coarse grained
MtlA	Mannitol-specific enzyme IICBA
MtlD	Mannitol-1-phosphate dehydrogenase
MWCO	Molecular weight cut off
NAT	Nucleobase ascorbate transporter
NBD	Nucleotide binding domain
NCS1	Nucleobase-cation-symporter 1
NE	Nuclear envelope
NETs	Nuclear envelope pransmembrane proteins
NLS	Nuclear localization signal
NMR	Nuclear magnetic resonance
NPC	Nuclear pore complexes
NSS	Neurotransmitter sodium symporter
Nup	Nucleoporin

ODV	Occlusion derived virus
OF	Outward facing (conformation)
OHS	Oligosaccharide/H^+ symporter
ONM	Outer nuclear membrane
PACE	Proteobacterial antimicrobial compound efflux
PBC	Periodic boundary conditions
PC	Phosphatidylcholine
PCR	Polymerase chain reaction
PDB	Protein Data Bank
PE	Preeclampsia
PEP	Phosphoenol pyruvate
PG	Phosphatidylglycerol
POPE	1-Palmitoyl-2-oleoyl-*sn*-glycero-3-phosphatidylethanolamine
PTEN	Phosphatase and tensin
PTM	Post–translational modification
PTS	Phosphoenolpyruvate-dependent phospotransferase
QM	Quantum mechanical
RDF	Radial distribution functions
RMSF	Root mean square fluctuations
RNAi	RNA interference
RND	Resistance-nodulation-division
ROS	Reactive oxygen species
S6K	S6 kinase
SAXS	Small-angle X-ray scattering
SBGP	Single binding center gated (model)
SDS	Sodium dodecyl sulphate
SDS-PAGE	Sodium dodecyl sulphate polyacrylamide gel electrophoresis
SHC	Src homology collagen
SMA	Styrene maleic acid
SMALP	Styrene maleic acid lipid particle
smFRAP	Single-molecule fluorescence recovery after photobleaching
SNR	Signal to noise ratio
SP	Sugar porter
SPEED	Single-point edge-excitation sub-diffraction (microscopy)

SREBP1c	Sterol regulatory element binding protein 1c
SSS	Solute/sodium symporter
SUN	Sad1p, UNC-84
TCP	Toxin co-regulated pilus
TIRF	Total internal reflection (microscopy)
TM	Transmembrane
TMH	Transmembrane helices
TPP	Tetraphenylporphyrin
TSC2	Tuberous sclerosis 2
UV	Ultraviolet
VcBMC	*V. cholerae* biofilm matrix cluster
VEGF	Vascular endothelial growth factor
VPI	*V. cholerae* pathogenicity island
VPS	Vibrio polysaccharide

Chapter One

1. BITTER–SWEET STORY OF THE IGF RECEPTORS IN CELL (MAL)FUNCTIONING

Dragana Robajac*, Miloš Šunderić, Nikola Gligorijević, Olgica Nedić
Institute for the Application of Nuclear Energy (INEP),
University of Belgrade, Belgrade, Serbia

ABSTRACT

The insulin–like growth factor (IGF) system contains multiple members including growth factors, their binding proteins and receptors. After binding of growth factors to their receptors, a cascade of signals is activated initiating a number of mitogenic and metabolic pathways. Being at the crossroad of different and sometimes opposing functions, dependent on structural modifications as well as cell surrounding, the IGF system represents an intriguing field of investigation. It is involved in cell growth, proliferation and energy metabolism, but also in cell apoptosis. The IGF system will be described in the following chapter, with the focus on the IGF receptors and functions associated with them. The data on membrane proteins, their N–glycome and oxidation status will be related to our findings on the receptors in different physiological and pathological conditions, such as normal and abnormal tissue growth and development. Placental and colorectal tissues will be used as examples.

Keywords: insulin–like growth factors, membrane receptors, placenta, diabetes, colon cancer

1.1. INTRODUCTION

The insulin–like growth factor (IGF) system consists of peptides (IGF–I and IGF–II), binding proteins (IGFBP–1–6), receptors (IGF–1R and IGF–2R) and

* Direct all correspondence to Dr. Dragana Robajac, Department of Metabolism at the Institute for the Application of Nuclear Energy (INEP), Belgrade, Serbia. E-mail: draganar@inep.co.rs.

IGFBP proteases, as presented in Figure 1. Being closely related to IGF peptides and IGF–1R, and due to a high degree of homology and crossreactivity, insulin and insulin receptors (IR) can also be observed as the part of the IGF system, as will be discussed in the following sections.

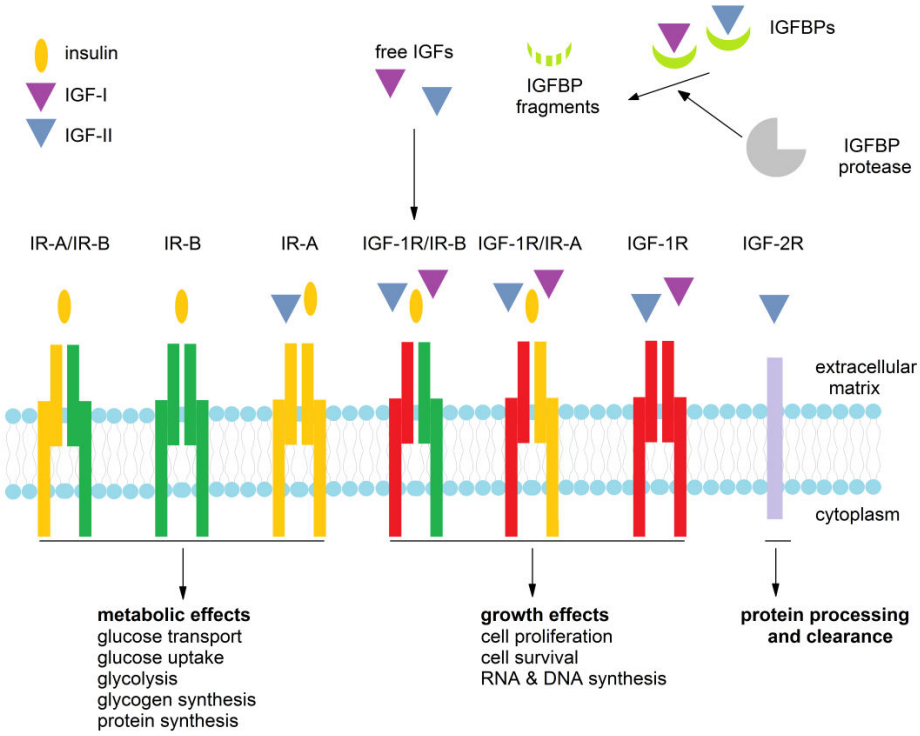

Figure 1. Members of the IGF system and the processes they control.

1.1.1. Peptides of the IGF system

Peptides of the IGF system are 7.5 kDa proteins, with amino acids arranged in four domains (B, C, A and D), and are mainly produced in the liver (Le Roith et al., 2001). IGF–I and IGF–II share 70% similarity, while the difference between IGFs and insulin is around 50% (Rinderknecht and Humbel, 1978). The main difference between IGFs and (pro)insulin is the existence of domains C and D (both are omitted from insulin while proinsulin contains domain C). A second difference originates from the specific amino acids in the IGFs located at positions 3, 4, 15 and 16, that are responsible for recognition and binding to IGFBPs. A third difference between IGFs and insulin is derived from the existence of

IGFBPs, which bind IGFs leaving rather minute amounts of free peptides, whereas binding proteins do not control insulin availability, allowing this peptide to be able to circulate freely (Annunziata, Granata and Ghigo, 2011).

The *IGF–I* gene is located in the 12q region, and after birth its expression (and the production of IGF–I responsible for growth and proliferation) is under the control of growth hormone. The *IGF–II* gene is located in the 11p region, whose anomalies result in abnormal foetal and postnatal growth, as well as increased risk of embryonic tumours in early life (Wakeling et al., 2017; Brioude et al., 2018). The term genomic imprinting is used to describe the monoallelic expression of genes based on their parental origin (Cassidy and Charalambous, 2018). Genomic imprinting is found to be of high importance as imprinting disorders share one common characteristic – developmental anomaly. As a result, altered growth and nutrient uptake are expressed already in early life. The placenta is a source of many proteins whose expression results in a genomic imprinting process, where some of these genes are found to be involved in the placentation process (Graves and Ranfree, 2013). *IGF–II* is maternally imprinted, and is normally inherited from the father, whereas the loss of *IGF–II* imprinting is related to an increased cell proliferation and tumour risk (Kaneda et al., 2007; Livingstone, 2013). IGFs are expressed ubiquitously in all tissues where they act in an autocrine/paracrine manner, affecting cell growth, differentiation and proliferation, mitogenesis and metabolism. Additionally, the expression of other members of the IGF system (e.g. IGFBPs, IGFBP proteases and IGF–Rs) regulates the bioavailability of these peptides and hence their numerous functions.

1.1.2. IGF binding proteins

There are six proteins belonging to the family of IGF binding proteins (IGFBP–1–6) and there is also a family of IGFBP–related proteins, that share some structural similarities with IGFBPs but bind IGFs with much lower affinity (Brahmkhatri, Prasanna and Atreya, 2015).

IGFBPs consist of 216–289 amino acids distributed in three domains (N, C, L), and it is the L domain that is not preserved between different IGFBPs, while the other two share high a degree of homology among IGFBPs and are responsible for high affinity binding of IGFs (Hwa et al., 1999). IGFBP–1, –3, and –4 bind both IGF peptides with the same affinity, while the affinity of IGFBP–2, –5 and –6 is higher for IGF–II compared to IGF–I (Firth and Baxter, 2002). IGFBPs are susceptible to different modifications: (i) IGFBP–1, –3 and –5 are phosphorylated (Jones et al., 1993; Hoeck and Mukku, 1994; Graham et al.,

2007), (ii) IGFBP–3 and –4 are N–glycosylated (Firth and Baxter, 1999; Zhou et al., 2003), (iii) IGFBP–5 and –6 are O–glycosylated (Neumann, Marinaro and Bach, 1998; Graham et al., 2007).

IGF peptides have higher affinity for IGFBPs than for receptors. Hence, IGFBPs regulate the availability of peptides acting as a storage system and also serve as protective molecules as they prolong the half–life of IGFs. Though all IGFBPs form binary complexes with IGFs, some IGFBPs (e.g. IGFBP –3 and –5) also form ternary complexes. The most abundant IGFBP in the circulation is IGFBP–3, which forms ternary complexes with IGFs and the acid labile subunit (ALS). After dissociation of the 150 kDa ternary complex, IGFs form binary complexes with other binding proteins, which further transport IGFs to target tissues (Le Roith et al., 2001).

Different (patho)physiological conditions may affect post–translational modifications of IGFBPs. For example, during pregnancy, placental alkaline phosphatase, produced by the syncytiotrophoblast, dephosphorylates blood IGFBP–1, thus reducing its affinity for IGF–I (Westwood et al., 1994), resulting in the prevalence of IGFBP–1 forms with lower affinities for IGFs, further leading to higher availability of free IGF–I (Forbes and Westwood, 2008).

1.2. RECEPTORS OF THE IGF SYSTEM

As already mentioned in this chapter, due to a high degree of homology between IGFs and insulin, receptors belonging to the IGF system are not only IGF type 1 (IGF–1R) and type 2 receptor (IGF–2R), but also insulin receptor (IR) and a hybrid receptor (HyR). Their structure, function and activating cascades will be discussed in the following sections and subsections of this chapter, with an emphasis on their impact on gestation and cancer development.

1.2.1. Type 1 insulin–like growth factor receptor – IGF–1R

The IGF–1R is a 420 kDa heterotetramer, a product of the *IGF–1R* gene located in the 15q region. Furin cleaves the IGF–1–pro–receptor into α (135 kDa) and β (95 kDa) subunits, while two pairs of αβ heterodimers are linked via disulphide bonds (Czech and Massague, 1982; Ward et al., 2001). IGF–1R is a transmembrane protein with two α–subunits located outside of the membrane, forming an extracellular ligand–binding domain, while tyrosine kinase domains are located at the intracellular part of the protein formed by two β–subunits. Tyrosine kinase domains are located between the juxtamembrane region and the

C–terminus, containing binding sites for phosphotyrosine from the signal molecules (Gatenby et al., 2013). It was shown that a heterozygous missense mutation in the *IGF–1R* gene can lead to severe foetal (intrauterine growth) restriction (IUGR) (Walenkamp et al., 2006), as can heterozygous mutations within the IGF–1R kinase domain (Kruis et al., 2010) or extracellular second fibronectin III domain (Wallborn et al., 2010). As high circulating levels of IGFs are found in these children, their condition is reflected by reduced IGF–1R tyrosine phosphorylation or altered cell surface expression of IGF–1R.

IGF–1R contains 16 asparagine (Asn) residues that are potential N–glycosylation sites; eleven are located in the α–subunit and five in the β–subunit (Ullrich et al., 1986). They are involved in the processing, stabilisation and localisation of the receptor (Itkonen and Mills, 2013), while the Asn^{913} N–glycan is found to be responsible for the IGF–1R transport to the plasma membrane (Kim et al., 2012). The importance of N–glycans is also noted at the level of sialic acid as its absence on the IGF–1R (desyalilation of the receptor) impairs cell proliferation in response to insulin (Arabkhari et al., 2010), as nicely reviewed by Ferreira et al. (2018). Under regular physiological conditions, actions of the IGFs are mediated mainly via IGF–1R.

1.2.1.1. IGF–1R cascades

Activation of the IGF–1R signalling pathway is a consequence of ligand–binding that induces conformational changes, facilitating autophosphorylation in the activation loop of the IGF–1R located in the α–subunit, leading to transphosphorylation of the opposing β–subunits (Hubbard and Till, 2000). As a result, activated IGF–1R further activates the PI3K–AKT cascade and MAPK–extracellular signal–regulated kinase (MEK)–extracellular signal–regulated kinase (ERK1/2) cascade (Coolican et al., 1997; Imai and Clemmons, 1999; Duan, Bauchat and Hsieh, 2000).

Once activated, IGF–1R interacts with adaptor proteins including Src homology collagen (SHC) proteins (p46/p52/p66) and insulin receptor substrate (IRS) (Dupont and LeRoith, 2001). SHC is primarily involved in the activation of p21ras–MAPK, which plays an important role in transduction of mitogenic signals initiated by different receptor tyrosine kinases, such as IGF–1R. After phosphorylation of IGF–1R, the receptor binds and phosphorylates SHC, leading to binding of adaptor protein growth factor–bound protein 2 (Grb2), which complexes with SOS, a p21ras guanine nucleotide exchange factor (Sasaoka et al., 2001). This action ends with ERK–1 and ERK activation, which leads to phosphorylation of cytoplasmic substrates and translocation and activation of transcription factors, enabling pro–proliferative and anti–apoptotic effects (Kolch,

2000). IGF–1R substrates are numerous: IRS, SHC, 14.3.3, CRK, CSK, PI3–kinase, SHP–2 phosphatase, Grb10 and others (Girnita et al., 2014).

IGF–1R can also utilize the components of the G–protein coupled receptor (GPCR) signalling, found to be essential for migratory and pro–survival functions controlled by IGF–I (Girnita et al., 2014). IGF–1R levels and functions are regulated by multiple post–translational modifications such as ubiquitination, sumoylation, phosphorylation and dephosphorylation (Girnita et al., 2014). Interestingly, IGF–1R propagates some completely opposing processes – growth and proliferation on one side and differentiation on the other, as well as cell adhesion on one side and motility on the other. Which process will be activated depends on the surrounding of the receptor and cell context. For example, IRS–1 is the main mediator of the mitogenic signals; however, cells that do not express IRS–1 will instead activate SHC and lead to differentiation (Romano, 2003).

1.2.2. Insulin receptor – IR

The IR is also a 420 kDa tetrameric transmembrane tyrosine kinase, encoded from the *IR* gene located in the 19p region. It is composed of two α– and two β–subunits. Approximately 95% of IR can be found in this heterotetrameric form, out of which 75% resides in the plasma membrane (Hwang and Frost, 1999). Due to alternative splicing, two IR isoforms exist: IR–A (a receptor isoform missing exon 11 – $Ex11^-$, which encodes 12 amino acids from the IRs' ectodomain at the C–terminus of α–subunit) and IR–B (a receptor isoform with preserved exon 11 – $Ex11^+$) (Seino and Bell, 1989). The IR–A isoform is preferenatially expressed in foetal and cancer tissues, although it can also be found in the majority of other tissues (Frasca et al., 1999). IR–B is predominantly expressed during adult life, in an insulin targeted tissues, such as liver, muscle, adipose tissue and kidney. IR–A and IR–B differ in the tyrosine kinase activity and the degree of the IR's internalisation, signal transduction and distribution in the plasma membrane depending on the membrane content of cholesterol and caveolin (Uhles et al, 2003).

IR has 18 potential N–glycosylation sites (14 on the α– and 4 on the β–subunit) out of which 16 are regularly glycosylated (Sparrow et al., 2008). The presence of sialic acid is important for IR activation after insulin binding (Dridi et al., 2013), and changes in the sialic acid content can affect receptor function (Pshezhetsky and Ashmarina, 2013).

1.2.2.1. IR cascades

Similary to IGF–1R activation, ligand binding to IR results in receptor autophosphorylation on cytoplasmic tyrosine residues and phosphorylation of the tyrosines of IRS proteins. Phosphotyrosine sites of IRS enable binding of the lipid kinase PI3K, responsible for the synthesis of phosphatidylinositol (3,4,5)–trisphosphate (PIP3) at the plasma membrane. This further activates phosphoinositide–dependent kinase that phosphorylates a threonine residue of AKT, while the serine residue of AKT is phosphorylated by mTORC2. Once activated AKT activates/phosphorylates other downstream substrates as the forkhead family box O (FOXO) transcription factors: (i) the protein tuberous sclerosis 2 (TSC2), which permits activation of mTORC1 and its downstream targets ribosomal protein S6 kinase (S6K) and sterol regulatory element binding protein 1c (SREBP1c); (ii) glycogen synthase kinase 3β (GSK3β); (iii) the RabGAP TBC1 domain family member 4 (TBC1D4). As a result of IR activation, metabolic processes are initiated as well as cell growth and differentiation. Alternative substrates of IR are Grb10, Grb14 and the suppressor of cytokine signalling (SOCS), which block IRS binding.

As can be seen for both described receptor protein kinases, phosphorylation is a crucial event for the activation or inactivation of IGF–1R and IR, e.g. tyrosine phosphorylation activates while serine/threonine phosphorylation inactivates IR and IRS proteins. These mechanisms of IR activation and inhibition of its signalling pathways are in detail and critically described in an exceptional review of Haeusler, McGraw and Accili (2018).

IR–A expression is related to a decrease in metabolic signalling of insulin and the actions of IGFs and the signalling path they trigger upon activation of IR–A. Consequent to IGF–II and proinsulin binding to IR–A, mitogenic signals are activated resulting in cell growth, proliferation and survival, being important in foetal and cancer tissues. IR–B expression, on the other hand, is associated with an increase in metabolic signalling of insulin, being important during adult life. Importantly, both IR and IGF–1R can translocate into the nucleus, thus regulating biological responses at the genomic level. This topic has been exstensively reviewed by Belfiore et al. (2017).

To increase the complexity of the IGF system, both IR and IGF–1R also have ligand–independent actions. For example, following ligand binding, due to catalytic activities of these receptors, anti–apoptotic signals are triggered enabling cell survival and resistance to apoptosis. However, unrelated to catalytic activities but only to receptors themselves, if lignads are absent and receptors are in a ligand–free form, they can support apoptosis. This effect can be reversed upon ligand binding (Belfiore et al., 2017).

1.2.2.2. IGF–1R/IR hybrid receptor – HyR

IR and IGF–1R share a high degree of similarity, ranging from 40–95% depending on the domain (Lou et al., 2006). Accordingly, one IGF–1R αβ heterodimer can dimerize with one IR αβ heterodimer (either A or B isoform) forming a hybrid receptor – HyR (Benyoucef et al., 2007). HyR can be found in tissues rich in both IR and IGF–1R, and considering there are two forms of IR, there are also two forms of HyR. Although HyR consists of the halves of two closely related receptors, there are indications that HyR is functionally much closer to IGF–1R, irrelevant to splicing, as it has rather low affinity for insulin and readily binds IGFs (Benyoucef et al., 2007).

1.2.3. Type 2 insulin–like growth factor receptor – IGF–2R

IGF–2R, also known as the cation–independent mannose–6–phosphate receptor, is a 270 kDa transmembrane protein encoded by the *IGF–2R* gene located in the 6q region. It mostly consists of the extracellular domain, while the transmembrane and cytoplasmic domains are much smaller (Lobel, Dahms and Kornfeld, 1988). IGF–2R is mostly expressed during foetal development (Sklar et al., 1992). Similar to other members of the IGF system, IGF–2R is also subjected to post–translational modifications. The extracellular domain contains 19 potential N–glycosylation sites, out of which at least two are glycosylated (Lobel et al., 1987). IGF–2R serves as a clearing route for IGF–II as, when bound to IGF–2R, it is directed towards lysosomal degradation (Kornfeld, 1992). There are, however, some indications of the potential signalling pathway involving IGF–2R.

1.2.3.1. IGF–2R cascades

Unlike IGF–1R and IR, IGF–2R does not contain tyrosine kinase activity or an autophosphorylation site. It is proposed that IGF–2R signalling is mediated by transactivating G protein–coupled sphingosine 1–phosphate receptors and that IGF–2R is involved in ERK1/2 activation (El–Shewy et al., 2007). Although it is thought that IGF–2R serves only for IGF–2 clearence and degradation, there are speculations that IGF–II binding to IGF–2R may be involved in mediating mitogenic effects in term placental explants (Harris et al., 2011). The exact mechanism of the potential signalling pathway mediated by IGF–2R has yet to be elucidated.

1.2.4. Physiology

Mitosis, cell growth, differentiation, migration, transformation and apoptosis are processes controlled by the IGFs. The control is exerted during embryonal development, postnatal life, maturation from childhood until adult age and ageing. As mentioned, the bioavailability and activity of IGFs are regulated by a network of IGFBPs, their proteases and IGF–Rs. In contrast to IGFs, insulin is mainly involved in metabolic processes (such as regulation of glucose concentration, protein and lipid metabolism), but mutual cross–reactivity enables IGFs to trigger metabolic responses and insulin to support cell growth (King et al., 1980). Malfunctioning in the IGF system may be associated with many pathophysiological states including cancer (Novosyadlyy and Le Roith, 2012; Nimptsch, Konigorski and Pischon, 2019).

In contrast to insulin, secreted by the pancreas, the majority of IGFs in the circulation are derived from the liver although many cells and organs can produce them locally. IGFs from the circulation exert predominantly endocrine functions, playing the role of a hormone. Peptides secreted locally exert paracrine and/or autocrine activities, expressing a role of cytokines or local growth factors. Liver is the principal organ that synthesises IGFBP–1, IGFBP–2 and IGFBP–3, but considerable quantities are produced by other organs as well, whereas synthesis of IGFBP–4, IGFBP–5 and IGFBP–6 occurs in a number of organs (Blum et al., 2018; Clemmons, 2018). IGFBPs are associated with lipid and carbohydrate metabolism, development of atherosclerosis, bone and skeletal muscle metabolism (Clemmons, 2018). Common to all IGFBPs is their capacity to control the amount of free, biologically active IGFs and, thus, to limit their presentation to cell membrane receptors. IGFBPs also protect them against proteolysis and assist in their trafficking within an organism.

IGFBPs can associate in specific complexes with other proteins beside IGFs and with other biomolecules, such as those from an extracellular matrix and glycosaminoglycans (Russo et al., 1997; Liu et al., 2014). Some IGFBPs can bind directly to cell membranes via their receptors, activating pathways other than those activated by insulin and IGFs, although they can still carry IGF ligands (Ingermann et al., 2010; Clemmons, 2018). This activity was considered as IGF–independent until recently, but a caution was drawn since some of the interactions of IGFBPs influence IGF signalling within the same cell. IGFBPs can be transported in the nucleus where they interact with nuclear proteins causing alteration of cellular physiology (Bach, 2018).

The portion of free IGFs in healthy adult persons is not greater than 1% (Juul, 2003). In contrast to insulin, stored in pancreatic granules and released upon metabolic demand, IGFs are mostly stored in blood as IGF/IGFBP complexes.

The high affinity of IGFBPs for IGFs maintains the equilibrium between protein–bound and free forms of these peptides. Upon demand for IGFs, IGFBP proteases modify IGFBPs reducing their affinity and enabling take–over by membrane receptors. Some IGFBPs are said to inhibit and the others to potentiate the activity of IGFs – the difference originates from the difference in the affinity of certain IGFBP compared to the affinity of receptors for IGFs (Le Roith, 2003; Clemmons, 2018).

It is worth mentioning that the IGF system is the only one having so many specific binding proteins (beside six high–affinity, there are several low–affinity), suggesting the need for very sensitive regulating mechanisms and fine tuning in respect to the actions of IGFs (Haywood et al., 2019). Regardless of the high degree of homology between insulin and IGFs, IGFBPs do not bind insulin (Annunziata, Granata and Ghigo, 2011). Physiological concentrations of insulin in healthy adults are in the range of pM whereas the concentrations of IGF–I and IGF–II are in nM (Juul, 2003; Heinemann, 2010). Thus, since IGFs are present in 100 to 1000–fold greater concentrations than insulin, their availability must be rigorously controlled.

IGF–I is a mediator of the activity of growth hormone (GH), as GH is an up–regulator of *IGF–I* gene expression (Annunziata, Granata and Ghigo, 2011). In contrast to IGF–I, IGF–II is not regulated by GH (Kaplan and Cohen, 2007). Insulin/IGF signalling has been identified as one of the most important pathways that controls lifespan (Novosyadlyy and Le Roith, 2012). Blood levels of IGF–I are related to age (O'Connor et al., 1998), but they differ markedly between healthy individuals. Total IGF–I, IGFBP–3 and their ratio within one individual, however, show only small changes with age over time (Janssen, 2019). Although it is generally assumed that lower concentrations of IGF–I correlate with longevity, experimental findings do not consistently support this assumption. Lower protein intake during life may favour longevity through a process that regulates the concentration of circulating IGF–I. There may be a specific optimal age–dependent "set point" for each individual for the GH/IGF system which co–determines survival (Janssen, 2019). Enhanced signalling through the GH/IGF axis was noted to accompany an age–related disease – cancer (Anisimov and Bartke, 2013). Therefore, maintaining equilibrium within the IGF system seems to be crucial for healthy living and ageing, and mechanisms that regulate lifespan and tumour incidence are mutually linked.

IGF–II was shown to exert growth–promoting actions in placenta and it influences prenatal growth and foetal development (Cianfarani, 2012). A physiological role of this peptide, however, still remains insufficiently known. Overexpression of the *IGF–II* gene can result in enlarged organs and the entire

body size at birth (Kadakia and Josefson, 2016). Specific polymorphisms of *IGF–II* have been related to an increased weight, obesity, metabolic complications and hypertension (Gaunt et al., 2001; Gu et al., 2002; Faienza et al., 2010). A degree of *IGF–II* methylation at birth seems to be a crucial factor for development of such changes in early childhood (Perkins et al., 2012) and it was proposed to be considered as a biomarker of intrauterine programming (Cianfarani, 2012).

IGF–1R binds IGF–I with high affinity. It also binds IGF–II and insulin but with six and a hundred fold lower affinity (Le Roith 2003; Annunziata, Granata and Ghigo, 2011). IR binds IGF–I with a hundred fold lower affinity than insulin (Ullrich et al., 1986). A hybrid IR/IGF–1R has twenty times greater affinity for IGF–I than for insulin (Sakai, Lowman and Clemmons, 2002). Tumour cells often demonstrate up–regulation or increased activity of IGF–1R (Novosyadlyy and Le Roith, 2012). As mentioned, IR exists in two isoforms where the form IR–A binds insulin and IGF–II, whereas IR–B binds predominantly insulin. The presence of specific isoforms may be associated with tumour development. Aggressive thyroid cancers, for example, overexpress IR–A, IGF–II and IGF–1R (Vella and Malaguarnera, 2018). IGF–2R binds IGF–II, but also mannose–6–phosphate (Man–6–P) and Man–6–P N–acetyl glucosamine (Nadimpalli and Amancha, 2010; Olson et al., 2014). IGF–II, after binding to IGF–2R, is most often degraded, so IGF–2R may be seen as a tumour–suppressor (Scott and Firth, 2004). Independently of the rest of the IGF system, IGF–2R acts as a lectin and regulates intracellular compartmentalisation of acid hydrolases containing Man–6–P residues (Nadimpalli and Amancha, 2010; Olson et al., 2014).

Post–translational modifications of IGFBPs and IGF–Rs, such as glycosylation, phosphorylation, oxidation and others can influence their affinity for IGFs. Phosphorylated IGFBP–1 has high affinity for IGF–I and usually inhibits its activity. During pregnancy, however, it is dephosphorylated by placental alkaline phosphatase to generate isoforms with lower affinity and consequently, increased IGF bioavailability (Solomon et al., 2014). In foetal blood, IGFBP–1 is the principal IGFBP. Maternal diabetes is associated with reduced IGFBP–1 phosphorylation in cord serum, suggesting that diabetes–related changes may additionally increase IGF–I bioavailability and stimulate foetal growth (Loukovaara et al., 2005). Phosphorylation of Ser^{111} enables IGFBP–3 to induce cell apoptosis (Jafari et al., 2018). Phosphorylation and O–glycosylation of IGFBP–5 affect its binding to heparin but not to IGFs (Graham et al., 2007). Glycosylation of IGFBP–3 does not seem to influence IGF binding or formation of protein complexes, but it influences the partitioning of IGFBP–3 between the extracellular milieu and the cell surface (Firth and Baxter, 1999). Post–translational modifications of the IGFBP–binding partners also affect the

formation of protein complexes. Oxidation of fibrinogen, for example, reduces its interaction with IGFBP–1 in patients with diabetes mellitus, which may be important for the duration of bleeding and the speed of wound healing (Gligorijević, Penezić and Nedić, 2017). Ageing or colon cancer caused altered glycosylation of alpha–2–macroglobulin resulting in decreased binding of IGFBP–2, increasing the amount of the free, physiologically active form of IGFBP–2 (Šunderić et al., 2019).

Both IR and IGF–1R belong to a tyrosine kinase family of receptors and they are therapeutic targets for the treatment of malignancy. Tumour cells develop resistance to targeted therapies over time by activating alternative signalling pathways. Enzymatic alteration and regulation of the N–linked glycosylation process are seen as novel targets for developing approaches to sensitize tumour cells to cytotoxic therapies (Contessa et al., 2008; de–Freitas–Junior et al., 2017). Inhibition of N–linked glycosylation of receptors in patients with congenital disorders of glycosylation (CDG) was found to impair receptor processing and surface localization (Klaver et al., 2019). Reduced fucosylation of IGF–1R, due to impaired activity of fucosyltransferase, was shown to suppress proliferation, epithelial–mesenchymal transition, migration and invasion of specific placental cells (Yu et al., 2019). Pathophysiological conditions characterised by an increased oxidative stress, such as colorectal carcinoma, may induce oxidation of IGF receptors reducing their affinity for IGFs (Nedić et al., 2013).

Growing evidence suggests that IGFBP–1 and IGFBP–2 are favourably linked with insulin sensitivity and preclinical data implicate their direct involvement in the regulation of insulin signalling and adiposity (Haywood et al., 2019). These two IGFBPs have been under investigation as therapeutic targets for obesity, metabolic disorders and diabetes. Cancer treatment, on the other hand, most often includes strategies which enable lowering of the IGF concentration and inhibition of IGF–1R signalling (Ryan and Goss, 2008; Caban et al., 2019). A major future need is to identify cell membrane receptors and intracellular proteins which bind individual forms of IGFBPs and the signalling pathways that are activated following these interactions. This information will be useful in creating new therapeutic approaches for altering the activity of IGFs in different diseases.

1.3. PLACENTA

The main barrier as well as the bond between mother and the foetus is the placenta, a multifunctional organ representing the crucial determinant for foetal growth and development. The placenta is the filter that enables transport of

oxygen and all nutrients in the direction of mother–foetus, but it is also a gland that secretes hormones (estrogen, progesterone, growth hormone, human placental lactogen). These hormones additionally support communication between the mother and foetus, in order to regulate maternal physiological adaptation to pregnancy and, more importantly, to fulfil different foetal needs. Placental characteristics, both morphological and functional (such as vascularisation, thickness, cell composition, presence and abundance of different transporter/signalling molecules, hormones, etc.) alter throughout gestation (Fowden et al., 2009; Sandovici et al., 2012).

To understand the processes in the placental cell, the structure of the placenta is shown in Figure 2.

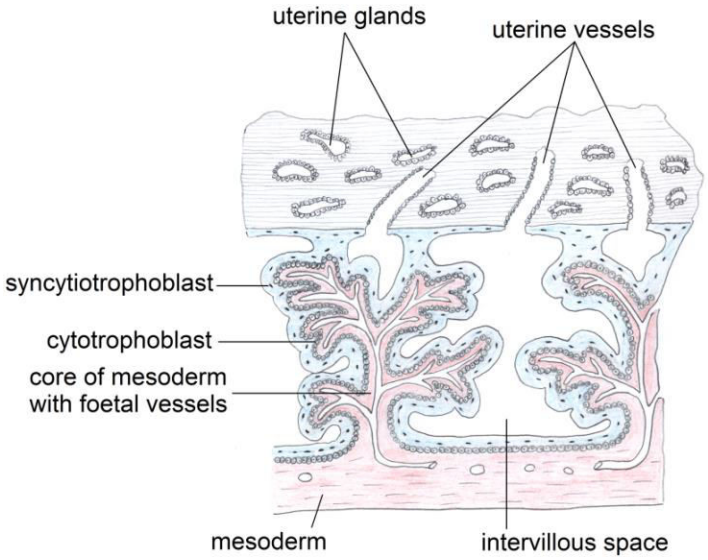

Figure 2. Schematic representation of human placental structures.

In chorionic villi, the cytotrophoblast proliferates and differentiates into extravillous trophoblast or syncytiotrophoblast (Forbes and Westwood, 2008). Extravillous trophoblasts are oriented towards the maternal endometrium into which they migrate and invade and remodel spiral arteries enabling the flow of oxygen and nutrients to the placenta and foetus. The syncytiotrophoblast is a multinucleated layer that ensures nutrient and gas exchange and also serves as a protective barrier (Kingdom et al., 2000). Underneath the syncytiotrophoblast is the mesenchymal core that contains placental capillaries and different cells such as fibroblasts (Kingdom et al., 2000). As this multinucleated layer has no

transcriptional activities, it is reconstituted due to continuous proliferation, differentiation and fusion of cytotrophoblasts (Forbes and Westwood, 2008). The rate of trophoblast turnover is associated with different tissue pathologies and is related to impaired foetal growth – both enhanced and reduced (Jansson and Powell, 2006). Placental nutrient transporters are localized on the syncytiotrophoblast, which is orientated towards the mother and is soaked in maternal blood (Forbes and Westwood, 2008).

1.3.1. The IGF system in healthy placenta

1.3.1.1. IGFs and IGFBPs

IGF–I is known to regulate differentiation of cytotrophoblasts to syncytiotrophoblasts and extravillous trophoblasts (Bhaumick et al., 1992; Milio, Hu and Douglas, 1994; Aplin et al., 2000; Lacey et al., 2002). IGF–I that is synthesized in the villous mesenchyme stimulates extravillous trophoblast migration in a paracrine manner (Lacey et al., 2002). The placenta also produces IGF–II, which has an important role in promoting trophoblast invasion (Hamilton et al., 1998) by inhibiting IGFBP–1 and TIMP3, molecules synthesized by the decidua to limit trophoblast infiltration into maternal tissues (Irwin et al., 2001). IGFBP–3 is the only IGFBP expressed by trophoblasts, fibroblasts of the villous stroma and the amnion and chorion laeve of the foetal membrane (Han et al., 1996; Rogers et al., 1996).

1.3.1.2. IGF–Rs and IR

IGF–1R is located in the trophoblast, villous endothelium and mesenchymal core (Fang et al., 1997; Holmes et al., 1999). In the first trimester of pregnancy IGF–1R is more expressed in the proliferating cytotrophoblasts, whereas at term the main expression site of IGF–1R is the basal membrane of the syncytiotrophoblast and the villous cytotrophoblast – thus, the expression exerts spatial–temporal change (Maruo et al., 1995; Hills et al., 2004). Being located at the basal membrane and the villous cytotrophoblast, IGF–1R is able to bind foetal IGF–I and IGF–II, whose levels can be elevated as a consequence of maternal diabetes. As a result, in such pregnancies, foetal IGF–I may overstimulate processes dependent of this peptide (Hiden et al., 2009).

IGF–1R and IR (as well as HyR) are abundantly expressed in placenta. At the beginning of gestation, in the first trimester, IR is predominantly expressed on the microvillous membrane of the syncytiotrophoblast, and to a lesser extent in the villous cytotrophoblasts, oriented to the maternal circulation. With gestation

advancing, IR expression shifts towards the placental endothelium directed to the foetal blood. Consequently, it is maternal insulin that triggers placental IR in the first trimester of pregnancy, while throughout the pregnancy it is slowly being displaced with foetal insulin, shifting insulin–dependent processes from mother to foetus (Desoye et al., 1994; Hiden et al., 2006; Hiden et al., 2009). At term, IR localisation on the proliferation sites indicates its involvement in the vascular growth which is in accordance with *in situ* data showing enhanced branching angiogenesis in gestational diabetes mellitus (Jirkovská et al., 2002). Elevated levels of foetal insulin can stimulate endothelial cell proliferation and vascular branching via binding to IR present on the sites of villus ramification (Hiden et al., 2009).

IGF–2R is expressed in the microvillous and plasma membranes of trophoblasts (Fang et al., 1997), and after proteolytic cleavage a soluble form of IGF–2R is released. Binding of soluble IGF–2R to IGF–II leads to degradation of this peptide and, hence, inhibition of its effects. It is reported that the molar ratio of IGF–II and the soluble, circulating form of IGF–2R, are related to placental development and the weight of the newborn (Ong et al., 2000). In experiments performed using a human trophoblast–derived choriocarcinoma cell line (BeWo) and placental explants, it was demonstrated that IGF–II protected IGF–2R–expressing BeWo cells from apoptosis, and the salvation of cytotrophoblast from apoptosis was found to be significant in a tissue with normal IGF–2R expression (Harris et al., 2011).

Exploring the N–glycosylation of placental membrane proteins, we demonstrated that gestation affects overall content of N–glycans, by increasing the abundance of core–fucosylated and multiantennary N–glycans, meanwhile lowering the abundance of bisected biantennary N–glycans and terminal α2,3–sialylation (Robajac et al., 2014). During gestation: (i) the content of total fucosylated, core–fucosylated biantennary N–glycans and α2,6–sialylated N–glycans decreases in IR; (ii) the content of total fucosylated and α 2,6–sialylated N–glycans decreases, whereas the content of core–fucosylated biantennary N–glycans increases in IGF–1R; (iii) overall fucosylation of IGF–2R increases together with the content of core–fucosylated biantennary N–glycans (Robajac et al., 2016a). The observed changes were not in accordance with the general pattern of glycosylation of placental membrane proteins, and even receptors differed between themselves.

Placental membrane proteins can be and are differently glycosylated. Most often these (glyco)proteins have been isolated using non–ionic (Triton or Tween) or anionic (sodium dodecyl sulphate, SDS) detergents. However, considering that glycans affect the polarity of (glyco)proteins, and other modifications contribute

with their specific groups, it was demonstrated that the choice of detergent may be crucial for isolation of a specific membrane (glyco)protein. Receptors of the IGF system are not an exception and one must bear this in mind when designing and conducting experiments that are based on the analysis of membrane proteins (Robajac et al., 2017).

1.3.1.3. IGF–Rs/IR signalling in placenta

It was demonstrated *in vitro* that IGF–I and IGF–II prevent apoptosis and enhance proliferation, migration and invasion of human placental villous explants, primary trophoblast cultures and trophoblast cell lines from the first trimester and term, as reviewed by Sferruzzi–Perri et al. (2017). Quantum dot experiments revealed the existence of a trans–syncytial pathway that allows mitotic signals to penetrate from the maternal side to the inner progenitor cells (from syncytium into the cytoplasm of the underlying cytotrophoblast), which proliferate in order to assist placental and foetal growth (Karolczak–Bayatti et al., 2019). Proliferative effects of IGFs are mediated through IGF–1R activation and subsequent triggering of the MAPK signalling pathway, whereas anti–apoptotic effects are mediated via the PI3K–AKT signalling pathway (Forbes et al., 2008). IGF–II effects on the first trimester of human extravillous trophoblast invasiveness (stimulation of cell migration) are mediated via IGF–2R signalling, involving inhibitory G proteins and activation of the MAPK pathway (McKinnon et al., 2001).

Trophoblast migration and invasion are induced via IGFs binding to IGF–1R, and possibly to IR and, again, subsequent activation of the MAPK and PI3K–AKT signalling pathways (Diaz et al., 2007; Mayama et al., 2013). In the primary human trophoblasts, amino acid transporter activity, mediated by insulin and IGF–I, relies on the mTOR pathway (Roos et al., 2009). Insulin–related processes include the control of cell survival, differentiation and proliferation, as well as amino acid metabolism (Ruiz–Palacios et al., 2017). Glucose uptake is regulated by insulin only in the first trimester of pregnancy, while in the third trimester of pregnancy it is not (Ericsson et al., 2005). Insulin binding to IR in placenta activates the Ras–ERK and IRS–PI3K–AKT–mTOR pathways (Knofler et al., 2005; Colomiere et al., 2009). The PI3K–AKT–mTOR pathway affects cell apoptosis and proliferation, but its main responsibility is for nutrient metabolism. The role of AKT in placenta is unknown, although in peripheral tissues AKT triggers mechanisms for translocation of the glucose transporter (GLUT4) from the cytoplasm to the membrane. This mechanism is still poorly understood, as GLUT1, and not GLUT4, is present in placenta (Ruiz–Palacios et al., 2017).

1.3.2. Preeclampsia and intrauterine growth restriction

Preeclampsia (PE) is a condition characterised by increased blood pressure, proteinuria as well as other systemic disorders, diagnosed in women after the 20th week of gestation, and is a leading cause of foetal and maternal mortality, with an incidence of 5% worldwide (Mol and Roberts, 2016). Insufficient invasion of trophoblasts and further incomplete remodelling of spiral arteries are regularly present in the preeclamptic placenta. As a result, placental ischemia, low oxygen levels and oxidative stress are found in this type of placental pathology (Kanasaki and Kalluri, 2009). What is more, when complicated, PE can lead to intrauterine growth restriction (IUGR), and additionally to acute kidney injury, thrombocytopenia, haemolysis and placental abruption, a condition called haemolysis–elevated liver enzymes and low platelet number, also known as HELLP syndrome (Wang, Rana and Karumanchi, 2009).

Reduced foetal growth is closely related to aberrant placental development (Sibley et al., 2005). There are several reports on lower blood concentrations of IGF–I in mothers as well as lower expression of placental IGF–I (Peng, Xue and Xia, 2011; Dubova et al., 2014; Kharb et al., 2016; Kharb et al., 2017), and increased oxidation of placental IGF–1R (Robajac et al., 2015). Recent findings indicate that hypermethylation of the IGF–I promoter is associated with PE (Ma et al., 2018). Levels of IGF–1R were also found to be decreased in reduced foetal growth (Laviola et al., 2005) and elevated in pregnancies complicated by macrosomia (Jiang et al., 2009). Compared to normal placentas, those complicated by IUGR are characterised by a decreased content of IGF–1R, selective impairment of the IRS–2/PI3K pathway, and reduced p38 and c–Jun N–terminal kinase activation (Laviola et al., 2005). An increase in the placental protein content and an increase in the response to IGF–I of IGF–1R, IRS–1 and AKT was reported in small for gestational age placentas, which is, according to Iñiguez et al., a compensatory mechanism in response to IUGR (2014). The same authors recently reported that Klotho mRNA and protein concentration vary due to foetal growth and gestational age and down–regulate the activation induced by IGF–I on IGF–1R and AKT (Iñiguez et al., 2019).

PE is known as a hypoxic condition, and it was reported that hypoxia decreases expression of PI3K–AKT and mTORC1 signalling in trophoblast cell lines (Yung et al., 2012). Low oxygen tension and IGF–I can maintain the multipotency and proliferation of placental mesenchymal stem cell via IGF–1R signalling (Youssef, Iosef and Han, 2014). The same authors also demonstrated that culturing placental mesenchymal stem cells under low oxygen tension modifies IGF signalling through the IGF–1R or IR via ERK1/2 and AKT, also

showing the involvement of these kinases in regulation of stem cell destiny (Youssef and Han, 2016). They also indicated that multipotency of these cells can be mediated by IGF–I and IGF–II actions either via IGF–1R and/or IR (Youssef and Han, 2016). An increase in the content of IR and a decrease in the IGF–1R and IGF–2R content in placentas originating from mothers with diabetes mellitus (DM) and from those diagnosed with PE with IUGR was also reported (Robajac et al., 2015). Common to both DM and PE with IUGR is oxidative stress, and elevated levels of protein carbonyls were reported for samples originating from either pathology (Robajac et al., 2015). Contrary to the general increase of carbonyls in placenta, isolated receptors were affected differently. As can be expected based on their high degree of homology, both IR and IGF–1R carbonylation was increased in PE complicated with IUGR, while DM had no effect on the carbonylation status of these receptors. IGF–2R carbonylation levels were not affected in either of the investigated pathologies suggesting greater resistance of this receptor to oxidative stress (Robajac et al., 2015). The glycan content of membrane proteins was also affected by these conditions (consequences of DM will be discussed in the next section). The overall fucosylation and the content of high–mannose N–glycans with more residues was decreased while the presence of paucimannosidic and high–mannose structures with a lower number of mannose residues was increased in the placentas from pregnancies complicated by PE (Robajac et al., 2016b). Interestingly, changes observed at the level of receptors were found only in the case of IR α2,6–sialylation, which was decreased due to pathology (Robajac et al., 2016b). These findings undoubtedly demonstrated that there is no general pattern being followed by all proteins of the same origin (i.e. membrane proteins), and that each one of them is an entity that should be carefully characterised and its impact on/by different pathology investigated independently of other proteins. Knowing the role of the receptors of the IGF system, it is expected that the observed changes most probably affect downstream processes, as these conditions are characterised with newborns being labelled as either large (DM) or small (IUGR) for gestational age.

Novel findings also indicate a decrease in the expression of *IGF–2R* in placentas from pregnancies complicated by idiopathic IUGR (Harris et al., 2019). Placental expression of IGF–2R was found to be related to changes in the expression of homeobox genes that control cellular signalling pathways responsible for increased trophoblast cell apoptosis, one of the characteristics of IUGR (Harris et al., 2019). All these new reports on the IGF–2R are new arguments in favour of the receptors' role unrelated to simple IGF–II degradation.

1.4. DIABETES

Anomalies in the insulin signalling pathway which may occur either due to the lack of insulin or a reduced sensitivity to insulin of its target tissues, lead to several glucose–related metabolic complications. Before clinical diagnosis of type 1 diabetes, circulating autoantibodies against insulin, glutamic acid decarboxylase, the protein tyrosine phosphatase IA–2, and/or zinc transporter 8 can be detected. While individuals with a single autoantibody type frequently revert to negative status, reversion is rare in people with multiple autoantibodies. To diagnose type 1 diabetes mellitus (DM), a positive result in at least two tests for autoantibodies is required. The presence of islet autoantibodies reflects immune B– and T–cell response to β–cell antigens. This autoimmune response to β–cells leads to the loss of β–cell mass and function giving rise to glucose intolerance and ultimately clinical symptoms of diabetes occur (Skyler et al., 2017). Current estimation is the existence of 425 million people with diabetes and another 352 million with impaired glucose tolerance worldwide, while the long–term prognosis for the year 2045 is 629 million people with diabetes and 532 million of people with impaired glucose tolerance (IDF, 2017).

Type 2 DM develops when β–cells fail to secrete sufficient amounts of insulin in conditions of reduced insulin sensitivity. Although it has complex genetic and environmental aetiology, a major risk for development of type 2 DM is obesity. Ectopic fat deposition in liver and muscle leads to insulin resistance and insulin sensitivity in liver and muscle, which is improved by weight loss. Fat may also accumulate in the pancreas contributing to a reduced function of β–cells, inflammation and death of β–cells. Defects in insulin secretion are at least partially reversible with energy restriction and weight loss in pre–diabetes and recent–onset type 2 DM; however, in the case of long–standing diabetes, reversibility is very difficult (Skyler et al., 2017). While type 1 DM is a consequence of the immuno–mediated destruction of β–cells, and type 2 DM is mainly associated with insulin secretory defects, there is evidence that mechanisms of these two types of diabetes overlap and have some common characteristics. For example, patients with type 2 DM also have reduced β–cell mass (Butler et al., 2003), and, in both types of diabetes, the stress response induced by hyperglycaemia may have a role in β–cell apoptosis (Laybutt et al., 2002). A reduction in the number of functional β–cells is very important for the development of hyperglycaemia and subsequent complications of diabetes. Hence, understanding the functional and differentiation state of β–cells is very important for defining subtypes of diabetes (Skyler et al., 2017).

1.4.1. IGF system in diabetes

By binding to its receptor, insulin exerts multiple effects on metabolism, cell growth and differentiation, and studies have shown that components of the insulin signalling pathway also have a role in growth and secretion of pancreatic β–cells (Porzio et al., 1999; Federici et al., 2001). Some *in vitro* studies have shown that reduction of IGF–Rs enhances insulin sensitivity possibly by reducing the amount of HyR (Haywood et al., 2019). As already mentioned, insulin and IGF–I bind preferably to their specific receptors, although cross–reaction occurs since these hormones and their receptors are structurally very similar. Signalling pathways of these two hormones overlap at some points and may have the same consequences, such as translocation of the GLUT4 transporter on the cell surface (Figure 3).

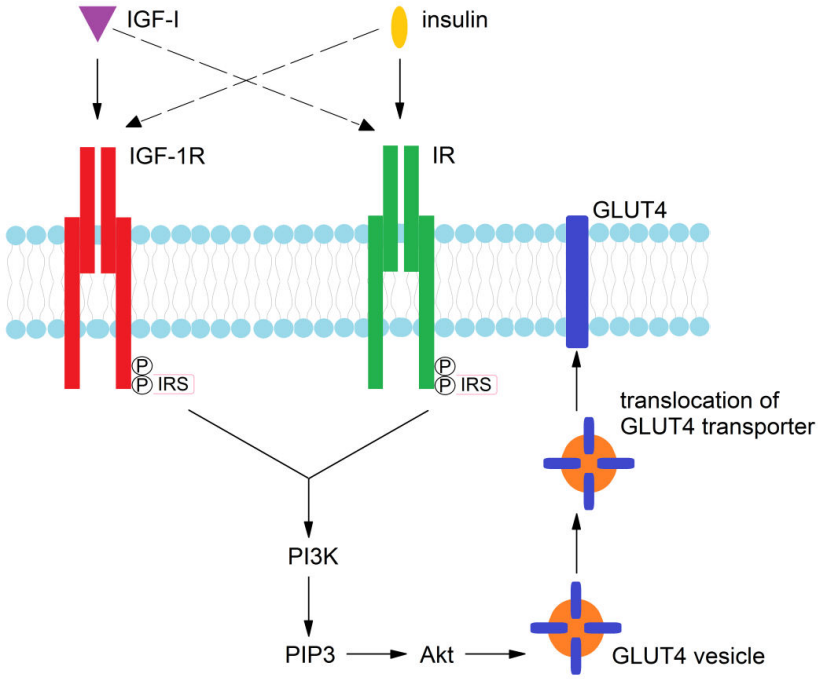

Figure 3. Involvment of the IR and IGF–1R in GLUT4 translocation.

This overlapping mechanism can explain why in normal, healthy conditions IGF–I acts with insulin to lower glucose levels (Sjögren et al., 2001). During the development of insulin resistance, when the glucose level is still within a normal

range, there is an increase in circulating IGF–I bioactivity. When a condition with impaired fasting glucose level develops, IGF–I bioactivity reaches a plateau. At the time when a person is finally diagnosed with type 2 diabetes, IGF–I bioactivity declines (Brugts et al., 2010). Some studies have shown that IGF–I levels are positively associated with insulin sensitivity and negatively with insulin secretion and diabetes in general (Succurro et al., 2009; Teppala et al., 2010). A large cross–sectional study in Denmark suggested a "U–shaped" association between IGF–I blood concentrations and insulin sensitivity, since both high and low IGF–I levels were associated with insulin resistance, compared to subjects with intermediate IGF–I levels (Friedrich et al., 2012). There is, however, no firm biological explanation for this observation. It is suggested that the concentration of IGF–I alone is not sufficient for the assessment of this complex pathological condition. IGF–I is currently not considered as a potential therapeutic agent – while it lowers blood glucose levels it also shows some negative side effects (Moses et al., 1996).

A discovery that two insulin receptor isoforms have distinct functional characteristics created a hypothesis that alterations in the relative amount of these two isoforms may have a causal role in the development of insulin resistance, which is a feature of type 2 diabetes. Studies that explored the expression of two mRNA transcripts, for $Ex11^-$ and $Ex11^+$, offered opposing results. Three studies reported that the expression of these two mRNA species is changed in skeletal muscle of both pre–diabetic insulin–resistant and type 2 diabetic subjects when compared to persons with normal insulin sensitivity (Mosthaf et al., 1991; Mosthaf et al., 1993; Norgren et al., 1993), whilst another three studies failed to confirm these results (Benecke, Flier and Moller, 1992; Anderson et al., 1993; Hansen et al., 1993). Different results were also obtained when relative amounts of two isoforms were analysed. Two studies showed that expression of the IR isoforms is changed in isolated adipocytes and in skeletal muscle membranes in subjects with type 2 DM (Sesti et al., 1991; Kellerer et al., 1993). A third study reported that the expression of the low–affinity IR–B form is significantly increased in fat and skeletal muscle from obese and type 2 diabetic subjects, when compared to non–obese controls (Sesti et al., 1995). An increased expression of the IR–B form significantly correlated with body mass index and fasting glucose levels. However, there is also a report not confirming any difference in the relative proportion of the two IR isoforms in the skeletal muscle of healthy, obese persons without diabetes and obese persons with type 2 DM (Benecke, Flier and Moller, 1992). A caution must be taken, as a small number of subjects involved in the latter study might explain the reported findings and the absence of a difference between the investigated groups. In patients with insulinoma, expression of the

IR–B isoform is significantly increased in their skeletal muscles compared to healthy persons. This increase is positively correlated with the concentration of plasma insulin and negatively with insulin sensitivity (Sbraccia et al., 1996). Noted inconsistencies between reported studies may be a result of differences in PCR protocols, sites of biopsies, control groups used for comparison, metabolic status of the examined subjects and possible contamination of muscle tissue specimens.

1.4.1.1. IR gene mutations and insulin resistance

Insulin resistance syndromes originate from IR malfunction (Ardon et al., 2014; Saito–Hakoda et al., 2018). The *IR* gene is located on the short arm of chromosome 19 and is composed of 22 exons. Mutations that affect the IR coding gene lead to insulin–resistant syndromes such as Leprechaunism, also known as the Donohue syndrome, Rabson–Mendenhall syndrome and type A insulin resistance syndrome. The first two are autosomal recessive disorders, characterised by intrauterine and postnatal growth retardation, dysmorphic features, altered glucose homeostasis, and early mortality. Type A insulin resistance is an autosomal dominant disorder and is characterised, besides insulin resistance, by *acanthosis nigricans* and hyperandrogenism such as polycystic ovarian syndrome. Since type A insulin resistance includes hyperandrogenism, this diagnosis is usually reserved for females, however, diagnosis could be generalized to men as well. Men can have insulin resistance with *acanthosis nigricans*, but without other clinical features such as lipoatrophy (Taylor et al., 1992).

The most severe of the insulin resistance syndromes is Leprechaunism. It is characterised by IUGR, loss of glucose homeostasis and hyperinsulinemia. Dysmorphic features are also present and include prominent eyes, thick lips, upturned nostrils, low–set posteriorly rotated ears, thick skin with lack of subcutaneous fat, distended abdomen, and enlarged genitalia in males and cystic ovaries in females (Longo et al., 1995). Cells from these patients have also markedly reduced insulin binding. A less severe syndrome is Rabson–Mendenhall. This condition was first described in three siblings with dental and skin anomalies, early dentition, coarse senile–looking faces, intellectual disability, prognathism, thick fingernails and *acanthosis nigricans*. Furthermore, insulin–resistant DM, ketoacidosis, intercurrent infections and pineal hyperplasia were also present (Rabson and Mendenhall, 1956). The life–span of patients with this syndrome can be longer than one year, during which they develop constant hyperglycaemia followed by diabetic ketoacidosis and death. This condition is accompanied by a constant reduction of insulin levels, which finally becomes

insufficient to prevent glucose synthesis by liver and the release of fatty acids by adipocytes (Longo, Wang and Pasquali, 1999). Until now, more than one hundred disease–causing mutations on the *IR* gene have been reported and approximately a half of them were identified as type A insulin resistance (Ardon et al., 2014). It has also been reported that mutations with a strong effect on the insulin binding are associated with more severe phenotypes, while a longer survival rate has been reported for mutations where IR function is partially preserved. Definitive correlations, however, cannot be drawn due to the rarity of these conditions and a scarcity of the available experimental data from functional analyses (Longo et al., 2002). The greatest number of the reported mutations in the *IR* gene are categorized as missense (64%), followed by nonsense (13%), while the splice site mutations, deletions and insertions in the coding sequence are less common. Most of the mutations that are located in the first 11 exons result in Leprechaunism, while those in the gene responsible for β–subunit expression are found frequently in patients with Rabson–Mendenhall syndrome (Ardon et al., 2014).

Some variations in the *IR* gene are also thought to have influence on the increased risk for development of type 2 diabetes. Different populations were tested for a Val→Met^{985} mutation, giving no conclusive data since only some of these studies support the role of this mutation as a risk factor for diabetes predisposition (Hart et al., 1999), whereas others do not (Hansen et al., 1997). Barroso and co–workers identified seven single nucleotide polymorphisms in the *IR* gene and found that the one present in the sixth intron on the 46th nucleotide base pair (IVS6+43) is associated with an increased risk for developing type 2 DM (Barroso et al., 2003).

1.4.1.2. IR antibodies

Autoantibodies specific for the IR were also detected (Flier et al., 1975; Chon et al., 2011). This rare phenomenon is also called type B insulin resistance and represents a condition where autoantibodies against cell surface proteins are produced. In general, it is similar to Graves' disease, where antibodies against the thyrotropin receptor are produced, and myasthenia gravis where antibodies against the acetylcholine receptor are produced. Due to this condition, both hyper– and hypoglycaemia may occur with the latter being more frequent (Braund et al., 1987). Whether hyper– or hypoglycaemia will occur depends on the consequence of autoantibody binding to IR. If the binding inhibits signal transducing activity, hyperglycaemia occurs, and if the binding stimulates signal transduction, hypoglycaemia occurs (Jeong et al., 2010; Maiza et al., 2013). Type B insulin resistance is characterised by an extreme insulin resistance, dramatic weight loss, severe hyperandrogenism and a widespread skin condition known as *acanthosis*

nigricans. Medical treatment is usually based on general immunosuppression, and the one including rituximab, cyclophosphamide and pulse steroids in the form of dexamethasone and methylprednisone gave satisfactory results. Nonetheless, the lack of a randomized, placebo–controlled trial is the main disadvantage for testing this treatment approach due to rarity of this disease (Malek et al., 2010).

In one clinical study, which included six non–obese women, severe insulin resistance and *acanthosis nigricans* were detected (Flier et al., 1975). Both basal and glucose stimulated insulin concentrations in plasma of these women were 10– to 100–fold increased. Their response to the injected insulin was markedly reduced, with some of them having to receive 1000 times higher than usual doses of insulin in order to control blood glucose levels. Autoantibodies to insulin were not detected in the blood of these patients and it was proposed that antibody to IR is responsible for this condition (Flier et al., 1975). In another single case study, patient's auto–anti–IR antibody was associated with hypoinsulinemia. Patient's serum and purified immunoglobulins activated IR β–subunit and IRS–1, which led subsequently to phosphorylation of AKT kinase, thus mimicking insulin hormone. After corticosteroid therapy, both IR autoantibody and the occurrence of hypoglycaemia disappeared (Maiza et al., 2013). In the young and adolescent study group, where insulin resistance was already detected, 9.8% of participants had anti–IR antibodies. They had clinical signs of obesity and *acanthosis nigricans*, and no clinical features of autoimmunity. It was suggested that the insulin receptor autoimmunity was responsible for the insulin resistance. These findings highlighted the importance of examining for the existence of anti–IR antibodies in patients with the childhood onset of insulin resistance, as they represent a considerable number of individuals, and are suitable for the development of new treatment approaches (Zhou et al., 2008).

Two types of antibodies against IR were reported to exist in the blood of persons diagnosed with type 1 and type 2 DM: those that inhibit insulin binding and those that immunoprecipitate solubilized receptors without affecting insulin binding, thus interacting with the regions outside of the insulin binding domain (Batarseh et al., 1988). Predominant types of IR antibodies in patients with DM are of the IgM class, different to anti–insulin antibodies found in patients with insulin resistance, where IgG is a dominant class. Patients with type 2 DM included in the study, who were on insulin treatment and had anti–insulin antibodies, had also anti–IR antibodies. In contrast, other patients with type 2 DM who were also on insulin therapy but did not have anti–insulin antibodies also had no anti–IR antibodies. There was no correlation between anti–insulin and anti–IR antibodies in patients with type 1 DM. A highly significant correlation between

the dose of insulin used and anti–IR antibody activity was detected (Batarseh et al., 1988).

In the plasma of patients with type 2 DM or pre–diabetes state, increased protease activity was found compared to healthy persons. A further increase in the proteolytic activity was measured following a high–carbohydrate meal in all three groups. It was suggested that higher proteolytic activity in patients with type 2 DM can cause more intensive cleavage of IR, thus contributing to an increased insulin resistance (Modestino et al., 2019).

1.4.1.3. HyR in diabetes

An increase in HyR abundance would be expected to reduce insulin sensitivity in target tissues, leading to an increased insulin resistance. One study showed that the proportion of HyR was significantly higher in skeletal muscles from patients with type 2 DM than in healthy subjects (Federici et al., 1996). The proportion of HyR was found to correlate with a decrease in both insulin binding affinity and insulin sensitivity, as measured by an insulin tolerance test. When adipose tissue from patients with type 2 DM was analysed, similar results were reported (Federici et al., 1997). Four studies tested whether the observed alterations in the HyR abundance are primarily defects associated with type 2 DM or represent anomalies associated with other common states of insulin resistance. One study revealed that the amount of IR and HyR was increased in the placenta of the insulin resistant women with gestational hypertension (Valensise et al., 1996). The second study showed that the abundance of HyR was increased in the skeletal muscle of the obese subjects and was correlated to an increased body mass index and decreased insulin sensitivity (Federici et al., 1998a). A greater abundance of HyR was also discovered in the skeletal muscle of patients with insulinoma (Federici et al., 1998b) and correlated with both increased plasma insulin levels and a reduced insulin–mediated glucose uptake (Federici et al., 1998a). The abundance of HyR in the skeletal muscle was compared between lean, glucose–tolerant, non–obese subjects with a different degree of insulin sensitivity, and non–diabetic, overweight subjects (Spampinato et al., 2000). Only in subjects with lower insulin sensitivity, the HyR/IR ratio was found to be slightly increased (Spampinato et al., 2000). In general, these studies support the hypothesis that changes in the proportion of HyR may contribute to an impaired insulin action in insulin resistant subjects due to a lower affinity of receptors for insulin. It was suggested that an increased expression of HyR may represent a general defect associated with different states of insulin resistance (Sesti et al., 2001).

1.4.1.4. Acanthosis nigricans

Acanthosis nigricans, a skin condition associated with dark spots, may be manifested in persons with insulin resistance (both A and B types). At physiological concentrations, insulin regulates carbohydrate, lipid and protein metabolism by binding specifically to IR. On the other hand, at higher concentrations, insulin can promote growth, through binding to IGF–1R (Andersen et al., 2017). Binding of insulin to IGF–1R may stimulate proliferation of keratinocytes and fibroblasts, leading to *acanthosis nigricans* (Cruz and Hud, 1992; Phiske, 2014). Both IGFBP–1 and IGFBP–2 are decreased in obese subjects with hyperinsulinemia, thus increasing plasma concentrations of free IGF–I, which promotes cell growth and differentiation. There are several observations supporting the idea that insulin–dependent activation of IGF–1R can facilitate *acanthosis nigricans* development: (i) IGF-Rs are present in cultured fibroblasts and keratinocytes; (ii) insulin can cross the dermoepidermal junction and can stimulate growth and replication of fibroblasts at high concentrations; (iii) the severity of *acanthosis nigricans* in obesity positively correlates with the fasting insulin concentration. It is therefore proposed that insulin may promote development of this condition through direct activation of the IGF–I signalling pathway. Areas such as neck and axillae are most often affected, suggesting that sweating and/or friction may be necessary co–events (Phiske, 2014). Although it seemed that the severity of *acanthosis nigricans* correlated with the level of insulin resistance, this is not always the case. In a case study on a Japanese girl who was diagnosed with type A insulin resistance, *acanthosis nigricans* was not observed (Saito–Hakoda et al., 2018). A new hypothesis was made – that IGF–I resistance in skin cells at a receptor or post–receptor level, or even inhibitory action of the mutant IR on IGF–1R signalling, can contribute to this condition.

1.4.1.5. The impact of diabetes on the cardiovascular system

Cardiovascular complications are the most common complications of diabetes. There is evidence suggesting that the reduction in IGF–1R levels exerts some benefit on the endothelial function in atherosclerosis, although the results are mostly based on animal models (Cubbon, Kearney and Wheatcroft, 2016). DM is also considered as a hypercoagulable state, since diabetic patients are under an increased risk of the development of thrombosis (Tripodi et al., 2011), a condition involved in approximately 80% of diabetes–related deaths. The concentrations of many clotting factors, such as fibrinogen, thrombin, tissue factors, coagulation factors VII, VIII, XI, XII, kallikrein and von Willebrand factor, are increased in diabetes (Carr, 2001; Vazzana et al., 2012). Besides changes in the concentration, chemical modification (glyco–oxidation) of

fibrinogen occurs contributing to thrombosis in diabetes (Dunn et al., 2006; Gligorijević, Penezić and Nedić, 2017). In general, DM induces increased reactivity of platelets, due to several factors: (i) higher mobilisation of Ca^{2+}; (ii) glycation of the platelet membrane which may lead to increased expression of some receptors, including P–selectin, glycoprotein Ib–IX and fibrinogen receptor IIb/IIIa (Kim, Bae and Kim, 2013; Pomero et al., 2015); (iii) a decrease in cAMP concentration (Kakouros et al., 2011). It was recently found that platelets from DM2 patients express high levels of the activated P2Y12 receptor (Hu et al., 2017). All these changes lead to an increased sensitivity of platelets to agonists such as thrombin, ADP and collagen, and also to aspirin resistance (Di Minno et al., 2012).

Results on the effect of insulin on the function of platelets are controversial, since some researchers detected insulin–related inhibitory effects, while others found no change at all (Randriamboavonjy and Fleming, 2009; Ferreiro et al., 2010). IGF–I has a stimulatory effect on wound healing, alone or in coordination with other molecules. Its impaired interaction with IGF–1R is believed to cause delayed skin wound repair in patients with DM (Aghdam et al., 2012). Platelets express IR, IGF–1R and HyR at their surface (Hunter and Hers, 2009). Alone, IGF–I is not able to activate platelets but it potentiates their higher activation in the presence of different activators (Hers, 2007; Kim et al., 2007).

IGF–I is present in α granules which are released upon platelet activation, thus increasing the local concentration of IGF–I at the site of injury. It was reported that platelets from patients with type 2 DM express higher amount of IGF–1R than platelets from healthy controls, whereas the amount of IR was not significantly affected by DM (Gligorijević, Robajac and Nedić, 2019). Although it was suspected that insulin has an inhibitory effect on platelets (Ferreiro et al., 2010), recent results suggest that there is no correlation (Moore et al., 2015). An increased binding of exogenous IGF–I to platelets potentiates their thrombin–induced aggregation, the effect being more pronounced in the case of platelets derived from patients with DM2 (Gligorijević, Robajac and Nedić, 2019). According to the obtained results, it seems that the concentration of IGF–I in the circulation may be one of the factors influencing platelet activation in patients with DM. A weak positive correlation between the concentration of HbA1c and the speed of thrombin–induced platelet activation due to exogenous IGF–I implicates that the severity of DM2 may be related to the effect of IGF–I. An increase in IGF–1R may be one of the mechanisms responsible for the observed effect (Gligorijević, Robajac and Nedić, 2019). In patients with diabetic neuropathy, significantly lower amounts of IGF–1R on erythrocytes were detected compared to control subjects without diabetes and those with diabetes but without

neuropathy (Migdalis et al., 1995). Taken all into consideration regarding IGF–1R, it seems that the expression and the role of this receptor in diabetes differ in a tissue specific manner. Depending on the tissue, both an increase and a decrease of IGF–I signalling can be detected and the potential effects can be either beneficial or detrimental.

Due to a worldwide increased incidence of diabetes, especially in developed countries, attention is drawn to the development of new and effective drugs to either disable transition of glucose intolerance to type 2 DM or to slow down or revert this process. One of the main obstacles in performing this task is the homology between insulin and IGFs, IR and IGF–1R and the overlapping of signalling cascades. It is desirable to construct a molecule being able to bind only to IR, and even more, to interfere only with the metabolic pathway and not the mitogenic. To fulfil this purpose, different orthosteric and antagonistic antibodies have been developed, as well as small peptides and aptamers (Escribano et al., 2017). Still, a successful solution is far from being found and the thorny road is ahead of scientists trying to untangle this riddle.

1.4.2. Gestational diabetes

Maternal insulin resistance appears during gestation to ensure sufficient energy for the foetus. However, when the maternal body is not able to encompass these changes, gestational DM (GDM) develops, and its prevalence in Europe is around 5% (Eades, Cameron and Evans, 2017). GDM is the type of diabetes diagnosed in the second trimester of pregnancy, and is associated with an increased oxidative stress and inflammation in the placenta and foetus (Radaelli et al., 2003; Mrizaki et al., 2014). GDM is associated with different perinatal complications (e.g. macrosomia) which may later in adult life increase a risk of obesity, type 2 diabetes, cardiovascular diseases and metabolic syndrome (Buchanan and Xiang, 2005). This condition is classified as a pre–diabetic state as GDM represents an increased risk of developing type 2 DM later in life (Lee et al., 2008). GDM affects placental structure, altering the transport of nutrients to the foetus (Brett et al., 2014; Araujo et al., 2015). Although glucose transport in the placenta takes place independently of IR – mainly via GLUT1, the placenta is rich in IR and maternal insulin activates IR signalling pathways, affecting placental metabolism (Hiden et al., 2006). Altered expression of IRs is found in the fetoplacental endothelium of GDM women (Lassance et al., 2013), but IR expression is restored by insulin treatment, establishing normal endothelial function and healthy newborns (Guzmán–Gutiérrez et al., 2014).

In the placenta of obese women, the expression of IGF signalling components and nutrient transporters is altered, and is dependent on the maternal body fat mass, gestational weight gain, and the observed macrosomia (Jansson et al., 2013; Brett et al., 2016; Martino et al., 2016). Increased levels of IGF–I and IGF–II in GDM lead to up–regulation of placental amino acid transporters, resulting in an increase in the placental amino acid levels (Cetin et al., 2005). In the obese and mothers with GDM or type 1 diabetes, esterification of fatty acids forms triglycerides which are stored in the placenta (in syncytiotrophoblast) in the form of lipid droplets (Diamant et al., 1982; Elchalal et al., 2005). The key mediators of these actions are fatty acids (Pathmaperuma et al., 2010) and insulin (Hirschmugl et al., 2017). Statins, 3–hydroxy–3–methylglutaryl–coenzyme A reductase inhibitors, are used to lower high levels of the circulating cholesterol, usually diagnosed in the obese and women with metabolic syndrome or type 2 DM. Forbes et al. (2015) demonstrated that in the first trimester villous tissue explants statins attenuated proliferation induced by IGF–I or IGF–II. Altered IGF–1R distribution in trophoblasts was reported to result from the reduced levels of complex N–glycans, responsible for expression of the immature receptor at the cell surface (Forbes et al., 2015).

Although insulin secretion increases in pregnancy due to hyperplasia of pancreatic β–cells (Butler et al., 2010), pregnancy is characterised by a relative insulin resistance state, which favours the metabolic needs of the developing foetus, especially in the third trimester (Tan and Tan, 2013). Investigating the effect of pregestational insulin–dependent DM on the content of placental IGF–Rs and IR N–glycans, we found no changes compared to healthy controls (Robajac et al., 2012). The investigated cohort was very small, consisting of only 5 samples in each group, and the pregnant women had regular check–ups and glycaemic control. Our findings implied that a careful control of glucose levels and an adequate therapy enable the maintenance of physiological homeostasis during pregnancy, thus providing normal foetal growth. When considering the number of cases which can be included in the study, one must bear in mind that most pregnancies with uncontrolled diabetes end with either stillbirth or preterm delivery when babies are too small, underdeveloped and with very little chance of survival.

Activation of IR triggers mTOR, a positive regulator of amino acid transport that stimulates cell proliferation and growth. Therefore, a placentomegaly (an increase in the placental size) and foetal macrosomia (overgrowth of the foetus) that are often found in obese and pregnancies complicated with GDM can be a result of mTORC1 signalling (Jansson et al., 2013). Activation of the mTOR cascade is related to cell survival, metabolism, growth, proliferation and

autophagy and is a sensor of nutrients from the placenta (Jansson, Aye and Goberdhan, 2012). The expression of amino acid carriers is regulated by the mTOR pathway. It is important to mention that this pathway can be activated not only by insulin but also by other growth factors. The expression of amino acid transporters can be regulated via the mTOR pathway by the levels of amino acids (Roos et al, 2009). This is also found in GDM, where an increased food intake may activate the mTOR pathway, further activating amino acid transporters, which can be related to overgrowth and macrosomia (Jansson et al., 2013). Amino acid transporter systems A and L are positively regulated by mTORC1, which is critical for foetal growth (Dimasuay et al., 2016).

As previously stated, some proteins in the placenta can interfere with the signalling pathway of insulin, such as Annexin 2 and 14–3–3 proteins, which are overexpressed in GDM placentas and can block the insulin signalling pathway, contributing to insulin resistance found in GDM (Liu et al., 2012). A decrease in AKT levels (Ruiz–Palacios et al., 2017b) and an increase in levels of the PI3K subunit p85α (Alonso et al., 2006; Colomiere et al., 2009) occur in the placental insulin resistance in GDM treated with diet. Because the insulin signalling pathway is not much damaged in the GDM placenta, it is probable that insulin resistance can be treated by exogenous insulin therapy (Ruiz–Palacios et al., 2017).

1.5. CANCER

Next to cardiovascular diseases, the malignant diseases are the leading cause of mortality in the modern world. Lung, prostate, colorectal, stomach and liver cancers are the most common types of cancer in men, while breast, colorectal, lung, cervix and thyroid cancer are the most common among women. During the last year, 9.6 million people died from conditions associated with cancer (WHO).

Cancer arises as a consequence of neoplastic transformation of cells and tissues – a disturbance of tissue homeostasis in the direction of uncontrolled cell proliferation and inhibition of cell death by apoptosis. Neoplastic transformation is a multistep process, as presented in Figure 4.

Each step is characterised by gene alterations which lead to normal cell transformation into the malignant one. It is known that during the transformation, the cell loses control mechanisms, which leads to an increased growth potential, alterations on cell membranes, karyotype anomalies and various morphological and biochemical changes (Harley et al., 1994).

The traditional view, in which cancer is regarded as a simple lump of cells that uncontrollably divide is discarded, since new findings show that they are complex tissues comprised of many heterogeneous cells which interact in multiple ways. The surrounding of the cancer cells is also very important in tumour genesis and progression, as it plays an active role in the incitement of cancer cell dynamics (Hanahan and Weinberg, 2011).

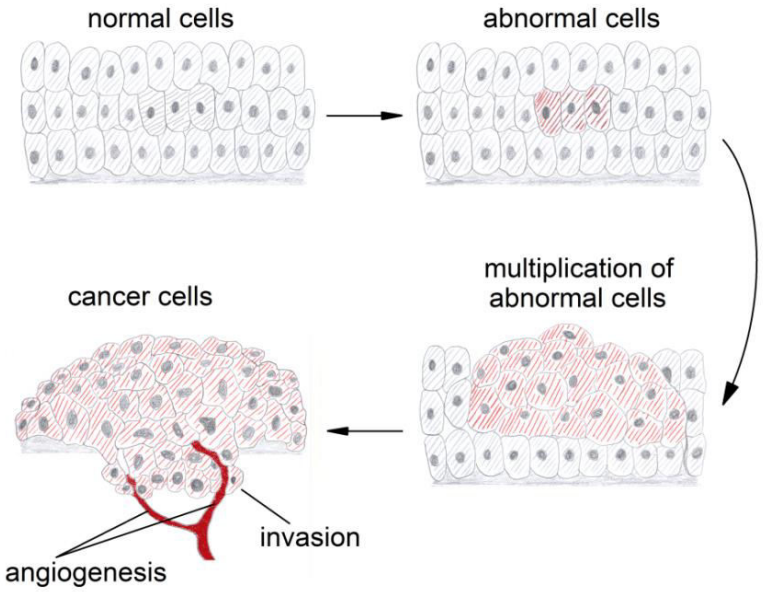

Figure 4. Neoplastic transformation of cells.

1.5.1. General characteristics of cancer cells

Each cancer cell is distinguished by six determinants which enable the cell to evade or circumvent the limiting mechanisms that check that everything is under control. There are ten so–called "hallmarks of cancer" (Fiaschi and Chiarugi, 2012) and each of them will be carefully addressed in the following paragraphs, as cancer has become a hot topic for the last few decades and understanding of its mechanisms is set among the top scientific priorities.

1.5.1.1. ***Self–sufficiency of proliferative signals*****.** One of the best–known characteristics of the cancer cell is its potential for chronic proliferation. Normal tissues possess control mechanisms which carefully "weigh" the amount of

growth–promoting and growth–inhibiting signals that are produced, directing cells to some point of the growth/division cycle. Cancer cells acquire a transformed phenotype, which is characterised by disordered signalling cascades, allowing cells to grow and divide uncontrollably (Sever and Brugge, 2015).

Growth signals, which direct normal cell cycle, are usually produced in a paracrine fashion, spatially and temporally conditioned, and often "stored" in the pericellular space, where their action is controlled by a multitude of enzymes which activate them in a tissue localized manner. Experimental study of this kind of regulation is demanding and hardly accessible, which is the reason why we do not know much about that level of regulatory mechanism (Kataoka et al., 2003).

On the other hand, cancer cells pave their own way through the "wilderness", without letting neighbouring cells decide on their fate. Growth factors which they produce act in an autocrine manner, binding to surface receptors which are either structurally altered to become more sensitive to ligand binding and/or are produced in greater quantities, making them more responsive to limiting amounts of ligands (Walsh et al., 1991). Beside altered upstream members of the signalling cascade (ligands and receptors), the downstream elements can also be changed becoming hyperactive, usually through somatic mutations that render them constitutively active. One of the downstream signalling molecules that is very often mutated in cancer cells is the catalytic subunit of PI3K (Yuan and Cantley, 2008; Jiang and Liu, 2009).

1.5.1.2. ***Insensitivity to anti–proliferative signals*****.** One of the ways to control cell growth and division is through negative–feedback mechanisms. Consequently, the cell can respond to various signals to which it is exposed (Amit et al., 2007). Any disturbance in the circuit can lead to continuous proliferation. It is documented that in various types of cancer, some stage of this control becomes defective. For instance, mTOR is one of the key regulators that influences the flux of information in the cell, upstream and downstream of the PI3K pathway. When this switch gets hampered, the loss of the negative–feedback mechanism leads to a prolonged activation of PI3K and its effector AKT/PKB, thus disabling the anti–proliferative role of mTOR (Sudarsanam et al., 2010).

Although excess signalling leads to cellular proliferation, it was shown that overexpression of oncogenes leads to a state called senescence and/or apoptosis. Mooi and Peeper (2006) found cells with morphological features of senescence in some cases of melanoma, so it seems that this is an obstacle that transformed cells must overcome in order to achieve pro–proliferative characteristics.

Tumour–suppressor genes are another level of protection from the unconstrained cell cycle. They have an ability to abort the progression of a cell through cyclic changes if they "sense" something is wrong, by integration of

signals from extracellular and intracellular sources. One of the prototypical tumour–suppressor genes is the one that expresses Rb (retinoblastoma–associated) (Burkhart and Sage, 2008) and TP53 proteins (Soussi and Wiman, 2015). Rb protein usually filters the signals from the extracellular milieu, while TP53 monitors the intracellular changes, such as the supply of oxygen and nutrients, changes in genome structure etc. When the messages that the cell receives are unfavourable, the programs for senescence or apoptosis are activated. If the expression of these proteins is somehow inhibited, the cell is left without a break and is free to grow and divide without any limitation.

Another way in which the proliferative potential of the cell is kept under control is through contact inhibition, which prevents cells to migrate and divide, when in contact with the neighbouring cells. Cancer cells are insensitive to this mechanism and will keep moving across adjacent cells and dividing, forming disordered, multi–layered patterns. Since contact inhibition is preserved in normal cells, they will stop dividing in the contact with the cancer cells. This can be one of the mechanisms by which cancer affects distant tissues that it colonises during metastasis, where it leads to shrinkage of the affected organ (Ribatti, 2017).

1.5.1.3. ***Invasion and metastasis*****.** After some time, proliferating cancer cells start to populate surrounding tissues, as a single cell or as a group of cells interconnected by adhesion molecules and other communication junctions. The first step in this process is detachment of the cell from its environment, e.g. other cells and the extracellular matrix, followed by a change in its shape, enabling it to overcome spatial restrictions and to migrate without constraint. Cancer cells develop a phenotype that is a feature of embryonic tissues when cells actively migrate and proliferate in the process of organogenesis (Berx and van Roy, 2009).

Invasion is the first step in the cascade of events, with the final act being dissemination to distant, receptive tissues (metastasis). The second step in the metastasis process is intravasation, when cells escape the primary site of origin and enter the circulatory system through local blood and lymphatic vessels. When they reach a certain organ, the cell(s) leave the vessels lumina (extravasion), and populate it, forming small clusters which grow into a micrometastatic lesions and finally to a macroscopic tumour (colonization) (Seyfried and Huysentruyt, 2013). What is interesting is that certain tumour cells prefer to colonize only specified organs (the “seed and soil” theory). It is believed that cancer cells can thrive only in the environment that is similar to the place where the primary tumour developed. For example, prostate cancer usually metastasizes to bones, colon cancer has a tendency to metastasize to the liver, while in women stomach cancer often metastasises to the ovary (Akhtar et al., 2019).

The cancer cells' environment is not just a silent observer in the process of metastasis, but an active helper. Cancer cells manipulate the normal cells around them, by sending signals which activate them. It is known that macrophages at the periphery of the tumour, after activation by cancer cells, secrete proteases which degrade the extracellular matrix, helping cancer cells in invasion and colonization (Kessenbrock, Plaks and Werb, 2010). This type of metastasis is termed "mesenchymal", and is characteristic of cancers that arise from epithelial tissues (carcinomas). There are two other ways in which cancer cells can invade and colonize distant tissues. One way is called "collective" invasion and involves a set of cells which travel together into adjacent tissues, and the other is "amoeboid" invasion, in which cells take a more plastic form, enabling them to squeeze through cracks in the extracellular matrix, rather than degrade it (Krakhmal et al., 2015).

1.5.1.4. ***Limitless replication*****.** The main characteristic of a normal cell is its mortality. After a certain number of growth/division cycles the cell enters a state in which it is viable, but without the possibility to replicate, the so called senescence. If the cell goes on beyond that point, it enters a crisis and succumbs to cellular death, apoptosis. These two points (senescence and crisis) represent checkpoints which prevent cells to enter a limitless replication sequence. One of the structures that prevents this are small repeats at the end of chromosomes, called telomeres. After each division cycle, a telomere shortens slightly, eventually losing its ability to protect the chromosome from end–to–end fusion, resulting in a disruption of karyotype stability, thus triggering a program of conducted cellular death. Cancer cells, however, gain the possibility to overcome this hurdle. Their telomeres do not shorten, enabling them to become immortal. The majority of cancer cells produce a telomerase, which extends telomeric DNA after division, making cells prone to endless division (Jafri et al., 2016).

1.5.1.5. ***Continuous angiogenesis*****.** Like any other cell, the cancer cell also needs nutrients, oxygen and a waste disposal system to survive. These needs are satisfied via blood vessels, which deliver nutrients and oxygen and remove carbon–dioxide and metabolic waste products. During embryogenesis, blood vessels are continuously formed. Endothelial cells are differentiated into capillaries and bigger blood vessels, and new sprouts of capillaries are formed from existing ones, making the circulatory system of the body (Folkman, 2007). During adulthood, angiogenesis occurs rarely, only in specific cases such as wound healing and during the female reproductive cycle (Tepper et al., 2005). The occurrence of intensive angiogenesis is noticed in neoplastic transformation of cells. As cancer cells divide and grow they get further and further away from the nearest capillary and the source of vital components dries out. The locally

induced hypoxia can activate the expression of vascular endothelial growth factor (VEGF), a pro–angiogenic factor that stimulates the formation of new blood vessels (Katayama et al., 2019). Oncogenes can also activate the expression of this protein. A number of angiogenic inhibitors can be detected in the circulation. They are usually fragments of proteins that are not inhibitors themselves (plasmin, collagen). Inactivation of these entities can lead to neoplastic transformation in cells (Ribatti, 2009a).

1.5.1.6. ***Escaping apoptosis*****.** Programmed cell death, or apoptosis is a mechanism through which cells commit voluntary suicide, and it happens when proper functioning is irreparable and if there are no other possibilities for rescue. The most manifested stressors inducing this mechanism are disturbances in signalling (survival signals) and anomalies in the DNA. The cellular fate is determined by a fine balance between pro– and anti–apoptotic factors which belong to the Bcl–2 family. The main pro–apoptotic proteins are Bax and Bak, and they are found in the outer mitochondrial membrane. The three main anti–apoptotic proteins are Bcl–2, Bcl–x_L and Bcl–w (Adams and Cory, 2007).

As previously mentioned, TP53 is one of the main tumour supressors in the cell, and its activation induces a signalling cascade which leads to apoptosis. Cancer cells evolve a mechanism to inactivate this protein, thus, eliminating a critical sensor (Zawacka–Pankau and Selivanova, 2015). They can also produce pro–surviving factors, such as IGFs (Yu and Rohan, 2000), which can deceive the cell disabling its apoptosis. Down–regulation of pro–apoptotic proteins is another strategy for survival (Igney and Krammer, 2002).

1.5.1.7. ***Change in cell metabolism.*** When supplied with sufficient oxygen, cells synthesize ATP through a process of oxidative phosphorylation: glycolysis is executed in the cytosol, glucose is transformed to pyruvate and then to carbon dioxide in mitochondria. Under anaerobic conditions, the pyruvate is not directed to mitochondria and the amount of ATP produced per 1 mol of glucose is very low. The German physiologist and doctor Otto Warburg noticed that cancer cells prefer to produce ATP solely under the glycolytic condition, the state being called “aerobic glycolysis” (Warburg, 1956). In cancerous tissue, as a result of inflammation, the availability of nutrients and hence glucose are reduced. The metabolic shift is partially achieved through an up–regulation of GLUT1 transporters which increase the influx of glucose in the cell. Activated oncogenes are among the main stimulators of glycolysis (Hsu and Sabatini, 2008). It is not known why cancer cells use the aerobic glycolysis mechanism for creating energy, especially since this production is nutritionally costly. One plausible explanation is that, in this way, the intermediates of the path are redirected

towards synthesis of important molecules such as nucleotides and certain amino acids (Vander Heiden, Cantley and Thompson, 2009).

1.5.1.8. ***Escaping immune destruction.*** The immune system monitors every irregularity and destroys cells which are not inherent to an organism, or which are in some way transformed. This is a way to halt any process which leads to destructive changes. Cells of the innate and adaptive immune system constantly patrol through the body, and if they detect changed structures, they destroy the affected cell. Tumours and, eventually cancer, arises as a consequence of transformed cells managing to escape the immune system surveillance. Cancer cells possess the ability to modify their antigens in order to trick the immune system, and survive. The cells of the immune system can destroy a certain portion of transformed cells, but a small number of them that acquired favourable mutations, remain and become dominant over the immune system, by establishing an immunosuppressive environment (Ribatti, 2017b).

1.5.1.9. ***Genome instability and mutation.*** Cancer cells are prone to a high mutation rate, where subpopulation of cells achieves a favourable phenotype, enabling them to gain a selective advantage and to thrive (Negrini, Gorgoulis and Halazonetis, 2010). This genomic instability arises as a consequence of increased sensitivity to mutagenic signals and inactivation of proteins which take part in the maintenance of the genome. These proteins detect and repair mistakes made during genomic expression, and neutralise potentially damaging agents (Jackson and Bartek, 2009). An increased rate of general mutation is also a consequence of mutational inactivation of tumour suppressor genes, which monitor the activities inside the cell and, if necessary, direct cells to senescence or apoptosis, such as *TP53* (Lane, 1992).

1.5.1.10. ***Tumour–promoting inflammation.*** The constituent parts of tumour tissue are immune cells, equally originating from innate and adaptive arms of the immune system (Man et al., 2013). The most obvious explanation for their appearance is an attempt by the immune system to eradicate tumour cells. By trying to eliminate the transformed cells, they secrete a variety of signalling molecules, which is similar to the immune response to invading pathogens or in wound healing. But these molecules, which should help healthy cells, this time do more harm than good. It was previously said that cancer cells gain the advantage by escaping the immune surveillance. When they do so, they are free to replicate and proliferate, helped by stimulatory molecules that immune cells secrete (various growth factors, such as EGF and VEGF, pro–angiogenic factors, chemokines) (Grivennikov, Greten and Karin, 2010).

1.5.2. IGF system and cancer

The IGF system is a very important mediator which orchestrates cellular actions that lead to growth, division, differentiation or programmed cellular death. It must be tightly controlled, since any mistake can potentially lead to disturbances which, in the case of cancer, may end up with uncontrolled cell division (Samani et al., 2007).

An increased expression of IGF–I, IGF–II, IGF–1R or the combination of these molecules was found in many types of tumours such as glioblastoma (Sandberg et al., 1988), neuroblastoma (Lichtor, Kurpakus and Gurney, 1993), breast cancer (Gebauer, Jäger and Lang, 1998), colorectal (Freier et al., 1999), pancreatic (Bergmann et al., 1995) and ovarian cancer (Sayer et al., 2005). The elements of the IGF system act as paracrine and/or autocrine factors in the stimulation of tumour growth *in situ* or during tumour progression, and their roles depend upon type of the tissue. As mentioned earlier, the *IGF–II* gene is expressed only from the paternal allele, through a mechanism known as imprinting, which silences the mother's copy of the gene. The loss of imprinting activates both alleles, and raises significantly the amount of IGF–II in the circulation. An increased expression of IGF–II was noted in Wilms' tumour (Ogawa et al., 1993) and subsequently in various gynaecological (Chen et al., 2000) and gastrointestinal neoplasias (Cui et al., 2003).

The action of IGFs is restrained, as they are bound to IGFBPs which control their action, i.e. restrict them from binding to IGF–1R. The change in the amount of these proteins can influence the amount of IGF bound to a cognate receptor (Clemmons et al., 1995). IGFBP–3 is the most abundant binding protein, so the variation in its concentration exerts the greatest influence on the availability of IGFs. *In vitro* experiments have shown that IGFBP–3 plays a protective role against cancer, through direct binding of IGFs or through IGF independent actions, since it can directly interact with specific receptors on the surface of the cell or inside it, and activate the apoptotic cascade (Grimberg, 2000). Anti–apoptotic properties of IGFBP–3 were so far confirmed only in *in vitro* studies (Grill, Sivaprasad and Cohick, 2002), the results being inconsistent in epidemiological studies (Renehan et al., 2004). IGFBPs can also have pro–tumorigenic actions, by expressing their IGF independent effects. It was shown that IGFBP–2 can inhibit the action of PTEN, a major tumour suppressor (Zeng et al., 2015), and the positive correlation between serum IGFBP–2 concentration and cancer cell invasiveness was found in patients with colorectal (Šunderić et al., 2014), prostate (Uzoh et al., 2011), and breast (So et al., 2008) cancers and various types of leukaemia (Kühnl et al., 2011).

Metastasis is a process that includes interplay between the cancer cell and its surrounding. In order to leave its original habitat and to invade other regions, the cell must surpass many barriers, and usually not so welcome microenvironment. Some of the obstacles that it must overcome are: (i) the need for nutrients and oxygen; (ii) the existence of an extracellular matrix; (iii) tissue barriers; (iv) adaptation for survival in a new environment (Chambers, Groom and MacDonald, 2002). The elements of the IGF system can provide the cell much needed help in any of these steps.

The main characteristic of the cancer cell is its fast rate of growth and proliferation. In order to keep up with such a hectic pace, the cell's metabolism craves for nutrients and oxygen. As the cell grows and divides, it becomes more and more remote from the nearest capillary as a source of nutrient/fuel, so it must overcome this problem. One of the solutions is to secrete factors which stimulate the formation of new blood vessels in the process known as neovascularisation. The main trigger for this stimulation can be local hypoxia. IGFs and insulin can precede and/or augment the hypoxic stimulus (Samani et al., 2007). Experiments with cultured cells demonstrated that IGF–I/II can induce expression of hypoxia–inducible factor 1α (HIF–1α) (Feldser et al., 1999), which can activate the HIF–1/arylhydrocarbon receptor nuclear complex involved in the activation of genes that contain the hypoxia response element, such as VEGF, a major tumour–induced pro–angiogenic factor (Zelzer et al., 1998). IGFs act via the MAPK and PI3K pathways. The other way in which IGF peptides can stimulate angiogenesis is through direct stimulation of endothelial cells for migration and differentiation. IGFs play a paracrine role by entering the surrounding capillaries, where they participate in cell survival and stability (Grulich–Henn et al., 2002). The hypoxia can, on the other hand, induce production of IGFs. Experiments performed on the human hepatocellular carcinoma cell line (HepG2), confirmed that IGF–II production is up–regulated by hypoxia, through involvment of Erg–1 transcription factor and Wilms' tumour (WT) 1 suppressor gene. Hypoxia activates Erg–1 and induces expression of the IGF–II promoter gene, while the WT1 suppressor gene is silenced (Kim et al., 1998).

If they want to leave their place of origin, cancer cells must break through a network of intertwined threads that constitute the extracellular matrix. In order to do so, they must degrade the matrix by the action of several enzymes called matrix metalloproteinases (MMPs), especially MMP–2 and MMP–9, which are associated with angiogenesis and tumour invasion. It was shown that elements of the IGF system can regulate expression of these MMPs, thus promoting cell migration and invasion (Long, Navab and Brodt, 1998; Mira et al., 1999).

1.5.2.1. IGF–1R/IR and cancer

Biological actions of IGF peptides, as already mentioned, are achieved through binding to three types of receptors: IR, IGF–1R and HyR (IR/IGF–1R). In adult, healthy tissues, IR is responsible for signals that stimulate metabolic actions, while IGF–1R transfers the information that stimulates cellular growth and division. In transformed cells, this is not so clear–cut, as the signalling pathways can become interconected and synergistic (Malaguarnera and Belfiore, 2011). Cancer cells usally overexpress the IR–A isoform by 60% to even 100% compared to healthy cells (Malaguarnera and Belfiore, 2011). Since this type of receptor has a high binding affinity for IGF–II and IGF–1R for IGF–I and IGF–II, stimulatory effects of IGFs can be maximized.

IGF–2R acts as a tumour suppressor since it binds IGF–II leading it to degradation inside the cell. Various structural aberrations, such as mutations, loss of heterozygosity and microsatellite instability, can alter the activity of this receptor, as was found in many tumours (Souza et al., 1999). Although the primary function of IGF–2R is to bind and sequester IGF–II from the extracellular space, it was discovered that it can activate TGF–β1 (O'Gorman et al., 2002), a growth inhibitor for most types of cells, and influence the sensitivity of cancer cells to the host immune system (Motyka et al., 2000).

Activation of IGF–1R leads to a series of cascade events, with a main goal to save the cell from apoptosis and to stimulate its growth and division (Figure 5). Binding of IGF–I/II to IGF–1R activates the PI3K–AKT–mTOR pathway, which results in protein synthesis, growth and preparation of the cell to replicate (Butler et al., 1998).

The activity of PI3K is controlled by a PTEN, a well–known tumour suppressor. It acts as phosphatase, causing dephosphorylation of PI3K, thus inhibiting the downstream signalling process. The PTEN molecule is the second most commonly deactivated tumour–suppressor in human cancer. Activation of the PI3K–AKT pathway enables the cell to avoid pro–apoptotic signals by inactivation of the pro–apoptotic Bcl–2–associated agonist of cell death, known as Bad protein (Moorehead et al., 2003).

Reactive oxygen species (ROS) are by–products of cell metabolism, arising from processes responsible for energy production, cell signalling and destruction of foreign “invaders”, among other processes. The cell holds an intrinsic balance which is based on a delicate equilibrium between produced ROS and molecules that act as their neutralizers (antioxidants). When this state becomes disrupted, the cell enters a condition called oxidative stress (Betteridge, 2000). Oxidative stress usually has devastating effects on a cell, by inducing death or senescence at least, but this is not always the case. Generated ROS can induce positive reinforcement

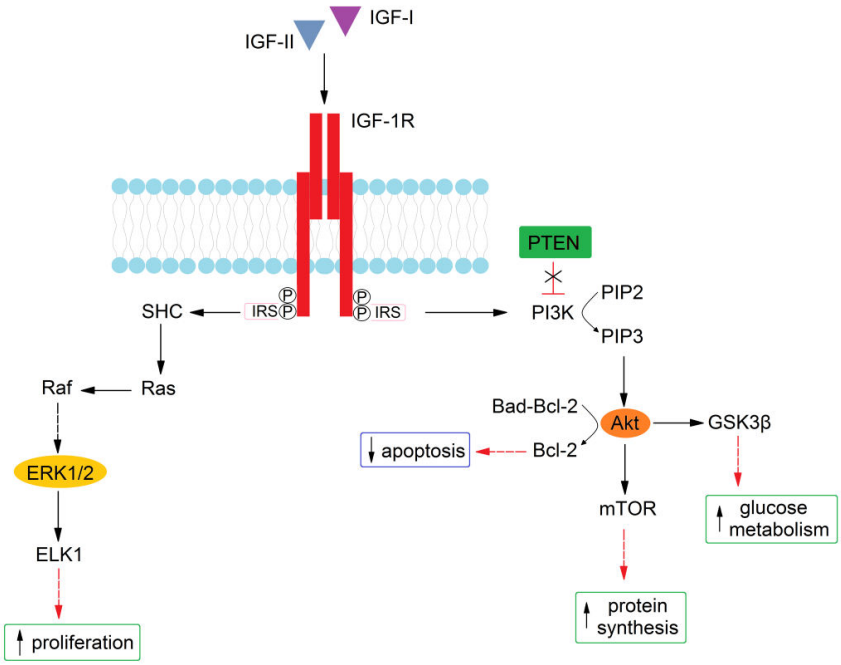

Figure 5. IGF–1R signaling pathway in cancer.

on each step the cell needs in order to transform itself to a malignant form (Reuter et al., 2010). One of the first steps in this transformation cycle is the so called "epithelial–mesenchymal" (EMT) transition, in which a cell gains properties which enable it to acquire a more aggressive phenotype. ROS can influence a number of signalling pathways involved in this process, particularly those involving an extracellular matrix (ECM) (Mani et al., 2008).

It is already known that a change in the glycosylation pattern accompanies the shift towards neoplastic transformation. Cancer cells often exhibit novel glycan structures, which are not present in normal cells; however, many of them are being expressed in the foetal phase (Dennis and Laferte, 1987). Each step of the malignant transformation is followed by some alteration in the glycan structure. Inside the transformed cell, the expression levels of certain glycosyl–transferases are altered, in order to encourage metastasis and cancer spreading (Gu et al., 2009). It is known that some tumour types are characterised by altered glycosylation patterns, and this feature can serve to establish biomarkers, if further clinical investigations show their tissue specificity (Adamczyk, Tharmalingam and Rudd, 2012). IGF–1R is glycosylated and possesses a unique

glycan signature, which enables proper functioning, reflected in ligand binding and signal transduction. A change in the glycosylation pattern can influence these characteristics and alter the responsiveness of the receptor to its ligands.

1.5.2.2. IGF system and colorectal cancer

Colorectal cancer is the third most common cancer diagnosed in the general population. In 2018, there were over 1.8 million new cases worldwide. Out of 25 countries with the highest incidence rate of this type of cancer, Hungary leads, with 51.2 new cases per 100,000 people, in both sexes (World Cancer Research Fund/American Institute for Cancer Research).

Colorectal cancer is derived from the epithelial cells that coat the inner surface of the colon and rectum (De Rosa et al., 2015). The initial investigations, which consisted of immunostaining of the higher–grade and higher–stage cancer tissues, showed strong response to anti–IGF–1R antibody, in adenocarcinomas and their metastases (Hakam et al., 1999). The colorectal cancer cell lines (CaCo–2) demonstrated a higher expression rate of IGF–II and IGF–1R (Zarrilli et al., 1994).

Although the preclinical data is convincing, the epidemiological studies are not so straightforward. The study on UK patients with acromegaly revealed no higher risk for the occurrence of colorectal cancer than in the healthy population, although they have increased level of IGF–I in the circulation (Orme et al., 1998). On the other hand, in a prospective study conducted on 210 colorectal cancer patients that underwent resection, immunohistochemical analysis showed that expression of IGF–I and IGF–1R seems to increase with tumour size (Shiratsuchi et al., 2011).

1.5.2.3. Post–translational changes of IGF receptors in colorectal cancer (an experimental model)

Post–translational modifications (PTM) represent a tool by which the structure and function of proteins can be manipulated, exerting a fine tuning control of proteins and enabling them to change their activity in accordance with changing environmental conditions. The majority of PTMs are enzymatically controlled and coordinated, but sometimes proteins can be modified randomly, in an unplanned manner (Walsh et al., 2005). As a consequence, they can even lose their function, or gain a new one, such as antigenicity (Kurien et al., 2006).

One such modification is protein oxidation, caused by ROS. Cancer is a state with elevated oxidative stress, which reflects on proteins as one of the targets. By employing a radioreceptor assay, we showed that ^{125}I–IGF–I was able to bind more strongly to IGF–1R in tumour samples than in non–tumour samples,

whereas the binding of ^{125}I–IGF–II to IGF–1/2R was the same in both groups of samples (Nedić et al., 2013). Although oxidative stress accompanies malignant processes in the cell and its environment, not all proteins are equally exposed or susceptible to modification. Whether proteins will be oxidatively modified depends on their structure, location, concentration and nature, as well as on the concentration and type of ROS present (Barelli et al., 2008). DNP modification of membrane proteins isolated from colon tissue revealed that total membrane proteins are only slightly modified in tumour samples (Nedić et al., 2013). Unlike oxidized IGF–2R, the oxidized IGF–1R could be detected only in fragments, suggesting that oxidation of IGF–1R makes it more susceptible to degradation than oxidation of IGF–2R. An increased binding of ^{125}I–IGF–I to IGF–1R in tumour samples, without increased concentration of the receptor compared to healthy tissues, led to a conclusion that structural changes induced an increase in affinity, which may be a result of the oxidative alteration of the protein (Nedić et al., 2013).

Aberrant glycosylation is a common feature of neoplastic changes in the cell. The glycan moiety is mostly found on the cell surface and extracellular matrix, and participates in cellular interactions (Ohtsubo and Marth, 2006). Since the cell–environment contact is very important in cancer spreading, changes in the glycan structure of proteins can be more predictive than changes in the structure of the protein itself. As already mentioned, IGF–Rs are glycosylated and IGF–1R is overactive in cancer pathology. Until now, there is no data on the glycosylation pattern of IGF receptors in colon cancer. In an unpublished study (Robajac et al., 2020), use of a reverse–phase lectin microarray revealed the strongest interaction of IGF–Rs isolated from colon cancer tissue and adjacent non–tumour tissue, with lectins MAL–II and WGA, implying that receptors are rich in terminal α2,3 Sia (MAL–II) and GlcNAc β1,4 GlcNAc or Sia (WGA). Our preliminary results with lectins ConA and AAL suggest that IGF–Rs in tumour tissues are exposed to an increased fucosylation and mannosylation; both of these glycosylation changes are already known to accompany cell transformation to cancer phenotype. The glycans of IGF–Rs most probably affect their structure, ligand binding, signalling, and interaction with physiological lectins.

1.5.2.4. IGF in therapy

Radio–/chemotherapy is still a primary choice for treating cancer. Although cells are exposed to agents which act as cytostatics (unfortunately, healthy cells are also affected), after some time, cancer cells can escape the inhibitory effect of therapy and become resistant, or even appear as a more aggressive phenotype (Jones, 2016). IGF–1R plays a significant role in acquiring such features. Some of

the mechanisms involved in the resistance to therapy are: (i) loss of the inhibitory effect of a number of molecules such as WT1 and miRNA on IGF–1R expression (Chen et al., 2011; Wang et al., 2014); (ii) overactivation of IGF–1R by constitutively secreted IGF–I (Montazami et al., 2015); (iii) overactivation of IGF–1R by the Src oncogene (Werner and Le Roith, 2000). Signals originating from IGF–1R control the expression of the multidrug resistance protein 1 (MDR1) (Benabbou et al., 2014), a member of the ABC (ATP–binding cassette transporter) protein family, which act as importers and exporters of different molecules in a cell. Their elevated expression in cancer leads to an increased efflux of cytostatic drugs and consequential decrease in the therapeutic response (Zhang et al., 2015). In addition to residing in the cell membrane, IGF–1R can be translocated into the nucleus where it acts as a transcriptional regulator, by controling the expression of genes responsible for cell cycle progression (Sarfstein et al., 2012; Vesel et al., 2017).

There have been trials to design a therapeutic medium that will interfere with IR/IGF–1R signalling, in order to silence the signalling cascade that stimulates cancer cells to divide in an uncontroled manner. The first targets are IGF peptides. Chen et al. (2018) designed an antibody that neutralised both IGF–I and IGF–II, preventing them from binding to IGF–1R. This antibody inhibited growth of the breast cancer cell line by as much as 40%, at the lowest concentration added to the culture medium. Another direction of intervention is to use anti–receptor antibodies, that would compete with IGFs for binding to IGF–1R, but without activation of the signalling cascade. Investigations of that type have even reached phase III of clinical investigation (figitumumab), but the outcome was rather disappointing. Anti–receptor antibodies were not efficient enough and caused metabolic toxicity (Langer et al., 2014). The problem with anti–receptor antibodies was that, although designed not to interact with IR, they nevertheless caused hyperinsulinemia and hyperglycaemia. The explanation can be found in activation of the feedback mechanism, since the pituitary gland senses insufficient IGF activity and secretes higher amounts of growth hormone. Growth hormone causes depression of insulin sensitivity in tissues, which ultimately leads to hyperinsulinemia, and consequently to hyperglycaemia (Pollak, 2012).

1.6. CONCLUSION

Two very distinct but profoundly related processes of placental development and carcinogenesis have been used as model systems throughout this chapter to explain the roles of membrane receptors. As discussed, they are both characterised

by fast cell growth and proliferation, high invasiveness and cell migration. One of them mimics tumour metastasis while the other one is an actual process of tumour metastasis, the only difference being tight regulation of oncogenes and oncogenic processes during placentation, as extensively reviewed by West, Bouma and Winger (2018). We examined the role of IGF–1R, IR and IGF–2R in these processes, as these membrane glycoproteins are responsible for glucose metabolism, protein and nucleic acid synthesis, cell growth, proliferation, survival and apoptosis. As explained in this chapter, all of these closely related and to some extent opposite processes intertwine and the plethora of overlapping signals settles the IGF system at the crossroad between the good (desirable) and bad (harmful) pathophysiological events. It is the surrounding and, hence, the phenotype that is the driving force to reach the final verdict on *whether the story will be bitter or sweet*.

ACKNOWLEDGMENTS

This work was supported by the Ministry of Education, Science and Technological Development of the Republic of Serbia, under the project number 173042. Data reported in this chapter resulted from several national and bilateral projects.

REFERENCES

Adamczyk B, Tharmalingam T, Rudd PM. Glycans as cancer biomarkers. *Biochim Biophys Acta*. 2012;1820(9):1347–1353.

Adams JM, Cory S. The Bcl–2 apoptotic switch in cancer development and therapy. *Oncogene*. 2007;26(9):1324–1337.

Aghdam SY, Eming SA, Willenborg S, Neuhaus B, Niessen CM, Partridge L, Krieg T, Bruning JC. Vascular endothelial insulin/IGF–1 signaling controls skin wound vascularization. *Biochem Biophys Res Comm*. 2012;421(2):197–202.

Akhtar M, Haider A, Rashid S, Al–Nabet ADMH. Paget's "Seed and Soil" theory of cancer metastasis: An idea whose time has come. *Adv Anat Pathol*. 2019;26(1):69–74.

Alonso A, Del Rey CG, Navarro A, Tolivia J, Gonzalez CG. Effects of gestational diabetes mellitus on proteins implicated in insulin signalling in human placenta. *Gynecol Endocrinol*. 2006;22(9):526–535.

Amit I, Citri A, Shay T, Lu Y, Katz M, Zhang F, Tarcic G, et al. A module of negative feedback regulators defines growth factor signaling. *Nat Genet*. 2007;39(4):503–512.

Andersen M, Nørgaard–Pedersen D, Brandt J, Pettersson I, Slaaby R. IGF1 and IGF2 specificities to the two insulin receptor isoforms are determined by insulin receptor amino acid 718. *PLoS One*. 2017;12(6):e0178885.

Anderson CM, Henry RR, Knudson PE, Olefsky JM, Webster JG. Relative expression of insulin receptor isoforms does not differ in lean, obese, and noninsulin–dependent diabetes mellitus subjects. *J Clin Endocrinol Metab*. 1993;76(5):1380–1382.

Anisimov VN, Bartke A. The key role of growth hormone–insulin–IGF–I signaling in ageing and cancer. *Crit Rev Oncol/Hematol*. 2013;87(3):201–223.

Annunziata M, Granata R, Ghigo E. The IGF system. *Acta Diabetol*. 2011;48(1):1–9.

Aplin JD, Lacey H, Haigh T, Jones CJ, Chen CP, Westwood M. Growth factor–extracellular matrix synergy in the control of trophoblast invasion. *Biochem Soc Trans*. 2000;28(2):199–202.

Arabkhari M, Bunda S, Wang Y, Wang A, Pshezhetsky AV, Hinek A. Desialylation of insulin receptors and IGF–1 receptors by neuraminidase–1 controls the net proliferative response of L6 myoblasts to insulin. *Glycobiology*. 2010;20(5):603–16.

Araujo JR, Keating E, Martel F. Impact of gestational diabetes mellitus in the maternal–to–fetal transport of nutrients. *Curr Diab Rep*. 2015;15(2):569.

Ardon O, Procter M, Tvrdik T, Longo N, Mao R. Sequencing analysis of insulin receptor defects and detection of two novel mutations in *INSR* gene. *Mol Genet Metab Rep.* 2014;1:71–84.

Bach LA. IGF–binding proteins. *J Mol Endocrinol*. 2018;61(1):T11–T28.

Barelli S, Canellini G, Thadikkaran L, Crettaz D, Quadroni M, Rossier JS, Tissot JD, Lion N. Oxidation of proteins: Basic principles and perspectives for blood proteomics. *Proteomics Clin Appl*. 2008;2(2):142–157.

Barroso I, Luan J, Middelberg RPS, Harding AH, Franks PW, Jakes RW, Clayton D, Schafer AJ, O'Rahilly S, Wareham NJ. Candidate gene association study in type 2 diabetes indicates a role for genes involved in β–cell function as well as insulin action. *PloS Biology*. 2003;1(1):41–55.

Batarseh H, Thompson RA, Odugbesan O, Barnett AH. Insulin receptor antibodies in diabetes mellitus. *Clin Exp Immunol*. 1988;71(1):85–90.

Belfiore A, Malaguarnera R, Vella V, Lowrence MC, Sciacca L, Frasca F, Morrione A, Vigneri R. Insulin receptor isoforms in physiology and disease: an updated view. *Endocr Rev*. 2017;38(5):379–431.

Benabbou N, Mirshahi P, Bordu C, Faussat AM, Tang R, Therwath A, Soria J, Marie JP, Mirshahi M. A subset of bone marrow stromal cells regulate ATP–binding cassette gene expression via insulin–like growth factor–I in a leukemia cell line. *Int J Oncol*. 2014;45(4):1372–1380.

Benecke H, Flier JS, Moller DE. Alternatively spliced variants of the insulin receptor protein. Expression in normal and diabetic human tissues. *J Clin Invest*. 1992;89(6):2066–2070.

Benyoucef S, Surinya KH, Hadaschik D, Siddle K. Characterization of insulin/IGF hybrid receptors: contributions of the insulin receptor L2 and Fn1 domains and the alternatively spliced exon 11 sequence to ligand binding and receptor activation. *Biochem J*. 2007;403(3):603–613.

Bergmann U, Funatomi H, Yokoyama M, Beger HG, Korc M. Insulin–like growth factor I overexpression in human pancreatic cancer: evidence for autocrine and paracrine roles. *Cancer Res*. 1995;55(10):2007–2011.

Berx G, van Roy F. Involvement of members of the cadherin superfamily in cancer. *Cold Spring Harb Perspect Biol*. 2009;1(6):a003129.

Betteridge DJ. What is oxidative stress? *Metabolism*. 2000;49(2 Suppl 1):3–8.

Bhaumick B, George D, Bala RM. Potentiation of epidermal growth factor–induced differentiation of cultured human placental cells by insulin–like growth factor–I. *J Clin Endocrinol Metab*. 1992;74(5):1005–1011.

Blum WF, Alherbish A, Alsagheir A, El Awwa A, Kaplan W, Koledova E, Savage M. The growth hormone–insulin–like growth factor–I axis in the diagnosis and treatment of growth disorders. *Endocr Connect*. 2018;7(6):R212–R222.

Brahmkhatri VP, Prasanna C, Atreya HS. Insulin–like growth factor system in cancer: novel targeted therapies. *Biomed Res Int*. 2015;538019.

Braund WJ, Williamson DH, Clark A, Naylor BA, Buley ID, Chapel HM. Autoimmunity to insulin receptor and hypoglycaemia in patient with Hodgkin's disease. *Lancet*. 1987;1(8527):237–240.

Brett KE, Ferraro ZM, Holcik M, Adamo KB. Placenta nutrient transport–related gene expression: the impact of maternal obesity and excessive gestational weight gain. *J Matern Fetal Neonatal Med*. 2016;29(9):1399–1405.

Brett KE, Ferraro ZM, Yockell–Lelievre J, Gruslin A, Adamo KB. Maternal–fetal nutrient transport in pregnancy pathologies: The role of the placenta. *Int J Mol Sci*. 2014;15(9):16153–16185.

Brioude F, Kalish JM, Mussa A, Foster AC, Bliek J, Ferrero GB, Boonen SE, et al. Expert consensus document: Clinical and molecular diagnosis, screening and

management of Beckwith–Wiedemann syndrome: an international consensus statement. *Nat Rev Endocrinol*. 2018;14(4):229–249.

Brugts MP, van Duijn CM, Hofland LJ, Witteman JC, Lamberts SW, Janssen JA. IGF–I bioactivity in an elderly population: Relation to insulin sensitivity, insulin levels, and the metabolic syndrome. *Diabetes*. 2010;59(2):505–508.

Buchanan TA, Xiang AH. Gestational diabetes mellitus. *J Clin Invest*. 2005;115(3):485–491.

Burkhart DL, Sage J. Cellular mechanisms of tumour suppression by the retinoblastoma gene. *Nat Rev Cancer*. 2008;8(9):671–682.

Butler AE, Cao–Minh L, Galasso R, Rizza RA, Corradin A, Cobelli C, Butler PC. Adaptive changes in pancreatic beta cell fractional area and beta cell turnover in human pregnancy. *Diabetologia*. 2010;53(10):2167–76.

Butler AE, Janson J, Bonner–Weir S, Ritzel R, Rizza RA, Butler PC. β–Cell deficit and increased β–cell apoptosis in humans with type 2 diabetes. *Diabetes*. 2003;52(1):102–110.

Butler AA, Yakar S, Gewolb IH, Karas M, Okubo Y, LeRoith D. Insulin–like growth factor–I receptor signal transduction: At the interface between physiology and cell biology. *Comp Biochem Physiol B Biochem Mol Biol*. 1998;121(1):19–26.

Caban M, Owczarek K, Chojnacka K, Lewandowska U. Overview of polyphenols and polyphenol–rich extracts as modulators of IGF–1, IGF–1R, and IGFBP expression in cancer diseases. *J Funct Foods*. 2019;52:389–407.

Carr ME. Diabetes mellitus. A hypercoagulable state. *J Diabetes Complications*. 2001;15(1):44–45.

Cassidy FC, Charalambous M. Genomic imprinting, growth and maternal–fetal interactions. *J Exp Biol*. 2018;221(Suppl 1).pii: jeb164517.

Cetin I, de Santis MS, Taricco E, Radaelli T, Teng C, Ronzoni S, Spada E, Milani S, Pardi G. Maternal and fetal amino acid concentrations in normal pregnancies and in pregnancies with gestational diabetes mellitus. *Am J Obstet Gynecol*. 2005;192(2):610–617.

Chambers AF, Groom AC, MacDonald IC. Dissemination and growth of cancer cells in metastatic sites. *Nat Rev Cancer*. 2002;2(8):563–572.

Chen MY, Clark AJ, Chan DC, Ware JL, Holt SE, Chidambaram A, Fillmore HL, Broaddus WC. Wilms' tumor 1 silencing decreases the viability and chemoresistance of glioblastoma cells in vitro: A potential role for IGF–1R de–repression. *J Neurooncol*. 2011;103(1):87–102.

Chen CL, Ip SM, Cheng D, Wong LC, Ngan HY. Loss of imprinting of the IGF–II and H19 genes in epithelial ovarian cancer. *Clin Cancer Res*. 2000;6(2):474–479.

Chen Z, Liu J, Chu D, Shan Y, Ma G, Zhang H, Zhang XD, et al. A dual–specific IGF–I/II human engineered antibody domain inhibits IGF signaling in breast cancer cells. *Int J Biol Sci*. 2018;14(7):799–806.

Chon S, Choi MC, Lee YJ, Hwang YC, Jeong IK, Oh S, Ahn KJ, et al. Autoimmune hypoglycemia in a patient with characterization of insulin receptor autoantibodies. *Diabetes Metab J*. 2011:35(1):80–85.

Cianfarani S. Insulin–like growth factor–II: new roles for an old actor. *Front Endocrinol*. 2012;3:118.

Clemmons DR. Role of IGF–binding proteins in regulating IGF responses to changes in metabolism. *J Mol Endocrinol*. 2018;61(1):T139–T169.

Clemmons DR, Busby WH, Arai T, Nam TJ, Clarke JB, Jones JI, Ankrapp DK. Role of insulin–like growth factor binding proteins in the control of IGF actions. *Prog Growth Factor Res*. 1995;6(2-4):357–366.

Colomiere M, Permezel M, Riley C, Desoye G, Lappas M. Defective insulin signaling in placenta from pregnancies complicated by gestational diabetes mellitus. *Eur J Endocrinol*. 2009;160(4):567–578.

Contessa JN, Bhojani MS, Freeze HH, Rehemtulla A, Lawrence TS. Inhibition of n–linked glycosylation disrupts receptor tyrosine kinase signaling in tumor cells. *Cancer Res*. 2008;68(10):3803–3809.

Coolican SA, Samuel DS, Ewton DZ, McWade FJ, Florini JR. The mitogenic and myogenic actions of insulin–like growth factors utilize distinct signaling pathways. *J Biol Chem*. 1997;272(10):6653–6662.

Cruz PD, Hud JA. Excess insulin binding to insulin–like growth factor receptors: proposed mechanism for acanthosis nigricans. *J Invest Dermatol*. 1992;98(6 Suppl):82S–85S.

Cubbon RM, Kearney MT, Wheatcroft SB. Endothelial IGF–1 Receptor signalling in diabetes and insulin resistance. *Trends Endocrinol Metab*. 2016;27(2):96–104.

Cui H, Cruz–Correa M, Giardiello FM, Hutcheon DF, Kafonek DR, Brandenburg S, Wu Y, He X, Powe NR, Feinberg AP. Loss of IGF2 imprinting: A potential marker of colorectal cancer risk. *Science*. 2003;299(5613):1753–1755.

Czech MP, Massague J. Subunit structure and dynamics of the insulin receptor. *Fed Proc*. 1982;41(11):2719–2723.

de–Freitas–Junior JCM, Andrade–da–Costa J, Silva MC, Pinho SS. Glycans as regulatory elements of the insulin/IGF system: impact in cancer progression. *Int J Mol Sci*. 2017;18(9):1921.

Dennis JW, Laferte S. Tumor cell surface carbohydrate and the metastatic phenotype. *Cancer Metastasis Rev*. 1987;5(3):185–204.

De Rosa M, Pace U, Rega D, Costabile V, Duraturo F, Izzo P, Delrio P. Genetics, diagnosis and management of colorectal cancer. *Oncol Rep*. 2015;34(3):1087–1896.

Desoye G, Hartmann M, Blaschitz A, Dohr G, Hahn T, Kohnen G, Kaufmann P. Insulin receptors in syncytiotrophoblast and fetal endothelium of human placenta. Immunohistochemical evidence for developmental changes in distribution pattern. *Histochemistry*. 1994;101(4):277–285.

Di Minno MND, Lupoli R, Palmieri NM, Russolillo A, Buonauro A, Di Minno G. Aspirin resistance, platelet turnover, and diabetic angiopathy: A 2011 update. *Thromb Res*. 2012;129(3):341–344.

Diamant YZ, Metzger BE, Freinkel N, Shafrir E. Placental lipid and glycogen content in human and experimental diabetes mellitus. *Am J Obstet Gynecol*. 1982;144(1):5–11.

Diaz LE, Chuan YC, Lewitt M, Fernandez–Perez L, Carrasco–Rodríguez S, Sanchez–Gomez M, Flores–Morales A. IGF–II regulates metastatic properties of choriocarcinoma cells through the activation of the insulin receptor. *Mol Hum Reprod*. 2007;13(8):567–576.

Dimasuay KG, Boeuf P, Powell TL, Jansson T. Placental responses to changes in the maternal environment determine fetal growth. Front Physiol. 2016;7:12.

Dridi L, Seyrantepe V, Fougerat A, Pan X, Bonneil E, Thibault P, Moreau A, et al. Positive regulation of insulin signaling by neuraminidase 1. *Diabetes*. 2013;62(7):2338–2346.

Duan C, Bauchat JR, Hsieh T. Phosphatidylinositol 3–kinase is required for insulin–like growth factor–I–induced vascular smooth muscle cell proliferation and migration. *Circ Res*. 2000;86(1):15–23.

Dubova EA, Pavlov KA, Lyapin VM, Kulikova GV, Shchyogolev AI, Sukhikh GT. Expression of insulin–like growth factors in the placenta in preeclampsia. *Bull Exp Biol Med*. 2014;157(1):103–107.

Dunn EJ, Philippou H, Ariëns RAS, Grant PJ. Molecular mechanisms involved in the resistance of fibrin to clot lysis by plasmin in subjects with type 2 diabetes mellitus. *Diabetologia*. 2006;49(5):1071–1080.

Dupont J, LeRoith D. Insulin and insulin–like growth factor I receptors: similarities and differences in signal transduction. *Horm Res*. 2001;55(Suppl 2):22–26.

Eades CE, Cameron DM, Evans JMM. Prevalence of gestational diabetes mellitus in Europe: A meta–analysis. *Diabetes Res Clin Pract*. 2017;129:173–181.

Elchalal U, Schaiff WT, Smith SD, Rimon E, Bildirici I, Nelson DM, Sadovsky Y. Insulin and fatty acids regulate the expression of the fat droplet–associated protein adipophilin in primary human trophoblasts. *Am J Obstet Gynecol*. 2005;193(5):1716–1723.

El–Shewy HM, Lee MH, Obeid LM, Jaffa AA, Luttrell LM. The insulin–like growth factor type 1 and insulin–like growth factor type 2/mannose–6–phosphate receptors independently regulate ERK1/2 activity in HEK293 cells. *J Biol Chem*. 2007;282:26150–26157.

Ericsson A, Hamark B, Jansson N, Johansson BR, Powell TL, Jansson T. Hormonal regulation of glucose and system A amino acid transport in first trimester placental villous fragments. *Am J Physiol Regul Integr Comp Physiol*. 2005;288(3):R656–662.

Escribano O, Beneit N, Rubio–Longás C, López–Pastor AR, Gómez–Hernández A. The role of insulin receptor isoforms in diabetes and its metabolic and vascular complications. *J Diabetes Res*. 2017;1403206.

Faienza MF, Santoro N, Lauciello R, Calabrò R, Giordani L, Di Salvo G, Ventura A, et al. IGF2 gene variants and risk of hypertension in obese children and adolescents. *Pediatr Res*. 2010;67(4):340–344.

Fang J, Furesz TC, Lurent RS, Smith CH, Fant ME. Spatial polarization of insulin–like growth factor receptors on the human syncytiotrophoblast. *Pediatr Res*. 1997;41(2):258–265.

Federici M, Hribal ML, Ranalli M, Marselli L, Porzio O, Lauro D, Borboni P, et al. The common Arg972 polymorphism in insulin receptor substrate–1 causes apoptosis of human pancreatic islets. *FASEB J*. 2001;15(1):22–24.

Federici M, Lauro D, D'Adamo M, Giovannone B, Porzio O, Mellozzi M, Tamburrano G, Sbraccia P, Sesti G. Expression of insulin/IGF–I hybrid receptors is increased in skeletal muscle of patients with chronic primary hyperinsulinemia. *Diabetes*. 1998b;47(1):87–92.

Federici M, Porzio O, Lauro D, Borboni P, Giovannone B, Zucaro L, Hribal ML, Sesti G. Increased abundance of insulin/insulin–like growth factor–i hybrid receptors in skeletal muscle of obese subjects is correlated with *in vivo* insulin sensitivity. *J Clin Endocrinol Metab*. 1998a;83(8):2911–2915.

Federici M, Porzio O, Zucaro L, Giovannone B, Borboni P, Marini MA, Lauro D, Sesti G. Increased abundance of insulin/IGF–I hybrid receptors in adipose tissue from NIDDM patients. *Mol Cell Endocrinol*. 1997;135(1):41–47.

Federici M, Zucaro L, Porzio O, Massoud R, Borboni P, Lauro D, Sesti G. Increased expression of insulin/insulin–like growth factor–I hybrid receptors in skeletal muscle of noninsulin–dependent diabetes mellitus subjects. *J Clin Invest*. 1996;98(12):2887–2893.

Feldser D, Agani F, Iyer NV, Pak B, Ferreira G, Semenza GL. Reciprocal positive regulation of hypoxia–inducible factor 1alpha and insulin–like growth factor 2. *Cancer Res*. 1999;59(16):3915–3918.

Ferreira IG, Pucci M, Venturi G, Malagolini N, Chiricolo M, Dall'Olio F. Glycosylation as a main regulator of growth and death factor receptors signaling. *Int J Mol Sci*. 2018;19(2).pii: E580.

Ferreiro JL, Gómez–Hospital JA, Angiolillo DJ. Platelet abnormalities in diabetes mellitus. *Diab Vasc Dis Res*. 2010;7(4):251–259.

Fiaschi T, Chiarugi P. Oxidative stress, tumor microenvironment, and metabolic reprogramming: a diabolic liaison. *Int J Cell Biol*. 2012:762825.

Firth SM, Baxter RC. Characterisation of recombinant glycosylation variants of insulin–like growth factor binding protein–3. *J Endocrinol*. 1999;160(3):379–387.

Firth SM, Baxter RC. Cellular actions of the insulin–like growth factor binding proteins. *Endocr Rev*. 2002;23(6):824–854.

Flier JS, Kahn CR, Roth J, Bar RS. Antibodies that impair insulin receptor binding in an unusual diabetic syndrome with severe insulin resistance. *Science*. 1975;190(4209):63–65.

Folkman J. Angiogenesis: An organizing principle for drug discovery? *Nat Rev Drug Discov*. 2007;6(4):273–286.

Forbes K, Shah VK, Siddals K, Gibson JM, Aplin JD, Westwood M. Statins inhibit insulin–like growth factor action in first trimester placenta by altering insulin–like growth factor1receptor glycosylation. *Mol Hum Rep*. 2015;21(1):105–114.

Forbes K, Westwood M. The IGF Axis and Placental Function. *Horm Res*. 2008;69(3):129–137.

Forbes K, Westwood M, Baker PN, Aplin JD. Insulin–like growth factor I and II regulate the life cycle of trophoblast in the developing human placenta. *Am J Physiol Cell Physiol*. 2008;294(6):C1313–1322.

Fowden AL, Sferruzzi–Perri AN, Coan PM, Constancia M, Burton GJ. Placental efficiency and adaptation: endocrine regulation. *J Physiol*. 2009;587(Pt 14):3459–3472.

Frasca F, Pandini G, Scalia P, Sciacca L, Mineo R, Costantino A, Goldfine ID, Belfiore A, Vigneri R. Insulin receptor isoform A, a newly recognized, high–affinity insulin–like growth factor II receptor in fetal and cancer cells. *Mol Cell Biol*. 1999;19(5):3278–3288.

Freier S, Weiss O, Eran M, Flyvbjerg A, Dahan R, Nephesh I, Safra T, Shiloni E, Raz I. Expression of the insulin–like growth factors and their receptors in adenocarcinoma of the colon. *Gut*. 1999;44(5):704–708.

Friedrich N, Thuesen B, Jørgensen T, Juul A, Spielhagen C, Wallaschofksi H, Linneberg A. The association between IGF–I and insulin resistance: a general population study in Danish adults. *Diabetes Care*. 2012;35(4):768–773.

Gatenby VK, Imrie H, Kearney M. The IGF–1 receptor and regulation of nitric oxide bioavailability and insulin signalling in the endothelium. *Eur J Physiol*. 2013;465(8):1065–1074.

Gaunt TR, Cooper JA, Miller GJ, Day IN, O'Dell SD. Positive associations between single nucleotide polymorphisms in the IGF2 gene region and body mass index in adult males. *Hum Mol Genet*. 2001;10(14):1491–1501.

Gebauer G, Jäger W, Lang N. mRNA expression of components of the insulin–like growth factor system in breast cancer cell lines, tissues, and metastatic breast cancer cells. *Anticancer Res*. 1998;18(2A):1191–1195.

Girnita L, Worrall C, Takahashi S, Seregard S, Girnita A. Something old, something new and something borrowed: emerging paradigm of insulin–like growth factor type 1 receptor (IGF–1R) signaling regulation. *Cell Mol Life Sci*. 2014;71(13):2403–2427.

Gligorijević N, Penezić A, Nedić O. Influence of glyco–oxidation on complexes between fibrin(ogen) and insulin–like growth factor binding protein–1 in patients with diabetes mellitus type 2. *Free Radic Res*. 2017;51(1): 64–72.

Gligorijević N, Robajac D, Nedić O. Enhanced platelet sensitivity to IGF-1 in patients with type 2 diabetes mellitus. *Biochem. (Mosc)* 2019;84(10):1213-1219.

Graham ME, Kilby DM, Firth SM, Robinson PJ, Baxter RC. The *in vivo* phosphorylation and glycosylation of human insulin–like growth factor–binding protein–5. *Mol Cell Proteomics*. 2007;6(8):1392–1405.

Graves JA, Renfree MB. Marsupials in the age of genomics. *Annu Rev Genomics Hum Genet*. 2013;14:393–420.

Grill CJ, Sivaprasad U, Cohick WS. Constitutive expression of IGF–binding protein–3 by mammary epithelial cells alters signaling through Akt and p70S6 kinase. *J Mol Endocrinol*. 2002;29(1):153–162.

Grimberg A. P53 and IGFBP–3: Apoptosis and cancer protection. *Mol Genet Metab*. 2000;70(2):85–98.

Grivennikov SI, Greten FR, Karin M. Immunity, inflammation, and cancer. *Cell*. 2010;140(6):883–899.

Grulich–Henn J, Ritter J, Mesewinkel S, Heinrich U, Bettendorf M, Preissner KT. Transport of insulin–like growth factor–I across endothelial cell monolayers and its binding to the subendothelial matrix. *Exp Clin Endocrinol Diabetes*. 2002;110(2):67–73.

Gu D, O'Dell SD, Chen XH, Miller GJ, Day IN. Evidence of multiple causalsites affecting weight in the IGF2–INS–TH region of human chromosome 11. *Hum Genet*. 2002;110(2):173–181.

Gu J, Sato Y, Kariya Y, Isaji T, Taniguchi N, Fukuda T. A mutual regulation between cell–cell adhesion and N–glycosylation: implication of the bisecting GlcNAc for biological functions. *J Proteome Res*. 2009;8(2):431–435.

Guzmán–Gutiérrez E, Arroyo P, Salsoso R, Fuenzalida B, Sáez T, Leiva A, Pardo F, Sobrevia L. Role of insulin and adenosine in the human placenta microvascular and macrovascular endothelial cell dysfunction in gestational diabetes mellitus. *Microcirculation*. 2014;21(1):26–37.

Haeusler RA, McGraw TE, Accili D. Biochemical and cellular properties of insulin receptor signalling. Nat Rev *Mol Cell Biol*. 2018;19(1):31–44.

Hakam A, Yeatman TJ, Lu L, Mora L, Marcet G, Nicosia SV, Karl RC, Coppola D. Expression of insulin–like growth factor–1 receptor in human colorectal cancer. *Hum Pathol*. 1999;30(10):1128–1133.

Hamilton GS, Lysiak JJ, Han VK, Lala PK. Autocrine–paracrine regulation of human trophoblast invasiveness by insulin–like growth factor (IGF)–II and IGF–binding protein (IGFBP)–1. *Exp Cell Res*. 1998;244(1):147–156.

Han VK, Bassett N, Walton J, Challis JR. The expression of insulin–like growth factor (IGF) and IGF–binding protein (IGFBP) genes in the human placenta and membranes: evidence for IGF–IGFBP interactions at the feto–maternal interface. *J Clin Endocrinol Metab*. 1996;81(7):2680–2693.

Hanahan D, Weinberg RA. Hallmarks of cancer: The next generation. *Cell*. 2011;144(5):646–674.

Hansen T, Bjørbaek C, Vestergaard H, Grønskov K, Bak JF, Pedersen O. Expression of insulin receptor spliced variants and their functional correlates in muscle from patients with non–insulin–dependent diabetes mellitus. *J Clin Endocrinol Metab*. 1993;77(6):1500–1505.

Hansen L, Hansen T, Clausen JO, Echwald SM, Urhammer SA, Rasmussen SK, Pedersen O. The Val985Met insulin–receptor variant in the Danish Caucasian population: Lack of associations with non–insulin–dependent diabetes mellitus or insulin resistance. Am J *Hum Genet*. 1997;60(6):1532–1535.

Harley CB, Kim NW, Prowse KR, Weinrich SL, Hirsch KS, West MD, Bacchetti S, Hirte HW, Counter CM, Greider CW. Telomerase, cell immortality, and cancer. *Cold Spring Harb Symp Quant Biol*. 1994;59:307–315.

Harris LK, Crocker IP, Baker PN, Aplin JD, Westwood M. IGF2 actions on trophoblast in human placenta are regulated by the insulin–like growth factor 2 receptor, which can function as both a signaling and clearance receptor. *Biol Reprod*. 2011;84(3):440–446.

Harris LK, Pantham P, Yong HEJ, Pratt A, Borg AJ, Crocker I, Westwood M, Aplin J, Kalionis B, Murthi P. The role of insulin–like growth factor 2 receptor–mediated

homeobox gene expression in human placental apoptosis, and its implications in idiopathic fetal growth restriction. *Mol Hum Rep*. 2019;25(9):572-585.

Hart LM, Stolk RP, Dekker JM, Nijpels G, Grobbee DE, Heine RJ, Maassen A. Prevalence of variants in candidate genes for type 2 diabetes mellitus in the Netherlands: the Rotterdam study and the Hoorn study. *J Clin Endocrinol Metab*. 1999;84(3):1002–1006.

Haywood NJ, Slater TA, Matthews CJ, Wheatcroft SB. The insulin like growth factor and binding protein family: Novel therapeutic targets in obesity and diabetes. *Mol Metab*. 2019;19:86–96.

Heinemann l. Insulin assay standardization: leading to measures of insulin sensitivity and secretion for practical clinical care. *Diabetes Care*. 2010;33(6):e83.

Hers I. Insulin–like growth factor–1 potentiates platelet activation via the IRS–PI3Kα pathway. *Blood*. 2007;110(13):4243–4252.

Hiden U, Glitzner E, Hartmann M, Desoye G. Insulin and the IGF system in the human placenta of normal and diabetic pregnancies. *J Anat*. 2009;215(1):60–68.

Hiden U, Maier A, Bilban M, Ghaffari–Tabrizi N, Wadsack C, Lang I, Dohr G, Desoye G. Insulin control of placental gene expression shifts from mother to foetus over the course of pregnancy. *Diabetologia*. 2006;49(1):123–131.

Hills FA, Elder MG, Chard T, Sullivan MH. Regulation of human villous trophoblast by insulin–like growth factors and insulin–like growth factor–binding protein–1. *J Endocrinol*. 2004;183(3):487–496.

Hirschmugl B, Desoye G, Catalano P, Klymiuk I, Scharnagl H, Payr S, Kitzinger E, et al. Maternal obesity modulates intracellular lipid turnover in the human term placenta. *Int J Obes (Lond)*. 2017;41(2):317–323.

Hoeck WG, Mukku VR. Identification of the major sites of phosphorylation in IGF binding protein 3. *J Cell Biochem*. 1994;56(2):262–273.

Holmes R, Porter H, Newcomb P, Holly JM, Soothill P. An immunohistochemical study of type I insulin–like growth factor receptors in the placentae of pregnancies with appropriately grown or growth restricted fetuses. *Placenta*. 1999;20(4):325–330.

Hsu PP, Sabatini DM. Cancer cell metabolism: Warburg and beyond. *Cell*. 2008;134(5):703–707.

Hu L, Chang L, Zhang Y, Zhai L, Zhang S, Qi Z, Yan H, et al. Platelets express activated P2Y12 receptor in patients with diabetes mellitus. *Circulation*. 2017;136(9):817–833.

Hubbard SR, Till JH. Protein tyrosine kinase structure and function. *Annu Rev Biochem*. 2000;69:373–398.

Hunter RW, Hers I. Insulin/IGF–1 hybrid receptor expression on human platelets: consequences for the effect of insulin on platelet function. *J Thromb Haemost*. 2009;7(12):2123–2130.

Hwa V, Oh J, Rosenfeld RG. The insulin–like growth factor–binding protein (IGFBP) superfamily. *Endocr Rev*. 1999;20(6):761–787.

Hwang JB, Frost SC. Effect of alternative glycosylation on insulin receptor processing. *J Biol Chem*. 1999;274(32):22813–22820.

Igney FH, Krammer PH. Death and anti–death: tumour resistance to apoptosis. *Nat Rev Cancer*. 2002;2(4):277–288.

Imai Y, Clemmons DR. Roles of phosphatidylinositol 3–kinase and mitogen–activated protein kinase pathways in stimulation of vascular smooth muscle cell migration and deoxyriboncleic acid synthesis by insulin–like growth factor–I. *Endocrinology*. 1999;140(9):4228–4235.

Ingermann AR, Yang YF, Han J, Mikami A, Garza AE, Mohanraj L, Fan L, et al. Identification of a novel cell death receptor mediating IGFBP–3–induced anti–tumor effects in breast and prostate cancer. *J Biol Chem*. 2010;285(39):30233–30246.

Iñiguez G, Castro JJ, Garcia M, Kakarieka E, Johnson MC, Cassorla F, Mericq V. IGF–IR signal transduction protein content and its activation by IGF–I in human placentas: relationship with gestational age and birth weight. *PLoS One*. 2014;9(7):e102252.

Iñiguez G, Gallardo P, Castro JJ, Gonzalez R, Garcia M, Kakarieka E, San Martin S, Johnson MC, Mericq V, Cassorla F. Klotho gene and protein in human placentas according to birth weight and gestational age. *Front Endocrinol (Lausanne)*. 2019;9:797.

International Diabetes Federation, IDF Diabetes Atlas, International Diabetes Federation, Brussels, Belgium, 8th edition, 2017, http://www.diabetesatlas.org.

Irwin JC, Suen LF, Faessen GH, Popovici RM, Giudice LC. Insulin–like growth factor (IGF)–II inhibition of endometrial stromal cell tissue inhibitor of metalloproteinase–3 and IGF–binding protein–1 suggests paracrine interactions at the decidua:trophoblast interface during human implantation. *J Clin Endocrinol Metab*. 2001;86(5):2060–2064.

Itkonen HM, Mills IG. N–linked glycosylation supports cross–talk between receptor tyrosine kinases and androgen receptor. *PLoS One*. 2013;8(5):e65016.

Jackson SP, Bartek J. The DNA–damage response in human biology and disease. *Nature*. 2009;461(7267):1071–1078.

Jafari E, Gheysarzadeh A, Mahnam K, Shahmohammadi R, Ansari A, Bakhtyari H, Mofid MR. *In silico* interaction of insulin–like growth factor binding protein 3 with insulin–like growth factor 1. *Res Pharmaceut Sci*. 2018;13(4):332–342.

Jafri MA, Ansari SA, Alqahtani MH, Shay JW. Roles of telomeres and telomerase in cancer, and advances in telomerase–targeted therapies. *Genome Med*. 2016;8:69.

Janssen JAMJL. IGF–I and the endocrinology of aging. *Curr Opin Endocr Metab Res*. 2019;5:1–6.

Jansson T, Aye IL, Goberdhan DC. The emerging role of mTORC1 signaling in placental nutrient–sensing. *Placenta*. 2012;33(Suppl 2):e23–e29.

Jansson N, Rosario FJ, Gaccioli F, Lager S, Jones HN, Roos S, Jansson T, Powell TL. Activation of placental mTOR signaling and amino acid transporters in obese women giving birth to large babies. *J Clin Endocrinol Metab*. 2013;98(1):105–113.

Jansson T, Powell TL. Human placental transport in altered fetal growth: does the placenta function as a nutrient sensor? *Placenta*. 2006;27(Suppl A):91–97.

Jeong KH, Oh SJ, Chon S, Lee MH. Generalized acanthosis nigricans related to type B insulin resistance syndrome: A case report. *Cutis*. 2010;86(6):299–302.

Jiang BH, Liu LZ. PI3K/PTEN signaling in angiogenesis and tumorigenesis. *Adv Cancer Res*. 2009;102:19–65.

Jiang H, Xun P, Luo G, Wang Q, Cai Y, Zhang Y, Yu B. Levels of insulin–like growth factors and their receptors in placenta in relation to macrosomia. *Asia Pac J Clin Nutr*. 2009;18(2):171–178.

Jirkovská M, Kubínová L, Janácek J, Moravcová M, Krejcí V, Karen P. Topological properties and spatial organization of villous capillaries in normal and diabetic placentas. *J Vasc Res*. 2002;39(3):268–278.

Jones R. Cytotoxic chemotherapy: Clinical aspects. *Medicine*. 2016;44(1):25–29.

Jones JI, Busby WH Jr, Wright G, Smith CE, Kimack NM, Clemmons DR. Identification of the sites of phosphorylation in insulin–like growth factor binding protein–1. Regulation of its affinity by phosphorylation of serine 101. *J Biol Chem*. 1993;268(2):1125–1131.

Juul A. Serum levels of insulin–like growth factor I and its binding proteins in health and disease. *Growth Horm IGF Res*. 2003;13(4):113–170.

Kadakia R, Josefson J. The relationship of insulin–like growth factor 2 to fetal growth and adiposity. *Horm Res Paediatr*. 2016;85(2):75–82.

Kakouros N, Rade JJ, Kourliouros A, Resar JR. Platelet function in patients with diabetes mellitus: From a theoretical to a practical perspective. Int *J Endocrinol*. 2011:742719.

Kanasaki K, Kalluri R. The biology of preeclampsia. *Kidney Int*. 2009;76(8):831–837.

Kaneda A, Wang CJ, Cheong R, Timp W, Onyango P, Wen B, Iacobuzio–Donahue CA, et al. Enhanced sensitivity to IGF–II signaling links loss of imprinting of IGF2 to increased cell proliferation and tumor risk. *Proc Natl Acad Sci USA*. 2007;104(52):20926–20931.

Kaplan S, Cohen P. The somatomedin hypothesis 2007: 50 years later. *J Cin Endocrinol Metab*. 2007;92(12):4529–4535.

Karolczak–Bayatti M, Forbes K, Horn J, Teesalu T, Harris LK, Westwood M, Aplin JD. IGF signalling and endocytosis in the human villous placenta in early pregnancy as revealed by comparing quantum dot conjugates with a soluble ligand. *Nanoscale*. 2019;11(25):12285–12295.

Kataoka H, Tanaka H, Nagaike K, Uchiyama S, Itoh H. Role of cancer cell–stroma interaction in invasive growth of cancer cells. *Hum Cell*. 2003;16(1):1–14.

Katayama Y, Uchino J, Chihara Y, Tamiya N, Kaneko Y, Yamada T, Takayama K. Tumor neovascularization and developments in therapeutics. *Cancers (Basel)*. 2019;11(3):316.

Kellerer M, Sesti G, Seffer E, Obermaier–Kusser B, Pongratz DE, Mosthaf L, Häring HU. Altered pattern of insulin receptor isotypes in skeletal muscle membranes of Type 2 (non–insulin–dependent) diabetic subjects. *Diabetologia*. 1993;36(7):628–632.

Kessenbrock K, Plaks V, Werb Z. Matrix metalloproteinases: regulators of the tumor microenvironment. *Cell*. 2010;141(1):52–67.

Kharb S, Nanda S. Patterns of biomarkers in cord blood during pregnancy and preeclampsia. *Curr Hypertens Rev*. 2017;13(1):57–64.

Kharb S, Panjeta P, Ghalaut VS, Bala J, Nanda S. Biomarkers in preeclamptic women with normoglycemia and hyperglycemia. *Curr Hypertens Rev*. 2016;12(3):228–233.

Kim JH, Bae HY, Kim SY. Clinical marker of platelet hyperreactivity in diabetes mellitus. *Diabetes Metab J*. 2013;37(6):423–428.

Kim KW, Bae SK, Lee OH, Bae MH, Lee MJ, Park BC. Insulin–like growth factor II induced by hypoxia may contribute to angiogenesis of human hepatocellular carcinoma. *Cancer Res*. 1998;58(2):348–351.

Kim S, Garcia A, Jackson SP, Kunapuli SP. Insulin–like growth factor–1 regulates platelet activation through PI3–Kα isoform. *Blood*. 2007;110(13):4206–4213.

Kim JG, Kang MJ, Yoon YK, Kim HP, Park J, Song SH, Han SW, et al. Heterodimerization of glycosylated insulin–like growth factor–1 receptors and insulin receptors in cancer cells sensitive to anti–IGF1R antibody. *PLoS One*. 2012;7(3):e33322.

King GL, Kahn CR, Rechler MM, Nissley SP. Direct demonstration of separate receptors for growth and metabolic activities of insulin and multiplication–stimulating activity (an insulin–like growth factor) using antibodies to the insulin receptor. *J Clin Invest*. 1980;66(1):130–140.

Kingdom J, Huppertz B, Seaward G, Kaufmann P. Development of the placental villous tree and its consequences for fetal growth. *Eur J Obstet Gynecol Reprod Biol*. 2000;92(1):35–43.

Klaver E, Zhao P, May M, Flanagan–Steet H, Freeze HH, Gilmore R, Wells L, Contessa J, Steet R. Selective inhibition of N–linked glycosylation impairs receptor tyrosine kinase processing. *Dis Models Mechan*. 2019;12(6):pii:dmm039602.

Knofler M, Sooranna SR, Daoud G, Whitley GS, Markert UR, Xia Y, Cantiello H, Hauguel–de–Mouzon S. Trophoblast signalling: Knowns and unknowns – a workshop report. *Placenta*. 2005;26(Suppl A):S49–S51.

Kolch W. Meaningful relationships: The regulation of the Ras/Raf/MEK/ERK pathway by protein interactions. *Biochem J*. 2000;351(Pt 2):289–305.

Kornfeld S. Structure and function of the mannose 6–phosphate/insulinlike growth factor II receptors. *Annu Rev Biochem*. 1992;61:307–330.

Krakhmal NV, Zavyalova MV, Denisov EV, Vtorushin SV, Perelmuter VM. Cancer invasion: Patterns and mechanisms. *Acta Naturae*. 2015;7(2):17–28.

Kruis T, Klammt J, Galli–Tsinopoulou A, Wallborn T, Schlicke M, Müller E, Kratzsch J, et al. Heterozygous mutation within a kinase–conserved motif of the insulin–like growth factor I receptor causes intrauterine and postnatal growth retardation. *J Clin Endocrinol Metab*. 2010;95(3):1137–1142.

Kühnl A, Kaiser M, Neumann M, Fransecky L, Heesch S, Radmacher M, Marcucci G, et al. High expression of IGFBP2 is associated with chemoresistance in adult acute myeloid leukemia. *Leuk Res*. 2011;35(12):1585–1590.

Kurien BT, Hensley K, Bachmann M, Scofield RH. Oxidatively modified autoantigens in autoimmune diseases. *Free Radic Biol Med*. 2006;41:549–556.

Lacey H, Haigh T, Westwood M, Aplin JD. Mesenchymally–derived insulin–like growth factor 1 provides a paracrine stimulus for trophoblast migration. *BMC Dev Biol.* 2002;2:5.

Lane DP. Cancer. p53, guardian of the genome. *Nature*. 1992;358(6381):15–16.

Langer CJ, Novello S, Park K, Krzakowski M, Karp DD, Mok T, Benner RJ, Scranton JR, Olszanski AJ, Jassem J. Randomized, phase III trial of first–line figitumumab in combination with paclitaxel and carboplatin versus paclitaxel and carboplatin alone in patients with advanced non–small–cell lung cancer. *J Clin Oncol*. 2014;32(19):2059–2066.

Lassance L, Miedl H, Absenger M, Diaz–Perez F, Lang U, Desoye G, Hiden U. Hyperinsulinemia stimulates angiogenesis of human fetoplacental endothelial cells: A possible role of insulin in placental hypervascularization in diabetes mellitus. *J Clin Endocrinol Metab*. 2013;98(9):E1438–1447.

Laviola L, Perrini S, Belsanti G, Natalicchio A, Montrone C, Leonardini A, Vimercati A, et al. Intrauterine growth restriction in humans is associated with abnormalities in placental insulin–like growth factor signaling. *Endocrinology*. 2005;146(3):1498–1505.

Laybutt DR, Kaneto H, Hasenkamp W, Grey S, Jonas JC, Sgroi DC, Groff A, et al. Increased expression of antioxidant and antiapoptotic genes in islets that may contribute to β–cell survival during chronic hyperglycemia. *Diabetes*. 2002;51(2):413–423.

Le Roith D. The insulin–like growth factor system. *Exp Diabesity Res*. 2003;4(4):205–212.

Le Roith D, Bondy C, Yakar S, Liu JL, Butler A. The somatomedin hypothesis: 2001. *Endocr Rev*. 2001;22(1):53–74.

Lee H, Jang HC, Park HK, Metzger BE, Cho NH. Prevalence of type 2 diabetes among women with a previous history of gestational diabetes mellitus. *Diabetes Res Clin Pract*. 2008;81(1):124–129.

Lichtor T, Kurpakus MA, Gurney ME. Expression of insulin–like growth factors and their receptors in human meningiomas. *J Neurooncol*. 1993;17(3):183–190.

Liu B, Xu Y, Voss C, Qiu FH, Zhao MZ, Liu YD, Nie J, Wang ZL. Altered protein expression in gestational diabetes mellitus placentas provides insight into insulin resistance and coagulation/fibrinolysis pathways. *PLoS One*. 2012;7(9):e44701.

Liu D, Zhang X, Gao J, Palombo M, Gao D, Chen P, Sinko PJ. Core functional sequence of C–terminal GAG–binding domain directs cellular uptake of IGFBP–3–derived peptides. *Protein Pept Lett*. 2014;21(2):124–131.

Livingstone C. IGF2 and cancer. *Endocr Relat Cancer*. 2013;20(6):R321–339.

Lobel P, Dahms NM, Breitmeyer J, Chirgwin JM, Kornfeld S. Cloning of the bovine 215–kDa cation–independent mannose 6–phosphate receptor. *Proc Natl Acad Sci USA*. 1987;84(8):2233–2237.

Lobel P, Dahms NM, Kornfeld S. Cloning and sequence analysis of the cation–independent mannose 6–phosphate receptor. *J Biol Chem*. 1988;263(5):2563–2570.

Long L, Navab R, Brodt P. Regulation of the Mr 72,000 type IV collagenase by the type I insulin–like growth factor receptor. *Cancer Res*. 1998;58(15):3243–3247.

Longo N, Langley SD, Griffin LD, Elsas LJ. Two mutations in the insulin receptor gene of a patient with Leprechaunism: Application to prenatal diagnosis. *J Clin Endocrinol Metab*. 1995;80(5):1496–1501.

Longo N, Wang Y, Pasquali M. Progressive decline in insulin levels in Rabson–Mendenhall syndrome. *J Clin Endocrinol Metab*. 1999;84(8):2623–2629.

Longo N, Wang Y, Smith SA, Langley SD, DiMeglio LA, Giannella–Neto D. Genotype–phenotyte correlation in inherited severe insulin resistance. *Hum Mol Genet*. 2002;11(12):1465–1475.

Lou M, Garrett TPJ, McKern NM, Hoyne PA, Epa VC, Bentley JD, Lovrecz GO, Cosgrove LJ, Frenkel MJ, Ward CW. The first three domains of the insulin receptor differ structurally from the insulin–like growth factor 1 receptor in the regions governing ligand specificity. *Proc Natl Acad Sci USA*. 2006;103(33):12429–12434.

Loukovaara M, Leinonen P, Teramo K, Nurminen E, Andersson S, Rutanen EM. Effect of maternal diabetes on phosphorylation of insulin–like growth factor binding protein–1 in cord serum. *Diab Med*. 2005;22(4):434–439.

Ma M, Zhou QJ, Xiong Y, Li B, Li XT. Preeclampsia is associated with hypermethylation of IGF–1 promoter mediated by DNMT1. *Am J Transl Res*. 2018;10(1):16–39.

Maiza JC, Caron–Debarle M, Vigouroux C, Schneebeli S. Anti–insulin receptor antibodies related to hypoglycemia in a previously diabetic patient. *Diabetes Care*. 2013;36(6):e77.

Malaguarnera R, Belfiore A. The insulin receptor: a new target for cancer therapy. *Front Endocrinol (Lausanne)*. 2011;2:93.

Malek R, Chong AY, Lupsa BC, Lungu AO, Cochran EK, Soos MA, Semple RK, Balow JE, Gorden P. Treatment of type B insulin resistance: A novel approach to reduce insulin receptor autoantibodies. *J Clin Endocrinol Metab*. 2010;95(8):3641–3647.

Man YG, Stojadinovic A, Mason J, Avital I, Bilchik A, Bruecher B, Protic M, et al. Tumor–infiltrating immune cells promoting tumor invasion and metastasis: Existing theories. *J Cancer*. 2013;4(1):84–95.

Mani SA, Guo W, Liao MJ, Eaton EN, Ayyanan A, Zhou AY, Brooks M, et al. The epithelial–mesenchymal transition generates cells with properties of stem cells. *Cell*. 2008;133(4):704–715.

Martino J, Sebert S, Segura MT, García–Valdés L, Florido J, Padilla MC, Marcos A, et al. Maternal body weight and gestational diabetes differentially influence placental and pregnancy outcomes. *J Clin Endocrinol Metab*. 2016;101(1):59–68.

Maruo T, Murata K, Matsuo H, Samoto T, Mochizuki M. Insulin–like growth factor–I as a local regulator of proliferation and differentiated function of the human trophoblast in early pregnancy. *Early Pregnancy*. 1995;1(1):54–61.

Mayama R, Izawa T, Sakai K, Suciu N, Iwashita M. Improvement of insulin sensitivity promotes extravillous trophoblast cell migration stimulated by insulin–like growth factor–I. *Endocr J*. 2013;60(3):359–368.

McKinnon T, Chakraborty C, Gleeson LM, Chidiac P, Lala PK. Stimulation of human extravillous trophoblast migration by IGF–II is mediated by IGF type 2 receptor involving inhibitory G protein(s) and phosphorylation of MAPK. *J Clin Endocrinol Metab*. 2001;86(8):3665–3674.

Migdalis IN, Kalogeropoulou K, Kalantzis L, Nounopoulos C, Bouloukos A, Samartzis M. Insulin–like growth factorI and IGF–I receptors in diabetic patients with neuropathy. *Diabetic Med*. 1995;12(9):823–827.

Milio LA, Hu J, Douglas GC. Binding of insulin–like growth factor I to human trophoblast cells during differentiation in vitro. *Placenta*. 1994;15(6):641–651.

Mira E, Mañes S, Lacalle RA, Márquez G, Martínez–A C. Insulin–like growth factor I–triggered cell migration and invasion are mediated by matrix metalloproteinase–9. *Endocrinology*. 1999;140(4):1657–1664.

Modestino AE, Skowronski EA, Pruitt C, Taub PR, Herbst K, Schmid–Schönbein GW, Heller MJ, Mills PJ. Elevated resting and postprandial digestive proteolytic activity in peripheral blood of individuals with type–2 diabetes mellitus, with uncontrolled cleavage of insulin receptors. *J Am Coll Nutr*. 2019;38(6):485-492.

Mol BWJ, Roberts CT, Thangaratinam S, Magee LA, de Groot CJM, Hofmeyr GJ. Pre–eclampsia. *Lancet*. 2016;387(10022):999–1011.

Montazami N, Aghapour M, Farajnia S, Baradaran B. New insights into the mechanisms of multidrug resistance in cancers. *Cell Mol Biol (Noisy–le–grand)*. 2015;61(7):70–80.

Mooi WJ, Peeper DS. Oncogene–induced cell senescence – halting on the road to cancer. *N Engl J Med*. 2006;355(10):1037–1046.

Moore SF, Williams CM, Brown E, Blair TA, Harper MT, Coward RJ, Poole AW, Hers I. Loss of the insulin receptor in murine megakaryocytes/platelets causes thrombocytosis and alterations in IGF signaling. *Cardiovasc Res*. 2015;107(1):9–19.

Moorehead RA, Hojilla CV, De Belle I, Wood GA, Fata JE, Adamson ED, Watson KL, Edwards DR, Khokha R. Insulin–like growth factor–II regulates PTEN expression in the mammary gland. *J Biol Chem*. 2003;278(50):50422–50427.

Moses AC, Young SC, Morrow LA, O'Brien M, Clemmons DR. Recombinant human insulin–like growth factor I increases insulin sensitivity and improves glycemic control in type II diabetes. *Diabetes*. 1996;45(1):91–100.

Mosthaf L, Eriksson J, Häring HU, Groop L, Widen E, Ullrich A. Insulin receptor isotype expression correlates with risk of non–insulin–dependent diabetes. *Proc Natl Acad Sci USA*. 1993;90(7):2633–2635.

Mosthaf L, Vogt B, Häring HU, Ullrich A. Altered expression of insulin receptor types A and B in the skeletal muscle of non–insulin–dependent diabetes mellitus patients. *Proc Natl Acad Sci USA*. 1991;88(11):4728–4730.

Motyka B, Korbutt G, Pinkoski MJ, Heibein JA, Caputo A, Hobman M, Barry M, et al. Mannose 6–phosphate/insulin–like growth factor II receptor is a death receptor for granzyme B during cytotoxic T cell–induced apoptosis. *Cell*. 2000;103(3):491–500.

Mrizak I, Grissa O, Henault B, Fekih M, Bouslema A, Boumaiza I, Zaouali M, Tabka Z, Khan NA. Placental infiltration of inflammatory markers in gestational diabetic women. *Gen Physiol Biophys*. 2014;33(2):169–176.

Nadimpalli SK, Amancha PK. Evolution of mannose 6–phosphate receptors (MPR300 and 46): Lysosomal enzyme sorting proteins. *Curr Protein Pept Sci*. 2010;11(1):68–90.

Nedić O, Robajac D, Šunderić M, Miljuš G, Đukanović B, Malenković V. Detection and identification of the oxidized insulin–like growth factor binding proteins and receptors in patients with colorectal carcinoma. *Free Rad Biol Med*. 2013;65:1195–1200.

Negrini S, Gorgoulis VG, Halazonetis TD. Genomic instability – an evolving hallmark of cancer. Nat Rev *Mol Cell Biol*. 2010;11(3):220–228.

Neumann GM, Marinaro JA, Bach LA. Identification of N–glycosylation sites and partial characterization of carbohydrate structure and disulfide linkages of human insulin–like growth factor binding protein 6. *Biochemistry*. 1998;37(18):6572–6585.

Nimptsch K, Konigorski S, Pischon T. Diagnosis of obesity and use of obesity biomarkers in science and clinical medicine. *Metab Clin Exp*. 2019;92:61–70.

Norgren S, Zierath J, Galuska D, Wallberg–Henriksson H, Luthman H. Differences in the ratio of RNA encoding two isoforms of the insulin receptor between control and NIDDM Patients. The RNA variant without exon 11 predominates in both groups. *Diabetes*. 1993;42(5):675–681.

Novosyadlyy R, Le Roith D. Insulin–like growth factors and insulin: at the crossroad between tumor development and longevity. *J Gerontol A Bio Sci Med Sci.* 2012;67(6):640–651.

O'Connor KG, Tobin JD, Harman SM, Plato CC, Roy TA, Sherman SS, Blackman MR. Serum levels of insulin–like growth factor–I are related to age and not to body composition in healthy women and man. *J Gerontol Med Sci*. 1988;53A(3):M176–M182.

Ogawa O, Becroft DM, Morison IM, Eccles MR, Skeen JE, Mauger DC, Reeve AE. Constitutional relaxation of insulin–like growth factor II gene imprinting associated with Wilms' tumour and gigantism. *Nat Genet*. 1993;5(4):408–412.

O'Gorman DB, Weiss J, Hettiaratchi A, Firth SM, Scott CD. Insulin–like growth factor–II/mannose 6–phosphate receptor overexpression reduces growth of

choriocarcinoma cells in vitro and in vivo. *Endocrinology*. 2002;143(11):4287–4294.

Ohtsubo K, Marth JD. Glycosylation in cellular mechanisms of health and disease. *Cell*. 2006;126(5):855–867.

Olson LJ, Castonguay AC, Lasanajak Y, Peterson FC, Cummings RD, Smith DF, Dahms NM. Identification of a fourth mannose 6–phosphate binding site in the cation–independent mannose 6–phosphate receptor. *Glycobiology*. 2014;25(6):591–606.

Ong K, Kratzsch J, Kiess W, Costello M, Scott C, Dunger D. Size at birth and cord blood levels of insulin, insulin–like growth factor I (IGF–I), IGF–II, IGF–binding protein–1 (IGFBP–1), IGFBP–3, and the soluble IGF–II/mannose–6–phosphate receptor in term human infants. The ALSPAC Study Team. Avon Longitudinal Study of Pregnancy and Childhood. *J Clin Endocrinol Metab*. 2000;85(11):4266–4269.

Orme SM, McNally RJ, Cartwright RA, Belchetz PE. Mortality and cancer incidence in acromegaly: A retrospective cohort study. United Kingdom Acromegaly Study Group. *J Clin Endocrinol Metab*. 1998;83(8):2730–2734.

Pathmaperuma AN, Mana P, Cheung SN, Kugathas K, Josiah A, Koina ME, Broomfield A, et al. Fatty acids alter glycerolipid metabolism and induce lipid droplet formation, syncytialisation and cytokine production in human trophoblasts with minimal glucose effect or interaction. *Placenta*. 2010;31(3):230–239.

Peng HY, Xue M, Xia AB. Study on changes of IGF–I and leptin levels in serum and placental tissue of preeclampsia patients and their associativity. *Xi Bao Yu Fen Zi Mian Yi Xue Za Zhi*. 2011;27(2):192–194.

Perkins E, Murphy SK, Murtha AP, Schildkraut J, Jirtle RL, Demark–Wahnefried W, Forman MR, et al. Insulin–like growth factor 2/H19 methylation at birth and risk of overweight and obesity in children. *J Pediatr*. 2012;161(1):31–39.

Phiske MM. An approach to acanthosis nigricans. *Indian Dermatol Online J*. 2014;5(3):239–249.

Pollak M. The insulin receptor/insulin–like growth factor receptor family as a therapeutic target in oncology. *Clin Cancer Res*. 2012;18(1):40–50.

Pomero F, Di Minno MND, Fenoglio L, Gianni M, Ageno W, Dentali F. Is diabetes a hypercoagulable state? A critical appraisal. *Acta Diabetol*. 2015;52(6):1007–1016.

Porzio O, Federici M, Hribal ML, Lauro D, Accili D, Lauro R, Borboni P, Sesti G. The Gly^{972}→Arg amino acid polymorphism in IRS–1 impairs insulin secretion in pancreatic β cells. *J Clin Invest*. 1999;104(3):357–364.

Pshezhetsky AV, Ashmarina LI. Desialylation of surface receptors as a new dimension in cell signaling. *Biochemistry (Moscow)*. 2013;78(7):736–745.

Rabson SM, Mendenhall EN. Familial hypertrophy of pineal body, hyperplasia of adrenal cortex and diabetes mellitus. *Am J Clin Pathol*. 1956;26(3):283–290.

Radaelli T, Varastehpour A, Catalano P, Hauguel–de–Mouzon S. Gestational diabetes induces placental genes for chronic stress and inflammatory pathways. *Diabetes*. 2003;52(12):2951–2958.

Randriamboavonjy V, Fleming I. Insulin, insulin resistance, and platelet signaling in diabetes. *Diabetes Care*. 2009;32(4):528–530.

Renehan AG, Zwahlen M, Minder C, O'Dwyer ST, Shalet SM, Egger M. Insulin–like growth factor (IGF)–I, IGF binding protein–3, and cancer risk: Systematic review and meta–regression analysis. *Lancet*. 2004;363(9418):1346–1453.

Reuter S, Gupta SC, Chaturvedi MM, Aggarwal BB. Oxidative stress, inflammation, and cancer: How are they linked? *Free Radic Biol Med*. 2010;49(11):1603–1616.

Ribatti D. Endogenous inhibitors of angiogenesis: a historical review. *Leuk Res*. 2009;33(5):638–644.

Ribatti D. A revisited concept: Contact inhibition of growth. From cell biology to malignancy. *Exp Cell Res*. 2017a;359(1):17–19.

Ribatti D. The concept of immune surveillance against tumors. The first theories. *Oncotarget*. 2017b;8(4):7175–7180.

Rinderknecht E, Humbel RE. The amino acid sequence of human insulin–like growth factor I and its structural homology with proinsulin. *J Biol Chem*. 1978;253(8):2769–2776.

Robajac D, Križáková M, Masnikosa R, Miljuš G, Šunderić M, Nedić O, Katrlík J. Sensitive glycoprofiling of insulin–like growth factor receptors isolated from colon tissue of patients with colorectal carcinoma using lectin-based protein microarray. *Int J Biol Macromol*. 2020;144:932–937.

Robajac D, Masnikosa R, Filimonović D, Miković Ž, Nedić O. N–glycosylation pattern of human placental insulin–like growth factor and insulin receptors in well–controlled pregestational diabetes mellitus. *J Med Biochem*. 2012;31(3):205–210.

Robajac D, Masnikosa R, Miković Ž, Mandić V, Nedić O. Oxidation of placental insulin and insulin–like growth factor receptors in mothers with diabetes mellitus or preeclampsia complicated with intrauterine growth restriction. *Free Radic Res*. 2015;49(8):984–989.

Robajac D, Masnikosa R, Miković Ž, Nedić O. Gestation–associated changes in the glycosylation of placental insulin and insulin–like growth factor receptors. *Placenta*. 2016a ;39:70–76.

Robajac D, Masnikosa R, Vanhooren V, Libert C, Miković Ž, Nedić O. The N–glycan profile of placental membrane glycoproteins alters during gestation and ageing. *Mech Ageing Dev*. 2014;138:1–9.

Robajac D, Vanhooren V, Masnikosa R, Miković Ž, Mandić V, Libert C, Nedić O. Preeclampsia transforms membrane N–glycome in human placenta. *Exp Mol Pathol*. 2016b;100(1):26–30.

Robajac D, Zámorová M, Katrlík J, Miković Ž, Nedić O. Screening for the best detergent for the isolation of placental membrane proteins. *Int J Biol Macromol*. 2017;102:431–437.

Rogers J, Wiltrout L, Nanu L, Fant ME. Developmentally regulated expression of IGF binding protein–3 (IGFBP–3) in human placental fibroblasts: Effect of exogenous IGFBP3 on IGF–1 action. *Regul Pept*. 1996;61(3):189–195.

Romano G. The complex biology of the receptor for the insulin–like growth factor–1. *Drug News Perspect*. 2003;16(8):525–531.

Roos S, Lagerlof O, Wennergren M, Powell TL, Jansson T. Regulation of amino acid transporters by glucose and growth factors in cultured primary human trophoblast cells is mediated by mTOR signaling. *Am J Physiol Cell Physiol*. 2009;297(3):C723–C731.

Ruiz–Palacios M, Prieto–Sánchez M, Ruiz–Alcaraz A, Blanco–Carnero J, Sanchez–Campillo M, Parrilla J, Larqué E. Insulin treatment may enhance fatty acid carriers in placentas from gestational diabetes subjects. *Int J Mol Sci*. 2017b;18(6). pii: E1203.

Ruiz–Palacios M, Ruiz–Alcaraz AJ, Sanchez–Campillo M, Larqué E. Role of insulin in placental transport of nutrients in gestational diabetes mellitus. *Ann Nutr Metab*. 2017;70(1):16–25.

Russo VC, Bach LA, Fosang AJ, Baker NL, Werther GA. Insulin like growth factor binding protein–2 binds to cell surface proteoglycans in the rat brain olfactory bulb. *Endocrinology*. 1997;138(11):4858–4856.

Ryan PD, Goss PE. The emerging role of the insulin–like growth factor pathway as a therapeutic target in cancer. *Oncologist*. 2008;13:16–24.

Saito–Hakoda A, Nishii A, Uchida T, Kikuchi A, Kanno J, Fujiwara I, Kure S. A follow–up during puberty in a Japanese girl with type A insulin resistance due to a novel mutation in *INSR*. *Clin Pediatr Endocrinol*. 2018;27(1):53–57.

Sakai K, Lowman HB, Clemmons DR. Increases in free, unbound insulin–like growth factor I enhance insulin responsiveness in human hepatoma G2 cells in culture. *J Biol Chem*. 2002;277(16):13620–13627.

Samani AA, Yakar S, LeRoith D, Brodt P. The role of the IGF system in cancer growth and metastasis: Overview and recent insights. *Endocr Rev*. 2007;28(1):20–47.

Sandberg AC, Engberg C, Lake M, von Holst H, Sara VR. The expression of insulin–like growth factor I and insulin–like growth factor II genes in the human fetal and adult brain and in glioma. *Neurosci Lett*. 1988;93(1):114–119.

Sandovici I, Hoelle K, Angiolini E, Constância M. Placental adaptations to the maternal–fetal environment: Implications for fetal growth and developmental programming. *Reprod Biomed Online*. 2012;25(1):68–89.

Sarfstein R, Pasmanik–Chor M, Yeheskel A, Edry L, Shomron N, Warman N, Wertheimer E, Maor S, Shochat L, Werner H. Insulin–like growth factor–I receptor (IGF–IR) translocates to nucleus and autoregulates IGF–IR gene expression in breast cancer cells. *J Biol Chem*. 2012;287(4):2766–2776.

Sasaoka T, Ishiki M, Wada T, Hori H, Hirai H, Haruta T, Ishihara H, Kobayashi M. Tyrosine phosphorylation–dependent and –independent role of Shc in the regulation of IGF–1–induced mitogenesis and glycogen synthesis. *Endocrinology*. 2001;142(12):5226–5235.

Sayer RA, Lancaster JM, Pittman J, Gray J, Whitaker R, Marks JR, Berchuck A. High insulin–like growth factor–2 (IGF–2) gene expression is an independent predictor of poor survival for patients with advanced stage serous epithelial ovarian cancer. *Gynecol Oncol*. 2005;96(2):355–361.

Sbraccia P, D'Adamo M, Leonetti F, Caiola S, Iozzo P, Giaccari A, Buongiorno A, Tamburrano G. Chronic primary hyperinsulinaemia is associated with altered insulin receptor mRNA splicing in muscle of patients with insulinoma. *Diabetologia*. 1996;39(2):220–225.

Scott CD, Firth SM. The role of the M6P/IGF–II receptor in cancer: Tumor suppression or garbage disposal? *Horm. Metab. Res*. 2004;36(5):261–271.

Seino S, Bell GI. Alternative splicing of human insulin receptor messenger RNA. *Biochem Biophys Res Commun*. 1989;159(1):312–316.

Sesti G, D'Alfonso R, Punti MDV, Frittitta L, Trischitta V, Liu YY, Borboni P, Longhi R, Montemurro A, Lauro R. Peptide–based radioimmunoassay for the two isoforms of the human insulin receptor. *Diabetologia*. 1995;38(4):445–453.

Sesti G, Federici M, Lauro D, Sbraccia P, Lauro R. Molecular mechanism of insulin resistance in type 2 diabetes mellitus: Role of the insulin receptor variant forms. *Diabetes Metab Res Rev*. 2001;17(5):363–373.

Sesti G, Marini MA, Tullio AN, Montemurro A, Borboni P, Fusco A, Accili D, Renato Lauro R. Altered expression of the two naturally occurring human insulin receptor variants in isolated adipocytes of non–insulin–dependent diabetes mellitus patients. *Biochem Biophys Res Commun*. 1991;181(3):1419–1424.

Sever R, Brugge JS. Signal transduction in cancer. *Cold Spring Harb Perspect Med*. 2015;5(4):pii:a006098.

Seyfried TN, Huysentruyt LC. On the origin of cancer metastasis. *Crit Rev Oncog*. 2013;18(1-2):43–73.

Sferruzzi–Perri AN, Sandovici I, Constancia M, Fowden AL. Placental phenotype and the insulin–like growth factors: resource allocation to fetal growth. *J Physiol*. 2017;595(15):5057–5093.

Shiratsuchi I, Akagi Y, Kawahara A, Kinugasa T, Romeo K, Yoshida T, Ryu Y, Gotanda Y, Kage M, Shirouzu K. Expression of IGF–1 and IGF–1R and their relation to clinicopathological factors in colorectal cancer. *Anticancer Res*. 2011;31(7):2541–2545.

Sibley CP, Turner MA, Cetin I, Ayuk P, Boyd CA, D'Souza SW, Glazier JD, Greenwood SL, Jansson T, Powell T. Placental phenotypes of intrauterine growth. *Pediatr Res*. 2005;58(5):827–832.

Sjögren K, Wallenius K, Liu J, Bohlooly M, Pacini G, Svensson L, Törnell J, et al. Liver–derived IGF–I is of importance for normal carbohydrate and lipid metabolism. *Diabetes*. 2001;50(7):1539–1545.

Sklar MM, Thomas CL, Municchi G, Roberts CT Jr, LeRoith D, Kiess W, Nissley P. Developmental expression of rat insulin–like growth factor II/mannose 6–phosphate receptor messenger ribonucleic acid. *Endocrinology*. 1992;130(6):3484–3491.

Skyler JS, Bakris GL, Bonifacio E, Darsow T, Eckel RH, Groop L, Groo PH, et al. Differentiation of diabetes by pathophysiology, natural history, and prognosis. *Diabetes*. 2017;66(2):241–255.

So AI, Levitt RJ, Eigl B, Fazli L, Muramaki M, Leung S, Cheang MC, Nielsen TO, Gleave M, Pollak M. Insulin–like growth factor binding protein–2 is a novel therapeutic target associated with breast cancer. *Clin Cancer Res*. 2008;14(21):6944–6954.

Solomon AL, Siddals KW, Baker PN, Gibson JM, Aplin JD, Westwood M. Placental alkaline phosphatase de–phosphorylates insulin–like growth factor (IGF)–binding protein–1. *Placenta*. 2014;35(7):520–522.

Soussi T, Wiman KG2. TP53: An oncogene in disguise. *Cell Death Differ*. 2015;22(8):1239–49.

Souza RF, Wang S, Thakar M, Smolinski KN, Yin J, Zou TT, Kong D, Abraham JM, Toretsky JA, Meltzer SJ. Expression of the wild–type insulin–like growth factor II receptor gene suppresses growth and causes death in colorectal carcinoma cells. *Oncogene*. 1999;18(28):4063–4068.

Spampinato D, Pandini G, Iuppa A, Trischitta V, Vigneri R, Frittitta L. Insulin/insulin–like growth factor I hybrid receptors overexpression is not an early defect in insulin–resistant subjects. *J Clin Endocrinol Metab*. 2000;85(11):4219–4223.

Sparrow LG, Lawrence MC, Gorman JJ, Strike PM, Robinson CP, McKern NM, Ward CW. N–linked glycans of the human insulin receptor and their distribution over the crystal structure. *Proteins*. 2008;71(1):426–439.

Succurro E, Andreozzi F, Marini MA, Lauro R, Hribal ML, Perticone F, Sesti G. Low plasma insulin–like growth factor–1 levels are associated with reduced insulin sensitivity and increased insulin secretion in nondiabetic subjects. *Nutr Metab Cardiovasc Dis*. 2009;19(10):713–719.

Sudarsanam S, Johnson DE. Functional consequences of mTOR inhibition. *Curr Opin Drug Discov Devel*. 2010;13(1):31–40.

Šunderić M, Đukanović B, Malenković V, Nedić O. Molecular forms of the insulin–like growth factor–binding protein–2 in patients with colorectal cancer. *Exp Mol Pathol*. 2014;96(1):48–53.

Šunderić M, Križakova M, Malenković V, Ćujić D, Katrlik J, Nedić O. Changes due to ageing in the glycan structure of alpha–2–macroglobulin and its reactivity with ligands. *Prot J*. 2019;38(1):23–29.

Tan EK, Tan EL. Alterations in physiology and anatomy during pregnancy. *Best Pract Res Clin Obstet Gynaecol*. 2013;27(6):791–802.

Taylor SI, Cama A, Accili D, Barbetti F, Quon MJ, de la Luz Sierra M, Suzuki Y, et al. Mutations in the insulin receptor gene. *Endocr Rev*. 1992;13(3):566–595.

Teppala S, Shankar A. Association between serum IGF–1 and diabetes among US adults. *Diabetes Care*. 2010;33(10):2257–2259.

Tepper OM, Capla JM, Galiano RD, Ceradini DJ, Callaghan MJ, Kleinman ME, Gurtner GC. Adult vasculogenesis occurs through in situ recruitment, proliferation, and tubulization of circulating bone marrow–derived cells. *Blood*. 2005;105(3):1068–1077.

Tripodi A, Branchi A, Chantarangkul V, Clerici M, Merati G, Artoni A, Mannucci PM. Hypercoagulability in patients with type 2 diabetes mellitus detected by a thrombin generation assay. *J Thromb Thrombolysis*. 2011;31(2):165–172.

Uhles S, Moede T, Leibiger B, Berggren PO, Leibiger IB. Isoform–specific insulin receptor signaling involves different plasma membrane domains. *J Cell Biol*. 2003;163(6):1327–1237.

Ullrich A, Gray A, Tam AW, Yang–Feng T, Tsubokawa M, Collins C, Henzel W, et al. Insulin–like growth factor 1 receptor primary structure: comparison with insulin receptor suggests structural determinants that define functional specificity. *EMBO J*. 1986;5(10):2503–2512.

Uzoh CC, Holly JM, Biernacka KM, Persad RA, Bahl A, Gillatt D, Perks CM. Insulin–like growth factor–binding protein–2 promotes prostate cancer cell growth via IGF–dependent or –independent mechanisms and reduces the efficacy of docetaxel. *Br J Cancer*. 2011;104(10):1587–1593.

Valensise H, Liu YY, Federici M, Lauro D, Dell'anna D, Romanini C, Sesti G. Increased expression of low–affinity insulin receptor isoform and insulin/insulin–like growth factor–I hybrid receptors in term placenta from insulin–resistant women with gestational hypertension. *Diabetologia*. 1996;39(8):952–960.

Vander Heiden MG, Cantley LC, Thompson CB. Understanding the Warburg effect: The metabolic requirements of cell proliferation. *Science*. 2009;324(5930):1029–1033.

Vazzana N, Ranalli P, Cuccurullo C, Davì G. Diabetes mellitus and thrombosis. *Thromb Res*. 2012;129(3):371–377.

Vella V, Malaguarnera R. The emerging role of insulin receptor isoforms in thyroid cancer: clinical implications and new perspectives. *Int J Mol Sci*. 2018;19(12):3814.

Vesel M, Rapp J, Feller D, Kiss E, Jaromi L, Meggyes M, Miskei G, et al. ABCB1 and ABCG2 drug transporters are differentially expressed in non–small cell lung cancers (NSCLC) and expression is modified by cisplatin treatment via altered Wnt signaling. *Respir Res*. 2017;18(1):52.

Wakeling EL, Brioude F, Lokulo–Sodipe O, O'Connell SM, Salem J, Bliek J, Canton AP, et al. Diagnosis and management of Silver–Russell syndrome: First international consensus statement. *Nat Rev Endocrinol*. 2017;13(2):105–24.

Walenkamp MJ, van der Kamp HJ, Pereira AM, Kant SG, van Duyvenvoorde HA, Kruithof MF, Breuning MH, Romijn JA, Karperien M, Wit JM. A variable degree of intrauterine and postnatal growth retardation in a family with a missense mutation in the insulin–like growth factor I receptor. *J Clin Endocrinol Metab*. 2006;91(8):3062–3070.

Wallborn T, Wüller S, Klammt J, Kruis T, Kratzsch J, Schmidt G, Schlicke M, et al. A heterozygous mutation of the insulin–like growth factor–I receptor causes retention of the nascent protein in the endoplasmic reticulum and results in intrauterine and postnatal growth retardation. *J Clin Endocrinol Metab*. 2010;95(5):2316–2324.

Walsh CT, Garneau–Tsodikova S, Gatto GJ Jr. Protein posttranslational modifications: The chemistry of proteome diversifications. *Angew Chem Int Ed Engl*. 2005;44(45):7342–7372.

Walsh JH, Karnes WE, Cuttitta F, Walker A. Autocrine growth factors and solid tumor malignancy. *West J Med*. 1991;155(2):152–163.

Wang T, Ge G, Ding Y, Zhou X, Huang Z, Zhu W, Shu Y, Liu P. MiR–503 regulates cisplatin resistance of human gastric cancer cell lines by targeting IGF1R and BCL2. *Chin Med J (Engl)*. 2014;127(12):2357–2362.

Wang A, Rana S, Karumanchi SA. Preeclampsia: The role of angiogenic factors in its pathogenesis. *Physiology (Bethesda)*. 2009;24:147–158.

Warburg O. On respiratory impairment in cancer cells. *Science*. 1956;124(3215):269–270.

Ward GM, Walters JM, Barton J, Alford FP, Boston RC. Physiologic modeling of the intravenous glucose tolerance test in type 2 diabetes: A new approach to the insulin compartment. *Metabolism*. 2001;50(5):512–519.

Werner H, Le Roith D. New concepts in regulation and function of the insulin–like growth factors: Implications for understanding normal growth and neoplasia. *Cell Mol Life Sci*. 2000;57(6):932–942.

West RC, Bouma GJ, Winger QA. Shifting perspectives from "oncogenic" to oncofetal proteins; how these factors drive placental development. *Reprod Biol Endocrinol*. 2018;16(1):101.

Westwood M, Gibson JM, Davies AJ, Young RJ, White A. The phosphorylation pattern of insulin–like growth factor binding protein–1 in normal plasma is different from that in amniotic fluid and changes during pregnancy. *J Clin Endocrinol Metab*. 1994;79(6):1735–1741.

WHO (World Health Organization), Health topics, Cancer [updated 2019]. Available from: (www.who.int/cancer/en/)

World Cancer Research Fund/American Institute for Cancer Research, Colorectal cancer statistsics, [updated 2019]. Available from: (https://www.wcrf.org/dietandcancer/cancer–trends/colorectal–cancer–statistics)

Youssef A, Han VK. Low oxygen tension modulates the insulin–like growth factor–1 or –2 signaling via both insulin–like growth factor–1 receptor and insulin receptor to maintain stem cell identity in placental mesenchymal stem cells. *Endocrinology*. 2016;157(3):1163–1174.

Youssef A, Iosef C, Han VK. Low–oxygen tension and IGF–I promote proliferation and multipotency of placental mesenchymal stem cells (PMSCs) from different gestations via distinct signaling pathways. *Endocrinology*. 2014;155(4):1386–1397.

Yu H, Rohan T. Role of the insulin–like growth factor family in cancer development and progression. *J Natl Cancer Inst*. 2000;92(18):1472–1489.

Yu M, Yuan C, Wang H, Liu J, Qin H, Liu S, Yan Q. FUT8 drives the proliferation and invasion of trophoblastic cells via IGF–1/IGF–1R signaling pathway. *Placenta*. 2019;75:45–53.

Yuan TL, Cantley LC. PI3K pathway alterations in cancer: Variations on a theme. *Oncogene*. 2008;27(41):5497–5510.

Yung HW, Cox M, Tissot van Patot M, Burton GJ. Evidence of endoplasmic reticulum stress and protein synthesis inhibition in the placenta of non–native women at high altitude. *FASEB J*. 2012:26(5):1970–1981.

Zarrilli R, Pignata S, Romano M, Gravina A, Casola S, Bruni CB, Acquaviva AM. Expression of insulin–like growth factor (IGF)–II and IGF–I receptor during proliferation and differentiation of CaCo–2 human colon carcinoma cells. *Cell Growth Differ*. 1994;5(10):1085–1091.

Zawacka–Pankau J, Selivanova G. Pharmacological reactivation of p53 as a strategy to treat cancer. *J Intern Med*. 2015;277(2):248–259.

Zelzer E, Levy Y, Kahana C, Shilo BZ, Rubinstein M, Cohen B. Insulin induces transcription of target genes through the hypoxia–inducible factor HIF–1alpha/ARNT. *EMBO J*. 1998;17(17):5085–5094.

Zeng L, Perks CM, Holly JM. IGFBP–2/PTEN: A critical interaction for tumours and for general physiology? *Growth Horm IGF Res*. 2015;25(3):103–107.

Zhang YK, Wang YJ, Gupta P, Chen ZS. Multidrug resistance proteins (MRPs) and cancer therapy. *AAPS J*. 2015;17(4):802–812.

Zhou R, Diehl D, Hoeflich A, Lahm H, Wolf E. IGF–binding protein–4: Biochemical characteristics and functional consequences. *J Endocrinol*. 2003;178(2):177–193.

Zhou P, Ten S, Sinha S, Ramchandani N, Vogiatzi M, Maclaren N. Insulin receptor autoimmunity and insulin resistance. *J Pediatr Endocrinol Metab*. 2008;21(4):369–375.

Submitted: 10th Sept 2019, Revised: 24th Dec 2019, Accepted: 3rd Jan 2020

Chapter Two

2. IMAGING TRANSMEMBRANE PROTEIN TRANSPORT ACROSS THE NUCLEAR ENVELOPE

Mark Tingey, Steven J. Schnell, Yichen Li, Samuel Junod, Wenlan Yu, Weidong Yang*

Department of Biology, Temple University, Philadelphia, Pennsylvania, USA

ABSTRACT

The mechanism of membrane protein transport across the nuclear envelope remains a point of discussion among researchers resulting in four proposed models: diffusion-retention, ATP-dependent, nuclear localization signal–mediated, sorting motif–mediated. Confirming any of these models is hampered by the challenges of resolving proteins on the outer nuclear membrane and the inner nuclear membrane. Whilst differentiation via imaging is possible using immunogold-labeled electron microscopy as well as various super-resolution methods, typically these methods require the sample to be fixed or frozen, and provide limited information regarding the dynamic transport mechanisms of nuclear membrane proteins. Recently a number of dynamic single-molecule microscopy techniques that have been developed and utilized to elucidate the transport mechanism of membrane proteins in our laboratory. Here we evaluate the existing evidence for each model, the techniques used to obtain that evidence, and ways in which single-molecule microscopy can be used to further interrogate the question of nuclear envelope transmembrane protein transport.

Keywords: single-molecule microscopy, SPEED, NETs, transmembrane protein, nuclear envelope, transport, single-molecule FRAP, HiLo

* Direct all correspondence to Dr. Weidong Yang, Department of Biology, Temple University, Philadelphia, Pennsylvania. E-mail: Weidong.Yang@temple.edu

2.1. INTRODUCTION

The nuclear membrane of eukaryotic cells consists of two lipid bilayers, the inner nuclear membrane (INM) and the outer nuclear membrane (ONM). The INM and ONM are sperated by a perinuclear space of approximately 30-50 nm (Franke et al., 1981; Feldherr and Akin, 1990). Together, these structures form the nuclear envelope (NE), which functions as a barrier between the nucleus and the cytoplasm of the cell. Embedded within the INM and ONM are nuclear envelope transmembrane proteins (NETs). Each membrane contains a unique set of NETs that are targeted to their specific compartments after synthesis at the endoplasmic reticulum (ER). The ER is contiguous with the ONM and fuses with the INM where nuclear pore complexes (NPCs) are inserted (Gerace and Burke, 1988). The NPC is a large complex composed of more than 30 nucleoporin (Nup) proteins that function together to regulate the transport of proteins and RNA. The primary pathway for soluble proteins and RNA to pass through the NE is the central channel of the NPC. The central channel has a minimum diameter of approximately 50 nm and functions as a selectively permeable barrier against passive diffusion of large molecules (Beck et al., 2004; Lim, Fahrenkrog and Köser, 2007). The barrier in the central channel is formed by intrinsically disordered phenylalanine-glycine (FG) motifs on one third of the Nups (Frey et al., 2007). In addition to the central channel, the NPC also contains multiple peripheral channels, which are structures approximately 10 nm wide between the core protein structure of the NPC and the membrane (Reichelt et al., 1990; Hinshaw, Carragher and Milligan, 1992). These peripheral channels remain poorly described; however, they have been implicated in the transport of NETs from the ONM to the INM.

The transport of NETs to their appropriate locations on the ONM and INM is critical to the proper function of the cell. ONM and INM NETs have been shown to play a role in genome function as well as providing structure to their respective membranes. For instance, a variety of INM NETs bind the lamina intermediate filament network associated with the INM (Hetzer and Wente, 2009; Arib and Akhtar, 2011; de Las Heras, 2013). Furthermore, ONM NETs connect to all three major cytoplasmic filament systems as well as forming connections across the lumen of the NE to form the nucleoskeleton and cytoskeleton (LINC) complex critical to mechanosignal transduction based regulation of the genome as well as cell and nuclear mechanical stability (Crisp et al., 2006; Zuleger, Korfali and Schirmer, 2008; Östlund et al., 2009). Loss of function in these complex interactomes can result in a variety of pathologies, often termed *envelopathies* or *laminopathies*. These pathologies are often highly tissue-specific, thereby

highlighting the importance of INM protein function during development (Schirmer and Gerace, 2005; Chi, Chen and Jeang, 2009).

The topography of individual NETs also provides insight into the putative function and interactions between NETs and surrounding proteins. The KASH (Klarsicht, ANC-1, Syne homology); SUN (Sad1p, UNC-84); and LEM (lamin-associated protein [LAP]2, Emerin, MAN1) domains represent families of NETs with functions critical to proper cell function. The LEM domain is a globular approximately 40-residue helix-loop-helix motif found primarily in several unrelated INM NETs (Lin et al., 2000), including MAN1, Emerin, LEM2, and several alternatively spliced isoforms of LAP2 (Wagner and Krohne, 2007). Proteins containing the LEM domain directly interact with the highly conserved barrier-to-autointegration factor (BAF) protein, a DNA bridging protein. Furthermore, all LEM-domain containing proteins bind directly to A- or B-type lamins *in vitro* (Gruenbaum et al., 2005). LEM domain NETs have been implicated in many critical genome regulation processes, including regulation of transcription factors, signal transduction, and chromatin structure (Barton, Soshnev and Geyer, 2015).

The KASH domain is a highly hydrophobic domain approximately 60 residues long, consisting of an approximately 20-residue transmembrane region and an approximately 35-residue C-terminal region that lies between the INM and ONM (Wang et al., 2012). The KASH domain interacts with the SUN domain, a specialized form of the discoidin domain found in INM NETs (Mans et al., 2014). The interaction between the KASH domain and the SUN domain forms the LINC complex and mediates subsequent nuclear movement and positioning (Crisp et al., 2006; Cain et al., 2018).

The localization of INM-NETs to their proper regions is critical to proper cell function; therefore, the mechanism by which NETs translocate from the ER to the INM after synthesis is an area of interest to researchers. The exact mechanism of translocation remains a subject of debate, and four prevailing hypotheses will be discussed in this chapter. These models of the transport of NETs from the ER and ONM to the INM share a similar basic pathway; specifically, proteins are produced in the ER, then travel across the ONM and through the NPC to the INM. The key difference in the models lies in the associated proteins and requirements for this passage. Although there are some reports of NETs translocating to the INM in a manner bypassing the NPC (Dixon and Schirmer, 2018), this chapter focuses on the transport models of NETs passing through the NPC.

2.2. Proposed Models for Nuclear Envelope Transmembrane Protein Transport

2.2.1. Diffusion-Retention Model

The diffusion-retention model is also referred to as the *Lateral diffusion retention* model and was the uncontested model for NET transport across the NE for many years. The diffusion-retention model was first proposed following a pair of discoveries, the first being identification of an approximately 10-nm channel peripheral to the central channel of the NPC (Hinshaw, Carragher and Milligan, 1992), which pointed to the potential existence of transport channels beyond the canonical soluble protein transport routes through the central channel of the NPC. The second discovery was the observation that the small INM protein p55 is capable of translocation between nuclei in a fused cell (Powell and Burke, 1990).

These two discoveries make up the basis for the diffusion-retention model, The core idea being that proteins freely and rapidly diffuse between the ER, ONM, and INM. The model further postulates that the mechanism behind aggregation of INM proteins on the INM is due to lamins and peripheral chromatin binding to INM NETs (Figure 1).

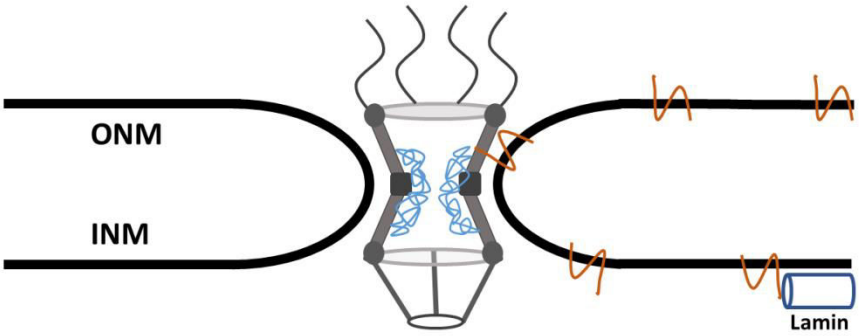

Figure 1. Diffusion-Retention Model of NETs Transport. NETs of a size ~70 kDa are synthesized at the ER. They then passively diffuse across the ONM, through the peripheral channel, and onto the INM. If they interact with a nuclear protein, i.e. lamin, they will be retained in the nucleus. If they do not interact with a nuclear protein, they will passivly diffuse from the INM to the ONM.

In the diffusion-retention model, translocation of a transmembrane protein begins at the ER. The transmembrane protein is either co-translationally or post-translationally inserted into the membrane of the ER, likely in a Sec61-dependent manner (Rapoport et al., 2004; Park and Rapoport, 2012; Katta, Smoyer and Jasperson 2014). Because the ER is contiguous to the ONM (Amar-Costesec et al., 1974), the protein is can freely diffuse from the ER to the ONM. Then, according to the diffusion-retention model, the protein diffuses through the peripheral channel of the NPC into the INM where it will bind to lamins and peripheral chromatin. If the protein does not have the required binding sites, it will then diffuse back through the peripheral channel to the ONM and ER (Katta, Smoyer and Jasperson, 2014; Dixon and Schirmer, 2018).

The supposition that INM proteins aggregate in the nucleus due to interactions between the NETs and proteins within the nucleus is supported experimentally by the observation that proteins that do not typically enrich at the INM will localize to the INM if a binding domain specific to nuclear proteins is added. Soullam and Worman first demonstrated this phenomenon by altering the transmembrane region of an ER-specific protein to express the lamin-binding region of an INM-specific NET, which subsequently localized to the INM (Soullam and Worman, 1993). This observation was further validated using other ER-specific proteins and a variety of INM NET-specific lamin-binding regions, providing further support for this model (Furukawa , Fritze and Gerace; Wu, Lin and Worman, 2002; Zuleger, Korfali and Schirmer, 2008).

A number of studies have assayed NETs for binding affinity for nuclear localized proteins and have shown that the vast majority of NETs directed to the INM exhibit binding affinity for chromatin or chromatin-associated proteins (Dixon and Schirmer, 2018). A good example of this affinity is the LEM domain family of NETs, which all contain a motif facilitating binding to the chromatin associated BAF protein, thereby enabling LEM domain NETs to aggregate on the INM (Brachner et al., 2005). Researchers have also made use of fluorescence recovery after photobleaching (FRAP) microscopy to determine the proportion of tagged mobile INM NETs as a method of assaying the diffusion-retention model. When FRAP of the fluorescently tagged INM-based Lamin B Receptor (LBR) was performed, it was shown that 60% of prephotobleach fluorescence failed to recover after photobleaching (Ellenberg et al., 1997). Approximately 60% of LBR on the INM is non-mobile and unable to diffuse. This observation strongly supports the assertion that proteins diffuse into the INM from the ONM, interact with proteins within the INM, and become immobile. Furthermore, numerous studies have shown a decrease in the mobility of NETs on the NE when compared to the ER, which suggests that the binding affinity in assayed NETs for nuclear

proteins inhibits mobility (Ostland et al., 1999; Shimi et al., 2004; Zuleger et al., 2011).

The approximately 10-nm peripheral channel is sufficient to allow membrane proteins to diffuse through the NE in a manner consistent with the measured diffusion rate, provided they have a nucleoplasmic or extraluminal domain approximately 40 kDa or smaller (Pain et al., 1975; Reichelt et al., 1990; Hinshaw, Carragher and Milligan, 1992; Maimon et al., 2012). The peripheral channel has been further implicated in NET transport to the INM in an experiment that blocked the peripheral channel. Researchers introduced a nuclear pore glycoprotein-210 (gp210) antibody, which binds to gp210. This gp210 antibody anchors the NPC to the membrane and is located near the peripheral channel (Greber, Senior and Gerace, 1990). In the presence of a gp210-specific antibody, the peripheral channel is occluded. Blocking the peripheral channel with the gp210-specific antibody severely impaired the ability of INM NETs to translocate to the INM (Ohba et al., 2004), further confirming that INM NETs require the peripheral channel for entry into the INM.

The diffusion-retention model is an energy independent model that relies on passive diffusion and is therefore limited by the size of the pheripheral channel. This limit has been confirmed in multiple studies that observed slowed transport as protein size increased or an inability to translocate if the protein became too large. Chimeric proteins of approximately 60 kDa and larger have been observed in multiple experiments to be unable to pass through the NPC into the INM, further supporting the size limitation proposed by the diffusion-retention model (Soullam and Worman, 1993; Soullam and Worman, 1995; Wu, Lin and Worman, 2002; Ohba et al., 2004; Boni et al. 2015; Ungricht and Kutay, 2015). For many years, the diffusion-retention model was mostly uncontested as the *de facto* model of NET transportation; however, many exceptions to this model have been observed, which suggests that the process is perhaps much more complex than is represented by this model.

2.2.2. ATP-Dependent Model

The diffusion-retention model of INM transport revolves around the concept of energy independence. Diffusion is a passive process that does not require adenosine triphosphate (ATP) to accomplish. To interrogate whether ATP is required for NETs to translocate to the INM, Ohba and colleagues developed a rapamycin trap assay that would enable them to assay whether or not ATP was required to transport NETs into the INM. This study used LAP2β, a type II integral protein of the INM, as a reporter. This reporter was then modified to have

the FRB (FKBP12/rapamycin-binding) domain of mTOR (mechanistic targeting of rapamycin) fused to the N-terminus and GFP fused to the C-terminus. The second component of this trap was a nuclear localized protein containing three repeats of FKBP12. In the presence of rapamycin, FRB and FKBP12 will bind, enabling researchers to determine if the reporter protein was successfully translocated to the INM (Ohba et al., 2004).

At reduced temperature and in the absence of ATP, translocation of the reporter to the INM was completely inhibited. However, reporters present on the ONM and ER were unaffected. This strongly suggests that ATP is required for translocation of NETs to the INM. However, it must also be noted that this experiment was performed with artificial markers, which may have also impacted translocation of NETs (Ohba et al., 2004).

The observations made by Ohba and colleagues led Zuleger, Korfali, and Schirmer to suggest a possible new transport model, initially dubbed gated lateral diffusion, wherein the authors suggest that Nup gp210 functions as a gatekeeper for the peripheral channel. This initial model proposed a mechanism in which proteins would be required to pay a *fee* of ATP to gp210, causing a conformational change allowing the proteins to then pass through the NPC into the INM (Zuleger, Korfali and Schirmer, 2008).

This idea was further refined in a subsequent study that also provided experimental support for the ATP-dependent model. In this study, authors assayed six proteins for their dependence upon ATP to translocate to the INM. Of the six proteins assayed, only emerin and SUN2 were found to require ATP to translocate to the INM (Zuleger et al., 2011). SUN2 and emerin exhibited decreased mobility on the ER as well as the ONM in the absence of ATP. This change suggests that ATP is not required as a fee to cause conformational changes in gp210; rather, ATP is required for a change to the protein prior to transport through the NPC. The ATP-dependent model begins with protein synthesis at the ER, where it is suggested that a chaperone or ER retention protein may be bound to the NETs. ATP is then required to release the NETs and allow translocation to the INM (Dixon and Schirmer, 2018). This model is still in its infancy, with little direct experimental evidence; however, as the most recently proposed model, this is to be expected (Figure 2).

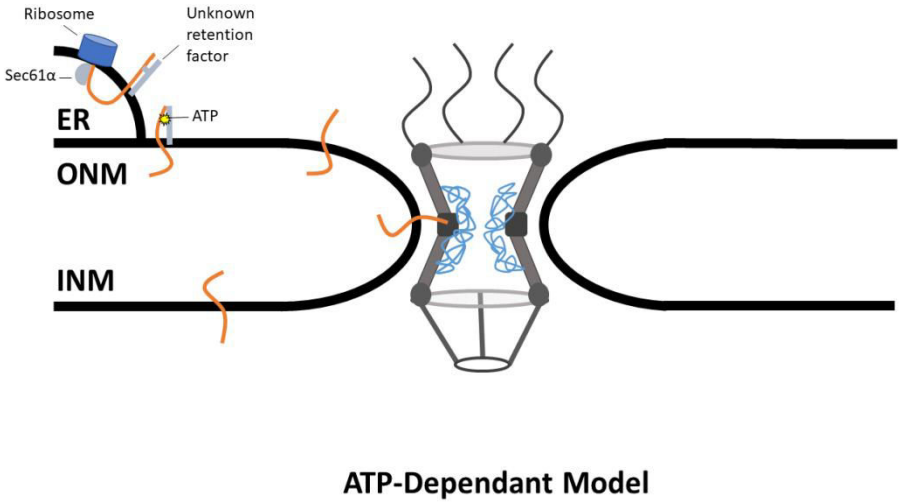

Figure 2. ATP-Dependant Model of NETs Transport. NETs are translated at the ER, where Sec61α inserts the protein into the membrane. The NET is then bound to an unknown retention factor, preventing the NET from diffusing across the NE. The bond between the NET and the retention factor is broken in an ATP dependent manner, and the NET then diffuses across the NE through the peripheral channel.

2.2.3. Nuclear Localization Signal–Mediated Model

Soluble protein transport into the nucleus, in a simplified model, takes place in three stages. First, the nuclear localization signal (NLS; a small <50 amino acid sequence) of a cargo protein is recognized by karyopherin-α/β. Second, the complex of the cargo and the karyopherin pass through the NPC by interacting with a subset of Nups enriched with FG repeats. Third, karyopherins release the cargo when stimulated by the small GTPase Ran in its GTP-bound form (Fried and Kutay, 2003; Lusk, Blobel and King, 2007).

In their 1995 paper, Soullam and Worman identified a signal in the N-terminal nucleoplasmic domain of chicken LBR that functioned similar to a canonical NLS. This indicated that there was, on some level, crossover between the membrane-bound and soluble protein transport pathways; however, the idea that the NLS may be critical for INM targeting was largely discarded; chimeric proteins containing NLS sequences were unable to translocate into the INM (Soullam and Worman, 1995).

This concept may have been discarded too soon. Ten years after Soullam and Worman published their findings, King and colleagues showed transport in

budding yeast of the membrane-bound LEM domain–containing proteins Heh1/Src1 and Heh2 relied upon karyopherins and the Ran GTPase cycle to aggregate in the INM. Furthermore, King and colleagues identified a sequence akin to the canonical NLS on Heh2 that binds to karyopherins and is required for transport into the INM. When the putative NLS was deleted from Heh2, the YFP-tagged proteins dispersed across the ER and ONM but were almost entirely excluded from the INM (King, Blobel and Lusk, 2006). Further analysis of the extralumenal domains of membrane proteins identified many putative NLS sites, suggesting that the phenomenon may not be isolated to Heh2, but is in fact widespread (Lusk, Bloble and King ,2007; Malik, Zuleger and Schirmer, 2009).

Observations made by Lusk, Blobel and King led them to publish "*Rules for the Road"*, a manuscript detailing a new transport model dubbed the "*Transport Factor–Mediated"* model. This model marries the diffusion-retention and the transport of soluble proteins models: a NET is synthesized at the ER and inserted into the membrane, then a karyopherin binds to an NLS in the extraluminal domain of the NET. The karyopherin then transports the NET through the NPC, where the karyopherin detaches in a RAN GTPase–dependent fashion (Lusk, Blobel and King, 2007; Katta, Smoyer and Jasperson, 2014) (Figure 3).

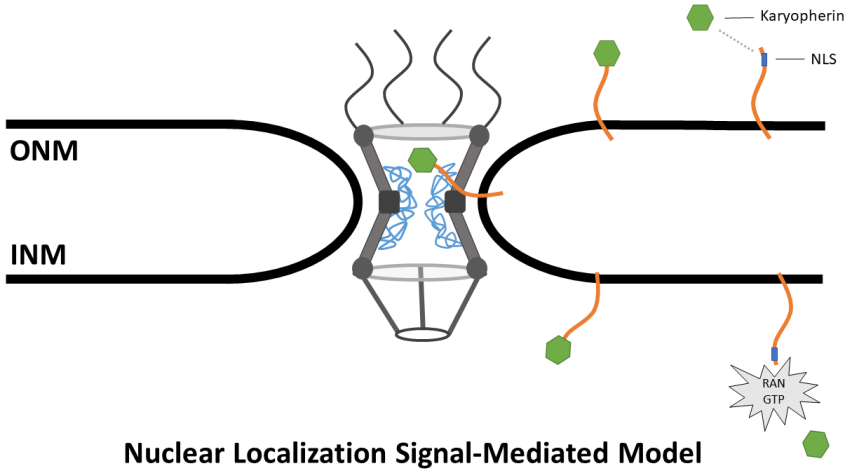

Figure 3. Nuclear localization signal-mediated model. NETs containing an NLS bind a karyopherin. The karyopherin then transports the NLS-containing terminus through the central channel of the NPC while the membrane bound terminus passes through the peripheral channel. The karyophern then disassociates from the NET in a RAN GTPase-dependent fashion.

In addition to proposing a new transport model, Lusk and colleagues codefied a series of rules for INM transport of NETs. These rules effectively amended the diffusion-retention model to have a lower size limitation for diffusion. The model states that proteins approximately 25 kDa or smaller can freely diffuse through the ER and ONM to the INM. These proteins may then aggregate in the INM due to interactions with other proteins within the nucleus. The size limitation is significantly smaller than the approximately 70 kDa limit of the diffusion-retention model, and excludes a large number of NETs from translocation via the diffusion-retention model.

To account for the larger proteins, the model states that NETs with an extraluminal domain between approximately 25 and 75 kDa require the assistance of an NLS to pass through the NPC. Furthermore, the strength of the NLS determines the specificity of the localization. For instance, a weak NLS would be enough to target a protein to the INM, but not to confer exclusive localization to the INM, whereas a strong NLS would target to a protein to the INM as well as confer exclusive localization to the INM.

This model raises the question that if NETs are making use of karyopherins to transport into the INM, do they also use the central channel of the NPC? A karyopherin bound to the extraluminal domain of a large NET is difficult to imagine passing through the peripheral channel of the NPC. To answer this question, Meinema and colleagues designed a rather elegant experiment to interrogate this question, wherein a synthetic INM NET was generated that fused the Heh2 NLS, linker and transmembrane region to the human protein FKBP12 tagged with eGFP. This protein then was expressed within a line containing a modified Nup Nsp1 fused to FRB. In the presence of rapamycin, FKBP12 and FRB will bind; therefore, if the synthetic Heh2 passes through the central channel of the NPC in the presence of rapamycin, it will bind to the FRB fused to Nsp1. If the synthetic NETs pass through the peripheral channel rather than the central pore, the FRB and FKBP12 will not bind. In addition to this experiment, combinations of FG Nups also were deleted. It was observed that the synthetic Heh2 aggregated in a manner consistent with central pore transport (Meinema et al., 2011).

Perhaps the most interesting conclusion drawn by Meinema and colleagues is the observation that a disordered linker is required for the NETs to make use of the central pore. They examined linkers of different lengths and compositions and determined that a linker consisting of at least 120 residues was required to facilitate transport. This indicates that the linker connects the transmembrane domain with the region that is interacting with the FG Nups, whereas the

disordered linker slices through the NPC scaffold in an as of yet uncharacterized manner (Meinema et al., 2011).

The assertion that NETs associate with karyopherins to facilitate nuclear transport was further supported by the observation that the deletion of different combinations of FG Nups directly impacted the efficacy by which the synthetic Heh2 was able to translocate to the INM (Meinema et al., 2011). Together, these data make a very convincing case for the Nuclear Localization Signal–Mediated model.

2.2.4. Sorting Motif–Mediated Model

The NLS plays a large role in the translocation of NETs to the INM; however, not all proteins containing an NLS appear to rely upon that NLS for translocation to the INM. In fact, the deletion or mutation of the NLS has no impact upon NET translocation to the INM (Turgay et al., 2010; Tapley, Ly and Starr, 2011). The lack of effect of the deletion of the NLS on these NETs implies that another factor is targeting these proteins to the INM.

The bacculovirus Occlusion Derived Virus (ODV) follows a rather interesting infection methodology. The virus inserts into the ER and then migrates into the INM, where it forms a viral envelope. While investigating the transport route followed by this virus, it was discovered that the capsid protein ODV-E66 is directed to the INM by a short sequence of amino acids. This sequence, termed the *inner nuclear membrane sorting motif* (INM-SM), has two prominent characteristics: an extremely hydrophobic region of 18 amino acids and a number of positively charged amino acids close to the C-terminus of the hydrophobic region. Together with these features, a 33–amino acid sequence on the N-terminus of ODV-E66 was sufficient to traffic proteins to the INM (Braunagel et al., 2004).

The discovery of the transmembrane sequence (TMS) in viral proteins raised a very important question: Is there a sequence in host cells that perform a similar function? It was shown by Braunagel and colleagues that a sorting motif similar to that found in ODV-E66 is present in well-identified host INM NETs, including some LEM SUN domain– and SUN domain–containing proteins (Braunagel et al., 2004). On more thorough inspection, it was shown that both the viral and host INM-SM–containing proteins interact with the translocon in a similar fashion. However, they do interact with the translocon in a fashion distinct from other membrane proteins (Saskena et al., 2004).

Further investigation of the translocon showed that the INM-SM of both ODV-E66 and LBR interact with truncated membrane-bound karyopherin-α importin-α-16 (Braunegal et al., 2004, Saskena et al., 2004). The truncate lacks

the importin-β binding site that enables keryopherin-α to interact with keryopherin-β to form the dimeric karyopherin complex. This observation has led investigators to propose that importin-α-16 functions independently of the full length karyopherin-α (Rexach, 2006). Given the smaller size of importin-α-16, it is likely that it is able to transport through the peripheral channel of the NPC while associated with its cargo (Rexach 2006; Saskena et al., 2006).

An interesting feature of importin-α-16 is the presence of armadillo repeat motifs (ARMs), which interact with FG Nups. Whilst the majority of FG Nups are localized to the central channel of the NPC, several Nups containing FG repeats are closely localized to the peripheral channel of the NPC (Batrakou, Kerr and Schirmer, 2009; Kerr and Schirmer, 2009; von Appen and Beck, 2016; Kosinski et al., 2016). The potential interaction between the ARM repeats on importin-α-16 and the FG repeat–containing Nups in the peripheral channel has caused some researchers to propose that importin-α-16 negotiates the FG Nups at the peripheral channel in a manner similar to how the importin complex negotiates the FG Nups in the central channel, provided the FG Nups are indeed accessible in the peripheral channel (Dixon and Schirmer, 2018).

In addition to interacting with membrane proteins, it was shown that importin-α-16 interacts with Sec61α. This information together forms the basis for a model in which INM proteins are recognized by Sec61α upon synthesis and then transported through the NPC by importin-α-16 to the INM, where release of importin-α-16 is then stimulated by Nup50 or some other Ran-independent mechanism (Gilchrist and Rexach, 2003; Braunegal et al., 2004; Matsuura and Stewart, 2005; Rexach, 2006; Braunegal, Cox and Summers, 2009) (Figure 4).

In an odd twist, a study of Heh2 trafficking in yeast (which was initially used to develop the Nuclear Localization Signal–mediated model) has identified an INM-SM sequence. The sequence interacts with truncated forms of Kap60 (Importin-α), Kap60-30, and Kap60-40, which were subsequently shown to be necessary for INM localization of Heh2 (Liu et al., 2010). Furthermore, mutating a previously unidentified INM-SM sequence decreased the localization of Heh2 at the INM in yeast. Interestingly, deletion of the INM-SM still resulted in Heh2 localizing to the INM (Meinema et al., 2011). This incongruous result has led some researchers to argue that in Heh2 yeast, the INM-SM may be used to determine membrane topology (Laba, Steen and Veenhoff, 2014).

Considering this evidence, it has been proposed that some INM-SM–containing proteins have redundant systems of transport into the INM. The contrasting view remains that the sorting motif–mediated model is a two-step process, wherein the INM-SM is recognized by Sec61α during translation and thereby targeted to the INM (Dixon and Schirmer, 2018).

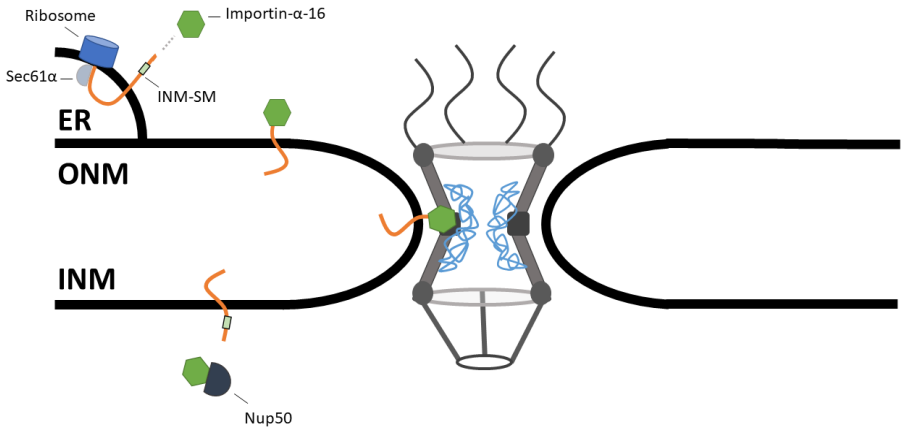

Figure 4. Sorting Motif-Mediated Model. NETs are recognized by Sec61α during translation and are inserted into the membrane. The INM-SM binds to Importin-α-16 which then transports the NETs to the INM. Importin-α-16 is then stimulated by Nup50 to release the INM-SM.

2.3. Classical Approaches to Study Structure and Function of NETs

2.3.1. Conventional fluorescence microscopy

Considering the foregoing evidence, it has been proposed that some INM-SM–containing proteins have redundant systems of transport into the INM. The contrasting view remains that the sorting motif–mediated model is a two-step process wherein the INM-SM is recognized by Sec61α during translation and thereby targeted to the INM (Dixon and Schirmer, 2018).

2.3.2. Immunofluorescence microscopy

In immunofluorescene microscopy, the specificity of antibodies to their respective antigens is used to target fluorescent dyes attached to specific target proteins in a cell. This specificty of targeting enables researchers to confidently visualize localization or distribution of target proteins. For example, localization of LBR and LAP1/2, the first NETs discovered, was accomplished by

immunofluorescence microscopy (Senior and Gerace, 1988; Worman et al., 1988; Foisner and Gerace, 1993); LBR and LAP1/2 were found to reside predominantly in the NE. In fact, several other NETs have been found to localize to the NE with immunofluorescence microscopy (Greber, Senior and Gerace, 1990; Manilal et al., 1996; Paulin-Levasseur et al., 1996; Malone et al., 1999; Hodzic et al., 2004). There are, however, several shortcomings inherent in immunofluorescene microscopy. The Abbe diffraction limit renders this approach unlikely to distinguish localizations of NETs on the INM from those on the ONM, because the two membrane bilayers are separated by a 40-nm perinuclear space (Bouchet-Marquis, Dubovhet and Fakan, 2006; Mudumbi, Schirmer and Yang, 2016). Also, immunofluorescene microscopy is limited to use in fixed cells as antibodies do not penetrate the cell membrane; this limitation deprives the researcher of studying the NETs in the natural environment of the live cell.

2.3.3. Live-cell fluorescence microscopy

Another labeling strategy is the use of genetically encoded fluorescent tags such as green fluorecent protein (GFP). The fluorescent protein is genetically inserted into the 5’ or 3’ end of the coding sequence of the target NET protein, and thus the live cell will express the NET with the fluorescent label attached; such labeling has enabled researchers to identify and localize NETs in the live cell. Rolls and colleagues utilized live-cell fluorescence microscopy to identify and characterize the INM protein nurim (Rolls et al., 1999). In order to avoid physical separation of the connected NE and ER caused by lysis and fixation in immunolabelling strategy, Rolls and colleagues constructed a baby hamster kidney (BHK) cell line stably expressing GFP-tagged nurim (having appended GFP into the 5’ end of nurim) and used live-cell fluorescence microscopy in this model to show that nurim was localized to the nuclear rim in live cells. Further, they compared the distributions of GFP-nurim and GFP-Nup62 and determined that whereas nurim is localized to the NE, it is not shown to localize at the NPC. Whereas both immunofluorescene or live-cell microscopy enable researchers to visualize the subcelluar localization of NET proteins, the latter provides information in an environment more closely to that of the physiological context of cell, as fixation and immunolabeling break subcellular structure to some extent.

Live-cell fluorescence microscopy has also been used to track real-time dynamic changes in the localization of NETs during mitosis. Haraguchi and colleagues examined spatial and temporal sequences of NE assembly by monitoring the behavior of GFP-fused NETs in living cells. With time-lapse fluorescence microscopy, Haraguchi and colleagues visualized and tracked

localization of individual NET proteins in live HeLa cells expressing corresponding GFP-fusion NETs (Haraguchi et al., 2008); these NETs, including LAP2β, LAP2α, emerin, MAN1, and LBR, were fused to GFP and transfected and studied spearately. Results showed movment of these NETs during the telophase, and the authors were able to draw a detailed diagram of NE formation in this period.

Studies such as these show that compared with immunofluorescence microsocpy, live-cell fluorescence microscopy not only can be used to elucidate the subcellular localization and distribution of NETs in physiological conditions, but also is the better method to monitor real-time movement of NETs in live cells. However, both approaches share the common limitation of the diffraction limit, which prevents either approach from determining the fine localization of NETs at sub-diffraction level, such as the difference between localization to the INM or ONM as mentioned above (Bouchet-Marquis, Dubochet and Fakan, 2006; Mudumbi, Schirmer and Yang, 2016).

2.3.4. Förster resonance energy transfer analysis

Förster resonance energy transfer (FRET) analysis is based on energy transfer between two chromophores (Cheng, 2006). The donor chromophore, when brought to its excited electronic state by the absorption of energy (delivered by laser), may transfer energy to an acceptor chromophore through nonradiative dipole–dipole coupling (Helms, 2008; Helms, 2018). Because the efficiency of this energy transfer is inversely proportional to the distance between donor and acceptor (Harris, 2010), FRET can be used to determine if two fluorophores are within a certain distance of each other, and as a result is considered to be an effective approach to detect interactions between biological molecules.

Employing a combination approach of live-cell fluorescence microscopy and FRET, Haraguchi and colleagues tested the interaction between BAF, a DNA-binding protein, NETs LAP2α and emerin (Haraguchi et al., 2008). To validate the utility of FRET to detect specific interactions, the authors showed detection of the strong FRET signal between BAF fused with mVenus and mCFP, consistent with BAF dimer or dodecamer formation *in vitro* (Haraguchi et al., 2001) as a positive control. As a negative control, the authors attempted detection of FRET interaction between BAF and a mutant emerin (emerin-m24) that does not bind to BAF either *in vivo* or *in vitro* (Haraguchi et al., 2001; Lee et al., 2001); no FRET signals were detected between mCFP-emerin-m24 and mVenus-BAF, suggesting that detected FRET signals are the result of specific interactions. The authors

cotransfected Hela cells with mVenus-BAF (donor) and mCFP (acceptor) fusions of LAP2α and emerin, respectively, and detected FRET interaction between mVenus-BAF and mCFP-LAP2 and mCFP-emerin, which suggests BAF directly binds emerin and LAP2α.

It is to be noted that there are several disadvantages to FRET. The fluorophores required are relatively larger compared with some target proteins. Also, attached fluorophores, especially fluorescent proteins, are sensitive to changes in environmental factors, such as pH, temperature and ionic concentrations (Leavesley and Rich, 2016). Moreover, FRET provides information only about the distance between the donor and acceptor molecules but cannot provide direct information about whether the donor and acceptor actually interact physically (Zheng, 2006).

2.3.5. Electron microscopy

In contrast to the limited spatial resolution of conventional fluorescence microscopy, electron microscopy (EM) can achieve subnanometer resolution to observe single protein molecules embedded in the NE or NPC (Erni et al., 2009). The excellent spatial resolution of EM is well suited to study fine detail in the structure and localization of NETs indistinguishable to conventional light microscopy. In fact, immunogold-label electron microscopy has been used to determine whether NETs localize on the ONM and INM (Paulin-Levasseur et al., 1996; Liu et al., 2003), that LAP1 localizes at the INM of isolated rat liver NE (Senior and Gerace 1988), and that most gp210 molecules are located inside the lumen of NEs in close vicinity to NPCs whereas relatively few were found at the cytoplasmic side of nuclear membranes in isolated rat liver NE (Greber, Senior and Gerace, 1990). However useful, EM suffers, similarly to immunofluorescence microscopy, the disadvantage of sample preparation via chemical fixation or freezing, which eliminates EM from use in researching the real-time dynamics in live cells.

2.3.6. DNA sequencing and protein structure deduction

In early studies of NET proteins (Hallberg, Wozniak and Blobel, 1993; Ye and Worman, 1994; Ye and Worman, 1996; Lin et al., 2000), the combination of sequencing and amino acid deduction was widely used to study primary structure and predict the potential function of NETs. For example, Worman and colleagues reported the cDNA sequence of LBR and deduced its primary structure and potential functions (Worman, Evans and Blobel, 1990). Specifically, the authors

first extracted NE from turkey erythrocytes (which contain few other intracellular membranes) with 1 M NaCl and 8 M urea; LBR was recognized by SDS-PAGE and anti-LBR.

Partial sequences of LBR were determined by gas-phase microsequencing. Based on these sequences, primers were synthesized for generating a probe via PCR. The probe enabled the authors to obtain the cDNA sequence of LBR, by which the amino acid sequence of LBR was deduced. By hydropathy analysis of the deduced primary structure of LBR (Kyte and Doolittle, 1982), the authors found that LBR has eight segments of hydrophobic amino acids that could function as transmembrane domains. Also, the amino-terminal region of LBR contains two consensus sites for phosphorylation by protein kinase A and three DNA-binding motifs that are found in gene regulatory proteins and histone. Such structural features of LBR suggests that LBR locates at the INM and that its amino-terminal region faces the nucleoplasm; in light of these features, it appears that LBR functions in gene regulation and chromatin organization. Whilst this sort of structure deduction provides rough information about potential functions of NETs, more detailed information requires exploration of other methods.

2.3.7. Coimmunoprecipitation

The mechanism of coimmunoprecipitation (Co-IP) consists of selecting an antibody against a known protein that is believed to interact with or bind other proteins in a larger complex; by targeting this known protein with an antibody, Co-IP can be used to pull the entire protein complex out of solution and thereby identify interaction partners of the known protein. It is because of this feature that Co-IP is a commonly used biochemical technique for detecting interaction or association between the proteins. It is with Co-IP that Goodchild and Dauer identified and characterized the interaction between NETs; the authors found that torsinA coimmunoprecipitates with LAP1 and proteins with lumenal domains such as LAP1 (LULL1) by anti-myc immunoprecipitations from lysates of BHK cells transfected with myc-LAP1 and lysates of myc-LULL1–transfected BHK cells, respectively (Goodchild and Dauer, 2005). Together, these results suggest that torsinA interacts with LAP1 and LULL1.

Although useful, Co-IP is not perfect, and has several disadvantages (Fields and Song, 1994; Adams, Seeholzer and Ohh, 2002; Borroto-Escuela et al. 2019; Hallberg, Wozniak and Blobel, 1993). Co-IP is not suitable to identify protein interactions of short time duration; also, Co-IP identifies proteins interacting within a complex but cannot distinguish whether members of a complex interact directly or indirectly (i.e. through a third member of the complex). Moreover, the

main disadvantage of Co-IP is the time and cost associated with preparation of the specific antibody, as it is often difficult to obtain a high-specificity antibody (Berggård, Linse and James, 2007; Miernyk and Thelen 2008). A widely remedial method is based on Co-IP of proteins from cells transiently expressing a tagged bait protein (Miernyk and Thelen, 2008); the commercially available antibodies against the tags are relatively specific and do not cross-react with the endogenous proteins (Berggård, Linse and James, 2007).

2.3.8. RNA interference

RNA Interference (RNAi) is a technique employed to study the physiological function of a protein by decreasing protein level (Kupferschmidt, 2013). RNA is synthesized with a sequence complementary to the gene being studied, and when introduced into the cell it serves to activate the RNAi pathway to knock down expression of the gene (Saurabh, Vidyarthi and Prasad, 2014; Weiss, Davidkova and Zhou, 1999). This classic function-analysis method can also be used to study NET function. With RNAi-mediated knockdown of MAN1 and emerin in *Caenorhabditis elegans*, Liu and colleagues showed that MAN1 and emerin have overlapping functions essential for chromosome segregation and cell division (Liu et al., 2003). Quantitative analysis showed an approximately 90% decrease in MAN1 and complete loss of emerin protein in RNAi-mediated knockdown embryos. The authors conducted simultaneous and separate knockdowns of MAN1 and emerin, causing 100% embryonic lethality in simultaneous knockdowns attributable to striking defects in chromosome segregation, whereas separate knockdown caused a mere 15% embryonic lethality. Liu and colleagues concluded that MAN1 and emerin perform at least one overlapping essential function in chromosome segregation of *C. elegans*. As a technique, RNAi also has several disadvantages, however, such as the incompleteness and potential nonspecificity of knockdowns (Boutros and Ahringer, 2008).

2.3.9. Proteomics

Proteomics is the large-scale experimental analysis of proteomes and often refers specifically to protein purification and mass spectrometry (Anderson and Anderson, 1998; Blackstock and Weir, 1999). This technique is widely used to identify NETs and reveal compositional complexity of NETs on the NE; however, this usefulness is confounded to some degree by the fact that the ONM and the ER are contiguous and have similar function (Schirmer and Gerace, 2005), and some

proteins localize to both the ONM and the ER. Dreger and colleagues and Shirmer and colleagues demonstrate two different proteomics strategies to identify NE-specific transmembrane proteins (Dreger et al., 2001; Schirmer et al., 2003; Schirmer and Gerace, 2005).

Dreger and colleagues used a comparative approach, hypothesizing that novel NE proteins would have the same biochemical extraction characteristics as the known transmembrane proteins of the lamina, whereas Schirmer and colleagues employed a subtractive proteomic analysis of rat liver nuclei to exclude peripheral ER proteins that were also present in the NE fraction. The comparative approach allowed them to identify the new NETs by comparing the NE proteins from two extractions, specifically transmembrane proteins and lamina-associated proteins. The protein would be identified as a NET if it identified in both extractions. However, this approach omitted NE proteins that are not associated with lamina. Furthermore, this approach recognized most previously characterized INM NETs. As for subtractive proteomic analysis, newly discovered NETs were identified by comparing transmembrane proteins from the peripheral ER and NE fractionations. Proteins found in the NE fraction but not the ER fraction were determined to be NETs. Compared with the comparative approach, the subtractive analysis exhibited more success identifying uncharacterized NETs without making use of prior 2D gel separation required in the comparative approach. Subtractive proteomics is therefore able to provide information on transmembrane proteins that poorly resolve on 2D gels (Santoni, Molloy and Rabilloud, 2000). Nevertheless, subtractive proteomics neglects proteins present and functional in both the ER and the NE. For example, torsinA, an ER protein present in both the ER and NE, and can interact with LAP1 and LULL1 (Goodchild and Dauer, 2005).

2.4. SINGLE MOLECULE IMAGING TECHNIQUES

2.4.1. Highly Inclined and Laminated Optical sheet microscopy

The reliable detection of single-molecule events requires the highest signal to noise ratio (SNR) possible. In the single-molecule environment, the signal represents the target fluorophore's image intensity and the noise originates in the background; these two factors can be controlled to some extent by optimizing the labeling strategy and the imaging setup, respectively. Here we review the approach of Serebryannyy and colleagues, who use the approach of using Highly Inclined and Laminated Optical sheet (HILO) microscopy with HaloTag-fused

lamins and NETs in the presence of Janelia Flour (JF) dyes (Serebryannyy et al., 2019) (Figure 5).

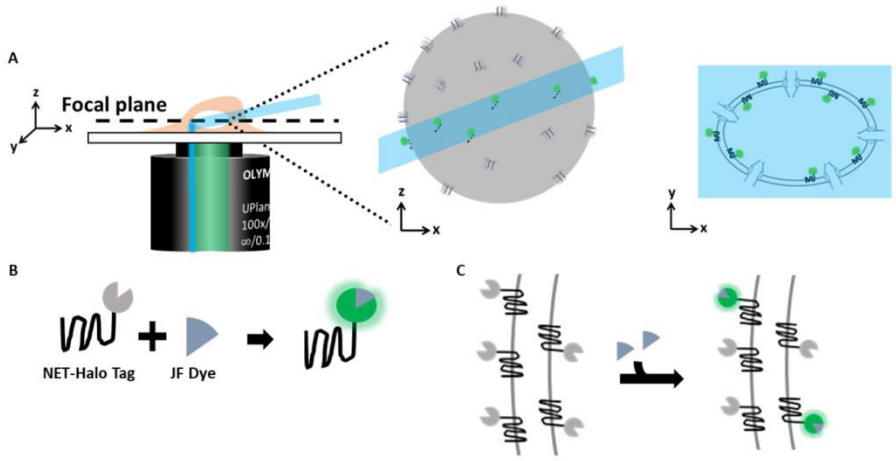

Figure 5. HILO technique for interrogating NETs diffusion constant across nuclear membranes. (**A**) High angle illumination pattern in blue with emitting fluorescent probes in green. (**B**) Terminally attached HaloTag to a NET with a bounded JF dye will emit when excited. (**C**) Addition of small amounts of JF dye to the NET-HaloTag.

Not to be confused with the HiLo microscopy technique (which fuses high- and low-resolution images and is similar to structural illumination microscopy (SIM) (Lim, Chu and Mertz, 2008), HILO was developed initially by Tokunaga and colleagues as a new method for detecting single-molecules (Tokunaga et al., 2008). HILO microscopy employs a sub-critical high-angle incident beam that excites a narrow slice through the target sample, allowing for the entire sample's emittance to be collected (Figure 5A high-angle illumination pattern in blue with emitting fluorescent probes in green). Compared with the no-angle (0^0) epifluorescence laser path, the narrow slice will significantly reduce the amount of noise from emitting background molecules, thus improving the SNR.

To illuminate intracellular molecules such as NETs, the position of the incident beam is positioned slightly away from the outermost edge of the objective, giving an illumination field depth of approximately 10 µm (Konopka and Bednarek, 2008). The beam position is significant for the HILO setup, because increasing the distance of the incident from the central position to a super-critical angle would induce an evanescent wave. This induced evanescent wave would illuminate only cell surface molecules of a depth of approximately

200 nm and is the primary feature of total internal reflection (TIRF) microscopy (Axelrod, 1981), a technique upon which HILO microscopy was built.

In addition to reducing the illumination area of the incident beam, SNR can be improved by controlling the amount of ligand present as well as creating either a spatial or temporal separation between emitting molecules; Serebryannyy and colleagues chose a ligand (JF dye) and receptor (HaloTag) labeling system, in which the authors control the concentration of ligand (Figure 5B terminally attached HaloTag to a NET with a bounded JF dye will emit when excited; [C] addition of small amounts of JF dye to the NET-HaloTag).

JF dye was designed by Grimm and colleagues, who focused on two challenges facing those conducting single-molecule studies in live-cells: photostability and membrane permeability (Grimm et al., 2015). Firstly, maintaining photostability requires a high ratio of photons absorbed to photons emitted (quantum yield); the more robust fluorophores will have a quantum yield close to 1.00. The higher the quantum yield, the more stable and resistant the target fluorophore is to photobleaching, allowing for longer trajectories over multiple frames. Secondly, to ensure high permeability of the dye, modifications to the original target molecule must be minimal and the entire construct be as small as possible. Both of these objectives were accomplished by replacing the *N,N*-dimethylamino substituents with four-membered azetidine rings to improve or maintain photostability while keeping the ligand small. As for the receptor, HaloTag, a modified haloalkane dehalogenase developed Los and colleagues, was used to covalently bind the synthetic ligands (Los et al., 2008). Because this is a protein tag, the HaloTag is transcribed and translated just like any other protein, making this receptor an excellent candidate when the experimenter can control the concentration of ligand (Figure 5C).

Since the release of JF dyes in 2015, this labeling system has been used for the bulk imaging of calcium channels in culture neuronal cells (Courtney et al., 2018), in single-molecule studies dealing with transcription factors in low-complexity sequence domains (Chong et al., 2018), and in the diffusion dynamics of lamins and NETs (Serebryannyy et al., 2019).

Using HILO microscopy and the JF dye–HaloTag labeling system, Serebryannyy and colleagues demonstrated how they were able to obtain 2D single-molecule localizations and calculate binding dynamics and dwell times of different types of lamins, lamin mutants, and NETs (Serbyannyy et al., 2019). To calculate the binding dynamics, the authors determined which molecules were either bound or unbound to the NE; for a molecule to be considered bound then it must maintain its position within 220 nm for 0.8 seconds (4 frames at 200 ms). Then the authors fit their data to a bi-exponential curve and found two binding

types, slow- or fast-binding molecules, and calculated the average dwell time for both event types.

Employing HILO microscopy with the JF dye-HaloTag labeling system, Serebryannyy and colleagues were able to obtain a whole slice of the NE to resolve lamin and NET dynamics. However, the limitations of this method include a slow camera speed and limited localization dimensions. Firstly, the slow camera speed may improve the resolution of events, but could cause underestimation of the speed of fast-bound molecules. Secondly, because only an x,y slice of the NE is taken, this method is limited to 2D localizations only; therefore z-dimensional diffusion, which can cause a molecule to leave, and subsequently return to, the focal plane, can cause the miscalculation of diffusion time.

2.4.2. Single-molecule Fluorescence Recovery After Photobleaching

A technique that lends itself well to the study of NETs is single-molecule fluorescence recovery after photobleaching (smFRAP). Whilst the HILO technique offers an excellent method to image a whole slice of the NE, the smFRAP technique can be used when observation of a smaller section is needed, with a 1-μm illumination area in the focal plane of the microscope. FRAP was, in part, developed for the study of the diffusion of proteins along the cell membrane (Axelrod et al., 1976), and has since been applied, sometimes in combination with other techniques, to study various membrane processes (Ellenberg et al., 1997; Coscoy et al., 2002; Sprague et al., 2004; Sprague and McNally, 2005; Zuleger et al., 2011; Fritzsche and Charras, 2015). In particular, combining FRAP with a single-molecule approach is useful to determine spatial locations of NETs along the INM and ONM to a resolution of 10 nm (Mudumbi, Schirmer and Yang, 2016), and is suited specifically to the live-cell environment.

Mudumbi and colleagues have used smFRAP to measure the diffusion coefficients and immobilized fractions of various NETS in live cells and determined the *in vivo* translocation rates and relative concentrations of various NETs along the ONM and INM (Mudumbi, Schirmer and Yang, 2016). The capability to calculate the diffusion rate of NETs through the NPC and the ability to determine the fixed and mobile fractions of NETs in the physiologic environment are important advancements in the study of NETs and related proteins.

Simply explained, smFRAP is the photobleaching of a small illumination volume of fluorescently tagged target proteins and measuring the return of mobile single molecules to the photobleached volume. Accurate and precise detection of the recovery of fluorescently tagged molecules to the area of interest is crucial to

the utility of the technique. The smFRAP technique is conducted with a small illumination volume (point spread function) near the diffraction limit in size; this point spread function is generated via a microscope objective of high numerical aperture. The illumination volume is trained upon the very edge of the nucleus at the focal plane of its greatest width (its equator). In this manner, use of smFRAP reduces the amount of background noise from (other) excited probes (Figure 6A; illumination pattern in blue with emitting fluorescent probes in green). The target proteins are photobleached in that area (Figure 6B), and their return is detected, molecule by molecule, at high temporal resolution (high frame rate) as new, unphotobleached molecules enter the area from the region outside that which is photobleached. The detected locations of tagged target proteins are compiled and used to form two-dimensional (Figure 6C) super-resolution images as described elsewhere (Figure 5C; compiled image of spatially and temporally separated NET molecules) (Ma and Yang, 2010; Goryaynov, Ma and Yang, 2012; Ma et al., 2013; Yang, 2013; Schnell, Ma and Yang, 2014; Li et al., 2019).

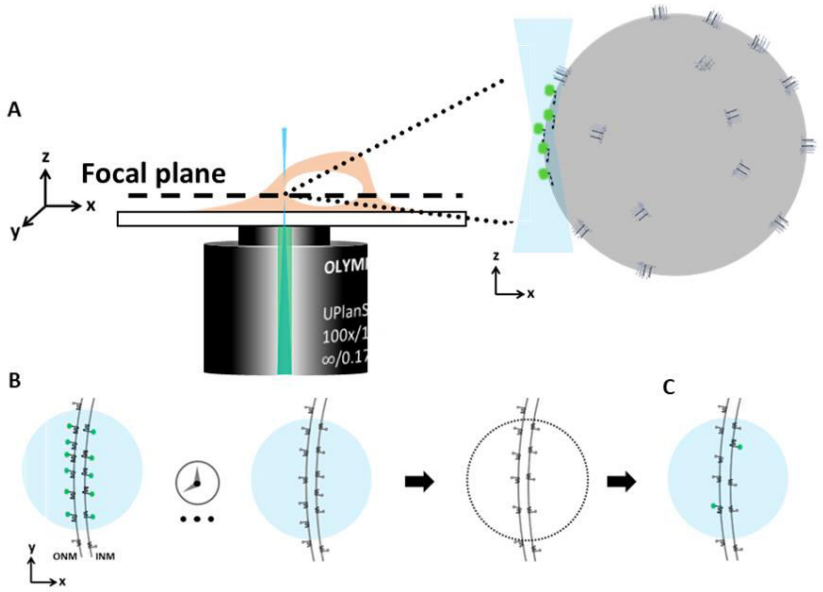

Figure 6. FRAP photobleaching techniques for resolving single-molecule locations. (**A**) Illumination pattern in blue with emitting fluorescent probes in green focused on the NE. (**B**) Photobleaching of fluorescent probe bound to NETs. (**C**) Imaging of spatially and temporally separated NET molecules.

2.4.3. Single-Point Edge-Excitation sub-Diffraction microscopy

Even more specialized than smFRAP is Single-Point Edge-Excitation Sub-Diffraction (SPEED) microscopy, a technique well described elsewhere (Ma and Yang, 2010; Goryaynov, Ma and Yang, 2012; Ma and Yang, 2013; Yang, 2013; Schnell, Ma and Yang, 2014; Li et al., 2019). Whilst with HILO, one can concentrate on a single slice of the NE, and with smFRAP can interrogate a small area of the membrane, SPEED microscopy can be used to limit investigation to just a single NPC itself with very high spatial and temporal resolution (Ma and Yang, 2010; Ma and Yang, 2013; Schnell, Ma and Yang, 2014; Yang, 2013; Goryaynov, Ma and Yang 2012; Li et al., 2019). Similar to smFRAP, positioning the single-point illumination of the laser at the edge of the equator of the NE serves to exclude illumination of NPCs other than the single NPC of interest (as the illumination area is smaller than the average distance between the nearest neighboring NPCs in many cells; see Figure 7A (illumination pattern in blue with emitting fluorescent probes in green) and Figure 7B (single NPC illumination area and emitting probes), but differs from smFRAP in taking advantage of the rotational symmetry of the NPC to glean information in three dimensions that cannot be obtained via smFRAP or HILO. Features of SPEED that allow for precise localization information are: the use of a small pixel area of a CCD camera (rather than a photomultiplier tube), which provides for a very fast detection speed, as fast as 0.2 ms per frame; a large number of photons generated, attributable to the high optical density of the illumination area; the aforementioned exclusion of fluorescence for NPCs other than the target NPC, resulting in a high SNR.

Some of the information that can be obtained with SPEED include the transport route (peripheral or central) of NETs as well as their transport direction, rate, and efficiency (rate of successful vs unsuccessful translocation through the NPC). Furthermore, varying the placement of the fluorophore (i.e. N- or C-terminus) on the target NET can provide information about whether the transport route of the protein lies in the peripheral channel only or whether the protein utilizes both the peripheral and central channel (i.e. if there is a disordered linker between domains of the protein). Moreover, the camera can be split to track two color channels (dual-channel SPEED), enabling the tracking of two fluorophores simultaneously, providing information about the relationship between molecules in the environment of the nuclear pore.

Obtained location information is compiled to make super-resolution 2D images as described above for smFRAP (Figure 7C, [simulated 2D localizations plotted with gray dotted lines to represent the NE]); however, the rotational

symmetry of the NPC can be leveraged with a transformation algorithm (Li et al., 2019) to reconstruct a 3D image with sub-diffraction level of detail (Figure 7D (Simulated 3D density map, with radial dimension, R, rotated by θ in the axial dimension, x) (Ma and Yang, 2010; Goryaynov, Ma and Yang, 2012; Ma and Yang, 2013; Yang, 2013; Schnell, Ma and Yang, 2014; Li et al., 2019).

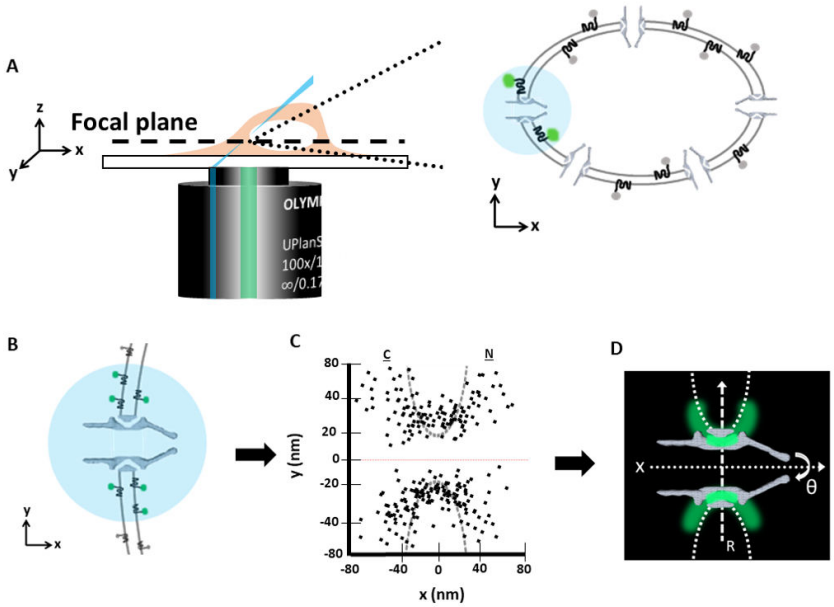

Figure 7. SPEED microscopy for interrogating pore dynamics and functions. (**A**) Illumination pattern in blue with emitting fluorescent probes in green focused on a single NPC from the perspective of the whole nucleus. (**B**) The single NPC illumination area and emitting probes. (**C**) Simulated 2D localizations plotted with gray dotted lines to represent the NE. (**D**) Simulated 3D density map, with radial dimension, *R*, rotated by θ in the axial dimension, *x*.

2.5. CONCLUSION

The obvious question pertaining to the transport models of NETs is: Which is correct? It has been proposed that these models are each correct under certain circumstances (Dixon and Schirmer, 2018). It is unclear at this time if any one model is more dominant than the others; however, some of this uncertainty can be resolved through the application of single-molecule microscopy techniques.

These techniques provide valuable tools to measure *in vivo* transport of NETs through the NPC, enabling researchers to accurately visualize the transport route of a molecule through both the central channel and the peripheral channel. For instance, in the case of the Nuclear Localization Signal–mediated model, SPEED microscopy in particular can provide the opportunity to tag each terminus with a different fluorophore and resolve the differing paths of the two termini.

In addition to confirmation of transport routes, the single-molecule techniques highlighted here provide researchers with the ability to derive dynamic transport kinetics from live cells. As has been shown here, relative concentrations of NETs on the ONM and INM can be derived using immunogold SEM. However, this does not provide *in vivo* information. Single-molecule FRAP enables researchers to determine concentrations in a live cell as well as calculate the transport rate of NETs of interest in the cell. This information provides novel insight into the behavior of molecules and will pave the way to a better understanding of transmembrane protein transport across the NE.

REFERENCES

Adams PD, Seeholzer S, Ohh M. Identification of associated proteins by coimmunoprecipitation. *Protein–protein interactions: A molecular cloning manual*. 2002:5.59–5.74.

Amar-Costesec A, Beaufay H, Wibo M, Thinès-Sempoux D, Feytmans E, Robbi M, Berthet J. Analytical study of microsomes and isolated subcellular membranes from rat liver. II. Preparation and composition of the microsomal fraction. *J Cell Biol*. 1974;61(1):201–212.

Anderson NL, Anderson NG. Proteome and proteomics: New technologies, new concepts, and new words. *Electrophoresis.* 1998;19(11):1853–1861.

Arib G, Akhtar A. Multiple facets of nuclear periphery in gene expression control. *Curr Opin Cell Biol.* 2011;23(3):346–353.

Axelrod D. Cell-substrate contacts illuminated by total internal reflection fluorescence. *J Cell Biol.* 1981;89(1):141–145.

Axelrod D, Koppel DE, Schlessinger J, Elson E, Webb WW. Mobility measurement by analysis of fluorescence photobleaching recovery kinetics. *Biophys J*. 1976;16(9):1055–1069.

Barton LJ, Soshnev AA, Geyer PK. Networking in the nucleus: A spotlight on LEM-domain proteins. *Curr Opin Cell Biol*. 2015;34:1–8.

Batrakou DG, Kerr AR, Schirmer EC. Comparative proteomic analyses of the nuclear envelope and pore complex suggests a wide range of heretofore unexpected functions. *J Proteomics*. 2009;72(1):56–70.

Beck M, Förster F, Ecke M, Plitzko JM, Melchior F, Gerisch G, Baumeister W, Medalia O. Nuclear pore complex structure and dynamics revealed by cryoelectron tomography. *Science*. 2004;306(5700):1387–1390.

Berggård T, Linse S, James P. Methods for the detection and analysis of protein-protein interactions. *Proteomics*. 2007;7(16):2833–2842.

Blackstock WP, Weir MP. Proteomics: Quantitative and physical mapping of cellular proteins. *Trends Biotechnol*. 1999;17(3):121–127.

Boni A, Politi AZ, Strnad P, Xiang W, Hossain MJ, Ellenberg J. Live imaging and modeling of inner nuclear membrane targeting reveals its molecular requirements in mammalian cells. *J Cell Biol*. 2015;209(5):705–720.

Borroto-Escuela DY, Hernández-Ramos I, Fuxe K, Borroto-Escuela DO. *Coimmunoprecipitation (Co-Ip) Analysis for Protein-Protein Interactions in the Neurons of the Cerebral Ganglia of the Land Snails of the Genus Polymita During Aestivation*. In Co-Immunoprecipitation Methods for Brain Tissue, Springer, 2019, pp147–56.

Bouchet-Marquis C, Dubochet J, Fakan S. Cryoelectron microscopy of vitrified sections: A new challenge for the analysis of functional nuclear architecture. *Histochem Cell Biol*. 2006;125(1-2):43–51.

Boutros M, Ahringer J. The art and design of genetic screens: RNA interference. *Nat Rev Genet*. 2008;9(7):554–566.

Brachner A, Reipert S, Foisner R, Gotzmann J. LEM2 is a novel MAN1-related inner nuclear membrane protein associated with A-type lamins. *J Cell Sci*. 2005;118(Pt 24):5797–5810.

Braunagel SC, Williamson ST, Saksena S, Zhong Z, Russell WK, Russell DH, Summers MD. Trafficking of ODV-E66 is mediated via a sorting motif and other viral proteins: facilitated trafficking to the inner nuclear membrane. *Proc Natl Acad Sci U S A*. 2004;101(22):8372–8377.

Cain NE, Jahed Z, Schoenhofen A, Valdez VA, Elkin B, Hao H, Harris NJ, et al. Conserved SUN-KASH interfaces mediate LINC complex-dependent nuclear movement and positioning. *Curr Biol*. 2018;28(19):3086–3097.

Cheng, P-C. *The Contrast Formation in Optical Microscopy*." In Handbook of Biological Confocal Microscopy, Springer, 2006, pp162–206.

Chi YH, Chen ZJ, Jeang KT. The nuclear envelopathies and human diseases. *J Biomed Sci*. 2009;16:96.

Chong S, Dugast-Darzacq C, Liu Z, Dong P, Dailey GM, Cattoglio C, Heckert A, et al. Imaging dynamic and selective low-complexity domain interactions that control gene transcription. *Science*. 2018;361(6400). pii: eaar2555.

Coscoy S, Waharte F, Gautreau A, Martin M, Louvard D, Mangeat P, Arpin M, Amblard F. Molecular analysis of microscopic ezrin dynamics by two-photon FRAP. *Proc Natl Acad Sci U S A*. 2002;99(20):12813–12818.

Courtney NA, Briguglio JS, Bradberry MM, Greer C, Chapman ER. Excitatory and inhibitory neurons utilize different Ca^{2+} sensors and sources to regulate spontaneous release. *Neuron*. 2018;98(5):977–991.e5.

Crisp M, Liu Q, Roux K, Rattner JB, Shanahan C, Burke B, Stahl PD, Hodzic D. Coupling of the nucleus and cytoplasm: role of the LINC complex. *J Cell Biol*. 2006;172(1):41–53.

de Las Heras JI, Meinke P, Batrakou DG, Srsen V, Zuleger N, Kerr AR, Schirmer EC. Tissue specificity in the nuclear envelope supports its functional complexity. *Nucleus*. 2013;4(6):460–477.

Dixon, CR, Schirmer EC. *Navigating the Nuclear Envelope: One or Multiple Transport Mechanisms for Integral Membrane Proteins?*. In Nuclear-Cytoplasmic Transport, Springer, 2018, pp151–177.

Dreger M, Bengtsson L, Schöneberg T, Otto H, Hucho F. Nuclear envelope proteomics: novel integral membrane proteins of the inner nuclear membrane. *Proc Natl Acad Sci U S A*. 2001;98(21):11943–11948.

Ellenberg J, Siggia ED, Moreira JE, Smith CL, Presley JF, Worman HJ, Lippincott-Schwartz J. Nuclear membrane dynamics and reassembly in living cells: Targeting of an inner nuclear membrane protein in interphase and mitosis. *J Cell Biol*. 1997;138(6):1193–1206.

Erni R, Rossell MD, Kisielowski C, Dahmen U. Atomic-resolution imaging with a sub-50-pm electron probe. *Phys Rev Lett*. 2009;102(9):096101.

Feldherr CM, Akin D. The permeability of the nuclear envelope in dividing and nondividing cell cultures. *J Cell Biol*. 1990;111(1):1–8.

Fields S, Song O-K. *System to Detect Protein-Protein Interactions*. Google Patents, 1994.

Foisner R, Gerace L. Integral membrane proteins of the nuclear envelope interact with lamins and chromosomes, and binding is modulated by mitotic phosphorylation. *Cell*. 1993;73(7):1267–1279.

Franke WW, Scheer U, Krohne G, Jarasch ED. The nuclear envelope and the architecture of the nuclear periphery. *J Cell Biol*. 1981;91(3 Pt 2):39s–50s.

Frey S, Richter RP, Görlich D. FG-rich repeats of nuclear pore proteins form a three-dimensional meshwork with hydrogel-like properties. *Science*. 2006;314(5800):815–817.

Fried H, Kutay U. Nucleocytoplasmic transport: taking an inventory. *Cell Mol Life Sci*. 2003;60(8):1659–1688.

Fritzsche M, Charras G. Dissecting protein reaction dynamics in living cells by fluorescence recovery after photobleaching. *Nat Protoc*. 2015;10(5):660–680.

Furukawa K, Fritze CE, Gerace L. The major nuclear envelope targeting domain of LAP2 coincides with its lamin binding region but is distinct from its chromatin interaction domain. *J Biol Chem*. 1998;273(7):4213–4219.

Gerace L, Burke B. Functional organization of the nuclear envelope. *Annu Rev Cell Biol*. 1988;4:335–374.

Gilchrist D, Rexach M. Molecular basis for the rapid dissociation of nuclear localization signals from karyopherin alpha in the nucleoplasm. *J Biol Chem*. 2003;278(51):51937–51949.

Goodchild RE, Dauer WT. The AAA+ protein torsinA interacts with a conserved domain present in LAP1 and a novel ER protein. *J Cell Biol*. 2005;168(6):855–862.

Goryaynov A, Ma J, Yang W. Single-molecule studies of nucleocytoplasmic transport: from one dimension to three dimensions. *Integr Biol (Camb)*. 2012;4(1):10–21.

Greber UF, Senior A, Gerace L. A major glycoprotein of the nuclear pore complex is a membrane-spanning polypeptide with a large lumenal domain and a small cytoplasmic tail. *EMBO J*. 1990;9(5):1495–1502.

Grimm JB, English BP, Chen J, Slaughter JP, Zhang Z, Revyakin A, Patel R, et al. A general method to improve fluorophores for live-cell and single-molecule microscopy. *Nat Methods*. 2015;12(3):244–250.

Gruenbaum Y, Margalit A, Goldman RD, Shumaker DK, Wilson KL. The nuclear lamina comes of age. *Nat Rev Mol Cell Biol*. 2005;6(1):21–31.

Hallberg E, Wozniak RW, Blobel G. An integral membrane protein of the pore membrane domain of the nuclear envelope contains a nucleoporin-like region. *J Cell Biol*. 1993;122(3):513–521.

Haraguchi T, Kojidani T, Koujin T, Shimi T, Osakada H, Mori C, Yamamoto A, Hiraoka Y. Live cell imaging and electron microscopy reveal dynamic processes of BAF-directed nuclear envelope assembly. *J Cell Sci*. 2008;121(Pt 15):2540–2554.

Haraguchi T, Koujin T, Segura-Totten M, Lee KK, Matsuoka Y, Yoneda Y, Wilson KL, Hiraoka Y. BAF is required for emerin assembly into the reforming nuclear envelope. *J Cell Sci*. 2001;114(Pt 24):4575–4585.

Helms V. *Fluorescence Resonance Energy Transfer*. In Principles of Computational Cell Biology. Weinheim: Wiley-VCH. 2008, p202.

Helms V. *Principles of Computational Cell Biology: From Protein Complexes to Cellular Networks*. John Wiley & Sons, 2018.

Hetzer MW, Wente SR. Border control at the nucleus: Biogenesis and organization of the nuclear membrane and pore complexes. *Dev Cell*. 2009;17(5):606–616.

Hinshaw JE, Carragher BO, Milligan RA. Architecture and design of the nuclear pore complex. *Cell*. 1992;69(7):1133–1141.

Hodzic DM, Yeater DB, Bengtsson L, Otto H, Stahl PD. Sun2 is a novel mammalian inner nuclear membrane protein. J Biol Chem. 2004;279(24):25805–25812.

Katta SS, Smoyer CJ, Jaspersen SL. Destination: inner nuclear membrane. *Trends Cell Biol*. 2014;24(4):221–229.

Konopka CA, Bednarek SY. Variable-angle epifluorescence microscopy: a new way to look at protein dynamics in the plant cell cortex. *Plant J*. 2008;53(1):186–196.

Kosinski J, Mosalaganti S, von Appen A, Teimer R, DiGuilio AL, Wan W, Bui KH, et al. Molecular architecture of the inner ring scaffold of the human nuclear pore complex. *Science*. 2016;352(6283):363–365.

Kupferschmidt K. A Lethal Dose of RNA. *Science*. 2013;341(6147) :732–733.

Kyte J, Doolittle RF. A simple method for displaying the hydropathic character of a protein. *J Mol Biol*. 1982;157(1):105–132.

Laba JK, Steen A, Veenhoff LM. Traffic to the inner membrane of the nuclear envelope. *Curr Opin Cell Biol*. 2014;28:36–45.

Leavesley SJ, Rich TC. Overcoming limitations of FRET measurements. *Cytometry A*. 2016;89(4):325–327.

Lee KK, Haraguchi T, Lee RS, Koujin T, Hiraoka Y, Wilson KL. Distinct functional domains in emerin bind lamin A and DNA-bridging protein BAF. *J Cell Sci*. 2001;114(Pt 24):4567–4573.

Li Y, Junod SL, Ruba A, Kelich JM, Yang W. Nuclear export of mRNA molecules studied by SPEED microscopy. *Methods*. 2019;153:46–62.

Lim D, Chu KK, Mertz J. Wide-field fluorescence sectioning with hybrid speckle and uniform-illumination microscopy. *Opt Lett*. 2008;33(16):1819–1821.

Lim RY, Fahrenkrog B, Köser J, Schwarz-Herion K, Deng J, Aebi U. Nanomechanical basis of selective gating by the nuclear pore complex. *Science*. 2007;318(5850):640–643.

Lin F, Blake DL, Callebaut I, Skerjanc IS, Holmer L, McBurney MW, Paulin-Levasseur M, Worman HJ. MAN1, an inner nuclear membrane protein that shares the LEM domain with lamina-associated polypeptide 2 and emerin. *J Biol Chem*. 2000;275(7):4840–4847.

Liu J, Lee KK, Segura-Totten M, Neufeld E, Wilson KL, Gruenbaum Y. MAN1 and emerin have overlapping function(s) essential for chromosome segregation and cell division in *Caenorhabditis elegans*. *Proc Natl Acad Sci U S A*. 2003;100(8):4598–4603.

Liu D, Wu X, Summers MD, Lee A, Ryan KJ, Braunagel SC. Truncated isoforms of Kap60 facilitate trafficking of Heh2 to the nuclear envelope. *Traffic*. 2010;11(12):1506–1518.

Los GV, Encell LP, McDougall MG, Hartzell DD, Karassina N, Zimprich C, Wood MG, et al. HaloTag: a novel protein labeling technology for cell imaging and protein analysis. *ACS Chem Biol*. 2008;3(6):373–382.

Lusk CP, Blobel G, King MC. Highway to the inner nuclear membrane: rules for the road. *Nat Rev Mol Cell Biol*. 2007;8(5):414–420.

Ma J, Liu Z, Michelotti N, Pitchiaya S, Veerapaneni R, Androsavich JR, Walter NG, Yang W. High-resolution three-dimensional mapping of mRNA export through the nuclear pore. *Nat Commun*. 2013;4:2414.

Ma J, Yang W. Three-dimensional distribution of transient interactions in the nuclear pore complex obtained from single-molecule snapshots. *Proc Natl Acad Sci U S A*. 2010;107(16):7305–7310.

Maimon T, Elad N, Dahan I, Medalia O. The human nuclear pore complex as revealed by cryo-electron tomography. *Structure*. 2012;20(6):998–1006.

Malik P, Zuleger N, Schirmer EC. *Transport of Inner Nuclear Membrane Proteins*. In Nuclear Transport, Landes Bioscience, 2009, pp133–145.

Malone CJ, Fixsen WD, Horvitz HR, Han M. UNC-84 localizes to the nuclear envelope and is required for nuclear migration and anchoring during *C. elegans* development. *Development*. 1999;126(14):3171–3181.

Manilal S, Man NT, Sewry CA, Morris GE. The Emery-Dreifuss muscular dystrophy protein, emerin, is a nuclear membrane protein. *Hum Mol Gen*. 1996;5(6) :801–808.

Mans BJ, Anantharaman V, Aravind L, Koonin EV. Comparative genomics, evolution and origins of the nuclear envelope and nuclear pore complex. *Cell Cycle*. 2004;3(12):1612–1637.

Matsuura Y, Stewart M. Nup50/Npap60 function in nuclear protein import complex disassembly and importin recycling. *EMBO J*. 2005;24(21):3681–3689.

Meinema AC, Laba JK, Hapsari RA, Otten R, Mulder FA, Kralt A, van den Bogaart G, et al. Long unfolded linkers facilitate membrane protein import through the nuclear pore complex. *Science*. 2011;333(6038):90–93.

Miernyk JA, Thelen JJ. Biochemical approaches for discovering protein-protein interactions. *Plant J*. 2008;53(4):597–609.

Mudumbi KC, Schirmer EC, Yang W. Single-point single-molecule FRAP distinguishes inner and outer nuclear membrane protein distribution. *Nat Commun*. 2016;7:12562.

Östlund C, Folker ES, Choi JC, Gomes ER, Gundersen GG, Worman HJ. Dynamics and molecular interactions of linker of nucleoskeleton and cytoskeleton (LINC) complex proteins. *J Cell Sci*. 2009;122(Pt 22):4099–4108.

Park E, Rapoport TA. Mechanisms of Sec61/SecY-mediated protein translocation across membranes. *Annu Rev Biophys*. 2012;41:21–40.

Paulin-Levasseur M, Blake DL, Julien M, Rouleau L. The MAN antigens are non-lamin constituents of the nuclear lamina in vertebrate cells. *Chromosoma*. 1996;104(5):367–379.

Powell L, Burke B. Internuclear exchange of an inner nuclear membrane protein (p55) in heterokaryons: *In vivo* evidence for the interaction of p55 with the nuclear lamina. *J Cell Biol*. 1990;111(6 Pt 1):2225–2234.

Rapoport TA, Goder V, Heinrich SU, Matlack KE. Membrane-protein integration and the role of the translocation channel. *Trends Cell Biol*. 2004;14(10):568–575.

Reichelt R, Holzenburg A, Buhle EL Jr, Jarnik M, Engel A, Aebi U. Correlation between structure and mass distribution of the nuclear pore complex and of distinct pore complex components. *J Cell Biol*. 1990;110(4):883–894.

Rexach MF. A sorting importin on Sec61. *Nat Struct Mol Biol*. 2006;13(6):476–478.

Rolls MM, Stein PA, Taylor SS, Ha E, McKeon F, Rapoport TA. A visual screen of a GFP-fusion library identifies a new type of nuclear envelope membrane protein. *J Cell Biol*. 1999;146(1):29–44.

Santoni V, Molloy M, Rabilloud T. Membrane proteins and proteomics: un amour impossible? *Electrophoresis*. 2000;21(6):1054–1070.

Saurabh S, Vidyarthi AS, Prasad D. RNA interference: concept to reality in crop improvement. *Planta*. 2014;239(3):543–564.

Schirmer EC, Gerace L. The nuclear membrane proteome: extending the envelope. *Trends Biochem Sci*. 2005;30(10):551–558.

Schnell SJ, Ma J, Yang W. Three-dimensional mapping of mRNA export through the nuclear pore complex. *Genes (Basel)*. 2014;5(4):1032–1049.

Senior A, Gerace L. Integral membrane proteins specific to the inner nuclear membrane and associated with the nuclear lamina. *J Cell Biol*. 1988;107(6 Pt 1):2029–2036.

Serebryannyy LA, Ball DA, Karpova TS, Misteli T. Single molecule analysis of lamin dynamics. *Methods*. 2019;157:56–65.

Shimi T, Koujin T, Segura-Totten M, Wilson KL, Haraguchi T, Hiraoka Y. Dynamic interaction between BAF and emerin revealed by FRAP, FLIP, and FRET analyses in living HeLa cells. *J Struct Biol*. 2004;147(1):31–41.

Soullam B, Worman HJ. The amino-terminal domain of the lamin B receptor is a nuclear envelope targeting signal. *J Cell Biol*. 1993;120(5):1093–1100.

Soullam B, Worman HJ. Signals and structural features involved in integral membrane protein targeting to the inner nuclear membrane. *J Cell Biol*. 1995;130(1):15–27.

Sprague BL, McNally JG. FRAP analysis of binding: proper and fitting. *Trends Cell Biol*. 2005;15(2):84–91.

Sprague BL, Pego RL, Stavreva DA, McNally JG. Analysis of binding reactions by fluorescence recovery after photobleaching. *Biophys J*. 2004;86(6):3473-3495.

Tapley EC, Ly N, Starr DA. Multiple mechanisms actively target the SUN protein UNC-84 to the inner nuclear membrane. *Mol Biol Cell*. 2011;22(10):1739–1752.

Tokunaga M, Imamoto N, Sakata-Sogawa K. Highly inclined thin illumination enables clear single-molecule imaging in cells. *Nat Methods*. 2008;5(2):159–161.

Turgay Y, Ungricht R, Rothballer A, Kiss A, Csucs G, Horvath P, Kutay U. A classical NLS and the SUN domain contribute to the targeting of SUN2 to the inner nuclear membrane. *EMBO J*. 2010;29(14):2262–2275.

Ungricht R, Kutay U. Establishment of NE asymmetry—targeting of membrane proteins to the inner nuclear membrane. *Curr Opin Cell Biol*. 2015;34:135–141.

von Appen A, Beck M. Structure determination of the nuclear pore complex with three-dimensional cryo electron microscopy. *J Mol Biol*. 2016;428(10 Pt A):2001–2010.

Wagner N, Krohne G. LEM-Domain proteins: New insights into lamin-interacting proteins. *Int Rev Cytol*. 2007;261:1–46.

Wang W, Shi Z, Jiao S, Chen C, Wang H, Liu G, Wang Q. Structural insights into SUN-KASH complexes across the nuclear envelope. *Cell Res*. 2012;22(10):1440–1452.

Washburn MP, Wolters D, Yates JR 3rd. Large-scale analysis of the yeast proteome by multidimensional protein identification technology. *Nat Biotechnol*. 2001;19(3):242–247.

Weiss B, Davidkova G, Zhou LW. Antisense RNA gene therapy for studying and modulating biological processes. *Cell Mol Life Sci*. 1999;55(3):334–358.

Worman HJ, Evans CD, Blobel G. The lamin B receptor of the nuclear envelope inner membrane: a polytopic protein with eight potential transmembrane domains. *J Cell Biol*. 1990;111(4):1535–1542.

Worman HJ, Yuan J, Blobel G, Georgatos SD. A lamin B receptor in the nuclear envelope. *Proc Natl Acad Sci U S A*. 1988;85(22):8531-8534.

Wu W, Lin F, Worman HJ. Intracellular trafficking of MAN1, an integral protein of the nuclear envelope inner membrane. *J Cell Sci*. 2002;115(Pt 7):1361–1371.

Yang W. Distinct, but not completely separate spatial transport routes in the nuclear pore complex. *Nucleus*. 2013;4(3):166–175.

Yang JW, Fu JX, Li J, Cheng XL, Li F, Dong JF, Liu ZL, Zhuang CX. A novel co-immunoprecipitation protocol based on protoplast transient gene expression for studying protein–protein interactions in rice. *Plant Mol Biol Rep*. 2014;32(1):153–161.

Ye Q, Worman HJ. Primary structure analysis and lamin B and DNA binding of human LBR, an integral protein of the nuclear envelope inner membrane. *J Biol Chem*. 1994;269(15):11306–11311.

Ye Q, Worman HJ. Interaction between an integral protein of the nuclear envelope inner membrane and human chromodomain proteins homologous to Drosophila HP1. *J Biol Chem*. 1996;271(25):14653–14656.

Zheng J. *Spectroscopy-Based Quantitative Fluorescence Resonance Energy Transfer Analysis*. In Ion Channels, Springer, 2006, pp65–77.

Zuleger N, Kelly DA, Richardson AC, Kerr AR, Goldberg MW, Goryachev AB, Schirmer EC. System analysis shows distinct mechanisms and common principles of nuclear envelope protein dynamics. *J Cell Biol*. 2011;193(1):109–123.

Zuleger N, Korfali N, Schirmer EC. Inner nuclear membrane protein transport is mediated by multiple mechanisms. *Biochem Soc Trans*. 2008;36(Pt 6):1373–1377.

Submitted: 10th Sept 2019, Revised: 28th Nov 2019, Accepted: 3rd Jan 2020

Chapter Three

3. SIMULATING MEMBRANE PROTEINS

Nilay K. Roy *

ITS-Research Computing, Northeastern University,
360 Huntington Avenue, Boston, MA 02115, USA

ABSTRACT

Membrane proteins may contain a significant portion of their mass within the interior of the membrane or are only associated to the membrane surface. The transmembrane (TM) part can be α-helical or have a β-sheet topology. The TM part can have a variety of sizes, molecular weights and conformations. Membrane proteins govern biological processes such as energy conversion, transport, signal recognition and transduction. Up to 30% of the encoded proteins in the genome of all organisms are such proteins, and they are 60% of all drug targets. Currently less than 1% of the protein structures deposited in the RCSB Protein Data Bank are membrane proteins. Simulating membrane proteins provides an alternative way to study them. Ion channels are a class of membrane proteins where passive transport is influenced by the membrane potentials. Many such ion channels have a selectivity filter and a gating mechanism embedded in the membrane core. Asymmetric ion concentrations across the membrane also affect transport and protein functions. These are difficult to study. Large scale molecular dynamics (MD) with coarse graining in both the membrane lipid bilayer and in parts of membrane protein itself is generally the method used in any simulation study to understand the mechanisms of such proteins' structure-function relationships and dynamic modes. Principal component analysis of the protein is also frequently used. This chapter gives an overview of the current simulation methods used to prepare and study membrane proteins. The focus is on large scale simulations with special emphasis on scalable parallel methods. Correctly relating molecular structures to the physiological properties of the protein is a major challenge in the field. All the effects of the inhomogeneous lipid bilayer, potentials, ion/anion concentrations, that cover both spatial and temporal scales must be included. This has challenges when systems have thousands of explicit atoms and require simulations on

* Current affiliation: The Charles Stark Draper Laboratory, Inc. (Draper), 555 Technology Square, Cambridge, MA 02139-3563. Tel:(617)258-1515. E-mail: nroy@draper.com.

the micro-second scale. We review these challenges and explain methods that have been used to overcome the shortcomings of explicit MD simulations.

Keywords: membrane proteins, transmembrane, genome, molecular dynamics, ion/cation concentrations, membrane potentials, force fields, semi-explicit methods, lipid, membrane curvature

3.1. INTRODUCTION

Molecular dynamics (MD) simulation is a molecular mechanics approach that is implemented using numerical methods that study the motion of a system of particles (atoms, molecules, entities) under the influence of internal and external forces (Chandler, 1987). These forces are interactions between the particles, which are influenced by other parameters such as temperature, pressure, and additional constraints (Lindahl, Hess and van der Spoel, 2001). Additional constraints include forces in steered or targeted MD. The empirical potential energy function that relates structure to energy and describes the forces between atoms using harmonic and periodic potentials to model covalent bond mediated interactions, as well as Coulomb and Lennard Jones-like potentials to represent electrostatic and van der Waals interactions, form the basis of MD force calcuations (MacKerell, 1998). These forces are called “force fields”. Typically calculated in a few femtosecond time steps they predict how each atom will move. Repeating the time step millions of times, a trajectory of all atoms in the system over time is generated that permits studying the dynamics of the (membrane) protein of interest and its microenvironment at a level of detail not accessible by laboratory experiments (Stansfeld and Sansom, 2011; Ingólfsson et al., 2016). By parallelizing the system using a large cluster of computers it is now possible to simulate a range of system sizes up to several million atoms even on a millisecond time scale (Allen et al., 2001; Rapaport, 2004; Klepeis et al., 2009). Several force fields have been developed like AMBER, CHARMM, and GROMOS (Patel et al., 2004; Case et al., 2005; Christen et al., 2005). Typically in MD simulations of very large explicit systems, it is well known that there are several problems. These include exponentially increasing equilibrium and non-equilibrium relaxation times, correlation times and lengths (Stanley, 1971). In very large systems there are problems like critical slowing down and other finite size effects that can take on special significance (Ceriotti, Bussi and Parrinello, 2010). Furthermore, with any simulation the full characterization must have reliable error estimates. This can only be obtained after several runs from a number of different initial starting

configurations. Figure 1 gives an example of time and length scales of different computational methods. In any MD system considerations must also include the ensemble to be used – for example NVE (micro-canonical), NPT or NVT (Leach, 1996). An important consideration here is if diffusion is needed. Then the density varies, and a grand-canonical enbsemble may be more favorable over the canonical NPT (Frenkel and Smit, 1996). NPT is generally also preferable if you want to equilibrate the system. NVT is then used to collect statistics of interest.

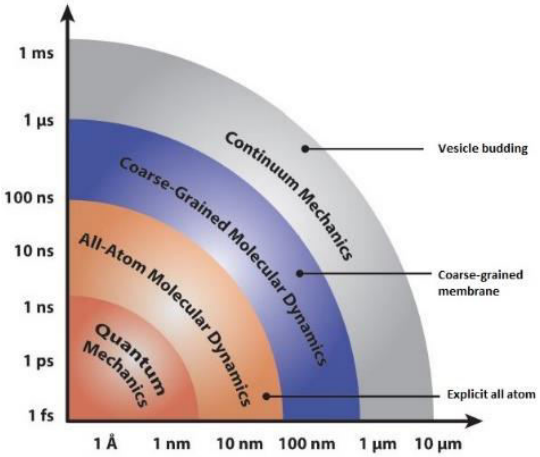

Figure 1. Computational methods over a range of length and time scales in membrane protein simulations.

Another important consideration is creating the starting structures and system of MD simulations. The membrane protein environment is characterized by two different chemical regions that have to be modelled correctly by the force field (Allen and Tildesley, 1987). This is done using implicit or explicit representations of the lipid and water phases. In general if the reported protein structure is used there are many defects. These include overlapping atoms, missing hydrogens, improper N and C terminus and so on. If modeled the total energy of the system would explode. The entire protein with the lipid membrane, water, and ion/counterions has to be systematically relaxed, overlapped and equilibrated. For water soluble proteins, generation of the initial system is completed by solvating the system with a water/ion solution (Marrink, Devries and Tieleman, 2009). However, membrane protein simulations require the additional working step of accommodating the protein in the bilayer. Here either the bilayer is constructed around the protein, or the protein is inserted into a pre-equilibrated bilayer. As shown in Figure 2 there are a number of tranmembrane protein toplogies.

Depending on the protein's shape, its cavity structure in the trans-membrane section, the number of membranes spanned by the protein and the membrane curvature (plane bilayer versus vesicles or micelles), individual challenges arise that have to be taken into account by both accommodation strategies (Van der Ploeg and Berendsen, 1983). Table 1 gives the times and sizes of some MD simulations of membranes (Stansfeld, Jefferys and Sansom, 2013; Chavent et al., 2015; Koldsø and Sansom, 2015; Reddy et al., 2015). These larger scale models also enable studies of the collective behaviour of multiple copies of membrane proteins, such as the influence of crowding of membrane proteins on their clustering and diffusion (Janosi et al., 2012; Chavent et al., 2014). The dynamic properties of membranes play a key role as regulatory mechanisms and will influence the mechanical properties of cell membranes.

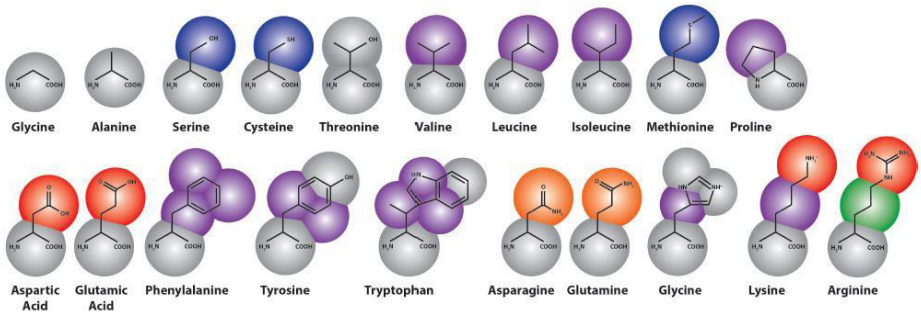

Figure 2. Martini coarse-grained model extension to amino acids, colored by bead type (where purple is apolar, blue and green are intermediate, gray and orange are polar and red represents charged particles).

MD system	Type	No. of entities	Time scale	Length scale	Size	Ref
Aqp0 in a PC bilayer	Atomistic	156 K atoms	100 ns	10 nm	5 GB	Stansfeld et al., 2013
EphA2 in a PC/PG bilayer	Coarse grained	292 K particles	10 µs	30 nm	100 GB	Chavent et al., 2015
144 GPCRs in a PM model	Coarse grained	2.6 M particles	10 µs	125 nm	1.1 TB	Koldsø and Sansom, 2015
Influenza A virion 10	Coarse grained	5 M particles	5 µs	90 nm	1.9 TB	Reddy et al., 2014

Table 1. For each MD system, the granularity of the simulation (atomistic versus coarse-grained), the number of atoms/particles (including water) in the simulation system, the duration of the production run simulation, the approximate linear dimension of the simulation box, and the resultant trajectory file size are given.

3.2. COARSE GRAINED MD SIMULATIONS

In coarse grained models the length-scale at which chemical components are modeled become important. Such a model necessarily lumps many atomic degrees of freedom into a single coarse-grained bead. As with the MD approach the coarse grained molecular model (CGMD) treats molecules classically. Newton's laws of motion are integrated according to potentials, which define the forces beween each bead in the system.

$$m_i \frac{\partial^2 \mathbf{r_i}}{dt^2} = \mathbf{F}_i, \mathbf{F}_i = -\frac{\partial V}{\partial \mathbf{r}_i}, i = 1 \ldots N \quad (1)$$

Eq 1 describes the motion of N particles, each with mass, m_i, experiencing a force, $\mathbf{F}_i$, due to a potential energy function, V, itself a function of the configuration of all atoms in the system that are close enough to exert a measurable force. NAMD (Phillips et al., 2005) integrators is one software package that can be used for CGMD to perform simulations. MD simulations make contact with observables, like temperature and pressure. Temperature is defined by the kinetic energy of the particles, while macroscopic pressure is defined by the average of the molecular virial given in Eq 2 and Eq 3, respectively.

$$\frac{1}{2} N_{df} k_B T = E_{kin}, E_{kin} = \frac{1}{2} \sum_i^N m_i \mathbf{v}_i \cdot \mathbf{v}_i \quad (2)$$

$$\mathbf{P} = \frac{2}{\mathbf{V}} [E_{kin} - \Lambda], \ \Lambda = -\frac{1}{2} \sum_{i<j} \mathbf{r}_{ij} \cdot \mathbf{F}_{ij} \quad (3)$$

V is the volume of the system, E_{kin} is the kinetic energy, $\mathbf{r}_{ij}$ is the distance vector between particles, i and j, $\mathbf{F}_{ij}$ is the corresponding force, N_{df} is the number of degrees of freedom (3N - 3 for N particles, minus any constraints) and Λ is the virial. The choice of these forces and the physical quantities they represent-dispersion forces, electrostatics and bonded forces-define themodel and determine its ability to reproduce observed physical phenomena. CGMD can be done on models built using structure-based, force-based and energy-based force-fields. Because coarse-graining requires a simplification of many degrees of freedom, it is impossible to build a model that simultaneously reproduces the all of the geometric, thermodynamic and kinetics features of a physical system. To build a coarse-grained model, it is therefore necessary to choose which physical properties are essential to the behavior of the target system. Examples of such

systems are reviewed extensively (Shelley et al., 2001; Izvekov and Voth, 2005; Ayton and Voth, 2009; Shinoda, DeVane and Klein, 2010).

In the "Center for Molecular Modeling Coarse-Grained" (CMM-CG) (Shinoda, DeVane and Klein, 2010) model the entire structural properties of the dimyristoylphosphatidylcholine (DMPC) bilayer is reproduced. The CMM-CG model maps three water molecules onto a single bead. Non-bonded forces are modeled with general Lennard-Jones (LJ) potentials with a potential well depth and zero-position, which is tuned to reproduce the desired structure and thermodynamic properties of the target system. The softer 12-4 potential is used to model dispersion forces in water by matching the melting temperature, density and vapor pressure observed in bulk and thin-film test simulations. A potential of mean force (PMF) between CG beads is then estimated using pair correlation functions, or radial distribution functions (RDF).

In the case of "Force Matching with the Multiscale Coarse Grained" (MS-CG) (Ayton and Voth, 2009) model, force-matching to develop a rigorous coarse-grained force field directly from forces measured in all-atom simulations was used. A variational method in which a coarse-grained force field is systematically developed from all-atom simulations under the correct thermodynamic ensemble. It is now possible to develop the exact many-body coarse-grained PMF from a trajectory of atomistic forces with a sufficiently detailed basis function.

Introducing protein detail to a coarse-grained force field requires an accurate model for both of the structure and dynamics of the protein itself, as well as the interactions with surrounding lipids and solvent. One example of such coarse graining is in the so called "Martini Proteins" (Marrink, de Vries and Mark, 2004). In the Martini force field, amino acids are mapped onto as many as five beads (Figure 2), one of which represents the polypeptide backbone. Residues with rings (His, Phe, Tyr, Trp) use a finer mapping and improper dihedral terms to preserve the topology of these rings. Intra-amino acid bonded potentials, angles and dihedrals have equilibrium values equal to the average of distributions measured from all bonded amino acid pairs found. These are sorted by helix, coil and extended secondary structure, as measured by the DSSP ("define secondary structure of proteins") prediction algorithm (Kabsch and Sander, 1983), so that the Martini model includes the effect of secondary structure on the apparent hydrophobicity and polarity of its constituent particles. This secondary structure remains fixed throughout the simulation. Thus the Martini model cannot sample secondary structure changes. It is possible to reconstitute atomistic details from a coarse-grained simulation using a "back-mapping" procedure similar to simulated annealing (Rzepiela et al., 2010). By tuning these models it is possible for CGMD to accurately explain protein-bilayer interactions, peptide self-assembly and

protein binding. These methods can also model internal structural changes that guide the biological functions of many proteins.

3.3. ASYMMETRIC ION CONCENTRATIONS

Differences in ion concentrations across the membrane that are established under the action of various membrane transport proteins can give rise to a difference in electric potential. Reproducing this set of conditions in computer simulations is not trivial. Several methods have been used successfully to simulate this effect. To allow for the simulation of ion channels with a realistic implementation of asymmetric ion concentration and transmembrane potential boundary conditions, a grand canonical Monte Carlo (GCMC)/Brownian dynamics (BD) was implemented in one case (Lee et al., 2012). Here asymmetric boundary conditions were imposed on a finite nonperiodic simulated system surrounded by concentration buffer regions. Insight into the factors governing the permeation of wide aqueous pores was possible. Imposing asymmetric concentrations in explicit solvent MD is difficult. Such explicit solvent MD simulations are normally performed with conventional periodic boundary conditions (PBCs), which are critical to reduce finite-size effects. Unavoidably, the PBCs also eliminate the distinction between the two sides of a membrane. Because there is a single continuous bulk solution where ions are free to diffuse and equilibrate, concentration gradients across the membrane cannot be simulated. To overcome this simulation of asymmetric ion concentrations in MD simulations with explicit solvent using a dual-membranes–dual-volumes strategy was tried (Delemotte et al., 2011). Two spatially separated membranes are included to create two disconnected bulk phases between them. In a more recent effort one of the two membranes is replaced by an artificial vacuum separator to reduce the computational burden (Delemotte et al., 2008). In another case manually adjusting the number of cations and anions in the two bulk regions makes it possible to set the effective membrane potential near some pre-chosen value V_m (Kutzner et al., 2011). These methods serve to increase computational costs. Other attempts include introducing energy steps at the boundaries of the periodic cells that separates the two solutions and generates a nonuniform distribution of the solute molecules across the cell boundaries with assymetric external fields. These result in a net charge imbalance across the membrane (Gumbart et al., 2012). There is no simple relationship between the energy step, the charge imbalance, and the resulting membrane potential.

3.4. INTERFACE OF MEMBRANES

One interesting set of problems concerns the mechanism by which small peptides and peripherally associated membrane proteins bind to and interact with the water/membrane interface. Studies include membrane lytic toxins, model peptides, fusion proteins, and peripherally associated signal transduction proteins and biosynthetic enzymes. For example in one study (Huang et al., 2003) implicit solvent calculations were used on cobra cardiotoxin CTX A3 to interpret polarized attenuated total internal reflection infrared spectroscopy data, suggesting modes of binding of this toxin to zwitterionic and anionic membranes. This toxin appeared to have a greater thinning effect on anionic phosphatidylglycerol monolayers than on those composed of zwitterionic phosphatidylcholine species.

A number of other membrane–water interface associated peptides have been investigated. One study used the HIV fusion protein gp41 and mutants in POPE bilayers (Wong, 2003), with comparison between simulations and attenuated total internal reflection infrared spectroscopy to determine the orientation of peptides relative to the bilayer. The simulation component of this study involved the removal of several lipids from one leaflet in order to accommodate protein inclusion.

Several larger peripheral membrane proteins have been investigated by MD. One study looked at cytochrome c in association with different alkanethiol self-assembled monolayers, with the aim of understanding the structural features of the protein in these complexes and the nature of the monolayer association. Many peripherally associated proteins have important roles in signal transduction and disease, and simulations continue to be a powerful method to understand the detailed lipid–protein interactions responsible for their activity.

Figure 3 shows an example of the membrane anchored protein prostaglandin H2-synthase. Its substrate, arachidonic acid, is a fatty acid in the membrane and cannot be found in the cytoplasm. The only way to effectively study such a protein is by using large scale simulations.

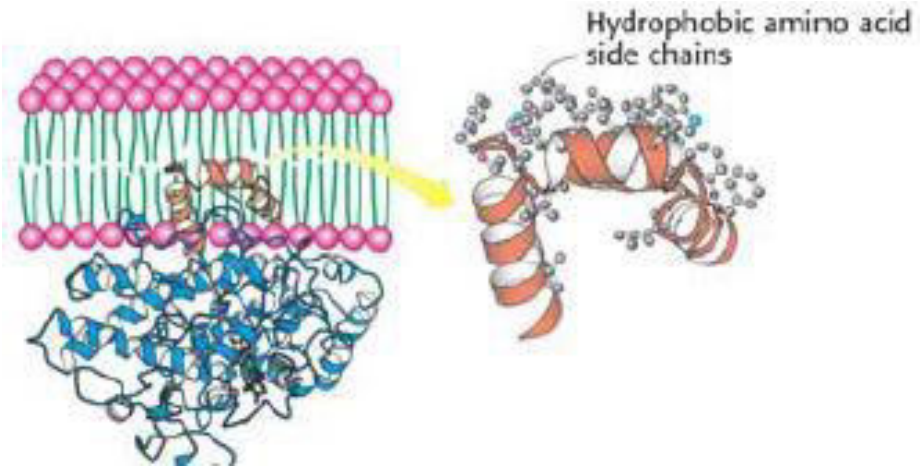

Figure 3. The membrane-anchored protein prostaglandin H2-synthase.

Figure 4 shows an example of hydration of the head group region in both coarse-grained (A) and all-atom models (B) of a membrane (lipids are removed). After large scale MD simulations reverse coarse-graining is done mapping back coarse-grained beads to the all-atom clusters, and resolvating the system. Minimization steps with simulated annealing while constraining atoms to the postion of the corresponding coarse-grained beads completes the process.

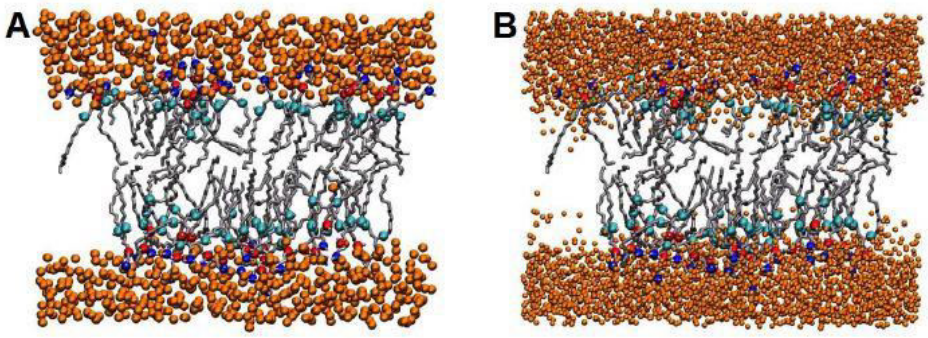

Figure 4. Hydration of the heads group region in both coarse-grained (**A**) and all-atom models (**B**) of a membrane protein. Lipids are removed.

3.5. TRANSMEMBRANE SIMULATIONS

It is known that membrane spanning helices can be considered the smallest autonomous membrane protein domains. Simulations can be done in order to study the properties of fundamental interest, such as the dynamics of isolated helices (Bright and Sansom, 2003), protein–lipid interactions (Petrache et al., 2002), helix association (Stockner et al., 2004), and the behaviour of simple channels such as those formed by certain fungal proteins and toxins (Tieleman and Sansom, 2001). MD simulations have also looked at the effects of hydrophobic mismatch on peptide and bilayer dynamics. Mismatch results when the effective hydrophobic thickness of the bilayer does not match that of a perfectly transmembrane-oriented helix (de Planque and Killian, 2003). Several mechanisms might compensate for this mismatch, including changes in peptide tilt, changes in secondary structure, peptide association, aggregation of different lipid species near the protein, and adaptation of bilayer structural properties like thickness or curvature. The dynamic properties of individual helices can be examined in detail with MD. A number of proline and glycine-containing sequence motifs have been extensively studied. Transmembrane helix flexibility mediated by specific sequence motifs have important consequences for the activity of membrane proteins such as gated ion channels (Capener and Sansom, 2002; Treptow, Marrink and Tarek, 2008; Nishizawa and Nishizawa, 2009; Delemotte et al., 2010; Khalili-Araghi et al., 2012; Li and Gong, 2015). The number of transmembrane helices in membrane proteins ranges from 1 to 14. A single transmembrane helix in bitopic membrane proteins are the most numerous. The second most numerous membrane proteins are those with seven transmembrane helices (Crozier et al., 2003), followed by proteins with 2, 4 and 12 transmembrane helices.

The dynamic properties of individual helices can be examined in detail with MD. Ion-channel pore helices like proline-kinked helices have been extensively studied. Proline and glycine are both thought to be important mediators of hinge-bending motions. Proline disrupts normal helical hydrogen bonding and participates in repulsive steric interactions with adjacent backbone atoms. A study on TMH-2 of the chemokine receptors identified a highly conserved TXP sequence motif by multiple sequence alignment (Govaerts et al., 2001). MD simulations were employed to investigate the effects of this sequence on the behavior of polyalanine in a hydrophobic environment. This indicated that the hydroxyl-containing amino acids also modulate the kink behavior of proline-containing sequences.

The interaction between α-helices is thought to be one of the most important determinants of membrane protein structure and function (Olivella et al., 2002). Proteins comprising pairs of α -helices can be employed as models for understanding these interactions. To get the interactions between pairs of helices simulated annealing and global searching MD (Kochva, Leonov and Arkin, 2003) or Monte-Carlo simulations (Kessel et al., 2003), either with an all-atom MD force field (Choma et al., 2001) or a simplified interaction potential function (Fleishman and Ben-Tal, 2002) is done.

Proton transport presents a special challenge to MD simulations because protons move between different water molecules and are not easily treated by a classical potential function. Viral and other small ion channels from small proteins (60-120 amino acids) are many such membrane proteins that have proton transport. Gramicidin A (Yu, Cukierman and Pomes, 2003), the influenza A M2 channel (Forrest, Tieleman and Sansom, 1999), and the engineered LS2 channel are examples. Different approaches have been developed for studying proton transport in membrane proteins. One method involves using the PM6 water model. PM6 is a polarizable and dissociable empirical water model consisting of O^{2-} and H^{+} units (Yu and Pomes, 2003). The empirical valence bond (EVB) theory has also been used to model the LS2 channel (Warshel, 2002). In all cases extensive MD simulations of a multitude of parameters and potential models are done to determine the best fit to experimental observations. These are all areas in which large-scale MD simulations do not provide correct answers.

Another area where explicit MD simulations need to be modified is in the proton exclusion problem, as seen in aquaporins (AQP). These membrane proteins allow water and glycerol to diffuse through while excluding protons, which would otherwise destroy the proton electrochemical gradient and starve cells to death. Several models for proton exclusion have been proposed (Zhu, Tajkhorshid and Schulten, 2001; deGroot et al., 2003; Ilan et al., 2004; Phongphanphanee, Yoshida and Hirata, 2008; Tani et al., 2009) and used with classical and steered (targeted) MD simulations. In simulations looking at water permeation, key structural features including the NPA motif, a constriction region (also termed ar/R), and the helix dipoles have been identified as contributors to this specificity. Methods to quantify water conduction properties such as osmotic permeability of AQP via MD simulation methods have also been developed. These methods involve inducing a hydrostatic pressure difference across a membrane with embedded AQP (Zhu, Tajkhorshid and Schulten, 2004).

In the case of mechanosensitive transmembrane channels (Perozo and Rees, 2003) a combination of MD simulations with normal mode analysis has been successfully used (Bilston and Mylvaganam, 2002; Anishkin et al., 2003; Valadie

et al., 2003). However, such simulations typically provide more than one mechanism for opening and closing. These multiple pathways provide a challenge in the absence of crystal structures on either the open or closed states for guidance. High-resolution structural methods cannot access these states. The crystal structures obtained of such states will most likely be a mutant one based on modeling. Figure 5 shows the two open states of the mechanosensitive ion channel MscL (Perozo et al., 2002).

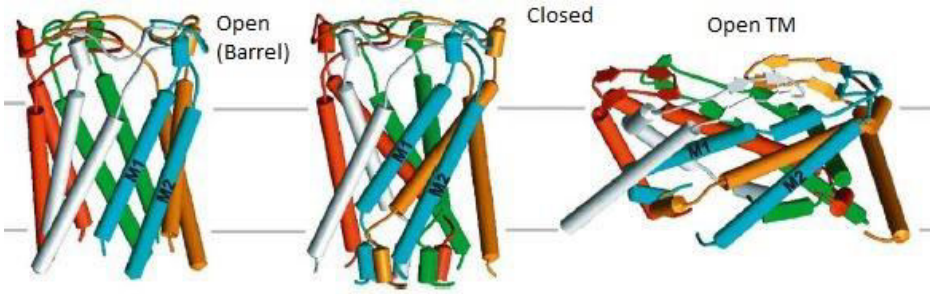

Figure 5. Two possible open states of the mechanosensitive ion channel MscL. MD simulations can predict both types of gating where the pore diameter of one open state (Barrel ~15 Å) is nearly half that of the other (Open TM pore diameter ~ 30 Å).

Direct MD simulations however are shown to be very effective in the case of ABC-type transporters (Higgins, 1992). As one of the largest superfamilies of proteins (Hopfner et al., 2000) ABC-transporters are involved in multidrug resistance in cancer cells and bacteria and in genetic diseases such as cystic fibrosis. They are present in eukaryotic and prokaryotic systems and have the characteristic LSGGQ signature motif in their ATPase domain. Using targeted MD (TMD) it has also been shown how MD can be used for structural modeling. The first reported crystal structure of a "complete" ABC-transporter, MsbA from *E. coli* (ECMsbA), was resolved at 4.5Å (Chang, 2003). This structure revealed only the C-α polypeptide trace of the protein, and coordinates for a significant part of the nucleotide binding domain (NBD) consisting of 78 residues including the conserved ATP binding "Walker A" motif could also not be determined due to disorder. Starting from the C-α polypeptide trace, the backbone and side chain atoms were generated, and the structure of the missing part of the NBD was modeled based on homology with known high-resolution structures of the NBDs of other ABC transporters. MD simulations were subsequently used to test the stability of the model. While the monomer was stable to MD simulations the dimer was not. In reorienting the transmembrane domains of ECMsbA with

respect to the NBDs in order to transform the "back-to-back" dimer into a "head-to-tail" model, a suitable template was found to model another ABC-transporter P-glycoprotein (Stenham et al., 2003).

Another avenue used to simulate membrane proteins is biased MD. Using the biasing forces on ATP synthase creates non-equlibrium MD simulations. Steering or acceleration may also be used. This is favored over the regular equilibirum MD. Events of interest like ATP binding or release occur on the millisecond time scale but the large size of the protein limits simulation to the nanosecond. One example is a biasing force to cause 120^{o} rotations of the cental stalk. The drawback with this method is that key relaxation events may be missed when a process that occurs in the millisecond time scale in nature is forced to occur on the nanosecond time scale accessible to protein MD simulations. Biased MD simulations thus do not yield a full transition path. However, useful mechanistic information can still be derived from such studies (Ma et al., 2002).

Finally, processes involving the breaking of chemical bonds cannot be studied using MD. A quantum mechanical (QM) treatment is needed, but QM is computationally expensive and currently limited to a few hundred atoms. The QM/MM (molecular mechanics) method is a technique used to study such systems. The reactive centre and its immediate surroundings are modeled in electronic detail using a quantum mechanical approach while the rest of the system is treated classically to atomic detail using MD. NAMD 2.12 and later (Melo et al., 2018) has this feature. Hybrid QM–MM simulations in NAMD divide the system into MM and QM regions, using a classical force field to treat the classical atoms and passing the information that describes the quantum atoms in the system to a quantum chemistry package, which is expected to calculate forces for all QM atoms, as well as the total energy of the QM region and the partial charges. All bonded and nonbonded interactions among MM atoms are handled by NAMD's CHARMM force field, whereas all interactions among QM atoms are handled by the quantum chemistry package in its chosen theory level. QM/MM methods can now be used for mechanical and electrostatic embedding, treatment of covalent bonds, link atoms, and point charge alteration and redistribution.

3.6. OUTER MEMBRANE PROTEIN SIMULATIONS

β-barrel membrane proteins are unique to the outer membranes of mitochondria, chloroplasts, and Gram-negative bacteria. The bacterial proteins, which range in size from 8 to 22 β-stranded barrels, perform a variety of

functions, from enzymatic lipid cleavage to nutrient uptake functions to iron transport (Schulz, 2002). MD simulations provide a useful tool for exploring the dynamics of outer membrane proteins, and interactions with their environment. In OmpA MD has been used to explore the behaviour of the protein in three different environments: a lipid bilayer, a detergent micelle, a (detergent-containing) crystal (Tamm et al., 2003). Figure 6 shows the structure at the beginning and end of a 25 ns simulation for a similar protein OmpX inserted in lipid DMPC with water and equilibration.

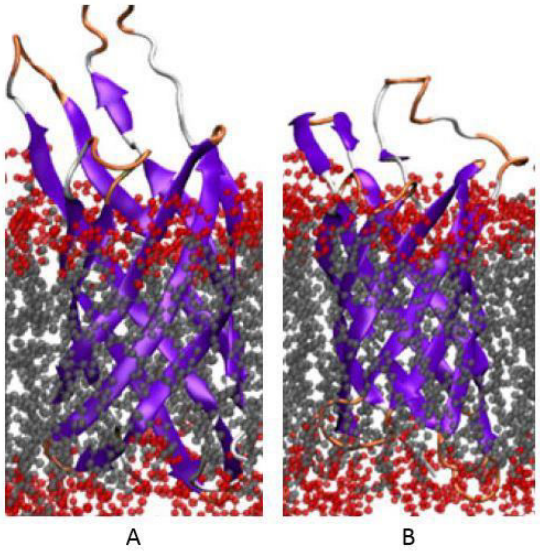

Figure 6. OmpX in a lipid bilayer. The end of the MD simulation (**B**) after 25 ns starting from initial equilibriated configuration (**A**). Waters are removed – however water is trapped in the protein via hydrogen bonds. See the text for more details.

In this case the simulation was stable with very small changes in the lipid layer. Water molecules trapped in the β-barrel due to hydrogen bonds are seen. There are large structural fluctutions on the extracelluar part of the protein. MD simulations can effectively study this. The problem is to sample adequately the conformational space accessible for the species of interest. In this case it may be a question of why water cannot pass through. In another case it may be the translocation mechanism and kinetics of the siderophore through FhuA (Ferguson et al., 2001). The sampling of conformational space when there is a large conformational change in the protein in the lipid layer can be difficult in MD runs

at the “ns” scale. While using several other methods like applying forces or pulling parts of the protein may result in inducing conformational changes in such simulations, in many instances other mechanisms are at work that cannot be studied using MD in such ways. For example, a significant conformational change in the plug domain of FhuA is required for the siderophore to either passively diffuse or be translocated into the periplasm. To study this by MD simulations requires long runs (ms scale) to trace the confomational changes as the diffusion occurs.

3.7. CONFORMATIONAL CHANGES IN SIMULATIONS

In many classes of membrane proteins like the voltage gated K channel KcsA (α-helical protein) or KvaP (Monticelli et al., 2004), the gating mechanism results in conformational changes (range of states) in the embedded region of the protein. Particularly in the selectivity filter regions. Here the large reaction force field in the pore region due to an extensive hyper-polarized/depolarized external membrane potential needs to be factored in. Figure 7 shows a system (Roy, 2019) where an extended dielectric region was used to get the reaction force in the pore and the corresponding conformational changes induced in KcsA in the pore. Simulations were 2ns, and the entire system had ~60K explicit atoms of a single membrane protein, lipids (5 shells), water and ions. Interhelix dynamics and force field maps can then help to understand the gating and related conformational changes.

Some membrane proteins like the bacterial leucine transporter (LeuT), a homologue of the eukaryotic Na^+/Cl^--dependent neurotransporters responsible for terminating synaptic transmission by driving the cellular uptake of neurotransmitters, including the biogenic amines, have a rare conformational change event (Gedeon et al., 2010). A large number of MD steps are necessary for these events to occur, which allow a system to overcome energy barriers and conformational transition from one potential energy minimum to another. Using a combination of accelerated MD (aMD) and PCA protein segments that are most involved in structural changes can be identified. The RMSF (root mean square fluctuations) calculation can be used to determine how much each residue moves during the trajectory. aMD simulations are routinely performed to assess time-dependent protein conformational change (Thomas et al., 2012) and are fully integrated into commonly used software packages including NAMD (Wang et al., 2011) and Amber (Shaw et al., 2010). These results can then be compared to experimental structures.

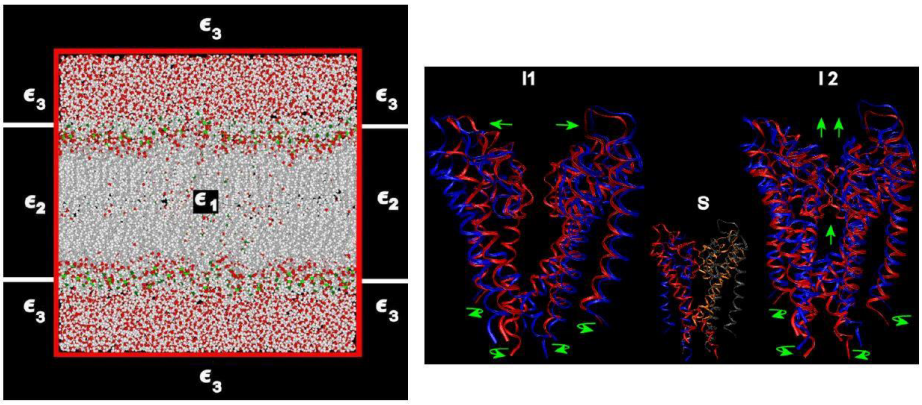

Figure 7. KcsA in DPPC surrounded by a dielectric continuum. The red region is the Helmholtz layer (**A**). In **B** with water and lipids removed the effects of the reaction force field is seen in conformational changes in KcsA. Straight green arrows show the relative translational motions between the chains from C (closed) to O (open) that occur with rotations of each of the four chains in KcsA shown with the curved arrows. These changes are reversible. See the text for details.

Cell membranes present barriers to the permeation/diffusion of polar molecules. Membrane transport proteins have evolved to facilitate the passage of specific molecules across this barrier. An example is the lactose permease (LacY) (Kaback, 1992). LacY performs the symport of lactose or other galactoside molecules with H^+ in a 1:1 stoichiometry. MD simulations of LacY in the apo state (without bound TDG) were run to discover whether substantial conformational changes would be observed (on a 25 ns timescale). Further from such runs the goal was to explore the possible relationship of such changes to the transport mechanism of LacY (longer timescale of 100 ms). Several references provide excellent results (Pang et al., 2003; Vardy et al., 2004; Kimanius, Lindahl and Andersson, 2018) using a variety of techniques, but based on the original classical MD approach.

3.8. CONCLUSION

MD simulations have contributed significantly to the understanding of protein structure-function relationships. MD has enabled an atomic-level description of

the interactions of channel-forming proteins with the solutes whose transport they mediate, characterization of ligand-binding processes, and in the case of voltage gated membrane proteins insights into the selectivity filter and gating mechanisms. Simulations of outer membrane proteins have provided information on the protein dynamics, role of the extracelluar structures and the relationship with the lipid layer embedded proteins in conferring selectivity to porins, or in water pathways. Mechanosensitive ion channel MD simulations have been used to study the relative flexibility throughout the protein, as a means by which insights into the mechanism of gating can be gained. MD simulations now contribute to the understanding of the structural, dynamical and functional properties of receptors. Extensive work is done to compare the structural dynamics with native crystal forms elucidated from ligand-free and bound forms. These include crystal structures from X-ray, and neutron, NMR and EPR studies and those augmented by threading and homology modeling (Nikolaev et al., 2018). The MD approach also allows for multiple random conformations to be taken at a time. These are validated after long equilibrium runs using experimental data. Here the experimental data is serving as limitations to be placed on the conformations (e.g. known distances between atoms). Only conformations that manage to remain within the limits set by the experimental data are accepted. This approach often applies large amounts of experimental data to the conformations which is a very computationally demanding task, but will result in valid conformations of open and closed states of membrane proteins that cannot be isolated by crystallization.

Methodological limitations do exist in large scale atomistic simulations of membrane proteins. Much of this relates to the force field used and the thermodynamic ensemble. While classical force fields (GROMOS, CHARMM, AMBER) have limited implementations of electronic polarizability (Lopes, Roux, and MacKerell Jr, 2009) others like reactive force fields and coarse-grained force fields have been shown to work well in many situations (Meuwly, 2019). Similarly there are a number of water models that can be used with ions/counter ions (Best and Mittal, 2010). There is also the question of the optimal method to embed a complex membrane protein within a lipid bilayer. In fact, the effect of the lipid composition of the bilayer model on the dynamics of membrane proteins is well established (Brown, 2012) and needs to be considered carefully before undertaking large-scale MD runs. All these limitations can however be overcome in judicious choices of the methods to use before undertaking large-scale MD runs.

Parallel techniques used in MD codes have now made possible the use of MD simulations for the routine study of systems consisting of thousands of atoms for multi-nanoseconds. On the temporal and spatial scales there are a number of

events that can occur. These can now be studied in more detail. The typical timescale for allosteric effects is usually from microseconds to milliseconds. During such complex events, the transitions between two stable states are separated by high free-energy barriers. Modified MD techniques are used for the study of such events. Coarse-grained models, steered MD, biased MD approaches, targeted MD, and alchemical free-energy pertubations. Another effect that is now being studied is the curvature of the lipid bilayer by using large systems that can be parallelized and an elastic curvature force field. In addition a flexible surface model (FSM) can be used. These enhancements are added to the usual large-scale MD simulations to include curvature stress.

The growth in the number of high-resolution membrane protein structures is encouraging. Simulations can provide additional dynamic details of the static snapshots given by membrane protein structures and can be used to investigate and build models of other conformational states. Models and simulations of open and closed states of membrane proteins, conformational substates of transporters, and dynamics linking the crystal structures of the different states will help in designing drugs, inhibitors, and understanding cell signaling and ligand docking. The ultimate goal of membrane MD simulations is to be able to do realistic simulations. Here effects of a controlled pH, metabolites and ions/counterions with a constant energy flow, and a wide variety of embedded and peripheral proteins are included with an actin skeleton. These billion atom explicit systems now model the plasma membrane in full complexity.

REFERENCES

Allen F, Almási G, Andreoni W, Beece D, Berne B J, Bright A, Brunheroto J, Cascaval C. Blue gene: A vision for protein science using a petaflop supercomputer. *IBM Syst J*. 2001;40(2):310–327.

Allen MP, Tildesley DJ. *Computer Simulation of Liquids*. Oxford University Press, New York, 1987.

Anishkin A, Gendel V, Sharifi NA, Chiang CS, Shirinian L, Guy HR, Sukharev S. On the conformation of the COOH-terminal domain of the large mechanosensitive channel MscL. *J Gen Physiol*. 2003;121(3):227-244.

Ayton GS, Voth GA. Hybrid coarse-graining approach for lipid bilayers at large length and time scales. *J Phys Chem B.* 2009;113(13): 4413–4424.

Best RB, Mittal J. Protein simulations with an optimized water model: Cooperative helix formation and temperature-induced unfolded state collapse. *J Phys Chem B*. 2010;114(46):14916-14923.

Bilston LE, Mylvaganam K. Molecular simulations of the large conductance mechanosensitive (MscL) channel under mechanical loading. *FEBS Lett*. 2002;512(1-3):185-190.

Bright JN, Sansom MSP. The flexing/twirling helix: exploring the flexibility about molecular hinges formed by proline and glycine motifs in transmembrane helices. *J Phys Chem B*. 2003;107(2):627–636.

Brown MF. Curvature forces in membrane lipid-protein interactions. *Biochemistry*. 2012;51(49):9782-9795.

Capener CE, Sansom MSP. Molecular dynamics simulations of a K+ channel model: Sensitivity to changes in ions, waters, andmembrane environment. *J Phys Chem*. 2002;106(17):4543–4551.

Case DA, Cheatham TE, Darden T, Gohlke H, Luo R, Merz KM, Onufriev A, Simmerling C, Wang B, Woods RJ. The Amber biomolecular simulation programs. *J Comput Chem*. 2005;26(16):1668–1688.

Ceriotti M, Bussi G, Parrinello M. Colored-noise thermostats à la carte. *J Chem Theory Comput*. 2010;6(4):1170–1180.

Chandler D. *Introduction to Modern Statistical Mechanics*. Oxford University Press, New York, 1987.

Chang G. Structure of MsbA from *Vibrio cholera*: A multidrug resistance ABC transporter homolog in a closed conformation. *J Mol Biol*. 2003;330(2):419-430.

Chavent M, Reddy T, Goose J, Dahl ACE, Stone JE, Jobard B, Sansom MSP. Methodologies for the analysis of instantaneous lipid diffusion in MD simulations of large membrane systems. *Faraday Discuss.* 2014;169:1–18.

Chavent M, Seiradake E, Jones EY, Sansom MSP. Structures of the EphA2 receptor at the membrane: Role of lipid interactions. *Structure*. 2015;24(2),337–347.

Choma CT, Tieleman DP, Cregut D, Serrano L, Berendsen HJC. Towards the design and computational characterization of a membrane protein. *J Mol Graph Model*. 2001;20(3):219-234.

Christen M, Hünenberger PH, Bakowies D, Baron R, Bürgi R, Geerke DP, Heinz TN, et al. The GROMOS software for biomolecular simulation: GROMOS05. *J Comput Chem*. 2005;26(16):1719–1751.

Crozier PS, Stevens MJ, Forrest LR, Woolf TB. (2003) Molecular dynamics simulations of dark-adapted rhodopsin in an explicit membrane bilayer: coupling between local retinal and larger scale conformational change. *J Mol Biol*. 2003;333(3):493-514.

Delemotte L, Dehez F, Treptow W, Tarek M. Modeling membranes under a transmembrane potential. *J Phys Chem B*. 2008;112(18):5547–5550.

Delemotte L, Tarek M, Klein ML, Amaral C, Treptow W. Intermediate states of the Kv1.2 voltage sensor from atomistic molecular dynamics simulations. *Proc Natl Acad Sci USA*. 2011;108(15):6109–6114.

Delemotte L, Treptow W, Klein ML, Tarek M. Effect of sensor domain mutations on the properties of voltage-gated ion channels: Molecular dynamics studies of the potassium channel Kv1.2. *Biophys J*. 2010;99(9):L72–L74.

de Groot BL, Frigato T, Helms V, Grubmuller H. The mechanism of proton exclusion in the aquaporin-1 water channel. *J Mol Biol*. 2003;333(2):279-293.

de Planque MR, Killian JA (2003) Protein–lipid interactions studied with designed transmembrane peptides: Role of hydrophobic matching and interfacial anchoring. *Mol Membr Biol*. 2003;20(4):271–284.

Ferguson AD, Kodding J, Walker G, Bos C, Coulton JW, Diederichs K, Braun V, Welte W. Active transport of an antibiotic rifamycin derivative by the outer membrane protein FhuA. *Structure*. 2001;9(8):707-716.

Fleishman SJ, Ben-Tal N. A novel scoring function for predicting the conformations of tightly packed pairs of transmembrane alphahelices. *J Mol Biol*. 2002;321(2):363-378.

Forrest LR, Tieleman DP, Sansom MSP. Defining the transmembrane helix of M2 protein from influenza A by molecular dynamics simulations in a lipid bilayer. *Biophys J*. 1999;76(4):1886-1896.

Frenkel D, Smit B. *Understanding Molecular Simulations. From Algorithms to Applications*. Academic Press, San Diego, California, 1996.

Gedeon PC, Indarte M, Surratt CK, Madura JD. Molecular dynamics of leucine and dopamine transporter proteins in a model cell membrane lipid bilayer. *Proteins*. 2010;78(4):797–811.

Govaerts C, Blanpain C, Deupi X, Ballet S, Ballesteros JA, Wodak SJ. Vassart G, Pardo L, Parmentier M. The TXP motif in the second transmembrane helix of CCR5-structural determinant of chemokine-induced activation. *J Biol Chem*. 2001;276(16):13217-13225.

Gumbart J, Khalili-Araghi M, Sotomayor M, Roux B. Constant electric field simulations of the membrane potential illustrated with simple systems. *Biochim Biophys Acta*. 2012;1818(2):294–302.

Higgins CF. ABC transporters-from microorganisms to man. *Annu Rev Cell Biol.* 1992;8:67-113.

Hopfner KP, Karcher A, Shin DS, Craig L, Arthur LM, Carney JP, Tainer JA. Structural biology of Rad50 ATPase: ATP driven conformational control in DNA double-strand break repair and the ABC-ATPase superfamily. *Cell*. 2000;101(7):789-800.

Huang WN, Sue SC, Wang DS, Wu PL, Wu WG. Peripheral binding mode and penetration depth of cobra cardiotoxin on phospholipid membranes as studied by a combined FTIR and computer simulation approach. *Biochemistry*. 2003;42(24):7457–7466.

Ilan B, Tajkhorshid E, Schulten K, Voth GA. The mechanism of proton exclusion in aquaporin channels. *Proteins*. 2004;55(2):223-228.

Ingólfsson HI, Arnarez C, Periole X, Marrink SJ. Computational 'microscopy' of cellular membranes. *J Cell Sci.* 2016;129(2):257–268.

Izvekov S, Voth GA. A multiscale coarse-graining method for biomolecular systems. *J Phys Chem B.* 2005;109(7):2469–2473.

Janosi L, Li Z, Hancock JF, Gorfe AA. Organization, dynamics, and segregation of Ras nanoclusters in membrane domains. *Proc Natl Acad Sci USA*. 2012;109(21):8097–8102.

Kaback HR. The lactose permease of *Escherichia coli*: A paradigm for membrane transport proteins. *Biochim Biophys Acta*. 1992;1101(2):210-213.

Kabsch W, Sander C. Dictionary of protein secondary structure: Pattern recognition of hydrogen-bonded and geometrical features. *Biopolymers*. 1983;22(12):2577–2637.

Kessel A, Shental-Bechor D, Haliloglu T, Ben-Tal N. Interactions of hydrophobic peptides with lipid bilayers: Monte Carlo simulations with M2 delta. *Biophys J*. 2003;85(6):3431-3444.

Khalili-Araghi F, Tajkhorshid E, Roux B, Schulten K. Molecular dynamics investigation of the ω-current in the Kv1.2 voltage sensor domains. *Biophys J*. 2012;102(2):258–267.

Kimanius, D., Lindahl, E. and Andersson, M. (2018) Uptake dynamics in the Lactose permease (LacY) membrane protein transporter. *Sci Rep*, 2018;8(1):14324.

Klepeis JL, Lindorff-Larsen K, Dror RO, Shaw DE. Long-timescale molecular dynamics simulations of protein structure and function. *Curr Opin Struct Biol*. 2009;19(2):120–127.

Kochva U, Leonov H, Arkin IT. Modeling the structure of the respiratory syncytial virus small hydrophobic protein by silentmutation analysis of global searching molecular dynamics. *Protein Sci*. 2003;12(12):2668-2674.

Koldsø H, Sansom MSP. Organization and dynamics of receptor proteins in a plasma membrane. *J Am Chem Soc*. 2015;137(46):14694–14704.

Kutzner C, Grubmüller H, de Groot BL, Zachariae U. Computational electrophysiology: The molecular dynamics of ion channel permeation and selectivity in atomistic detail. *Biophys J*. 2011;101(4):809–817.

Leach AR. *Molecular Modelling. Principles and Applications*. Addison Wesley Longman, Essex, England, 1996.

Lee KI, Jo S, Rui H, Egwolf B, Roux B, Pastor RW, Im W. Web interface for Brownian dynamics simulation of ion transport and its applications to beta-barrel pores. *J Comput Chem*. 2012;33(3):331–339.

Li Y, Gong H. Theoretical and simulation studies on voltage-gated sodium channels. *Protein Cell*. 2015;6(6):413–422.

Lindahl E, Hess B, van der Spoel D. GROMACS 3.0: A package for molecular simulation and trajectory analysis. *J Mol Model*. 2001;7(8):306–317.

Lopes PEM, Roux B, MacKerell Jr AD. Molecular modeling and dynamics studies with explicit inclusion of electronic polarizability. Theory and applications. *Theor Chem Acc*. 2009;124(1-2):11-28.

Ma J, Flynn TC, Cui Q, Leslie AG, Walker JE, Karplus M. A dynamic analysis of the rotation mechanism for conformational change in F(1)-ATPase. *Structure*. 2002;10(7):921-931.

MacKerell AD Jr. All-atom empirical potential for molecular modeling and dynamics studies of proteins. *J Phys Chem B*. 1998;102(18):3586–3616.

Marrink SJ, de Vries AH, Mark AE. Coarse grained model for semiquantitative lipid simulations. *J Phys Chem B*. 2004;108(2):750–760.

Marrink SJ, de Vries AH, Tieleman DP. Lipids on the move: Simulations of membrane pores, domains, stalks and curves. *Biochim Biophys Acta - Biomembranes*. 2009;1788(1):149–168.

Melo MCR, Bernardi RC, Rudack T, Scheurer M, Riplinger C, Phillips JC, Maia JDC, et al. NAMD goes quantum: An integrative suite for hybrid simulations. *Nature Methods*. 2018;15(5):351-354.

Meuwly M. Reactive molecular dynamics: From small molecules to proteins. *WIREs Comput Mol Sci*. 2019;9(1):e1386.

Monticelli L, Robertson KM, MacCallum JL, Tieleman DP. Computer simulation of the KvAP voltage-gated potassium channel: steered molecular dynamics of the voltage sensor. *FEBS Lett*. 2004;564(3):325-332.

Nikolaev DM, Shtyrov AA, Panov MS, Jamal A, Chakchir OB, Kochemirovsky VA, Olivucci M, Ryantsev MN. A comparative study of modern homology modeling algorithms for rhodopsin structure prediction. *ACS Omega* 2018;3(7):7555-7566.

Nishizawa M, Nishizawa K. Coupling of S4 helix translo-cation and S6 gating analyzed by molecular dynamics simulations of mutated K_v channels. *Biophys J*. 2009;97(1):90-100.

Olivella M, Deupi X, Govaerts C, Pardo L. Influence of the environment in the conformation of alpha-helices studied by protein database search and molecular dynamics simulations. *Biophys J*. 2002;82(6):3207-3213.

Pang A, Arinaminpathy Y, Sansom MSP, Biggin PC. Interdomain dynamics and ligand binding: molecular dynamics simulations of glutamine binding protein. *FEBS Lett*. 2003;550(1-3):168-174.

Patel S, Mackerell AD Jr, Brooks CL 3rd. CHARMM fluctuating charge force field for proteins: II protein/solvent properties from molecular dynamics simulations using a nonadditive electrostatic model. *J Comput Chem*. 2004;25(12):1504–1514.

Perozo E, Cortes DM, Sompornpisut P, Kloda A, Martinac B. Open channel structure of MscL and the gating mechanism of mechanosensitive channels. *Nature*. 2002;418(6901):942-948.

Perozo E, Rees DC. Structure and mechanism in prokaryotic mechanosensitive channels. *Curr Opin Struct Biol*. 2003;1(4):432-442.

Petrache HI, Zuckerman DM, Sachs JN, Killian JA, Koeppe RE, Woolf TB. Hydrophobic matching mechanism investigated by molecular dynamics simulations. *Langmuir*. 2002;18(4):1340–1351.

Phillips JC, Braun R, Wang W, Gumbart J, Tajkhorshid E, Villa E, Chipot C, Skeel RD, Kal´e L, Schulten K. Scalable molecular dynamics with NAMD. *J Comput Chem*. 2005;26(16):1781–1802.

Phongphanphanee S, Yoshida N, Hirata F. (2008) On the proton exclusion of aquaporins: A statistical mechanics study. *J Am Chem Soc*. 2008;130(5):1540-1541.

Rapaport DC. *The Art of Molecular Dynamics Simulation*. Cambridge University Press, Cambridge, UK, 2004.

Reddy T, Shorthouse D, Parton DL, Jefferys E, Fowler PW, Chavent M, Baaden M, Sansom MSP. Nothing to sneeze at: A dynamic and integrative computational model of an influenza A virion. *Structure*. 2015;23(3):584–597.

Roy NK. A new semi-explicit atomistic molecular dynamics simulation method for membrane proteins. *J Comput Methods Sci Eng*. 2019;19(1):259-286.

Rzepiela AJ, Schafer LV, Goga N, Risselada HJ, de Vries AH, Marrink SJ. Reconstruction of atomistic details from coarse-grained structures. *J Comput Chem.* 2010;31(6):1333–1343.

Schulz GE. The structure of bacterial outer membrane proteins. *Biochim Biophys acta - Biomembranes*. 2002;1565(2):308-317.

Shaw DE, Maragakis P, Lindorff-Larsen K, Piana S, Dror RO, Eastwood MP, Bank JA, et al. Atomic-level characterization of the structural dynamics of proteins. *Science*. 2020;330(6002):341-346.

Shelley JC, Shelley MY, Reeder RC, Bandyopadhyay S, Klein ML. A coarse grain model for phospholipid simulations. *J Phys Chem B.* 2001;105(40):4464–4470.

Shinoda W, DeVane R, Klein ML. Zwitterionic lipid assemblies: Molecular dynamics studies of monolayers, bilayers, and vesicles using a new coarse grain force field. *J Phys Chem B.* 2010;114(20):6836–6849.

Stanley HE. *Introduction of Phase Transitions and Critical Phenomena*. Oxford University Press, New York, 1971.

Stansfeld PJ, Jefferys E, Sansom, MSP. Multiscale simulations reveal conserved patterns of lipid interactions with aquaporins. *Structure*. 2013;21(5):810–819.

Stansfeld PJ, Sansom MSP. Molecular simulation approaches to membrane proteins. *Structure*. 2011;19:1562–1572.

Stenham DR, Campbell JD, Sansom MS, Higgins CF, Kerr ID, Linton KJ. An atomic detail model for the human ATP binding cassette transporter P-glycoprotein derived from disulfide cross-linking and homology modeling. *FASEB J*. 2003;17(15):2287-2289.

Stockner T, Ash WL, MacCallum JL, Tieleman DP. Direct simulation of transmembrane helix association: Role of asparagines. *Biophys J*. 2004;87(3):1650–1656.

Tamm LK, Abildgaard F, Arora A, Blad H, Bushweller JH. Structure, dynamics and function of the outer membrane protein A (OmpA) and influenza hemagglutinin fusion domain in detergent micelles by solutions NMR, *FEBS Lett*. 2003;555(1):139-143.

Tani K, Mitsuma T, Hiroaki Y, Kamegawa A, Nishikawa K, Tanimura Y, Fujiyoshi Y. Mechanism of aquaporin-4's fast and highly selective water conduction and proton exclusion. *J Mol Biol*. 2009;389(4):694-706.

Thomas JR, Gedeon PC, Grant BJ, Madura JD. LeuT conformational sampling utilizing accelerated molecular dynamics and principal component analysis. *Biophys J*. 2012;103(1):L1-L3.

Tieleman DP, Sansom MSP. Molecular dynamics simulations of antimicrobial peptides: From membrane binding to trans-membrane channels. *Int J Quantum Chem*. 2001;83(3-4):166–179.

Treptow W, Marrink SJ, Tarek M. Gating motions in voltage-gated potassium channels revealed by coarse-grained molecular dynamics simulations. *J Phys Chem*. 2008;B112(11):3277-3282.

Valadie H, Lacapcre JJ, Sanejouand YH, Etchebest C. Dynamical properties of the MscL of *Escherichia coli*: A normal mode analysis. *J. Mol. Biol*. 2003;332(3):657-674.

Van der Ploeg P, Berendsen HJC. Molecular-dynamics of a bilayer-membrane. *Mol Phys*. 1983;49(1):233–248.

Vardy E, Arkin IT, Gottschalk KE, Kaback HR, Schuldiner S. Structural conservation in the major facilitator superfamily as revealed by comparative modeling. *Protein Sci*. 2004;13(7):1832-1840.

Wang Y, Harrison C, Schulten K, McCammon JA. Implementation of accelerated molecular dynamics in NAMD. *Comput Sci Discov*. 2011;4(1):015002.

Warshel A. Molecular dynamics simulations of biological reactions. *Acc Chem Res*. 2002;35(6):385-395.

Wong TC. Membrane structure of the human immunodeficiency virus gp41 fusion peptide by molecular dynamics simulation II. The glycine mutants. *Biochim Biophys Acta – Biomembranes*. 2003;1609(1):45–54.

Yu CH, Cukierman S, Pomes R. Theoretical study of the structure and dynamic fluctuations of dioxolane-linked gramicidin channels. *Biophys J*. 2003;84(2 Pt 1), 816-831.

Yu CH, Pomes R. Functional dynamics of ion channels: Modulation of proton movement by conformational switches. *J Am Chem Soc*. 2003;125(45):13890-13894.

Zhu FQ, Tajkhorshid E, Schulten K. Molecular dynamics study of aquaporin-1 water channel in a lipid bilayer. *FEBS Lett*. 2001;504(3):212-218.

Zhu FQ, Tajkhorshid E, Schulten K. Theory and simulation of water permeation in aquaporin-1. *Biophys J*. 2004;86(1 Pt 1):50-57.

Submitted: 18th Oct 2019, Revised: 16th Nov 2019, Accepted: 3rd Jan 2020

Chapter Four

4. GENERAL PRINCIPLES OF SECONDARY ACTIVE TRANSPORTER FUNCTION

Oliver Beckstein*, *, Fiona Naughton
Department of Physics, Arizona State University, Tempe AZ 85287, USA

ABSTRACT

Transport of ions and small molecules across the cell membrane against electrochemical gradients is catalyzed by integral membrane proteins that use a source of free energy to drive the energetically uphill flux of the transported substrate. Secondary active transporters couple the spontaneous influx of a "driving" ion such as Na^+ or H^+ to the flux of the substrate. The thermodynamics of such cyclical non-equilibrium systems are well understood and recent work has focused on the molecular mechanism of secondary active transport. The fact that these transporters change their conformation between an inward-facing and outward-facing conformation in a cyclical fashion, called the alternating access model, is broadly recognized as the molecular framework in which to describe transporter function. However, only with the advent of high resolution crystal structures and detailed computer simulations has it become possible to recognize common molecular-level principles between disparate transporter families. Inverted repeat symmetry in secondary active transporters has shed light on how protein structures can encode a bi-stable two-state system. More detailed analysis (based on experimental structural data and detailed molecular dynamics simulations) indicates that transporters can be understood as gated pores with at least two coupled gates. These gates are not just a convenient cartoon element to illustrate a putative mechanism but map to distinct parts of the transporter protein. Enumerating all distinct gate states naturally includes occluded states in the alternating access picture and also suggests what kind of protein conformations might be observable. By connecting the possible conformational states and ion/substrate bound states in a kinetic

* Direct all correspondence to Prof. Oliver Beckstein, Department of Physics, Arizona State University, Tempe, AZ, USA. E-mail: oliver.beckstein@asu.edu.

model, a unified picture emerges in which symporter, antiporter, and uniporter function are extremes in a continuum of functionality.

Keywords: membrane protein, transporter, symmetry, molecular mechanisms

4.1. INTRODUCTION

Active transporters are integral membrane proteins that move substrate through the membrane against an electrochemical gradient by using a source of free energy. They are broadly classified as primary and secondary active transporters, depending on the free energy source (Mitchell, 1967). *Primary active transporters* harness chemical reactions (e.g., phosphorylation by ATP) or light. Some examples are the sodium-potassium pump (Na/K ATPase) (Morth et al., 2007), the rotary F_0F_1-ATPase and the light-driven proton pump bacteriorhodopsin (Buch-Pedersen et al., 2009), complex I in the respiratory chain (Sazanov, 2015), or ATP-driven ABC transporters such as p-glycoprotein (Lespine et al., 2009).

Secondary transport is driven by an electrochemical gradient in a *driving ion*, namely sodium or protons. Examples are neurotransmitter transporters SERT (serotonin) and DAT (dopamine) (Gouaux, 2009), sodium-proton exchangers (NHE) (Fuster and Alexander, 2014), the calcium exchanger (Ottolia et al., 2007), and AE1, the anion exchanger in red blood cells also known as Band 3 (Västermark et al., 2014). Secondary active transporters can be divided into two classes based on their physiological behavior (Mitchell, 1967). *Symporters* move their substrate in parallel with the driving ion (Figure 1A). Both driving ion and substrate are bound at the same time and move in the same direction. One part of the transport cycle consists of the movement of the substrate- and ion-free (apo) transporter.

In the *antiporter* transport cycle (Figure 1B), the driving ion is bound during one leg of the cycle while the substrate is bound in the other leg and is transported in the opposite direction.

Variations of the above scheme are common, though. For instance, many symporters transport another ion back instead of the apo leg of the transport cycle. Sometimes, the driving ion is effectively part of the substrate as in the AdiC transporter (Fang et al., 2009), which exchanges *L*-arginine with its decarboxylated product agmatine to effectively export protons.

A third class of related transporters consists of non-coupled transporters. These *uniporters* facilitate diffusion through the membrane. Although we specifically focus on active transporters, the discussion on transport cycles

(Section 6) will make clear that the uniporters are closely related to active transporters and it is plausible that small changes in the protein may convert between the two.

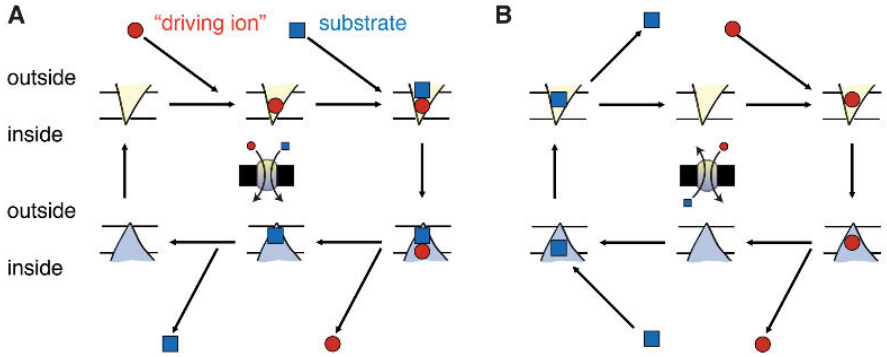

Figure 1. Secondary active transport cycles.
Schematic transport cycle of **A** a symporter (transport of substrate and driving ion in the same direction) and **B** an antiporter (transport in opposite directions). The central cartoon summarizes the physiological function. The V-shaped triangle symbolizes a membrane-embedded transporter protein in the outward facing conformation in which its binding sites are accessible from the outside. The hat-shaped triangle indicates the inward facing conformation. The driving ion is drawn as a circle while the transported substrate is shown as a square. The predominant direction of reactions is shown by arrows, with horizontal arrows indicating binding/unbinding and vertical arrows conformational transitions. The order of binding and unbinding events and the stoichiometry of substrate to driving ions may differ from this cartoon.

In this chapter we focus on overarching principles that are common across almost all secondary active transporters. We begin with the *alternating access model* which provides the "standard model" for explaining transporter function in a structural context (Section 2). Although evolution always finds ways to add a few exceptions to common rules (for instance, there are a few transporters that do not appear to follow the classical alternating access model), the physical principles under which transporters operate are not negotiable. Transporters function out of equilibrium as "physical enzymes" that catalyze transport by free energy transduction through cyclic processes (Section 3). Ten years ago, a remarkable insight was found into the evolutionary mechanism that can generate protein structures that can switch between the two states of the alternating access model: transporters contain so-called inverted repeat sequences that fold into structures with an internal pseudo two-fold symmetry. This symmetry is broken to

generate two different conformations, as discussed in Section 4. A complimentary view of transporters is that of a pore with multiple coupled gates; originally motivated by the description of ion channels as pores with a single gate, this cartoon model has proven valuable because transporters actually contain physical components that perform the functions of gates, as will be shown with selected examples in Section 5. When the alternating access/gated pore model is considered together with the cycle view of transport, a simple unified picture emerges that describes symporters, antiporters, and uniporters as ideals in a spectrum of functionality (Section 6).

4.2. THE ALTERNATING ACCESS MODEL

The *alternating access model* in its basic form was described by Jardetzky (1966) as a polymer molecule that contains binding sites for substrate and is able to assume two different conformations that alternatingly expose the binding sites to the interior and the exterior. The idea of a cyclical process facilitated by a molecule that changes accessibility was expressed by Mitchell (1967) in his "circulating carrier" model. Together these models describe in abstract terms a basic framework or model to understand driven transport across the cell membrane. The key insight was that coupling of two fluxes (substrate and driving ion) could be accomplished by binding to different conformations of the same molecule as discussed in more detail in the next Section 3. In particular, it is physically not possible to move substrate against a gradient through a continuous pore, i.e., one that is simultaneously accessible from both sides, regardless of any energy consuming mechanism to open or close the pore (Tanford, 1983). The consequence of this insight is that transporters cannot function if continuous pores are formed through the membrane. The alternating access model with its two distinct states provides a conceptual framework that avoids pore formation. However, it requires that a membrane protein is able to change between different conformations on the sub-millisecond time scale[1], a speed that is easily achievable for macromolecular conformational changes (Henzler-Wildman and Kern, 2007; Schwartz and Schramm, 2009).

---

1. Turnover numbers of transporters range from one transport event per millisecond (for sodium/proton exchangers) to one per second (some amino acid/cation transporters from thermophiles operating at room temperature) with a typical number on the order of one hundred events per second (e.g., lactose permease); see "transporter turnover rate" in the BioNumbers database https://bionumbers.hms.harvard.edu/ (Milo et al., 2010). This means that any step in the transport cycle, including the conformational transition, must be faster than 1 millisecond for the fastest transporters, and 10 milliseconds or 1 second for the slower ones.

The alternating access model also does not give any insights into the actual molecular structure of a transporter except the general requirement that substrate and ion binding sites must switch accessibility in different conformations. In order to obtain deeper mechanistic insights actual atomic-scale structures of transporters in multiple conformations are needed.

The first secondary active transporter for which the major states in the transport cycle were resolved at atomic resolution was the sodium-coupled symporter Mhp1, a member of the nucleobase-cation-symporter 1 (NCS1) family (Weyand et al., 2011; Jackson et al., 2013; Patching, 2018). The structures of wild-type Mhp1 revealed a sodium binding and a substrate binding site deep at the center of the transporter, roughly at the membrane midplane (Weyand et al., 2008). In one structure, these binding sites were accessible from the extracellular side, making this the outward facing (OF) conformation as shown in Figure 2.

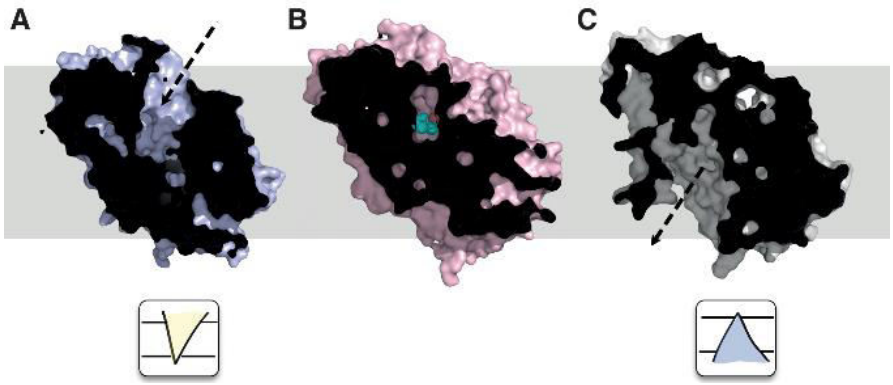

Figure 2. Conformations of the nucleobase/sodium-coupled symporter Mhp1 from X-ray crystallography.
A Outward-facing open conformation (PDB ID 2JLN) (Weyand et al., 2008). **B** Outward-facing occluded conformation with bound substrate benzylhydantoin (PDB ID 4D1B (Simmons et al., 2014); this structure superseded the original 2JLO structure (Weyand et al., 2008) but the structural differences are small). **C** Inward-facing open conformation (PDB ID 2X79; (Shimamura et al., 2010)). The approximate position in the membrane is indicated by the gray rectangle in the background. The two cartoons under **A** and **C** indicate the two states of the classical alternating access model as used in Figure 1.

Shimamura et al. (2010) managed to crystallize wild-type Mhp1 in an inward facing (IF) conformation in which the binding sites were exposed to the intracellular side. Together they represent the two key conformations required by the alternating access model. A third conformation was also found: in this

occluded conformation the binding sites were not accessible from any compartment (Weyand et al., 2008; Simmons et al., 2014). The alternating access model does not require such a conformation. As will be argued in Section 5, such occluded states are a necessary consequence of a molecular architecture in which the alternating access conformations are formed by gate domains.

The hallmark of the alternating access mechanism are relatively large conformational changes in protein conformation and these appear to exist in many secondary transporters for which this mechanism remains the standard structural framework in which to understand transporter function (Boudker and Verdon, 2010; Law, Maloney and Wang, 2008; Forrest and Rudnick, 2009; Gouaux, 2009; Krishnamurthy, Piscitelli and Gouaux, 2009; Abramson and Wright, 2009; Boudker and Verdon, 2010; Kaback et al., 2011; Forrest, Krämer and Ziegler, 2011; Schweikhard and Ziegler, 2012; Henzler-Wildman, 2012; Yan, 2013; Shi, 2013; Slotboom, 2014; Diallinas, 2014; Li et al., 2015; Drew and Boudker, 2016; Bai, Moraes and Reithmeier, 2017; Kazmier, Claxton and Mchaourab, 2017; Patching, 2018; Henderson, Fendler, and Poolman, 2019).

Although the alternating access model is the canonical model for active transporters, some transporters appear not to be described well within this framework. For example, chloride/proton antiporters are currently understood to function by small changes in a central glutamate residue that alternatingly binds chloride and protons (Miller, 2006; Accardi, 2015) and do not require the large conformational change—the "alternating access transition"—that is generally taken to be a key step in the classical alternating access model. However, it could be argued that the fundamental principle of alternating access and the need to maintain a pathway that cannot directly conduct ions and substrate always has to be maintained in order to support the cyclical reactions that are required for energy transduction (see the next Section 3) even though different models are also sometimes discussed (Klingenberg, 2007; Naftalin, 2010).

4.3. THERMODYNAMICS AND CYCLES

Transport is driven by spontaneous influx of a driving ion. The free energy dissipation from flowing down its electrochemical gradient is coupled to the vectorial transport of a substrate molecule or ion. Hill (1989) clearly explained the principle of free energy transduction in transporters (and enzymes) through a cyclic process that tightly couples driving ion flux and substrate flux. Following his treatment, we will first qualitatively explain how a cyclical process that operates out of equilibrium transduces energy. We will then briefly revisit the

thermodynamic driving forces of the process in order to motivate the idea that transporters are really enzymes that catalyze transport.

4.3.1. Transport is a non-equilibrium process

Consider, for instance, a hypothetical antiporter that uses one driving ion (red circle in Figure 3A) to move one substrate molecule (blue square). We initially imagine the system to exist in equilibrium, i.e., the net fluxes between all states are zero, also known as the detailed balance condition. The inside and outside populations i of particles are in Nernst equilibrium, i.e., when considering the concentrations on either side of the membrane and the membrane potential, no net flux of particles would occur if a pore selective for species i were opened in the membrane.[2] For example, the binding of a driving ion to the transporter in the outward facing conformation is the equilibrium reaction

$$T_1 + I \leftrightarrow T_2 : I \qquad (1)$$

and the isomerization between outward facing and inward facing conformation (the alternating access transition) is

$$T_2 : I \leftrightarrow T_3 : I \qquad (2)$$

Because all individual fluxes are zero, no net transport takes place. On average, for every substrate molecule that is moved from inside to outside in a given unit of time, the same number of molecules are moved from the outside to the inside.

We now perturb the system away from equilibrium by increasing the outside concentration of the driving ion, as indicated by the larger number of driving ions in Figure 3B. Following Le Chatelier's principle, the equilibrium of the binding reaction Eq. 1 is moved as to increase the concentration of products (Dill and Bromberg, 2003), i.e., the number of ion-loaded transporters $T_2 : I$ increases above its equilibrium value. Because the reactants (inputs) of the isomerization reaction Eq. 2 are provided by the products (output) of the binding reaction Eq. 1, which have increased, Le Chatelier's principle equally applies to the isomerization and pushes this equilibrium towards the ion-loaded inward facing conformation, $T_3 : I$.

---

2. It is also necessary that the transporter state populations are in equilibrium with each other and the ion and substrate concentrations. However, any imbalance in the transporter populations would soon move towards the equilibrium values, provided that the ion and substrate concentrations are at equilibrium. A transport cycle cannot be driven by the transporter; only the binding/dissociation of external ions and substrates can continuously draw on a source of free energy.

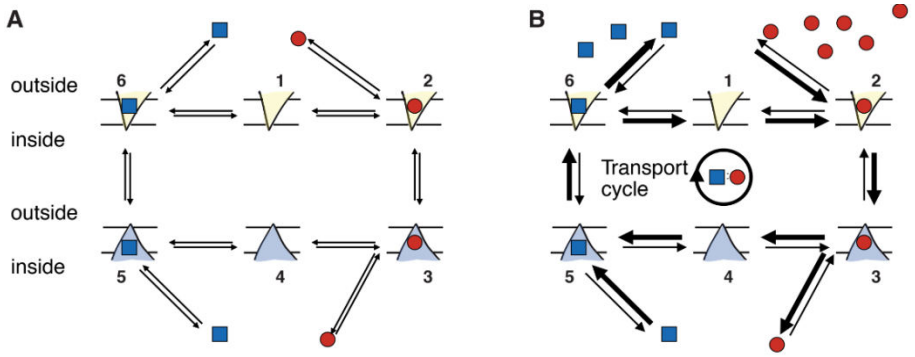

Figure 3. Transport by an antiporter is a cyclical out-of-equilibrium process. **A** Equilibrium—all concentrations are at equilibrium values and all reactions obey detailed balance. **B** Out-of-equilibrium—the outside ion concentration is raised over its equilibrium value, which leads to moving all states out of equilibrium. The states are numbered so that one can refer to, say, the outward facing apo state (neither ion nor substrate bound) of the transporter as T_1 or the inward facing, substrate-bound state as T_5 : S where the presence of the substrate is included for clarity even though the label "5" includes the presence of the substrate (as opposed to state 4, which does not include it).

The same reasoning is applied to each subsequent reaction and in this way, net flux of substrate from the inside to the outside is induced in steps 5→6. Crucially, the reactions form a cycle so that after the steps 1→2→3→4→5→6→1 the transporter is in exactly the same state as it was before. However, the environment has changed as one ion was transported from the outside to the inside and one substrate was transported from the inside to the outside with 1:1 stoichiometry, as expressed by the transport reaction of the antiporter,[3]

$$I_{\text{out}} + S_{\text{in}} \rightarrow I_{\text{in}} + S_{\text{out}}. \qquad (3)$$

The corresponding reaction of the symporter is

$$I_{\text{out}} + S_{\text{out}} \rightarrow I_{\text{in}} + S_{\text{in}}. \qquad (4)$$

Interested readers are referred to Hill (1989) who makes the above reasoning quantitative by considering how the net fluxes between states, which are zero in equilibrium, become biased in one direction when a component is perturbed.

3. Different stoichiometries require different stoichiometric coefficients. For instance, a 2:1 antiporter would be described with $2I_{\text{out}} + \text{Sin} \rightarrow 2I_{\text{in}} + S_{\text{out}}$.

Based on reaction kinetics he develops a theory of cycle fluxes that can be applied to arbitrarily complex cycles to compute steady state populations and fluxes. In particular, more realistic transporter schemes contain additional transitions such as the one between the two apo states $1 \rightleftharpoons 4$, often referred to as leaks or slippage. Such a transition would allow three cycles to become possible: The transport cycle that was just described and two leak cycles: cycle $1 \rightleftharpoons 2 \rightleftharpoons 3 \rightleftharpoons 4 \rightleftharpoons 1$ would dissipate the ionic gradient. Cells spend a substantial amount of their chemical energy to establish the driving ion gradient. In mammals an estimated 19%–28% of ATP are used to power the Na^+-K^+-ATPase that establishes the transmembrane sodium gradient (Rolfe and Brown, 1997). Therefore, dissipation of the sodium gradient is costly and reduces the organism's fitness. The other leak cycle $1 \rightleftharpoons 6 \rightleftharpoons 5 \rightleftharpoons 4 \rightleftharpoons 1$ would run in the opposite direction and let substrate molecules enter the cell, counter to the physiological necessity of the transporter to remove them from the cell. Under physiological conditions, leak cycles must be suppressed by decreasing the rate for slippage transitions such as $1 \rightleftharpoons 4$.

The qualitative discussion makes clear that energy transduction, i.e., the use of the free energy stored in the driving ion gradient, requires a complete cycle that contains both ion and substrate translocation steps. If any part of the cycle is broken, no energy transduction can take place. Thus, energy transduction is a property of complete cycles and not of individual states (Hill, 1989). Therefore, there is no specific step in the cycle that could be described as an "energized" state or a state where energy is "gained by a binding reaction" (Hill and Eisenberg, 1981).

In general, a protein that functions according to the alternating access mechanism cannot function if it presents a continuous, leaky pathway (Tanford, 1983) as this prevents energy coupling. Similarly, non-productive leak cycles also reduce the efficiency of a transporter. Although here we generally discuss ideal, fully efficient cycles to elucidate the basic principles, real transporters leak and therefore their transport stoichiometry is generally not the ideal one (Hill, 1989; Henderson, Fendler and Poolman, 2019). For example, instead of an ideal 1:1 stoichiometry one might measure only 1:0.75, i.e., on average 1.33 driving ions are needed to move one substrate because only 75% of the total flux comes from productive cycles (1:1 stoichiometry) and 25% comes from leak cycles (1:0).

The ion and substrate binding or dissociation steps are necessary components of the cycle because without them the cycle cannot be driven in a specific direction: these steps provide the only external "handle" to control the process (Zuckerman, 2019). Therefore, no cyclical process with a net flux in one direction exists in which only a protein changes through a repeated sequence of

conformational states; coupling to an external source of free energy is always necessary.

Finally, it is worth emphasizing that because the transporter protein moves cyclically through different conformations, it is not altered in any permanent way. In the energetic description of the process (see Section 3.2 below), the transporter does not appear. Thus, transporters act as enzymes for moving substrate, similar to how biochemical enzymes catalyze the formation and breaking of chemical bonds. In this sense, transporters are "physical enzymes" or "molecular machines" in that they catalyze a physical process instead of a chemical one. Other proteins of this kind are molecular motors, which turn chemical energy into movement of the protein itself, or rotary pumps such as the V-type and P-type ATPases, which turn chemical energy into rotary motion and movement of protons or ions across the cell membrane; the latter can run in reverse to turn rotary motion by ion flow into chemical bonds. Similarly, transporters run backwards if the concentrations are changed appropriately, which becomes obvious when analyzing the thermodynamic driving forces.

4.3.2. Driving forces

Quantitatively, the only thermodynamic driving forces X_i are the ones originating in electrochemical potential ($\mu' = \mu_0 + kT \ln c/c_0 + q\Psi$) differences of ions and substrates across the cell membrane (Dill and Bromberg, 2003); free energy differences due to the different states of the protein cancel in the whole cycle and play no role (Hill, 1989). The driving force for species $i \in \{I,S\}$ is

$$X_i = \mu'_{i,\text{in}} - \mu'_{i,\text{out}} = kT \ln(c_{i,\text{in}}/c_{i,\text{out}}) + q_i\Delta\Psi \qquad (5)$$

where c_i is the concentration (or activity) on the indicated side of the membrane, q_i the charge, $\Delta\Psi = \Psi_{\text{in}} - \Psi_{\text{out}}$ is the transmembrane potential, T is the temperature and k is Boltzmann's constant. The membrane potential is typically negative, $\Delta\Psi < 0$. Thus, for typical driving cations (Na^+, H^+ with $q = +1e$) and $\Delta\Phi \approx 100$mV the membrane potential contributes at $T = 298$ K about $q_I\Delta\Psi \approx -3.9\ kT$. Typical sodium concentrations are on the order of 100 mM on the outside and 10 mM inside a cell and hence $kT \ln c_I,\text{in}/c_I,\text{out} = -2.3\ kT$. If the substrate is neutral (the electrostatic component is zero for $q_S = 0$) then a positive net charge is moved into the cell down an electrostatic potential and a sizable fraction of the available free energy will be provided from the membrane potential component. In general, any

electrogenic transport (movement of a net charge) is affected by the membrane potential.

Denote by J_i the flux at which particle i is transported across the membrane (in particles per unit time), with the direction out→in counting as $J_i < 0$ and the reverse as $J_i > 0$. Note that in a simple cycle such as the one in Figure 1, exactly one ion is moved for each substrate molecule and hence the absolute values of these fluxes must be the same, $|J_I| = |J_S|$ but the signs will differ, depending on symport or antiport processes.

When the driving force is negative, e.g., $X_I < 0$, then spontaneous movement occurs, such as influx of the driving ion and hence $J_I < 0$. The antiporter is supposed to move substrate against a gradient from the inside to the outside, i.e., against the opposing driving force $X_S < 0$ under which S particles would spontaneously move into the cell. The rate of free energy dissipation is

$$\Phi = J_I X_I + J_S X_S \geq 0. \qquad (6)$$

$\Phi = 0$ holds in equilibrium but then no transport occurs (see Section 3.1). The second law of thermodynamics requires $\Phi > 0$ in non-equilibrium steady state, i.e., when concentrations remain fixed at their non-equilibrium values and do not change (Hill, 1989). In steady-state, the transporter moves ions and substrates at a constant flux. Under which conditions will the antiporter move S from inside to outside, i.e., given $J_S > 0$ (even though $X_S < 0$), what is required of I? Rearranging Eq. 6

$$J_I X_I > -J_S X_S \qquad (7)$$

and noting that the right hand side is positive, it follows that $J_I X_I$ also has to be positive, i.e., the driving ion must flow down its electrochemical gradient from the outside to the inside ($J_I < 0$, $X_I < 0$). In other words, spontaneous fluxes always dissipate free energy, which can be coupled to the substrate flux. This free energy dissipation rate must be larger than the rate of free energy required to move S against its driving force. For a simple antiporter cycle without leakage, $J_S = -J_I$ (for each I transported to the inside, one S is transported to the outside, in the same amount of time) and hence $-J_S X_I > -J_S X_S$ and with $J_S > 0$,

$$X_I < X_S \text{ (simple antiporter)} \qquad (8)$$

is required for transport. The amount of available free energy per driving ion translocation event must be larger (more negative) than the substrate gradient

against which S is moved because out of equilibrium not all free energy can be transformed into useful work and a fraction always increases the entropy of the universe in the form of heat, as required by the second law. The condition Eq. 7 can also be fulfilled with $J_I > 0$, $X_I > 0$, i.e., a spontaneous flux of ions from the inside to the outside. In this case the transporter would need to be able operate as a symporter to move driving ion and substrate together (it cannot happen in separate cycles (Hill, 1989)).

For a simple symporter with $X_I < 0$, $X_S > 0$ and $J_I = J_S < 0$, the condition equivalent to Eq. 8 reads

$$X_I < -X_S \text{ (simple symporter).} \qquad (9)$$

We will come back to the question of the relationship between symporters and antiporters in Section 6 where we will see that one can write a universal kinetic scheme that encompasses symporters, antiporters, and uniporters.

4.4. INVERTED REPEAT SYMMETRY

The alternating access model together with the thermodynamic cycle analysis explains how transporters function in principle, i.e., they describe the physical constraints under which any transporter protein has to operate. However, understanding *how* these principles are embodied in an actual biomolecule requires structural atomic-resolution data, primarily provided by X-ray crystallography and electron microscopy. The most important requirement of the alternating access model is the existence of *two states* that make binding sites accessible to the outside or the inside, generally referred to as an *outward facing* (*OF*) *conformation* and an *inward facing* (*IF*) *conformation*. It turns out that a viable evolutionary path to create a switchable two-state system in a single protein molecule can be based on an internal two-fold structural symmetry, so-called *inverted repeats*. This deep insight into a fundamental principle of transporter function was only recently discovered by Forrest et al. (2008) and since then broadly recognized as nearly universal (Forrest, 2013, 2015).

4.4.1. Inverted repeat structures

Structural symmetry is well represented among membrane proteins. These symmetries can arise due to oligomerization, often seen in cyclically symmetric channels and pores, or due to the presence of internal repeats within the protein

sequence (Forrest, 2015). Notably, internal repeats occur more frequently in membrane protein super-families than overall (Myers-Turnbull et al., 2014); in the case of secondary active transporters, most known structures show an *inverted repeat symmetry* (Bai, Moraes and Reithmeier, 2017; Shi, 2013)—that is, internal repeats which adopt similar folds but start on opposite sides of the membrane, giving rise to C_2 pseudosymmetry about an axis parallel to the membrane plane. Further common to most secondary active transporters is the presence of two bundles or domains, with the substrate binding sites located near the interface and often involving discontinuous helices (Shi, 2013). The exact number of transmembrane helices and distribution of the inverted repeats over the two domains differs, with several common folds observed (Figure 4):

(3 + 3) + (3 + 3): Major Facilitator Superfamily (MFS). The core MFS fold contains 12 transmembrane helices (TMs) (Law, Maloney and Wang, 2008; Yan, 2013). An Nand C-domain are each formed from a pair of 3 TM inverted repeats, and are themselves two-fold pseudosymmetric. The MFS is one of the largest transporter families found across multiple organisms; the first structures were reported for lactase permease LacY (Abramson et al., 2003) and glycerol-3-phosphate transporter GlpT (Huang et al., 2003), with many determined since.

(5 + 5): LeuT fold. The LeuT fold consists of 5 TM inverted repeats, with the first two helices from each repeat forming a core bundle (i.e. TMs 1, 2, 6, 7), while the next two (TMs 3, 4, 8, 9) form a scaffold/hash domain; TMs 5 and 10 may act as gates (Kazmier, Claxton and Mchaourab, 2017). First observed in the neurotransmitter/sodium symporter LeuT (Yamashita et al., 2005), several other transporters have been found to adopt this fold, including the sodium/hydantoin transporter Mhp1 (Weyand et al., 2008).

(5 + 5): NhaA fold. Also consisting of 5 TM repeats, the NhaA fold is observed in sodium/proton antiporters (e.g. NhaA (Hunte et al., 2005)) and the apical sodium dependent bile acid transporter (ASBT) family (e.g. ASBTNM (Hu et al., 2011)). The first two helices of each repeat (TMs 1, 2, 6, 7) form a panel or dimer domain, with the remaining three (TMs 3-5, 8-10) forming a core domain (Fuster and Alexander, 2014; Padan, 2014).

(7 + 7): 7-TM inverted repeat (7TMIR) fold. Relatively recently identified, transporters with this fold include the proton/uracil symporter UraA and chloride/bicarbonate antiporter AE1; four helices from each repeat (TMs 1-4, 8-

11) for a core domain, while the remaining three (TMs 5-7, 12-14) form a gate domain (Chang and Geertsma, 2017).

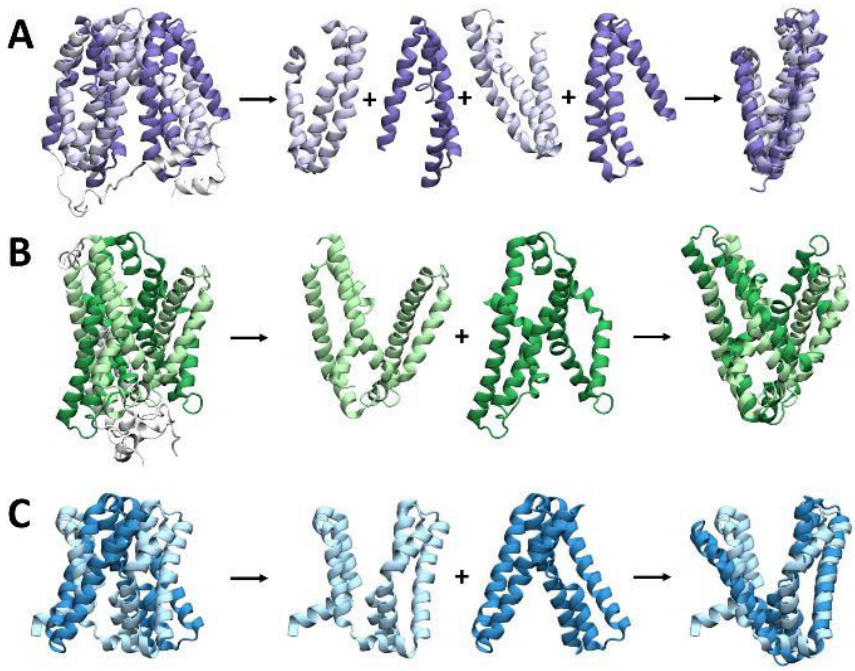

Figure 4. Representative structures of common secondary active transporter folds, highlighting the inverted repeats.
In each case, the protein is first shown whole, then with the repeats separated translationally, and finally with the second repeat rotated and overlayed on the first. **A** LacY (inward facing, MFS fold; PDB ID IPV6) **B** Mhp1 (outward facing, LeuT fold; PDB ID 2JLN) **C** ASBTNM (inward facing, NhaA fold; PDB ID 3ZUY).

Internal repeats such as these have been speculated to arise from the duplication of an ancestor gene and subsequent fusion event, in this case following a flip of one duplicate relative to the membrane; possible candidates showing these initial "half" folds have been identified in the DedA (for the LeuT fold) and SWEET (for the MFS fold) families (Keller, Ziegler and Schneider, 2014). The EmrE multidrug transporter is proposed to come together as an antiparallel dimer and function through an exchange of asymmetrical structures similar to that described below (Korkhov and Tate, 2009; Morrison et al., 2012), and represents a possible pre-fusion step in the proposed duplication-and-fusion evolutionary process of inverted repeat symmetry.

Distinct inward- and outward-facing conformations arise from asymmetry in the exact folds of the repeats composing the two domains (discussed in Section 4.2), which changes the relative locations/orientations of these domains. Several mechanisms for this relative motion have been proposed (Drew and Boudker, 2016; Forrest, Krämer and Ziegler, 2011): the domains may rotate about the substrate binding site to alternatively expose it to each side of the membrane, as in the *rocker-switch* (where the domains are structurally symmetric, proposed for e.g. for MFS transporters (Radestock and Forrest, 2011)) and *rocker-bundle* (where the domains are distinct, e.g. for LeuT fold transporters (Kazmier, Claxton, and Mchaourab, 2017)) mechanisms; or, as in the *elevator mechanism*, one domain predominantly containing the binding site may move perpendicular to the membrane, moving the binding site against to relatively fixed second domain to expose it to each side of the membrane in turn (proposed for e.g. for NhaA fold transporters (Padan, 2014)).

4.4.2. Asymmetry and alternating access

While inverted repeats share an overall fold, they are found to take on different conformations, giving rise to an asymmetry that allows the substrate binding site to be exposed to one side of the membrane while blocked from the other. By exchanging conformations between the two repeats—with the first repeat adopting the conformation of the second and vice versa—the protein is thus able to switch between an inward facing and an outward facing state (Forrest, Krämer, and Ziegler, 2011) (Figure 5).

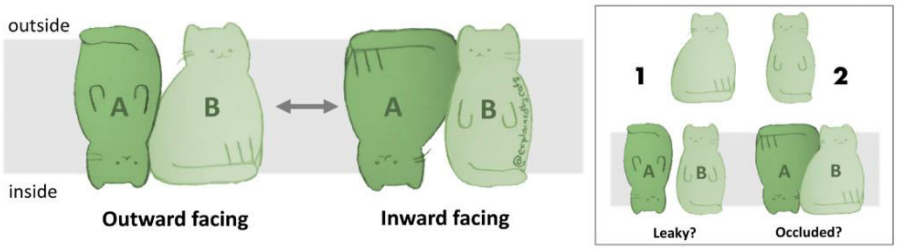

Figure 5. Cartoon showing how symmetry-broken inverted repeats generate the two major conformations in the alternating access mechanism.
Each repeat (labeled **A** and **B**) may take on one of two conformations (shown as 1 and 2 in the inset), giving rise to 2 x 2 = 4 possible conformations, though two (occluded and "leak" states, shown inset) are not part of the basic alternating access mechanism.

Exchanging conformations in this way means there is no or little net energetic change in the overall protein structure from the inward-to-outward or outward-to-inward transitions (Forrest, 2015). The presence of two possible conformations for each of the two repeats also brings up the question of whether the repeats can possess the same conformation at a given time; such overall conformations might form occluded (closed at both side) or leaky (open on both sides) states of the transporter (Figure 5; inset). The presence of occluded and leak states in the transport cycle is discussed further in Section 5.

The above described *repeat swapping* has been taken advantage of to generate homology models of transporters in different states, given a structure in only one state: the conformation of each repeat is used as a template for the other, forcing the exchange of conformations (Vergara-Jaque et al., 2015). This method was first applied to LeuT (Forrest et al., 2008), producing a structure that latter proved to be consistent with an experimental structure (Krishnamurthy and Gouaux, 2012), and has since been used to generate structures for a range of secondary active transporters, with subsequent experimental validation obtained in several cases; including the glutamate transporter GltPh (Crisman et al., 2009; Reyes, Ginter and Boudker, 2009), LacY (Radestock and Forrest, 2011), CcdaA (Zhou and Bushweller, 2018) and NhaA (Schushan et al., 2012).

4.5. TRANSPORTERS AS GATED PORES

Läuger (1980) envisaged ion channels as pores with a single free energy barrier, which can be identified with the gate of the channel that controls ion flow in response to external stimuli (Hille, 2001). He could model transporters as pores with two coupled barriers (Läuger, 1980); motivated by the suggestive original "gated pore model" (Klingenberg, 1979) (which was more precisely renamed the "single binding center gated model" (SBGP) (Klingenberg, 2007)) one may also call these two barriers gates (Figure 6) (Abramson and Wright, 2009; Krishnamurthy, Piscitelli and Gouaux, 2009; Forrest, Krämer and Ziegler, 2011). Such a gate should be thought of as a switch or bi-stable element that can exist in two states that are generally called "open" and "closed" although it might also carry the meaning "outward facing" or "inward facing". The gate picture reduces the nuanced view of free energy barriers with variable barrier height to one in which either a very high barrier exists ("closed") or the barrier is small compared to thermal fluctuations ("open"). This simplification allows one to broadly enumerate and categorize states and make general (but necessarily approximate) statements for whole classes of proteins. It also allows one to create simple

cartoons of transporter states that summarize transporter conformations succinctly. As will be shown below, the cartoon is a useful abstraction because gates correspond to physical molecular domains in transporter proteins (i.e., they have a molecular identity) and thus states generated from the gate picture directly correspond to observable protein conformations.

In ion channels, a change in membrane potential or binding of a signaling molecule opens the gate and ions spontaneously flow through the open pore down their electrochemical gradient (Hille, 2001), as shown for a pore with $N = 1$ gate in Figure 6.[4] In the "transporters as gated pores" picture, the coordinated movement of two (or more) gates creates the conformations of the alternating access model (Section 2). The outward facing open state is formed when the outer gate opens while the inner gate remains closed. Conversely, the inward facing state consists of the outer gate closed, while the inner one is open, as shown for a transporter with $N = 2$ gates in Figure 6. Simultaneous opening of both gates must be avoided—a "leak" state (see Figure 6)—to prevent leakage of the driving ion and dissipation of the ionic gradient. The coordination of the gates is termed "coupling". Furthermore, conformational changes (i.e., changes in the gates) must also be coupled to the binding/dissociation of driving ion(s) and substrate(s), a point that will be revisited below and explicitly included in Section 6. For simplicity, we will focus on the different conformational states of the protein while keeping in mind that the presence of ions and/or substrates will likely change the structure to some degree.

It has been observed experimentally that under certain conditions transporters can also function as channels (DeFelice and Goswami, 2007), a view that fits naturally in the picture of a transporter whose gates are not fully coordinated so that leak states may occur (see Figure 6) although many questions remain in this somewhat under-explored area. Channel-like behavior is characterized by spontaneous energetically downhill diffusion of ions (or substrates) in a non-stoichiometric and burst-like fashion, which differs from the leak cycles that can occur in the standard cycle due to loose coupling (Henderson, Fendler and Poolman, 2019) in that the latter still only move individual particles. Even for the channel-like behavior of transporters, it is not necessarily clear that the canonical transport pathway is used. It is possible that alternative pathways through the protein are responsible (Vandenberg, Huang and Ryan, 2008).

4. Describing a channel with a single gate is an oversimplified picture because many ion channels contain an activation gate and a separate inactivation gate, which switches the channel into a relatively long lasting inactive state (Hille 2001). These gates are typically coupled to some degree, e.g., the inactivation gate might only close when the activation gate has closed but the coupling is presumably different from the coupling between gates that enables energy transduction in transporters.

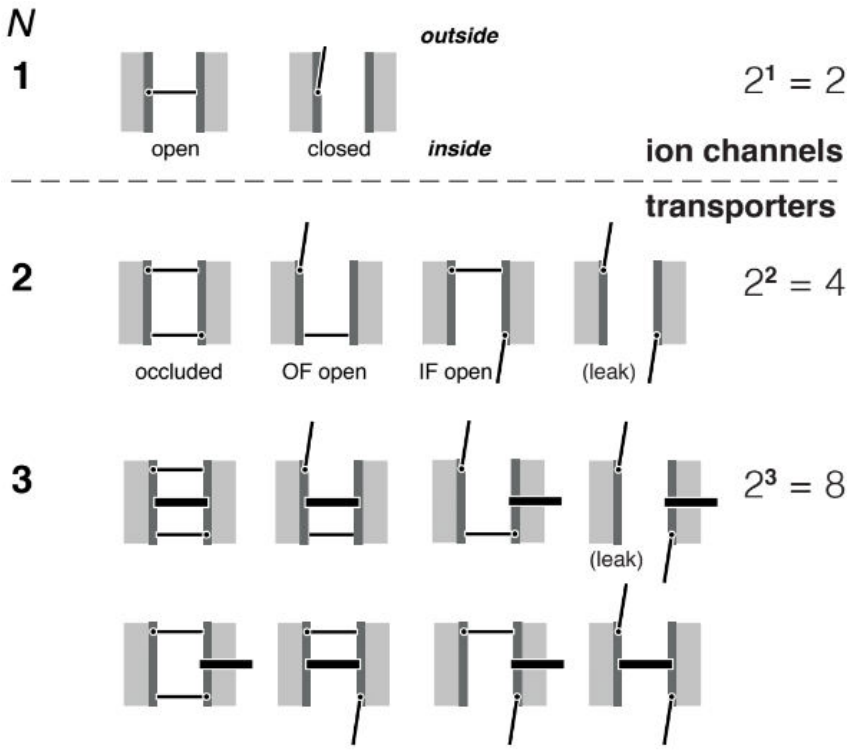

Figure 6. Ion channels and transporters as gated pores.
In this simplified picture, ion channels contain a single gate that is controlled by external stimuli. Transporters can implement alternating access by the coordinated movement of two or more gates. The number of gates N determines the total number of distinct states, 2^N. Not all states might be physiologically observed, and some, such as the leak states, will prevent energy transduction.

Nevertheless, the "transporters as gated pores" picture is more than just a convenient cartoon model because as we will discuss below, the gates generally represent a molecular reality, i.e., secondary transporters contain distinguishable parts that function as gates. Therefore, conformational states that are predicted from the gated pore model generally correspond to conformations with distinct structural arrangements of the corresponding gates.

4.5.1. Gates as molecular building blocks

Since X-ray crystallography has revealed the molecular structures of a range of transporters, various authors have identified domains of these proteins that

regulate access to binding sites with gates, as summarized by Forrest, Krämer and Ziegler (2011). A particular terminology of *thin* and *thick* gates originated in the structural analysis of LeuT-like transporters (Krishnamurthy, Piscitelli and Gouaux, 2009; Abramson and Wright, 2009). Thin gates are generally considered to be parts of the protein whose movement can prevent the exchange of ions or substrates with the intra- or extracellular solution. Perhaps somewhat confusingly, the conformational transition that is responsible for alternating access, or rather the sum of moving structural elements, is sometimes considered the thick gate. In other transporter families, such as the MFS transporters, no special distinction between thin and thick gates is commonly made.

Although there is some ambiguity in how to define gates, they are nevertheless recognizable molecular entities. Diallinas (2014) concludes, based on work in the purine transporter UapA, that physiological transport properties are determined by intramolecular interactions between binding sites and gating elements, similar to ones present in channels. LeVine et al. (2016) quantitatively analyzed the mechanism of the LeuT transporter with a particular emphasis on the allosteric coupling between ions, substrate, and the protein. Based on experimental and simulation data, they concluded that LeuT is best described with an allosteric gated pore alternating access mechanism in which gate movement is strongly coupled to binding and the other gates.

We will illustrate the physical reality of gates in transporters in an example, the Mhp1 transporter (a member of the LeuT-like family of APC (amino acid-polyamine-organoCation) transporters (Västermark et al., 2014)), and in Section 5.2, where also members of the major facilitator superfamily (MFS) (Marger and Saier,1993) will be included.

4.5.1.1. *Thin and thick gates in Mhp1*

The hydantoin permease Mhp1 from *Microbacterium liquefaciens* is a nucleobase-sodium symporter (Suzuki and Henderson, 2006), a member of the NCS1 family (Patching, 2018). It co-transports one sodium ion with one 5-substituted hydantoin. It shares a five-helix inverted repeat architecture with other members of the superfamily of LeuT-like transporters (Cameron, Beckstein and Henderson, 2013). X-ray crystallographic structures of Mhp1 in outward facing and inward facing conformations together with computer simulations revealed the structural basis for the alternating access mechanism in this secondary transporter (Weyand et al., 2008; Shimamura et al., 2010; Simmons et al., 2014). The transporter can be understood as a gated pore with two thin and one thick gate (Krishnamurthy, Piscitelli and Gouaux, 2009), i.e., as a pore with three gates: The thick gate regulates the passage through the center of the membrane by means of

the large conformational change that switches the transporter from its outward facing to its inward facing conformation. In Mhp1 it consists of the hash motif (formed by helices TM3, TM4 and their inverted-repeat counterparts TM8 and TM9; see Figures 7A, C and 4B) that can rotate by about 30° on an axis parallel to TM3 relative to the four-helix "bundle" (TM1, TM2 and TM6, TM7) (Shimamura et al., 2010). Thin gates are formed by the N-termini of the pseudo-symmetry related helices TM5 and TM10 and the linker to each preceding helix (Shimamura et al., 2010). The extracellular (EC) thin gate (TM10; Figure 7B) governs access to the substrate binding site from the periplasmic medium while the intracellular (IC; Figure 7D) gate fulfills the symmetrical role of controlling the pathway to the cytosol.

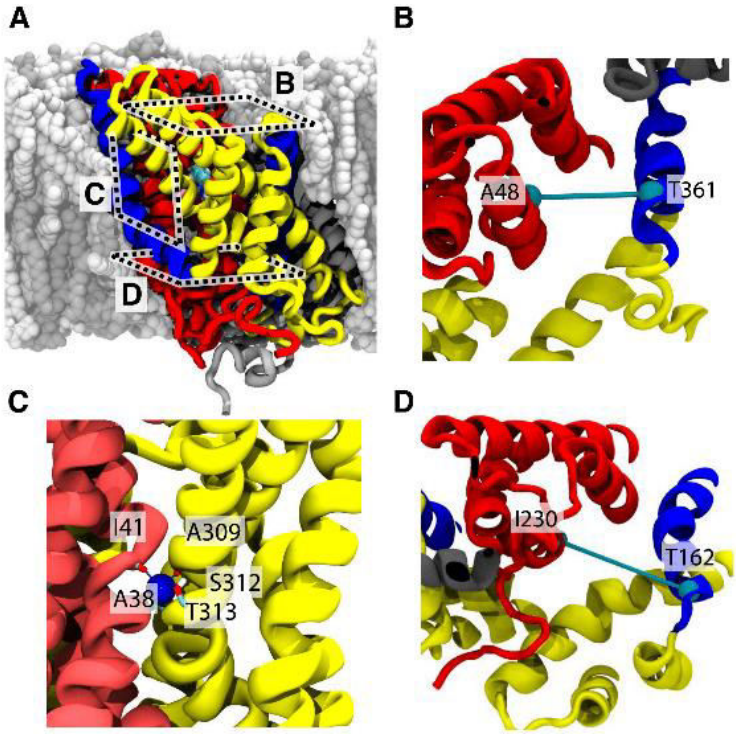

Figure 7. The three gates in Mhp1.
A Mhp1 in the membrane. The hash motif (helices 3, 4, 8, 9) is shown in yellow, the bundle (helices 1, 2, 6, 7) in red, flexible (thin gate) helices 5 and 10 in blue, and C-terminal helices 11 and 12 in gray. The views on the gates (B–D) are indicated by broken rectangles. **B** extracellular thin gate (formed by TM10). **C** thick gate, quantified by the distance across the Na2 sodium binding site. **D** intracellular thin gate (TM5).

The sodium binding site is formed between bundle and hash, so opening of the thick gate, i.e., the alternating-access transition, opens up the sodium binding site and weakens ion binding to ensure rapid diffusion of the ion into the cytosolic compartment and opening a pathway for the substrate to follow (Shimamura et al., 2010).

The role of the thin gates in Mhp1 appears to be more subtle (and might well differ from the role of thin gates in related NSS-like transporters such as LeuT (Kazmier, Sharma Islam, et al., 2014; Kazmier, Sharma Quick, et al., 2014; Kazmier, Claxton and Mchaourab, 2017). In Mhp1, the whole N-terminus of TM10 moves together with the linker between TM9 and TM10 (Weyand et al., 2008; Shimamura et al., 2010; Kazmier, Sharma Islam, et al., 2014), thus forming a distinct gate structure that is mirrored in TM5 and the TM 4-5 linker, which are related to TM9/10 through the inverted-repeat symmetry as described in Section 4 and shown in Figure 4B.

As discussed in Section 2, a protein that functions according to the alternating access mechanism cannot function if it presents a continuous, leaky pathway (Tanford, 1983) [or if it allows too many non-productive leak cycles to occur (Section 3)]. The EC gate appears to prevent Mhp1 from leaking the driving ion, Na^+, as demonstrated by modeling: Figure 8B shows that in the inward facing conformation, with the EC gate closed, the solvent accessible surface only extends from the IC side into the binding site at the center of the protein. However, when the EC gate is removed (the atoms were deleted from the structure as a simple model of a hypothetical inward facing conformation with an open EC gate) a pathway opens up through the membrane (Figure 8D). The calculated electrostatic solvation free energy (Born energy) in the volume of the pathway shows that Na^+ ions could traverse the membrane because a low-energy path is visible (Figure 8D). On the contrary, in all other states, no low energy path can be found for a sodium ion (Figures 8A–C) because either the thick gate or the EC gate blocks the passage. Thus, the EC gate fulfills an important role in preventing a sodium ion leak. It is required because the switch in the thick gate does not just simply change the conformation from outward to inward facing but it really acts as a gate that is open for inward facing and closed for outward facing.

Additionally, the EC gate is involved in substrate selectivity (Simmons et al., 2014). Mhp1 transports 5-substituted hydantoins (Patching, 2011; 2017) where the substituent must be a bulky hydrophobic moiety such as a benzyl or indolylmethyl group. However, if the 5-substituent is too voluminous such as a naphthyl group, transport is inhibited even though the molecule binds tightly. A crystal structure of outward-facing Mhp1 with 5-(2-naphthylmethyl)-*L*-hydantoin bound revealed that the EC gate was trapped in an open conformation due to a

steric clash of the naphthyl ring with Leu363 (Simmons et al., 2014; Patching 2017, 2018). A Leu363Ala mutant of Mhp1, which removes the clash, was competitive for transporting 5-(2-naphthylmethyl)-*L*-hydantoin.

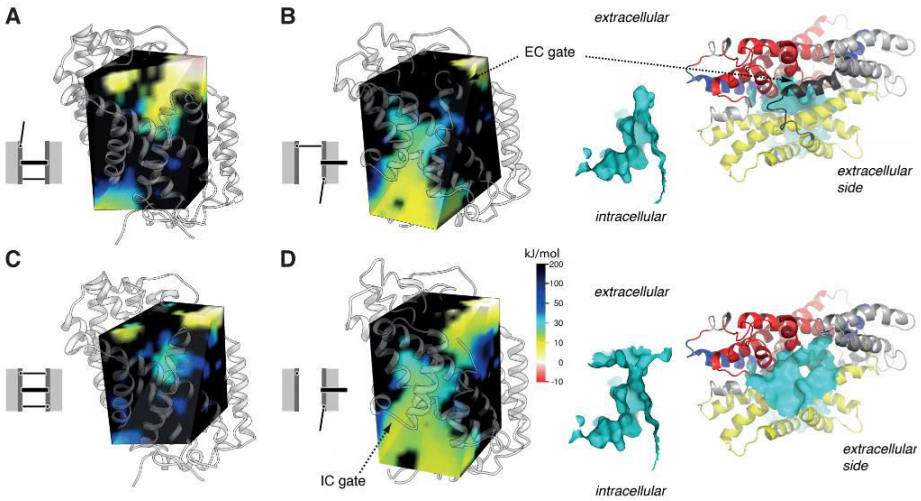

Figure 8. The putative role of the extracellular (EC) gate of Mhp1 is to prevent a sodium leak when the thick gate is open.

The left four panels show a cut through the electrostatic solvation free energy (Born energy) landscape of a Na^+ ion inside Mhp1 for different conformations of the transporter, computed with the Poisson-Boltzmann equation. Red (-10 $kJ.mol^{-1}$) to yellow (+10 $kJ.mol^{-1}$) regions can be considered accessible for sodium ions under typical conditions. (The Na^+ Born energy was calculated as described previously (Stelzl et al., 2014).) The gate cartoons in **A**–**C** represent some of the states for the triple-gated transporter in Figure 6; the cartoon in **D** symbolizes a leaky state that was artificially modeled by removal of the EC-gate portion of TM10. **A** Outward facing open conformation (EC gate open, thick gate closed). **B** Inward facing open conformation (EC gate closed, thick gate and IC gate open). The solvent accessible surface (cyan) is shown from the side in the context of the protein helices (view on the surface from the top). The color scheme for the helices is the same as in Figure 7, except that the N-terminal half of the EC gate (TM10) is shown in black. The closed EC gate prevents a continuous sodium pathway. **C** Outward facing occluded conformation (EC gate closed, thick gate closed). **D** Simple model for a hypothetical inward facing open, leaky conformation with IC gate an thick gate open and EC gate removed. The solvent accessible surface representation and the electrostatic free energy show a sodium pathway through the membrane-spanning portion of the transporter.

These results strongly suggest that closure of the EC gate is required for the alternating access transition to occur. In the language of the gated pore view, the thin EC gate is coupled to the thick gate. Structural comparison suggests that this coupling is due to the geometrical architecture and the direct connection of the rotating hash motif to the EC gate through the 9-10 linker. The thick gate cannot move into the space occupied by the open EC gate and therefore is prevented from closing. Conversely, the open thick gate appears to latch the EC gate in its closed position (Shimamura et al., 2010).

4.5.2. Gate states

Thinking of transporters as consisting of N gating elements that can individually switch between two states (such as open and closed as in Figure 6) suggests a simple count to enumerate the possible number of conformations,

$$n_C = 2^N. \qquad (10)$$

For a transporter with two gates, four states are possible, and eight states for $N = 3$.[5] The simple count ignores the fact that gate movement must be coordinated in some fashion. The type of coupling will depend on the individual molecule and may even depend on the substrate (Henderson, Fendler and Poolman, 2019) but for canonical transport one might want to assume that a leak state with all gates open plays no important role and so $n_C = 2^N - 1$.[6]

The primary advantage of such a simple enumeration is to provide a framework in which to place experimentally or computationally observed conformations. Forrest, Krämer and Ziegler (2011) proposed a similar classification with eight states, consisting of different conformations and with differing substrate occupancy. Their scheme makes use of thin gates but places central importance on the major conformational switch between inward and outward conformations. It has been successfully used to, e.g., categorize the wealth of structural data for APC transporter BetP, for which crystal structures are obtained for most states (Ressl et al., 2009; Perez et al., 2012; Perez et al., 2014), and to analyze four LeuT-fold transporter simulated transitions (Jeschke, 2013).

---

5. We equate a state with a conformation of the transporter, assuming that each state is formed by an distinguishable ensemble of conformers near the specific conformation. This typically implies that there is a kinetic separation between states. Although this is not necessarily always the case in practice, we will nevertheless use state and conformation interchangeably to keep the discussion simple.

6. One could write $n_C = 2^N - F$ where $0 \leq F < 2^N$ is the number of "forbidden" conformations if one knew through other means which conformations were not accessible.

An almost trivial prediction of the gated pore model is the existence of occluded states. In an occluded state, the transporter obtains a conformation in which the binding sites are not accessible from either compartment. In the doubly-gated pore, the occluded state naturally arises when the two gates are closed (N = 2 in Figure 6). The alternating access model and the associated kinetic and thermodynamic analysis do not require occluded states for energy transduction and vectorial transport. Therefore, the existence of occluded states, which are not strictly necessary for function, could be interpreted as a consequence of the structural constraints of the implementation of alternating access (via inverted repeat symmetry) in proteins. Below we will show some structural evidence for occluded states. But it is also noteworthy to point out that molecular dynamics (MD) computer simulations have been able to generate occluded states when started from crystallographic conformations corresponding to inward or outward facing states: For example, Latorraca et al. (2017) simulated the LbSemiSWEET transporter with unbiased MD and observed full transitions from outward to inward facing states that passed through an occluded state. The simulation spontaneously reached experimentally determined structures for inward open and occluded LbSemiSWEET. They found that the transitions were driven by favorable inter-helical interactions when either the extracellular or the intracellular gate closed and and unfavorable helix configuration when both gates were closed. The two gates became tightly coupled, which prevented simultaneous gate opening, which would result in a leak state. Other simulation examples are discussed below, which all point to the insight that molecular gates are a simple way to generate alternating-access states. Without specific coupling that prevents two gates from closing at the same time, occluded states will occur.

4.5.2.1. MFS transporters: two gates

MFS transporters all share a common fold with four inverted repeats (Figure 4A). It was originally believed that alternating access would proceed by a rigid body movement whereby the two halves of the protein would move relative to each other in a “rocker switch” manner (Law, Maloney and Wang, 2008). Discussion concentrated on LacY for which an alternative model described the protein as more flexible, with cytoplasmic and periplasmic openings governing access to the binding site, effectively describing gates (Kaback et al., 2007). The existence of an occluded state in LacY corroborated the gated pore model for its mechanism. Stelzl et al. (2014) hypothesized that LacY functioned as a pore with two coupled gates that could both close at the same time. With this assumption they could perform biased MD simulations to generate a model of occluded LacY with both gates closed. The model broadly agreed with double electron-electron resonance

(DEER) spectroscopy data. Recent experimental evidence for an occluded mutant) (Smirnova, Kasho and Kaback, 2018) corroborated the model.

The MFS transporter $PepT_{So}$ is a proton-coupled bacterial symporter for which only inward facing crystal structures are known (Newstead et al., 2011; Fowler et al., 2015). An open question has been the nature and molecular mechanism of the conformational transition between inward and outward conformation. Fowler et al. (2015) used an array of experimental and computational techniques, including X-ray crystallography, DEER and MD, to elucidate the dynamics of $PepT_{So}$. They found that $PepT_{So}$ is representative for a large number of MFS transporters in that the ends of the first two helices in each of the four inverted repeats (see Figure 4A) form gates at the EC and IC entrance. A wealth of structural data exists for the MFS transporters (Yan, 2013) with many transporter structures having been solved to atomic resolution in different conformations. Fowler et al. (2015) analyzed 33 MFS structures in terms of the minimal pore radius near the periplasmic (extracellular, EC) and cytoplasmic (intracellular, IC) entrance (Figure 9). The structure could neatly be categorized as outward or inward facing, or occluded, based either on geometrical constriction radius (Figure 9A) or on distances of the inverted-repeat gates (Figure 9B).

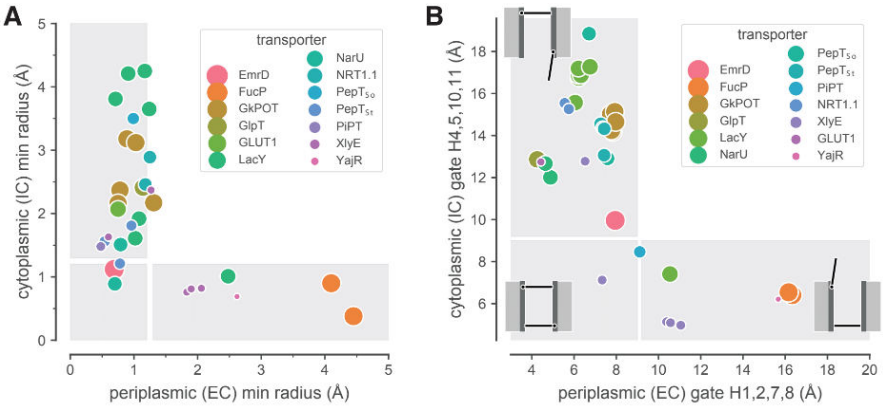

Figure 9. Conformational state of MFS transporters from crystal structures. The gray rectangles approximately indicate classification of the structures as outward open, occluded, or inward open. **A** Minimal pore radii *R* computed with HOLE (Smart et al., 1996) near the periplasmic and cytoplasmic entrance. A conformation is classified as occluded if both R ≤ 1.2 Å. **B** Gate distances *d*, calculated as the minimum distance between the C_α atoms of the relevant pairs of helix tips H1,2,7,8 (periplasmic gate) or H4,5,10,11 (cytoplasmic gate) (Fowler et al., 2015). A conformation is classified as occluded for both $d \leq 9$ Å. Figure drawn after Fowler et al. (2015).

Using multiple MD simulation with a Markov state model, Selvam, Mittal and Shukla (2018) sampled conformational transitions from the inward facing conformation through an occluded state to an outward facing conformation of $PepT_{So}$. Their computational results were validated by comparison of simulated with experimental DEER spectroscopy data. The occluded state forms by closure of both ends of the protein. In a computed free energy landscape, the occluded state is a stable local minimum, as expected for a thermodynamic state.

Overall, the evidence suggests that MFS transporters can be described as transporters with two gates. The gates are related to their internal repeat symmetry. Coupling allows occluded states to occur, which were found to exist in crystal structures and MD simulations.

4.5.2.2. Mhp1: three gates

As an example of a transporter that can be described with three gates we look at Mhp1 again. The crystallographic structures in Figure 2 show an occluded state (Weyand et al., 2008; Simmons et al., 2014) in addition to the outward (Weyand et al., 2008) and inward facing states (Shimamura et al., 2010) that are necessary for alternating access. Given the definition of the three gates (see Figure 7), the crystallographic occluded structure is in an outward-facing occluded conformation because the thick gate is closed (outward facing) and both thin gates are also closed. MD simulations had shown that the thin gates can change conformations on the 100-ns time scale (Shimamura et al., 2010). A detailed analysis of the simulations in terms of the gate distances (Figure 10A) showed that the EC gate was mobile when the thick gate was closed (outward facing conformation) and the simulations sampled both outward open and outward occluded conformations. The IC thin gate remained locked, though. Conversely, once the thick gate was open (inward facing conformation), the EC gate was locked and the IC gate could sample open and closed conformations. The dynamic behavior of the thin gates reflects the two-fold symmetry that is imposed by the inverted repeat symmetry (Figure 4B). Using site-directed spin labeling and DEER spectroscopy, Kazmier et al. (2014) showed that the IC gate formed by TM5 undergoes motions between open and closed conformations, in agreement with the computational results.

The crystallographic inward facing structure shows the IC gate in a wide open position[7], corresponding to an inward open structure. The MD simulations with the thick and both thin gates closed showed that a second occluded state might exist (Figure 10B,C), as predicted by a pore with three gates (Figure 6).

The MD simulations sampled one conformation predicted for a triple-gated pore, bringing the total observed to 4 out of 7 (discounting the leak state). They also suggest that some other conformations are not observable because of

coupling between thick and thin gates. For example, opening of the thick gate while the EC gate was open was experimentally ruled out (Simmons et al., 2014) (also see discussion in Section 5.1); conversely the MD suggested that EC gate will remain closed when the thick gate is open. These observations rule out two more putative states (EC open/thick open/IC open and EC open/thick open/IC closed). The remaining state (EC closed/thick close/IC open) seems unlikely based on the MD, which showed that the IC gate is locked when the thick gate is closed. Based on this analysis, only 4 out of 8 possible states, namely the three crystal conformations (OF open, OF occluded, IF open) and the MD prediction for IF occluded, should be the only observable conformations for Mhp1.

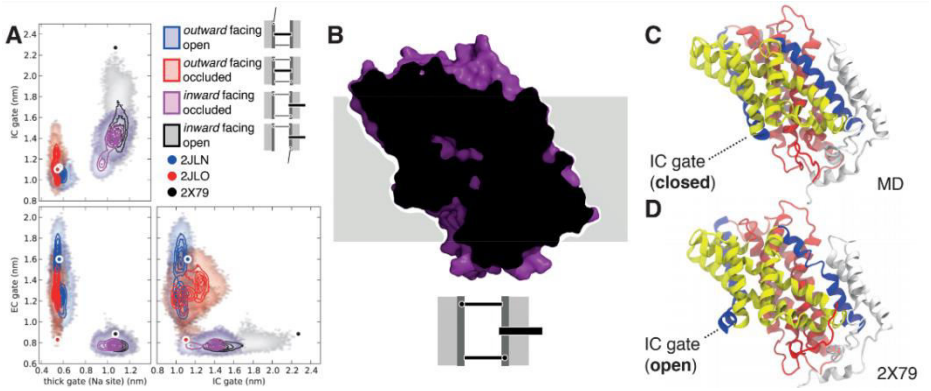

Figure 10. MD simulations sample an inward facing occluded state of Mhp1. **A** Gate distances (see Figure 7) from 100-ns MD trajectories of Mhp1 with a Na^+ ion in the Na2 site (simulations from Shimamura et al. (2010) and additional unpublished data). Contour lines are drawn at 20% increments of probability density. The shaded area indicates the full extent of order parameters explored in the simulation. Simulations started from crystal structures (circles) in three different conformational states (represented by the PDB ID), except for the magenta trajectories, which were started from a frame of the *inward facing open* simulation (gray) that showed an almost closed intracellular gate. Data for three independent simulations each starting from the outward facing states (blue and red) are shown together with one from the *inward facing open* (gray) and two from the *inward facing occluded* (magenta) states. **B**, **C** Putative inward-facing occluded conformation of Mhp1 (snapshot from the high-probability region of the inward facing occluded trajectory (magenta) in **A**). The cut through the transporter is shown in the same way as the crystal structures in Figure 2. **D** Inward facing open crystal structure (PDB ID 2X79) with the open IC gate.

An analysis based on gate states is general but limited in important details and must be augmented with additional information about the relative stability of the states. For example, under physiological conditions, the inward facing conformation is more prevalent than the outward facing one although this can be changed with the addition of substrate (Kazmier et al., 2014; Calabrese et al., 2017). The DEER experiments suggest that some conformations such as the inward facing occluded might be much shorter lived than other ones (Kazmier et al., 2014). Such quantitative information is crucial in order to interpret kinetic reaction diagrams based on the predicted states.

4.6. UNIFIED TRANSPORT CYCLE MODEL

In our enumeration of gate states we have implicitly assumed that these states do not depend on the binding of driving ions or substrate. Such an assumption is not warranted. For instance, the symporter in Figure 1A must avoid leak cycles that involve a slippage transition between the inward- and outward-facing transporter conformations when only the ion is bound or it would just dissipate the ion gradient. Mechanistically, the absence of the substrate when the ion is present must be changing the free energy landscape of the transition (Läuger, 1980) in such a way that the ion-only transition faces a much higher barrier than the fully loaded transporter. In other words, binding of an ion *and* a substrate unlocks the transporter and enables the conformational transition to occur as experimentally found for the aspartate-sodium symporter GltPh (Akyuz et al., 2015). A similar argument can be made for the antiporter cycle in Figure 1B where the transition between the empty inward and outward-facing states needs to be suppressed to avoid leak cycles that only dissipate the ion. In this case, binding of the ion *or* the substrate unlocks the transporter. In both cases it is clear that presence or absence of bound ion and/or substrate corresponds to a protein with different energetics from, say, the unloaded conformation.

Consequently, the number of available states of a transporter will be the product of the number conformational states n_C with the number of ways to bind driving ions and substrates. We can estimate n_C from the gate model as $n_C = 2^N - 1$ for N gates and a leak state excluded. Assuming an ion:substrate stoichiometry of

---

7. The crystals that produced the inward facing open structure with PDB ID 2X79 only formed when cells were grown on minimal medium with seleno-*L*-methionine (Shimamura et al., 2010). The electron density map of 2X79 contains a blob of unidentified density in the inward facing cavity that appears to have wedged open the IC gate and stabilized the IF conformation. It is possible that the unidentified molecule(s) held the IC gate in an especially wide open position from which it relaxes in the MD.

ν_I:ν_S and making the simplifying assumption that there are ν_I ion binding sites and ν_S substrate binding sites, there are $n_j = \sum_{k=0}^{\nu_j} \binom{\nu_j}{k} = 2^{\nu_j}$ ways to distribute zero to ν_j particles over ν_j binding sites. Hence the number of states in the model is

$$\Omega(N, \nu_I, \nu_S) = n_C n_I n_S = (2^N - 1)\, 2^{\nu_I + \nu_S} \qquad (11)$$

(If ions and substrates compete for overlapping binding sites then Ω is less than the value given by Eq. 11.)

For example, for the transporters in Figure 1, $\nu_I = \nu_S = 1$ and with $N = 2$, Ω = 3 x 4 = 12 different states should be considered, as shown in Figure 11. In principle, all theoretically possible transitions between states (arrows in Figure 11) contribute to a overall transport process (Hill, 1989). In our example, occluded states are included fo completeness. However, occluded states (numbers 5–8) cannot exchange with each othe and their effect could be replaced with an effective rate constant between the outward facing and inward facing conformations that are connected by the occluded state.

If we follow Zuckerman (2019) and consider three different idealized processes, in which certain transitions are suppressed by virtue of low kinetic rate constants (Hill and Eisenberg, 1981) (grayed out in Figure 11), then we recognize the transport cycle for a symporter (Figure 11A) and for an antiporter (Figure 11B). Furthermore, by suppressing transitions that involve the driving ion and only retaining a cycle that contains the alternating access transition with either substrate bound or the empty transporter, a simple uniporter model emerges (Figure 11C). In this case, no energy coupling occurs and the substrate will move down its electrochemical gradient by facilitated diffusion.

The idealized cycles could be made more realistic by retaining all transitions related to ion and substrate binding (1–4 and 9–12 in Figure 11) while still suppressing the undesirable conformational transition (e.g., the ion leak pathway 2↔11 for the symporter in Figure 11A). With these additional transitions included, different sequences of binding or dissociation reactions would be included in the models for the symporter and antiporter. A uniporter might be able to bind a driving ion but not transport it. Overall, the three physiologically very different types of transporters only differ in which of the alternating-access transitions is forbidden (or strongly suppressed). One can imagine that mutations may differentially change the transition rates and so switch the function of transporter from, say, a symporter to a uniporter (as seen in MFS sugar transporters (Madej et al., 2014)) or an antiporter to a symporter (Henderson,

Fendler and Poolman, 2019). Occluded states are now seen as a possible control point to tune the function: e.g., in order to block an outward↔inward transition, only one partial transition to or from the occluded state need be blocked.

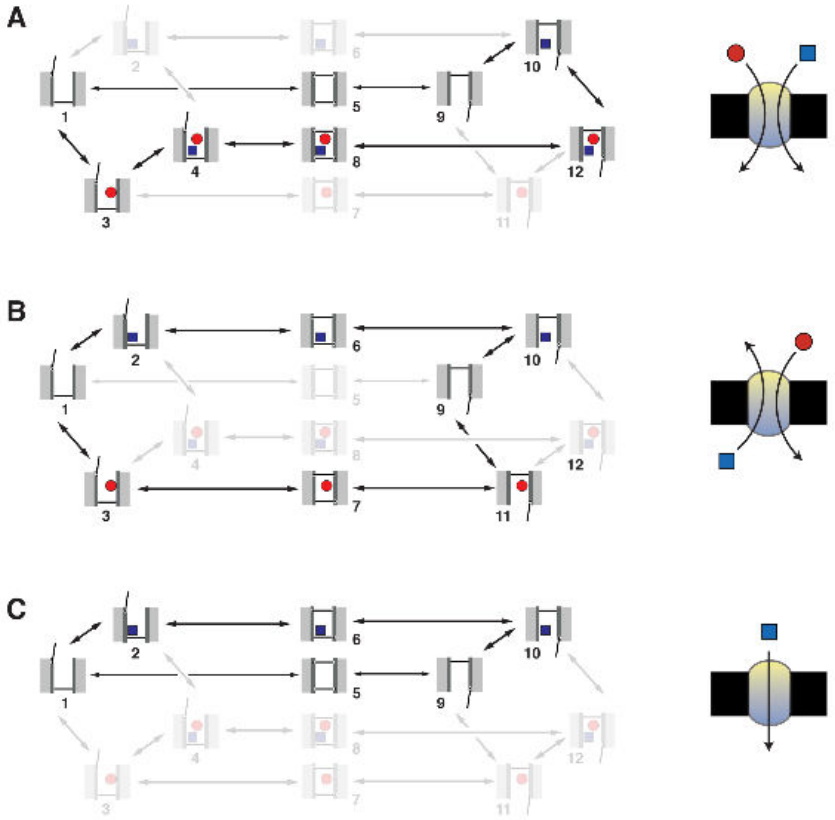

Figure 11. Unified picture of transporter function.
Unified picture for a hypothetical transporter with a 1:1 stoichiometry between driving ion (red circle) and substrate (blue square) and two gates. All combinations of conformational states with bound ion and/or substrate are listed. Leak states are omitted for simplicity. When an ion or substrate is shown, the corresponding binding or dissociation reaction is implied. Depending on the physiological function (symbol on the right), only certain sequences of states are visited (in the idealized case) while others (grayed out) are not part of the cycle. **A** Symporter. (The cycle drawn here corresponds to the one in Figure 1A; the alternative binding sequences 1↔2↔4 and 9↔11↔12 might also occur.) **B** Antiporter. (The cycle corresponds to the one in Figure 1B; the alternative binding sequences 2↔4↔3 and 10↔12↔11 might also occur.) **C** Uniporter.

4.7. CONCLUSION

We have provided a perspective on broad and general principles that apply to secondary active transporters. Transporters are seen as catalysts or "physical enzymes" that enable transport across the cell membrane against an electrochemical gradient by transducing free energy from the electrochemical gradient of a driving ion. Energy transduction requires cyclical reactions that include both driving ion and transported substrate. The alternating access model provides a simple scheme through which such cycles can be established. The protein must exist in at least two distinct conformations in which the binding sites are exposed only to either the outside or the inside solution. Importantly, no energy transduction is possible if a continuous pore is established. The two protein conformations that are needed for the two alternating access states are related by a structural two-fold pseudo symmetry that originates in inverted repeats in the protein's genetic sequence. A description of transporters as gated pores is fruitful in many cases because gates (two state switches) can be identified with structural elements in the transporter. Enumerating all distinct gate states naturally includes occluded states in the alternating access picture and also suggests what kind of protein conformations might be observable. By connecting the possible conformational states and ion/substrate bound states in a kinetic model, a unified picture emerges in which symporter, antiporter, and uniporter function are extremes in a continuum of functionality.

Many open questions remain. For example, the molecular mechanism of coupling between conformational changes and ion/substrate binding and allosteric interactions between gates need to be evaluated for most known transporters. General theories of allosteric coupling will likely be helpful to define the specific quantitative questions that need to be asked (LeVine et al., 2016). Occluded states were explained as a consequence of the existence of gates in transporters, so a natural question to ask is if all transporters have occluded states, and if so, are they ultimately a consequence of the symmetries of the inverted repeats? It is tempting to speculate that occluded states are the fully symmetrical high energy conformations whose energy is lowered by symmetry breaking. There remain classes of transporters for which we do not have sufficient structural evidence to answer the question although simulations (as shown here) have started filling this gap. The unified model indicates that transporter function forms a continuum. However, how difficult is it to move through this continuum, what are the minimal changes to change physiological function? Could such changes be achieved with allosteric modulators (small molecules) or changes in external

conditions such as membrane tension, pressure, temperature, or transmembrane voltage?

More broadly speaking, it has also been recognized that channels and transporters form a spectrum (Gadsby, 2009; Henderson, Fendler and Poolman, 2019), or as expressed by Läuger (1980): "Channel and carrier [transporter] models should therefore not be regarded as mutually exclusive possibilities, but rather as limiting cases of a more general mechanism." There seems to be value in stepping back and asking what the general principles are under which a class of proteins has to operate.

ACKNOWLEDGMENTS

We thank Philip Fowler for providing us with the data for Figure 9. Research reported in this work was supported by the National Institute of General Medical Sciences of the National Institutes of Health under Awards Number R01GM118772.

REFERENCES

Abramson J, Smirnova I, Kasho V, Verner G, Kaback HR, Iwata S. Structure and mechanism of the lactose permease of *Escherichia coli*. *Science*. 2003;301 (5633):610–615. DOI: 10.1126/science.1088196.

Abramson J, Wright EM. Structure and function of Na^+-symporters with inverted repeats. *Curr Opin Struct Biol*. 2009;19(4):425–432. DOI: 10.1016/j.sbi.2009.06.002.

Accardi A. Structure and gating of CLC channels and exchangers. *J Physiol*. 2015;593(Pt 18):4129–4138. DOI: 10.1113/JP270575.

Akyuz N, Georgieva ER, Zhou Z, Stolzenberg S, Cuendet MA, Khelashvili G, Altman RB, Terry DS, Freed JH, Weinstein H, Boudker O, Blanchard SC. Transport domain unlocking sets the uptake rate of an aspartate transporter. *Nature*. 2015;518(7537):68–73. DOI: 10.1038/nature14158.

Bai X, Moraes TF, Reithmeier RAF. Structural biology of solute carrier (SLC) membrane transport proteins. *Mol Membr Biol*. 2017;34(1-2):1–32. DOI: 10.1080/09687688.2018.1448123.

Boudker O, Verdon G. Structural perspectives on secondary active transporters. *Trends Pharmacol Sci*. 2010;31(9):418–426. DOI: 10.1016/j .tips.2010.06.004.

Buch-Pedersen MJ, Pedersen BP, Veierskov B, Nissen P, Palmgren MG. Protons and how they are transported by proton pumps. *Pflügers Arch*. 2009;457(3):573–579. DOI: 10.1007/s00424-008-0503-8.

Calabrese AN, Jackson SM, Jones LN, Beckstein O, Heinkel F, Gsponer J, Sharples D, Sans M, Kokkinidou M, Pearson AR, Radford SE, Ashcroft AE, Henderson PJF. Topological dissection of the membrane transport protein Mhp1 derived from cysteine accessibility and mass spectrometry. *Anal Chem*. 2017;89(17):8844–8852. DOI: 10.1021/acs.analchem.7b01310.

Cameron AD, Beckstein O, Henderson PJF. The five-helix inverted repeat superfamily of membrane transport proteins. In Encylopedia of Biophysics, edited by Roberts G, 2013;1481–1485. Springer. DOI: 10.1007/978-3-642-16712-6_772.

Chang Y-N, Geertsma ER. The novel class of seven transmembrane segment inverted repeat carriers. *Biol Chem*. 2017;398(2):165–174. DOI: 10.1515/hsz-2016-0254.

Crisman TJ, Qu S, Kanner BI, Forrest LR. Inward facing conformation of glutamate transporters as revealed by their inverted-topology structural repeats. *Proc Natl Acad Sci USA*. 2009;106(49):20752–20757. DOI: 10.1073/pnas.0908570106.

DeFelice LJ, Goswami T. Transporters as channels. *Annu Rev Physiol*. 2007;69:87–112. DOI: 10.1146/annurev.physiol.69.031905.164816.

Diallinas G. Understanding transporter specificity and the discrete appearance of channel-like gating domains in transporters. *Front Pharmacol*. 2014;5(207). DOI: 10.3389/fphar.2014.00207.

Dill KA, Bromberg S. Molecular Driving Forces: Statistical Thermodynamics in Biology, Chemistry, Physics, and Nanoscience. New York: Garland Science, 2010.

Drew D, Boudker O. Shared molecular mechanisms of membrane transporters. *Ann Rev Biochem*. 2016;85(1):543–572. DOI: 10.1146/annurev-biochem-060815-014520.

Fang Y, Jayaram H, Shane T, Kolmakova-Partensky L, Wu F, Williams C, Xiong Y, Miller C. Structure of a prokaryotic virtual proton pump at 3.2 A resolution. *Nature*. 2009;460(7258):1040–1043. DOI: 10.1038/nature08201.

Forrest LR. Structural biology. (Pseudo-)symmetrical transport. *Science*. 2013;339(6118):399–401. DOI: 10.1126/science.1228465.

Forrest LR. Structural symmetry in membrane proteins. *Ann Rev Biophys*. 2015;44(1):311–337. DOI: 10.1146/annurev-biophys-051013-023008.

Forrest LR, Krämer R, Ziegler C. The structural basis of secondary active transport mechanisms. *Biochim Biophys Acta*. 2011;1807(2):167–188. DOI: 10.1016/j.bbabio.2010.10.014.

Forrest LR, Rudnick G. The rocking bundle: A mechanism for ion-coupled solute flux by symmetrical transporters. *Physiology*. 2009;24:377–386. DOI: 10.1152/physiol.00030.2009.

Forrest LR, Zhang Y-W, Jacobs MT, Gesmonde J, Xie L, Honig BH, and Rudnick G. Mechanism for alternating access in neurotransmitter transporters. *Proc Natl Acad Sci USA*. 2008;105(30):10338–10343. DOI: 10.1073/pnas.0804659105.

Fowler PW, Orwick-Rydmark M, Radestock S, Solcan N, Dijkman PM, Lyons JA, Kwok J, Caffrey M, Watts A, Forrest LR, Newstead S. Gating topology of the proton-coupled oligopeptide symporters. *Structure*. 2015;23(2):290–301. DOI: 10.1016/j.str.2014.12.012.

Fuster DG, Alexander RT. Traditional and emerging roles for the SLC9 Na^+/H^+ exchangers. *Pflügers Archiv - Europ J Physiol*. 2014;466(1):61–76. DOI: 10.1007/s00424-013-1408-8.

Gadsby DC. Ion channels versus ion pumps: the principal difference, in principle. *Nat Rev Mol Cell Biol*. 2009;10(5):344–352. DOI: 10.1038/nrm2668.

Gouaux E. The molecular logic of sodium-coupled neurotransmitter transporters. *Philos Trans R Soc Lond B Biol Sci*. 2009;364(1514):149–154. DOI: 10.1098/rstb.2008.0181.

Henderson RK, Fendler K, Poolman B. Coupling efficiency of secondary active transporters. *Curr Opin Biotechnol*. 2019;58:62–71. DOI: 10.1016/j.copbio.2018.11.005.

Henzler-Wildman K. Analyzing conformational changes in the transport cycle of EmrE. *Curr Opin Struct Biol*. 2012;22(1):38–43. DOI: 10.1016/j.sbi.2011.10.004.

Henzler-Wildman K, Kern D. Dynamic personalities of proteins. *Nature*. 2007;450(7172):964–972. DOI: 10.1038/nature06522.

Hill TL. Free energy transduction in biology and biochemical cycle kinetics. 1989 New York: Springer.

Hill TL, Eisenberg E. Can free energy transduction be localized at some crucial part of the enzymatic cycle? *Q Rev Biophys*. 1981;14(4):463–511. DOI: 10.1017/s0033583500002468.

Hille B. Ion Channels of Excitable Membranes. 3rd ed. Sunderland MA, 2001 U.S.A., Sinauer Associates.

Hu N-J, Iwata S, Cameron AD, Drew D. Crystal structure of a bacterial homologue of the bile acid sodium symporter ASBT. *Nature*. 2011;478(7369):408–411. DOI: 10.1038/nature10450.

Huang Y, Lemieux MJ, Song J, Auer M, Wang D-N. Structure and mechanism of the glycerol-3-phosphate transporter from *Escherichia coli*. *Science*. 2003;301(5633):616–620. DOI: 10.1126/science.1087619.

Hunte C, Screpanti E, Venturi M, Rimon A, Padan E, Michel H. Structure of a Na^+/H^+ antiporter and insights into mechanism of action and regulation by pH. *Nature*. 2005;435(7046):1197–1202. DOI: 10.1038/nature03692.

Jackson SM, Ivanova E, Simmons S, Patching SG, Weyand S, Shimamura T, Brückner F, Iwata S, Sharples DJ, Baldwin SA, Sansom MSP, Beckstein O, Cameron AD, Henderson PJF. Na^+-Hydantoin Membrane Transport Protein, Mhp1. In Encylopedia of Biophysics, edited by Gordon Roberts, 2013;1514–1521. Springer. DOI: 10.1007/978-3-642-16712-6_670.

Jardetzky O. Simple allosteric model for membrane pumps. *Nature*. 1966;211(5052):969–970. DOI: 10.1038/211969a0.

Jeschke G. A comparative study of structures and structural transitions of secondary transporters with the LeuT fold. *Eur Biophys J*. 2013;42(2-3):181–197. DOI: 10.1007/s00249-012-0802-z.

Kaback HR, Dunten R, Frillingos S, Venkatesan P, Kwaw I, Zhang W, Ermolova N. Site-directed alkylation and the alternating access model for LacY. *Proc Natl Acad Sci USA*. 2007;104(2):491–494. DOI: 10.1073/pnas.0609968104.

Kaback HR, Smirnova I, Kasho V, Nie Y, Zhou Y. The alternating access transport mechanism in LacY. *J Membr Biol*. 2011;239(1-2):85–93. DOI: 10.1007/s00232-010-9327-5.

Kazmier K, Claxton DP, Mchaourab HS. Alternating access mechanisms of LeuT-fold transporters: trailblazing towards the promised energy landscapes. *Curr Opin Struct Biol*. 2017;45:100–108. DOI: 10.1016/j.sbi.2016.12.006.

Kazmier K, Sharma S, Islam SM, Roux B, Mchaourab HS. Conformational cycle and ion-coupling mechanism of the Na+/hydantoin transporter Mhp1. *Proc Natl Acad Sci USA*. 2014;111(41):14752–14757. DOI: 10.1073/pnas.1410431111.

Kazmier K, Sharma S, Quick M, Islam SM, Roux B, Weinstein H, Javitch JA, Mchaourab HS. Conformational dynamics of ligand-dependent alternating access in LeuT. *Nat Struct Mol Biol*. 2014;21(5):472–479. DOI: 10.1038/nsmb.2816.

Keller R, Ziegler C, Schneider D. When two turn into one: Evolution of membrane transporters from half modules. *Biol Chem*. 2014;395(12):1379–1388. DOI: 10.1515/hsz-2014-0224.

Klingenberg M. The ADP,ATP shuttle of the mitochondrion. *Trends Biochem Sci*. 1979;4(11):249–252. DOI: 10.1016/0968-0004(79)90215-9.

Klingenberg M. Transport viewed as a catalytic process. *Biochimie*. 2007;89(9):1042–1048. DOI: 10.1016/j.biochi.2007.02.010.

Korkhov VM, Tate CG. An emerging consensus for the structure of EmrE. *Acta Crystallographica Section D*. 2009;65(2):186–192. DOI: 10.1107/S0907444908036640.

Krishnamurthy H, Gouaux E. X-ray structures of LeuT in substrate free outward-open and apo inward-open states. *Nature*. 2012;481:469–474. DOI: 10.1038/nature10737.

Krishnamurthy H, Piscitelli CL, Gouaux E. Unlocking the molecular secrets of sodium-coupled transporters. *Nature*. 2009;459(7245):347–355. DOI: 10.1038/nature08143.

Latorraca NR, Fastman NM, Venkatakrishnan AJ, Frommer WB, Dror RO, Feng L. Mechanism of substrate translocation in an alternating access transporter. *Cell*. 2017;169(1):96–107.e12. DOI: 10.1016/j.cell.2017.03.010.

Läuger P. Kinetic properties of ion carriers and channels. *J Membr Biol*. 1980;57(3):163–178. DOI: 10.1007/BF01869585.

Law CJ, Maloney PC, Wang D-N. Ins and outs of major facilitator superfamily antiporters. *Annu Rev Microbiol*. 2008;62:289–305. DOI: 10.1146/annurev.micro.61.080706.093329.

Lespine A, Dupuy J, Alvinerie M, Comera C, Nagy T, Krajcsi P, Orlowski S. Interaction of macrocyclic lactones with the multidrug transporters: the bases of the pharmacokinetics of lipid-like drugs. *Curr Drug Metab*. 2009;10(3):272–288. DOI: 10.2174/138920009787846297.

LeVine MV, Cuendet MA, Khelashvili G, Weinstein H. Allosteric mechanisms of molecular machines at the membrane: Transport by sodium-coupled symporters. *Chem Rev*. 2016;116(11):6552–6587. DOI: 10.1021/acs.chemrev.5b00627.

Li J, Wen P-C, Moradi M, Tajkhorshid E. Computational characterization of structural dynamics underlying function in active membrane transporters. *Curr Opin Struct Biol*. 2015;31:96–105. DOI: 10.1016/j.sbi.2015.04.001.

Madej MG, Sun L, Yan N, Kaback HR. Functional architecture of MFS D-glucose transporters. *Proc Natl Acad Sci USA*. 2014;111(7):E719–E727. DOI: 10.1073/pnas.1400336111.

Marger MD, Saier Jr MH. A major superfamily of transmembrane facilitators that catalyse uniport, symport and antiport. *Trends Biochem Sci*. 1993;18(1):13–20. DOI: 10.1016/0968-0004(93)90081-W.

Miller C. ClC chloride channels viewed through a transporter lens. *Nature*. 2006;440:484–489. DOI: 10.1038/nature04713.

Milo R, Jorgensen P, Moran U, Weber G, Springer M. BioNumbers–the database of key numbers in molecular and cell biology. *Nucleic Acids Res*. 2010;38(Database issue):D750–D753. DOI: 10.1093/nar/gkp889.

Mitchell P. Translocations through natural membranes. Chapter 2 in Advances in Enzymology and Related Areas of Molecular Biology, edited by Nord FF, 1967;29:33–87. New York: John Wiley & Sons, Inc. DOI: 10.1002/9780470122747.ch2.

Morrison EA, Dekoster GT, Dutta S, Vafabakhsh R, Clarkson MW, Bahl A, Kern D, Ha T, Henzler-Wildman KA. Antiparallel EmrE exports drugs by exchanging between asymmetric structures. *Nature*. 2012;481:45–50. DOI: 10.1038/nature10703.

Morth JP, Pedersen BP, Toustrup-Jensen MS, Sørensen TL-M, Petersen J, Andersen JP, Vilsen B, Nissen P. Crystal structure of the sodium-potassium pump. *Nature*. 2007;450(7172):1043–1049. DOI: 10.1038/nature06419.

Myers-Turnbull D, Bliven SE, Rose PW, Aziz ZK, Youkharibache P, Bourne PE, Prli´c A. Systematic detection of internal symmetry in proteins using CE-Symm. *J Mol Biol*. 2014;426(11):2255–2268. DOI: 10.1016/j.jmb.2014.03.010.

Naftalin RJ. Reassessment of models of facilitated transport and cotransport. *J Membr Biol*. 2010;234(2):75–112. DOI: 10.1007/s00232-010-9228-7.

Newstead S, Drew D, Cameron AD, Postis VLG, Xia X, Fowler PW, Ingram JC, Carpenter EP, Sansom MSP, McPherson MJ, Baldwin SA, Iwata S. Crystal structure of a prokaryotic homologue of the mammalian oligopeptide-proton symporters, PepT1 and PepT2. *EMBO J*. 2011;30:417–426. DOI: 10.1038/emboj.2010.309.

Ottolia M, John S, Xie Y, Ren X, Philipson KD. Shedding light on the Na^+/Ca^{2+} exchanger. *Ann N Y Acad Sci*. 2007;1099:78–85. DOI: 10.1196/annals.1387.044.

Padan E. Functional and structural dynamics of NhaA, a prototype for Na^+ and H^+ antiporters, which are responsible for Na^+ and H^+ homeostasis in cells. *Biochimica et Biophysica Acta – Bioenergetics*. 2014;1837(7):1047–1062. DOI: 10.1016/j.bbabio.2013.12.007.

Patching SG. Efficient syntheses of ^{13}C- and ^{14}C-labelled 5-benzyl and 5-indolylmethyl *L*-hydantoins. *J Labelled Comp Radiopharm*. 2011;54(2):110-114.

Patching SG. Synthesis, NMR analysis and applications of isotope-labelled hydantoins. *Journal of Diagnostic Imaging in Therapy*. 2017;4(1):3-26.

Patching SG. Recent developments in Nucleobase Cation Symporter-1 (NCS1) family transport proteins from bacteria, archaea, fungi and plants. *J Biosci*. 2018;43(4):797-815. DOI: 10.1007/s12038-018-9780-3.

Perez C, Faust B, Mehdipour AR, Francesconi KA, Forrest LR, Ziegler C. Substrate-bound outward-open state of the betaine transporter BetP provides insights into Na^+ coupling. *Nat Commun*. 2014;5:4231. DOI: 10.1038/ncomms5231.

Perez C, Koshy C, Yildiz O, Ziegler C. Alternating access mechanism in conformationally asymmetric trimers of the betaine transporter BetP. *Nature*. 2012;490:126–130. DOI: 10.1038/nature11403.

Radestock S, Forrest LR. The alternating-access mechanism of MFS transporters arises from inverted-topology repeats. *J Mol Biol*. 2011;407(5):698–715. DOI: 10.1016/j.jmb.2011.02.008.

Ressl S, Terwisscha van Scheltinga AC, Vonrhein C, Ott V, Ziegler C. Molecular basis of transport and regulation in the Na^+/betaine symporter BetP. *Nature*. 2009;458(7234):47–52. DOI: 10.1038/nature07819.

Reyes N, Ginter C, Boudker O. Transport mechanism of a bacterial homologue of glutamate transporters. *Nature*. 2009;462(7275):880–885. DOI: 10.1038/nature08616.

Rolfe DF, Brown GC. Cellular energy utilization and molecular origin of standard metabolic rate in mammals. *Physiol Rev*. 1997;77(3):731–758. DOI: 10.1152/physrev.1997.77.3.731.

Sazanov LA. A giant molecular proton pump: structure and mechanism of respiratory complex I. *Nat Rev Mol Cell Biol*. 2015;16(6):375–388. DOI: 10.1038/nrm3997.

Schushan M, Rimon A, Haliloglu T, Forrest LR, Padan E, and Ben-Tal N. A model-structure of a periplasm-facing state of the NhaA antiporter suggests the molecular underpinnings of pH-induced conformational changes. *J Biol Chem*. 2012;287(22):18249–18261. DOI: 10.1074/jbc.M111.336446.

Schwartz SD, Schramm VL. Enzymatic transition states and dynamic motion in barrier crossing. *Nat Chem Biol*. 2009;5(8):551–558. DOI: 10.1038/nchembio.202.

Schweikhard ES, Ziegler CM. Amino acid secondary transporters: toward a common transport mechanism. Chapter 1 in Co-Transport Systems, edited by Bevensee MO, 2012;70:1–28. *Curr Top Membranes*. Elsevier Inc. DOI: 10.1016/B978-0-12-394316-3.00001-6.

Selvam B, Mittal S, Shukla D. Free energy landscape of the complete transport cycle in a key bacterial transporter. *ACS Cent Sci*. 2018;4(9):1146–1154. DOI: 10.1021/acscentsci.8b00330.

Shi Y. Common folds and transport mechanisms of secondary active transporters. *Ann Rev Biophys*. 2013;42(1):51–72. DOI: 10.1146/annurevbiophys-083012-130429.

Shimamura T, Weyand S, Beckstein O, Rutherford NG, Hadden JM, Sharples D, Sansom MSP, Iwata I, Henderson PJF, Cameron AD. Molecular basis of alternating access membrane transport by the sodium-hydantoin transporter Mhp1. *Science*. 2010;328(5977):470–473. DOI: 10.1126/science.1186303.

Simmons KJ, Jackson SM, Brückner F, Patching SG, Beckstein O, Ivanova E, Geng T, Weyand S, Drew D, Lannigan J, Sharples DJ, Sansom MSP, Iwata S, Fishwick CWG, Johnson AP, Cameron AD, Henderson PJF. The molecular mechanism of ligand recognition by membrane transport protein, Mhp1. *EMBO J*. 2014;33:1831–1844. DOI: 10.15252/embj.201387557.

Slotboom DJ. Structural and mechanistic insights into prokaryotic energycoupling factor transporters. *Nat Rev Microbiol*. 2014;12(2):79–87. DOI: 10.1038/nrmicro3175.

Smart OS, Neduvelil JG, Wang X, Wallace BA, Sansom MSP. HOLE: A program for the analysis of the pore dimensions of ion channel structural models. *J Mol Graph*. 1996;14:354–360. DOI: 10.1016/s0263-7855(97)00009-x.

Smirnova I, Kasho V, Kaback HR. Engineered occluded apointermediate of LacY. *Proc Natl Acad Sci USA*. 2018;115(50):12716–12721. DOI: 10.1073/pnas.1816267115.

Stelzl LS, Fowler PW, Sansom MSP, Beckstein O. Flexible gates generate occluded intermediates in the transport cycle of LacY. *J Mol Biol*. 2014;426:735–751. DOI: 10.1016/j.jmb.2013.10.024.

Suzuki S, Henderson PJF. The hydantoin transport protein from *Microbacterium liquefaciens*. *J Bacteriol*. 2006;188(9):3329–3336. DOI: 10.1128/JB.188.9.3329-3336.2006.

Tanford C. Translocation pathway in the catalysis of active transport. *Proc Natl Acad Sci USA*. 1983;80(12):3701–3705.

Vandenberg RJ., Huang S, Ryan RM. Slips, leaks and channels in glutamate transporters. *Channels*. 2008;2(1):51–58.

Västermark Å, Wollwage S, Houle ME, Rio R, Saier Jr MH. Expansion of the APC superfamily of secondary carriers. *Proteins*. 2014;82(10):2797–2811. DOI: 10.1002/prot.24643.

Vergara-Jaque A, Fenollar-Ferrer C, Kaufmann D, Forrest LR. Repeat-swap homology modeling of secondary active transporters: updated protocol and prediction of elevator-type mechanisms. *Front Pharmacol*. 2015;6:183 DOI: 10.3389/fphar.2015.00183.

Weyand S, Shimamura T, Beckstein O, Sansom MSP, Iwata S, Henderson PJF, Cameron AD. The alternating access mechanism of transport as observed in the sodium-hydantoin transporter Mhp1. *J Synchrotron Rad*. 2011;18(1):20–23. DOI: 10.1107/S0909049510032449.

Weyand S, Shimamura T, Yajima S, Suzuki S, Mirza O, Krusong K, Carpenter EP, Rutherford NG, Hadden JM, O'Reilly J, Ma P, Saidijam M, Patching SG, Hope RJ, Norbertczak HT, Roach PCJ, Iwata S, Henderson PJF, Cameron AD. Structure and molecular mechanism of a nucleobase-cation-symport-1 family transporter. *Science*. 2008;322(5902):709–713. DOI: 10.1126/science.1164440.

Yamashita A, Singh SK, Kawate T, Jin Y, Gouaux E. Crystal structure of a bacterial homologue of Na^+/Cl^--dependent neurotransmitter transporters. *Nature*. 2005;437(7056):215–223. DOI: 10.1038/nature03978.

Yan N. Structural advances for the major facilitator superfamily (MFS) transporters. *Trends Biochem Sci*. 2013;38(3):151–159. DOI: 10.1016/j.tibs.2013.01.003.

Zhou Y, Bushweller JH. Solution structure and elevator mechanism of the membrane electron transporter CcdA. *Nat Struct Mol Biol*. 2018;25(2):163–169. DOI: 10.1038/s41594-018-0022-z.

Zuckerman DM. Physical lens on the cell. 2019 online. https://www.physicallensonthecell.org/.

Submitted: 8th Dec 2019, Revised: 23rd Jan 2020, Accepted: 28th Jan 2020

Chapter Five

5. EMERGING STRUCTURAL INSIGHTS INTO MULTIDRUG RECOGNITION AND EXTRUSION BY MATE AND MFS TRANSPORTERS

Min Lu*, Katherine Si-Jia Lu
Department of Biochemistry & Molecular Biology, Rosalind Franklin University of Medicine & Science, North Chicago, Illinois, USA

ABSTRACT

Integral membrane proteins known as multidrug transporters promote multidrug resistance by extruding chemically and structurally dissimilar drugs across the cell membrane, often by utilizing the H^+ or Na^+ electrochemical gradient. As the current pace of drug discovery is inadequate to address the rapid increase of multidrug resistance, multidrug transporters pose urgent and catastrophic threats to human health by diminishing the efficacy of existing and new therapeutic drugs. Despite such clinical relevance, currently we still lack a deep and mechanistic understanding of how multidrug transporters recognize and extrude different therapeutic drugs. The recent structure determination of several substrate-bound H^+- and Na^+-dependent multidrug transporters has offered an excellent opportunity to better understand the underlying mechanism of multidrug extrusion. This chapter provides an updated account of the X-ray structures of substrate-bound MATE (Multidrug and Toxic Compound Extrusion) and MFS (Major Facilitator Superfamily) multidrug transporters, as well as their mechanistic implications. Beyond discussing the molecular basis of multidrug recognition and extrusion by MATE and MFS transporters, this chapter may engender new thoughts and ideas about how to curtail efflux-mediated multidrug resistance.

Keywords: multidrug resistance, multidrug extrusion, multidrug transporters, substrate recognition, cation coordination, transport mechanism

---

*Direct all correspondence to Dr. Min Lu, Department of Biochemistry and Molecular Biology, Rosalind Franklin University of Medicine and Science, 3333 Green Bay Road, North Chicago, Illinois 60064, USA. E-mail: min.lu@rosalindfranklin.edu.

5.1. INTRODUCTION

The ongoing explosion of multidrug resistance continues to plague global and US health care (Higgins, 2007; Fischbach and Walsh, 2009). Multidrug-resistant infectious diseases alone claim more than 2 million lives and cost more than $170 billion per year (Hall et al., 2018). Our arsenal of new therapeutic drugs is being outstripped by the increase in drug resistance (Fischbach and Walsh, 2009).

For instance, no new approved antibiotic class has been discovered over the past 40 years, signaling the worst drought in antibiotic discovery since 1928 (Hall et al., 2018). Needless to say, the public-health crisis caused by multidrug resistance cannot be solved without a deep knowledge of the underlying mechanisms.

Multidrug efflux has emerged as a major mechanism underlying multidrug resistance (Higgins, 2007). Integral membrane proteins known as multidrug transporters curtail the efficacy of existing and new therapeutics by extruding them across the cell membrane (Saier and Paulsen, 2001; Chitsaz and Brown, 2017). Multidrug transporters pose catastrophic and growing threats to humankind because they confer multidrug resistance to pathogenic microorganisms and human cells, making the associated diseases untreatable (Hall et al., 2018).

Thus far, seven families of multidrug transporters have been discovered: namely the ABC (ATP-Binding Cassette), AbgT (*p*-Aminobenzoyl-glutamate Transporter), DMT (Drug/Metabolite Transporter), MATE (Multidrug and Toxic Compound Extrusion), MFS (Major Facilitator Superfamily), PACE (Proteobacterial Antimicrobial Compound Efflux), and RND (Resistance-Nodulation-Division) families (Saier and Paulsen, 2001; Chitsaz and Brown, 2017; Ahmad et al., 2018; Ahmad et al., 2020).

Nearly half of the membrane transport proteins known to date are from the ABC and MFS protein families (Chitsaz and Brown, 2017). The ABC multidrug transporters are “primary” active membrane transport proteins powered by ATP hydrolysis (Saier and Paulsen, 2001). By contrast, the DMT, MATE, MFS and RND families of multidrug transporters are “secondary” active transporters that utilize the transmembrane H^+ or Na^+ electrochemical gradient to translocate drugs (Chitsaz and Brown, 2017).

The DMT, MFS, and RND multidrug transporters typically employ the H^+ gradient to extrude drugs, whereas the MATE transporters use either the H^+ or Na^+ gradient (Chitsaz and Brown, 2017). Based on amino-acid sequence similarity, the ~900 MATE transporters can be classified into the NorM, DinF (DNA damage-inducible protein F) and eukaryotic subfamilies (Brown et al., 1999; Omote et al., 2006; Kuroda and Tsuchiya, 2009; Lu, 2016).

Members of the NorM and DinF subfamilies can utilize the H^+ or Na^+ electrochemical gradient, whereas the eukaryotic MATE proteins are H^+-dependent (Morita et al., 2000; He et al., 2004; Otsuka et al., 2005a; for additional references see Lu, 2016). Both the NorM and DinF subfamilies contain eubacterial and archaeal members, which share rather modest amino-acid sequence similarity (Lu, 2016). MATE transporters can extrude polyaromatic drugs that carry positive charges at physiological pH, although these drugs exhibit rather diverse chemical structures and properties (Omote et al., 2006; Kuroda and Tsuchiya, 2009).

The more than 1 million sequenced MFS proteins, on the other hand, comprise the largest family of solute transport proteins and at least 82 subfamilies (for review see Saier and Paulsen, 2001; Yan, 2013; Quistgaard et al., 2016). Previous studies of MFS transporters such as LacY (lactose permease) and GLUTs (glucose transporters), which are from the Oligosaccharide/H^+ Symporter (OHS) and Sugar Porter (SP) subfamilies, respectively, revealed the shared MFS transporter architecture and provided critical insights into the transport mechanism (for review see Kaback and Guan, 2019; Yan, 2017).

MdfA, a polyspecific MFS multidrug transporter from the ubiquitous Drug/H^+ Antiporter-1 (DHA1) subfamily, can export physicochemically disparate compounds that lack a common chemical structure (Edgar and Bibi, 1997; for review see Fluman and Bibi, 2009; Yardeni et al., 2017). Previous studies suggested that MdfA is mechanistically distinct from the substrate-specific MFS transporters such as LacY, likely representing a new paradigm for membrane transport proteins (Fluman et al., 2012; Tirosh et al., 2012; Fluman et al., 2014).

Unfortunately, we are now on the losing side of the war against multidrug resistance because the current pace of drug discovery is woefully inadequate to tackle multidrug efflux (Fischbach and Walsh, 2009). This doomsday scenario cannot be averted unless we understand how multidrug transporters extrude drugs. At the present time, we do not fully understand how these drug-exporting proteins select their substrates, how they move therapeutic drugs across the cell membrane, or how they can be countervailed for potential therapeutic benefit (Lu, 2016).

Over the past 6 years, major strides have been made toward illuminating how MATE and MFS multidrug transporters recognize and extrude drugs, but these new mechanistic insights have yet to be reviewed collectively (Lu, 2016; Wu et al. 2019). This chapter summarizes these recent findings, focuses on what has been learned from the crystal structures of substrate-bound MATE and MFS multidrug transporters (Lu et al., 2013a; Lu et al., 2013b; Wu et al., 2019), and asks new questions that need to be addressed by future work.

5.2. THE SUBSTRATE-BOUND STRUCTURE OF NORM-NG

The X-ray structures of at least eight MATE transporters have been published, including NorM from *Vibrio cholerae* (NorM-VC; He et al., 2010), NorM from *Neisseria gonorrhoeae* (NorM-NG; Lu et al., 2013b), DinF from *Pyrococcus furiosus* (PfMATE; Tanaka et al., 2013), DinF from *Bacillus halodurans* (DinF-BH; Lu et al., 2013a), DinF from *Escherichia coli* (ClbM; Mousa et al., 2016), DinF from *Vibrio cholerae* (VcmN; Kusakizako et al. 2019), eukaryotic MATE transporter from *Camelina sativa* (CasMATE; Tanaka et al. 2017), and eukaryotic MATE protein from *Arabidopsis thaliana* (AtDTX14; Miyauchi et al., 2017).

Among them, the drug-bound structures of only three MATE transporters, NorM-NG, PfMATE and DinF-BH, have been reported. Since the function of PfMATE is questionable (Zakrzewska et al., 2019), the mechanistic implications of the drug-bound PfMATE structure remain controversial (Lu, 2016) and hence is excluded from this chapter.

The first substrate-bound structure of any MATE transporter, i.e., that of NorM-NG, captures the transporter in an outward-facing, substrate-bound state (Lu et al., 2013b). NorM-NG traverses the membrane bilayer twelve times giving rise to twelve membrane-spanning segments (TM1-TM12). Near the middle of the lipid bilayer, similarly folded N (TM1-TM6) and C (TM7-TM12) domains point away from one another toward the periplasm, yielding a V-shaped conformation (Figure 1a).

TM1-TM12 are connected by eleven intracellular and extracellular loops, denoted L1-2 to L11-12. Among them, L3-4, L9-10 and L6-7 are conspicuously long (Lu et al., 2013b). The intracellular L6-7 delimits the N and C domains of NorM-NG, whereas the extracellular L3-4 and L9-10 insert into a cavity formed between the N and C domains.

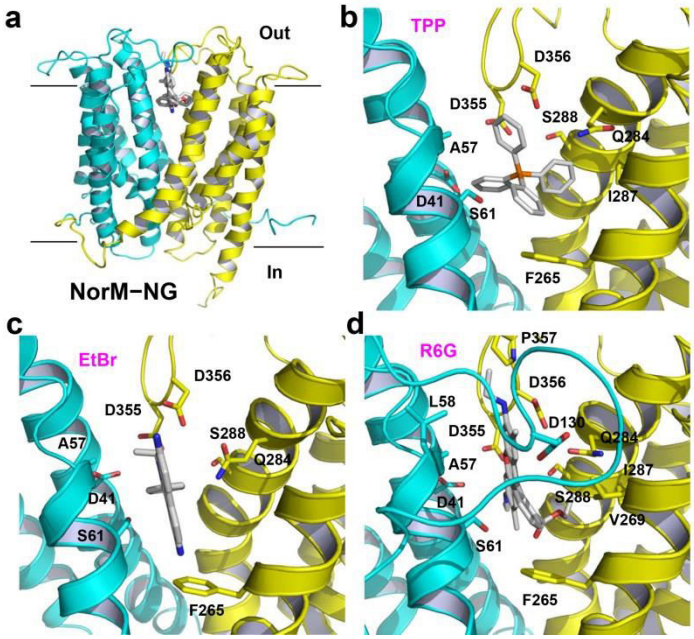

Figure 1. Structure of the multidrug-binding site in NorM-NG. (**a**) NorM-NG is drawn as a ribbon and viewed from the membrane plane, whereas the three substrates are in stick representation and colored grey. The N (residues 5-230) and C (residues 231-459) domains of NorM-NG are colored cyan and yellow, respectively. (**b**),(**c**),(**d**) Close-up of the binding site for TPP (PDB 4HUK), ethidium (PDB 4HUM), and R6G (PDB 4HUN), respectively. Relevant amino acids are illustrated as sticks. IL3-4 was omitted in (**b**) and (**c**) for clarity.

The bottom of this cavity is situated about half way through the membrane and is defined by D41, S61, F265 and I292, which are from TM1, TM2, TM7 and TM8, respectively (Lu et al., 2013b). The cavity is sealed from the cytoplasmic side by highly ordered protein structure, ~20 Å thick. The wall of the cavity is formed by T42, A57, L58, V269, Q284, V285, I287 and S288; and the extracellular loops L3-4 and L9-10, which donate S129, D130, D355, D356 and P357 into the cavity.

Except for D130, V269 and P357, all the amino acids surrounding this cavity are conserved or semi-conserved in the NorM subfamily. The interior of the cavity exhibits a surplus of negative charges, suggesting potential electrostatic attraction for cations or zwitterions (Lu et al., 2013b).

5.3. THE MULTIDRUG-BINDING SITE IN NORM-NG

Since NorM-NG was crystallized in the absence of added monovalent cations including Na^+, the TPP-, ethidium- and R6G-bound NorM-NG structures were interpreted to depict a Na^+-free, substrate-bound state of the transporter (Lu et al., 2013b). Each of the three substrates buries ~70% of accessible surface area upon binding NorM-NG, which is similar to values obtained for multidrug-binding transcription factors (Bachas et al., 2011; Newberry et al., 2008). Also akin to these water-soluble transcription factors, the docking locations for TPP, ethidium and R6G are similar in NorM-NG, which are near the membrane-periplasm interface (Lu et al., 2013b).

Numerous interactions were observed between NorM-NG and the bound substrates (Lu et al., 2013b). In particular, the side chains of three acidic amino acids, D41, D355 and D356, make long-range electrostatic interactions with the bound substrates (Figures 1b,c,d). The distances between the side-chain carboxyl groups and the positively charged atoms in the substrates are from 3.4 to 7.2 Å (Lu et al., 2013b).

Moreover, the side chains of S61, Q284 and S288 also contribute to charge complementation, which make charge-dipole interactions with the bound substrates, because the side-chain hydroxyl and carbonyl groups are within 5 Å of the positively charged atoms in the substrates. Surprisingly, the hydrophobic interactions between NorM-NG and the bound substrates are scarce, involving only A57 and F265. F265 in particular makes an edge-to-face aromatic stacking interaction with the substrates (Figures 1b,c,d).

To validate the biological relevance of the multidrug-binding site, the amino acids involved in the binding of all three substrates were substituted. These single mutations, with the exception of S61A, severely impaired the ability of NorM-NG to confer resistance to *E. coli* against TPP, ethidium or R6G (Lu et al., 2013b). Congruent with these observations, these inactivating mutations exerted deleterious effects on the Na^+-dependent drug efflux function.

Altogether, the data suggested that D41, F265, Q284, D355 and D356 play critical roles in multidrug transport, thereby supporting the functional importance of the observed multidrug-binding site. Furthermore, mutations of the counterparts of S266 and S288 in the human MATE protein hMATE1 affected the drug-binding affinity (Otsuka et al., 2005b; Matsumoto et al., 2008), implying a common substrate-binding site among the NorM and eukaryotic MATE transporters (Lu et al., 2013b; Lu, 2016).

Interestingly, in contrast to the multidrug transporters from the ABC, DMT, and MFS families, which utilize numerous aromatic amino acids to bind their

substrates (Chen et al., 2007; Aller et al., 2009; Heng et al., 2015), NorM-NG employs a small number of hydrophobic residues to interact with drugs (Lu et al., 2013b).

At least three acidic residues are used by NorM-NG to neutralize the substrates, which may be important for preventing negatively charged or electroneutral compounds from binding and transport by the protein, thus conferring substrate specificity. The paucity of aromatic and non-polar residues may enable NorM-NG to avoid overly tight association with hydrophobic drugs when the transporter is poised to release substrate (Lu et al., 2013b).

In addition, there are no substantial changes in the positions of amino-acid side chains upon binding different substrates in NorM-NG, similar to what had been observed in the multidrug-binding transcription factors (Bachas et al., 2011; Newberry et al., 2008). The multiple acidic residues in NorM-NG may allow versatile orientation and charge complementation of structurally dissimilar cationic drugs without the need to drastically alter the structure of the multidrug-binding site (Lu et al., 2013b).

Additionally, extracellular loops L3-4 and L9-10 cover the multidrug-binding cavity, which may provide flexibility to optimize transporter-substrate interactions. Indeed, it was subsequently discovered that these extracellular loops can undergo structural changes when NorM-NG interacts with different ligands (Radchenko et al., 2015).

5.4. THE CATION-BINDING SITE IN NORM-NG

Besides the Na^+-free, substrate-bound structures of NorM-NG, the Cs^+-bound structure of NorM-VC was also reported (Lu et al., 2013b). The Cs^+-bound structure represents a “drug”-bound, cation-bound NorM-NG wherein an unidentified ligand acts as a substrate surrogate. This co-structure exhibited no significant conformational difference from that of Na^+-free, drug-bound NorM-NG (rms deviation ~0.5 Å).

This finding is unexpected because the canonical antiport mechanism predicts that the counter-transported cation and substrate compete for a shared binding-site in the transporter, and that substrate and cation must not bind the protein simultaneously (for review see Schuldiner, 2014).

In the Cs^+-bound structure of NorM-NG, the carboxyl group of a conserved E261 and the aromatic ring of a conserved Y294 are within 3.2 Å and 4.4 Å of the cation, respectively, implicating E261 and Y294 as the Na^+-coordinating residues (Figure 2a). Notably, no substrate-binding amino acids in NorM-NG directly

coordinate Cs^+, which mimics the counter-transported Na^+. Interestingly, Y294 makes an uncommon cation-π interaction (Dougherty, 1996).

Of note, membrane protein-ligand interactions mediated by cation-π interactions usually involve positively charged amines, which had been found in a number of ligand-gated acetylcholine receptors and G-protein-coupled receptors, as well as the betaine and carnitine transporters (for review see Zacharis and Dougherty, 2002; Ressel et al., 2009; Tang et al., 2010; Schulze et al., 2010).

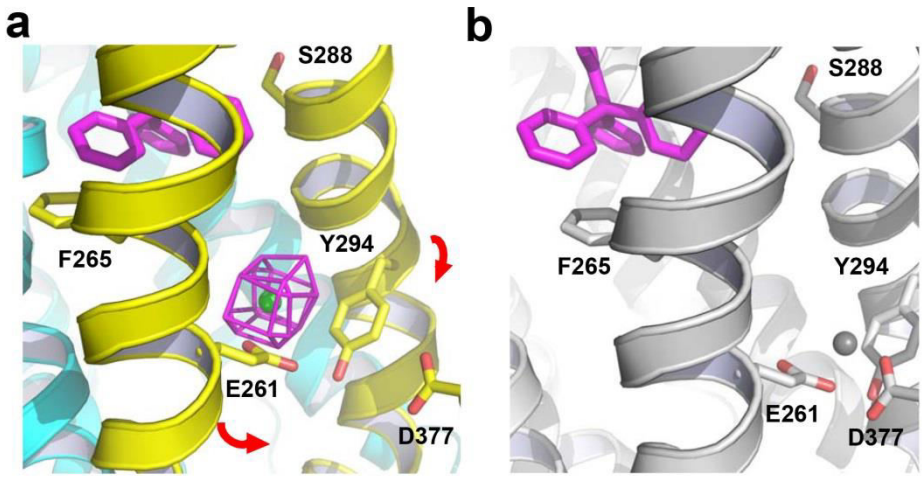

Figure 2. Structure of the cation-binding site in NorM-NG. (**a**) Cs^+-bound structure of NorM-NG (PDB 4HUL). Cs^+ (green sphere) is overlaid with difference isomorphous Fourier map (magenta mesh) contoured at 6 σ. Red arrows indicate a proposed movement of TM7 and TM8 towards TM10. TPP (magenta) taken from the TPP-bound structure (PDB 4HUK) is shown in stick representation to indicate the multidrug-binding site. (**b**) Hypothetical Na^+ (gray sphere) coordination arrangement, relevant amino acids are depicted as stick models and NorM-NG is colored gray.

Generally speaking, cation-π interactions are largely electrostatic in nature and thus well-suited for molecular interaction within a hydrophobic environment, including the lipid bilayer (Dougherty, 1996). Nonetheless, a Na^+-π interaction had never been observed in any membrane protein prior to structure determination of NorM-NG (Lu et al., 2013b). Y294 in NorM-NG presumably makes a cation-π interaction with Na^+, which is also the preferred counter-transported cation (Long et al., 2008).

This cation selectivity likely results from the side-chain carboxylate of E261 being a high-field-strength ligand that favors Na^+ over K^+, as well as from a

higher binding affinity for the Na^+-π relative to K^+-π interaction (Noskov and Roux, 2008; Remko and Soralova, 2012). Furthermore, the relatively weak Na^+-π interaction may offer kinetic advantages, for example, faster rates of Na^+-binding and/or unbinding, as compared with the more common Na^+-coordination arrangement that exclusively involves oxygen atoms (Harding, 2002; Xue et al., 2008).

Mutation of either E261 or Y294 was found to impair the transport function of NorM-NG, therefore supporting the functional importance of the observed cation-binding site (Lu et al., 2013b). Furthermore, although the distance between the carboxyl group of D377 and Cs^+ exceeds 7.2 Å in NorM-NG, previous studies suggested the counterpart of D377 in NorM-VC as a Na^+-coordinating residue in a cation-bound, substrate-free state (He et al., 2010; Lu et al., 2013b).

Mutational studies of D377 counterparts in yet another two MATE proteins, NorM-VP and hMATE1, also indicated that D377 plays an important role in multidrug transport (Otsuka et al., 2005; Matsumoto et al., 2008). Thus, it was concluded that D377 likely coordinates Na^+ in the substrate-free NorM-NG (Figure 2b).

5.5. THE TRANSPORT MECHANISM OF NORM-NG

Based on available biochemical data and structure comparison between the cation-bound, drug-free NorM-VC and drug-bound NorM-NG, a transport mechanism was proposed (Lu et al., 2013b; Lu, 2016). This mechanism predicts that the outward-facing, drug-bound NorM-NG utilizes E261 and Y294 to initiate Na^+-binding from the periplasmic side (Figure 3). Subsequently, D377 becomes involved in Na^+-coordination as TM7 and TM8 shift toward TM10.

As a consequence, F265, Q284 and S288 move away from the multidrug-binding site, thereby triggering the release of bound drug. The Na^+-bound, drug-free NorM-NG then transitions into the inward-open conformation to capture a new drug. Afterwards, TM7 and TM8 move back towards the central cavity upon drug binding, which drives the release of Na^+ into the cytoplasm. The drug-bound, Na^+-free NorM-NG finally switches to the outward-facing conformation to start a new transport cycle (Figure 3).

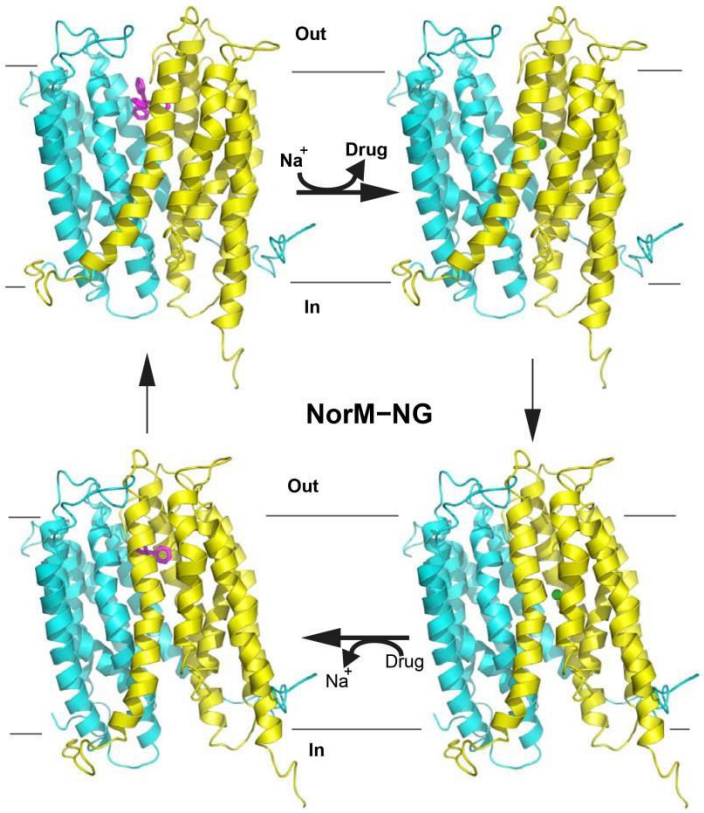

Figure 3. Proposed transport mechanism for NorM-NG. The protein is shown in ribbon representation; TPP (magenta) is drawn as a stick model and Na^+ as a green sphere. The N (residues 5-230) and C (231-459) domains of NorM-NG are colored cyan and yellow, respectively. Na^+ binding to the outward-facing, drug-bound NorM-NG (top left) triggers the release of drug. Subsequently, the Na^+-bound, outward-facing NorM-NG (top right) then switches to the Na^+-bound, inward-facing state (bottom right). Drug binding to NorM-NG promotes the dissociation of Na^+ from the transporter to yield the drug-bound, inward-facing state (bottom left), which eventually returns to the drug-bound, outward-facing conformation (top left).

This mechanism suggests that Na^+ and substrate alternately bind to two spatially distinct sites in NorM-NG during the transport cycle, rather than competing for a common subset of amino acids (Lu et al., 2013b; Lu, 2016). This non-canonical, indirect competition based antiport mechanism involves a fully-loaded intermediate state in which the substrate and counter-transported cation

bind to the transporter simultaneously, as supported by the Cs^+-bound NorM-NG structure (Lu et al., 2013b). In this mechanism, the coupling between drug and counter-transported Na^+ is mediated by structural changes within the transporter (Lu, 2016).

5.6. THE STRUCTURE OF SUBSTRATE-BOUND DINF-BH

Besides NorM-NG, the substrate-bound structure of DinF-BH was also published (Lu et al., 2013a). In contrast to NorM-NG, which is a Na^+-coupled antiporter, DinF-BH is H^+-dependent. Moreover, in NorM-NG, the N domain (TM1-TM6) is structurally related to the C domain (TM7-TM12) around a pseudo-twofold rotational symmetry axis normal to the membrane plane, and the structures of the two domains can be superimposed onto each other with an rms deviation of 2.4 Å (Lu et al., 2013b).

By contrast, structural superimposition of the two domains in DinF-BH results in an rms deviation of 3.3 Å, with the largest difference being in the extracellular halves of TM7-TM8 and their counterparts in TM1-TM2 (Lu et al., 2013a). If those protein residues are excluded, the rms deviation can be lowered to 2.5 Å. Of note, TM7 and TM8 in DinF-BH are more bent near their midsections than TM1 and TM2, respectively.

The bending of TM7 and TM8 in DinF-BH creates a crevice in the C domain (Figure 4a), which is accessible to the periplasm and outer membrane leaflet (Lu, et al. 2013a). This crevice separates the C domain into two layers, with TM7 and TM8 in one and TM9 to TM12 in the other. This helical arrangement suggests that in order to form a similar cation-binding site to that of NorM-NG (Lu et al., 2013b), the unbending or straightening of both TM7 and TM8 is required (Lu et al., 2013a).

In addition, the DinF subfamily lacks the cation-binding motif identified in NorM-NG, which involves E261 (TM7), Y294 (TM8) and D377 (TM10). These data implied that the cation-binding site of DinF-BH differs from that of NorM-NG (Lu, 2016). Indeed, further structural and biochemical studies revealed that the drug/cation coupling mechanism is different between NorM-NG and DinF-BH (Lu et al., 2013a; Radchenko et al., 2015).

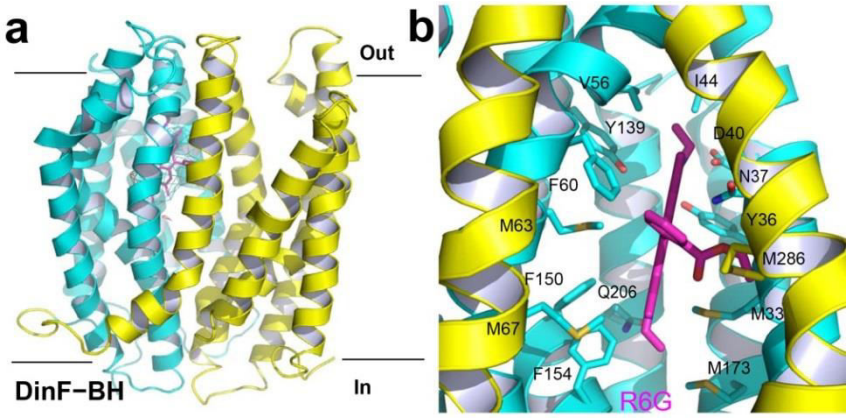

Figure 4. Structure of the substrate-binding site in DinF-BH. (**a**) DinF-BH is shown in ribbon rendition as viewed from the membrane plane, with residues 3-227 and 228-448 colored cyan and yellow, respectively (PDB 4LZ9). The bound R6G is drawn as magenta sticks, which is overlaid with the experimental electron density map (cyan mesh) contoured at 1.5 σ. (**b**) Close-up of the drug-binding chamber, R6G (magenta) and relevant amino acids are displayed in stick representation.

In DinF-BH, TM1-TM8 collectively forms an internal chamber that shelters the bound substrate R6G (Lu et al. 2013a). This chamber harbors numerous hydrophobic amino acids, whose bulky side chains can shield R6G from the external environment (Figure 4b). Additionally, TM7 and TM8 define a lateral opening through which protons from the solvent-filled crevice can enter the chamber.

At the widest point within the membrane bilayer, the opening is 10 Å wide, which is spatially sufficient to allow R6G to diffuse out of the chamber and into the crevice (Lu et al., 2013a). The access to the chamber from the cytoplasmic side, however, is blocked by highly ordered protein structure, suggesting that the R6G-bound structure captures DinF-BH in an outward-facing state.

5.7. DRUG/PROTON COUPLING IN DINF-BH

Within the drug-binding chamber of DinF-BH, the side chains of M33, I44, V56, F60, M63, M67, F150, F154, M173, M286 make van der Waals interactions with R6G; whereas those of Y36, N37, D40, Y139, and Q206 make charge-dipole or charge-charge interactions with bound substrate (Figure 4b). Among them, D40

is conserved within the DinF subfamily and makes the only charge-charge interaction with R6G (Lu et al., 2013a; Lu, 2016). Moreover, the functional importance of the observed transporter-R6G interactions was confirmed by mutational and biochemical studies (Lu et al., 2013a). These studies suggested that M33, D40, I44, V56, M67, M173, Q206 and M286 in DinF-BH play pivotal roles in multidrug transport.

D40 serves as a substrate-binding residue as well as the protonation site, with a calculated and measured pK_a of 7.4 and 7.2, respectively (Lu et al., 2013a). Apparently, the hydrophobicity of the R6G-binding chamber in DinF-BH shifts the pK_a of side-chain carboxylates of D40 upward, and the R6G-bound structure portrays a deprotonated transporter. Based on additional structural and biochemical studies (Lu et al., 2013a; Radchenko et al., 2015), a direct competition based antiport mechanism was proposed for DinF-BH (Figure 5).

This mechanism suggests that protons disrupt drug-binding by competing directly for D40 in the outward-facing, drug-bound DinF-BH. Subsequently, the outward-facing, protonated transporter switches to the inward-facing and protonated state. Drug binding then triggers deprotonation of the transporter by directly competing for D40. Finally, the inward-facing, drug-bound transporter returns to the outward-facing, drug-bound state to begin a new transport cycle.

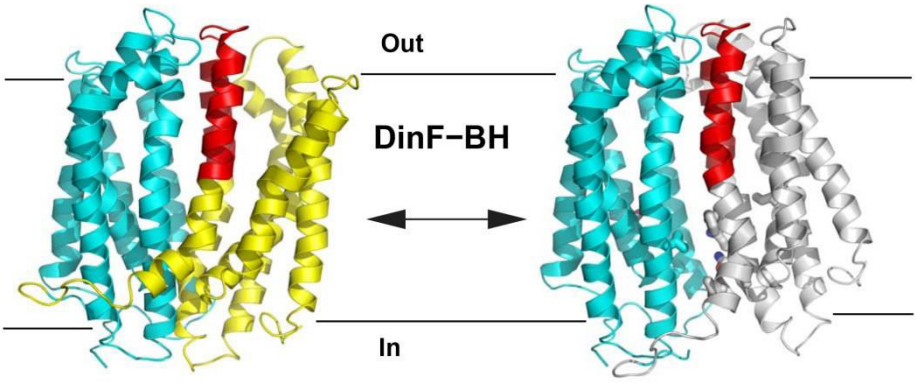

Figure 5. Proposed transport mechanism for DinF-BH. Structure of the outward-facing transporter (left, PDB 4LZ9) and model of the inward-facing state (right) are viewed from the membrane. Residues 3-227 are colored cyan, whereas residues 228-448 are colored yellow (outward-facing structure) or gray (inward-facing model), except for residues 253-288, which are colored red to highlight the bending of TM7 and TM8.

Significantly, these results highlighted a key difference between NorM-NG and DinF-BH in the coupling between substrate and counter-transported cation (Lu et al., 2013a; Lu, 2016). In NorM-NG, the Na^+- and substrate-binding sites are spatially separated, and Na^+ induces drug extrusion indirectly via protein conformational changes. By contrast, in DinF-BH, H^+ triggers drug release by directly competing for the substrate-binding D40, during which no substantial rearrangement of transmembrane helices is needed. This mechanistic difference argued against the view that MATE transporters share a common antiport mechanism (Tanaka et al., 2013).

5.8. THE SUBSTRATE-BOUND STRUCTURE OF I239T/G354E

Although the crystal structures of at least twenty five MFS transporters have been published (for review see Yan, 2013; Quistgaard et al., 2016), the structures of only three multidrug transporters, EmrD, YajR, and MdfA, have been reported (Yin et al., 2008; Jiang et al., 2013; Heng et al., 2015; Liu et al., 2016; Nagarathinam et al., 2018; Zomot et al., 2018; Wu et al., 2019). Notably, EmrD, YajR, and MdfA all belong to the DHA1 subfamily within MFS.

Among them, the drug-bound structures of three MdfA mutants, Q131R, Q131R/L339E, and I239T/G354E, are known (Heng et al., 2015; Zomot et al., 2018; Wu et al., 2019). Since the mutation Q131R or Q131R/L339E severely impairs the transport function of MdfA (Zomot et al., 2018), this chapter focuses on the drug-bound structures of I239T/G354E, which is functionally active (Tirosh et al., 2012; Wu et al., 2019).

MdfA is one of the best characterized MFS multidrug transporters (for review see Fluman and Bibi, 2009; Yardeni et al., 2017). Previous biochemical studies showed that MdfA possesses an extremely broad spectrum of drug recognition and can couple the export of cationic, electroneutral, and zwitterionic drugs to the import of H^+, with a drug/H^+ stoichiometry of 1:1 (Edgar and Bibi, 1997; Fluman et al., 2012). Moreover, prior studies suggested that the membrane-embedded D34 in MdfA serves as the protonation site (Fluman et al., 2012).

Furthermore, a number of MdfA mutants with different transport properties from those of the wild type transporter have been identified, including I239T/G354E (Sigal et al., 2009; Tirosh et al., 2012). In stark contrast to MdfA, which cannot extrude short dicationic compounds such as the neurotoxicant

methyl viologen, I239T/G354E exports both monocationic and short dicationic drugs, with a variable drug/H^+ stoichiometry of 1:2 or 2:2 (Tirosh et al., 2012).

The crystal structure of I239T/G354E in complex with substrate LDAO has been published (Wu et al., 2019), which revealed a structure fold typical of MFS transporters of known structure and virtually identical to that of Q131R (Heng et al., 2015). I239T/G354E is comprised of twelve membrane-spanning segments (TM1-TM12), which form the similarly folded N (TM1-TM6) and C (TM7-TM12) domains (Figure 6a).

The LDAO-binding cavity is located at the interface between these two domains, which is accessible only to the cytoplasm, indicating that the LDAO-bound structure captures I239T/G354E in an inward-facing state (Figure 6b). Unexpectedly, the experimental electron density maps revealed two bound LDAO molecules in I239T/G354E, denoted LDAO1 and LDAO2 (Wu et al., 2019).

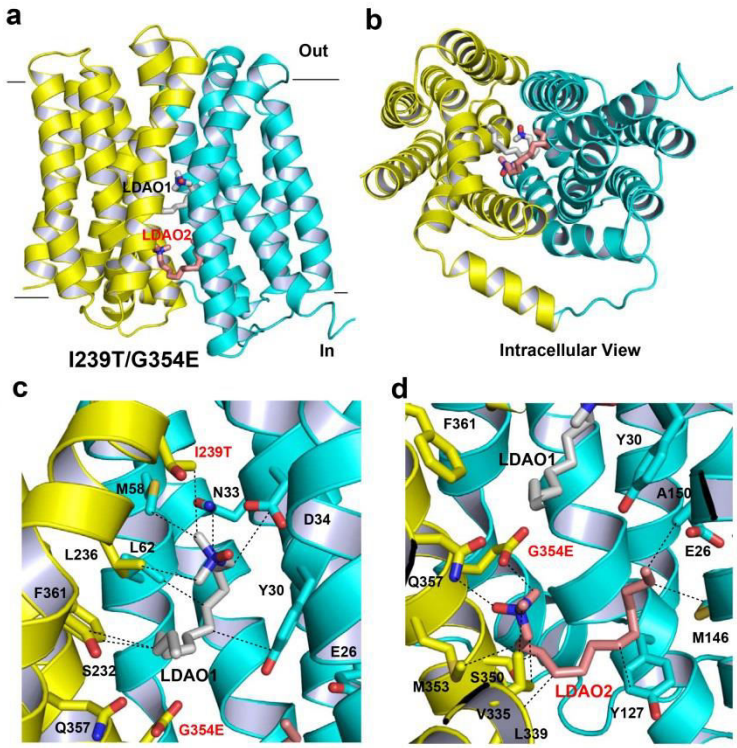

Figure 6. Structure of the LDAO-bound I239T/G354E. (**a**) Structure of I239T/G354E as viewed from the membrane (PDB 6OOM). I239T/G354E is drawn as a ribbon diagram, with the N (9-205) and C (206-400) domains colored cyan and yellow, respectively. The bound LDAO molecules are shown as stick

models and are colored grey and light pink, respectively. (**b**) Cytoplasmic view of the I239T/G354E structure, highlighting the inward-facing conformation of the transporter. (**c**) Close-up view of the LDAO1-binding site, LDAO1 (grey) and relevant amino acids are shown in stick models and close-range interactions are highlighted as dashed lines. (**d**) Structure of the LDAO2-binding site, LDAO2 (light pink) and relevant amino acids are drawn as sticks, dashed lines indicate the interactions between LDAO2 and I239T/G354E.

5.9. THE SUBSTRATE-BINDING SITES IN I239T/G354E

The binding site of LDAO1 (Figure 6c) is similar to that seen in the LDAO-bound structure of MdfA mutant Q131R, which is situated halfway into the lipid bilayer, at about equal distance between the extracellular and intracellular surfaces of the membrane (Heng et al., 2015). The binding site of LDAO2 (Figure 6d), by contrast, is between the LDAO1-binding site and the cytoplasm-membrane interface, ~6 Å from the latter and solvent-accessible (Wu et al., 2019).

Since LDAO1 is more than 5 Å from LDAO2, the two LDAO molecules likely bind the transporter independently. Of note, the structures of LDAO-binding sites in Q131R and I239T/G354E are similar, suggesting that the binding of one LDAO molecule is unlikely to affect the binding of the other allosterically by changing the protein structure (Wu et al., 2019).

LDAO1 engages in polar or electrostatic interactions with the side chains of N33 and D34, and van der Waals interactions with the side chains Y30, N33, M58, L62, S232, L236, I239T, and F361 (Wu et al., 2019). The interactions between LDAO1 and I239T/G354E closely resemble those between LDAO and Q131R (Heng et al., 2015), implying that the LDAO-binding site in MdfA is not affected by the double mutation I239T/G354E (Wu et al., 2019).

On the other hand, LDAO2 makes long-range electrostatic interactions with the side chain of G354E, H-bonds with the side chain of Q357, and forms van der Waals interactions with the side chains of Y127, M146, A150, V335, L339, S350, M353, and G354E (Wu et al., 2019).

Furthermore, it was observed that mutation of Y30, D34, M58, L62, Y127, L236, V335, L339, or F361 abolished the ability of I239T/G354E to confer LDAO resistance to *E. coli* (Wu et al., 2019). Additionally, alanine substitution of N33, M146, I239T, M353 or Q357 suppressed the transport function of I239T/G354E, although to a lesser degree.

These data suggested that the observed interactions between I239T/G354E and LDAO in the crystal structure are functionally important, and that the

majority of the LDAO1- and LDAO2-binding protein residues play pivotal roles in the LDAO-efflux function of I239T/G354E (Wu et al., 2019).

These results argued that I239T/G354E contains two discrete, non-overlapping binding sites for zwitterionic and possibly monocationic drugs (Tirosh et al., 2012; Wu et al., 2019). As such, this finding provided the first direct evidence for a second drug-binding site in any multidrug transporter. Besides I239T/G354E, other multidrug transporters from the ABC, MFS, and RND families may also contain more than one drug-binding site (Putmann et al., 1999; Loo et al., 2003; Nakashima et al., 2011). Thus, the LDAO-bound structure of I239T/G354E serves as an important starting point for understanding how a multidrug transport recognizes and extrudes two drugs in general.

To elucidate the drug/proton coupling mechanism of I239T/G354E, additional mutational and functional studies were carried out (Wu et al., 2019). These studies suggested that during transport, LDAO1 and LDAO2 trigger the release of protons from the side-chain carboxylate of D34 and G354E, respectively. Given the experimental conditions and the measured and calculated pK_a for D34 and G354E, the LDAO-bound structure likely represents a deprotonated I239T/G354E (Wu et al., 2019).

Interestingly, the two substrate- and proton-binding protein residues (D34 and G354E) in I239T/G354E are functionally distinct: the centrally located D34 plays a more important role than the peripherally located G354E (Wu et al., 2019). One plausible explanation for this functional difference is that the binding of drug and/or proton to D34 triggers the protein structural changes required for transport more effectively than that of G354E.

5.10. DRUG/PROTON STOICHIOMETRY AND COUPLING

I239T/G354E, but not MdfA, can also extrude short dicationic drugs such as methyl viologen (MV). The MV-bound structure of I239T/G354E was also reported, which is similar to that of the LDAO-bound complex (Wu et al., 2019). The experimental electron density maps revealed the bound MV, which is located at the apex of the cytoplasm-facing cavity in I239T/G354E (Figure 7a).

MV resides half way into the lipid bilayer and makes numerous contacts with I239T/G354E. Specifically, MV engages in hydrophobic interactions with the side chains of Y30, L119, S232, L235, L236, I327, and Y361 in I239T/G354E. Additionally, the side-chain carboxylate groups of D34 and G354E make long-range charge-charge interactions with bound MV (Wu et al., 2019).

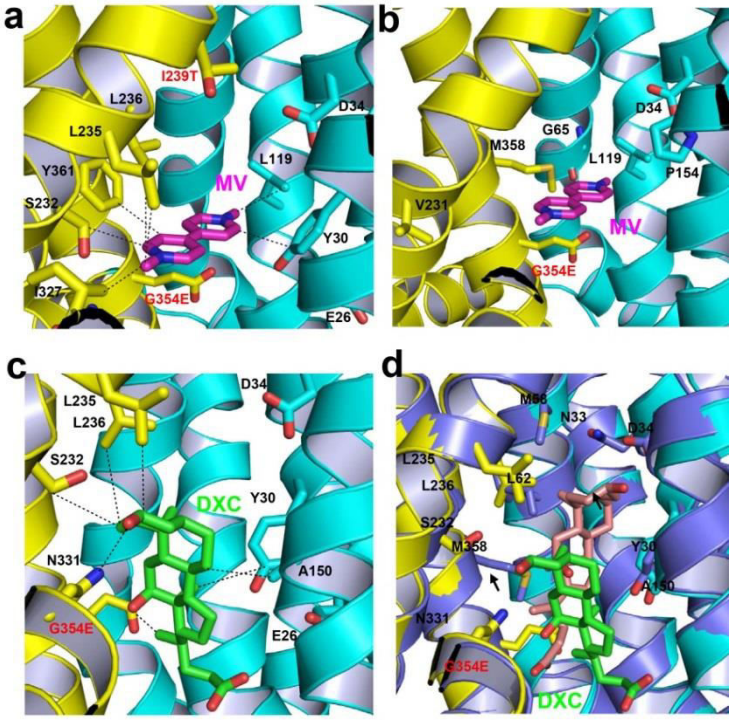

Figure 7. Structures of the MV- and DXC-binding sites in I239T/G354E. (**a**) Close-up view of the MV-binding site in I239T/G354E, with the N and C domains colored cyan and yellow, respectively (PDB 6OOP). The bound MV is drawn in stick models and colored magenta. The relevant amino acids are shown in stick models and close-range interactions are highlighted by dashed lines. (**b**) Location of the mutated amino acids that resulted in the new functionality of transporting short dicationic compounds. The bound MV (magenta) and relevant amino acids are shown in stick models. (**c**) Close-up view of the DXC-binding site within I239T/G354E (PDB 6OOQ). The bound DXC (green) and relevant amino acids are shown in stick models, and the close-range interactions are highlighted by dashed lines. (**d**) Overlay of the DXC-bound Q131R (light blue, PDB 4ZP0) and I239T/G354E, with the DXC-binding amino acids and DXC drawn as stick models. The Q131R-bound DXC is colored light pink and the C1-OH groups are highlighted by black arrows.

The functional importance of transporter-MV interactions was confirmed by mutagenesis and biochemical studies, which revealed that most of the MV-binding amino acids play crucial roles in the I239T/G354E-mediated extrusion of MV (Wu et al., 2019). Since the binding site of MV overlaps with that of LDAO1,

the ability of LDAO-binding site mutants to confer MV resistance was also examined in the presence of LDAO (Wu et al., 2019).

These studies indicated that LDAO competitively inhibits the export of MV by I239T/G354E, and vice versa, which further validated the biological relevance of the LDAO- and MV-bound structures. Further biochemical studies suggested that I239T/G354E catalyzes the exchange of one MV for two protons during transport, with MV inducing the release of two protons from D34 and G354E, which helps to explain why I239T, but not MdfA, can export short dicationic drugs (Tirosh et al., 2012; Wu et al., 2019).

Besides I239T/G354E, previous biochemical studies showed that the MdfA single mutants G65E, L119E, P154E, V231E, G354E and M358E can also extrude short dicationic drugs (Tirosh et al., 2012). The MV-bound structure of I239T/G354E offers an explanation for these observations (Figure 7b), arguing that the side chains of G65E, L119E, P154E, V231E, G354E and M385E interact with the dicationic substrate through long-range electrostatic interactions in the corresponding mutants (Wu et al., 2019).

Since these mutated residues are located within the hydrophobic multidrug-binding cavity, the pK_a of the side-chain carboxylate in the mutated residue is shifted upward, thus enabling the mutated residue to serve as a protonation site in MdfA *in vivo* (Tirosh et al., 2012). Overall, these findings suggested how new functionality can be engineered into MdfA and how its drug/proton stoichiometry is affected by the number of protonation sites (Wu et al., 2019).

5.11. THE STRUCTURE OF INHIBITOR-BOUND I239T/G354E

Aside from LDAO and MV, I239T/G354E and MdfA interact with anionic deoxycholate (DXC) differently. Although the structure of DXC-bound I239T/G354E is similar to that of Q131R, the structure of DXC-binding site is different (Wu et al., 2019). In I239T/G354E, DXC engages in van der Waals interactions with the side chains of Y30, A150, S232, L235, L236, and G354E, whereas the side chain of N331 H-bonds with the C1-OH from DXC (Figure 7c).

If the DXC from the I239T/G354E structure is overlaid onto its counterpart in the DXC-bound Q131R by superimposing the protein structures, the distance between the two C1-OH groups in DXC exceeds 8.6 Å (Figure 7d). Thus, the G354E mutation drastically changed the binding pose of DXC in the transporter (Wu et al., 2019).

In keeping with these structural differences, MdfA, but not I239T/G354E, can extrude DXC (Wu et al., 2019). Although DXC is not transportable by I239T/G354E, it potentiated the bactericidal activity of LDAO or MV. This result can be understood in light of the I239T/G354E structures, which revealed that the binding site of DXC overlaps with those of LDAO1, LDAO2 and MV (Wu et al., 2019).

Therefore, DXC hinders the binding of LDAO or MV to I239T/G354E by acting as a competitive inhibitor. In Q131R, an H-bond is formed between the side-chain carboxylate of D34 and C1-OH of DXC, which may trigger the deprotonation of D34; in I239T/G354E, however, no H-bond is made between DXC and D34 or G354E (Wu et al., 2019).

These findings shed new light on the fundamental difference between substrate and inhibitor, suggesting that effective therapeutic drugs may be designed to evade extrusion by any H^+-coupled multidrug antiporter if they lack the chemical groups to stimulate deprotonation of the drug transporter (Wu et al., 2019).

Take chloramphenicol (Cm) for example. In the Cm-bound Q131R structure, both the C4-OH and C5-OH in Cm H-bond with the side-chain carboxylate of D34, likely to trigger the deprotonation of the transporter (Heng et al., 2015). In principle, if both the C4-OH and C5-OH are methylated or replaced by hydrogen and/or fluorine atoms, the modified Cm would not deprotonate D34 and hence can no longer be exported by MdfA. Evasion of the transporter-mediated efflux by the modified Cm, and any other antimicrobial agent, will increase the intracellular concentration of these compounds and augment their therapeutic efficacy (Wu et al., 2019).

5.12. THE ANTIPORT MECHANISM OF I239T/G354E

The crystal structures of I239T/G354E and of outward-facing MdfA can be used together to infer a unified transport mechanism for I239T/G354E (Nagarathinam et al., 2018; Wu et al., 2019). Briefly, substrate can induce the release of two protons from D34 and G354E in the inward-facing transporter, via charge-charge and/or H-bonding interactions (Wu et al., 2019). The substrate-bound, deprotonated I239T/G354E subsequently adopts the outward-facing conformation (Figure 8), which is followed by the protonation of D34 and G354E, thereby triggering the release of substrate. The substrate-free, protonated transporter returns to the inward-facing conformation to acquire substrate in a new round of transport.

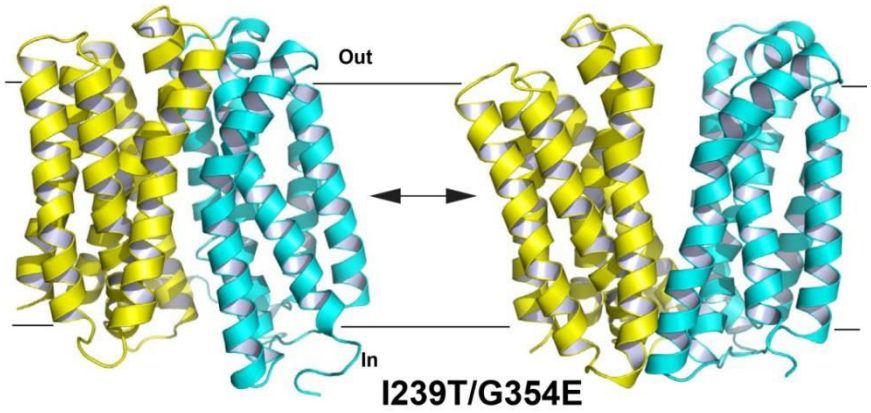

Figure 8. Proposed transport mechanism for I239T-G354E. Structure of the inward-facing transporter (left, PDB 6OOM) and model of the outward-facing state (right) are viewed from the membrane. Residues 9-205 are colored cyan, whereas residues 206-400 are colored yellow.

Among the three membrane-embedded acidic amino acids within I239T/G354E, D34 and G354E are the shared binding sites for substrate(s) and H^+; E26, with a calculated pK_a of >8, may facilitate substrate binding and perhaps H^+ translocation (Wu et al., 2019).

Notably, in I239T/G354E, the LDAO1- and MV-binding sites are overlapping; whereas in QacA, another MFS multidrug transporter, the binding sites for dicationic and monocationic substrates are different (Wu et al., 2019;), highlighting the mechanistic diversity among MFS multidrug antiporters. In accord with this difference, I239T/G354E catalyzes electroneutral exchange of H^+ for monocationic substrate, whereas the QacA-mediated drug/H^+ antiport is electrogenic (Mitchell et al., 1999; Tirosh et al., 2012).

Furthermore, although the outward-facing structure of I239T/G354E is unknown, the outward-facing MdfA structure can be utilized to model the transporter-drug interactions in the outward-facing I239T/G354E (Nagarathinam et al., 2018). This analysis revealed that the positioning of LDAO1 or MV is largely compatible with the outward-facing I239T/G354E, although some of the interactions between the inward-facing transporter and LDAO1 or MV may be ruptured in the outward-facing state.

The modeling also implied that steric clash between the transporter and bound ligand would arise if the positioning of LDAO2 or DXC remains unchanged in the outward-facing I239T/G354E. It is conceivable that the malleable LDAO2 would alter its binding pose to accommodate the outward-facing I239T-G354E, while

the relatively rigid DXC would not, implying that DXC only targets inward-facing I239T/G354E.

5.13. HIGHLIGHTS AND OUTLOOK

This chapter gives an updated account of the substrate-bound structures of MATE and MFS multidrug transporters, which bear similar and yet distinct protein folds (He et al., 2010). These structures suggest that multidrug transporters interact with distinct substrates differently: they use several H-bonds to recognize electroneutral and anionic substrates, while they recognize zwitterionic and cationic substrates via charge-charge interactions (Heng et al., 2015; Wu et al., 2019).

The broad substrate specificity results from the preponderance of non-specific hydrophobic interactions between the substrate and transporter, such as in DinF-BH and I239T/G354E (Lu et al., 2013a; Wu et al., 2019), in addition to the involvement of long-range charge-charge interactions, such as in NorM-NG and I239T/G354E (Lu et al., 2013b; Radchenko et al., 2015; Wu et al., 2019). Furthermore, the existence of two discrete drug-binding sites, as seen in LDAO-bound I239T/G354E, accommodate two drugs of various sizes and shapes, further broadening the substrate specificity (Wu et al., 2019).

The long-range electrostatic interactions can be enhanced by more than 10-fold by the low-dielectric environment in lipid bilayer, which lack stringent geometric requirements but are functionally important for the following reasons (Wu et al., 2019). First, they mediate substrate-induced proton release (Radchenko et al., 2015; Wu et al., 2019). Second, they allow the transporter to preferably export substrates carrying positive charges, especially if the transporter contains two or more protonatable, acidic amino acids in the multidrug-binding site (Lu, 2016).

MATE and MFS multidrug transporters are therefore polyspecific rather than nonspecific: specificity arises because specific H-bonds, although small in number, are used to select electroneutral or anionic drugs (Heng et al., 2015), and the overall size and shape of bound drugs must fit the multidrug-binding site (Lu, 2016; Wu et al., 2019); whereas promiscuity or non-specificity exists because structurally dissimilar drugs with positive charges can be recognized through long-range charge-charge interactions (Radchenko et al., 2015; Wu et al., 2019).

In terms of the drug/cation coupling mechanism, I239T/G354E and DinF-BH are similar, in which the drug and H^+ compete for a shared binding site, even though DinF-BH exhibits structural asymmetry due to the bending of TM7 and

TM8 (Lu, 2016; Wu et al., 2019). The coupling mechanism of NorM-NG is unusual, which involves rearrangement of transmembrane helices in the C domain, including TM7 and TM8. Nonetheless, based on the amino-acid sequence analysis, the drug/cation coupling mechanism of NorM-NG may be shared by the eukaryotic MATE transporters (Lu, 2016).

Furthermore, a direct competition based antiport mechanism in principle is more likely to tolerate alteration of the multidrug- and proton-binding residues than that of indirect competition. Indeed, prior studies demonstrated that the transport function of MdfA can be retained despite the relocation of D34 (Sigal et al., 2009).

Besides I239T/G354E, some other membrane transporters can also interact with two substrates simultaneously (Schultz et al., 2010; Li et al., 2015; Quick et al., 2018), including the betaine-choline-carnitine-transporter (BCCT), neurotransmitter/sodium symporter (NSS) and solute/sodium symporter (SSS). In BCCT, NSS and likely SSS, however, the second bound substrate facilitates the transport of the first substrate, acting as an allosteric regulator.

Thus, BCCT, NSS and SSS proteins function differently from I239T/G354E since in the former, the second substrate binds the transporter throughout the transport cycle and is not transported along with the first, primary substrate (Schultz et al., 2010). Furthermore, two substrate molecules interact with I239T/G354E independently, rather than allosterically (Tirosh et al., 2012; Wu et al., 2019).

In theory, membrane transporters with a sufficiently large substrate-binding pocket and two or more protonation sites, such as I239T/G354E, can transport two substrates during the same transport cycle. By contrast, those transporters with a relatively small substrate-binding pocket, tend to translocate only one substrate per cycle. In this regard, multidrug transporters are well suited for extruding two drugs simultaneously because they generally possess a voluminous drug-binding pocket and two or more membrane-embedded protonatable amino acids (Fluman and Bibi, 2009).

Although important mechanistic insights can be garnered from the structures of substrate-bound MATE and MFS multidrug transporters (Lu et al., 2013a; Lu et al., 2013b; Wu et al., 2019), major gaps in our knowledge remain unaddressed. In particular, the outward-facing structure of NorM-NG, DinF-BH, or I239T/G354E, is unknown, which greatly hampers our understanding of the alternating access transport mechanism (Lu, 2016). Furthermore, the substrate-bound structure of any eukaryotic MATE transporter is lacking, which must be tackled by future work in order to gain new insights into the antiport mechanism

of MATE proteins as well as the mechanistic similarity and difference among the different subfamilies of MATE transporters.

ACKNOWLEDGEMENTS

We thank the past and present members of the Lu laboratory for their contributions to the research on MATE and MFS multidrug transporters. This work was in part supported by the US National Institutes of Health (R01-GM094195).

REFERENCES

Ahmad I, Nawaz N, Ur Rahman S, Sajid A, Khan FA, Khan SB, Mustafa MZ, Patching SG. Multifaceted roles of efflux proteins in prokaryotes. *AJBLS*. 2018;7(1):1-7.

Ahmad I, Nawaz N, Dermani FK, Kohlan AK, Saidijam M, Patching SG. Bacterial multidrug efflux proteins: A major mechanism of antimicrobial resistance. *Curr Drug Targets*. 2020 DOI: 10.2174/1389450119666180426103300.

Aller SG, Yu J, Ward A, Weng Y, Chittaboina S, Zhuo R, Harrell PM, et al. Structure of P-glycoprotein reveals a molecular basis for poly-specific drug binding. *Science*. 2009;323(5922):1718–1722.

Bachas S, Eginton C, Gunio D, Wade H. Structural contributions to multidrug recognition in the multidrug resistance (MDR) gene regulator, BmrR. *Proc Natl Acad Sci U S A*. 2011;108(27):11046–11051.

Brown MH, Paulsen IT, Skurray RA. The multidrug efflux protein NorM is a prototype of a new family of transporters. *Mol Microbiol*. 1999;31(1):394–395.

Chen YJ, Pornillos O, Lieu S, Ma C, Chen AP, Chang G. X-ray structure of EmrE supports dual topology model. *Proc Natl Acad Sci U S A*. 2007;104(48):18999–19004.

Chitsaz M, Brown MH**.** The role played by drug efflux pumps in bacterial multidrug resistance. *Essays Biochem*. 2017;61(1):127–139.

Dougherty DA. Cation-pi interactions in chemistry and biology: a new view of benzene, Phe, Tyr, and Trp. *Science*. 1996;271(5246):163–168.

Edgar R, Bibi E. MdfA, an *Escherichia coli* multidrug resistance protein with an extraordinarily broad spectrum of drug recognition. *J Bacteriol*. 1997;179(7):2274–2280.

Fischbach MA, Walsh CT. Antibiotics for emerging pathogens. *Science*. 2009;325(5944):1089–1093.

Fluman N, Adler J, Rotenberg SA, Brown MH, Bibi E. Export of a single drug molecule in two transport cycles by a multidrug efflux pump. *Nat Commun*. 2014;5:4615.

Fluman N, Bibi E. Bacterial multidrug transport through the lens of the major facilitator superfamily. *Biochim Biophys Acta*. 2009;1794(5):738–747.

Fluman N, Ryan CM, Whitelegge JP, Bibi E. Dissection of mechanistic principles of a secondary multidrug efflux protein. *Mol Cell*. 2012;47(5):777–787.

Hall W, McDonnell A, O'Nell J. *Superbugs, An Arms Race Against Bacteria*. Harvard University Press, 2018, pp40–45.

Harding MM. Metal-ligand geometry relevant to proteins and in proteins: sodium and potassium. *Acta Crystallogr D Biol Crystallogr*. 2002;58(Pt 5):872–874.

He GX, Kuroda T, Mima T, Morita Y, Mizushima T, Tsuchiya T. An H(+)-coupled multidrug efflux pump, PmpM, a member of the MATE family of transporters, from *Pseudomonas aeruginosa. J Bacteriol*. 2004;186(1):262–265.

He X, Szewczyk P, Karyakin A, Evin M, Hong WX, Zhang Q, Chang G. Structure of a cation-bound multidrug and toxic compound extrusion transporter. *Nature*. 2010;467(7318):991–994.

Heng J, Zhao Y, Liu M, Liu Y, Fan J, Wang X, Zhao Y, Zhang XC. Substrate-bound structure of the *E. coli* multidrug resistance transporter MdfA. *Cell Res*. 2015;25(9):1060–1073.

Higgins CF. Multiple molecular mechanisms for multidrug resistance transporters. *Nature*. 2007;446(7137):749–757.

Jiang D, Zhao Y, Wang X, Fan J, Heng J, Liu X, Feng W, et al. Structure of the YajR transporter suggests a transport mechanism based on the conserved motif A. *Proc Natl Acad Sci U S A*. 2013;110(36):14664–14669.

Kaback HR, Guan L. It takes two to tango: The dance of the permease. *J Gen Physiol*. 2019;151(7):878–886.

Kuroda T, Tsuchiya T. Multidrug efflux transporters in the MATE family. *Biochim Biophys Acta*. 2009;1794(5):763–768.

Kusakizako T, Claxton DP, Tanaka Y, Maturana AD, Kuroda T, Ishitani R, Mchaourab HS, Nureki O. Structural basis of H^+-dependent conformational change in a bacterial MATE transporter. *Structure*. 2019;27(2):293–301.e3.

Liu M, Heng J, Gao Y, Wang X. Crystal structures of MdfA complexed with acetylcholine and inhibitor reserpine. *Biophys Rep*. 2016;2(2):78–85.

Long F, Rouquette-Loughlin C, Shafer WM, Yu EW. Functional cloning and characterization of the multidrug efflux pumps NorM from *Neisseria gonorrhoeae*

and YdhE from *Escherichia coli*. *Antimicrob Agents Chemother*. 2008;52(9):3052–3060.

Lu M. Structures of multidrug and toxic compound extrusion transporters and their mechanistic implications. *Channels (Austin)*. 2016;10(2):88–100.

Lu M, Radchenko M, Symersky J, Nie R, Guo Y. Structural insights into H^+-coupled multidrug extrusion by a MATE transporter. *Nat Struct Mol Biol*. 2013;20(11):1310–1317.

Lu M, Symersky J, Radchenko M, Koide A, Guo Y, Nie R, Koide S. Structures of a Na^+-coupled, substrate-bound MATE multidrug transporter. *Proc Natl Acad Sci U S A*. 2013;110(6):2099–2104.

Loo TW, Bartlett MC, Clarke DM. Simultaneous binding of two different drugs in the binding pocket of the human multidrug resistance P-glycoprotein. *J Biol Chem*. 2003;278(41):39706–39710.

Matsumoto T, Kanamoto T, Otsuka M, Omote H, Moriyama Y. Role of glutamate residues in substrate recognition by human MATE1 polyspecific H^+/organic cation exporter. *Am J Physiol Cell Physiol*. 2008;294(4):C1074–C1078.

Mitchell BA, Paulsen IT, Brown MH, Skurray RA. Bioenergetics of the Staphylococcal multidrug export protein QacA. Identification of distinct binding sites for monovalent and divalent cations. *J Biol Chem.* 1999;274:3541–3548.

Miyauchi H, Moriyama S, Kusakizako T, Kumazaki K, Nakane T, Yamashita K, Hirata K, et al. Structural basis for xenobiotic extrusion by eukaryotic MATE transporter. *Nat Commun*. 2017;8(1):1633.

Morita Y, Kataoka A, Shiota S, Mizushima T, Tsuchiya T. NorM of *Vibrio parahaemolyticus* is an Na(+)-driven multidrug efflux pump. *J Bacteriol*. 2000;182(23):6694–6697.

Mousa JJ, Yang Y, Tomkovich S, Shima A, Newsome RC, Tripathi P, Oswald E, Bruner SD, Jobin C. MATE transport of the *E. coli*-derived genotoxin colibactin. *Nat Microbiol*. 2016;1:15009.

Nagarathinam K, Nakada-Nakura Y, Parthier C, Terada T, Juge N, Jaenecke F, Liu K, et al. Outward open conformation of a Major Facilitator Superfamily multidrug/H^+ antiporter provides insights into switching mechanism. *Nat Commun*. 2018;9(1):4005.

Nakashima R, Sakurai K, Yamasaki S, Nishino K, Yamaguchi A. Structures of the multidrug exporter AcrB reveal a proximal multisite drug-binding pocket. *Nature*. 2011;480(7378):565–569.

Newberry KJ, Huffman JL, Miller MC, Vazquez-Laslop N, Neyfakh AA, Brennan RG. Structures of BmrR-drug complexes reveal a rigid multidrug binding pocket and transcription activation through tyrosine expulsion. *J Biol Chem*. 2008;283(39):26795–26804.

Noskov SY, Roux B. Control of ion selectivity in LeuT: two Na+ binding sites with two different mechanisms. *J Mol Biol*. 2008;377(3):804–818.

Omote H, Hiasa M, Matsumoto T, Otsuka M, Moriyama Y. The MATE proteins as fundamental transporters of metabolic and xenobiotic organic cations. *Trends Pharmacol Sci*. 2006;27(11):587–593.

Otsuka M, Matsumoto T, Morimoto R, Arioka S, Omote H, Moriyama Y. A human transporter protein that mediates the final excretion step for toxic organic cations. *Proc Natl Acad Sci U S A*. 2005;102(50):17923–17928.

Otsuka M, Yasuda M, Morita Y, Otsuka C, Tsuchiya T, Omote H, Moriyama Y. Identification of essential amino acid residues of the NorM Na^+/multidrug antiporter in *Vibrio parahaemolyticus*. *J Bacteriol*. 2005;187(5):1552–1558.

Putman M, Koole LA, van Veen HW, Konings WN. The secondary multidrug transporter LmrP contains multiple drug interaction sites. *Biochemistry*. 1999;38(42):13900–13905.

Quistgaard EM, Löw C, Guettou F, Nordlund P. Understanding transport by the major facilitator superfamily (MFS): structures pave the way. *Nat Rev Mol Cell Biol*. 2016;17(2):123–132.

Radchenko M, Symersky J, Nie R, Lu M. Structural basis for the blockade of MATE multidrug efflux pumps. *Nat Commun*. 2015;6:7995.

Remko M, Šoralová S. Effect of water coordination on competition between π and non-π cation binding sites in aromatic amino acids: L-phenylalanine, L-tyrosine, and L-tryptophan Li^+, Na^+, and K^+ complexes. *J Biol Inorg Chem*. 2012;17(4):621–630.

Ressl S, Terwisscha van Scheltinga AC, Vonrhein C, Ott V, Ziegler C. Molecular basis of transport and regulation in the Na(+)/betaine symporter BetP. *Nature*. 2009;458(7234):47–52.

Saier MH Jr, Paulsen IT. Phylogeny of multidrug transporters. *Semin Cell Dev Biol*. 2001;12(3):205–213.

Schuldiner S. Competition as a way of life for H(+)-coupled antiporters. *J Mol Biol*. 2014;426(14):2539–2546.

Schulze S, Köster S, Geldmacher U, Terwisscha van Scheltinga AC, Kühlbrandt W. Structural basis of Na(+)-independent and cooperative substrate/product antiport in CaiT. *Nature*. 2010;467(7312):233–236.

Sigal N, Fluman N, Siemion S, Bibi E. The secondary multidrug/proton antiporter MdfA tolerates displacements of an essential negatively charged side chain. *J Biol Chem.* 2009;284(11):6966–6971.

Tanaka Y, Hipolito CJ, Maturana AD, Ito K, Kuroda T, Higuchi T, Katoh T, et al. Structural basis for the drug extrusion mechanism by a MATE multidrug transporter. *Nature*. 2013;496(7444):247–251.

Tanaka Y, Iwaki S, Tsukazaki T. Crystal structure of a plant multidrug and toxic compound extrusion family protein. *Structure*. 2017;25(9):1455–1460.e2.

Tang L, Bai L, Wang WH, Jiang T. Crystal structure of the carnitine transporter and insights into the antiport mechanism. *Nat Struct Mol Biol*. 2010;17(4):492–496.

Tirosh O, Sigal N, Gelman A, Sahar N, Fluman N, Siemion S, Bibi E. Manipulating the drug/proton antiport stoichiometry of the secondary multidrug transporter MdfA. *Proc Natl Acad Sci U S A*. 2012;109(31):12473–12478.

Wu HH, Symersky J, Lu M. Structure of an engineered multidrug transporter MdfA reveals the molecular basis for substrate recognition. *Commun Biol*. 2019;2(1):210.

Xue Y, Davis AV, Balakrishnan G, Stasser JP, Staehlin BM, Focia P, Spiro TG, Penner-Hahn JE, O'Halloran TV. Cu(I) recognition via cation-pi and methionine interactions in CusF. *Nat Chem Biol*. 2008;4(2):107–109.

Yan N. Structural advances for the major facilitator superfamily (MFS) transporters. *Trends Biochem Sci*. 2013;38(3):151–159.

Yan N. A glimpse of membrane transport through structures-advances in the structural biology of the GLUT glucose transporters. *J Mol Biol*. 2017;429(17):2710–2725.

Yardeni EH, Zomot E, Bibi E. The fascinating but mysterious mechanistic aspects of multidrug transport by MdfA from *Escherichia coli*. *Res Microbiol*. 2018;169(7–8):455–460.

Yin Y, He X, Szewczyk P, Nguyen T, Chang G. Structure of the multidrug transporter EmrD from *Escherichia coli*. *Science*. 2006;312(5774):741–744

Zacharias N, Dougherty DA. Cation-pi interactions in ligand recognition and catalysis. *Trends Pharmacol Sci*. 2002;23(6):281–287.

Zakrzewska S, Mehdipour AR, Malviya VN, Nonaka T, Koepke J, Muenke C, Hausner W, Hummer G, Safarian S, Michel H. Inward-facing conformation of a multidrug resistance MATE family transporter. *Proc Natl Acad Sci U S A*. 2019;116(25):12275–12284.

Zomot E, Yardeni EH, Vargiu AV, Tam HK, Malloci G, Ramaswamy VK, Perach M, Ruggerone P, Pos KM, Bibi E. A new critical conformational determinant of multidrug efflux by an MFS transporter. *J Mol Biol*. 2018;430(9):1368–1385.

Submitted: 7th Nov 2019, Revised: 5th Dec 2019, Accepted: 3rd Jan 2020

Chapter Six

6. *VIBRIO CHOLERAE* MEMBRANE PROTEINS IN ANTIMICROBIAL RESISTANCE AND VIRULENCE

Manjusha Lekshmi[1], Nicholas Wenzel[2], Sanath H. Kumar[1], Manuel F. Varela[2,*]

[1]Post Harvest Technology, ICAR-Central Institute of Fisheries Education, Seven Bungalows, Andheri (W), Mumbai, 400061, India

[2]Department of Biology, Eastern New Mexico University, Portales, NM 88130, USA

ABSTRACT

Vibrio cholerae, the causative agent of cholera, is a common estuarine bacterium and a versatile human pathogen. The success of this pathogen can be attributed to the myriad of membrane proteins that contribute to its physiology of persistence in the aquatic environment and its virulence characters. Membrane proteins also contribute to antimicrobial resistance in *V. cholerae*. The ToxR-regulated outer membrane protein OmpU is an important virulence protein of *V. cholerae*, which is also essential for its survival in hostile environments. OmpU, along with another membrane protein, OmpT, mediates resistance to bile, detergents and antimicrobial peptides. In *V. cholerae*, antimicrobial resistance is mediated by efflux pumps belonging to the RND (resistance-nodulation-division) family such as VexABDK and to the MFS (major facilitator superfamily) such as the EmrD3 transporter. Some RND efflux pumps such as VexB, VexD, and VexK contribute to the virulence of *V. cholerae*, and the mutants lacking these proteins were attenuated in a mouse model. The production of cholera toxin and the toxin co-regulated protein, two important virulence proteins of *V. cholerae*, were significantly reduced in RND-negative mutants. The proton-driven EmrD3 efflux pump of *V. cholerae* confers resistance to an

* Direct all correspondence to Dr. Manuel Varela; Department of Biology, Eastern New Mexico University, Portales, NM 88130, USA. E-mail: manuel.varela@enmu.edu.

array of anionic detergents, dyes and antibiotics. Inhibition of efflux pumps with synthetic or natural compounds can reduce the virulence of *V. cholerae* and restore its susceptibility to conventional antibiotic treatment. A complex network involving quorum sensing, efflux pumps and virulence gene expression has also been elucidated in *V. cholerae*, suggesting that membrane proteins represent a hub of molecular activities regulating multiple physiologies and virulence of pathogenic bacteria such as *V. cholerae*.

Keywords: *Vibrio cholerae*, virulence, efflux pump, outer membrane proteins, ToxRS, biofilm

6.1. *VIBRIO CHOLERAE* - A VERSATILE HUMAN PATHOGEN

Cholera disease caused by *Vibrio cholerae* can affect up to 4 million people each year and, of those infected annually, between 28,000–130,000 may succumb to the disease (WHO, 2004; GBD 2015 Mortality and Causes of Death Collaborators, 2016). Increased prevalence of cholera infection occurs in underdeveloped and overcrowded regions of the world, where food and water sanitation practices are inadequate (WHO, 2004). In addition to its occurrence as an endemic disease in these underdeveloped regions, cholera can cause large-scale epidemic outbreaks in more developed middle-income countries.

Cholera disease owes its pathogenicity to toxigenic serotypes of *V. cholerae* (Foster, Aliabadi and Slonczewski, 2018). *V. cholerae* is most often spread via fecal-oral transmission of contaminated food and water sources (CDC, 2019). Infected individuals gradually begin to suffer from acute but severe watery diarrhea, which contains billions of organisms that can make their way into water systems used by others (Azman et al., 2013; NIH, 2017). Those suffering from a severe cholera infection often experience rapid dehydration and hyponatremia, both of which can be fatal if not treated (Foster, Aliabadi and Slonczewski, 2018). Accelerated oral or intravenous rehydration with isotonic liquids is the basis for treating an infected individual (Harris et al., 2012). Successful rehydration care can reduce the mortality of a severe cholera infection to less than 0.2% (Sack et al., 2004). Prevention of the disease is focused around preparedness, surveillance, and effective sanitation methods (WHO, 2004). Vaccination provides an additional level of cholera prevention, and several killed oral whole cell vaccines against cholera are in the market (Sinclair et al., 2011). Appropriate administration of these vaccines can prevent 50–60% of cholera incidents; however their adoption into the regular vaccination routines of affected countries

is dependent on the cost-effectiveness as a result of the prevalence of infection and access to rehydration therapy in the area.

6.1.1. Virulence of *V. cholerae*

V. cholerae is a motile, Gram-negative, curved rod-shaped bacterium of the family *Vibrionaceae*. Based on the structure of their cell surface lipopolysaccharides, *V. cholerae* strains are classified into more than 200 serogroups. Of these, only the O1 and O139 serotypes can produce the cholera toxin (CT) and cause severe pandemic cholera (Kaper, Morris and Levine, 1995). The O1 serotype is further classified into the classical and El Tor biotypes based on phenotypic differences such as their susceptibility to polymyxin B and phage infection pattern (Conner et al., 2016).

V. cholerae is an opportunistic pathogen that causes human infections through contaminated food and water. The organism has to pass the gastric acid barrier of the stomach before it can reach the upper small intestine, where it typically colonizes and causes infection. To continue its life cycle, *V. cholerae* exits the host during excretion and then find its way back to an aquatic environment (Reidl and Klose, 2002).

Cholera toxin (CT) belonging to the AB_5 family of ADP-ribosyltransferase, and a toxin co-regulated pilus (TCP) that mediates adherence and microcolony formation are the major factors contributing to virulence of *V. cholerae* (Kaper, Morris and Levine, 1995). The enterotoxin affects ion transport by intestinal epithelial cells and TCP helps the organism to colonize the small intestinal epithelium. Excessive loss of water and electrolytes following infection leads to severe diarrhea which is characteristic of cholera (Silva and Benitez, 2016). The cholera toxin subunits are encoded by the genes *ctxA* and *ctxB*. The genes required for TCP biogenesis form a large cluster known as the *V. cholerae* pathogenicity island (VPI). Within this cluster, *tcpA* encodes the major pilus subunit (Karaolis et al., 1998).

6.1.2. Life of *V. cholerae* outside the host, in the environment

V. cholerae spends the majority of its life cycle outside of the human host in estuarine and coastal environments. Many strains of *V. cholerae* including the toxigenic ones are present naturally in aquatic ecosystems and hence exist as facultative human pathogens (Colwell, Kaper and Joseph, 1977). Within the

marine environment, they attach to surfaces provided by plants, copepods (zooplankton), crustaceans, and insects (Huq et al., 1983). In order to survive in the marine and estuarine environment, *V. cholerae* makes use of several mechanisms to tide over the adverse conditions. Some of these include biofilm formation, shifting to a viable but non-culturable state, nutrient storage and initiation of protective responses to specific physiological and biological stressors. While inhabiting aquatic environments, *V. cholerae* can be found as biofilms or free swimming *vibrios* (Sack et al., 2004).

Biofilms are mutli-cellular microbial communities that are composed of cells attached to a substratum, an interface, or to each other and are embedded in a self-produced matrix. Biofilms can be present on a variety of surfaces such as living tissues or even plastics and metals (Varela et al., 2017). Biofilms contribute to the environmental persistence of *V. cholerae* and provide protection from a number of environmental stresses, including nutrient limitation and predation by protozoa and bacteriophages (Conner et al., 2016). *V. cholerae* biofilm formation is a well-regulated process that can be triggered by quorum sensing and the subsequent up or down regulation of *Vibrio* pathogenicity island-1 (VPI-1) or *V. cholerae* biofilm matrix cluster (VcBMC)-associated genes (Teschler et al., 2015; Lekshmi et al., 2018). Biofilm formation begins with the *V. cholerae* type IV pilus attaching to a surface, after which bacteria begin to form microcolonies and secrete *Vibrio* polysaccharide (VPS) (Watnick and Kolter, 1999). The development of highly organized, three-dimensional biofilm structures occurs following the formation of microcolonies. The extracellular matrix is composed of *Vibrio* polysaccharides, the biofilm matrix proteins, and extracellular nucleic acids, each playing unique roles in infection by *V. cholerae* (Watnick and Kolter, 1999). VPS is the structural basis for the three-dimensional lattice that is the *V. cholerae* biofilm (Mukherjee et al., 2016). Growth and transcription profiles of these biofilms follow an altered phenotype (Silva and Benitez, 2016). Once biofilm formation is complete, *V. cholerae* begin to reduce the production of both motility structures and the expression of certain virulence genes, as they become unnecessary (Moorthy and Wanick 2004; Tischler and Camilli 2004). The gene expression pattern of a mature biofilm provides resistance to environmental stressors. The formation of biofilms alone are enough to confer antimicrobial resistance to *V. cholerae* (Mukherjee et al., 2016). *V. cholerae* must be capable of adopting both motile and biofilm lifestyles during the infective process to successfully colonize the intestine and result in characteristic diarrhea (Fong and Yildiz, 2008).

6.2. STRUCTURAL AND FUNCTIONAL FEATURES OF MAJOR MEMBRANE PROTEINS OF *V. CHOLERAE*

The efflux pumps and porins situated in the membrane of *V. cholerae* are accompanied by many other additional proteins. The well-studied type II secretion system (T2SS) of *V. cholerae* and *E. coli* are a common class of such membrane proteins (Dunstan et al., 2013; Natarajan, Singh and Rapaport, 2019). Secretion systems are common in Gram-negative bacteria and in *V. cholerae, a* particular T2SS is responsible for the secretion of CT (Korotkov, Sandkvist and Hol, 2012). *V. cholerae* T2SS is a complex multiprotein system consisting of inner and outer membrane portions of the Gram-negative cell wall, which together facilitate the translocation of the CT protein through the bacterial membrane and into the exoplasm of a bacterial cell (Johnson et al., 2006). During this process, the fully formed CT protein must pass through a gated channel in the outer bacterial membrane, which is composed of many secretin proteins (Kubori, 2016; Natarajan, Singh and Rapaport, 2019). Individual *V. cholerae* secretin proteins called GspD, form the T2SS secretin complex–a complex that is conserved across all classes of secretion systems (DeAngelis et al., 2019). GspD has also recently been shown to associate with phage shock protein (Psp), a stress response pathway triggered by inner membrane damage (DeAngelis et al., 2019). The complex of *V. cholerae* membrane proteins ultimately aid in the virulence and pathogenicity of *V. cholerae.*

6.2.1. ToxR - A global regulator of virulence genes in *V. cholerae*

V. cholerae has a characteristic 3-component global regulator ToxRST, which controls the expression of genes in response to environmental signals (Pfau and Taylor, 1998). ToxR is a 32-kDA transmembrane protein belonging to the OmpR family of transcriptional regulators, with a dimeric periplasmic domain and a monomeric membrane domain (Miller, Taylor and Mekalanos, 1987; Mizuno and Tanaka, 1997; Chatterjee, Saha and Chakrabarti, 2007). ToxR regulates important virulence factors of *V. cholerae* such as the CT and the toxin-coregulated pilus (TCP) (Miller, Taylor and Mekalanos, 1987). ToxR is influenced by environmental stimuli such as pH, temperature, osmolarity, oxygen tension etc, which in turn regulates several physiological functions in *V. cholerae* (Faruque, Albert and Mekalanos, 1998; Pfau and Taylor, 1998). ToxS, a 19 kDA transmembrane protein, stimulates the activity of ToxR by interacting with its

perisplasmic domain, and together, these two proteins perform co-ordinated regulation of the expression of genes (DiRita and Mekalanos, 1991). The third regulatory element in the system is a 32-kDa protein ToxT, which controls the expression of some genes within the ToxR regulon. Expression of the *toxT* gene is controlled by ToxR itself. ToxT is a member of the AraC family of bacterial transcriptional activators, which play very important roles in regulating the expression of virulence factors (DiRita, 1992).

6.2.2. Outer membrane porins

Several membrane proteins help *V. cholerae* in efficient colonization of the small intestine, such as the ToxR-regulated outer membrane porin proteins OmpU and OmpT (Miller and Mekalanos, 1988). ToxR binds to a 7-bp tandemly repeated DNA sequence 5'-TTTTGAT-3' in the cholera toxin promoter region and regulates its expression (Chatterjee, Saha and Chakrabarti, 2007). ToxR is influenced by environmental stimuli, which in turn regulates several physiological functions in *V. cholerae* (Faruque, Albert and Mekalanos, 1998). The expression of OmpU is increased by ToxR, while the expression of OmpT is repressed (Li et al., 2000; Provenzano and Klose, 2000). The 40-kDa OmpT, and the 38-kDa OmpU have been purified to homogeneity and their pore–forming ability has been demonstrated using liposomes (Chakrabarti et al., 1996). These porins play important roles in solute transport and respond to diverse environmental stimuli (Miller and Mekalanos, 1988; Wibbenmeyer et al., 2002). Both OmpU and OmpT are involved in bile transport, the latter being more permeable to bile salts (Provenzano and Klose 2000). ToxR-mediated overexpression of OmpT and repression of OmpU result in increased bile sensitivity and altered solute flux across the outer membrane, consequently influencing virulence gene expression (Reidl and Klose, 2002).

V. cholerae has a distinct regulator mechanism that responds to low iron concentration by stimulating the expression of genes encoding hemolysins and outer membrane proteins (Sigel and Payne, 1982; Faruque, Albert and Mekalanos, 1998). This mechanism is mediated by Fur protein, which represses the expression of iron-regulated proteins in the presence of iron by binding to the promoter region upstream of these genes (Goldberg, Boyko and Calderwood, 1990). Studies on one of the iron-regulated proteins IrgA showed that insertional inactivation of *irgA* resulted in the loss of a 77-kDa major outer membrane protein in *V. cholerae* (Goldberg, Boyko and Calderwood, 1990; 1991). Further, the transcription of *irgA* is regulated by a 900-bp open reading frame (*irgB*) upstream

of the *irgA* promoter in an inverse orientation to *irgA* (Goldberg, Boyko and Calderwood, 1991). IrgB resembles the LysR family of positive transcriptional activators, and both *irgA* and *irgB* are negatively regulated by the Fur protein under iron-limiting conditions (Goldberg, Boyko and Calderwood, 1991). ViuA is a 74 kDa iron-regulated outer membrane protein of *V. cholerae*, which acts as the receptor for the iron-siderophore complex, ferric vibriobactin (Butterton et al., 1992). Subsequent studies have revealed that ViuA performs early steps in the biosynthesis of vibriobactin and is part a gene cluster comprising *vibA*, *vibB*, *vibC*, *vibE* and *vibF* (Wyckoff et al., 1997; Butterton et al., 2000).

V. cholerae is capable of living in both an aquatic environment and within the intestine of a human host (DeAngelis et al., 2019). In order to survive these very different environments, *V. cholerae* has evolved various methods to respond to environmental stresses that it may encounter (Saul-McBeth and Matson, 2019). One such method of response that has recently been described is centered on the SipA protein, which is found in the periplasmic space of *V. cholerae* membranes (Saul-McBeth and Matson, 2019). SipA is crucial for bacterial survival in different environments, namely in the presence of antimicrobial peptides (AMPs). SipA binds AMPs from the environment and interacts with outer membrane proteins, such as OmpA, to aid in removal of AMPs from the cell and promote *V. cholerae* survival.

6.2.3. Efflux pumps of *V. cholerae* – Role in antibiotic resistance and virulence

Antimicrobial efflux pumps of *V. cholerae* represent a crucial resistance mechanism (Kitaoka et al., 2011; Andersen et al., 2015; Varela, 2019). While such multidrug efflux resistance systems may potentially compromise the chemotherapeutic efficacy of severe cholera cases, the resistance mechanisms nevertheless make promising targets for resistance modulation in key bacterial pathogens (Varela et al., 2017). These and other antimicrobial efflux systems in bacteria consist of either secondary or primary active transporters (Konings, Poolman and van Veen, 1994). We discuss below related antimicrobial efflux systems from *V. cholerae* from a phylogenetic perspective.

6.2.3.1. V. cholerae and the major facilitator superfamily

The multidrug efflux pump VceB from *V. cholerae* consists of 14-transmembrane domains and is associated with the VceCAB operon on the bacterial genome (Colmer, Fralick and Hamood, 1998). VceB is a member of the

large superfamily of solute transporters (Andersen et al., 2015). Like its homologous counterpart EmrAB system in *E. coli*, VceB participates in a tripartite complex system in which VceB resides in the inner cytoplasmic membrane, VceA is located in the periplasm, and VceC is integral to the outer membrane of the bacterial cell wall (Woolley et al., 2005). Together, as a multi-component transport system in the *V. cholerae* cell wall, resistance to the quinolone nalidixic acid, deoxycholate, phenylmercuric acetate, and carbonyl-m-chlorophenylhydrazone (CCCP) is brought about (Colmer, Fralick and Hamood, 1998; Woolley et al., 2005). Expression of the VceCAB system is negatively controlled by the VceR repressor (Alatoom et al., 2007), which is structurally homologous to the TetR repressor (Cuthbertson and Nodwell, 2013).

From a toxigenic strain of *V. cholerae* O395, our laboratory cloned a multidrug efflux pump system referred to as EmrD-3, which is a member of the major facilitator superfamily of transporters (Smith, Kumar and Varela, 2009). We showed that the *emrD-3* determinant encodes a 397 amino acid polypeptide chain with 12 predicted transmembrane domains and the N- and C-termini residing at the cytoplasmic side of the inner membrane. We also found that host cells containing EmrD-3 conferred resistance to linezolid, rifampin, erythromycin, chloramphenicol, rhodamine 6G, and tetraphenylphosphonium chloride (Smith, Kumar and Varela, 2009). Further, we demonstrated that host cells harboring EmrD-3 actively transported ethidium bromide, an essential multidrug efflux substrate (Smith, Kumar and Varela, 2009). More recently, we discovered that extract of garlic (*Allium sativum*) and one of its bioactive components called allyl sulfide specifically inhibits the growth of host cells harboring EmrD-3 (Bruns et al., 2017). We found that relatively low extract concentrations targeted the EmrD-3 multidrug efflux pump, while higher concentrations appeared to affect the respiratory chain, possibly collapsing the proton-motive force (Bruns et al., 2017).

More recently, five new related multidrug efflux pumps called MFS pumps numbered 1 through 5, were discovered in *V. cholerae*, and were shown to be controlled under the regulator of transcription, a protein called MfsR, which is related to the well-known LysR family of regulators (Chen et al., 2013). Mutagenic analyses of the *msf* determinants showed reduced resistance to tetracycline and crude bile (Chen et al., 2013).

6.2.3.2. V. cholerae and the multidrug and toxic compound extrusion superfamily

The *V. cholerae* non-O1 bacterium harbors the VcrM antimicrobial transporter, which confers resistance to multiple agents such as acriflavine, ethidium bromide, rhodamine 6G, and tetraphenylphosphonium chloride (Huda et

al., 2003). Interestingly, VcrM is a sodium-driven transporter of the so-called multidrug and toxic compound extrusion (MATE) superfamily (Kuroda and Tsuchiya, 2009). Additional members of the MATE superfamily of transporters from non-O1 *V. cholerae* include VcmB, VcmD, and VcmH, which were also shown to be Na^+-dependent, but VcmN was found to be independent of the sodium motive force (Begum et al., 2005).

6.2.3.3. V. cholerae and the resistance-nodulation-cell division superfamily

Members of the resistance-nodulation-cell division (RND) superfamily from *V. cholerae* include VexB, VexD, VexF, VexH, VexK, and VexM (Bina et al., 2006; Taylor, Bina and Bina, 2012; Kunkle, Bina and Bina, 2017;). Interestingly, these RND transporters participate in forming a tripartite system composed of three components lining the cell wall, such as the outer and inner membranes and the periplasm (Destoumieux-Garzón et al., 2014). Furthermore, these RND systems are located within operons on the *V. cholerae* genome and are regulated (Nikaido, 2018).

6.2.3.4. V. cholerae and the ATP-binding cassette superfamily

A critical member of the sizeable ATP-binding cassette (ABC) superfamily from *V. cholerae* includes the VcaM transporter (Huda et al., 2003). Hydrolysis of ATP is the prime mode of energization (Orelle, Mathieu and Jault, 2019; Cui and Davidson, 2011). The ABC transporter confers resistance to ciprofloxacin, norfloxacin, tetracycline, doxorubicin, daunomycin, and dyes such as 4′,6-diamidino-2-phenylindole (DAPI) and Hoechst 33342 (Huda et al., 2003). More recently, evidence was reported that VcaM relies on the outer-membrane component TolC for active extrusion from host cells (Lu et al., 2018).

6.2.4. Carbohydrate transporters of *V. cholerae*

Nutrient acquisition is an important physiological function of bacteria which possess a robust machinery to accomplish this goal. Many cellular activities such as motility, chemotaxis, enzymes degrading macromolecules, membrane transporters, etc are dedicated to nutrient acquisition, transport and digestion (Dills et al., 1980). Bacteria have a peptidoglycan cell wall covering the outside of their cell membrane, and in the case of Gram-negative bacteria, a relatively thin peptidoglycan cell wall is surrounded by an additional envelope called the outer membrane made of lipopolysaccharide (Silhavy, Kahne and Walker, 2010). Gram-positive bacteria have a thick cell wall that lacks the outer membrane, but in

some bacteria such as *Staphylococcus aureus* the cell wall is surrounded by a teichoic acid layer. Cellular metabolism requires that the essential compounds are transported from the external environment into the bacterial cytoplasm. At the same time, extrusion of toxic metabolites of cellular metabolism is also important. Carbohydrate transport across the membrane is critical for survival of the bacterium and these mechanisms are either passive or active (Dills et al., 1980). The passive mechanism of sugar transport works by simple diffusion across the membrane (e.g. transport of glycerol), and this mechanism does not facilitate transport against a concentration gradient. On the other hand, the active transport mechanism is energized by a proton gradient or ATP, and this method can transport macromolecules against their concentration gradients. Bacterial metabolism generates a proton electrochemical potential difference across the membrane, which energizes several membrane-associated activities including macromolecular transport (Mitchell, 1961). This mechanism is termed secondary active transport, which is accomplished by three different ways namely symport, antiport and uniport mechanisms. Symport is a common mechanism of carbohydrate transport in bacteria which is coupled to H^+ electrochemical gradient. The other equally important carbohydrate transport mechanism is mediated by phosphoenolpyruvate-dependent phospotransferase systems (PTSs) (Kundig, Ghosh and Roseman, 1964). In this mechanism, the substrate is chemically modified for it to be transported across the membrane. The PTS is a high affinity system in bacteria, which helps to sequester carbohydrate present in low concentrations in the environment. This efficient system helps bacteria to survive under nutrient limiting conditions, such as in seawater in the case of *V. cholerae.*

The PTS catalyzes concomitant phosphorylation and transport of a series of carbohydrates by a process known as group translocation, which involves the phosphorylation of a number of carbohydrates with phosphoenol pyruvate (PEP) as the phosphoryl donor (Postma, Lengeler and Jacobson, 1993; Lengeler, Jahreis and Wehmeier, 1994; Barabote and Saier, 2005). The multi-component PTS consist of at least three proteins, two of which are cytoplasmic soluble proteins namely the heat stable protein (HPr) and enzyme I, and the third protein is a membrane bound transporter Enzyme II (EII). Enzyme I and HPr catalyze the phosphorylation of carbohydrates with the utilization of a phosphoenol pyruvate (PEP) resulting in phosphoenzyme I and pyruvate. Phosphoenzyme I in turn phosphorylates an intermediate phospho carrier protein HPr to form phospho HPr, and the phosphoryl group is finally transferred to the carbohydrate via the PTS enzyme II complex (Postma, Lengeler, and Jacobson 1993). The phosphorylated carbohydrate is subsequently taken up by Enzyme II (Postma, Lengeler and

Jacobson, 1993). Enzyme II is generally made of A, B and C components (Kumar et al., 2011). The *V. cholerae* mannitol operon is a 3.9-kb operon comprised of *mtlADR*, encoding a mannitol-specific enzyme IICBA (EIIMtl) component (MtlA), a mannitol-1-phosphate dehydrogenase (MtlD), and a repressor (MtlR) (Kumar et al., 2011). In marine bacteria such as vibrios, mannitol derived from decaying seaweeds is an important source of carbon, which also plays an important role in osmoregulation and stress tolerance (Stoop and Mooibroek, 1998; Efiuvwevwere et al., 1999).

Mannitol fermentation is an important biochemical feature of many vibrios. In *V. cholerae*, the rate of mannitol fermentation is an important distinguishing factor between toxigenic strains and non-toxigenic strains (Wang et al., 2007). Unlike the non-toxic *V. cholera*, which utilize mannitol very rapidly, the toxigenic strains of *V. cholerae* ferment mannitol very slowly (Kumar et al., 2011). A study has found that a small regulatory RNA (MtlS sRNA) transcribed antisense to the 5' untranslated region of mannitol post-transcriptionally binds to *mtlA* mRNA, thus preventing it from being translated (Mustachio et al., 2012).

A comparative genomic study revealed that about 36% and 27% of the genes are involved in membrane transport activities in non-toxigenic and toxigenic strains of *V. cholerae*, respectively (Mukherjee et al., 2016). These studies have identified the presence of multiple PTSs, particularly the specific EIIC domain in *V. cholerae* which are responsible for transport of important carbohydrate such as glucose, lactose, cellobiose, etc (Houot et al., 2010; Mukherjee et al., 2014; Mukherjee et al., 2016; Hayes, Dalia and Dalia, 2017;). Several recent studies have revealed the critical roles that *V. cholerae* PTSs play in its virulence and environmental persistence. For instance, when glucose or pyruvate is provided as a carbon source, phosphorylation of HPr and FPr by EI suppresses biofilm formation (Houot and Watnick, 2008). Two PTS pathways involving glucose- and nitrogen-specific Enzyme II independently control biofilm formation and colonization of the germ-free mouse intestine by *V. cholerae* (Houot et al., 2010). Thus, PTS in *V. cholerae* plays a critical role in regulating virulence gene expression ostensibly by modulating the levels of intracellular cyclic AMP (Wang et al., 2015).

6.3. CONCLUSION

To conclude, *V. cholerae* is a versatile bacterium which possesses an intelligent network of genes involved in a myriad of functions enabling this estuarine bacterium to succeed as a powerful human pathogen. Comparative

genomic analyses have revealed distinct differences between toxigenic and non-toxigenic strains with respect to pathogenicity and environmental survival, and these traits have been associated with distinct differences in their genetic make-ups. *V. cholerae* serves as a model pathogen to understand how production of toxin alone does not define a successful pathogen, but a number of well co-ordinated mechanisms direct bacterial response to the host and the environment, and ensure its persistence and successful infection of the host.

REFERENCES

Alatoom AA, Aburto R, Hamood AN, Colmer-Hamood JA. VceR negatively regulates the vceCAB MDR efflux operon and positively regulates its own synthesis in *Vibrio cholerae 569B*. *Can J Microbiol*. 2007;53(7):888–900.

Andersen JL, He GX, Kakarla P, K C R, Kumar S, Lakra WS, Mukherjee MM, et al. Multidrug efflux pumps from *Enterobacteriaceae*, *Vibrio cholerae* and *Staphylococcus aureus* bacterial food pathogens. *Int J Environ Res Public Health*. 2015;12(2):1487–1547.

Azman AS, Rudolph KE, Cummings DA, Lessler J. The incubation period of cholera: A systematic review. *J Infect*. 2013;66(5):432–438.

Barabote RD, Saier MH Jr. Comparative genomic analyses of the bacterial phosphotransferase system. *Microbiol Mol Biol Rev*. 2005;69(4):608–634.

Begum A, Rahman MM, Ogawa W, Mizushima T, Kuroda T, Tsuchiya T. Gene cloning and characterization of four MATE family multidrug efflux pumps from *Vibrio cholerae non-O1*. *Microbiol Immunol*. 2005;49(11):949–957.

Bina JE, Provenzano D, Wang C, Bina XR, Mekalanos JJ. Characterization of the *Vibrio cholerae* vexAB and vexCD efflux systems. *Arch Microbiol*. 2006;186(3):171–181.

Bruns MM, Kakarla P, Floyd JT, Mukherjee MM, Ponce RC, Garcia JA, Ranaweera I, et al. Modulation of the multidrug efflux pump EmrD-3 from *Vibrio cholerae* by *Allium sativum* extract and the bioactive agent allyl sulfide plus synergistic enhancement of antimicrobial susceptibility by *A. sativum* extract. *Arch Microbiol*. 2017;199(8):1103–1112.

Butterton JR, Choi MH, Watnick PI, Carroll PA, Calderwood SB. *Vibrio cholerae* VibF is required for vibriobactin synthesis and is a member of the family of nonribosomal peptide synthetases. *J Bacteriol*. 2000;182(6):1731–1738.

Butterton JR, Stoebner JA, Payne SM, Calderwood SB. Cloning, sequencing, and transcriptional regulation of viuA, the gene encoding the ferric vibriobactin receptor of *Vibrio cholerae*. *J Bacteriol*. 1992;174(11):3729–3738.

CDC. 2019. Cholera - *Vibrio cholerae* infection | Cholera | CDC." June 24, 2019. https://www.cdc.gov/cholera/index.html.

Chakrabarti SR, Chaudhuri K, Sen K, Das J. Porins of *Vibrio cholerae*: purification and characterization of OmpU. *J Bacteriol*. 1996;178(2):524–530.

Chatterjee T, Saha RP, Chakrabarti P. Structural studies on *Vibrio cholerae* ToxR periplasmic and cytoplasmic domains. *Biochim Biophys Acta*. 2007;1774(10):1331–1338.

Chen S, Wang H, Katzianer DS, Zhong Z, Zhu J. LysR family activator-regulated major facilitator superfamily transporters are involved in *Vibrio cholerae* antimicrobial compound resistance and intestinal colonisation. *Int J Antimicrob Agents*. 2013;41(2):188–192.

Colmer JA, Fralick JA, Hamood AN. Isolation and characterization of a putative multidrug resistance pump from *Vibrio cholerae*. *Mol Microbiol*. 1998;27(1):63–72.

Colwell RR, Kaper J, Joseph SW. *Vibrio cholerae*, *Vibrio parahaemolyticus*, and other vibrios: occurrence and distribution in Chesapeake Bay. *Science*. 1977;198(4315):394–396.

Conner JG, Teschler JK, Jones CJ, Yildiz FH. Staying Alive: *Vibrio cholerae's* cycle of environmental survival, transmission, and dissemination. *Microbiol Spectr*. 2016;4(2).

Cui J, Davidson AL. ABC solute importers in bacteria. *Essays Biochem*. 2011;50(1):85–99.

Cuthbertson L, Nodwell JR. The TetR family of regulators. *Microbiol Mol Biol Rev*. 2013;77(3):440–475.

DeAngelis CM, Nag D, Withey JH, Matson JS. Characterization of the *Vibrio cholerae* phage shock protein response. *J Bacteriol*. 2019;201(14). pii: e00761–18.

Destoumieux-Garzón D, Duperthuy M, Vanhove AS, Schmitt P, Wai SN. Resistance to antimicrobial peptides in vibrios. *Antibiotics (Basel)*. 2014;3(4):540–563.

Dills SS, Apperson A, Schmidt MR, Saier MH Jr. Carbohydrate transport in bacteria. *Microbiol Rev*. 1980;44(3):385–418.

DiRita VJ. Co-ordinate expression of virulence genes by ToxR in *Vibrio cholerae*. *Mol Microbiol*. 1992;6(4):451–458.

DiRita VJ, Mekalanos JJ. Periplasmic interaction between two membrane regulatory proteins, ToxR and ToxS, results in signal transduction and transcriptional activation. *Cell*. 1991;64(1):29–37.

Dunstan RA, Heinz E, Wijeyewickrema LC, Pike RN, Purcell AW, Evans TJ, Praszkier J, et al. Assembly of the type II secretion system such as found in *Vibrio cholerae* depends on the novel Pilotin AspS. *PLoS Pathog*. 2013;9(1):e1003117

Efiuvwevwere BJO, Gorris LGM, Smid EJ, Kets EPW. Mannitol-enhanced survival of *Lactococcus lactis* subjected to drying. *Appl Microbiol Biotechnol*. 1999;51(1):100–104.

Faruque SM, Albert MJ, Mekalanos JJ. Epidemiology, genetics, and ecology of toxigenic *Vibrio cholerae*. *Microbiol Mol Biol Rev*. 1998;62(4):1301–1314.

Fong JC, Yildiz FH. Interplay between cyclic AMP-cyclic AMP receptor protein and cyclic di-GMP signaling in *Vibrio cholerae* biofilm formation. *J Bacteriol*. 2008;190(20):6646–6659.

Foster JW, Aliabadi Z, Slonczewski JL. *Microbiology: The Human Experienc*e. W.W. Norton & Company, Inc., 2018.

GBD 2015 Mortality and Causes of Death Collaborators. Global, regional, and national life expectancy, all-cause mortality, and cause-specific mortality for 249 causes of death, 1980-2015: A systematic analysis for the global burden of disease study 2015. *Lancet (London, England)*. 2016;388(10053):1459–1544.

Goldberg MB, Boyko SA, Calderwood SB. Transcriptional regulation by iron of a *Vibrio cholerae* virulence gene and homology of the gene to the *Escherichia coli* fur system. *J Bacteriol*. 1990;172(12):6863–6870.

Goldberg MB, Boyko SA, Calderwood SB. Positive transcriptional regulation of an iron-regulated virulence gene in *Vibrio cholerae*. *Proc Natl Acad Sci U S A*. 1991;88(4):1125–1129.

Harris JB, LaRocque RC, Qadri F, Ryan ET, Calderwood SB. "Cholera." *Lancet (London, England)*. 2012;379(9835):2466–2476.

Hayes CA, Dalia TN, Dalia AB. Systematic genetic dissection of PTS in *Vibrio cholerae* uncovers a novel glucose transporter and a limited role for PTS during infection of a mammalian host. *Mol Microbiol*. 2017;104(4):568–579

Houot L, Chang S, Absalon C, Watnick P. *Vibrio cholerae* phosphoenolpyruvate phosphotransferase system control of carbohydrate transport, biofilm formation, and colonization of the germfree mouse intestine. *Infect Immun*. 2010;78(4):1482–1494.

Houot L, Watnick P. A novel role for enzyme I of the *Vibrio cholerae* phosphoenolpyruvate phosphotransferase system in regulation of growth in a biofilm. J Bacteriol. 2008;190(1):311–320.

Huda MN, Chen J, Morita Y, Kuroda T, Mizushima T, Tsuchiya T. Gene cloning and characterization of VcrM, a Na^+-coupled multidrug efflux pump, from *Vibrio cholerae non-O1*. *Microbiol Immunol*. 2003;47(6):419–427.

Huq A, Small EB, West PA, Huq MI, Rahman R, Colwell RR. Ecological relationships between *Vibrio cholerae* and planktonic crustacean copepods. Appl *Environ Microbiol*. 1983;45(1):275–283.

Johnson TL, Abendroth J, Hol WG, Sandkvist M. Type II secretion: From structure to function. *FEMS Microbiol Lett*. 2006;255(2):175–186.

Kaper JB, Morris JG Jr, Levine MM. Cholera. *Clin Microbiol Rev*. 1995;8(1):48–86.

Karaolis DK, Johnson JA, Bailey CC, Boedeker EC, Kaper JB, Reeves PR. A *Vibrio cholerae* pathogenicity island associated with epidemic and pandemic strains. *Proc Natl Acad Sci U S A*. 1998;95(6):3134–3139.

Kitaoka M, Miyata ST, Unterweger D, Pukatzki S. Antibiotic resistance mechanisms of *Vibrio cholerae*. *J Med Microbiol*. 2011;60(Pt 4):397–407.

Konings WN, Poolman B, van Veen HW. Solute transport and energy transduction in bacteria. *Antonie Van Leeuwenhoek*. 1994;65(4):369–380.

Korotkov KV, Sandkvist M, Hol WG. The type II secretion system: biogenesis, molecular architecture and mechanism. *Nat Rev Microbiol*. 2012;10(5):336–351.

Kubori T. Life with bacterial secretion systems. *PLoS Pathog*. 2016;12(8):e1005562.

Kumar S, Smith KP, Floyd JL, Varela MF. Cloning and molecular analysis of a mannitol operon of phosphoenolpyruvate-dependent phosphotransferase (PTS) type from *Vibrio cholerae O395*. *Arch Microbiol*. 2011;193(3):201–208.

Kundig W, Ghosh, S, Roseman S. Phosphate bound to histidine in a protein as an intermediate in a novel phospho-transferase system. *Proc Natl Acad Sci U S A*. 1964;52:1067–1074.

Kunkle DE, Bina XR, Bina JE. The *Vibrio cholerae* VexGH RND efflux system maintains cellular homeostasis by effluxing vibriobactin. *mBio*. 2017;8(3). pii: e00126–17.

Kuroda T, Tsuchiya T. Multidrug efflux transporters in the MATE family. *Biochim Biophys Acta*. 2009;1794(5):763–768.

Lekshmi M, Parvathi A, Kumar S, Varela MF. *Efflux pump-mediated quorum sensing: New avenues for modulation of antimicrobial resistance and bacterial virulence*. In Biotechnological Applications of Quorum Sensing Inhibitors, Kalia VC (Ed.), Springer, Singapore, 2018, pp127–42.

Lengeler JW, Jahreis K, Wehmeier UF. Enzymes II of the phospho enol pyruvate-dependent phosphotransferase systems: their structure and function in carbohydrate transport. *Biochim Biophys Acta*. 1994;1188(1–2):1–28.

Li CC, Crawford JA, DiRita VJ, Kaper JB. Molecular cloning and transcriptional regulation of ompT, a ToxR-repressed gene in *Vibrio cholerae*. *Mol Microbiol*. 2000;35(1):189–203.

Lu WJ, Lin HJ, Janganan TK, Li CY, Chin WC, Bavro VN, Lin HV. ATP-binding cassette transporter VcaM from *Vibrio cholerae* is dependent on the outer membrane factor family for its function. *Int J Mol Sci*. 2018;19(4). pii: E1000.

Miller VL, Mekalanos JJ. A novel suicide vector and its use in construction of insertion mutations: osmoregulation of outer membrane proteins and virulence

determinants in *Vibrio cholerae* requires toxR. *J Bacteriol*. 1988;170(6):2575–2583.

Miller VL, Taylor RK, Mekalanos JJ. Cholera toxin transcriptional activator toxR is a transmembrane DNA binding protein. *Cell*. 1987;48(2):271–279.

Mitchell P. Coupling of phosphorylation to electron and hydrogen transfer by a chemi-osmotic type of mechanism. *Nature*. 1961;191:144–148.

Mizuno T, Tanaka I. Structure of the DNA-binding domain of the OmpR family of response regulators. *Mol Microbiol*. 1997;24(3):665–667.

Moorthy S, Watnick PI. Genetic evidence that the *Vibrio cholerae* monolayer is a distinct stage in biofilm development. *Mol Microbiol*. 2004;52(2):573–587.

Mukherjee M, Kakarla P, Kumar S, Gonzalez E, Floyd JT, Inupakutika M, Devireddy AR, et al. Comparative genome analysis of non-toxigenic non-O1 versus toxigenic O1 *Vibrio cholerae*. *Genom Discov*. 2014;2(1):1–15.

Mukherjee MM, Kumar S, Shrestha U, Ranaweera I, Ranjana KC, Kakarla P, Willmon TM, et al. Comparative genomics and discovery of novel cellular targets for the development of new therapeutics towards *Vibrio cholerae*, the causative agent of cholera disease. *Anti-Infective Agents*. 2016;2. DOI: 10.2174/2211352514666160816151125.

Mustachio LM, Aksit S, Mistry RH, Scheffler R, Yamada A, Liu JM. The *Vibrio cholerae* mannitol transporter is regulated posttranscriptionally by the MtlS small regulatory RNA. *J Bacteriol*. 2012;194(3):598–606.

Natarajan J, Singh N, Rapaport D. Assembly and targeting of secretins in the bacterial outer membrane. *Int J Med Microbiol*. 2019;309(7):151322.

NIH. Cholera Biology and Genetics. NIH: National Institute of Allergy and Infectious Diseases. 2017. https://www.niaid.nih.gov/diseases-conditions/cholera-biology-and-genetics.

Nikaido H. RND transporters in the living world. *Res Microbiol*. 2018;169(7–8):363–371.

Orelle C, Mathieu K, Jault JM. Multidrug ABC transporters in bacteria. *Res Microbiol*. 2019;170(8):381–391.

Pfau JD, Taylor RK. Mutations in toxR and toxS that separate transcriptional activation from DNA binding at the cholera toxin gene promoter. *J Bacteriol*. 1998;180(17):4724–4733.

Postma PW, Lengeler JW, Jacobson G. Phosphoenolpyruvate:carbohydrate phosphotransferase systems of bacteria. *Microbiol Rev*. 1993;57(3):543–594.

Provenzano D, Klose KE. Altered expression of the ToxR-regulated porins OmpU and OmpT diminishes *Vibrio cholerae* bile resistance, virulence factor expression, and intestinal colonization. *Proc Natl Acad Sci U S A*. 2000;97(18):10220–10224.

Reidl J, Klose KE. *Vibrio cholerae* and cholera: out of the water and into the host. *FEMS Microbiol Rev*. 2002;26(2):125–139.

Sack DA, Sack RB, Nair GB, Siddique AK. Cholera. *Lancet*. 2004;363(9404):223–233.

Saul-McBeth J, Matson JS. A periplasmic antimicrobial peptide-binding protein is required for stress survival in *Vibrio cholerae*. *Front Microbiol*. 2019;10:161.

Sigel SP, Payne SM. Effect of iron limitation on growth, siderophore production, and expression of outer membrane proteins of *Vibrio cholerae*. J *Bacteriol*. 1982;150(1):148–155.

Silhavy TJ, Kahne D, Walker S. The bacterial cell envelope. *Cold Spring Harb Perspect Biol*. 2010;2(5):a000414.

Silva AJ, Benitez JA. *Vibrio cholerae* biofilms and cholera pathogenesis. *PLoS Negl Trop Dis*. 2016;10(2):e0004330.

Sinclair D, Abba K, Zaman K, Qadri F, Graves PM. Oral vaccines for preventing cholera. *Cochrane Database Syst Rev*. 2011;(3):CD008603

Smith KP, Kumar S, Varela MF. Identification, cloning, and functional characterization of EmrD-3, a putative multidrug efflux pump of the major facilitator superfamily from *Vibrio cholerae O395*. *Arch Microbiol*. 2009;191(12):903–911.

Stoop JM, Mooibroek H. Cloning and characterization of NADP-mannitol dehydrogenase cDNA from the button mushroom, *Agaricus bisporus*, and its expression in response to NaCl stress. *Appl Environ Microbiol*. 1998;64(12):4689–4696.

Taylor DL, Bina XR, Bina JE. *Vibrio cholerae* VexH encodes a multiple drug efflux pump that contributes to the production of cholera toxin and the toxin co-regulated pilus. *PLoS One*. 2012;7(5):e38208.

Teschler JK, Zamorano-Sánchez D, Utada AS, Warner CJ, Wong GC, Linington RG, Yildiz FH. Living in the matrix: assembly and control of *Vibrio cholerae* biofilms. *Nat Rev Microbiol*. 2015;13(5):255–268.

Tischler AD, Camilli A. Cyclic diguanylate regulates *Vibrio cholerae* virulence gene expression. *Infect Immun*. 2005;73(9):5873–5882.

Varela MF. *Antimicrobial Efflux Pumps*. In Antibiotic Drug Resistance, John Wiley & Sons, Ltd., 2019, Chapter 8, pp167-179.

Varela MF, Andersen JL, Ranjana KC, Kumar S, Sanford LM, Hernandez AJ. *Bacterial Resistance Mechanisms and Inhibitors of Multidrug Efflux Pumps Belonging to the Major Facilitator Superfamily of Solute Transport Systems*, 2017. https://ebooks.benthamscience.com/book/9781681082912/chapter/152013/

Wang Q, Millet YA, Chao MC, Sasabe J, Davis BM, Waldor MK. A genome-wide screen reveals that the *Vibrio cholerae* phosphoenolpyruvate phosphotransferase

system modulates virulence gene expression. *Infect Immun*. 2015;83(9):3381–3395.

Wang HY, Yan MY, Zhao YW, Kan B. Transcriptional repressor gene--mtlR of mannitol PTS operon in *Vibrio cholerae*. *Wei Sheng Wu Xue Bao*. 2007;47(3):522–525.

Watnick PI, Kolter R. Steps in the development of a *Vibrio cholerae* El Tor biofilm. *Mol Microbiol*. 1999;34(3):586–595.

WHO. Cholera outbreak: Assessing the outbreak response and improving preparedness. WHO. 2004. https://www.who.int/cholera/publications/OutbreakAssessment/en/.

Wibbenmeyer JA, Provenzano D, Landry CF, Klose KE, Delcour AH. *Vibrio cholerae* OmpU and OmpT porins are differentially affected by bile. *Infect Immun*. 2002;70(1):121–126.

Woolley RC, Vediyappan G, Anderson M, Lackey M, Ramasubramanian B, Jiangping B, Borisova T, et al. Characterization of the *Vibrio cholerae* vceCAB multiple-drug resistance efflux operon in *Escherichia coli*. *J Bacteriol*. 2005;187(15):5500–5503.

Wyckoff EE, Stoebner JA, Reed KE, Payne SM. Cloning of a *Vibrio cholerae* vibriobactin gene cluster: identification of genes required for early steps in siderophore biosynthesis. *J Bacteriol*. 1997;179(22):7055–7062.

Submitted: 10th Oct 2019, Revised: 18th Dec 2019, Accepted: 3rd Jan 2020

Chapter Seven

7. THE COMMANDMENTS OF STUDYING INTEGRAL MEMBRANE PROTEINS

Raymond J. Turner *
Department of Biological Sciences, University of Calgary
Calgary, AB, Canada

ABSTRACT

As a budding biochemist, I was introduced to Arthur Kornberg's ten commandments of enzymology. After 25 years of working in the field of integral membrane protein (IMP) structure-function, my trainees and students of my class noticed that I would make statements on IMP research in the form of a commandment, in the guises of these early biochemistry commandments. Here I share my commandments around IMP expression and purification, IMP biochemistry, IMP functionality studies, and IMP high-resolution structures.

Keywords: integral membrane proteins, expression and purification, detergent solubilization, membrane mimetics, structure and function, biochemistry, hydropathy analysis, membrane topology, membrane sidedness

7.1. INTRODUCTION

A favorite read I give all my students on the introduction to the topic integral membrane protein (IMP) biochemistry is the story of a novice membrane protein biochemist and how he learns to love lysozyme (von Heijne, 1999). This article is an informative yet playfully written review by Gunner von Hejine, where he good-humouredly highlighted the frustrations encapsulated in being a biochemist trying to study integral membrane proteins. Although considerable advancements

* Direct all correspondence to Prof. Raymond J. Turner; Department of Biological Sciences, 447 Biological Sciences Building, University of Calgary, 2500 University Dr. NW, Calgary, AB, Canada, T2N 1N4. E-mail: turnerr@ucalgary.ca.

in technology have occurred in the past 10 years since this review was written, IMPs are still notoriously more difficult to study than their soluble cousins.

This chapter aims to highlight some of the tripping points and mistakes to avoid or at least to be aware of, for those embarking down a path of study on an IMP. To deliver these thoughts in a highly consumable fashion, I will try to channel the great Arthur Kornberg's Ten Commandments of Enzymology (Kornberg, 2000, Kornberg, 2003), which I also consider mandatory reading for every budding biochemist. Each commandment is stated and then explained in the context of understanding IMP structure-function.

7.2. THE COMMANDMENTS

THOU SHALT…

7.2.1. COMMANDMENTS AROUND IMP EXPRESSION AND PURIFICATION

7.2.1.1. Not strive to OVER-express integral membrane proteins (sic)

Well let's just say it, over-expressing IMPs can be frustrating at best. But let's correct this wording; what is really meant here is enhancing functional protein accumulation and in this chapter we will refer to it as EFPA. Unfortunately, maximizing protein accumulation has been foolishly and incorrectly called "protein over-expression" for decades, leading to disgruntled comments from molecular biologists gleefully pointing out how dimwitted protein biochemists can be in their fundamental understanding of biology. This of course is not limited to IMPs, but all EFPA. So, let's not continue to propagate this language. Proteins do not express, genes are expressed, subsequently producing mRNA, which is further translated into proteins. Thus, for EFPA to occur, we need several steps to be working at their optimal levels and properly coordinated. The process is far more complex than we typically consider, as not only does a protein have to be efficiently translated but in many cases, they are assisted in their folding, cofactors need to be added, they require cellular targeting as well as potentially assisted to assemble into a multiprotein complex. In the case of IMPs, 'properly targeted' means to the membrane (and the correct membrane in the cell), inserted

into the membrane in the correct topology and post insertional folding and transmembrane segment assembly/interactions to occur (for a more complete description of these processes see the review by Cymer, von Heijne and White [2015]).

EFPA is notoriously challenging with IMPs as the volume of protein capture in a cell (the membrane itself) is considerably more limiting than the cytoplasm, particularly when we consider prokaryotic expression systems. EFPA of IMPs is typically plagued with problems of protein aggregation and inclusion bodies through the transmembrane helices (TMH) miss folding into beta-strands. Additionally, misfolded or slowly folding proteins will have exposed regions leading to degrees of proteolytic degradation (Schlegel et al., 2014).

Expression and translation at a high rate for some proteins can lead to high cellular stress. EFPA of a transporter can lead to uncoupling of the proton motive force (Winstone, Duncalf and Turner, 2002) or miss directed and non-specific transport across the membrane, both of which can lead to cellular stress or lethality. The stress of producing the IMP can actually lead to loss of expression through the selection of cells that are producing less IMP and thus more physiologically fit. This fitness selection can lead to plasmid curing and expression loss within yeast and bacterial expression systems.

Here it is also important to have some words about heterologous IMP expression. We observe that often IMPs do not have their codons optimized. The use of rare codons may be present to decrease the translation rate to coordinate more closely with the folding, targeting and insertion of the protein. Thus, methods to optimize codon usage for the expression of IMPs can lead to folding and assembly problems and reduce IMP production (Schlegel et al., 2012). However, recently groups have gone after this issue exploring optimization of transcription rates and codon usage, which appears promising (see Claassens et al. (2017) and citations within for work in this area).

Overall, considerable time, effort, resources, and ‘luck’ must be put forward to optimize EFPA of IMPs as there are no effective rules of thumb. Of course, if going after a homolog or similar IMP family member, where previous work has provided a template toward EFPA, it is worth starting with such information and optimizing around it. But, for the most part, EFPA of IMPs is imperially determined. Thus, it should be considered (but is more often overlooked), that it is often more resource-efficient to accept the low initial yields one may start to get and simply do multiple preparations to get enough material for targeted experiments. Yet optimizing EFPA can be a wonderful learning experience for a graduate trainee, and gleefully fun for those that enjoy dancing with experimental conditions.

7.2.1.2. Not to forget about the detergent

Throughout this chapter, I use the term 'membrane mimetic' rather than just detergent, as recently, alternative compounds have been explored to overcome issues with classical detergents. Regardless, most IMP researchers still use detergents (surfactant, amphiphiles, tensides, soaps) to solubilize their IMP of interest from their lipid home. To date, finding the best membrane mimetic is still mostly empirically determined, and various detergent companies now provide small samples in detergent array kits to explore detergent ‘space’ for your IMP of interest. Yet there are some things to consider. A key thing to remember is that one is trying to mimic the natural lipid environment as closely as possible.

Detergents are made up of essentially two parts. 1) The head, which is polar and can be anionic, cationic, zwitterionic, or non-ionic. 2) The tail, which is hydrophobic and can be flexible, straight, branched, or more ridged and steroid-like. Important considerations of working with detergents are overviewed in Tables 1 and 2.

Parameter	**What to think about**
Critical micellar concentration (CMC)	Concentration of transition to begin forming micelles Dependent on T, pH, ionic strength
Hydrophile-lipophile balance (HLB)	Expression of hydrophilic character HLB of 12-14.5 for IMPs
Critical micellular concentration (CMT)	Also referred to as the ghost point as below the CMT Detergents precipitate out into ghost white solution
Effect on biophysical parameters	Adds to molecular weight Adds to hydrodynamic radius (Stokes radius) Influences migration on PAGE Can influence/inhibit ligand binding
Presence of aromatic rings	Can contribute to protein absorbance at 280 nm

Table 1. Important parameters of detergents.

Experimental factor	Effect
Temperature	CMT; working T
pH	Detergent head group pKa; net charge
Ionic strength	Increased counter ion decreases CMC
Detergent concentration	CMC
Multivalent ions	Can cluster charged detergents and precipitate
Purity	Peroxides and aldehydes damage proteins Increased purity -> increased price
Organics	Decrease dielectric increase CMC
Protein concentration	Do you have enough detergent to solubilize your target protein?

Table 2. Factors that affect detergent performance.

Alternatives to the use of classical detergents are still limited. Amphipols have been explored for some time, which are essentially polar or charged polymers decorated with acyl chains which are thought to wrap around the nonpolar domains of IMP providing aqueous solubility (Popot, 2010). Attempts to use perfluorinated surfactants have shown some success as they can maintain IMP lipid contacts (Popot, 2010). Another interesting group is the maltose neopentyl glycol amphiphiles, which gives two heads and two tails linked (Chae et al., 2010). The detergent alternative that has received the most hype recently are SMALPs. These are a Styrene Maleic Acid copolymer (SMA), which is considered to extract the IMP along with a small amount of the natural lipid bilayer encircled by the polymer to generate SMA Lipid Particles. SMALP scaffolded IMPs have quickly become popular with structural biochemists, particularly those using electron microscopy (Knowles et al., 2009; Postis et al., 2015).

Issues around the choice of detergent that are often overlooked include that the IMP may have considerably different thermal and kinetic stability when solubilized in detergent compared to its natural lipid bilayer. Further, the detergent may not be a ‘neutral’ player and could potentially act as an inhibitor or allosteric regulator to IMP activity.

To avoid issues around biochemical experiments in detergents, IMPs can be reconstituted into lipid bilayer (typically of defined lipid content) vesicles to try to

return to a natural state. Here one must consider the size of the vesicle and if membrane curvature could influence the biochemistry of the IMP of interest.

A few tricks exist to avoid the use of amphiphiles for purifying the IMP with its natural lipids. Along with SMALPs, bicelles (Sanders and Prosser, 1998) and lipid nanodisks (Baybur and Sligar, 2010) allow for natural lipid bilayer encapsulation but they are small enough for structural studies. An approach to avoid detergent and lipid completely has been introduced by expressing the IMP as a protein-peptide fusion construct referred to as the SIMPLEx system (Mizrachi et al., 2015). The IMP remains soluble and folded correctly with the amphipathic peptide providing a hydrophobic shield around the IMP.

Regardless of which membrane mimetic is chosen one needs to remember that it is NOT the natural environment of the IMP and changes to dynamics and stability will occur. Even with the lipid-based systems of SMALPs, bicelles, and nanodisks, the lateral pressure and diffusability will be different, and of course, the sidedness of the protein will be lost. Additionally, one should consider that detergents can have deleterious interactions with the extramembranous soluble domains (Yang et al., 2014). It is fundamental to remember that a solubilized IMP is a fish out of water, still a fish, but its behaviour can be very different.

7.2.1.3. Not to overlook the additional challenges of IMP purification

For IMPs the first challenge is optimizing EFPA, but one typically wants to purify the protein for structure-functional studies. For the most part, one can follow the plethora of protein purification approaches used for soluble proteins (see Deutscher [1990] as a classical excellent resource). As with soluble proteins, one must be concerned about the variables of cell lysis approaches and the protection of protein from proteases and oxidative stressors. Yet, the choice of temperature, buffers, and metal/salt ions and concentrations becomes more complicated due to the need to use membrane mimetics to solubilize the protein (see other commandments as well).

The factors highlighted in Tables 1 and 2 can lead to serious issues in protein purification as the net charge of the protein is influenced by the charges of the detergent and the size of the protein is increased with the detergent shell. Thus, chromatographic purification approaches behave considerably different as well as how the protein will behave when centrifuged. A common error in purifying a detergent-solubilized IMP with ion-exchange chromatography is forgetting the net charge of the head group of the detergent and only focusing on the calculated pI

of the target protein. The reader is directed to sections I and II of Hunte, von Jagow and Schagger (2003), for examples and more detail on the considerations of each purification method.

An extremely popular approach to facilitate protein purification is to add an affinity tag through molecular biology approaches. The most frequently used tag is that of the hexa-histidine (His_6) peptide added for use on immobilized metal ion absorption/affinity chromatography (IMAC). Undoubtedly, affinity-affinity tags (Terpe, 2003) have been the most significant technological advancement helping accelerate protein biochemistry. However, there are issues with such tags influencing and changing the activity and stability of the tagged target protein (Majorek et al., 2014; Mohanty and Weiner, 2014; Booth et al., 2018). An example of the influence of a His_6 tag on an IMP transporter is seen with the bacterial multidrug resistance transporter EmrE where the *in vivo* resistance profile was changed as well as changes of *in vitro* structural observations regarding multimeric state equilibrium and ligand binding upon the addition of the tag (Qazi et al., 2015). Therefore, one can still utilize affinity tag approaches to initiate the purification, but do not consider that your protein will behave as wildtype *in vivo* or reconstituted and that the tag may lead to miss-interpretations in structural and functional studies.

7.2.2. COMMANDMENTS AROUND IMP BIOCHEMISTRY

7.2.2.1. Understand the differences in stability compared to globular proteins

IMPs are remarkably thermodynamically stable in the lipid bilayer. This comes from the hydrogen bonds fully satisfied in the hydrophobic environment where the weakly coulombic nature of the H-bond is enhanced in the hydrophobic environment. Similarly, salt bridges are stronger and the intimate contacts of the van der Waals interactions between helices provide large enthalpic contributions in addition to the balance of the lipophobic effect and hydrophobic matching towards entropy contributions (White and Wimley, 1999; Engelman et al., 2003; Bowie, 2005).

The mixed solvation conditions (lipid environment and bulk aqueous phase) leads to unexpected behavior in traditional biochemical protein manipulation conditions. Consider denaturation using urea or guanidinium ion. Both of these denature a protein by competing out H-bonds. In the case of an IMP in a lipid or membrane mimetic, the extra membrane domains will denature but the

transmembrane polypeptide remains inaccessible to these compounds and does not denature. Thermal denaturation is different as well due to the large enthalpy and many IMPs do not thermally denature. If they do, upon cooling they often aggregate into beta-strand based amyloid structures. Certainly, the delipidated protein is highly unstable and the reason why IMPs are manipulated in membrane mimetics.

A traditional storage approach of proteins is lyophilization, or -20°C storage. Lyophilisation can concentrate salt ions leading to aggregation events with detergents. The freezing step can trap crystallization water within the detergent protein complex dissociating TMHs leading to protein aggregation. As with any protein storage conditions, tests for protein aggregation need to be conducted.

Many small IMPs with short extra membrane loops do not denature (linearize) in sodium dodecyl sulfate (SDS). In fact they can maintain their structure and ligand binding properties in such detergents (Tulumello and Deber, 2012). The use of this detergent in electrophoresis techniques is standard biochemistry and migration comparisons are based on the ratio of SDS molecules with molecular weight to define a charge to mass ratio. For IMPs, they can bind differential amounts of SDS (depending on the degree of TMH-TMH interactions are disrupted) leading to anomalous migration on SDS-PAGE (Rath et al., 2009). There is also the issue of the competitive ability of SDS to outcompete the membrane mimetic used for the solubilization steps.

Tips to deal with these issues experimentally are provided in Hunte, von Jagow and Schagger (2003), but overall it is important to recognize stability differences compared to globular proteins.

7.2.2.2. Think carefully of experimental conditions

Biochemists will think carefully of their experimental physicochemical conditions: pH and buffering compound, ionic strength, counterions, dielectric constant, redox potential, temperature, protein concentration/density. These conditions are chosen with their protein of interest in mind to try to mimic the natural physiological conditions as well as stabilize their system while doing experiments. In this regard, we work in a biological buffer with a mixture of various compounds and concentrations to define the ideal condition.

However, when working with IMPs we have an additional compound, the membrane mimetic, which is either influenced or influences the other biological buffer components. If we don’t want our detergent, and subsequently our IMP,

precipitating out we need to consider how the biological buffer components will influence the detergent performance (consider Tables 1 and 2).

Temperature is likely the most frequent mistake of the novice IMP biochemist in the lab. This comes from the standard of doing all protein experiments on ice or in the cold room. Yet, many detergents have their CMT between 4 and 24 °C, which leads to the detergents crystalizing and precipitating out or forming gel-like phases.

Another consideration is in moving from the detergent or detergent-like compounds being used as membrane mimetics to reconstitution into proteoliposomes. Considering first that reconstitution is an art form in itself and this process is often different for each unique IMP. Then one must consider the lipid composition of the liposome as well as the size. Will curvature strain be an issue for ones given IMP; i.e. does it originate from a membrane with high curvature or more planar? Or more fundamentally, are your chosen lipids appropriately hydrophobically matched (Killian, 1998)? Even considering the head group and lipid mixture is of importance regarding maintaining topology. Biological lipids have different lipid compositions in each leaflet of the bilayer and protein sequences have evolved to match.

It is extremely difficult, if not impossible to mimic accurately all the biological conditions. So beyond knowing this as a biochemist, here I leave the warning to be extremely careful about the interpretation from your model system as to what is going on in the cell.

7.2.3. COMMANDMENTS AROUND IMP FUNCTIONALITY STUDIES

7.2.3.1. Not to ignore ligand binding differences

Kinetics and diffusion in three-dimensional space are considerably different than in the two-dimensional plane. Here we consider the differences in the ability to bind ligand. The ability of a substrate to find the binding site of an IMP transporter or receptor in a lipid bilayer will be different than when it is solubilized in a membrane mimetic allowing extra degrees of freedom. This will affect the ‘on rates’ and subsequently the binding constant. Differences in this diffusion property on the kinetics are complemented by differences in thermodynamic energy properties of ligand-protein binding. The dynamics of the

peptide chain and subsequent movements of amino acid side chains would be modulated differently by the membrane mimetic compared to the lipid bilayer.

Thus the on/off rates can be different leading to very different binding constants. An early study evaluating nucleoside transporters noted that different detergents needed to be screened to find one that got close to retaining the high ligand affinity observed *in vivo* (Hammond and Zarenda, 1996). A study illustrating these differences of membrane mimetic on structure and dynamics, circular dichroism and fluorescence were performed on the model multi-ligand transporter, EmrE. Remarkable differences were observed with the protein solubilized in different detergents as well as vesicle systems and solvents (Federkeil et al., 2003). A follow-up study using isothermal titration calorimetry confirmed the above statements with K_d values for the same substrate ranging over 10 fold (Sikora and Turner, 2005). A more recent example is seen with P-glycoprotein, where modulators stimulated ATPase activity compared to inhibition in native membranes (Shukla et al., 2017).

The issues around detergent selection for maintaining activity have been recognized since the 1960s with studies of different detergents on mitochondrial enzymes (for example see Soltysiak and Kaniuga [1970]). Unfortunately, such issues became forgotten with high throughput purification methods, as there are very few studies evaluating changes to the structure, binding with a change of membrane mimetics. Yet this issue is found in various early texts on membrane proteins (early attention to this issue brought up in Gennis [1989]). Few would do activity comparisons under different solubilization conditions as, well, why would they? If after a frustrating timeframe optimizing EFPA and detergent selection and purification, finally finding something that worked, few would want to start again.

So this commandment is simply to note that there is a strong likelihood that different solubilization and physicochemical conditions will give different answers about your IMP of interest.

7.2.3.2. Remember that membrane sidedness is lost

This seems obvious, but it tends to be forgotten or ignored. Upon solubilization of an IMP in a membrane mimetic, it is important to recognize that the biological sidedness of the protein has now been lost. The biological membrane is referred to in most textbooks as a semi-permeable barrier and divides different environments. Consider the protein in Figure 1. Each side of the membrane has completely different physicochemical environments. There can be

remarkable differences in pH, ionic strength, specific ions and ion concentrations, dielectric constant, redox potential, and both low and high molecular weight metabolites and biomolecules (peptides, proteins, carbohydrates, nucleic acids). There will also be differences in fluidity in the lipid leaflet on each side of the membrane with conditions of side influencing the protein dynamics, ligand binding and catalytic activity.

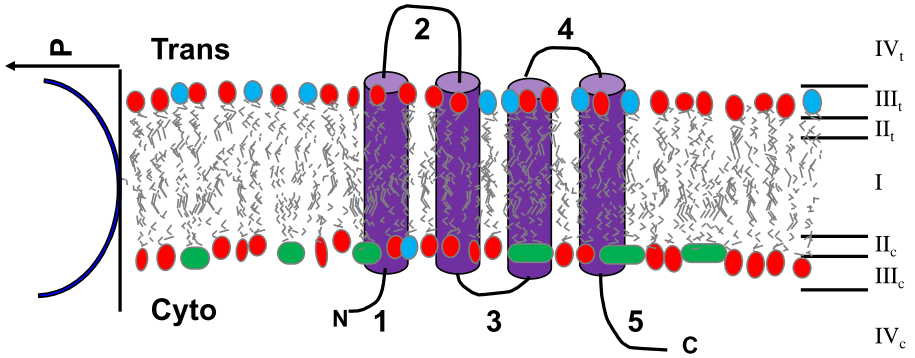

Figure 1. Depiction of a biomembrane with a protein topology sketch. Cartooned here is a bilayer demonstrating a different lipid composition between the two leaflets of the membrane. The two sides of the membrane are defined as the cytoplasmic side or cis side (subscript 'c') and the outside or trans side (subscript 't'). On the right in roman numerals indicates the different regions of the membrane: I as the acyl chain lipid core; II as the slightly polar glycerol region of the glycerol lipids; III as the highly polar and/or charged lipid head group region potentially also influenced by a phosphoester bridging group; IV the bulk solvent. The subscripts of these regions are to depict that their physicochemical environments are different to each other. Considering the potential of differential saturation of acyl chains, once could also divide region I to the c and t leaflets as the dynamics and packing pressure can also be different. The graph depiction on the left illustrates the nature of the hydrophobic (polarity; P) gradient that exists, and that it is not an instant transition. A topology model of a 4 transmembrane helix protein is also shown with the numbers indicating the different extra membrane loops. From this diagram one should recognize that the chemical environments of loops 1, 3, and 5 would be different from loops 2 and 4.

Biologically, an IMP has evolved so that the amino acid sequence on the different sides of the membrane is well suited to those specific physicochemical conditions. Thus, once the protein is solubilized, the extramembrane domains are now exposed to identical conditions, defined by the experimentalist, which may or may not be relevant to either side of the membrane. Replacing detergent membrane mimetics with bilayer disks can solve the issues around the accuracy of

the detergent to replicate the bilayer, yet the sidedness is still lost leaving the extra membrane domains exposed to the same conditions.

7.2.3.3. Not to confuse *in vitro* vs *in vivo* activity

I have been amused over the years receiving reviewer comments asking for activity measurements of the detergent-solubilized transporters I have worked on. Given that a transporter moves a ligand from one side of the membrane to the other, such activity by definition is lost once solubilized. A similar issue exists for ion channels and receptors. This is the ramification of the biomembrane sidedness and solubilization causing forfeiture of physicochemical condition separation as in the comments above. One can still measure ligand binding as a proxy, but the binding observed will likely be somewhat disconnected to the *in vivo* state. Not to say such experiments are not worth doing to compare mutants, ligand specificity, and inhibitors.

For the most part, it is still impossible to obtain biochemical structure-function information of an IMP while in its natural cellular environment *in vivo*. Certainly, experiments in proteoliposomes, defined detergent vesicle, or black membrane systems provide closer to *in vivo* realities, but may still not be able to provide exactly replicated conditions. Yet combining genetic phenotype experiments beside good cell biology, complemented with *in vitro* biochemical and structural studies a considerable wealth of knowledge has been amassed on IMPs. The message here is simply to recognize that our experimental model systems still do not precisely mimic those of a cell.

7.2.4. COMMANDMENTS AROUND IMP STRUCTURE

7.2.4.1. Not to put all faith in hydropathy plots

I still find myself shocked when in a graduate student committee meeting where they are announcing they have cloned a gene responsible for this or that, and they had performed bioinformatic analysis and go on to define it as an IMP and show me a picture of the TMH winding back and forth through a double-lined membrane followed by excitement around some domain of residues as binding site or the like. Such meetings remind me of the blind faith students (and senior researchers) often have in some of our tools, using them as black boxes. But in the case of IMPs, not understanding the issues around hydropathy analysis and various prediction algorithms frequently leads to wrong models and subsequent

downstream problems in experimental interpretations. It is not to say many of the present programs work remarkably well, however they may never be 100% accurate.

The first comment on this issue is the choice of hydropathy scale that is applied to the primary amino acid sequence. For the uninitiated, this first step is considered trivial. Assign a value of hydrophobicity to each amino acid and apply these values to the primary sequence as initially applied by Kyte and Doolittle (1982). However, it is remarkably challenging to agree on such a value for each amino acid. More than 80 hydrophobicity/hydrophilicity indices existed by 1989, and the next two decades saw on the order of 2-4 new hydropathy scales proposed per year. Some became favored for various regions, but often would be chosen by default or random and applied to a sequence to generate hydropathy plots predicting TMH regions, which were taken on faith to be accurate, but overall were disappointing error-prone (Elofsson and von Heijne, 2007).

Advancements came as the field recognized that some classes of IMP were more efficiently predicted with some scales versus others (Crimi and degli Esposti, 1991; Turner amd Weiner, 1993). Further improvements came through considering the ionized versus a neutral form of amino acid, as well as considering possible charge pairing that would neutralize charges for membrane insertion (Jayasinghe, Hristova and White, 2001a). Another advancement was to recognize the regions in the membrane (Figure 1) and that the hydropathy values should not be weighted equally to the core of the membrane versus the membrane barrier as there is a polarity gradient in the natural membrane (von Heijne and Rees, 2008).

Issues with hydropathy analysis are nicely illustrated by applying different scales to the same protein, which will often lead to different outcomes. Yet even with applying the learned concepts the scale outputs are getting closer to an agreement. However, using different approaches still leads to differences in the confidence of the final predictions (MacCallum and Tieleman, 2011).

Using hydropathy knowledge in combination with homology sequence alignments and computational learning increased the predictability of multispanning IMPs to be over 80% accurate (Viklund and Elofsson, 2004). However, the false positive and false negative rates (either predicting a region to be in the membrane or missing a transmembrane region) for most algorithms are still on the order of 20-30% (Zhao et al., 2006). An explanation given for why we may not be able to reach 100% accuracy is that some TMHs could be fully hidden from the hydrophobic lipids and thus ‘look like’ a soluble helix. Further, some sequences in a large soluble protein may be sufficiently hydrophobic, being they are hidden from the polar aqueous environment by the remainder of the protein

(Zhao et al., 2006). Thus some TMHs may be impossible to distinguish from helices in soluble globular proteins and *visa versa*. Furthermore, even with the significant improvements of prediction algorithms, it is still very difficult to predict marginally hydrophobic TMHs, disrupted TMHs, and re-entrant loops such as what seems to occur in the glutamate transporter and some ion channels.

Even with this knowledge, taking a quick look online gives the observation that there are still a large number of servers that default to a single Kyte and Doolittle scale and simple calculations. A list of good predictor algorithms was put together by Tsirigos et al. (2013). The recommendation here is to use different algorithms, choosing different hydropathy scales and selectivity limits and take the average result as your working model.

7.2.4.2. Not to believe blindly the predicted topology

Moving from the prediction of the TMHs by hydropathy analysis, one normally takes the subsequent leap to define the topology of the protein in the membrane; the winding of the peptide sequence back and forth across the membrane defining the location of specific extra membrane loops/domains and location of the N and C-termini. This was initially considered a trivial exercise as one should be able to define if the protein has a cleavable signal sequence or not, and then just wind the protein back and forth across the membrane from that start position. However, it is now recognized that IMP biogenesis can follow many pathways for insertion, folding and maturation (Cymer, von Heijne G and White, 2015; White, 2015), complicating this early assumption.

An early improvement to hydropathy analysis was the recognition that prokaryotic proteins had a sidedness preference of charged amino acids allowing one to test the predicted number of helices to the positive-inside rule (von Heijne, 1992). However, a complication to this rule has come from recognizing that lipid type also influences the topology (Dowhan and Bogdanov, 2009; Dowhan, Vitrac and Bogdanov, 2019). A further cautionary note recognizes that protein topology can vary between members of the same functional family (Tsirigos et al., 2018).

There are a wide range of sidedness fusion tags and probes for both eukaryotic and prokaryotic IMPs to experimentally test the predicted topology (van Geest and Lolkema, 2000). Additionally, a curated database of IMP topologies, MPtopo (initially beginning from Jayasinghe, Hristova and White [2001b]). A value of this database is that it is conservative, containing only experimentally validated transmembrane segments.

Overall, the two-dimensional topology model is the first step to move forward for structure-functional biochemistry. Having the topology very early on helps guide experiments towards a biological mechanism. If one misinterprets the topology, one will be plagued with confusing results moving forward.

7.2.4.3. Be skeptical of high-resolution structures

The literature is full of studies that point out the gap between the number of sequences representing IMPs in sequenced genomes – typically on the order of 30% - and the low number of known unique IMP structures (see https://blanco.biomol.uci.edu/mpstruc). This differential illuminates the challenges along the structure determination path for IMPs.

A degree of cautionary thought of a structure's accuracy should be considered for all structural biology, as in the case of crystallography one is growing crystals outside the *in vivo* physicochemical conditions. It is often forgotten that the final structure is a model to represent the data. Considering when it comes to IMPs solved in a membrane mimetic, one's skepticism should be heightened. This is not to say that the three-dimensional structures are wrong. Certainly, the polypeptide folded and interacted in a way that promoted an ordered crystal and this growth was under the conditions that the experimentalist screened to find the ideal conditions for this growth. But these final conditions are rarely what one would find *in vivo*; nature evolved not to crystalize their proteins for the most part. So with such aggressive processing of the sample and the difficulty of mimicking the natural conditions, one should not be surprised that artifacts slip in. The challenge is to understand the relevance of the given structure to the *in vivo* state, and in the context, here, in a lipid bilayer of a specific membrane/cellular environment. Additionally, heterologous protein-protein interactions are typically lost or ignored as one is crystalizing the minimal unit (as with the majority of studies in the past). It is extremely difficult to mimic the conditions *in vivo* for a soluble protein, and exceedingly more complicated for an IMP where there are multiple physicochemical regions as lamented on in other commandments.

In earlier times, prior to about 2015, we did not appreciate the role of lipids in modulating the structure of IMPs, thus most deposited structures solved by X-ray crystallography methods used IMPs solubilized in detergents. The lipid was considered a contaminant and if found as part of the structure the molecules were considered an experimental artifact in the same manner of a buffer molecule found tightly bound in a soluble protein structure. This led to several structures deposited, that although were solved correctly, did not represent the correct

biologically functional lipid constrained structure. If one accepts that any given type of IMP will have a unique annular lipid and specific lipid-protein interactions (Corradi et al., 2019). Using different membrane mimetics for a given IMP should lead to at least subtle variations in the resulting structures. Similarly, using the same membrane mimetic for different proteins one should expect variations of influence on the different structures. This, of course, has lead to the frustrations between different groups' data and interpretations.

It was also remarkable to see structures discussed with great enthusiasm towards mechanism interpretation, even though the unique detergent-solubilized form did not correspond to the biochemistry performed to date in other membrane mimetics. The worst cases of these involved early structures of the transporters P-glycoprotein and EmrE where structures needed to be retracted (although I note they are still accessible). Different membrane mimetics can lead to the stabilization of different structural states over others. An example is seen with the ryanodine receptor (Willegems and Efremov, 2018). This recent and many early studies show the importance of caution in interpretation, without which has lead to biases and assumptions on IMP structures and subsequent interpretations in function.

Unfortunately, little work has been done to decipher the mechanisms that are influencing the structure of an IMP in protein-detergent complexes and the effects of different folding states. In the past decade, more researchers are appreciating that the choice of detergent has to go beyond getting a good extraction and protein purification yield. It is no longer acceptable to ignore that a chosen membrane mimetic may not retain the correct structural and physical properties of the protein (Anandan and Vrielink, 2016). The modulations may be as subtle as a TMH rotated away from its native contacts, a TMH kinked differently, or even to the extent that a TMH is no longer defined in the bilayer. Up to about 2010, it was defined that the transmembrane structure of an IMP was either all beta or all alpha helix. Albeit, it was recognized that different pitches could occur within a given helix. It was also considered that once the polypeptide strand penetrated the lipid bilayer it would continue all the way through as a transmembrane segment (either helix or beta). With this bias of interpretation in mind, if a structure was solved with transmembrane segment abnormalities, the structure was typically thrown out. Since then structures of mixed secondary structure within the membrane have been solved, with several having interrupted secondary structure and those with an incomplete transmembrane strand turning to return to the same side. Another striking failure of earlier structures was defining membrane sidedness to a detergent-solubilized structure in *ab initio* of other biochemical data.

Combining the advances in cryo-electron microscopy with lipid disk membrane mimetic approaches leads us into a new revolution in IMP structural biology. The warning here is to be careful not to get seduced by the hype and continue to recognize potential experimental artifacts creeping into structures to mislead mechanistic interpretations.

7.2.4.4. Remember the importance of the lipid

A theme through many of these commandments is that the solvent of IMPs is a multiphasic mixture of ionic water and lipids. There is now considerable support to appreciate the role of lipids in IMP folding. We also now appreciate the regions of a membrane better, which includes: the core where the acyl chains reside, the glycerol region of the lipid, the head group region (Figure 1, regions I, II, II). The dynamics and dielectric constant of these regions are quite different as well as the ability of water to penetrate which leads to preferences of where amino acids sit in the membrane. Additionally, the two leaflets of the lipid bilayer can be remarkably different in lipid content leading to different thicknesses and bilayer dynamics (Ingolfsson et al., 2014). The differences in lipid composition can also flip the topology of an IMP (Bay and Turner, 2013). For a more detailed discussion of lipids and IMPs see reviews by Corradi et al. (2018; 2019).

Serious improvements in solubilization methods and novel membrane mimetics have been developed to allow the reconstitution of IMPs into lipid disk environments suitable for structure evaluation by cryo-EM, NMR, SAXS, neutron scattering and using cubic lipids for crystallography. These systems have allowed biophysical chemists to overcome earlier limitations. Also, structures are now complemented with computational modeling and molecular dynamics has led towards increased faith of the resulting structure.

Yet, still, the majority of the biochemical and structural work is done with the IMP purified and solubilized in membrane mimetic environments, particularly detergents. Regardless, with the advancement of computational approaches, structures solved in detergent can be placed into a lipid bilayer in silico and molecular dynamics simulations performed to 'solve' a more biologically relevant structure. The group of Sansom produced a platform to facilitate putting IMPs into lipid membranes - MemProtMD (Stansfeld et al., 2015).

7.3. ENVOI

By no means do I consider to hold a candle to the protein prowess of G. Von Heijne and A. Kornberg for their experience with proteins that lead to their informative prose (von Heijne, 1999; Kornberg, 2003). Regardless, the above commandments come from my >25 years of biochemical experimental studies on IMP structure function and all the love and hate that such an experience brings. Some of these commandments relate to issues around our early naivety in the field's perceived understanding of the influence that various experimental parameters have on IMP structure and function. It is impossible to know how much dogmatic information we have accumulated on specific IMPs that could be unwittingly infected by breaks in these commandments leading to factual artifacts awash in the literature. This chapter was not meant to be an extensive review of each of the issues highlighted, only to lead the novice membrane protein biochemist towards finding the right path(s). IMPs are arguably the most important, coding a third of genomes (no bias here, honest) and thus drive the adventurous and courageous towards lifelong relationships. Therefore, I leave these commandments to the IMP research field to consider for both moving forward as well as when contemplating literature of the past.

REFERENCES

Anandan A, Vrielink A. Detergents in membrane protein purification and crystallisation. *Adv Exp Med Biol*. 2016;922:13–28.

Bay DC, Turner RJ. Membrane composition influences the topology bias of bacterial integral membrane proteins. *Biochim Biophys Acta - Biomembranes*. 2013;1828(2):260–270.

Bayburt TH, Sligar SG. Membrane protein assembly into nanodiscs. *FEBS Lett*. 2010;584(9):1721–1727.

Booth WT, Schlachter CR, Pote S, Ussin N, Mank NJ, Klapper V, Offermann LR, Tang C, Hurlburt BK, Chruszcz M. Impact of an N-terminal polyhistidine tag on protein thermal stability. *ACS Omega*. 2018;3(1):760–768.

Bowie JU. Solving the membrane protein folding problem. *Nature*. 2005;438(7068):581–589.

Chae PS, Rasmussen SG, Rana RR, Gotfryd K, Chandra R, Goren MA, Kruse AC, et al. Maltose-neopentyl glycol (MNG) amphiphiles for solubilization, stabilization and crystallization of membrane proteins. *Nat Methods*. 2010;7(12):1003–1008.

Claassens NJ, Siliakus MF, Spaans SK, Creutzburg SCA, Nijsse B, Schaap PJ, Quax TEF, van der Oost J. Improving heterologous membrane protein production in

Escherichia coli by combining transcriptional tuning and codon usage algorithms. *PLoS One*. 2017;12(9):e0184355.

Corradi V, Mendez-Villuendas E, Ingólfsson HI, Gu RX, Siuda I, Melo MN, Moussatova A, et al. Lipid-protein interactions are unique fingerprints for membrane proteins. *ACS Cent Sci*. 2018;4(6):709–717.

Corradi V, Sejdiu BI, Mesa-Galloso H, Abdizadeh H, Noskov SY, Marrink SJ, Tieleman DP. Emerging diversity in lipid-protein interactions. *Chem Rev*. 2019;119(9):5775–5848.

Crimi M, Degli Esposti M. Structural predictions for membrane proteins: the dilemma of hydrophobicity scales. *Trends Biochem Sci*. 1991;16(3):119.

Cymer F, von Heijne G, White SH. Mechanisms of integral membrane protein insertion and folding. *J Mol Biol*. 2015;427(5):999–1022.

Deutscher MP. Guide to protein purification. *Methods Enzymol*. 1990;182:1–818.

Dowhan W, Bogdanov M. Lipid-dependent membrane protein topogenesis. *Annu Rev Biochem*. 2009;78:515–540.

Dowhan W, Vitrac H, Bogdanov M. Lipid-assisted membrane protein folding and topogenesis. *Protein J*. 2019;38(3):274–288.

Elofsson A, von Heijne G. Membrane protein structure: prediction versus reality. *Annu Rev Biochem*. 2007;76:125–140.

Engelman DM, Chen Y, Chin CN, Curran AR, Dixon AM, Dupuy AD, Lee AS, et al. Membrane protein folding: beyond the two stage model. *FEBS Lett*. 2003;555(1):122–125.

Federkeil S, Winstone TL, Jicking G, Turner RJ. Spectroscopic analysis of EmrE in various membrane mimicking environments. *Biochem Cell Biol*. 2003;81(70):61–70.

Gennis RB. *Biomembranes, Molecular Structure and Function*. Springer-Verlag, 1989.

Hammond JR, Zarenda M. Effect of detergents on ligand binding and translocation activities of solubilized/reconstituted nucleoside transporters. *Arch Biochem Biophys*. 1996;332(2):313–322.

Hunte C, von Jagow G, Schagger H. *Membrane Protein Purification and Crystallization. A practical Guide.* Academic Press, 2003.

Ingólfsson HI, Melo MN, van Eerden FJ, Arnarez C, Lopez CA, Wassenaar TA, Periole X, de Vries AH, Tieleman DP, Marrink SJ. Lipid organization of the plasma membrane. *J Am Chem Soc*. 2014;136(41):14554–14559.

Jayasinghe S, Hristova K, White SH. Energetics, stability, and prediction of transmembrane helices. *J Mol Biol*. 2001a;312(5):927–934.

Jayasinghe S, Hristova K, White SH. MPtopo: A database of membrane protein topology. *Protein Sci*. 2001b;10(2):455–458.

Killian JA. Hydrophobic mismatch between proteins and lipids in membranes. *Biochim Biophys Acta*. 1998;1376(3):401–415.

Knowles TJ, Finka R, Smith C, Lin YP, Dafforn T, Overduin M. Membrane proteins solubilized intact in lipid containing nanoparticles bounded by styrene maleic acid copolymer. *J Am Chem Soc*. 2009;131(22):7484–7485.

Kornberg A. Ten commandments: Lessons from the enzymology of DNA replication. *J Bacteriol*. 2000;182(13):3613–3618.

Kornberg A. Ten commandments of enzymology, amended. *Trends Biochem Sci*. 2003;28(10):515–517.

Kyte J, Doolittle RF. A simple method for displaying the hydropathic character of a protein. *J Mol Biol*. 1982;157(1):105–132.

MacCallum JL, Tieleman DP. Hydrophobicity scales: A thermodynamic looking glass into lipid-protein interactions. *Trends Biochem Sci*. 2011;36(12):653–662.

Majorek KA, Kuhn ML, Chruszcz M, Anderson WF, Minor W. Double trouble-Buffer selection and His-tag presence may be responsible for nonreproducibility of biomedical experiments. *Protein Sci*. 2014;23(10):1359–1368.

Mizrachi D, Chen Y, Liu J, Peng HM, Ke A, Pollack L, Turner RJ, Auchus RJ, DeLisa MP. Making water-soluble integral membrane proteins *in vivo* using an amphipathic protein fusion strategy. *Nat Commun*. 2015;6:6826.

Mohanty AK, Wiener MC. Membrane protein expression and production: effects of polyhistidine tag length and position. *Protein Expr Purif*. 2004;33(2):311–325.

Popot JL. Amphipols, nanodiscs, and fluorinated surfactants: three nonconventional approaches to studying membrane proteins in aqueous solutions. *Annu Rev Biochem*. 2010;79:737–775.

Postis V, Rawson S, Mitchell JK, Lee SC, Parslow RA, Dafforn TR, Baldwin SA, Muench SP. The use of SMALPs as a novel membrane protein scaffold for structure study by negative stain electron microscopy. *Biochim Biophys Acta*. 2015;1848(2):496–501.

Qazi SJS, Chew R, Bay DC, Turner RJ. Structural and functional comparison of hexahistidine tagged and untagged forms of small multidrug resistance protein, EmrE. *Biochem Biophys Rep*. 2015;1:22–32.

Rath A, Glibowicka M, Nadeau VG, Chen G, Deber CM. Detergent binding explains anomalous SDS-PAGE migration of membrane proteins. *Proc Natl Acad Sci U S A*. 2009;106(6):1760–1765.

Sanders CR, Prosser RS. Bicelles: A model membrane system for all seasons? *Structure*. 1998;6(10):1227–1234.

Schlegel S, Hjelm A, Baumgarten T, Vikström D, de Gier JW. Bacterial-based membrane protein production. *Biochim Biophys Acta*. 2014;1843(8):1739–1749.

Schlegel S, Löfblom J, Lee C, Hjelm A, Klepsch M, Strous M, Drew D, Slotboom DJ, de Gier JW. Optimizing membrane protein overexpression in the *Escherichia coli* strain Lemo21(DE3). *J Mol Biol*. 2012;423(4):648–659.

Shukla S, Abel B, Chufan EE, Ambudkar SV. Effects of a detergent micelle environment on P-glycoprotein (ABCB1)-ligand interactions. *J Biol Chem*. 2017;292(17):7066–7076.

Sikora CW, Turner RJ. Investigation of ligand binding to the multidrug resistance protein EmrE by isothermal titration calorimetry. *Biophys J*. 2005;88(1):475–482.

Soltysiak D, Kaniuga Z. The effect of triton X-100 on the respiratory chain enzymes of a heart-muscle preparation. *Eur J Biochem*. 1970;14(1):70–74.

Stansfeld PJ, Goose JE, Caffrey M, Carpenter EP, Parker JL, Newstead S, Sansom MS. MemProtMD: Automated insertion of membrane protein structures into explicit lipid membranes. *Structure*. 2015;23(7):1350–1361.

Terpe K. Overview of tag protein fusions: from molecular and biochemical fundamentals to commercial systems. *Appl Microbiol Biotechnol*. 2003;60(5):523–533.

Tsirigos KD, Govindarajan S, Bassot C, Västermark Å, Lamb J, Shu N, Elofsson A. Topology of membrane proteins-predictions, limitations and variations. *Curr Opin Struct Biol*. 2018;50:9–17.

Tsirigos KD, Hennerdal A, Käll L, Elofsson A. A guideline to proteome-wide α-helical membrane protein topology predictions. *Proteomics*. 2012;12(14):2282–2294.

Tulumello DV, Deber CM. Efficiency of detergents at maintaining membrane protein structures in their biologically relevant forms. *Biochim Biophys Acta*. 2012;1818(5):1351–1358.

Turner RJ, Weiner JH. Evaluation of transmembrane helix prediction methods using the recently defined NMR structures of the coat proteins from bacteriophages M13 and Pf1. *Biochim Biophys Acta*. 1993;1202(1):161–168.

Viklund H, Elofsson A. Best alpha-helical transmembrane protein topology predictions are achieved using hidden Markov models and evolutionary information. *Protein Sci*. 2004;13(7):1908–1917.

van Geest M, Lolkema JS. Membrane topology and insertion of membrane proteins: Search for topogenic signals. *Microbiol Mol Biol Rev*. 2000;64(1):13–33.

von Heijne G. Membrane protein structure prediction. Hydrophobicity analysis and the positive-inside rule. *J Mol Biol*. 1992;225(2):487–494.

von Heijne G. A day in the life of Dr K. or how I learned to stop worrying and love lysozyme: A tragedy in six acts. *J Mol Biol*. 1999;293(2):367–379.

von Heijne G, Rees D. Membranes: reading between the lines. *Curr Opin Struct Biol*. 2008;18(4):403–405.

White SH. The messy process of guiding proteins into membranes. *Elife*. 2015;4. pii: e12100.

White SH, Wimley WC. Membrane protein folding and stability: Physical principles. *Annu Rev Biophys Biomol Struct*. 1999;28:319–365.

Willegems K, Efremov RG. Influence of lipid mimetics on gating of ryanodine receptor. *Structure*. 2018;26(10):1303–1313.e4.

Winstone TL, Duncalf KA, Turner RJ. Optimization of expression and the purification by organic extraction of the integral membrane protein EmrE. *Protein Expr Purif*. 2002;26(1):111–121.

Yang Z, Wang C, Zhou Q, An J, Hildebrandt E, Aleksandrov LA, Kappes JC Membrane protein stability can be compromised by detergent interactions with the extramembranous soluble domains. *Protein Sci*. 2014;23(6):769–789.

Zhao G, London E. An amino acid "transmembrane tendency" scale that approaches the theoretical limit to accuracy for prediction of transmembrane helices: Relationship to biological hydrophobicity. *Protein Sci*. 2006;15(8):1987–2001.

Submitted: 3rd Jan 2020, Revised: 26th Jan 2019, Accepted: 28th Jan 2020

Chapter Eight

8. CLONING, AMPLIFIED EXPRESSION, FUNCTIONAL CHARACTERISATION AND PURIFICATION OF *VIBRIO PARAHAEMOLYTICUS* NCS1 CYTOSINE TRANSPORTER VPA1242

Irshad Ahmad[1], Pikyee Ma[2], David J. Sharples, Peter J. F. Henderson[*], Simon G. Patching[*]

School of BioMedical Sciences and Astbury Centre for Structural Molecular Biology, University of Leeds, Leeds, LS2 9JT, UK

ABSTRACT

The Nucleobase Cation Symporter-1 (NCS1) family of secondary active transport proteins comprises over 2,500 sequenced members from bacteria, archaea, fungi and plants. In bacteria NCS1 transporters function in salvage pathways for nucleobases and nucleosides, hydantoins and other related compounds. To-date only three bacterial NCS1 proteins are experimentally characterised: Mhp1 (5-arylhydantoins), PucI (allantoin), CodB (cytosine). In this work we cloned the gene for *Vibrio parahaemolyticus* protein VPA1242 (412 residues) into plasmid pTTQ18 with concomitant introduction of a C-terminal hexahistidine-tag and achieved amplified expression in *Escherichia coli* BL21(DE3). VPA1242 is predicted to contain twelve transmembrane spanning α-helices with both N- and C-terminal ends in the cytoplasm and it shares high sequence homology with CodB (75.2% identical plus 14.3% highly similar residues). In transport assays, VPA1242 mediated uptake of ^{3}H-cytosine into energised whole cells and no significant

* Direct all correspondence to Prof. Simon Patching or Prof. Peter Henderson, Astbury Building, Faculty of Biological Sciences, University of Leeds, Leeds, LS2 9JT, UK. E-mail: s.g.patching@leeds.ac.uk, simonpatching@yahoo.co.uk, p.j.f.henderson@leeds.ac.uk.

1. Current address: Institute of Basic Medical Sciences, Khyber Medical University, Peshawar, Pakistan

2. Current address: Laboratory of Biomolecular Research, Paul Scherrer Institute, 5232 Villigen PSI, Switzerland

uptake of any other tested radiolabelled compounds. ^{3}H-cytosine uptake was not dependent on sodium, suggesting that VPA1242 transport is driven by a proton gradient. Based on competition of ^{3}H-cytosine uptake by unlabelled compounds, VPA1242 was highly specific for cytosine. The only other compounds that had small but significant competitive effects were hydantoin, benzyhydantoin, and uracil, which share some structural similarity to cytosine. VPA1242 was stable to detergent solubilisation and purification using a Ni-NTA resin, achieving a purity of ~85% and a yield of ~0.9 mg/litre from fermentor cultures, and had stable α-helical content, all making it tractable to further structural and biophysical characterisation.

Keywords: bacteria, cloning strategy, CodB, cytosine, NCS1, nucleobase cation symporter, protein purification, substrate specificity, transport protein

8.1. INTRODUCTION

The Nucleobase Cation Symporter-1 (NCS1) family of secondary active transport proteins comprises over 2,500 sequenced members derived from Gram-negative and Gram-positive bacteria, archaea, fungi and plants (de Koning and Diallinas, 2000; Pantazopoulou and Diallinas, 2007; Saier et al., 2009; Weyand et al., 2010; Witz et al., 2014; Krypotou et al., 2015; Ma et al., 2016; Sioupouli et al., 2017; Patching, 2018). These proteins generally function in salvage pathways as transporters for purine and pyrimidine nucleobases and nucleosides, hydantoins and other related compounds including pyridoxine, thiamine and uric acid. NCS1 family proteins are usually 419-635 amino acid residues in length and are usually predicted to possess twelve transmembrane spanning α-helices (Saier et al., 2009; Witz et al., 2014) and function using a symport mechanism driven by a proton or sodium gradient (Krypotou et al., 2015). The common transport mechanism catalysed by NCS1 family proteins is simplified as: Nucleobase or Hydantoin or Vitamin (out) + H^+ or Na^+ (out) → Nucleobase or Hydantoin or Vitamin (in) + H^+ or Na^+ (in). NCS1 proteins show no sequence similarity to the NCS2 family, also known as the Nucleobase Ascorbate Transporter (NAT) family (Goudela et al., 2005; Gournas et al., 2008; Diallinas and Gournas, 2008; Frillingos, 2012). The first structural model for the NCS1 family was the sodium-coupled hydantoin transport protein, Mhp1, from *Microbacterium liquefaciens* (Suzuki and Henderson, 2006; Jackson et al., 2013; Patching, 2017; Patching, 2018), for which crystal structures have been determined with the protein in three different conformations i.e. outward-facing open, occluded with substrate and inward-facing open (Weyand et al., 2008; Shimamura et al., 2010; Simmons et al., 2014). Mhp1 has provided a principal model for the alternating access mechanism of

membrane transport and for the mechanism of ion-coupling (Shimamura et al., 2010; Weyand et al., 2011; Adelman et al., 2011; Shi, 2013; Kazmier et al., 2014; Kazmier et al., 2017). The function and substrate specificities of only 25 NCS1 proteins (3 bacterial, 16 fungal, 6 plant) have so far been characterised experimentally (Schwacke et al., 2003; Krypotou et al. 2015; Patching, 2018). The two other characterised bacterial NCS1 proteins are allantoin transporter PucI from *Bacillus subtilis* (Ma et al., 2016) and cytosine transporter CodB from *Escherichia coli* (Danielsen et al., 1995).

Studies suggest that the two distinct fungal NCS1 subfamilies and the plant homologues originated through independent horizontal transfers from prokaryotes and demonstrate that transport activities in NCS1 proteins appeared independently by convergent evolution (Hamari et al., 2009; Krypotou et al., 2015). This is one explanation for the observation that substrate specificities of (fungal and plant) NCS1 proteins cannot be predicted by simple amino acid sequence comparisons, by phylogenetic analyses or from comparisons of amino acid residues in the major substrate binding site. Indeed, comparisons performed with Fur-type and Fcy-type NCS1 fungal transporters showed how identical or highly similar residues can provide different substrate specificities due to convergent evolution within the major substrate binding site (Hamari et al., 2009; Krypotou et al., 2015). Further investigations into the origins of substrate specificity in the wider NCS1 family are therefore warranted, especially those from bacteria. In this work we present results for cloning, amplified expression, functional characterisation and purification of NCS1 transport protein VPA1242 from *Vibrio parahaemolyticus* (UniProt entry Q87GS3).

V. parahaemolyticus is a Gram-negative marine bacterium and is a worldwide leading cause of foodborne gastroenteritis in humans, especially in the areas with high consumption of raw or undercooked seafoods (Letchumanan et al., 2014; Letchumanan et al., 2015). The organism is naturally found in estuarine, marine and coastal environments and possesses enormous adaptive capabilities: a planktonic cell or attached to submerged inert surfaces, such as the underside of boats or to other ocean surfaces like fish, shellfish and zooplankton (McCarter, 1999; Iwamoto et al., 2010; Nelapati et al., 2012). *V. parahaemolyticus* exists either as a swimmer cell or a swarmer cell, adapted for locomotion in various environments (Sar et al., 1990; Makino et al., 2003). Under appropriate circumstances the organism has an exceptionally short generation time of 8-12 minutes (Ulitzur, 1974; Makino et al., 2003). A haemolysin is thought to be an important virulence factor produced by the bacterium but the mechanisms of pathogenesis are still unclear (Hiyoshi et al., 2010; West et al., 2013; Lee et al., 2015; Kumaran and Citarasu, 2016). The only predicted NCS1 family transporter

in *V. parahaemolyticus* is VPA1242, which is closely related to cytosine transporter CodB from *E. coli* (Danielsen et al., 1995).

For investigating *V. parahaemolyticus* protein VPA1242, we used a well-established strategy for cloning bacterial transport proteins with a C-terminal hexahistidine tag in *E. coli* using plasmid pTTQ18, followed by optimisation of conditions for amplified expression. The functional activity of VPA1242-His_6 was characterized in terms of substrate and ion specificity and ligand recognition. VPA1242-His_6 was purified by immobilised metal affinity chromatography (IMAC) with a Ni-NTA resin, followed by analysis of secondary structure integrity and thermal stability using circular dichroism spectroscopy.

8.2. MATERIALS AND METHODS

8.2.1. General

Chemicals, reagents and media of the highest available quality were obtained from Sigma-Aldrich Co., Fisher Scientific UK Ltd, Melford Laboratories Ltd, BDH Chemical Supplies or Difco Laboratories, unless stated otherwise. All media, buffers and other solutions were prepared using either deionised water or MilliQ™ water. All media were sterilised by autoclaving or for thermally-sensitive solutions by passage through 0.2 μM Minisart® high-flow sterile syringe-driven filters (Sartorius) or using vacuum-driven 0.2 μM filters (Stericup®) from Millipore. Cellulose nitrate 25 mm ø filters (0.45 μM pore size) for radiolabelled substrate assays and cellulose ester GSTF 25 mm ø filters (0.22 μm pore size) (Whatman®) for protein determinations were from Millipore (UK) Ltd. DNA purification kits were from QIAGEN Ltd. Restriction endonucleases and T4 DNA ligase were from New England Biolabs, Pfu TurboTM DNA polymerase was from Agilent Technologies UK, and 1 kb DNA ladder and SYBR Safe™ DNA gel stain was from Invitrogen. PCR amplification of DNA was performed using a Peltier Thermal cycler from MJ Research. Cell disruption was performed using a Constant Systems disruptor. Protein determinations used the method of Schaffner and Weissmann (1973) or a BCA assay using Pierce® BCA protein assay reagent A from Thermo Scientific. SDS-PAGE was performed by the method of Laemmli (1970), refined for membrane proteins as described by Henderson and Macpherson (1986) using 4% stacking gels and 15% resolving gels in a BioRad Mini PROTEAN 3 apparatus. Acrylamide (40%) and bisacrylamide (2%) solutions were from BioRad Laboratories and SDS-7 protein molecular weight markers were from Sigma-Aldrich Co. Western blotting was performed by semi-dry transfer using a BioRad TRANS-BLOT® SD apparatus;

RGS-His_6 antibody was from QIAGEN Ltd, SuperSignal® West Pico luminal enhancer solution and stable peroxide solution were from Perbio Science UK and Fluorotrans™ membrane was from Pall BioSupport, UK. High-range Rainbow molecular weight markers were from Amersham Biosciences UK Ltd.

8.2.2. Gene cloning and amplified expression

Cloning and amplification of expression of *V. parahaemolyticus* protein VPA1242 in *E. coli* was achieved using a strategy that we and others have found successful with a wide range of bacterial and archaeal membrane proteins (Ward et al., 1999; Saidijam et al., 2003; Saidijam et al., 2005; Clough et al., 2006; Suzuki and Henderson, 2006; Szakonyi et al., 2007; Gordon et al., 2008; Ma et al., 2008; Bettaney et al., 2013; Ma et al., 2013; Ma et al., 2016). This involved design of PCR primers (Forward: 5'-CCGGAATTCGCATATGGCTGGAGACAATAACTACAGTCTTGGACCAG-3'; Reverse: 5'-AAAACTGCAGCC GCT GGCTGTGAAGCCAGTGCTTTTTTGTTGAG-3') to extract and amplify the specific gene from genomic DNA of *V. parahaemolyticus*, introducing *Eco*RI and *Pst*I restriction sites at the 5' and 3' ends, respectively. The restriction-digested PCR product was ligated into plasmid pTTQ18 (Stark, 1987) immediately upstream from a hexahistidine (His_6) tag coding sequence and the resultant pTTQ18-gene(His_6) construct was used to transform *E. coli* BL21(DE3) cells. Expression tests were initially performed using small scale cultures (50 ml) in LB medium supplemented with carbencillin (100 µg/ml), induction with IPTG (0.5 mM) at A_{600} = 0.6 and then growth for a further 2 hours. Total (inner plus outer) membranes from induced and uninduced cells were isolated using the water lysis procedure (Witholt et al., 1976; Ward et al., 2000) and analysed by SDS-PAGE and Western blotting using an antibody to the His_6 epitope for detection of amplified protein bands. Conditions for optimising the amplified expression level of VPA1242-His_6 were tested by using ranges in the concentration of IPTG for induction (0-1 mM) and the length of induction (2-5 hours) and using three different types of media for cell growth (LB, 2TY, M9 minimal).

8.2.3. Scale up and membrane preparation

To provide sufficient quantities of protein for purification and further analysis, optimised culture conditions were scaled up to volumes of 10 litres in flasks or 30 litres in a fermentor. Typically a total of 10 litres of cells were grown to an A_{600} of 0.4-0.6, then induced with IPTG (0.5 mM) and grown for a further 3

hours before harvesting by centrifugation (6000 x g, 15 min, 4 °C) and storage at -80 °C. At a later time the cells were thawed, suspended in Tris-EDTA buffer (20 mM Tris, pH 7.5 with 0.5 mM EDTA) and disrupted by passing twice through a cell disrupter (Constant Systems) at 30 kpsi. Undisrupted cells and cell debris were removed by centrifugation at 12000 x g for 45 minutes at 4 °C. The supernatant containing total (inner plus outer) membranes was collected and retained. Inner/outer membranes were separated by sucrose gradient ultracentrifugation and prepared as described in Ward et al. (2000), followed by washing and resuspension in Tris buffer (20 mM, pH 7.5), dispensing into aliquots, rapid freezing in liquid nitrogen and storage at -80 °C.

8.2.4. Whole cell transport and competition assays

Measurements of uptake of radiolabelled compounds into energised whole cells of *E. coli* were performed using a method based on that of Henderson et al. (1977). Radiolabelled compounds were synthesised in-house (Patching, 2009; Patching, 2011; Patching, 2017) or from Perkin Elmer Ltd, UK. Cells were grown in LB medium supplemented with glycerol (20 mM) and carbenicillin (100 μg/ml) in volumes of 50 or 100 ml at 37 °C in 250 ml or 500 ml baffled conical flasks with aeration at 220 rpm to an A_{600} of ~0.8. The cells were then either left uninduced or induced with IPTG (0.2 mM) and grown for a further 1 hour. After harvesting by centrifugation (4,000 rpm, 10 min, in Falcon tubes using a bench-top instrument), the cells were washed three times with 40 ml transport buffer (150 mM KCl, 5 mM MES, pH 6.6) and then resuspended in the same buffer to an A_{680} of 2.0. The basic method for the assay is described as follows. Cells were energised for building up the proton gradient to drive substrate transport by incubating aliquots of the suspension (955 μl) with 20 mM glycerol (20 μl of 1 M) and with bubbled air in a bijou bottle held in a water jacket at 25 °C. After exactly 3 minutes, radiolabelled substrate at a concentration of 50 μM (25 μl of a 2 mM stock solution) was added with brief mixing. At time points of 0.25, 1, 2, 5, 7.5 and 10 minutes after adding the radiolabelled substrate, 100 μl aliquots were transferred to cellulose nitrate filters (0.45 μm pore size), pre-soaked in transport buffer, on a vacuum manifold and washed immediately with transport buffer (3 ml) three times. The filters were transferred to scintillation vials with 10 ml Emulsifier Safe liquid scintillation fluid (Perkin Elmer Ltd, UK) and incubated overnight. The level of radioactivity retained by the cells was measured by liquid scintillation counting (Packard Tri-Carb 2100TR instrument). Background counts were measured from washing filters under vacuum in the absence of cells or radiolabelled substrate. Standard counts were measured by transferring 4 μl of the

radiolabelled substrate stock solution (containing 8 nmol) directly to a washed filter in the vial. The uptake of radiolabelled substrate into the cells was calculated using the following equation: Uptake (nmol/mg cells) = (Cell counts – Background counts) x (Total assay volume/Sample taken volume) x (1/mg of cells) x (Moles of standard/Standard counts); where dry weight of cells (mg) = Total assay volume (ml) x A_{680} x 0.68. The times of sampling and/or of added radiolabelled substrate concentration were varied for kinetic analyses. To test the effect of potential competing compounds on ^{3}H-cytosine uptake the unlabelled compound was added from a stock solution (50 mM) in 100% DMSO to the cells prior to the energisation period, the final concentration of the unlabelled compound was 500 μM and the final concentration of DMSO was 1%. Relative uptake values were measured as a percentage of those obtained from samples in the absence of any added unlabelled compound or DMSO.

8.2.5. Protein solubilisation and purification

Inner membranes were solubilised for up to 4 hours at 4 °C in solubilisation buffer [20% (v/v) glycerol, 300 mM NaCl, 1% (w/v) SDS, 20 mM imidazole, 20 mM Tris-HCl (pH 8.0)]. The membranes were then sedimented at 131,000 x g for 1 hour at 4 °C to remove the insoluble fraction. For purification by immobilised-metal affinity chromatography (IMAC), the supernatant was incubated with Ni-NTA resin for 2 hours at 4 °C with mixing and then transferred to a BioRad column and the supernatant was run through the column to elute unbound components. The resin was washed with 150-200 ml of wash buffer 1 [10% (v/v) glycerol, 0.05% (w/v) SDS, 20 mM imidazole, 10 mM Tris-HCl (pH 8.0)] to remove any remaining unbound material. The His_6-tagged protein was removed by addition of elution buffer [2.5% (v/v) glycerol, 0.05% (w/v) SDS, 200 mM imidazole, 10 mM Tris-HCl (pH 8.0)]. Volumes of eluted samples were reduced to 3 ml using Vivaspin 20 tube concentrators (4,000 xg) with molecular weight cut off (MWCO) 100 kDa. The 3 ml sample was then applied to a BioRadEcono-pac 10 DG desalting column to remove the high concentration of imidazole. When the sample had run into the column, 4.5 ml of wash buffer 2 [2.5% (v/v) glycerol, 0.05% (w/v) SDS, 10 mM Tris-HCl (pH 8.0)] was applied and the eluted fraction was collected in a Vivaspin 6 tube (MWCO 100 kDa) and spun at 4,000 x g. Purified protein concentrated to 5-30 mg/ml was dispensed into aliquots, flash frozen in liquid nitrogen and stored at -80 °C.

8.2.6. Circular dichroism spectroscopy

The secondary structure content of purified protein was measured by far-UV circular dichroism (CD) spectroscopy using a CHIRASCAN instrument (Applied Photophysics, UK) at 20 ºC with constant nitrogen flushing. Protein samples (0.15 mg/ml) in 10 mM NaPi (pH 7.5) buffer plus 0.05% DDM were analysed in a Hellma quartz cuvette with a 1.0 mm pathlength. Measurements in the wavelength range 180-260 nm used a scan rate of 1 nm/second. A spectrum of buffer alone was subtracted from all sample spectra. Thermal stability was analysed by ramping the temperature from 5-90 ºC and finally back to 5 ºC, where each increment was held for 60 seconds before a measurement was made. Changes in secondary structure were monitored at 209 nm. Melting temperatures were estimated using Global Analysis CD software-3. CD ellipticity values were converted to mean residue ellipiticity (MRE, $deg.cm^{-2}.dmol^{-1}$).

8.3. RESULTS AND DISCUSSION

8.3.1. Database and computational analysis of *V. parahaemolyticus* protein VPA1242

According to the Kyoto Encyclopedia of Genes and Genomes (KEGG) database (http://www.genome.jp/kegg/) (Kanehisa et al., 2016), the gene for *V. parahaemolyticus* protein VPA1242 (UniProt entry Q87GS3, 412 residues) is predicted to code for a cytosine permease and is immediately upstream from the gene that codes for protein VPA1243, which is predicted to be a cytosine deaminase. Indeed, VPA1242 shares 75.2% sequence identity with *E. coli* cytosine permease CodB and the *E. coli* cytosine-inducible operon codBA encodes CodB (UniProt entry P0AA82) followed by a cytosine deaminase CodA (UniProt entry P25524) (Danielsen et al., 1992; Qi and Turnbough, 1995). *E. coli* can utilise cytosine as its sole source of nitrogen by using CodB to mediate uptake of exogenous cytosine and CodA to catalyse hydrolytic deamination of cytosine to uracil (a source of pyrimidines) and ammonia (a source of nitrogen) (Danielsen et al., 1992). Based on separate sequence alignments with characterised bacterial NCS1 family proteins, VPA1242 shares overall sequence homologies of 47.3% (22.8% identical, 24.5% highly similar) with Mhp1, 45.1% (24.8% identical, 20.3% highly similar) with PucI and 89.5% (75.2% identical, 14.3% highly

similar) with CodB. This further confirms that VPA1242 is most closely related with *E. coli* CodB and suggests that VPA1242 is a transporter of cytosine.

Analysis of the VPA1242 amino acid sequence using the prediction tools TMHMM (http://www.cbs.dtu.dk/services/TMHMM/) (Krogh et al., 2001) and TOPCONS (http://topcons.cbr.su.se/) (Bernsel et al., 2009) suggested that protein contains eleven or twelve transmembrane-spanning α-helices, respectively (Figure 1). Based on structurally characterised NCS1 family proteins and a demonstrated reliability for TOPCONS (Hennerdal and Elofsson, 2011; Tsirigos et al., 2015; Saidijam et al., 2018), twelve transmembrane helices is most likely to be correct. In this case, both the N- and C-terminal ends of the protein are predicted to reside at the cytoplasmic side of the membrane (Figure 2). This is the same as the membrane topology predicted for *E. coli* CodB (Danielsen et al., 1995). Locations of the twelve transmembrane helices predicted by TOPCONS in the sequence of VPA1242 align relatively well with those of transmembrane regions in the Mhp1 sequence based on its crystal structure (Figure 3).

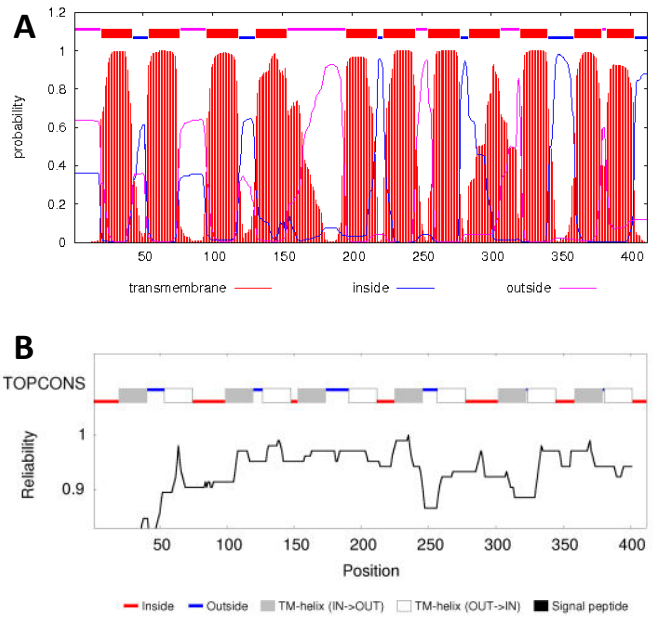

Figure 1. Predictions of transmembrane helices in *V. parahaemolyticus* protein VPA1242. The amino acid sequence of VPA1242 was taken from the UniProt KnowledgeBase (http://www.uniprot.org/) and analysed by membrane topology prediction tools TMHMM (http://www.cbs.dtu.dk/services/TMHMM/) (Krogh et al., 2001) (**A**) and TOPCONS (http://topcons.cbr.su.se/) (Bernsel et al., 2009) (**B**).

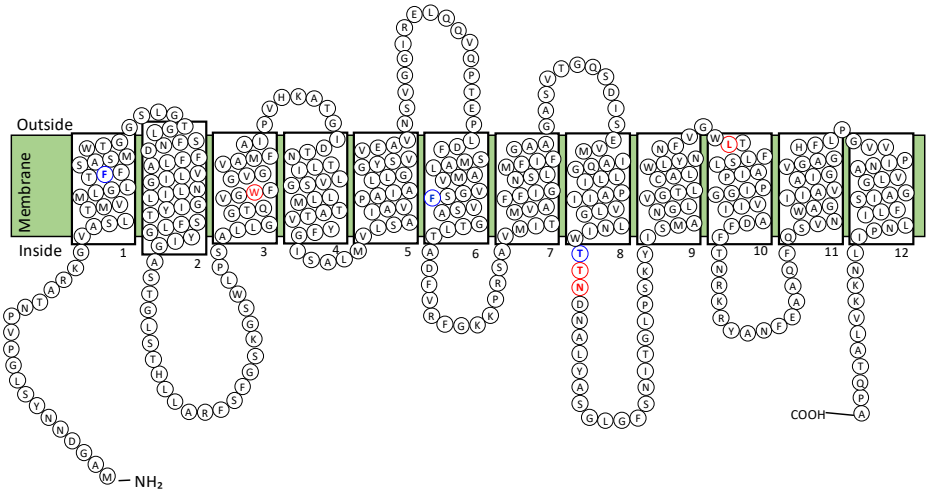

Figure 2. Predicted membrane topology of *V. parahaemolyticus* transport protein VPA1242. Diagram for the putative membrane topology of the VPA1242 transport protein of *V. parahaemolyticus* based on TOPCONS prediction for transmembrane helices (Figure 1). Twelve transmembrane-spanning α-helices are predicted and residues are coloured to show those that are identical (*red*) or highly similar (*blue*) compared with corresponding positions in the sodium and substrate binding site of Mhp1.

Based on the nine residues involved in substrate binding in Mhp1 (Simmons et al., 2014), we can compare the residues at corresponding positions in other characterised bacterial NCS1 proteins to look for possible explanations about the origin of substrate specificity (Table 1 and Figure 3). Out of these residues, only three VPA1242 residues (Ala35, Trp108, Leu325) are identically conserved with those in Mhp1, whilst all nine residues are identically conserved in VPA1242 and CodB. In comparison, five out of nine residues are identically conserved in PucI and Mhp1. Only two out of nine VPA1242/CodB residues (Trp108, Leu325) are identically conserved with those in PucI. These differences appear to account for the significantly different substrate specificities of VPA1242 and CodB compared with Mhp1and PucI. These observations further confirm the close relationship between VPA1242 and CodB. Cautions should of course be made about making possible structural explanations for differences in substrate specificity between NCS1 proteins, as demonstrated by studies on the fungal transporters (Hamari et al., 2009; Krypotou et al. 2015).

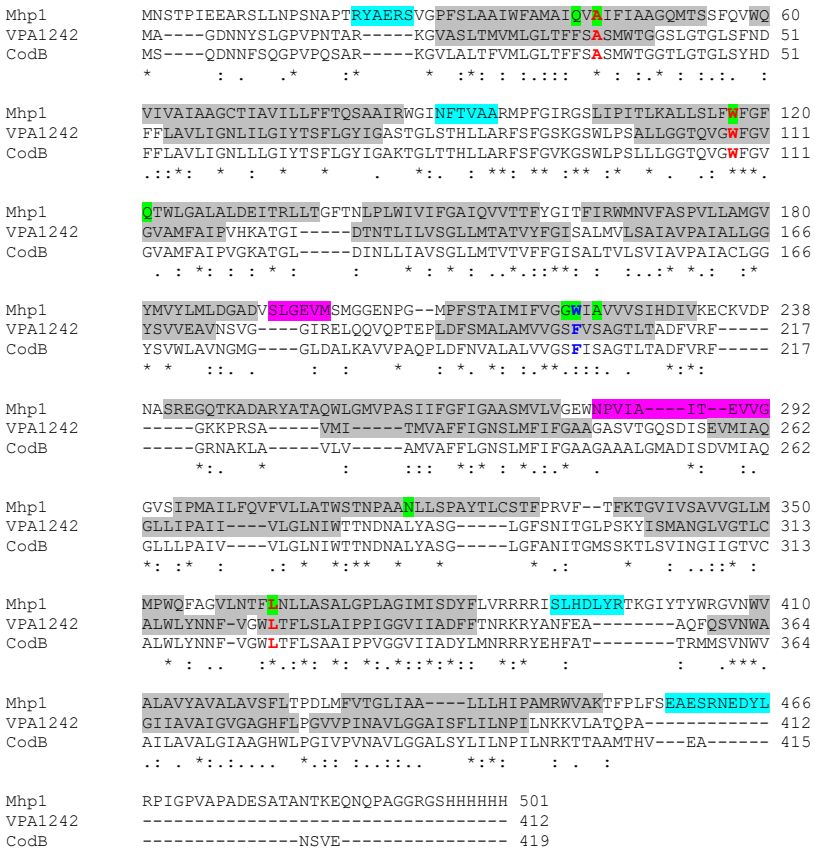

Figure 3. Conservation of residues between *V. parahaemolyticus* protein VPA1242, Mhp1 and CodB. Amino acid sequences of VPA1242 from *V. parahaemolyticus* (Q87GS3), Mhp1 from *M. liquefaciens* (D6R8X8) and CodB from *E. coli* (P0AA82) were taken from the UniProt KnowledgeBase (http://www.uniprot.org/) and aligned using Clustal Omega (http://www.ebi.ac.uk/Tools/msa/clustalo/) (Sievers et al., 2011). Conserved residues are indicated below the sequences as identical (*), highly similar (:) and similar (.). Residues in the substrate binding site of Mhp1 are highlighted (*green*) and residues at these positions are coloured for those that are identical (*red*) or highly similar (*blue*) in the three proteins. Helical regions in Mhp1 based on the crystal structure of Mhp1 with bound benzylhydantoin (PDB 4D1B) (Simmons et al., 2014) are highlighted: transmembrane helix (*grey*), internal helix (*cyan*), external helix (pink). Putative transmembrane helices in VPA1242 based on TOPCONS prediction are also highlighted (*grey*).

Mhp1		PucI	CodB	VPA
TMI	**Gln42**	**Asn43**	Phe33	Phe33
	Ala44	Pro45	**Ala35**	**Ala35**
TMIII	**Trp117**	**Trp119**	**Trp108**	**Trp108**
	Gln121	**Gln123**	Gly112	Gly112
TMVI	**Gly219**	Ile239	Ser203	Ser203
	Trp220	**Trp240**	**Phe204**	**Phe204**
	Ala222	Thr242	Ser206	Ser206
TMVIII	**Asn318**	**Asn329**	Leu284	Leu284
TMX	**Leu363**	**Leu377**	**Leu325**	**Leu325**

Table 1. Conservation of substrate binding residues in characterised bacterial NCS1 family proteins. Residues in the substrate binding site of crystallographically defined Mhp1 (5-arylhydantoins) are compared with those at the corresponding positions in PucI (allantoin), CodB (cytosine) and VPA1242 (cytosine) based on sequence alignments. Residues are coloured to indicate those that are identically conserved (*red*) or highly similar (*blue)* compared with residues in Mhp1.

8.3.2. Gene cloning and amplified expression of *V. parahaemolyticus* protein VPA1242 in *E. coli*

V. parahaemolyticus protein VPA1242 was tractable to an established strategy for amplified expression in *E. coli* of bacterial NCS1 family proteins using plasmid pTTQ18 with concomitant introduction of a C-terminal His_6 tag to assist protein purification (Ward et al., 1999; Saidijam et al., 2003; Saidijam et al., 2005; Clough et al., 2006; Suzuki and Henderson, 2006; Szakonyi et al., 2007; Gordon et al., 2008; Ma et al., 2008, 2013; Bettaney et al., 2013; Ma et al., 2016). Criteria included availability of genomic DNA for the organism of origin, absence of internal *Eco*RI and *Pst*I restriction sites in the gene for the protein of interest, a predicted cytoplasmic location of the protein C-terminus and availability of radiolabelled potential substrates for transport activity assays.

The *V. parahaemolyticus* gene that encodes VPA1242 was successfully amplified by PCR (Figure 4A) and ligated into plasmid pTTQ18, as confirmed by restriction digestion analysis (Figure 4B) and DNA sequencing. The plasmid construct was transformed into *E. coli* strain BL21(DE3) and small-scale growth

in LB medium showed amplified expression of VPA1242-His_6 based on detection of protein bands by SDS-PAGE and Western blotting against the C-terminal His_6 epitope (Figure 5). Based on various parameters that can be altered for improving the level of recombinant protein expression (Ahmad et al., 2018), growth and induction conditions for amplifying expression of VPA1242-His6 in *E. coli* BL21(DE3) were optimised and found to be LB medium supplemented with 20 mM glycerol, induction with 0.25 mM IPTG and a post-induction period of 3 hours (not shown).

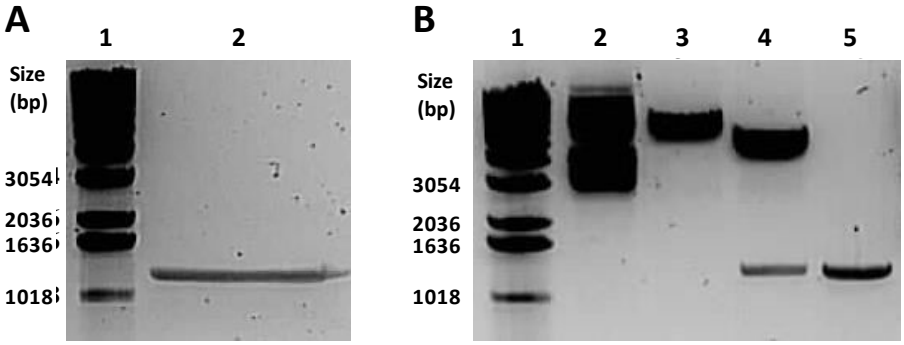

Figure 4. PCR amplification of the gene for *V. parahaemolyticus* protein VPA1242 and cloning into plasmid pTTQ18. Analysis on 1% agarose gels of **A**. The PCR product for amplifying the gene of *V. parahaemolyticus* protein VPA1242 (1 = DNA base pairs ladder, 2 = PCR product) and **B**. Restriction digestion of the plasmid construct for amplifying expression of *V. parahaemolyticus* protein VPA1242 (1 = DNA base pairs ladder, 2 = undigested plasmid, 3 = *Eco*RI-digested plasmid, 4 = *Eco*RI/*PstI*-digested plasmid, 5 = *Eco*RI/*Pst*I-digested PCR product).

8.3.3. Substrate and ion specificities of *V. parahaemolyticus* protein VPA1242

Initial time-dependence measurements for uptake of radiolabelled potential NCS1 substrates (50 μM) into energised *E. coli* cells induced for amplified expression of VPA1242 suggested that VPA1242 is a transporter of cytosine (not shown). Uptake of ^{3}H-cytosine was significantly greater in induced cells compared with uninduced cells with values after 1 minute of around 2.6 and 0.25 nmol mg-1 cells, respectively. None of the other compounds tested showed significant transport activity, including ^{3}H-uracil. Transport of ^{3}H-cytosine by

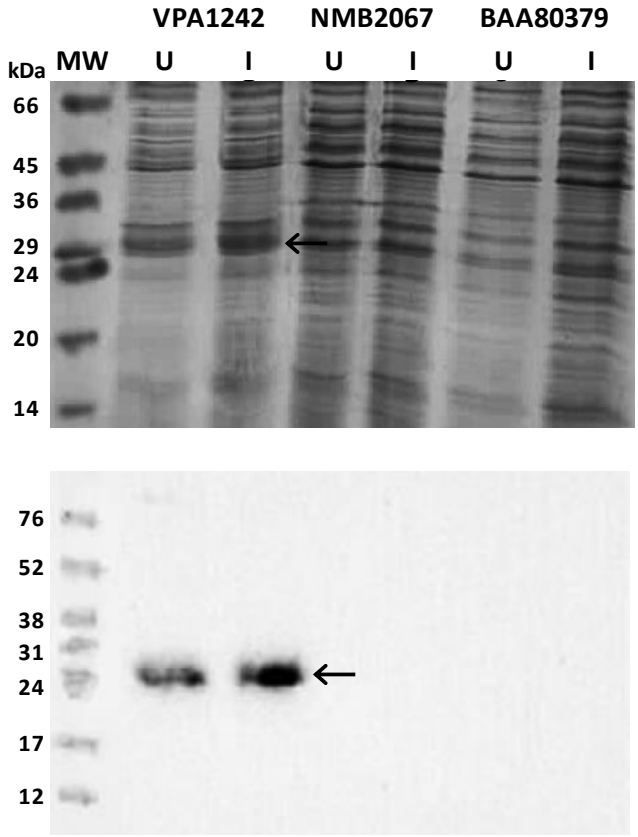

Figure 5. Test for amplified expression of *V. parahaemolyticus* protein VPA1242 in *E. coli*. Coomassie-stained SDS-PAGE (top) and Western blot (bottom) analyses of total membrane preparations from *E. coli* BL21(DE3) cells containing pTTQ18-derived plasmids for amplifying expression of *V. parahaemolyticus* protein VPA1242-His_6 alongside *Niesseria meningitides* protein NMB2067-His_6 and *Aeropyrum pernix* protein BAA80379-His_6 (as negative comparisons) from cultures in LB medium that were left uninduced (U) or induced with 0.5 mM IPTG for 2 hours (I). MW = molecular weight markers. The arrow indicates the position of VPA1242-His_6.

VPA1242 was confirmed by comparing uptake into induced versus uninduced cells and also into cells containing plasmid pTTQ18 with no gene insert (Figure 3 Figure 6). There was some uptake into uninduced cells, which was attributed to leaky expression from the plasmid, and low uptake into cells containing pTTQ18. After a time point of 1 minute, there was a rapid decrease in ^{3}H-cytosine uptake

into induced cells. This may be due to metabolism of ^{3}H-cytosine inside the cells, which likely leads to loss of ^{3}H as ^{3}H2O. Transport of ^{3}H-cytosine by VPA1242 showed no dependence on sodium over the concentration range 0-150 mM (Figure 7), suggesting that the protein is driven by a proton gradient. These results confirm that cytosine is a substrate of VPA1242, which was expected based on the close evolutionary relationship of VPA1242 with CodB from *E. coli*.

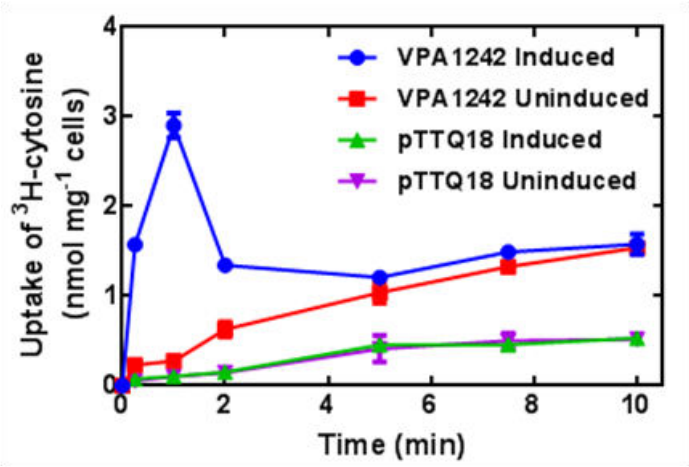

Figure 6. Confirmation of ^{3}H-cytosine transport by *V. parahaemolyticus* protein VPA1242. Uptake of ^{3}H-cytosine (50 µM) into *E. coli* BL21(DE3) cells harbouring the plasmid pTTQ18/VPA1242 or the empty plasmid pTTQ18/no gene from cultures grown in LB medium supplemented with 20 mM glycerol and 100 µg/ml of carbenicillin at 37°C with shaking at 220 rpm. Cells were left uninduced or were induced at A_{680} = 0.6 with IPTG (0.25 mM) and then grown for a further 1 hour. Harvested cells were washed three times using transport assay buffer (150 mM KCl, 5 mM MES pH 6.6) and resuspended in the same buffer to an accurate A_{680} of around 2.0. Cells were energised with glycerol (20 mM) and tested for uptake ^{3}H-cytosine at the given time points. Data points represent the average of duplicate measurements and the plots were produced using GraphPad Prism 7 software.

8.3.4. Ligand recognition by *V. parahaemolyticus* protein VPA1242

The specificity of ligand recognition by VPA1242 was tested through competition of ^{3}H-cytosine transport (50 µM) with a ten-fold excess of unlabelled NCS1 substrates and related compounds (500 µM) (Figures 8 and 9). By far the greatest

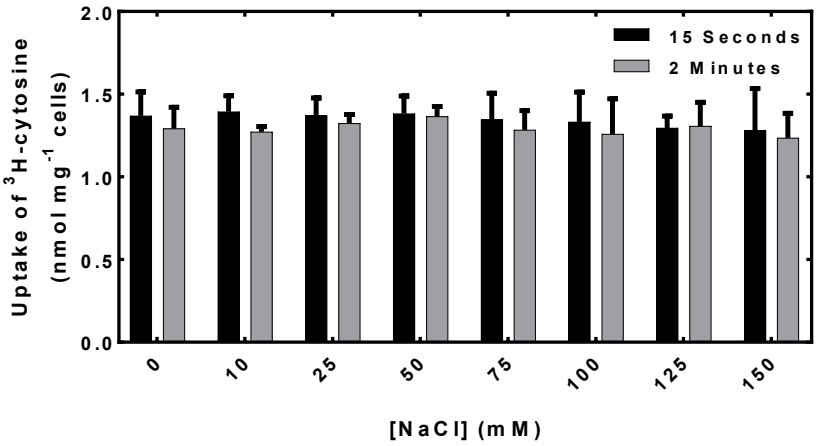

Figure 7. Effect of sodium ion concentration on uptake of ^{3}H-cytosine by *V. parahaemolyticus* protein VPA1242. *E. coli* BL21(DE3) cells harbouring plasmid pTTQ18/VPA1242 were grown in LB medium supplemented with glycerol (20 mM) and carbenicillin (100 µg/ml) at 37 °C with shaking at 220 rpm. Cells were induced at A_{680} = 0.6 with IPTG (0.25 mM) and then grown for a further 1 hour. Harvested cells were washed three times using transport assay buffer containing 5 mM MES (pH 6.6) and a range of NaCl concentrations from 0-150 mM, balanced by a range of KCl concentrations to maintain an overall salt concentration of 150 mM. Under conditions of zero NaCl, crown ether at a concentration of 10 mM was included to mop up any traces of NaCl. Cells were resuspended in the same buffer to an accurate A_{680} of around 2.0. Aliquots of cells were energised with glycerol (20 mM) and tested for uptake of ^{3}H-cytosine (50 µM) at the given time points. Data represent the average of duplicate measurements.

competitive effect was produced by cytosine, which reduced transport activity to 10.7% and 11.5% at time points of 15 seconds and 2 minutes, respectively. The next most effective competitors were hydantoin, benzylhydantoin and uracil which reduced uptake to 52.7/70.7%, 58.1/86.1% and 58.4/87.8% after 15 seconds and 2 minutes, respectively. These compounds share some structural similarity with cytosine. Except for uracil at 15 seconds, none of the other tested nucleobases had a substantial effect on ^{3}H-cytosine transport. Overall the results demonstrate high specificity for recognition of cytosine by VPA1242.

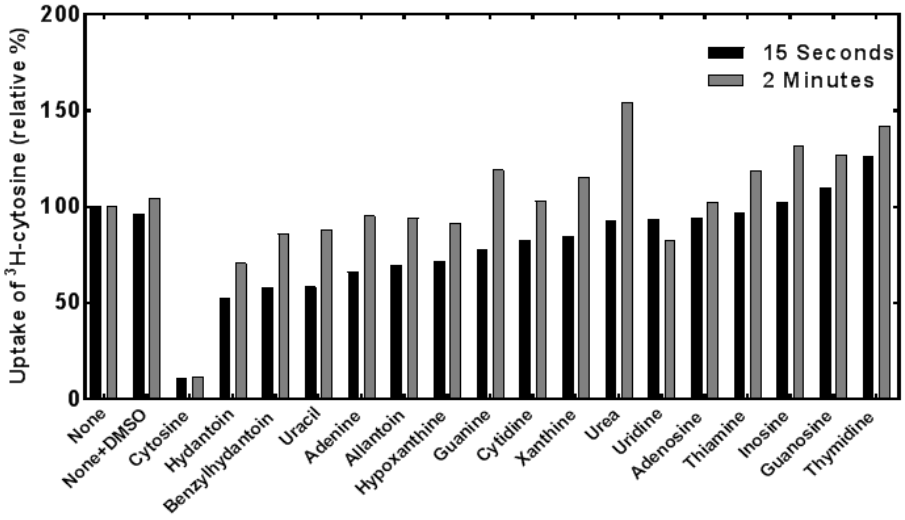

Figure 8. Ligand specificity of *V. parahaemolyticus* protein VPA1242. Competition of ^{3}H-cytosine (50 µM) uptake into *E. coli* BL21(DE3) cells expressing VPA1242-His_6 in presence of a ten-fold molar excess of potential unlabelled competitors. Non-competed uptake was taken as 100% corresponding to 15 seconds and 2 minutes post-addition of ^{3}H-cytosine. All data represent the average of duplicate measurements. None = no competitors.

8.3.5. Detergent solubilisation and purification of *V. parahaemolyticus* protein VPA1242

In order to provide sufficient material for purification of VPA1242-His_6, optimised growth and induction conditions were scaled up to 30 litre cultures in a fermentor followed by isolation of inner membranes. VPA1242-His_6 was solubilised from inner membranes using the detergent DDM (1%) and then purified by IMAC using a Ni-NTA resin with imidazole at a concentration of 20 mM for incubation and washing steps and 200 mM for elution (Figure 10). The relative amount of VPA1242-His_6 in the supernatant was similar to that in inner membranes, indicating that the large majority of membrane proteins had been solubilised. Negligible VPA1242-His_6 in the unbound fraction suggested that most of the VPA1242-His_6 protein was bound to the resin. This resulted in a purity for VPA1242-His_6 of ~85% based on densitometric analysis of the Coomassie-stained gel and a purification yield of ~0.9 mg/litre of cell culture.

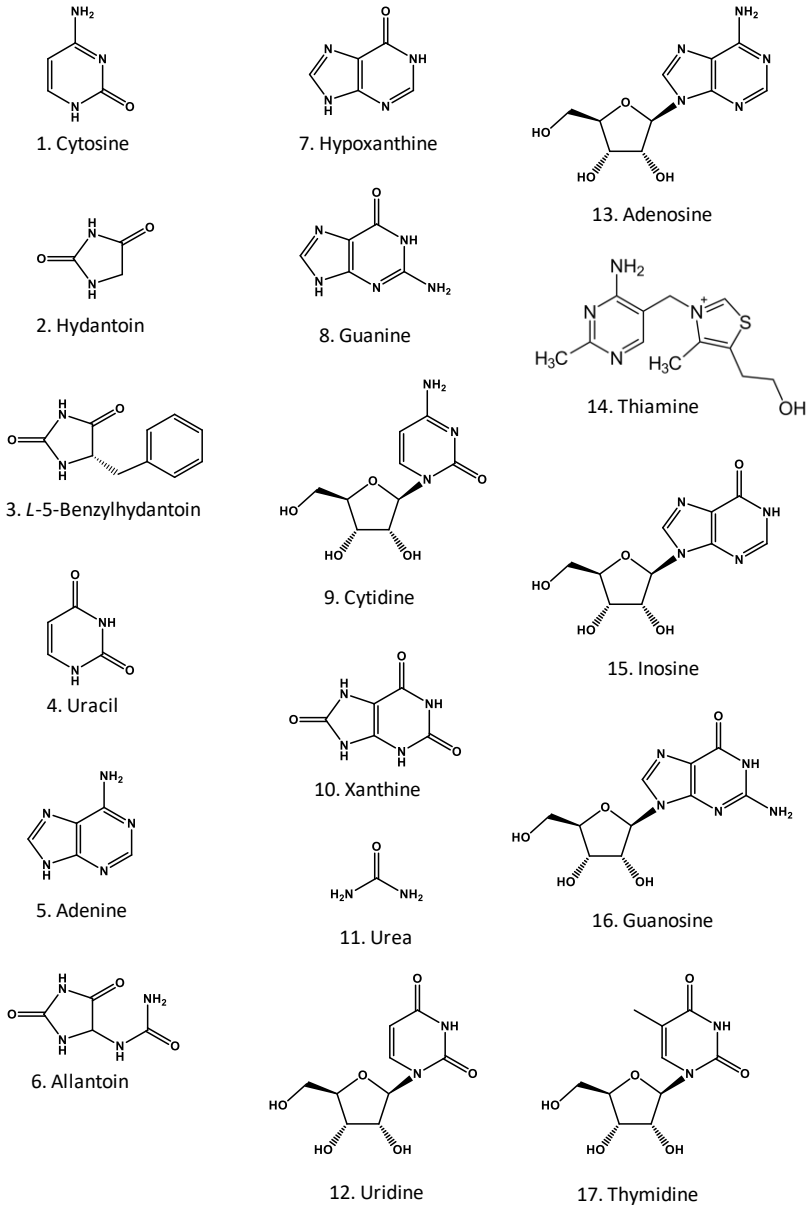

Figure 9. Structures of compounds used as potential competitors of VPA1242-mediated ^{3}H-cytsosine uptake into whole cells. The structures 1-17 are arranged in order of decreasing competitive effect on VPA1242-mediated ^{3}H-cytsosine uptake into whole cells as shown in Figure 8.

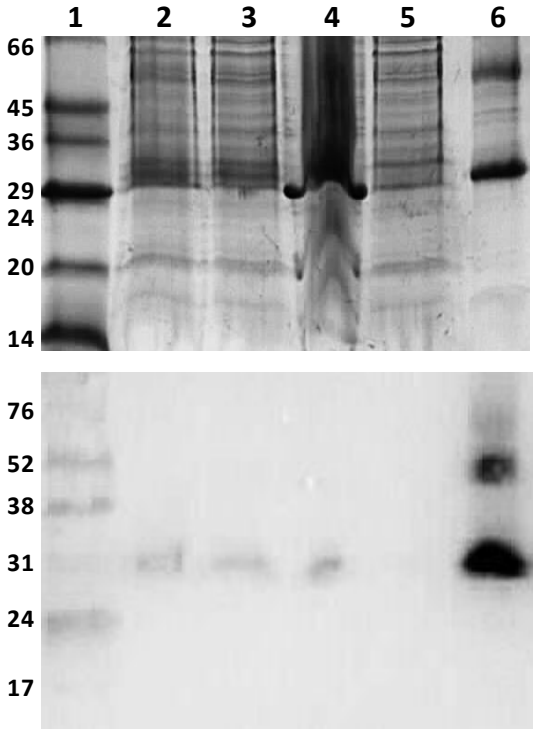

Figure 10. Solubilisation and purification of *V. parahaemolyticus* protein VPA1242 from inner membranes. Coomassie-stained SDS-PAGE (*top*) and Western blot (*bottom*) analyses for solubilisation (1% DDM) and IMAC purification of VPA1242-His_6 from inner membranes. Samples were loaded on the gel (16 μg) and blot (4 μg) as follows: 1 = molecular weight markers, 2 = inner membranes, 3 = supernatant (soluble fraction), 4 = membrane pellet (unsoluble fraction), 5 = column flow-through (unbound fraction), 6 = eluted and concentrated protein.

The monomeric form of VPA1242-His_6 migrates by SDS-PAGE at a molecular weight position of around 30 kDa, which is lower than the calculated molecular weight of 42,821 Da. Visible on both SDS-PAGE gels and Western blots, the band migrating at around 50 kDa is likely to be the dimeric form of VPA1242 (Figure 5). Migration at a lower molecular weight position is consistent with SDS-PAGE analysis of other NCS1 family proteins, which migrate at approximately 62-74% of their predicted sizes (Suzuki and Henderson, 2006; Bettaney, 2008; Ma, 2010; Ma et al., 2016). It is widely recognised that membrane proteins migrate anomalously on SDS-PAGE gels at lower molecular

weight positions than their actual molecular weights predicted from amino acid composition due to their hydrophobic nature, high binding of SDS or retention of secondary structure that facilitates migration through the gel (Ward et al., 2000; Rath et al., 2009; Rath and Deber, 2013).

Purified VPA1242-His_6 had α-helix content according to far-UV circular dichroism spectroscopy (Figure 11), thus confirming secondary structure integrity of the DDM-solubilised protein. A thermal ramping experiment produced a melting temperature of 42.8 ºC and showed that the VPA1242-His_6 protein is reasonably stable for performing biophysical assays using a temperature range of 18-25 ºC (Figure 11).

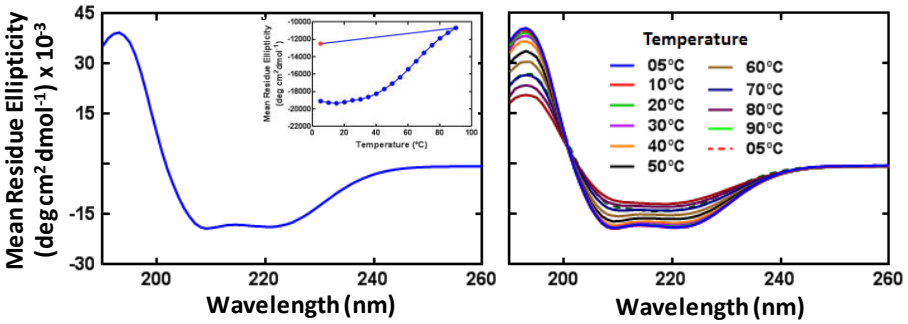

Figure 11. Secondary structure integrity of purified VPA1242-His_6. Far-UV (180-260 nm) circular dichroism spectrum for purified VPA1242-His_6 acquired using a CHIRASCAN instrument (Applied Photophysics, UK) at 20 ºC with constant nitrogen flushing (*left*). The sample was prepared in a Hellma quartz cuvette of 1.0 mm pathlength at a final protein concentration of 0.15 mg/ml in CD buffer (10 mM NaPi pH 7.5, 0.05% DDM). Inset is a thermal unfolding profile over the temperature range 5-90 ºC and finally back to 5 ºC monitored at a wavelength of 209 nm. Full spectra from the thermal unfolding experiment are also shown (*right*).

8.4. CONCLUSION

In this study, the gene for *V. parahaemolyticus* protein VPA1242 was successfully cloned into plasmid pTTQ18 and conditions for amplified expression of VPA1242-His_6 in *E. coli* were optimised. Consistent with a close relationship to CodB from *E. coli*, cytosine was confirmed as the main substrate of VPA1242. The protein was tractable to large scale production, detergent solubilisation and

purification. A reasonable purification yield, secondary structure integrity and stability of VPA1242-His_6 make it a promising candidate for crystallisation trials and for study of structure, ligand binding and dynamics using further biochemical and biophysical techniques. Mutagenesis studies should help us to better understand the origins of substrate specificity in VPA1242 and in other bacterial NCS1 transport proteins.

REFERENCES

Adelman JL, Dale AL, Zwier MC, Bhatt D, Chong LT, Zuckerman DM, Grabe M. Simulations of the alternating access mechanism of the sodium symporter Mhp1. *Biophys J*. 2011;101(10):2399-2407.

Ahmad I, Nawaz N, Darwesh NM, ur Rahman S, Mustafa MZ, Khan SB, Patching SG. Overcoming challenges for amplified expression of recombinant proteins using *Escherichia coli*. *Protein Expr Purif*. 2018;144:12-18.

Bernsel A, Viklund H, Hennerdal A, Elofsson A. TOPCONS: consensus prediction of membrane protein topology. *Nucleic Acids Res*. 2009;37(Web Server issue):W465-W468.

Bettaney KE, Sukumar P, Hussain R, Siligardi G, Henderson PJ, Patching SG. A systematic approach to the amplified expression, functional characterization and purification of inositol transporters from *Bacillus subtilis*. *Mol Membr Biol*. 2013;30(1):3-14.

Clough J, Saidijam M, Bettaney KE, Szakonyi G, Patching SG, Mueller J, Shibayama K, Bacon M, Barksby E, Groves m, Herbert RB, Phillips-Jones M, Ward A, Gunn-Moore F, O'Reilly J, Rutherford NG, Bill R, Henderson PJF. Prokaryotic membrane transport proteins: Amplified expression and purification. In Lundstrom KH (Ed) Structural genomics on membrane proteins. Taylor and Francis 2006;21-42.

Danielsen S, Boyd D, Neuhard J. Membrane topology analysis of the *Escherichia coli* cytosine permease. *Microbiology*. 1995;141(Pt 11):2905-2913.

de Koning H, Diallinas G. Nucleobase transporters (review). *Mol Membr Biol*. 2000;17(2):75-94.

Diallinas G, Gournas C. Structure-function relationships in the nucleobase-ascorbate transporter (NAT) family: lessons from model microbial genetic systems. *Channels (Austin)*. 2008;2(5):363-372.

Frillingos S. Insights to the evolution of Nucleobase-Ascorbate Transporters (NAT/NCS2 family) from the Cys-scanning analysis of xanthine permease XanQ. *Int J Biochem Mol Biol*. 2012;3(3):250-272.

Gordon E, Horsefield R, Swarts HG, de Pont JJ, Neutze R, Snijder A. Effective high-throughput overproduction of membrane proteins in *Escherichia coli*. *Protein Expr Purif*. 2008;62:1-8.

Goudela S, Karatza P, Koukaki M, Frillingos S, Diallinas G.Comparative substrate recognition by bacterial and fungal purine transporters of the NAT/NCS2 family. *Mol Membr Biol*. 2005;22(3):263-275.

Gournas C, Papageorgiou I, Diallinas G. The nucleobase-ascorbate transporter (NAT) family: genomics, evolution, structure-function relationships and physiological role. *Mol Biosyst*. 2008;4(5):404-416.

Hamari Z, Amillis S, Drevet C, Apostolaki A, Vágvölgyi C, Diallinas G, Scazzocchio C. Convergent evolution and orphan genes in the Fur4p-like family and characterization of a general nucleoside transporter in *Aspergillus nidulans*. *Mol Microbiol*. 2009;73(1):43-57.

Henderson PJ, Giddens RA, Jones-Mortimer MC. Transport of galactose, glucose and their molecular analogues by *Escherichia coli* K12. *Biochem J*. 1977;162(2):309-320.

Henderson PJ, Macpherson AJ. Assay, genetics, proteins, and reconstitution of proton-linked galactose, arabinose, and xylose transport systems of *Escherichia coli*. *Methods Enzymol*. 1986;125:387-429.

Hennerdal A, Elofsson A. Rapid membrane protein topology prediction. *Bioinformatics*. 2011;27(9):1322-1323.

Hiyoshi H, Kodama T, Iida T, Honda T. Contribution of *Vibrio parahaemolyticus* virulence factors to cytotoxicity, enterotoxicity, and lethality in mice. *Infect Immun*. 2010;78(4):1772-1780.

Iwamoto M, Ayers T, Mahon BE, Swerdlow DL. Epidemiology of seafood-associated infections in the United States. *Clin. Microbiol Rev*. 2010;23(2):399-411.

Jackson SM, Patching SG, Ivanova E, Simmons KJ, Weyand S, Shimamura T, Brueckner F, Suzuki S, So Iwata, Sharples DJ, Baldwin SA, Sansom MPS, Beckstein O, Cameron AD, Henderson PJF. Mhp1, the Na(+)-hydantoin membrane transport protein. In Gordon CK Roberts (ed) Encyclopedia of Biophysics, Springer, 2013; 1514-1521.

Kanehisa M, Furumichi M, Tanabe M, Sato Y, Morishima K. KEGG: New perspectives on genomes, pathways, diseases and drugs. *Nucleic Acids Res*. 2017;45(D1):D353-D361.

Kazmier K, Claxton DP, Mchaourab HS. Alternating access mechanisms of LeuT-fold transporters: trailblazing towards the promised energy landscapes. *Curr Opin Struct Biol*. *Curr Opin Struct Biol*. 2017;45:100-108.

Kazmier K, Sharma S, Islam SM, Roux B, Mchaourab HS. Conformational cycle and ion-coupling mechanism of the Na^+/hydantoin transporter Mhp1. *Proc Natl Acad Sci U S A*. 2014;111(41):14752-14757.

Krogh A, Larsson B, von Heijne G, Sonnhammer EL. Predicting transmembrane protein topology with a hidden Markov model: Application to complete genomes. *J Mol Biol*. 2001;305(3):567-580.

Krypotou E, Evangelidis T, Bobonis J, Pittis AA, Gabaldón T, Scazzocchio C, Mikros E, Diallinas G. Origin, diversification and substrate specificity in the family of NCS1/FUR transporters. *Mol Microbiol*. 2015;96(5):927-950.

Kumaran T, Citarasu T. Isolation and characterization of virulence-related properties of pathogenic *Vibrio Parahaemolyticus* isolated from aquatic environments. *Environ J*. 2016;2:57-65.

Laemmli UK. Cleavage of structural proteins during the assembly of the head of bacteriophage T4. *Nature*. 1970;227(5259):680-685.

Lee CT, Chen IT, Yang YT, Ko TP, Huang YT, Huang JY, Huang MF, Lin SJ, Chen CY, Lin SS, Lightner DV, Wang HC, Wang AH, Wang HC, Hor LI, Lo CF. The opportunistic marine pathogen *Vibrio parahaemolyticus* becomes virulent by acquiring a plasmid that expresses a deadly toxin. *Proc Natl Acad Sci U S A*. 2015;112(34):10798-10803.

Letchumanan V, Chan K-G, Lee L-H. *Vibrio parahaemolyticus*: a review on the pathogenesis, prevalence, and advance molecular identification techniques. *Front Microbiol*. 2014;5:705.

Letchumanan V, Pusparajah P, Tan LT-H, Yin W-F, Lee L-H, Chan K-G. Occurrence and antibiotic resistance of *Vibrio parahaemolyticus* from shellfish in Selangor, Malaysia. *Front Microbiol*. 2015;6:1417.

Ma P, Patching SG, Ivanova E, Baldwin JM, Sharples D, Baldwin SA, Henderson PJ.Allantoin transport protein, PucI, from *Bacillus subtilis*: evolutionary relationships, amplified expression, activity and specificity. *Microbiology*. 2016;162(5):823-836.

Ma P, Varela F, Magoch M, Silva AR, Rosário AL, Brito J, Oliveira TF, Nogly P, Pessanha M, Stelter M, Kletzin A, Henderson PJ, Archer M. An efficient strategy for small-scale screening and production of archaeal membrane transport proteins in *Escherichia coli*. *PLoS One*. 2013;8(10):e76913.

Ma P, Yuille HM, Blessie V, Göhring N, Iglói Z, Nishiguchi K, Nakayama J, Henderson PJ, Phillips-Jones MK. Expression, purification and activities of

the entire family of intact membrane sensor kinases from *Enterococcus faecalis*. *Mol Membr Biol*. 2008;25(6-7):449-473.

Makino K, Oshima K, Kurokawa K, Yokoyama K, Uda T, Tagomori K, Iijima Y, Najima M, Nakano M, Yamashita A, Kubota Y, Kimura S, Yasunaga T, Honda T, Shinagawa H, Hattori M, Iida T. Genome sequence of *Vibrio parahaemolyticus*: A pathogenic mechanism distinct from that of *V. cholerae*. *Lancet*. 2003;361(9359):743-749.

McCarter L. The multiple identities of *Vibrio parahaemolyticus*. *J Mol Microbiol Biotechnol*. 1999;1(1):51-57.

Minton JA, Rapp M, Stoffer AJ, Schultes NP, Mourad GS. Heterologous complementation studies reveal the solute transport profiles of a two-member nucleobase cation symporter 1 (NCS1) family in *Physcomitrella patens*. *Plant Physiol Biochem*. 2016;100:12-17.

Mourad GS, Tippmann-Crosby J, Hunt KA, Gicheru Y, Bade K, Mansfield TA, Schultes NP. Genetic and molecular characterization reveals a unique nucleobase cation symporter 1 in Arabidopsis. *FEBS Lett*. 2012;586(9):1370-1378.

Nelapati S, Nelapati K, Chinnam B. *Vibrio parahaemolyticus*-An emerging foodborne pathogen-A Review. *Vet World*. 2012;5(1):48-62.

Pantazopoulou A, Diallinas G. Fungal nucleobase transporters. *FEMS Microbiol Rev*. 2007;31(6):657-675.

Patching SG. Synthesis of highly pure ^{14}C-labelled *DL*-allantoin and ^{13}C NMR analysis of labelling integrity. *J Labelled Comp Radiopharm*. 2009;52(9):401–404.

Patching SG. Efficient syntheses of ^{13}C- and ^{14}C-labelled 5-benzyl and 5-indolylmethyl *L*-hydantoins. *J Label Compd Radiopharm*. 2011;54(2):110–114.

Patching SG. Synthesis, NMR analysis and applications of isotope-labelled hydantoins. *Journal of Diagnostic Imaging in Therapy*. 2017;4(1):3-26.

Patching SG. Recent developments in Nucleobase Cation Symporter-1 (NCS1) family transport proteins from bacteria, archaea, fungi and plants. *J Biosci*. 2018;43(4):797-815.

Qi F, Turnbough Jr CL. Regulation of codBA operon expression in *Escherichia coli* by UTP-dependent reiterative transcription and UTP-sensitive transcriptional start site switching. *J Mol Biol*. 1995;254(4):552-565.

Rapp M, Schein J, Hunt KA, Nalam V, Mourad GS, Schultes NP. The solute specificity profiles of nucleobase cation symporter 1 (NCS1) from Zea mays and Setaria viridis illustrate functional flexibility. *Protoplasma*. 2016;253(2):611-623.

Rath A, Deber CM. Correction factors for membrane protein molecular weight readouts on sodium dodecyl sulfate-polyacrylamide gel electrophoresis. *Anal Biochem*. 2013;434(1):67-72.

Rath A, Glibowicka M, Nadeau VG, Chen G, Deber CM. Detergent binding explains anomalous SDS-PAGE migration of membrane proteins. *Proc Natl Acad Sci U S A*. 2009;106(6):1760-1765.

Saidijam M, Azizpour S, Patching SG. Comprehensive analysis of the numbers, lengths and amino acid compositions of transmembrane helices in prokaryotic, eukaryotic and viral integral membrane proteins of high-resolution structure. *J Biomol Struct Dyn*. 2018;36(2):443-464.

Saidijam M, Bettaney KE, Szakonyi G, Psakis G, Shibayama K, Suzuki S, Clough JL, Blessie V, Abu-Bakr A, Baumberg S, Meuller J, Hoyle CK, Palmer SL, Butaye P, Walravens K, Patching SG, O'reilly J, Rutherford NG, Bill RM, Roper DI, Phillips-Jones MK, Henderson PJ. Active membrane transport and receptor proteins from bacteria. *Biochem Soc Trans*. 2005;33(Pt 4):867-872.

Saidijam M, Psakis G, Clough JL, Meuller J, Suzuki S, Hoyle CJ, Palmer SL, Morrison SM, Pos MK, Essenberg RC, Maiden MC, Abu-bakr A, Baumberg SG, Neyfakh AA, Griffith JK, Stark MJ, Ward A, O'Reilly J, Rutherford NG, Phillips-Jones MK, Henderson PJ. Collection and characterisation of bacterial membrane proteins. *FEBS Lett*. 2003;555(1):170-175.

Saier MH Jr, Yen MR, Noto K, Tamang DG, Elkan C. The Transporter Classification Database: Recent advances. *Nucleic Acids Res*. 2009;37(Database issue):D274-D278.

Sar N, McCarter L, Simon M, Silverman M. Chemotactic control of the two flagellar systems of *V. parahaemolyticus*. *J Bacteriol*. 1990;172(1):334-341.

Schaffner W, Weissmann C. A rapid, sensitive, and specific method for the determination of protein in dilute solution. *Anal Biochem*. 1973;56(2):502-514.

Schein JR, Hunt KA, Minton JA, Schultes NP, Mourad GS. The nucleobase cation symporter 1 of *Chlamydomonas reinhardtii* and that of the evolutionarily distant *Arabidopsis thaliana* display parallel function and establish a plant-specific solute transport profile. *Plant Physiol Biochem*. 2013;70:52-60.

Schwacke R, Schneider A, van der Graaff E, Fischer K, Catoni E, Desimone M, Frommer WB, Flügge UI, Kunze R. ARAMEMNON, a novel database for Arabidopsis integral membrane proteins. *Plant Physiol*. 2003;131(1):16-26.

Shi Y. Common folds and transport mechanisms of secondary active transporters. *Annu Rev Biophys*. 2013;42:51-72.

Shimamura T, Weyand S, Beckstein O, Rutherford NG, Hadden JM, Sharples D, Sansom MS, Iwata S, Henderson PJ, Cameron AD. Molecular basis of alternating access membrane transport by the sodium-hydantoin transporter Mhp1. *Science*. 2010;328(5977):470-473.

Sievers F, Wilm A, Dineen D, Gibson TJ, Karplus K, Li W, Lopez R, McWilliam H, Remmert M, Söding J, Thompson JD, Higgins DG. Fast, scalable generation of high-quality protein multiple sequence alignments using Clustal Omega. *Mol Syst Biol*. 2011;7:539.

Simmons KJ, Jackson SM, Brueckner F, Patching SG, Beckstein O, Ivanova E, Geng T, Weyand S, Drew D, Lanigan J, Sharples DJ, Sansom MS, Iwata S, Fishwick CW, Johnson AP, Cameron AD, Henderson PJ. Molecular mechanism of ligand recognition by membrane transport protein, Mhp1. *EMBO J*. 2014;33(16):1831-1844.

Sioupouli G, Lambrinidis G, Mikros E, Amillis S, Diallinas G. Cryptic purine transporters in *A. nidulans* reveal the role of specific residues in the evolution of specificity in the NCS1 family. *Mol Microbiol*. 2017;103(2):319-332.

Stark MJ. Multicopy expression vectors carrying the lac repressor gene for regulated high-level expression of genes in *Escherichia coli*. *Gene*. 1987;51(2-3):255-267.

Suzuki S, Henderson PJ. The hydantoin transport protein from *Microbacterium liquefaciens*. *J Bacteriol*. 2006;188(9):3329-3336.

Szakonyi G, Leng D, Ma P, Bettaney KE, Saidijam M, Ward A, Zibaei S, Gardiner AT, Cogdell RJ, Butaye P, Kolsto AB, O'reilly J, Hope RJ, Rutherford NG, Hoyle CJ, Henderson PJ. A genomic strategy for cloning, expressing and purifying efflux proteins of the major facilitator superfamily. *J Antimicrob Chemother*. 2007;59(6):1265-1270.

Tsirigos KD, Peters C, Shu N, Käll L, Elofsson A. The TOPCONS web server for consensus prediction of membrane protein topology and signal peptides. *Nucleic Acids Res*. 2015;43(W1):W401-W407.

Ulitzur S. *Vibrio parahaemolyticus* and *Vibrio alginolyticus*: Short generation-time marine bacteria. *Microb Ecol*. 1974;1(1):127-135.

Ward A, O'Reilly J, Rutherford NG, Ferguson SM, Hoyle CK, Palmer SL, Clough JL, Venter H, Xie H, Litherland GJ, Martin GE, Wood JM, Roberts PE, Groves MA, Liang WJ, Steel A, McKeown BJ, Henderson PJ. Expression of prokaryotic membrane transport proteins in Escherichia coli. *Biochem Soc Trans*. 1999;27(6):893-899.

Ward A, Sanderson NM, O'Reilly J, Rutherford NG, Poolman B, Henderson PJF. The amplified expression, identification, purification, assay and properties of hexahistidine tagged bacterial membrane transport proteins. In Baldwin SA

(Ed) Membrane transport – a Practical Approach, 2000;141–166. Oxford: Blackwell.

West CKG, Klein SL, Lovell CR. High frequency of virulence factor genes tdh, trh, and tlh in *Vibrio parahaemolyticus* strains isolated from a pristine estuary. *Appl Environ Microbiol*. 2013;79(7):2247-2252.

Weyand S, Ma P, Saidijam M, Baldwin J, Beckstein O, Jackson S, Suzuki S, Patching SG, Shimamura T, Sansom MS, Iwata S, Cameron AD, Baldwin SA, Henderson PJ. 2010. The Nucleobase-Cation-Symport-1 family of membrane transport proteins. 11. In Handbook of Metalloproteins, John Wiley and Sons. DOI: 10.1002/0470028637.met268

Weyand S, Shimamura T, Beckstein O, Sansom MS, Iwata S, Henderson PJ, Cameron AD. The alternating access mechanism of transport as observed in the sodium-hydantoin transporter Mhp1. *J Synchrotron Radiat*. 2011;18(1):20-23.

Weyand S, Shimamura T, Yajima S, Suzuki S, Mirza O, Krusong K, Carpenter EP, Rutherford NG, Hadden JM, O'Reilly J, Ma P, Saidijam M, Patching SG, Hope RJ, Norbertczak HT, Roach PC, Iwata S, Henderson PJ, Cameron AD. Structure and molecular mechanism of a nucleobase-cation-symport-1 family transporter. *Science*. 2008;322(5902):709-713.

Witholt B, Boekhout M, Brock M, Kingma J, Heerikhuizen HV, Leij LD. An efficient and reproducible procedure for the formation of spheroplasts from variously grown *Escherichia coli*. *Anal Biochem*. 1976;74(1):160-170.

Witz S, Panwar P, Schober M, Deppe J, Pasha FA, Lemieux MJ, Möhlmann T. Structure-function relationship of a plant NCS1 member-homology modeling and mutagenesis identified residues critical for substrate specificity of PLUTO, a nucleobase transporter from Arabidopsis. *PLoS One*. 2014;9(3):e91343.

Submitted: 10th Nov 2019, Revised: 30th Dec 2019, Accepted: 3rd Jan 2020

Chapter Nine

9. FULL LIST OF REFERENCES

Abramson J, Smirnova I, Kasho V, Verner G, Kaback HR, Iwata S. Structure and mechanism of the lactose permease of *Escherichia coli*. *Science*. 2003;301 (5633):610–615.

Abramson J, Wright EM. Structure and function of Na^+-symporters with inverted repeats. *Curr Opin Struct Biol*. 2009;19(4):425–432.

Accardi A. Structure and gating of CLC channels and exchangers. *J Physiol*. 2015;593(Pt 18):4129–4138.

Adamczyk B, Tharmalingam T, Rudd PM. Glycans as cancer biomarkers. *Biochim Biophys Acta*. 2012;1820(9):1347–1353.

Adams JM, Cory S. The Bcl–2 apoptotic switch in cancer development and therapy. *Oncogene*. 2007;26(9):1324–1337.

Adams PD, Seeholzer S, Ohh M. Identification of associated proteins by coimmunoprecipitation. *Protein–protein interactions: A molecular cloning manual*. 2002:5.59–5.74.

Adelman JL, Dale AL, Zwier MC, Bhatt D, Chong LT, Zuckerman DM, Grabe M. Simulations of the alternating access mechanism of the sodium symporter Mhp1. *Biophys J*. 2011;101(10):2399-2407.

Aghdam SY, Eming SA, Willenborg S, Neuhaus B, Niessen CM, Partridge L, Krieg T, Bruning JC. Vascular endothelial insulin/IGF–1 signaling controls skin wound vascularization. *Biochem Biophys Res Comm*. 2012;421(2):197–202.

Ahmad I, Nawaz N, Darwesh NM, ur Rahman S, Mustafa MZ, Khan SB, Patching SG. Overcoming challenges for amplified expression of recombinant proteins using *Escherichia coli*. *Protein Expr Purif*. 2018;144:12-18.

Ahmad I, Nawaz N, Dermani FK, Kohlan AK, Saidijam M, Patching SG. Bacterial multidrug efflux proteins: A major mechanism of antimicrobial resistance. *Curr Drug Targets*. 2020 DOI: 10.2174/1389450119666180426103300.

Ahmad I, Nawaz N, Ur Rahman S, Sajid A, Khan FA, Khan SB, Mustafa MZ, Patching SG. Multifaceted roles of efflux proteins in prokaryotes. *AJBLS*. 2018;7(1):1-7.

Akhtar M, Haider A, Rashid S, Al–Nabet ADMH. Paget's "Seed and Soil" theory of cancer metastasis: An idea whose time has come. *Adv Anat Pathol*. 2019;26(1):69–74.

Akyuz N, Georgieva ER, Zhou Z, Stolzenberg S, Cuendet MA, Khelashvili G, Altman RB, Terry DS, Freed JH, Weinstein H, Boudker O, Blanchard SC. Transport domain unlocking sets the uptake rate of an aspartate transporter. *Nature*. 2015;518(7537):68–73.

Alatoom AA, Aburto R, Hamood AN, Colmer-Hamood JA. VceR negatively regulates the vceCAB MDR efflux operon and positively regulates its own synthesis in *Vibrio cholerae 569B*. *Can J Microbiol*. 2007;53(7):888–900.

Allen F, Almási G, Andreoni W, Beece D, Berne B J, Bright A, Brunheroto J, Cascaval C. Blue gene: A vision for protein science using a petaflop supercomputer. *IBM Syst J*. 2001;40(2):310–327.

Allen MP, Tildesley DJ. *Computer Simulation of Liquids*. Oxford University Press, New York, 1987.

Aller SG, Yu J, Ward A, Weng Y, Chittaboina S, Zhuo R, Harrell PM, et al. Structure of P-glycoprotein reveals a molecular basis for poly-specific drug binding. *Science*. 2009;323(5922):1718–1722.

Alonso A, Del Rey CG, Navarro A, Tolivia J, Gonzalez CG. Effects of gestational diabetes mellitus on proteins implicated in insulin signalling in human placenta. *Gynecol Endocrinol*. 2006;22(9):526–535.

Amar-Costesec A, Beaufay H, Wibo M, Thinès-Sempoux D, Feytmans E, Robbi M, Berthet J. Analytical study of microsomes and isolated subcellular membranes from rat liver. II. Preparation and composition of the microsomal fraction. *J Cell Biol*. 1974;61(1):201–212.

Amit I, Citri A, Shay T, Lu Y, Katz M, Zhang F, Tarcic G, et al. A module of negative feedback regulators defines growth factor signaling. *Nat Genet*. 2007;39(4):503–512.

Anandan A, Vrielink A. Detergents in membrane protein purification and crystallisation. *Adv Exp Med Biol*. 2016;922:13–28.

Andersen JL, He GX, Kakarla P, K C R, Kumar S, Lakra WS, Mukherjee MM, et al. Multidrug efflux pumps from *Enterobacteriaceae*, *Vibrio cholerae* and *Staphylococcus aureus* bacterial food pathogens. *Int J Environ Res Public Health*. 2015;12(2):1487–1547.

Andersen M, Nørgaard–Pedersen D, Brandt J, Pettersson I, Slaaby R. IGF1 and IGF2 specificities to the two insulin receptor isoforms are determined by insulin receptor amino acid 718. *PLoS One*. 2017;12(6):e0178885.

Anderson NL, Anderson NG. Proteome and proteomics: New technologies, new concepts, and new words. *Electrophoresis.* 1998;19(11):1853–1861.

Anderson CM, Henry RR, Knudson PE, Olefsky JM, Webster JG. Relative expression of insulin receptor isoforms does not differ in lean, obese, and noninsulin–

dependent diabetes mellitus subjects. *J Clin Endocrinol Metab*. 1993;76(5):1380–1382.

Anishkin A, Gendel V, Sharifi NA, Chiang CS, Shirinian L, Guy HR, Sukharev S. On the conformation of the COOH-terminal domain of the large mechanosensitive channel MscL. *J Gen Physiol*. 2003;121(3):227-244.

Anisimov VN, Bartke A. The key role of growth hormone–insulin–IGF–I signaling in ageing and cancer. *Crit Rev Oncol/Hematol*. 2013;87(3):201–223.

Annunziata M, Granata R, Ghigo E. The IGF system. *Acta Diabetol*. 2011;48(1):1–9.

Aplin JD, Lacey H, Haigh T, Jones CJ, Chen CP, Westwood M. Growth factor–extracellular matrix synergy in the control of trophoblast invasion. *Biochem Soc Trans*. 2000;28(2):199–202.

Arabkhari M, Bunda S, Wang Y, Wang A, Pshezhetsky AV, Hinek A. Desialylation of insulin receptors and IGF–1 receptors by neuraminidase–1 controls the net proliferative response of L6 myoblasts to insulin. *Glycobiology*. 2010;20(5):603–16.

Araujo JR, Keating E, Martel F. Impact of gestational diabetes mellitus in the maternal–to–fetal transport of nutrients. *Curr Diab Rep*. 2015;15(2):569.

Ardon O, Procter M, Tvrdik T, Longo N, Mao R. Sequencing analysis of insulin receptor defects and detection of two novel mutations in *INSR* gene. *Mol Genet Metab Rep.* 2014;1:71–84.

Arib G, Akhtar A. Multiple facets of nuclear periphery in gene expression control. *Curr Opin Cell Biol.* 2011;23(3):346–353.

Axelrod D. Cell-substrate contacts illuminated by total internal reflection fluorescence. *J Cell Biol.* 1981;89(1):141–145.

Axelrod D, Koppel DE, Schlessinger J, Elson E, Webb WW. Mobility measurement by analysis of fluorescence photobleaching recovery kinetics. *Biophys J*. 1976;16(9):1055–1069.

Ayton GS, Voth GA. Hybrid coarse-graining approach for lipid bilayers at large length and time scales. *J Phys Chem B.* 2009;113(13): 4413–4424.

Azman AS, Rudolph KE, Cummings DA, Lessler J. The incubation period of cholera: A systematic review. *J Infect*. 2013;66(5):432–438.

Bach LA. IGF–binding proteins. *J Mol Endocrinol*. 2018;61(1):T11–T28.

Bachas S, Eginton C, Gunio D, Wade H. Structural contributions to multidrug recognition in the multidrug resistance (MDR) gene regulator, BmrR. *Proc Natl Acad Sci U S A*. 2011;108(27):11046–11051.

Bai X, Moraes TF, Reithmeier RAF. Structural biology of solute carrier (SLC) membrane transport proteins. *Mol Membr Biol*. 2017;34(1-2):1–32.

Barabote RD, Saier MH Jr. Comparative genomic analyses of the bacterial phosphotransferase system. *Microbiol Mol Biol Rev*. 2005;69(4):608–634.

Barelli S, Canellini G, Thadikkaran L, Crettaz D, Quadroni M, Rossier JS, Tissot JD, Lion N. Oxidation of proteins: Basic principles and perspectives for blood proteomics. *Proteomics Clin Appl*. 2008;2(2):142–157.

Barroso I, Luan J, Middelberg RPS, Harding AH, Franks PW, Jakes RW, Clayton D, Schafer AJ, O'Rahilly S, Wareham NJ. Candidate gene association study in type 2 diabetes indicates a role for genes involved in β–cell function as well as insulin action. *PloS Biology*. 2003;1(1):41–55.

Barton LJ, Soshnev AA, Geyer PK. Networking in the nucleus: A spotlight on LEM-domain proteins. *Curr Opin Cell Biol*. 2015;34:1–8.

Batarseh H, Thompson RA, Odugbesan O, Barnett AH. Insulin receptor antibodies in diabetes mellitus. *Clin Exp Immunol*. 1988;71(1):85–90.

Batrakou DG, Kerr AR, Schirmer EC. Comparative proteomic analyses of the nuclear envelope and pore complex suggests a wide range of heretofore unexpected functions. *J Proteomics*. 2009;72(1):56–70.

Bay DC, Turner RJ. Membrane composition influences the topology bias of bacterial integral membrane proteins. *Biochim Biophys Acta - Biomembranes*. 2013;1828(2):260–270.

Bayburt TH, Sligar SG. Membrane protein assembly into nanodiscs. *FEBS Lett*. 2010;584(9):1721–1727.

Beck M, Förster F, Ecke M, Plitzko JM, Melchior F, Gerisch G, Baumeister W, Medalia O. Nuclear pore complex structure and dynamics revealed by cryoelectron tomography. *Science*. 2004;306(5700):1387–1390.

Begum A, Rahman MM, Ogawa W, Mizushima T, Kuroda T, Tsuchiya T. Gene cloning and characterization of four MATE family multidrug efflux pumps from *Vibrio cholerae non-O1*. *Microbiol Immunol*. 2005;49(11):949–957.

Belfiore A, Malaguarnera R, Vella V, Lowrence MC, Sciacca L, Frasca F, Morrione A, Vigneri R. Insulin receptor isoforms in physiology and disease: an updated view. *Endocr Rev*. 2017;38(5):379–431.

Benabbou N, Mirshahi P, Bordu C, Faussat AM, Tang R, Therwath A, Soria J, Marie JP, Mirshahi M. A subset of bone marrow stromal cells regulate ATP–binding cassette gene expression via insulin–like growth factor–I in a leukemia cell line. *Int J Oncol*. 2014;45(4):1372–1380.

Benecke H, Flier JS, Moller DE. Alternatively spliced variants of the insulin receptor protein. Expression in normal and diabetic human tissues. *J Clin Invest*. 1992;89(6):2066–2070.

Benyoucef S, Surinya KH, Hadaschik D, Siddle K. Characterization of insulin/IGF hybrid receptors: contributions of the insulin receptor L2 and Fn1 domains and the alternatively spliced exon 11 sequence to ligand binding and receptor activation. *Biochem J*. 2007;403(3):603–613.

Berggård T, Linse S, James P. Methods for the detection and analysis of protein-protein interactions. *Proteomics*. 2007;7(16):2833–2842.

Bergmann U, Funatomi H, Yokoyama M, Beger HG, Korc M. Insulin–like growth factor I overexpression in human pancreatic cancer: evidence for autocrine and paracrine roles. *Cancer Res*. 1995;55(10):2007–2011.

Bernsel A, Viklund H, Hennerdal A, Elofsson A. TOPCONS: consensus prediction of membrane protein topology. *Nucleic Acids Res*. 2009;37(Web Server issue):W465-W468.

Berx G, van Roy F. Involvement of members of the cadherin superfamily in cancer. *Cold Spring Harb Perspect Biol*. 2009;1(6):a003129.

Best RB, Mittal J. Protein simulations with an optimized water model: Cooperative helix formation and temperature-induced unfolded state collapse. *J Phys Chem B*. 2010;114(46):14916-14923.

Bettaney KE, Sukumar P, Hussain R, Siligardi G, Henderson PJ, Patching SG. A systematic approach to the amplified expression, functional characterization and purification of inositol transporters from *Bacillus subtilis*. *Mol Membr Biol*. 2013;30(1):3-14.

Betteridge DJ. What is oxidative stress? *Metabolism*. 2000;49(2 Suppl 1):3–8.

Bhaumick B, George D, Bala RM. Potentiation of epidermal growth factor–induced differentiation of cultured human placental cells by insulin–like growth factor–I. *J Clin Endocrinol Metab*. 1992;74(5):1005–1011.

Bilston LE, Mylvaganam K. Molecular simulations of the large conductance mechanosensitive (MscL) channel under mechanical loading. *FEBS Lett*. 2002;512(1-3):185-190.

Bina JE, Provenzano D, Wang C, Bina XR, Mekalanos JJ. Characterization of the *Vibrio cholerae* vexAB and vexCD efflux systems. *Arch Microbiol*. 2006;186(3):171–181.

Blackstock WP, Weir MP. Proteomics: Quantitative and physical mapping of cellular proteins. *Trends Biotechnol*. 1999;17(3):121–127.

Blum WF, Alherbish A, Alsagheir A, El Awwa A, Kaplan W, Koledova E, Savage M. The growth hormone–insulin–like growth factor–I axis in the diagnosis and treatment of growth disorders. *Endocr Connect*. 2018;7(6):R212–R222.

Boni A, Politi AZ, Strnad P, Xiang W, Hossain MJ, Ellenberg J. Live imaging and modeling of inner nuclear membrane targeting reveals its molecular requirements in mammalian cells. *J Cell Biol*. 2015;209(5):705–720.

Booth WT, Schlachter CR, Pote S, Ussin N, Mank NJ, Klapper V, Offermann LR, Tang C, Hurlburt BK, Chruszcz M. Impact of an N-terminal polyhistidine tag on protein thermal stability. *ACS Omega*. 2018;3(1):760–768.

Borroto-Escuela DY, Hernández-Ramos I, Fuxe K, Borroto-Escuela DO. *Coimmunoprecipitation (Co-Ip) Analysis for Protein-Protein Interactions in the Neurons of the Cerebral Ganglia of the Land Snails of the Genus Polymita During Aestivation*. In Co-Immunoprecipitation Methods for Brain Tissue, Springer, 2019, pp147–56.

Bouchet-Marquis C, Dubochet J, Fakan S. Cryoelectron microscopy of vitrified sections: A new challenge for the analysis of functional nuclear architecture. *Histochem Cell Biol*. 2006;125(1-2):43–51.

Boudker O, Verdon G. Structural perspectives on secondary active transporters. *Trends Pharmacol Sci*. 2010;31(9):418–426.

Boutros M, Ahringer J. The art and design of genetic screens: RNA interference. *Nat Rev Genet*. 2008;9(7):554–566.

Bowie JU. Solving the membrane protein folding problem. *Nature*. 2005;438(7068):581–589.

Brachner A, Reipert S, Foisner R, Gotzmann J. LEM2 is a novel MAN1-related inner nuclear membrane protein associated with A-type lamins. *J Cell Sci*. 2005;118(Pt 24):5797–5810.

Brahmkhatri VP, Prasanna C, Atreya HS. Insulin–like growth factor system in cancer: novel targeted therapies. *Biomed Res Int*. 2015;538019.

Braunagel SC, Williamson ST, Saksena S, Zhong Z, Russell WK, Russell DH, Summers MD. Trafficking of ODV-E66 is mediated via a sorting motif and other viral proteins: facilitated trafficking to the inner nuclear membrane. *Proc Natl Acad Sci U S A*. 2004;101(22):8372–8377.

Braund WJ, Williamson DH, Clark A, Naylor BA, Buley ID, Chapel HM. Autoimmunity to insulin receptor and hypoglycaemia in patient with Hodgkin's disease. *Lancet*. 1987;1(8527):237–240.

Brett KE, Ferraro ZM, Holcik M, Adamo KB. Placenta nutrient transport–related gene expression: the impact of maternal obesity and excessive gestational weight gain. *J Matern Fetal Neonatal Med*. 2016;29(9):1399–1405.

Brett KE, Ferraro ZM, Yockell–Lelievre J, Gruslin A, Adamo KB. Maternal–fetal nutrient transport in pregnancy pathologies: The role of the placenta. *Int J Mol Sci*. 2014;15(9):16153–16185.

Bright JN, Sansom MSP. The flexing/twirling helix: exploring the flexibility about molecular hinges formed by proline and glycine motifs in transmembrane helices. *J Phys Chem B*. 2003;107(2):627–636.

Brioude F, Kalish JM, Mussa A, Foster AC, Bliek J, Ferrero GB, Boonen SE, et al. Expert consensus document: Clinical and molecular diagnosis, screening and management of Beckwith–Wiedemann syndrome: an international consensus statement. *Nat Rev Endocrinol*. 2018;14(4):229–249.

Brown MF. Curvature forces in membrane lipid-protein interactions. *Biochemistry*. 2012;51(49):9782-9795.

Brown MH, Paulsen IT, Skurray RA. The multidrug efflux protein NorM is a prototype of a new family of transporters. *Mol Microbiol*. 1999;31(1):394–395.

Brugts MP, van Duijn CM, Hofland LJ, Witteman JC, Lamberts SW, Janssen JA. IGF–I bioactivity in an elderly population: Relation to insulin sensitivity, insulin levels, and the metabolic syndrome. *Diabetes*. 2010;59(2):505–508.

Bruns MM, Kakarla P, Floyd JT, Mukherjee MM, Ponce RC, Garcia JA, Ranaweera I, et al. Modulation of the multidrug efflux pump EmrD-3 from *Vibrio cholerae* by *Allium sativum* extract and the bioactive agent allyl sulfide plus synergistic enhancement of antimicrobial susceptibility by *A. sativum* extract. *Arch Microbiol*. 2017;199(8):1103–1112.

Buchanan TA, Xiang AH. Gestational diabetes mellitus. *J Clin Invest*. 2005;115(3):485–491.

Buch-Pedersen MJ, Pedersen BP, Veierskov B, Nissen P, Palmgren MG. Protons and how they are transported by proton pumps. *Pflügers Arch*. 2009;457(3):573–579.

Burkhart DL, Sage J. Cellular mechanisms of tumour suppression by the retinoblastoma gene. *Nat Rev Cancer*. 2008;8(9):671–682.

Butler AE, Cao–Minh L, Galasso R, Rizza RA, Corradin A, Cobelli C, Butler PC. Adaptive changes in pancreatic beta cell fractional area and beta cell turnover in human pregnancy. *Diabetologia*. 2010;53(10):2167–76.

Butler AE, Janson J, Bonner–Weir S, Ritzel R, Rizza RA, Butler PC. β–Cell deficit and increased β–cell apoptosis in humans with type 2 diabetes. *Diabetes*. 2003;52(1):102–110.

Butler AA, Yakar S, Gewolb IH, Karas M, Okubo Y, LeRoith D. Insulin–like growth factor–I receptor signal transduction: At the interface between physiology and cell biology. *Comp Biochem Physiol B Biochem Mol Biol*. 1998;121(1):19–26.

Butterton JR, Choi MH, Watnick PI, Carroll PA, Calderwood SB. *Vibrio cholerae* VibF is required for vibriobactin synthesis and is a member of the family of nonribosomal peptide synthetases. *J Bacteriol*. 2000;182(6):1731–1738.

Butterton JR, Stoebner JA, Payne SM, Calderwood SB. Cloning, sequencing, and transcriptional regulation of viuA, the gene encoding the ferric vibriobactin receptor of *Vibrio cholerae*. *J Bacteriol*. 1992;174(11):3729–3738.

Caban M, Owczarek K, Chojnacka K, Lewandowska U. Overview of polyphenols and polyphenol–rich extracts as modulators of IGF–1, IGF–1R, and IGFBP expression in cancer diseases. *J Funct Foods*. 2019;52:389–407.

Cain NE, Jahed Z, Schoenhofen A, Valdez VA, Elkin B, Hao H, Harris NJ, et al. Conserved SUN-KASH interfaces mediate LINC complex-dependent nuclear movement and positioning. *Curr Biol*. 2018;28(19):3086–3097.

Calabrese AN, Jackson SM, Jones LN, Beckstein O, Heinkel F, Gsponer J, Sharples D, Sans M, Kokkinidou M, Pearson AR, Radford SE, Ashcroft AE, Henderson PJF. Topological dissection of the membrane transport protein Mhp1 derived from cysteine accessibility and mass spectrometry. *Anal Chem*. 2017;89(17):8844–8852.

Cameron AD, Beckstein O, Henderson PJF. The five-helix inverted repeat superfamily of membrane transport proteins. In Encylopedia of Biophysics, edited by Roberts G, 2013;1481–1485. Springer.

Capener CE, Sansom MSP. Molecular dynamics simulations of a K+ channel model: Sensitivity to changes in ions, waters, andmembrane environment. *J Phys Chem*. 2002;106(17):4543–4551.

Carr ME. Diabetes mellitus. A hypercoagulable state. *J Diabetes Complications*. 2001;15(1):44–45.

Case DA, Cheatham TE, Darden T, Gohlke H, Luo R, Merz KM, Onufriev A, Simmerling C, Wang B, Woods RJ. The Amber biomolecular simulation programs. *J Comput Chem*. 2005;26(16):1668–1688.

Cassidy FC, Charalambous M. Genomic imprinting, growth and maternal–fetal interactions. *J Exp Biol*. 2018;221(Suppl 1).pii: jeb164517.

CDC. Cholera - *Vibrio cholerae* infection | Cholera | CDC." June 24, 2019. https://www.cdc.gov/cholera/index.html.

Ceriotti M, Bussi G, Parrinello M. Colored-noise thermostats à la carte. *J Chem Theory Comput*. 2010;6(4):1170–1180.

Cetin I, de Santis MS, Taricco E, Radaelli T, Teng C, Ronzoni S, Spada E, Milani S, Pardi G. Maternal and fetal amino acid concentrations in normal pregnancies and in pregnancies with gestational diabetes mellitus. *Am J Obstet Gynecol*. 2005;192(2):610–617.

Chae PS, Rasmussen SG, Rana RR, Gotfryd K, Chandra R, Goren MA, Kruse AC, et al. Maltose-neopentyl glycol (MNG) amphiphiles for solubilization, stabilization and crystallization of membrane proteins. *Nat Methods*. 2010;7(12):1003–1008.

Chakrabarti SR, Chaudhuri K, Sen K, Das J. Porins of *Vibrio cholerae*: purification and characterization of OmpU. *J Bacteriol*. 1996;178(2):524–530.

Chambers AF, Groom AC, MacDonald IC. Dissemination and growth of cancer cells in metastatic sites. *Nat Rev Cancer*. 2002;2(8):563–572.

Chandler D. *Introduction to Modern Statistical Mechanics*. Oxford University Press, New York, 1987.

Chang G. Structure of MsbA from *Vibrio cholera*: A multidrug resistance ABC transporter homolog in a closed conformation. *J Mol Biol*. 2003;330(2):419-430.

Chang Y-N, Geertsma ER. The novel class of seven transmembrane segment inverted repeat carriers. *Biol Chem*. 2017;398(2):165–174.

Chatterjee T, Saha RP, Chakrabarti P. Structural studies on *Vibrio cholerae* ToxR periplasmic and cytoplasmic domains. *Biochim Biophys Acta*. 2007;1774(10):1331–1338.

Chavent M, Reddy T, Goose J, Dahl ACE, Stone JE, Jobard B, Sansom MSP. Methodologies for the analysis of instantaneous lipid diffusion in MD simulations of large membrane systems. *Faraday Discuss.* 2014;169:1–18.

Chavent M, Seiradake E, Jones EY, Sansom MSP. Structures of the EphA2 receptor at the membrane: Role of lipid interactions. *Structure*. 2015;24(2),337–347.

Chen MY, Clark AJ, Chan DC, Ware JL, Holt SE, Chidambaram A, Fillmore HL, Broaddus WC. Wilms' tumor 1 silencing decreases the viability and chemoresistance of glioblastoma cells in vitro: A potential role for IGF–1R de–repression. *J Neurooncol*. 2011;103(1):87–102.

Chen CL, Ip SM, Cheng D, Wong LC, Ngan HY. Loss of imprinting of the IGF–II and H19 genes in epithelial ovarian cancer. *Clin Cancer Res*. 2000;6(2):474–479.

Chen Z, Liu J, Chu D, Shan Y, Ma G, Zhang H, Zhang XD, et al. A dual–specific IGF–I/II human engineered antibody domain inhibits IGF signaling in breast cancer cells. *Int J Biol Sci*. 2018;14(7):799–806.

Chen YJ, Pornillos O, Lieu S, Ma C, Chen AP, Chang G. X-ray structure of EmrE supports dual topology model. *Proc Natl Acad Sci U S A*. 2007;104(48):18999–19004.

Chen S, Wang H, Katzianer DS, Zhong Z, Zhu J. LysR family activator-regulated major facilitator superfamily transporters are involved in *Vibrio cholerae* antimicrobial compound resistance and intestinal colonisation. *Int J Antimicrob Agents*. 2013;41(2):188–192.

Cheng, P-C. *The Contrast Formation in Optical Microscopy*." In Handbook of Biological Confocal Microscopy, Springer, 2006, pp162–206.

Chi YH, Chen ZJ, Jeang KT. The nuclear envelopathies and human diseases. *J Biomed Sci*. 2009;16:96.

Chitsaz M, Brown MH**.** The role played by drug efflux pumps in bacterial multidrug resistance. *Essays Biochem*. 2017;61(1):127–139.

Choma CT, Tieleman DP, Cregut D, Serrano L, Berendsen HJC. Towards the design and computational characterization of a membrane protein. *J Mol Graph Model*. 2001;20(3):219-234.

Chon S, Choi MC, Lee YJ, Hwang YC, Jeong IK, Oh S, Ahn KJ, et al. Autoimmune hypoglycemia in a patient with characterization of insulin receptor autoantibodies. *Diabetes Metab J*. 2011:35(1):80–85.

Chong S, Dugast-Darzacq C, Liu Z, Dong P, Dailey GM, Cattoglio C, Heckert A, et al. Imaging dynamic and selective low-complexity domain interactions that control gene transcription. *Science*. 2018;361(6400). pii: eaar2555.

Christen M, Hünenberger PH, Bakowies D, Baron R, Bürgi R, Geerke DP, Heinz TN, et al. The GROMOS software for biomolecular simulation: GROMOS05. *J Comput Chem*. 2005;26(16):1719–1751.

Cianfarani S. Insulin–like growth factor–II: new roles for an old actor. *Front Endocrinol*. 2012;3:118.

Claassens NJ, Siliakus MF, Spaans SK, Creutzburg SCA, Nijsse B, Schaap PJ, Quax TEF, van der Oost J. Improving heterologous membrane protein production in *Escherichia coli* by combining transcriptional tuning and codon usage algorithms. *PLoS One*. 2017;12(9):e0184355.

Clemmons DR. Role of IGF–binding proteins in regulating IGF responses to changes in metabolism. *J Mol Endocrinol*. 2018;61(1):T139–T169.

Clemmons DR, Busby WH, Arai T, Nam TJ, Clarke JB, Jones JI, Ankrapp DK. Role of insulin–like growth factor binding proteins in the control of IGF actions. *Prog Growth Factor Res*. 1995;6(2-4):357–366.

Clough J, Saidijam M, Bettaney KE, Szakonyi G, Patching SG, Mueller J, Shibayama K, Bacon M, Barksby E, Groves m, Herbert RB, Phillips-Jones M, Ward A, Gunn-Moore F, O'Reilly J, Rutherford NG, Bill R, Henderson PJF. Prokaryotic membrane transport proteins: Amplified expression and purification. In Lundstrom KH (Ed) Structural genomics on membrane proteins. Taylor and Francis 2006;21-42.

Colmer JA, Fralick JA, Hamood AN. Isolation and characterization of a putative multidrug resistance pump from *Vibrio cholerae*. *Mol Microbiol*. 1998;27(1):63–72.

Colomiere M, Permezel M, Riley C, Desoye G, Lappas M. Defective insulin signaling in placenta from pregnancies complicated by gestational diabetes mellitus. *Eur J Endocrinol*. 2009;160(4):567–578.

Colwell RR, Kaper J, Joseph SW. *Vibrio cholerae*, *Vibrio parahaemolyticus*, and other vibrios: occurrence and distribution in Chesapeake Bay. *Science*. 1977;198(4315):394–396.

Conner JG, Teschler JK, Jones CJ, Yildiz FH. Staying Alive: *Vibrio cholerae's* cycle of environmental survival, transmission, and dissemination. *Microbiol Spectr*. 2016;4(2).

Contessa JN, Bhojani MS, Freeze HH, Rehemtulla A, Lawrence TS. Inhibition of n–linked glycosylation disrupts receptor tyrosine kinase signaling in tumor cells. *Cancer Res*. 2008;68(10):3803–3809.

Coolican SA, Samuel DS, Ewton DZ, McWade FJ, Florini JR. The mitogenic and myogenic actions of insulin–like growth factors utilize distinct signaling pathways. *J Biol Chem*. 1997;272(10):6653–6662.

Corradi V, Mendez-Villuendas E, Ingólfsson HI, Gu RX, Siuda I, Melo MN, Moussatova A, et al. Lipid-protein interactions are unique fingerprints for membrane proteins. *ACS Cent Sci*. 2018;4(6):709–717.

Corradi V, Sejdiu BI, Mesa-Galloso H, Abdizadeh H, Noskov SY, Marrink SJ, Tieleman DP. Emerging diversity in lipid-protein interactions. *Chem Rev*. 2019;119(9):5775–5848.

Coscoy S, Waharte F, Gautreau A, Martin M, Louvard D, Mangeat P, Arpin M, Amblard F. Molecular analysis of microscopic ezrin dynamics by two-photon FRAP. *Proc Natl Acad Sci U S A*. 2002;99(20):12813–12818.

Courtney NA, Briguglio JS, Bradberry MM, Greer C, Chapman ER. Excitatory and inhibitory neurons utilize different Ca^{2+} sensors and sources to regulate spontaneous release. *Neuron*. 2018;98(5):977–991.e5.

Crimi M, Degli Esposti M. Structural predictions for membrane proteins: the dilemma of hydrophobicity scales. *Trends Biochem Sci*. 1991;16(3):119.

Crisman TJ, Qu S, Kanner BI, Forrest LR. Inward facing conformation of glutamate transporters as revealed by their inverted-topology structural repeats. *Proc Natl Acad Sci USA*. 2009;106(49):20752–20757.

Crisp M, Liu Q, Roux K, Rattner JB, Shanahan C, Burke B, Stahl PD, Hodzic D. Coupling of the nucleus and cytoplasm: role of the LINC complex. *J Cell Biol*. 2006;172(1):41–53.

Crozier PS, Stevens MJ, Forrest LR, Woolf TB. (2003) Molecular dynamics simulations of dark-adapted rhodopsin in an explicit membrane bilayer: coupling between local retinal and larger scale conformational change. *J Mol Biol*. 2003;333(3):493-514.

Cruz PD, Hud JA. Excess insulin binding to insulin–like growth factor receptors: proposed mechanism for acanthosis nigricans. *J Invest Dermatol*. 1992;98(6 Suppl):82S–85S.

Cubbon RM, Kearney MT, Wheatcroft SB. Endothelial IGF–1 Receptor signalling in diabetes and insulin resistance. *Trends Endocrinol Metab*. 2016;27(2):96–104.

Cui H, Cruz–Correa M, Giardiello FM, Hutcheon DF, Kafonek DR, Brandenburg S, Wu Y, He X, Powe NR, Feinberg AP. Loss of IGF2 imprinting: A potential marker of colorectal cancer risk. *Science*. 2003;299(5613):1753–1755.

Cui J, Davidson AL. ABC solute importers in bacteria. *Essays Biochem*. 2011;50(1):85–99.

Cuthbertson L, Nodwell JR. The TetR family of regulators. *Microbiol Mol Biol Rev*. 2013;77(3):440–475.

Cymer F, von Heijne G, White SH. Mechanisms of integral membrane protein insertion and folding. *J Mol Biol*. 2015;427(5):999–1022.

Czech MP, Massague J. Subunit structure and dynamics of the insulin receptor. *Fed Proc*. 1982;41(11):2719–2723.

Danielsen S, Boyd D, Neuhard J. Membrane topology analysis of the *Escherichia coli* cytosine permease. *Microbiology*. 1995;141(Pt 11):2905-2913.

DeAngelis CM, Nag D, Withey JH, Matson JS. Characterization of the *Vibrio cholerae* phage shock protein response. *J Bacteriol*. 2019;201(14). pii: e00761–18.

DeFelice LJ, Goswami T. Transporters as channels. *Annu Rev Physiol*. 2007;69:87–112.

de–Freitas–Junior JCM, Andrade–da–Costa J, Silva MC, Pinho SS. Glycans as regulatory elements of the insulin/IGF system: impact in cancer progression. *Int J Mol Sci*. 2017;18(9):1921.

de Groot BL, Frigato T, Helms V, Grubmuller H. The mechanism of proton exclusion in the aquaporin-1 water channel. *J Mol Biol*. 2003;333(2):279-293.

de Koning H, Diallinas G. Nucleobase transporters (review). *Mol Membr Biol*. 2000;17(2):75-94.

de Las Heras JI, Meinke P, Batrakou DG, Srsen V, Zuleger N, Kerr AR, Schirmer EC. Tissue specificity in the nuclear envelope supports its functional complexity. *Nucleus*. 2013;4(6):460–477.

Delemotte L, Dehez F, Treptow W, Tarek M. Modeling membranes under a transmembrane potential. *J Phys Chem B*. 2008;112(18):5547–5550.

Delemotte L, Tarek M, Klein ML, Amaral C, Treptow W. Intermediate states of the Kv1.2 voltage sensor from atomistic molecular dynamics simulations. *Proc Natl Acad Sci USA*. 2011;108(15):6109–6114.

Delemotte L, Treptow W, Klein ML, Tarek M. Effect of sensor domain mutations on the properties of voltage-gated ion channels: Molecular dynamics studies of the potassium channel Kv1.2. *Biophys J*. 2010;99(9):L72–L74.

Dennis JW, Laferte S. Tumor cell surface carbohydrate and the metastatic phenotype. *Cancer Metastasis Rev*. 1987;5(3):185–204.

de Planque MR, Killian JA (2003) Protein–lipid interactions studied with designed transmembrane peptides: Role of hydrophobic matching and interfacial anchoring. *Mol Membr Biol*. 2003;20(4):271–284.

De Rosa M, Pace U, Rega D, Costabile V, Duraturo F, Izzo P, Delrio P. Genetics, diagnosis and management of colorectal cancer. *Oncol Rep*. 2015;34(3):1087–1896.

Desoye G, Hartmann M, Blaschitz A, Dohr G, Hahn T, Kohnen G, Kaufmann P. Insulin receptors in syncytiotrophoblast and fetal endothelium of human placenta. Immunohistochemical evidence for developmental changes in distribution pattern. *Histochemistry*. 1994;101(4):277–285.

Destoumieux-Garzón D, Duperthuy M, Vanhove AS, Schmitt P, Wai SN. Resistance to antimicrobial peptides in vibrios. *Antibiotics (Basel)*. 2014;3(4):540–563.

Deutscher MP. Guide to protein purification. *Methods Enzymol*. 1990;182:1–818.

Diallinas G. Understanding transporter specificity and the discrete appearance of channel-like gating domains in transporters. *Front Pharmacol*. 2014;5(207).

Diallinas G, Gournas C. Structure-function relationships in the nucleobase-ascorbate transporter (NAT) family: lessons from model microbial genetic systems. *Channels (Austin)*. 2008;2(5):363-372.

Diamant YZ, Metzger BE, Freinkel N, Shafrir E. Placental lipid and glycogen content in human and experimental diabetes mellitus. *Am J Obstet Gynecol*. 1982;144(1):5–11.

Diaz LE, Chuan YC, Lewitt M, Fernandez–Perez L, Carrasco–Rodríguez S, Sanchez–Gomez M, Flores–Morales A. IGF–II regulates metastatic properties of choriocarcinoma cells through the activation of the insulin receptor. *Mol Hum Reprod*. 2007;13(8):567–576.

Dill KA, Bromberg S. Molecular Driving Forces: Statistical Thermodynamics in Biology, Chemistry, Physics, and Nanoscience. New York: Garland Science, 2010.

Dills SS, Apperson A, Schmidt MR, Saier MH Jr. Carbohydrate transport in bacteria. *Microbiol Rev*. 1980;44(3):385–418.

Di Minno MND, Lupoli R, Palmieri NM, Russolillo A, Buonauro A, Di Minno G. Aspirin resistance, platelet turnover, and diabetic angiopathy: A 2011 update. *Thromb Res*. 2012;129(3):341–344.

Dimasuay KG, Boeuf P, Powell TL, Jansson T. Placental responses to changes in the maternal environment determine fetal growth. Front Physiol. 2016;7:12.

DiRita VJ. Co-ordinate expression of virulence genes by ToxR in *Vibrio cholerae*. *Mol Microbiol*. 1992;6(4):451–458.

DiRita VJ, Mekalanos JJ. Periplasmic interaction between two membrane regulatory proteins, ToxR and ToxS, results in signal transduction and transcriptional activation. *Cell*. 1991;64(1):29–37.

Dixon, CR, Schirmer EC. *Navigating the Nuclear Envelope: One or Multiple Transport Mechanisms for Integral Membrane Proteins?*. In Nuclear-Cytoplasmic Transport, Springer, 2018, pp151–177.

Dougherty DA. Cation-pi interactions in chemistry and biology: a new view of benzene, Phe, Tyr, and Trp. *Science*. 1996;271(5246):163–168.

Dowhan W, Bogdanov M. Lipid-dependent membrane protein topogenesis. *Annu Rev Biochem*. 2009;78:515–540.

Dowhan W, Vitrac H, Bogdanov M. Lipid-assisted membrane protein folding and topogenesis. *Protein J*. 2019;38(3):274–288.

Dreger M, Bengtsson L, Schöneberg T, Otto H, Hucho F. Nuclear envelope proteomics: novel integral membrane proteins of the inner nuclear membrane. *Proc Natl Acad Sci U S A*. 2001;98(21):11943–11948.

Drew D, Boudker O. Shared molecular mechanisms of membrane transporters. *Ann Rev Biochem*. 2016;85(1):543–572.

Dridi L, Seyrantepe V, Fougerat A, Pan X, Bonneil E, Thibault P, Moreau A, et al. Positive regulation of insulin signaling by neuraminidase 1. *Diabetes*. 2013;62(7):2338–2346.

Duan C, Bauchat JR, Hsieh T. Phosphatidylinositol 3–kinase is required for insulin–like growth factor–I–induced vascular smooth muscle cell proliferation and migration. *Circ Res*. 2000;86(1):15–23.

Dubova EA, Pavlov KA, Lyapin VM, Kulikova GV, Shchyogolev AI, Sukhikh GT. Expression of insulin–like growth factors in the placenta in preeclampsia. *Bull Exp Biol Med*. 2014;157(1):103–107.

Dunn EJ, Philippou H, Ariëns RAS, Grant PJ. Molecular mechanisms involved in the resistance of fibrin to clot lysis by plasmin in subjects with type 2 diabetes mellitus. *Diabetologia*. 2006;49(5):1071–1080.

Dunstan RA, Heinz E, Wijeyewickrema LC, Pike RN, Purcell AW, Evans TJ, Praszkier J, et al. Assembly of the type II secretion system such as found in *Vibrio cholerae* depends on the novel Pilotin AspS. *PLoS Pathog*. 2013;9(1):e1003117.

Dupont J, LeRoith D. Insulin and insulin–like growth factor I receptors: similarities and differences in signal transduction. *Horm Res*. 2001;55(Suppl 2):22–26.

Eades CE, Cameron DM, Evans JMM. Prevalence of gestational diabetes mellitus in Europe: A meta–analysis. *Diabetes Res Clin Pract*. 2017;129:173–181.

Edgar R, Bibi E. MdfA, an *Escherichia coli* multidrug resistance protein with an extraordinarily broad spectrum of drug recognition. *J Bacteriol*. 1997;179(7):2274–2280.

Efiuvwevwere BJO, Gorris LGM, Smid EJ, Kets EPW. Mannitol-enhanced survival of *Lactococcus lactis* subjected to drying. *Appl Microbiol Biotechnol*. 1999;51(1):100–104.

Elchalal U, Schaiff WT, Smith SD, Rimon E, Bildirici I, Nelson DM, Sadovsky Y. Insulin and fatty acids regulate the expression of the fat droplet–associated protein adipophilin in primary human trophoblasts. *Am J Obstet Gynecol*. 2005;193(5):1716–1723.

Ellenberg J, Siggia ED, Moreira JE, Smith CL, Presley JF, Worman HJ, Lippincott-Schwartz J. Nuclear membrane dynamics and reassembly in living cells: Targeting of an inner nuclear membrane protein in interphase and mitosis. *J Cell Biol*. 1997;138(6):1193–1206.

Elofsson A, von Heijne G. Membrane protein structure: prediction versus reality. *Annu Rev Biochem*. 2007;76:125–140.

El–Shewy HM, Lee MH, Obeid LM, Jaffa AA, Luttrell LM. The insulin–like growth factor type 1 and insulin–like growth factor type 2/mannose–6–phosphate receptors independently regulate ERK1/2 activity in HEK293 cells. *J Biol Chem*. 2007;282:26150–26157.

Engelman DM, Chen Y, Chin CN, Curran AR, Dixon AM, Dupuy AD, Lee AS, et al. Membrane protein folding: beyond the two stage model. *FEBS Lett*. 2003;555(1):122–125.

Ericsson A, Hamark B, Jansson N, Johansson BR, Powell TL, Jansson T. Hormonal regulation of glucose and system A amino acid transport in first trimester placental villous fragments. *Am J Physiol Regul Integr Comp Physiol*. 2005;288(3):R656–662.

Erni R, Rossell MD, Kisielowski C, Dahmen U. Atomic-resolution imaging with a sub-50-pm electron probe. *Phys Rev Lett*. 2009;102(9):096101.

Escribano O, Beneit N, Rubio–Longás C, López–Pastor AR, Gómez–Hernández A. The role of insulin receptor isoforms in diabetes and its metabolic and vascular complications. *J Diabetes Res*. 2017;1403206.

Faienza MF, Santoro N, Lauciello R, Calabrò R, Giordani L, Di Salvo G, Ventura A, et al. IGF2 gene variants and risk of hypertension in obese children and adolescents. *Pediatr Res*. 2010;67(4):340–344.

Fang J, Furesz TC, Lurent RS, Smith CH, Fant ME. Spatial polarization of insulin–like growth factor receptors on the human syncytiotrophoblast. *Pediatr Res*. 1997;41(2):258–265.

Fang Y, Jayaram H, Shane T, Kolmakova-Partensky L, Wu F, Williams C, Xiong Y, Miller C. Structure of a prokaryotic virtual proton pump at 3.2 A resolution. *Nature*. 2009;460(7258):1040–1043.

Faruque SM, Albert MJ, Mekalanos JJ. Epidemiology, genetics, and ecology of toxigenic *Vibrio cholerae*. *Microbiol Mol Biol Rev*. 1998;62(4):1301–1314.

Federici M, Hribal ML, Ranalli M, Marselli L, Porzio O, Lauro D, Borboni P, et al. The common Arg972 polymorphism in insulin receptor substrate–1 causes apoptosis of human pancreatic islets. *FASEB J*. 2001;15(1):22–24.

Federici M, Lauro D, D'Adamo M, Giovannone B, Porzio O, Mellozzi M, Tamburrano G, Sbraccia P, Sesti G. Expression of insulin/IGF–I hybrid receptors is increased in skeletal muscle of patients with chronic primary hyperinsulinemia. *Diabetes*. 1998b;47(1):87–92.

Federici M, Porzio O, Lauro D, Borboni P, Giovannone B, Zucaro L, Hribal ML, Sesti G. Increased abundance of insulin/insulin–like growth factor–i hybrid receptors in

skeletal muscle of obese subjects is correlated with *in vivo* insulin sensitivity. *J Clin Endocrinol Metab*. 1998a;83(8):2911–2915.

Federici M, Porzio O, Zucaro L, Giovannone B, Borboni P, Marini MA, Lauro D, Sesti G. Increased abundance of insulin/IGF–I hybrid receptors in adipose tissue from NIDDM patients. *Mol Cell Endocrinol*. 1997;135(1):41–47.

Federici M, Zucaro L, Porzio O, Massoud R, Borboni P, Lauro D, Sesti G. Increased expression of insulin/insulin–like growth factor–I hybrid receptors in skeletal muscle of noninsulin–dependent diabetes mellitus subjects. *J Clin Invest*. 1996;98(12):2887–2893.

Federkeil S, Winstone TL, Jicking G, Turner RJ. Spectroscopic analysis of EmrE in various membrane mimicking environments. *Biochem Cell Biol*. 2003;81(70):61–70.

Feldherr CM, Akin D. The permeability of the nuclear envelope in dividing and nondividing cell cultures. *J Cell Biol*. 1990;111(1):1–8.

Feldser D, Agani F, Iyer NV, Pak B, Ferreira G, Semenza GL. Reciprocal positive regulation of hypoxia–inducible factor 1alpha and insulin–like growth factor 2. *Cancer Res*. 1999;59(16):3915–3918.

Ferguson AD, Kodding J, Walker G, Bos C, Coulton JW, Diederichs K, Braun V, Welte W. Active transport of an antibiotic rifamycin derivative by the outer membrane protein FhuA. *Structure*. 2001;9(8):707-716.

Ferreira IG, Pucci M, Venturi G, Malagolini N, Chiricolo M, Dall'Olio F. Glycosylation as a main regulator of growth and death factor receptors signaling. *Int J Mol Sci*. 2018;19(2).pii: E580.

Ferreiro JL, Gómez–Hospital JA, Angiolillo DJ. Platelet abnormalities in diabetes mellitus. *Diab Vasc Dis Res*. 2010;7(4):251–259.

Fiaschi T, Chiarugi P. Oxidative stress, tumor microenvironment, and metabolic reprogramming: a diabolic liaison. *Int J Cell Biol*. 2012:762825.

Fields S, Song O-K. *System to Detect Protein-Protein Interactions*. Google Patents, 1994.

Firth SM, Baxter RC. Characterisation of recombinant glycosylation variants of insulin–like growth factor binding protein–3. *J Endocrinol*. 1999;160(3):379–387.

Firth SM, Baxter RC. Cellular actions of the insulin–like growth factor binding proteins. *Endocr Rev*. 2002;23(6):824–854.

Fischbach MA, Walsh CT. Antibiotics for emerging pathogens. *Science*. 2009;325(5944):1089–1093.

Fleishman SJ, Ben-Tal N. A novel scoring function for predicting the conformations of tightly packed pairs of transmembrane alphahelices. *J Mol Biol*. 2002;321(2):363-378.

Flier JS, Kahn CR, Roth J, Bar RS. Antibodies that impair insulin receptor binding in an unusual diabetic syndrome with severe insulin resistance. *Science*. 1975;190(4209):63–65.

Fluman N, Adler J, Rotenberg SA, Brown MH, Bibi E. Export of a single drug molecule in two transport cycles by a multidrug efflux pump. *Nat Commun*. 2014;5:4615.

Fluman N, Bibi E. Bacterial multidrug transport through the lens of the major facilitator superfamily. *Biochim Biophys Acta*. 2009;1794(5):738–747.

Fluman N, Ryan CM, Whitelegge JP, Bibi E. Dissection of mechanistic principles of a secondary multidrug efflux protein. *Mol Cell*. 2012;47(5):777–787.

Foisner R, Gerace L. Integral membrane proteins of the nuclear envelope interact with lamins and chromosomes, and binding is modulated by mitotic phosphorylation. *Cell*. 1993;73(7):1267–1279.

Folkman J. Angiogenesis: An organizing principle for drug discovery? *Nat Rev Drug Discov*. 2007;6(4):273–286.

Fong JC, Yildiz FH. Interplay between cyclic AMP-cyclic AMP receptor protein and cyclic di-GMP signaling in *Vibrio cholerae* biofilm formation. *J Bacteriol*. 2008;190(20):6646–6659.

Forbes K, Shah VK, Siddals K, Gibson JM, Aplin JD, Westwood M. Statins inhibit insulin–like growth factor action in first trimester placenta by altering insulin–like growth factor1receptor glycosylation. *Mol Hum Rep*. 2015;21(1):105–114.

Forbes K, Westwood M. The IGF Axis and Placental Function. *Horm Res*. 2008;69(3):129–137.

Forbes K, Westwood M, Baker PN, Aplin JD. Insulin–like growth factor I and II regulate the life cycle of trophoblast in the developing human placenta. *Am J Physiol Cell Physiol*. 2008;294(6):C1313–1322.

Forrest LR. Structural biology. (Pseudo-)symmetrical transport. *Science*. 2013;339(6118):399–401.

Forrest LR. Structural symmetry in membrane proteins. *Ann Rev Biophys*. 2015;44(1):311–337.

Forrest LR, Krämer R, Ziegler C. The structural basis of secondary active transport mechanisms. *Biochim Biophys Acta*. 2011;1807(2):167–188.

Forrest LR, Rudnick G. The rocking bundle: A mechanism for ion-coupled solute flux by symmetrical transporters. *Physiology*. 2009;24:377–386.

Forrest LR, Tieleman DP, Sansom MSP. Defining the transmembrane helix of M2 protein from influenza A by molecular dynamics simulations in a lipid bilayer. *Biophys J*. 1999;76(4):1886-1896.

Forrest LR, Zhang Y-W, Jacobs MT, Gesmonde J, Xie L, Honig BH, and Rudnick G. Mechanism for alternating access in neurotransmitter transporters. *Proc Natl Acad Sci USA*. 2008;105(30):10338–10343.

Fowden AL, Sferruzzi–Perri AN, Coan PM, Constancia M, Burton GJ. Placental efficiency and adaptation: endocrine regulation. *J Physiol*. 2009;587(Pt 14):3459–3472.

Fowler PW, Orwick-Rydmark M, Radestock S, Solcan N, Dijkman PM, Lyons JA, Kwok J, Caffrey M, Watts A, Forrest LR, Newstead S. Gating topology of the proton-coupled oligopeptide symporters. *Structure*. 2015;23(2):290–301.

Franke WW, Scheer U, Krohne G, Jarasch ED. The nuclear envelope and the architecture of the nuclear periphery. *J Cell Biol*. 1981;91(3 Pt 2):39s–50s.

Frasca F, Pandini G, Scalia P, Sciacca L, Mineo R, Costantino A, Goldfine ID, Belfiore A, Vigneri R. Insulin receptor isoform A, a newly recognized, high–affinity insulin–like growth factor II receptor in fetal and cancer cells. *Mol Cell Biol*. 1999;19(5):3278–3288.

Freier S, Weiss O, Eran M, Flyvbjerg A, Dahan R, Nephesh I, Safra T, Shiloni E, Raz I. Expression of the insulin–like growth factors and their receptors in adenocarcinoma of the colon. *Gut*. 1999;44(5):704–708.

Frenkel D, Smit B. *Understanding Molecular Simulations. From Algorithms to Applications*. Academic Press, San Diego, California, 1996.

Frey S, Richter RP, Görlich D. FG-rich repeats of nuclear pore proteins form a three-dimensional meshwork with hydrogel-like properties. *Science*. 2006;314(5800):815–817.

Fried H, Kutay U. Nucleocytoplasmic transport: taking an inventory. *Cell Mol Life Sci*. 2003;60(8):1659–1688.

Friedrich N, Thuesen B, Jørgensen T, Juul A, Spielhagen C, Wallaschofksi H, Linneberg A. The association between IGF–I and insulin resistance: a general population study in Danish adults. *Diabetes Care*. 2012;35(4):768–773.

Frillingos S. Insights to the evolution of Nucleobase-Ascorbate Transporters (NAT/NCS2 family) from the Cys-scanning analysis of xanthine permease XanQ. *Int J Biochem Mol Biol*. 2012;3(3):250-272.

Fritzsche M, Charras G. Dissecting protein reaction dynamics in living cells by fluorescence recovery after photobleaching. *Nat Protoc*. 2015;10(5):660–680.

Furukawa K, Fritze CE, Gerace L. The major nuclear envelope targeting domain of LAP2 coincides with its lamin binding region but is distinct from its chromatin interaction domain. *J Biol Chem*. 1998;273(7):4213–4219.

Fuster DG, Alexander RT. Traditional and emerging roles for the SLC9 Na^+/H^+ exchangers. *Pflügers Archiv - Europ J Physiol*. 2014;466(1):61–76.

Gadsby DC. Ion channels versus ion pumps: the principal difference, in principle. *Nat Rev Mol Cell Biol*. 2009;10(5):344–352.

Gatenby VK, Imrie H, Kearney M. The IGF–1 receptor and regulation of nitric oxide bioavailability and insulin signalling in the endothelium. *Eur J Physiol*. 2013;465(8):1065–1074.

Gaunt TR, Cooper JA, Miller GJ, Day IN, O'Dell SD. Positive associations between single nucleotide polymorphisms in the IGF2 gene region and body mass index in adult males. *Hum Mol Genet*. 2001;10(14):1491–1501.

GBD 2015 Mortality and Causes of Death Collaborators. Global, regional, and national life expectancy, all-cause mortality, and cause-specific mortality for 249 causes of death, 1980-2015: A systematic analysis for the global burden of disease study 2015. *Lancet (London, England)*. 2016;388(10053):1459–1544.

Gebauer G, Jäger W, Lang N. mRNA expression of components of the insulin–like growth factor system in breast cancer cell lines, tissues, and metastatic breast cancer cells. *Anticancer Res*. 1998;18(2A):1191–1195.

Gedeon PC, Indarte M, Surratt CK, Madura JD. Molecular dynamics of leucine and dopamine transporter proteins in a model cell membrane lipid bilayer. *Proteins*. 2010;78(4):797–811.

Gennis RB. *Biomembranes, Molecular Structure and Function*. Springer-Verlag, 1989.

Gerace L, Burke B. Functional organization of the nuclear envelope. *Annu Rev Cell Biol*. 1988;4:335–374.

Gilchrist D, Rexach M. Molecular basis for the rapid dissociation of nuclear localization signals from karyopherin alpha in the nucleoplasm. *J Biol Chem*. 2003;278(51):51937–51949.

Girnita L, Worrall C, Takahashi S, Seregard S, Girnita A. Something old, something new and something borrowed: emerging paradigm of insulin–like growth factor type 1 receptor (IGF–1R) signaling regulation. *Cell Mol Life Sci*. 2014;71(13):2403–2427.

Gligorijević N, Penezić A, Nedić O. Influence of glyco–oxidation on complexes between fibrin(ogen) and insulin–like growth factor binding protein–1 in patients with diabetes mellitus type 2. *Free Radic Res*. 2017;51(1): 64–72.

Gligorijević N, Robajac D, Nedić O. Enhanced platelet sensitivity to IGF-1 in patients with type 2 diabetes mellitus. *Biochem. (Mosc)* 2019;84(10):1213-1219.

Goldberg MB, Boyko SA, Calderwood SB. Transcriptional regulation by iron of a *Vibrio cholerae* virulence gene and homology of the gene to the *Escherichia coli* fur system. *J Bacteriol*. 1990;172(12):6863–6870.

Goldberg MB, Boyko SA, Calderwood SB. Positive transcriptional regulation of an iron-regulated virulence gene in *Vibrio cholerae*. *Proc Natl Acad Sci U S A*. 1991;88(4):1125–1129.

Goodchild RE, Dauer WT. The AAA+ protein torsinA interacts with a conserved domain present in LAP1 and a novel ER protein. *J Cell Biol*. 2005;168(6):855–862.

Gordon E, Horsefield R, Swarts HG, de Pont JJ, Neutze R, Snijder A. Effective high-throughput overproduction of membrane proteins in *Escherichia coli*. *Protein Expr Purif*. 2008;62:1-8.

Goryaynov A, Ma J, Yang W. Single-molecule studies of nucleocytoplasmic transport: from one dimension to three dimensions. *Integr Biol (Camb)*. 2012;4(1):10–21.

Gouaux E. The molecular logic of sodium-coupled neurotransmitter transporters. *Philos Trans R Soc Lond B Biol Sci*. 2009;364(1514):149–154.

Goudela S, Karatza P, Koukaki M, Frillingos S, Diallinas G.Comparative substrate recognition by bacterial and fungal purine transporters of the NAT/NCS2 family. *Mol Membr Biol*. 2005;22(3):263-275.

Gournas C, Papageorgiou I, Diallinas G. The nucleobase-ascorbate transporter (NAT) family: genomics, evolution, structure-function relationships and physiological role. *Mol Biosyst*. 2008;4(5):404-416.

Govaerts C, Blanpain C, Deupi X, Ballet S, Ballesteros JA, Wodak SJ. Vassart G, Pardo L, Parmentier M. The TXP motif in the second transmembrane helix of CCR5-structural determinant of chemokine-induced activation. *J Biol Chem*. 2001;276(16):13217-13225.

Graham ME, Kilby DM, Firth SM, Robinson PJ, Baxter RC. The *in vivo* phosphorylation and glycosylation of human insulin–like growth factor–binding protein–5. *Mol Cell Proteomics*. 2007;6(8):1392–1405.

Graves JA, Renfree MB. Marsupials in the age of genomics. *Annu Rev Genomics Hum Genet*. 2013;14:393–420.

Greber UF, Senior A, Gerace L. A major glycoprotein of the nuclear pore complex is a membrane-spanning polypeptide with a large lumenal domain and a small cytoplasmic tail. *EMBO J*. 1990;9(5):1495–1502.

Grill CJ, Sivaprasad U, Cohick WS. Constitutive expression of IGF–binding protein–3 by mammary epithelial cells alters signaling through Akt and p70S6 kinase. *J Mol Endocrinol*. 2002;29(1):153–162.

Grimberg A. P53 and IGFBP–3: Apoptosis and cancer protection. *Mol Genet Metab*. 2000;70(2):85–98.

Grimm JB, English BP, Chen J, Slaughter JP, Zhang Z, Revyakin A, Patel R, et al. A general method to improve fluorophores for live-cell and single-molecule microscopy. *Nat Methods*. 2015;12(3):244–250.

Grivennikov SI, Greten FR, Karin M. Immunity, inflammation, and cancer. *Cell*. 2010;140(6):883–899.

Gruenbaum Y, Margalit A, Goldman RD, Shumaker DK, Wilson KL. The nuclear lamina comes of age. *Nat Rev Mol Cell Biol*. 2005;6(1):21–31.

Grulich–Henn J, Ritter J, Mesewinkel S, Heinrich U, Bettendorf M, Preissner KT. Transport of insulin–like growth factor–I across endothelial cell monolayers and its binding to the subendothelial matrix. *Exp Clin Endocrinol Diabetes*. 2002;110(2):67–73.

Gu D, O'Dell SD, Chen XH, Miller GJ, Day IN. Evidence of multiple causalsites affecting weight in the IGF2–INS–TH region of human chromosome 11. *Hum Genet*. 2002;110(2):173–181.

Gu J, Sato Y, Kariya Y, Isaji T, Taniguchi N, Fukuda T. A mutual regulation between cell–cell adhesion and N–glycosylation: implication of the bisecting GlcNAc for biological functions. *J Proteome Res*. 2009;8(2):431–435.

Gumbart J, Khalili-Araghi M, Sotomayor M, Roux B. Constant electric field simulations of the membrane potential illustrated with simple systems. *Biochim Biophys Acta*. 2012;1818(2):294–302.

Guzmán–Gutiérrez E, Arroyo P, Salsoso R, Fuenzalida B, Sáez T, Leiva A, Pardo F, Sobrevia L. Role of insulin and adenosine in the human placenta microvascular and macrovascular endothelial cell dysfunction in gestational diabetes mellitus. *Microcirculation*. 2014;21(1):26–37.

Haeusler RA, McGraw TE, Accili D. Biochemical and cellular properties of insulin receptor signalling. Nat Rev *Mol Cell Biol*. 2018;19(1):31–44.

Hakam A, Yeatman TJ, Lu L, Mora L, Marcet G, Nicosia SV, Karl RC, Coppola D. Expression of insulin–like growth factor–1 receptor in human colorectal cancer. *Hum Pathol*. 1999;30(10):1128–1133.

Hall W, McDonnell A, O'Nell J. *Superbugs, An Arms Race Against Bacteria*. Harvard University Press, 2018, pp40–45.

Hallberg E, Wozniak RW, Blobel G. An integral membrane protein of the pore membrane domain of the nuclear envelope contains a nucleoporin-like region. *J Cell Biol*. 1993;122(3):513–521.

Hamari Z, Amillis S, Drevet C, Apostolaki A, Vágvölgyi C, Diallinas G, Scazzocchio C. Convergent evolution and orphan genes in the Fur4p-like family and characterization of a general nucleoside transporter in *Aspergillus nidulans*. *Mol Microbiol*. 2009;73(1):43-57.

Hamilton GS, Lysiak JJ, Han VK, Lala PK. Autocrine–paracrine regulation of human trophoblast invasiveness by insulin–like growth factor (IGF)–II and IGF–binding protein (IGFBP)–1. *Exp Cell Res*. 1998;244(1):147–156.

Hammond JR, Zarenda M. Effect of detergents on ligand binding and translocation activities of solubilized/reconstituted nucleoside transporters. *Arch Biochem Biophys*. 1996;332(2):313–322.

Han VK, Bassett N, Walton J, Challis JR. The expression of insulin–like growth factor (IGF) and IGF–binding protein (IGFBP) genes in the human placenta and membranes: evidence for IGF–IGFBP interactions at the feto–maternal interface. *J Clin Endocrinol Metab*. 1996;81(7):2680–2693.

Hanahan D, Weinberg RA. Hallmarks of cancer: The next generation. *Cell*. 2011;144(5):646–674.

Hansen T, Bjørbaek C, Vestergaard H, Grønskov K, Bak JF, Pedersen O. Expression of insulin receptor spliced variants and their functional correlates in muscle from patients with non–insulin–dependent diabetes mellitus. *J Clin Endocrinol Metab*. 1993;77(6):1500–1505.

Hansen L, Hansen T, Clausen JO, Echwald SM, Urhammer SA, Rasmussen SK, Pedersen O. The Val985Met insulin–receptor variant in the Danish Caucasian population: Lack of associations with non–insulin–dependent diabetes mellitus or insulin resistance. Am J *Hum Genet*. 1997;60(6):1532–1535.

Haraguchi T, Kojidani T, Koujin T, Shimi T, Osakada H, Mori C, Yamamoto A, Hiraoka Y. Live cell imaging and electron microscopy reveal dynamic processes of BAF-directed nuclear envelope assembly. *J Cell Sci*. 2008;121(Pt 15):2540–2554.

Haraguchi T, Koujin T, Segura-Totten M, Lee KK, Matsuoka Y, Yoneda Y, Wilson KL, Hiraoka Y. BAF is required for emerin assembly into the reforming nuclear envelope. *J Cell Sci*. 2001;114(Pt 24):4575–4585.

Harding MM. Metal-ligand geometry relevant to proteins and in proteins: sodium and potassium. *Acta Crystallogr D Biol Crystallogr*. 2002;58(Pt 5):872–874.

Harley CB, Kim NW, Prowse KR, Weinrich SL, Hirsch KS, West MD, Bacchetti S, Hirte HW, Counter CM, Greider CW. Telomerase, cell immortality, and cancer. *Cold Spring Harb Symp Quant Biol*. 1994;59:307–315.

Harris LK, Crocker IP, Baker PN, Aplin JD, Westwood M. IGF2 actions on trophoblast in human placenta are regulated by the insulin–like growth factor 2 receptor, which can function as both a signaling and clearance receptor. *Biol Reprod*. 2011;84(3):440–446.

Harris JB, LaRocque RC, Qadri F, Ryan ET, Calderwood SB. "Cholera." *Lancet (London, England)*. 2012;379(9835):2466–2476.

Harris LK, Pantham P, Yong HEJ, Pratt A, Borg AJ, Crocker I, Westwood M, Aplin J, Kalionis B, Murthi P. The role of insulin–like growth factor 2 receptor–mediated homeobox gene expression in human placental apoptosis, and its implications in idiopathic fetal growth restriction. *Mol Hum Rep*. 2019;25(9):572-585.

Hart LM, Stolk RP, Dekker JM, Nijpels G, Grobbee DE, Heine RJ, Maassen A. Prevalence of variants in candidate genes for type 2 diabetes mellitus in the Netherlands: the Rotterdam study and the Hoorn study. *J Clin Endocrinol Metab*. 1999;84(3):1002–1006.

Hayes CA, Dalia TN, Dalia AB. Systematic genetic dissection of PTS in *Vibrio cholerae* uncovers a novel glucose transporter and a limited role for PTS during infection of a mammalian host. *Mol Microbiol*. 2017;104(4):568–579.

Haywood NJ, Slater TA, Matthews CJ, Wheatcroft SB. The insulin like growth factor and binding protein family: Novel therapeutic targets in obesity and diabetes. *Mol Metab*. 2019;19:86–96.

He GX, Kuroda T, Mima T, Morita Y, Mizushima T, Tsuchiya T. An H(+)-coupled multidrug efflux pump, PmpM, a member of the MATE family of transporters, from *Pseudomonas aeruginosa. J Bacteriol*. 2004;186(1):262–265.

He X, Szewczyk P, Karyakin A, Evin M, Hong WX, Zhang Q, Chang G. Structure of a cation-bound multidrug and toxic compound extrusion transporter. *Nature*. 2010;467(7318):991–994.

Heinemann l. Insulin assay standardization: leading to measures of insulin sensitivity and secretion for practical clinical care. *Diabetes Care*. 2010;33(6):e83.

Helms V. *Fluorescence Resonance Energy Transfer*. In Principles of Computational Cell Biology. Weinheim: Wiley-VCH. 2008, p202.

Helms V. *Principles of Computational Cell Biology: From Protein Complexes to Cellular Networks*. John Wiley & Sons, 2018.

Henderson RK, Fendler K, Poolman B. Coupling efficiency of secondary active transporters. *Curr Opin Biotechnol*. 2019;58:62–71.

Henderson PJ, Giddens RA, Jones-Mortimer MC. Transport of galactose, glucose and their molecular analogues by *Escherichia coli* K12. *Biochem J*. 1977;162(2):309-320.

Henderson PJ, Macpherson AJ. Assay, genetics, proteins, and reconstitution of proton-linked galactose, arabinose, and xylose transport systems of *Escherichia coli*. *Methods Enzymol*. 1986;125:387-429.

Hennerdal A, Elofsson A. Rapid membrane protein topology prediction. *Bioinformatics*. 2011;27(9):1322-1323.

Heng J, Zhao Y, Liu M, Liu Y, Fan J, Wang X, Zhao Y, Zhang XC. Substrate-bound structure of the *E. coli* multidrug resistance transporter MdfA. *Cell Res*. 2015;25(9):1060–1073.

Henzler-Wildman K. Analyzing conformational changes in the transport cycle of EmrE. *Curr Opin Struct Biol*. 2012;22(1):38–43.

Henzler-Wildman K, Kern D. Dynamic personalities of proteins. *Nature*. 2007;450(7172):964–972.

Hers I. Insulin–like growth factor–1 potentiates platelet activation via the IRS–PI3Kα pathway. *Blood*. 2007;110(13):4243–4252.

Hetzer MW, Wente SR. Border control at the nucleus: Biogenesis and organization of the nuclear membrane and pore complexes. *Dev Cell*. 2009;17(5):606–616.

Hiden U, Glitzner E, Hartmann M, Desoye G. Insulin and the IGF system in the human placenta of normal and diabetic pregnancies. *J Anat*. 2009;215(1):60–68.

Hiden U, Maier A, Bilban M, Ghaffari–Tabrizi N, Wadsack C, Lang I, Dohr G, Desoye G. Insulin control of placental gene expression shifts from mother to foetus over the course of pregnancy. *Diabetologia*. 2006;49(1):123–131.

Higgins CF. ABC transporters-from microorganisms to man. *Annu Rev Cell Biol.* 1992;8:67-113.

Hill TL. Free energy transduction in biology and biochemical cycle kinetics. 1989 New York: Springer.

Hill TL, Eisenberg E. Can free energy transduction be localized at some crucial part of the enzymatic cycle? *Q Rev Biophys*. 1981;14(4):463–511.

Hille B. Ion Channels of Excitable Membranes. 3rd ed. Sunderland MA, 2001 U.S.A., Sinauer Associates.

Hills FA, Elder MG, Chard T, Sullivan MH. Regulation of human villous trophoblast by insulin–like growth factors and insulin–like growth factor–binding protein–1. *J Endocrinol*. 2004;183(3):487–496.

Hinshaw JE, Carragher BO, Milligan RA. Architecture and design of the nuclear pore complex. *Cell*. 1992;69(7):1133–1141.

Hirschmugl B, Desoye G, Catalano P, Klymiuk I, Scharnagl H, Payr S, Kitzinger E, et al. Maternal obesity modulates intracellular lipid turnover in the human term placenta. *Int J Obes (Lond)*. 2017;41(2):317–323.

Hiyoshi H, Kodama T, Iida T, Honda T. Contribution of *Vibrio parahaemolyticus* virulence factors to cytotoxicity, enterotoxicity, and lethality in mice. *Infect Immun*. 2010;78(4):1772-1780.

Hodzic DM, Yeater DB, Bengtsson L, Otto H, Stahl PD. Sun2 is a novel mammalian inner nuclear membrane protein. J Biol Chem. 2004;279(24):25805–25812.

Hoeck WG, Mukku VR. Identification of the major sites of phosphorylation in IGF binding protein 3. *J Cell Biochem*. 1994;56(2):262–273.

Holmes R, Porter H, Newcomb P, Holly JM, Soothill P. An immunohistochemical study of type I insulin–like growth factor receptors in the placentae of pregnancies

with appropriately grown or growth restricted fetuses. *Placenta*. 1999;20(4):325–330.

Hopfner KP, Karcher A, Shin DS, Craig L, Arthur LM, Carney JP, Tainer JA. Structural biology of Rad50 ATPase: ATP driven conformational control in DNA double-strand break repair and the ABC-ATPase superfamily. *Cell*. 2000;101(7):789-800.

Houot L, Chang S, Absalon C, Watnick P. *Vibrio cholerae* phosphoenolpyruvate phosphotransferase system control of carbohydrate transport, biofilm formation, and colonization of the germfree mouse intestine. *Infect Immun*. 2010;78(4):1482–1494.

Houot L, Watnick P. A novel role for enzyme I of the *Vibrio cholerae* phosphoenolpyruvate phosphotransferase system in regulation of growth in a biofilm. J Bacteriol. 2008;190(1):311–320.

Hsu PP, Sabatini DM. Cancer cell metabolism: Warburg and beyond. *Cell*. 2008;134(5):703–707.

Hu L, Chang L, Zhang Y, Zhai L, Zhang S, Qi Z, Yan H, et al. Platelets express activated P2Y12 receptor in patients with diabetes mellitus. *Circulation*. 2017;136(9):817–833.

Hu N-J, Iwata S, Cameron AD, Drew D. Crystal structure of a bacterial homologue of the bile acid sodium symporter ASBT. *Nature*. 2011;478(7369):408–411.

Huang Y, Lemieux MJ, Song J, Auer M, Wang D-N. Structure and mechanism of the glycerol-3-phosphate transporter from *Escherichia coli*. *Science*. 2003;301(5633):616–620.

Huang WN, Sue SC, Wang DS, Wu PL, Wu WG. Peripheral binding mode and penetration depth of cobra cardiotoxin on phospholipid membranes as studied by a combined FTIR and computer simulation approach. *Biochemistry*. 2003;42(24):7457–7466.

Hubbard SR, Till JH. Protein tyrosine kinase structure and function. *Annu Rev Biochem*. 2000;69:373–398.

Huda MN, Chen J, Morita Y, Kuroda T, Mizushima T, Tsuchiya T. Gene cloning and characterization of VcrM, a Na^+-coupled multidrug efflux pump, from *Vibrio cholerae non-O1*. *Microbiol Immunol*. 2003;47(6):419–427.

Hunte C, Screpanti E, Venturi M, Rimon A, Padan E, Michel H. Structure of a Na^+/H^+ antiporter and insights into mechanism of action and regulation by pH. *Nature*. 2005;435(7046):1197–1202.

Hunte C, von Jagow G, Schagger H. *Membrane Protein Purification and Crystallization. A practical Guide.* Academic Press, 2003.

Hunter RW, Hers I. Insulin/IGF–1 hybrid receptor expression on human platelets: consequences for the effect of insulin on platelet function. *J Thromb Haemost*. 2009;7(12):2123–2130.

Huq A, Small EB, West PA, Huq MI, Rahman R, Colwell RR. Ecological relationships between *Vibrio cholerae* and planktonic crustacean copepods. Appl *Environ Microbiol*. 1983;45(1):275–283.

Hwa V, Oh J, Rosenfeld RG. The insulin–like growth factor–binding protein (IGFBP) superfamily. *Endocr Rev*. 1999;20(6):761–787.

Hwang JB, Frost SC. Effect of alternative glycosylation on insulin receptor processing. *J Biol Chem*. 1999;274(32):22813–22820.

Igney FH, Krammer PH. Death and anti–death: tumour resistance to apoptosis. *Nat Rev Cancer*. 2002;2(4):277–288.

Ilan B, Tajkhorshid E, Schulten K, Voth GA. The mechanism of proton exclusion in aquaporin channels. *Proteins*. 2004;55(2):223-228.

Imai Y, Clemmons DR. Roles of phosphatidylinositol 3–kinase and mitogen–activated protein kinase pathways in stimulation of vascular smooth muscle cell migration and deoxyriboncleic acid synthesis by insulin–like growth factor–I. *Endocrinology*. 1999;140(9):4228–4235.

Ingermann AR, Yang YF, Han J, Mikami A, Garza AE, Mohanraj L, Fan L, et al. Identification of a novel cell death receptor mediating IGFBP–3–induced anti–tumor effects in breast and prostate cancer. *J Biol Chem*. 2010;285(39):30233–30246.

Ingólfsson HI, Arnarez C, Periole X, Marrink SJ. Computational 'microscopy' of cellular membranes. *J Cell Sci.* 2016;129(2):257–268.

Ingólfsson HI, Melo MN, van Eerden FJ, Arnarez C, Lopez CA, Wassenaar TA, Periole X, de Vries AH, Tieleman DP, Marrink SJ. Lipid organization of the plasma membrane. *J Am Chem Soc*. 2014;136(41):14554–14559.

Iñiguez G, Castro JJ, Garcia M, Kakarieka E, Johnson MC, Cassorla F, Mericq V. IGF–IR signal transduction protein content and its activation by IGF–I in human placentas: relationship with gestational age and birth weight. *PLoS One*. 2014;9(7):e102252.

Iñiguez G, Gallardo P, Castro JJ, Gonzalez R, Garcia M, Kakarieka E, San Martin S, Johnson MC, Mericq V, Cassorla F. Klotho gene and protein in human placentas according to birth weight and gestational age. *Front Endocrinol (Lausanne)*. 2019;9:797.

International Diabetes Federation, IDF Diabetes Atlas, International Diabetes Federation, Brussels, Belgium, 8th edition, 2017, http://www.diabetesatlas.org.

Irwin JC, Suen LF, Faessen GH, Popovici RM, Giudice LC. Insulin–like growth factor (IGF)–II inhibition of endometrial stromal cell tissue inhibitor of

metalloproteinase–3 and IGF–binding protein–1 suggests paracrine interactions at the decidua:trophoblast interface during human implantation. *J Clin Endocrinol Metab*. 2001;86(5):2060–2064.

Itkonen HM, Mills IG. N–linked glycosylation supports cross–talk between receptor tyrosine kinases and androgen receptor. *PLoS One*. 2013;8(5):e65016.

Iwamoto M, Ayers T, Mahon BE, Swerdlow DL. Epidemiology of seafood-associated infections in the United States. *Clin. Microbiol Rev*. 2010;23(2):399-411.

Izvekov S, Voth GA. A multiscale coarse-graining method for biomolecular systems. *J Phys Chem B*. 2005;109(7):2469–2473.

Jackson SP, Bartek J. The DNA–damage response in human biology and disease. *Nature*. 2009;461(7267):1071–1078.

Jackson SM, Ivanova E, Simmons S, Patching SG, Weyand S, Shimamura T, Brückner F, Iwata S, Sharples DJ, Baldwin SA, Sansom MSP, Beckstein O, Cameron AD, Henderson PJF. Na^+-Hydantoin Membrane Transport Protein, Mhp1. In Encylopedia of Biophysics, edited by Gordon Roberts, 2013;1514–1521. Springer.

Jackson SM, Patching SG, Ivanova E, Simmons KJ, Weyand S, Shimamura T, Brueckner F, Suzuki S, So Iwata, Sharples DJ, Baldwin SA, Sansom MPS, Beckstein O, Cameron AD, Henderson PJF. Mhp1, the Na(+)-hydantoin membrane transport protein. In Gordon CK Roberts (ed) Encyclopedia of Biophysics, Springer, 2013; 1514-1521.

Jafari E, Gheysarzadeh A, Mahnam K, Shahmohammadi R, Ansari A, Bakhtyari H, Mofid MR. *In silico* interaction of insulin–like growth factor binding protein 3 with insulin–like growth factor 1. *Res Pharmaceut Sci*. 2018;13(4):332–342.

Jafri MA, Ansari SA, Alqahtani MH, Shay JW. Roles of telomeres and telomerase in cancer, and advances in telomerase–targeted therapies. *Genome Med*. 2016;8:69.

Janosi L, Li Z, Hancock JF, Gorfe AA. Organization, dynamics, and segregation of Ras nanoclusters in membrane domains. *Proc Natl Acad Sci USA*. 2012;109(21):8097–8102.

Janssen JAMJL. IGF–I and the endocrinology of aging. *Curr Opin Endocr Metab Res*. 2019;5:1–6.

Jansson N, Rosario FJ, Gaccioli F, Lager S, Jones HN, Roos S, Jansson T, Powell TL. Activation of placental mTOR signaling and amino acid transporters in obese women giving birth to large babies. *J Clin Endocrinol Metab*. 2013;98(1):105–113.

Jansson T, Aye IL, Goberdhan DC. The emerging role of mTORC1 signaling in placental nutrient–sensing. *Placenta*. 2012;33(Suppl 2):e23–e29.

Jansson T, Powell TL. Human placental transport in altered fetal growth: does the placenta function as a nutrient sensor? *Placenta*. 2006;27(Suppl A):91–97.

Jardetzky O. Simple allosteric model for membrane pumps. *Nature*. 1966;211(5052):969–970.

Jayasinghe S, Hristova K, White SH. Energetics, stability, and prediction of transmembrane helices. *J Mol Biol*. 2001;312(5):927–934.

Jayasinghe S, Hristova K, White SH. MPtopo: A database of membrane protein topology. *Protein Sci*. 2001;10(2):455–458.

Jeong KH, Oh SJ, Chon S, Lee MH. Generalized acanthosis nigricans related to type B insulin resistance syndrome: A case report. *Cutis*. 2010;86(6):299–302.

Jeschke G. A comparative study of structures and structural transitions of secondary transporters with the LeuT fold. *Eur Biophys J*. 2013;42(2-3):181–197.

Jiang BH, Liu LZ. PI3K/PTEN signaling in angiogenesis and tumorigenesis. *Adv Cancer Res*. 2009;102:19–65.

Jiang H, Xun P, Luo G, Wang Q, Cai Y, Zhang Y, Yu B. Levels of insulin–like growth factors and their receptors in placenta in relation to macrosomia. *Asia Pac J Clin Nutr*. 2009;18(2):171–178.

Jiang D, Zhao Y, Wang X, Fan J, Heng J, Liu X, Feng W, et al. Structure of the YajR transporter suggests a transport mechanism based on the conserved motif A. *Proc Natl Acad Sci U S A*. 2013;110(36):14664–14669.

Jirkovská M, Kubínová L, Janácek J, Moravcová M, Krejcí V, Karen P. Topological properties and spatial organization of villous capillaries in normal and diabetic placentas. *J Vasc Res*. 2002;39(3):268–278.

Johnson TL, Abendroth J, Hol WG, Sandkvist M. Type II secretion: From structure to function. *FEMS Microbiol Lett*. 2006;255(2):175–186.

Jones R. Cytotoxic chemotherapy: Clinical aspects. *Medicine*. 2016;44(1):25–29.

Jones JI, Busby WH Jr, Wright G, Smith CE, Kimack NM, Clemmons DR. Identification of the sites of phosphorylation in insulin–like growth factor binding protein–1. Regulation of its affinity by phosphorylation of serine 101. *J Biol Chem*. 1993;268(2):1125–1131.

Juul A. Serum levels of insulin–like growth factor I and its binding proteins in health and disease. *Growth Horm IGF Res*. 2003;13(4):113–170.

Kaback HR. The lactose permease of *Escherichia coli*: A paradigm for membrane transport proteins. *Biochim Biophys Acta*. 1992;1101(2):210-213.

Kaback HR, Dunten R, Frillingos S, Venkatesan P, Kwaw I, Zhang W, Ermolova N. Site-directed alkylation and the alternating access model for LacY. *Proc Natl Acad Sci USA*. 2007;104(2):491–494.

Kaback HR, Guan L. It takes two to tango: The dance of the permease. *J Gen Physiol*. 2019;151(7):878–886.

Kaback HR, Smirnova I, Kasho V, Nie Y, Zhou Y. The alternating access transport mechanism in LacY. *J Membr Biol*. 2011;239(1-2):85–93.

Kabsch W, Sander C. Dictionary of protein secondary structure: Pattern recognition of hydrogen-bonded and geometrical features. *Biopolymers*. 1983;22(12):2577–2637.

Kadakia R, Josefson J. The relationship of insulin–like growth factor 2 to fetal growth and adiposity. *Horm Res Paediatr*. 2016;85(2):75–82.

Kakouros N, Rade JJ, Kourliouros A, Resar JR. Platelet function in patients with diabetes mellitus: From a theoretical to a practical perspective. Int *J Endocrinol*. 2011:742719.

Kanasaki K, Kalluri R. The biology of preeclampsia. *Kidney Int*. 2009;76(8):831–837.

Kaneda A, Wang CJ, Cheong R, Timp W, Onyango P, Wen B, Iacobuzio–Donahue CA, et al. Enhanced sensitivity to IGF–II signaling links loss of imprinting of IGF2 to increased cell proliferation and tumor risk. *Proc Natl Acad Sci USA*. 2007;104(52):20926–20931.

Kanehisa M, Furumichi M, Tanabe M, Sato Y, Morishima K. KEGG: New perspectives on genomes, pathways, diseases and drugs. *Nucleic Acids Res*. 2017;45(D1):D353-D361.

Kaper JB, Morris JG Jr, Levine MM. Cholera. *Clin Microbiol Rev*. 1995;8(1):48–86.

Kaplan S, Cohen P. The somatomedin hypothesis 2007: 50 years later. *J Cin Endocrinol Metab*. 2007;92(12):4529–4535.

Karaolis DK, Johnson JA, Bailey CC, Boedeker EC, Kaper JB, Reeves PR. A *Vibrio cholerae* pathogenicity island associated with epidemic and pandemic strains. *Proc Natl Acad Sci U S A*. 1998;95(6):3134–3139.

Karolczak–Bayatti M, Forbes K, Horn J, Teesalu T, Harris LK, Westwood M, Aplin JD. IGF signalling and endocytosis in the human villous placenta in early pregnancy as revealed by comparing quantum dot conjugates with a soluble ligand. *Nanoscale*. 2019;11(25):12285–12295.

Kataoka H, Tanaka H, Nagaike K, Uchiyama S, Itoh H. Role of cancer cell–stroma interaction in invasive growth of cancer cells. *Hum Cell*. 2003;16(1):1–14.

Katayama Y, Uchino J, Chihara Y, Tamiya N, Kaneko Y, Yamada T, Takayama K. Tumor neovascularization and developments in therapeutics. *Cancers (Basel)*. 2019;11(3):316.

Katta SS, Smoyer CJ, Jaspersen SL. Destination: inner nuclear membrane. *Trends Cell Biol*. 2014;24(4):221–229.

Kazmier K, Claxton DP, Mchaourab HS. Alternating access mechanisms of LeuT-fold transporters: trailblazing towards the promised energy landscapes. *Curr Opin Struct Biol*. 2017;45:100–108.

Kazmier K, Sharma S, Islam SM, Roux B, Mchaourab HS. Conformational cycle and ion-coupling mechanism of the Na+/hydantoin transporter Mhp1. *Proc Natl Acad Sci USA*. 2014;111(41):14752–14757.

Kazmier K, Sharma S, Quick M, Islam SM, Roux B, Weinstein H, Javitch JA, Mchaourab HS. Conformational dynamics of ligand-dependent alternating access in LeuT. *Nat Struct Mol Biol*. 2014;21(5):472–479.

Keller R, Ziegler C, Schneider D. When two turn into one: Evolution of membrane transporters from half modules. *Biol Chem*. 2014;395(12):1379–1388.

Kellerer M, Sesti G, Seffer E, Obermaier–Kusser B, Pongratz DE, Mosthaf L, Häring HU. Altered pattern of insulin receptor isotypes in skeletal muscle membranes of Type 2 (non–insulin–dependent) diabetic subjects. *Diabetologia*. 1993;36(7):628–632.

Kessel A, Shental-Bechor D, Haliloglu T, Ben-Tal N. Interactions of hydrophobic peptides with lipid bilayers: Monte Carlo simulations with M2 delta. *Biophys J*. 2003;85(6):3431-3444.

Kessenbrock K, Plaks V, Werb Z. Matrix metalloproteinases: regulators of the tumor microenvironment. *Cell*. 2010;141(1):52–67.

Khalili-Araghi F, Tajkhorshid E, Roux B, Schulten K. Molecular dynamics investigation of the ω-current in the Kv1.2 voltage sensor domains. *Biophys J*. 2012;102(2):258–267.

Kharb S, Nanda S. Patterns of biomarkers in cord blood during pregnancy and preeclampsia. *Curr Hypertens Rev*. 2017;13(1):57–64.

Kharb S, Panjeta P, Ghalaut VS, Bala J, Nanda S. Biomarkers in preeclamptic women with normoglycemia and hyperglycemia. *Curr Hypertens Rev*. 2016;12(3):228–233.

Killian JA. Hydrophobic mismatch between proteins and lipids in membranes. *Biochim Biophys Acta*. 1998;1376(3):401–415.

Kim JH, Bae HY, Kim SY. Clinical marker of platelet hyperreactivity in diabetes mellitus. *Diabetes Metab J*. 2013;37(6):423–428.

Kim KW, Bae SK, Lee OH, Bae MH, Lee MJ, Park BC. Insulin–like growth factor II induced by hypoxia may contribute to angiogenesis of human hepatocellular carcinoma. *Cancer Res*. 1998;58(2):348–351.

Kim S, Garcia A, Jackson SP, Kunapuli SP. Insulin–like growth factor–1 regulates platelet activation through PI3–Kα isoform. *Blood*. 2007;110(13):4206–4213.

Kim JG, Kang MJ, Yoon YK, Kim HP, Park J, Song SH, Han SW, et al. Heterodimerization of glycosylated insulin–like growth factor–1 receptors and insulin receptors in cancer cells sensitive to anti–IGF1R antibody. *PLoS One*. 2012;7(3):e33322.

Kimanius, D., Lindahl, E. and Andersson, M. (2018) Uptake dynamics in the Lactose permease (LacY) membrane protein transporter. *Sci Rep*, 2018;8(1):14324.

King GL, Kahn CR, Rechler MM, Nissley SP. Direct demonstration of separate receptors for growth and metabolic activities of insulin and multiplication–

stimulating activity (an insulin–like growth factor) using antibodies to the insulin receptor. *J Clin Invest*. 1980;66(1):130–140.

Kingdom J, Huppertz B, Seaward G, Kaufmann P. Development of the placental villous tree and its consequences for fetal growth. *Eur J Obstet Gynecol Reprod Biol*. 2000;92(1):35–43.

Kitaoka M, Miyata ST, Unterweger D, Pukatzki S. Antibiotic resistance mechanisms of *Vibrio cholerae*. *J Med Microbiol*. 2011;60(Pt 4):397–407.

Klaver E, Zhao P, May M, Flanagan–Steet H, Freeze HH, Gilmore R, Wells L, Contessa J, Steet R. Selective inhibition of N–linked glycosylation impairs receptor tyrosine kinase processing. *Dis Models Mechan*. 2019;12(6):pii:dmm039602.

Klepeis JL, Lindorff-Larsen K, Dror RO, Shaw DE. Long-timescale molecular dynamics simulations of protein structure and function. *Curr Opin Struct Biol*. 2009;19(2):120–127.

Klingenberg M. The ADP,ATP shuttle of the mitochondrion. *Trends Biochem Sci*. 1979;4(11):249–252.

Klingenberg M. Transport viewed as a catalytic process. *Biochimie*. 2007;89(9):1042–1048.

Knofler M, Sooranna SR, Daoud G, Whitley GS, Markert UR, Xia Y, Cantiello H, Hauguel–de–Mouzon S. Trophoblast signalling: Knowns and unknowns – a workshop report. *Placenta*. 2005;26(Suppl A):S49–S51.

Knowles TJ, Finka R, Smith C, Lin YP, Dafforn T, Overduin M. Membrane proteins solubilized intact in lipid containing nanoparticles bounded by styrene maleic acid copolymer. *J Am Chem Soc*. 2009;131(22):7484–7485.

Kochva U, Leonov H, Arkin IT. Modeling the structure of the respiratory syncytial virus small hydrophobic protein by silentmutation analysis of global searching molecular dynamics. *Protein Sci*. 2003;12(12):2668-2674.

Kolch W. Meaningful relationships: The regulation of the Ras/Raf/MEK/ERK pathway by protein interactions. *Biochem J*. 2000;351(Pt 2):289–305.

Koldsø H, Sansom MSP. Organization and dynamics of receptor proteins in a plasma membrane. *J Am Chem Soc*. 2015;137(46):14694–14704.

Konings WN, Poolman B, van Veen HW. Solute transport and energy transduction in bacteria. *Antonie Van Leeuwenhoek*. 1994;65(4):369–380.

Konopka CA, Bednarek SY. Variable-angle epifluorescence microscopy: a new way to look at protein dynamics in the plant cell cortex. *Plant J*. 2008;53(1):186–196.

Korkhov VM, Tate CG. An emerging consensus for the structure of EmrE. *Acta Crystallographica Section D*. 2009;65(2):186–192.

Kornberg A. Ten commandments: Lessons from the enzymology of DNA replication. *J Bacteriol*. 2000;182(13):3613–3618.

Kornberg A. Ten commandments of enzymology, amended. *Trends Biochem Sci*. 2003;28(10):515–517.

Kornfeld S. Structure and function of the mannose 6–phosphate/insulinlike growth factor II receptors. *Annu Rev Biochem*. 1992;61:307–330.

Korotkov KV, Sandkvist M, Hol WG. The type II secretion system: biogenesis, molecular architecture and mechanism. *Nat Rev Microbiol*. 2012;10(5):336–351.

Kosinski J, Mosalaganti S, von Appen A, Teimer R, DiGuilio AL, Wan W, Bui KH, et al. Molecular architecture of the inner ring scaffold of the human nuclear pore complex. *Science*. 2016;352(6283):363–365.

Krakhmal NV, Zavyalova MV, Denisov EV, Vtorushin SV, Perelmuter VM. Cancer invasion: Patterns and mechanisms. *Acta Naturae*. 2015;7(2):17–28.

Krishnamurthy H, Gouaux E. X-ray structures of LeuT in substrate free outward-open and apo inward-open states. *Nature*. 2012;481:469–474.

Krishnamurthy H, Piscitelli CL, Gouaux E. Unlocking the molecular secrets of sodium-coupled transporters. *Nature*. 2009;459(7245):347–355.

Krogh A, Larsson B, von Heijne G, Sonnhammer EL. Predicting transmembrane protein topology with a hidden Markov model: Application to complete genomes. *J Mol Biol*. 2001;305(3):567-580.

Kruis T, Klammt J, Galli–Tsinopoulou A, Wallborn T, Schlicke M, Müller E, Kratzsch J, et al. Heterozygous mutation within a kinase–conserved motif of the insulin–like growth factor I receptor causes intrauterine and postnatal growth retardation. *J Clin Endocrinol Metab*. 2010;95(3):1137–1142.

Krypotou E, Evangelidis T, Bobonis J, Pittis AA, Gabaldón T, Scazzocchio C, Mikros E, Diallinas G. Origin, diversification and substrate specificity in the family of NCS1/FUR transporters. *Mol Microbiol*. 2015;96(5):927-950.

Kubori T. Life with bacterial secretion systems. *PLoS Pathog*. 2016;12(8):e1005562.

Kühnl A, Kaiser M, Neumann M, Fransecky L, Heesch S, Radmacher M, Marcucci G, et al. High expression of IGFBP2 is associated with chemoresistance in adult acute myeloid leukemia. *Leuk Res*. 2011;35(12):1585–1590.

Kumar S, Smith KP, Floyd JL, Varela MF. Cloning and molecular analysis of a mannitol operon of phosphoenolpyruvate-dependent phosphotransferase (PTS) type from *Vibrio cholerae O395*. *Arch Microbiol*. 2011;193(3):201–208.

Kumaran T, Citarasu T. Isolation and characterization of virulence-related properties of pathogenic *Vibrio Parahaemolyticus* isolated from aquatic environments. *Environ J*. 2016;2:57-65.

Kundig W, Ghosh, S, Roseman S. Phosphate bound to histidine in a protein as an intermediate in a novel phospho-transferase system. *Proc Natl Acad Sci U S A*. 1964;52:1067–1074.

Kunkle DE, Bina XR, Bina JE. The *Vibrio cholerae* VexGH RND efflux system maintains cellular homeostasis by effluxing vibriobactin. *mBio*. 2017;8(3). pii: e00126–17.

Kupferschmidt K. A Lethal Dose of RNA. *Science*. 2013;341(6147) :732–733.

Kurien BT, Hensley K, Bachmann M, Scofield RH. Oxidatively modified autoantigens in autoimmune diseases. *Free Radic Biol Med*. 2006;41:549–556.

Kuroda T, Tsuchiya T. Multidrug efflux transporters in the MATE family. *Biochim Biophys Acta*. 2009;1794(5):763–768.

Kusakizako T, Claxton DP, Tanaka Y, Maturana AD, Kuroda T, Ishitani R, Mchaourab HS, Nureki O. Structural basis of H^+-dependent conformational change in a bacterial MATE transporter. *Structure*. 2019;27(2):293–301.e3.

Kutzner C, Grubmüller H, de Groot BL, Zachariae U. Computational electrophysiology: The molecular dynamics of ion channel permeation and selectivity in atomistic detail. *Biophys J*. 2011;101(4):809–817.

Kyte J, Doolittle RF. A simple method for displaying the hydropathic character of a protein. *J Mol Biol*. 1982;157(1):105–132.

Laba JK, Steen A, Veenhoff LM. Traffic to the inner membrane of the nuclear envelope. *Curr Opin Cell Biol*. 2014;28:36–45.

Lacey H, Haigh T, Westwood M, Aplin JD. Mesenchymally–derived insulin–like growth factor 1 provides a paracrine stimulus for trophoblast migration. *BMC Dev Biol.* 2002;2:5.

Laemmli UK. Cleavage of structural proteins during the assembly of the head of bacteriophage T4. *Nature*. 1970;227(5259):680-685.

Lane DP. Cancer. p53, guardian of the genome. *Nature*. 1992;358(6381):15–16.

Langer CJ, Novello S, Park K, Krzakowski M, Karp DD, Mok T, Benner RJ, Scranton JR, Olszanski AJ, Jassem J. Randomized, phase III trial of first–line figitumumab in combination with paclitaxel and carboplatin versus paclitaxel and carboplatin alone in patients with advanced non–small–cell lung cancer. *J Clin Oncol*. 2014;32(19):2059–2066.

Lassance L, Miedl H, Absenger M, Diaz–Perez F, Lang U, Desoye G, Hiden U. Hyperinsulinemia stimulates angiogenesis of human fetoplacental endothelial cells: A possible role of insulin in placental hypervascularization in diabetes mellitus. *J Clin Endocrinol Metab*. 2013;98(9):E1438–1447.

Latorraca NR, Fastman NM, Venkatakrishnan AJ, Frommer WB, Dror RO, Feng L. Mechanism of substrate translocation in an alternating access transporter. *Cell*. 2017;169(1):96–107.e12.

Läuger P. Kinetic properties of ion carriers and channels. *J Membr Biol*. 1980;57(3):163–178.

Laviola L, Perrini S, Belsanti G, Natalicchio A, Montrone C, Leonardini A, Vimercati A, et al. Intrauterine growth restriction in humans is associated with abnormalities in placental insulin–like growth factor signaling. *Endocrinology*. 2005;146(3):1498–1505.

Law CJ, Maloney PC, Wang D-N. Ins and outs of major facilitator superfamily antiporters. *Annu Rev Microbiol*. 2008;62:289–305.

Laybutt DR, Kaneto H, Hasenkamp W, Grey S, Jonas JC, Sgroi DC, Groff A, et al. Increased expression of antioxidant and antiapoptotic genes in islets that may contribute to β–cell survival during chronic hyperglycemia. *Diabetes*. 2002;51(2):413–423.

Leach AR. *Molecular Modelling. Principles and Applications*. Addison Wesley Longman, Essex, England, 1996.

Leavesley SJ, Rich TC. Overcoming limitations of FRET measurements. *Cytometry A*. 2016;89(4):325–327.

Lee CT, Chen IT, Yang YT, Ko TP, Huang YT, Huang JY, Huang MF, Lin SJ, Chen CY, Lin SS, Lightner DV, Wang HC, Wang AH, Wang HC, Hor LI, Lo CF. The opportunistic marine pathogen *Vibrio parahaemolyticus* becomes virulent by acquiring a plasmid that expresses a deadly toxin. *Proc Natl Acad Sci U S A*. 2015;112(34):10798-10803.

Lee KK, Haraguchi T, Lee RS, Koujin T, Hiraoka Y, Wilson KL. Distinct functional domains in emerin bind lamin A and DNA-bridging protein BAF. *J Cell Sci*. 2001;114(Pt 24):4567–4573.

Lee H, Jang HC, Park HK, Metzger BE, Cho NH. Prevalence of type 2 diabetes among women with a previous history of gestational diabetes mellitus. *Diabetes Res Clin Pract*. 2008;81(1):124–129.

Lee KI, Jo S, Rui H, Egwolf B, Roux B, Pastor RW, Im W. Web interface for Brownian dynamics simulation of ion transport and its applications to beta-barrel pores. *J Comput Chem*. 2012;33(3):331–339.

Lekshmi M, Parvathi A, Kumar S, Varela MF. *Efflux pump-mediated quorum sensing: New avenues for modulation of antimicrobial resistance and bacterial virulence*. In Biotechnological Applications of Quorum Sensing Inhibitors, Kalia VC (Ed.), Springer, Singapore, 2018, pp127–42.

Lengeler JW, Jahreis K, Wehmeier UF. Enzymes II of the phospho enol pyruvate-dependent phosphotransferase systems: their structure and function in carbohydrate transport. *Biochim Biophys Acta*. 1994;1188(1–2):1–28.

Le Roith D. The insulin–like growth factor system. *Exp Diabesity Res*. 2003;4(4):205–212.

Le Roith D, Bondy C, Yakar S, Liu JL, Butler A. The somatomedin hypothesis: 2001. *Endocr Rev*. 2001;22(1):53–74.

Lespine A, Dupuy J, Alvinerie M, Comera C, Nagy T, Krajcsi P, Orlowski S. Interaction of macrocyclic lactones with the multidrug transporters: the bases of the pharmacokinetics of lipid-like drugs. *Curr Drug Metab*. 2009;10(3):272–288.

Letchumanan V, Chan K-G, Lee L-H. *Vibrio parahaemolyticus*: a review on the pathogenesis, prevalence, and advance molecular identification techniques. *Front Microbiol*. 2014;5:705.

Letchumanan V, Pusparajah P, Tan LT-H, Yin W-F, Lee L-H, Chan K-G. Occurrence and antibiotic resistance of *Vibrio parahaemolyticus* from shellfish in Selangor, Malaysia. *Front Microbiol*. 2015;6:1417.

LeVine MV, Cuendet MA, Khelashvili G, Weinstein H. Allosteric mechanisms of molecular machines at the membrane: Transport by sodium-coupled symporters. *Chem Rev*. 2016;116(11):6552–6587.

Li CC, Crawford JA, DiRita VJ, Kaper JB. Molecular cloning and transcriptional regulation of ompT, a ToxR-repressed gene in *Vibrio cholerae*. *Mol Microbiol*. 2000;35(1):189–203.

Li Y, Gong H. Theoretical and simulation studies on voltage-gated sodium channels. *Protein Cell*. 2015;6(6):413–422.

Li Y, Junod SL, Ruba A, Kelich JM, Yang W. Nuclear export of mRNA molecules studied by SPEED microscopy. *Methods*. 2019;153:46–62.

Li J, Wen P-C, Moradi M, Tajkhorshid E. Computational characterization of structural dynamics underlying function in active membrane transporters. *Curr Opin Struct Biol*. 2015;31:96–105.

Lichtor T, Kurpakus MA, Gurney ME. Expression of insulin–like growth factors and their receptors in human meningiomas. *J Neurooncol*. 1993;17(3):183–190.

Lim D, Chu KK, Mertz J. Wide-field fluorescence sectioning with hybrid speckle and uniform-illumination microscopy. *Opt Lett*. 2008;33(16):1819–1821.

Lim RY, Fahrenkrog B, Köser J, Schwarz-Herion K, Deng J, Aebi U. Nanomechanical basis of selective gating by the nuclear pore complex. *Science*. 2007;318(5850):640–643.

Lin F, Blake DL, Callebaut I, Skerjanc IS, Holmer L, McBurney MW, Paulin-Levasseur M, Worman HJ. MAN1, an inner nuclear membrane protein that shares the LEM domain with lamina-associated polypeptide 2 and emerin. *J Biol Chem*. 2000;275(7):4840–4847.

Lindahl E, Hess B, van der Spoel D. GROMACS 3.0: A package for molecular simulation and trajectory analysis. *J Mol Model*. 2001;7(8):306–317.

Liu M, Heng J, Gao Y, Wang X. Crystal structures of MdfA complexed with acetylcholine and inhibitor reserpine. *Biophys Rep*. 2016;2(2):78–85.

Liu J, Lee KK, Segura-Totten M, Neufeld E, Wilson KL, Gruenbaum Y. MAN1 and emerin have overlapping function(s) essential for chromosome segregation and

cell division in *Caenorhabditis elegans*. *Proc Natl Acad Sci U S A*. 2003;100(8):4598–4603.

Liu D, Wu X, Summers MD, Lee A, Ryan KJ, Braunagel SC. Truncated isoforms of Kap60 facilitate trafficking of Heh2 to the nuclear envelope. *Traffic*. 2010;11(12):1506–1518.

Liu B, Xu Y, Voss C, Qiu FH, Zhao MZ, Liu YD, Nie J, Wang ZL. Altered protein expression in gestational diabetes mellitus placentas provides insight into insulin resistance and coagulation/fibrinolysis pathways. *PLoS One*. 2012;7(9):e44701.

Liu D, Zhang X, Gao J, Palombo M, Gao D, Chen P, Sinko PJ. Core functional sequence of C–terminal GAG–binding domain directs cellular uptake of IGFBP–3–derived peptides. *Protein Pept Lett*. 2014;21(2):124–131.

Livingstone C. IGF2 and cancer. *Endocr Relat Cancer*. 2013;20(6):R321–339.

Lobel P, Dahms NM, Breitmeyer J, Chirgwin JM, Kornfeld S. Cloning of the bovine 215–kDa cation–independent mannose 6–phosphate receptor. *Proc Natl Acad Sci USA*. 1987;84(8):2233–2237.

Lobel P, Dahms NM, Kornfeld S. Cloning and sequence analysis of the cation–independent mannose 6–phosphate receptor. *J Biol Chem*. 1988;263(5):2563–2570.

Long L, Navab R, Brodt P. Regulation of the Mr 72,000 type IV collagenase by the type I insulin–like growth factor receptor. *Cancer Res*. 1998;58(15):3243–3247.

Long F, Rouquette-Loughlin C, Shafer WM, Yu EW. Functional cloning and characterization of the multidrug efflux pumps NorM from *Neisseria gonorrhoeae* and YdhE from *Escherichia coli*. *Antimicrob Agents Chemother*. 2008;52(9):3052–3060.

Longo N, Langley SD, Griffin LD, Elsas LJ. Two mutations in the insulin receptor gene of a patient with Leprechaunism: Application to prenatal diagnosis. *J Clin Endocrinol Metab*. 1995;80(5):1496–1501.

Longo N, Wang Y, Pasquali M. Progressive decline in insulin levels in Rabson–Mendenhall syndrome. *J Clin Endocrinol Metab*. 1999;84(8):2623–2629.

Longo N, Wang Y, Smith SA, Langley SD, DiMeglio LA, Giannella–Neto D. Genotype–phenotyte correlation in inherited severe insulin resistance. *Hum Mol Genet*. 2002;11(12):1465–1475.

Loo TW, Bartlett MC, Clarke DM. Simultaneous binding of two different drugs in the binding pocket of the human multidrug resistance P-glycoprotein. *J Biol Chem*. 2003;278(41):39706–39710.

Lopes PEM, Roux B, MacKerell Jr AD. Molecular modeling and dynamics studies with explicit inclusion of electronic polarizability. Theory and applications. *Theor Chem Acc*. 2009;124(1-2):11-28.

Los GV, Encell LP, McDougall MG, Hartzell DD, Karassina N, Zimprich C, Wood MG, et al. HaloTag: a novel protein labeling technology for cell imaging and protein analysis. *ACS Chem Biol*. 2008;3(6):373–382.

Lou M, Garrett TPJ, McKern NM, Hoyne PA, Epa VC, Bentley JD, Lovrecz GO, Cosgrove LJ, Frenkel MJ, Ward CW. The first three domains of the insulin receptor differ structurally from the insulin–like growth factor 1 receptor in the regions governing ligand specificity. *Proc Natl Acad Sci USA*. 2006;103(33):12429–12434.

Loukovaara M, Leinonen P, Teramo K, Nurminen E, Andersson S, Rutanen EM. Effect of maternal diabetes on phosphorylation of insulin–like growth factor binding protein–1 in cord serum. *Diab Med*. 2005;22(4):434–439.

Lu M. Structures of multidrug and toxic compound extrusion transporters and their mechanistic implications. *Channels (Austin)*. 2016;10(2):88–100.

Lu WJ, Lin HJ, Janganan TK, Li CY, Chin WC, Bavro VN, Lin HV. ATP-binding cassette transporter VcaM from *Vibrio cholerae* is dependent on the outer membrane factor family for its function. *Int J Mol Sci*. 2018;19(4). pii: E1000.

Lu M, Radchenko M, Symersky J, Nie R, Guo Y. Structural insights into H^+-coupled multidrug extrusion by a MATE transporter. *Nat Struct Mol Biol*. 2013;20(11):1310–1317.

Lu M, Symersky J, Radchenko M, Koide A, Guo Y, Nie R, Koide S. Structures of a Na^+-coupled, substrate-bound MATE multidrug transporter. *Proc Natl Acad Sci U S A*. 2013;110(6):2099–2104.

Lusk CP, Blobel G, King MC. Highway to the inner nuclear membrane: rules for the road. *Nat Rev Mol Cell Biol*. 2007;8(5):414–420.

Ma J, Flynn TC, Cui Q, Leslie AG, Walker JE, Karplus M. A dynamic analysis of the rotation mechanism for conformational change in F(1)-ATPase. *Structure*. 2002;10(7):921-931.

Ma J, Liu Z, Michelotti N, Pitchiaya S, Veerapaneni R, Androsavich JR, Walter NG, Yang W. High-resolution three-dimensional mapping of mRNA export through the nuclear pore. *Nat Commun*. 2013;4:2414.

Ma P, Patching SG, Ivanova E, Baldwin JM, Sharples D, Baldwin SA, Henderson PJ.Allantoin transport protein, PucI, from *Bacillus subtilis*: evolutionary relationships, amplified expression, activity and specificity. *Microbiology*. 2016;162(5):823-836.

Ma P, Varela F, Magoch M, Silva AR, Rosário AL, Brito J, Oliveira TF, Nogly P, Pessanha M, Stelter M, Kletzin A, Henderson PJ, Archer M. An efficient strategy for small-scale screening and production of archaeal membrane transport proteins in *Escherichia coli*. *PLoS One*. 2013;8(10):e76913.

Ma J, Yang W. Three-dimensional distribution of transient interactions in the nuclear pore complex obtained from single-molecule snapshots. *Proc Natl Acad Sci U S A*. 2010;107(16):7305–7310.

Ma P, Yuille HM, Blessie V, Göhring N, Iglói Z, Nishiguchi K, Nakayama J, Henderson PJ, Phillips-Jones MK. Expression, purification and activities of the entire family of intact membrane sensor kinases from *Enterococcus faecalis*. *Mol Membr Biol*. 2008;25(6-7):449-473.

Ma M, Zhou QJ, Xiong Y, Li B, Li XT. Preeclampsia is associated with hypermethylation of IGF–1 promoter mediated by DNMT1. *Am J Transl Res*. 2018;10(1):16–39.

MacCallum JL, Tieleman DP. Hydrophobicity scales: A thermodynamic looking glass into lipid-protein interactions. *Trends Biochem Sci*. 2011;36(12):653–662.

MacKerell AD Jr. All-atom empirical potential for molecular modeling and dynamics studies of proteins. *J Phys Chem B*. 1998;102(18):3586–3616.

Madej MG, Sun L, Yan N, Kaback HR. Functional architecture of MFS D-glucose transporters. *Proc Natl Acad Sci USA*. 2014;111(7):E719–E727.

Maimon T, Elad N, Dahan I, Medalia O. The human nuclear pore complex as revealed by cryo-electron tomography. *Structure*. 2012;20(6):998–1006.

Maiza JC, Caron–Debarle M, Vigouroux C, Schneebeli S. Anti–insulin receptor antibodies related to hypoglycemia in a previously diabetic patient. *Diabetes Care*. 2013;36(6):e77.

Majorek KA, Kuhn ML, Chruszcz M, Anderson WF, Minor W. Double trouble-Buffer selection and His-tag presence may be responsible for nonreproducibility of biomedical experiments. *Protein Sci*. 2014;23(10):1359–1368.

Makino K, Oshima K, Kurokawa K, Yokoyama K, Uda T, Tagomori K, Iijima Y, Najima M, Nakano M, Yamashita A, Kubota Y, Kimura S, Yasunaga T, Honda T, Shinagawa H, Hattori M, Iida T. Genome sequence of *Vibrio parahaemolyticus*: A pathogenic mechanism distinct from that of *V. cholerae*. *Lancet*. 2003;361(9359):743-749.

Malaguarnera R, Belfiore A. The insulin receptor: a new target for cancer therapy. *Front Endocrinol (Lausanne)*. 2011;2:93.

Malek R, Chong AY, Lupsa BC, Lungu AO, Cochran EK, Soos MA, Semple RK, Balow JE, Gorden P. Treatment of type B insulin resistance: A novel approach to reduce insulin receptor autoantibodies. *J Clin Endocrinol Metab*. 2010;95(8):3641–3647.

Malik P, Zuleger N, Schirmer EC. *Transport of Inner Nuclear Membrane Proteins*. In Nuclear Transport, Landes Bioscience, 2009, pp133–145.

Malone CJ, Fixsen WD, Horvitz HR, Han M. UNC-84 localizes to the nuclear envelope and is required for nuclear migration and anchoring during *C. elegans* development. *Development*. 1999;126(14):3171–3181.

Man YG, Stojadinovic A, Mason J, Avital I, Bilchik A, Bruecher B, Protic M, et al. Tumor–infiltrating immune cells promoting tumor invasion and metastasis: Existing theories. *J Cancer*. 2013;4(1):84–95.

Mani SA, Guo W, Liao MJ, Eaton EN, Ayyanan A, Zhou AY, Brooks M, et al. The epithelial–mesenchymal transition generates cells with properties of stem cells. *Cell*. 2008;133(4):704–715.

Manilal S, Man NT, Sewry CA, Morris GE. The Emery-Dreifuss muscular dystrophy protein, emerin, is a nuclear membrane protein. *Hum Mol Gen*. 1996;5(6) :801–808.

Mans BJ, Anantharaman V, Aravind L, Koonin EV. Comparative genomics, evolution and origins of the nuclear envelope and nuclear pore complex. *Cell Cycle*. 2004;3(12):1612–1637.

Marger MD, Saier Jr MH. A major superfamily of transmembrane facilitators that catalyse uniport, symport and antiport. *Trends Biochem Sci*. 1993;18(1):13–20.

Marrink SJ, de Vries AH, Mark AE. Coarse grained model for semiquantitative lipid simulations. *J Phys Chem B.* 2004;108(2):750–760.

Marrink SJ, de Vries AH, Tieleman DP. Lipids on the move: Simulations of membrane pores, domains, stalks and curves. *Biochim Biophys Acta - Biomembranes*. 2009;1788(1):149–168.

Martino J, Sebert S, Segura MT, García–Valdés L, Florido J, Padilla MC, Marcos A, et al. Maternal body weight and gestational diabetes differentially influence placental and pregnancy outcomes. *J Clin Endocrinol Metab*. 2016;101(1):59–68.

Maruo T, Murata K, Matsuo H, Samoto T, Mochizuki M. Insulin–like growth factor–I as a local regulator of proliferation and differentiated function of the human trophoblast in early pregnancy. *Early Pregnancy*. 1995;1(1):54–61.

Matsumoto T, Kanamoto T, Otsuka M, Omote H, Moriyama Y. Role of glutamate residues in substrate recognition by human MATE1 polyspecific H^+/organic cation exporter. *Am J Physiol Cell Physiol*. 2008;294(4):C1074–C1078.

Matsuura Y, Stewart M. Nup50/Npap60 function in nuclear protein import complex disassembly and importin recycling. *EMBO J*. 2005;24(21):3681–3689.

Mayama R, Izawa T, Sakai K, Suciu N, Iwashita M. Improvement of insulin sensitivity promotes extravillous trophoblast cell migration stimulated by insulin–like growth factor–I. *Endocr J*. 2013;60(3):359–368.

McCarter L. The multiple identities of *Vibrio parahaemolyticus*. *J Mol Microbiol Biotechnol*. 1999;1(1):51-57.

McKinnon T, Chakraborty C, Gleeson LM, Chidiac P, Lala PK. Stimulation of human extravillous trophoblast migration by IGF–II is mediated by IGF type 2 receptor involving inhibitory G protein(s) and phosphorylation of MAPK. *J Clin Endocrinol Metab*. 2001;86(8):3665–3674.

Meinema AC, Laba JK, Hapsari RA, Otten R, Mulder FA, Kralt A, van den Bogaart G, et al. Long unfolded linkers facilitate membrane protein import through the nuclear pore complex. *Science*. 2011;333(6038):90–93.

Melo MCR, Bernardi RC, Rudack T, Scheurer M, Riplinger C, Phillips JC, Maia JDC, et al. NAMD goes quantum: An integrative suite for hybrid simulations. *Nature Methods*. 2018;15(5):351-354.

Meuwly M. Reactive molecular dynamics: From small molecules to proteins. *WIREs Comput Mol Sci*. 2019;9(1):e1386.

Miernyk JA, Thelen JJ. Biochemical approaches for discovering protein-protein interactions. *Plant J*. 2008;53(4):597–609.

Migdalis IN, Kalogeropoulou K, Kalantzis L, Nounopoulos C, Bouloukos A, Samartzis M. Insulin–like growth factorI and IGF–I receptors in diabetic patients with neuropathy. *Diabetic Med*. 1995;12(9):823–827.

Miller C. ClC chloride channels viewed through a transporter lens. *Nature*. 2006;440:484–489.

Miller VL, Mekalanos JJ. A novel suicide vector and its use in construction of insertion mutations: osmoregulation of outer membrane proteins and virulence determinants in *Vibrio cholerae* requires toxR. *J Bacteriol*. 1988;170(6):2575–2583.

Miller VL, Taylor RK, Mekalanos JJ. Cholera toxin transcriptional activator toxR is a transmembrane DNA binding protein. *Cell*. 1987;48(2):271–279.

Milio LA, Hu J, Douglas GC. Binding of insulin–like growth factor I to human trophoblast cells during differentiation in vitro. *Placenta*. 1994;15(6):641–651.

Milo R, Jorgensen P, Moran U, Weber G, Springer M. BioNumbers–the database of key numbers in molecular and cell biology. *Nucleic Acids Res*. 2010;38(Database issue):D750–D753.

Minton JA, Rapp M, Stoffer AJ, Schultes NP, Mourad GS. Heterologous complementation studies reveal the solute transport profiles of a two-member nucleobase cation symporter 1 (NCS1) family in *Physcomitrella patens*. *Plant Physiol Biochem*. 2016;100:12-17.

Mira E, Mañes S, Lacalle RA, Márquez G, Martínez–A C. Insulin–like growth factor I–triggered cell migration and invasion are mediated by matrix metalloproteinase–9. *Endocrinology*. 1999;140(4):1657–1664.

Mitchell P. Coupling of phosphorylation to electron and hydrogen transfer by a chemi-osmotic type of mechanism. *Nature*. 1961;191:144–148.

Mitchell P. Translocations through natural membranes. Chapter 2 in Advances in Enzymology and Related Areas of Molecular Biology, edited by Nord FF, 1967;29:33–87. New York: John Wiley & Sons, Inc.

Mitchell BA, Paulsen IT, Brown MH, Skurray RA. Bioenergetics of the Staphylococcal multidrug export protein QacA. Identification of distinct binding sites for monovalent and divalent cations. *J Biol Chem.* 1999;274:3541–3548.

Miyauchi H, Moriyama S, Kusakizako T, Kumazaki K, Nakane T, Yamashita K, Hirata K, et al. Structural basis for xenobiotic extrusion by eukaryotic MATE transporter. *Nat Commun*. 2017;8(1):1633.

Mizrachi D, Chen Y, Liu J, Peng HM, Ke A, Pollack L, Turner RJ, Auchus RJ, DeLisa MP. Making water-soluble integral membrane proteins *in vivo* using an amphipathic protein fusion strategy. *Nat Commun*. 2015;6:6826.

Mizuno T, Tanaka I. Structure of the DNA-binding domain of the OmpR family of response regulators. *Mol Microbiol*. 1997;24(3):665–667.

Modestino AE, Skowronski EA, Pruitt C, Taub PR, Herbst K, Schmid–Schönbein GW, Heller MJ, Mills PJ. Elevated resting and postprandial digestive proteolytic activity in peripheral blood of individuals with type–2 diabetes mellitus, with uncontrolled cleavage of insulin receptors. *J Am Coll Nutr*. 2019;38(6):485-492.

Mohanty AK, Wiener MC. Membrane protein expression and production: effects of polyhistidine tag length and position. *Protein Expr Purif*. 2004;33(2):311–325.

Mol BWJ, Roberts CT, Thangaratinam S, Magee LA, de Groot CJM, Hofmeyr GJ. Pre–eclampsia. *Lancet*. 2016;387(10022):999–1011.

Montazami N, Aghapour M, Farajnia S, Baradaran B. New insights into the mechanisms of multidrug resistance in cancers. *Cell Mol Biol (Noisy–le–grand)*. 2015;61(7):70–80.

Monticelli L, Robertson KM, MacCallum JL, Tieleman DP. Computer simulation of the KvAP voltage-gated potassium channel: steered molecular dynamics of the voltage sensor. *FEBS Lett*. 2004;564(3):325-332.

Mooi WJ, Peeper DS. Oncogene–induced cell senescence – halting on the road to cancer. *N Engl J Med*. 2006;355(10):1037–1046.

Moore SF, Williams CM, Brown E, Blair TA, Harper MT, Coward RJ, Poole AW, Hers I. Loss of the insulin receptor in murine megakaryocytes/platelets causes thrombocytosis and alterations in IGF signaling. *Cardiovasc Res*. 2015;107(1):9–19.

Moorehead RA, Hojilla CV, De Belle I, Wood GA, Fata JE, Adamson ED, Watson KL, Edwards DR, Khokha R. Insulin–like growth factor–II regulates PTEN expression in the mammary gland. *J Biol Chem*. 2003;278(50):50422–50427.

Moorthy S, Watnick PI. Genetic evidence that the *Vibrio cholerae* monolayer is a distinct stage in biofilm development. *Mol Microbiol*. 2004;52(2):573–587.

Morita Y, Kataoka A, Shiota S, Mizushima T, Tsuchiya T. NorM of *Vibrio parahaemolyticus* is an Na(+)-driven multidrug efflux pump. *J Bacteriol*. 2000;182(23):6694–6697.

Morrison EA, Dekoster GT, Dutta S, Vafabakhsh R, Clarkson MW, Bahl A, Kern D, Ha T, Henzler-Wildman KA. Antiparallel EmrE exports drugs by exchanging between asymmetric structures. *Nature*. 2012;481:45–50.

Morth JP, Pedersen BP, Toustrup-Jensen MS, Sørensen TL-M, Petersen J, Andersen JP, Vilsen B, Nissen P. Crystal structure of the sodium-potassium pump. *Nature*. 2007;450(7172):1043–1049.

Moses AC, Young SC, Morrow LA, O'Brien M, Clemmons DR. Recombinant human insulin–like growth factor I increases insulin sensitivity and improves glycemic control in type II diabetes. *Diabetes*. 1996;45(1):91–100.

Mosthaf L, Eriksson J, Häring HU, Groop L, Widen E, Ullrich A. Insulin receptor isotype expression correlates with risk of non–insulin–dependent diabetes. *Proc Natl Acad Sci USA*. 1993;90(7):2633–2635.

Mosthaf L, Vogt B, Häring HU, Ullrich A. Altered expression of insulin receptor types A and B in the skeletal muscle of non–insulin–dependent diabetes mellitus patients. *Proc Natl Acad Sci USA*. 1991;88(11):4728–4730.

Motyka B, Korbutt G, Pinkoski MJ, Heibein JA, Caputo A, Hobman M, Barry M, et al. Mannose 6–phosphate/insulin–like growth factor II receptor is a death receptor for granzyme B during cytotoxic T cell–induced apoptosis. *Cell*. 2000;103(3):491–500.

Mourad GS, Tippmann-Crosby J, Hunt KA, Gicheru Y, Bade K, Mansfield TA, Schultes NP. Genetic and molecular characterization reveals a unique nucleobase cation symporter 1 in Arabidopsis. *FEBS Lett*. 2012;586(9):1370-1378.

Mousa JJ, Yang Y, Tomkovich S, Shima A, Newsome RC, Tripathi P, Oswald E, Bruner SD, Jobin C. MATE transport of the *E. coli*-derived genotoxin colibactin. *Nat Microbiol*. 2016;1:15009.

Mrizak I, Grissa O, Henault B, Fekih M, Bouslema A, Boumaiza I, Zaouali M, Tabka Z, Khan NA. Placental infiltration of inflammatory markers in gestational diabetic women. *Gen Physiol Biophys*. 2014;33(2):169–176.

Mudumbi KC, Schirmer EC, Yang W. Single-point single-molecule FRAP distinguishes inner and outer nuclear membrane protein distribution. *Nat Commun*. 2016;7:12562.

Mukherjee M, Kakarla P, Kumar S, Gonzalez E, Floyd JT, Inupakutika M, Devireddy AR, et al. Comparative genome analysis of non-toxigenic non-O1 versus toxigenic O1 *Vibrio cholerae*. *Genom Discov*. 2014;2(1):1–15.

Mukherjee MM, Kumar S, Shrestha U, Ranaweera I, Ranjana KC, Kakarla P, Willmon TM, et al. Comparative genomics and discovery of novel cellular targets

for the development of new therapeutics towards *Vibrio cholerae*, the causative agent of cholera disease. *Anti-Infective Agents*. 2016. DOI: 10.2174/2211352514666160816151125.

Mustachio LM, Aksit S, Mistry RH, Scheffler R, Yamada A, Liu JM. The *Vibrio cholerae* mannitol transporter is regulated posttranscriptionally by the MtlS small regulatory RNA. *J Bacteriol*. 2012;194(3):598–606.

Myers-Turnbull D, Bliven SE, Rose PW, Aziz ZK, Youkharibache P, Bourne PE, Prli´c A. Systematic detection of internal symmetry in proteins using CE-Symm. *J Mol Biol*. 2014;426(11):2255–2268.

Nadimpalli SK, Amancha PK. Evolution of mannose 6–phosphate receptors (MPR300 and 46): Lysosomal enzyme sorting proteins. *Curr Protein Pept Sci*. 2010;11(1):68–90.

Naftalin RJ. Reassessment of models of facilitated transport and cotransport. *J Membr Biol*. 2010;234(2):75–112.

Nagarathinam K, Nakada-Nakura Y, Parthier C, Terada T, Juge N, Jaenecke F, Liu K, et al. Outward open conformation of a Major Facilitator Superfamily multidrug/H^+ antiporter provides insights into switching mechanism. *Nat Commun*. 2018;9(1):4005.

Nakashima R, Sakurai K, Yamasaki S, Nishino K, Yamaguchi A. Structures of the multidrug exporter AcrB reveal a proximal multisite drug-binding pocket. *Nature*. 2011;480(7378):565–569.

Natarajan J, Singh N, Rapaport D. Assembly and targeting of secretins in the bacterial outer membrane. *Int J Med Microbiol*. 2019;309(7):151322.

Nedić O, Robajac D, Šunderić M, Miljuš G, Đukanović B, Malenković V. Detection and identification of the oxidized insulin–like growth factor binding proteins and receptors in patients with colorectal carcinoma. *Free Rad Biol Med*. 2013;65:1195–1200.

Negrini S, Gorgoulis VG, Halazonetis TD. Genomic instability – an evolving hallmark of cancer. Nat Rev *Mol Cell Biol*. 2010;11(3):220–228.

Nelapati S, Nelapati K, Chinnam B. *Vibrio parahaemolyticus*-An emerging foodborne pathogen-A Review. *Vet World*. 2012;5(1):48-62.

Neumann GM, Marinaro JA, Bach LA. Identification of N–glycosylation sites and partial characterization of carbohydrate structure and disulfide linkages of human insulin–like growth factor binding protein 6. *Biochemistry*. 1998;37(18):6572–6585.

Newberry KJ, Huffman JL, Miller MC, Vazquez-Laslop N, Neyfakh AA, Brennan RG. Structures of BmrR-drug complexes reveal a rigid multidrug binding pocket and transcription activation through tyrosine expulsion. *J Biol Chem*. 2008;283(39):26795–26804.

Newstead S, Drew D, Cameron AD, Postis VLG, Xia X, Fowler PW, Ingram JC, Carpenter EP, Sansom MSP, McPherson MJ, Baldwin SA, Iwata S. Crystal structure of a prokaryotic homologue of the mammalian oligopeptide-proton symporters, PepT1 and PepT2. *EMBO J*. 2011;30:417–426.

NIH. Cholera Biology and Genetics. NIH: National Institute of Allergy and Infectious Diseases. 2017. https://www.niaid.nih.gov/diseases-conditions/cholera-biology-and-genetics.

Nikaido H. RND transporters in the living world. *Res Microbiol*. 2018;169(7–8):363–371.

Nikolaev DM, Shtyrov AA, Panov MS, Jamal A, Chakchir OB, Kochemirovsky VA, Olivucci M, Ryantsev MN. A comparative study of modern homology modeling algorithms for rhodopsin structure prediction. *ACS Omega* 2018;3(7):7555-7566.

Nimptsch K, Konigorski S, Pischon T. Diagnosis of obesity and use of obesity biomarkers in science and clinical medicine. *Metab Clin Exp*. 2019;92:61–70.

Nishizawa M, Nishizawa K. Coupling of S4 helix translo-cation and S6 gating analyzed by molecular dynamics simulations of mutated K_v channels. *Biophys J*. 2009;97(1):90-100.

Norgren S, Zierath J, Galuska D, Wallberg–Henriksson H, Luthman H. Differences in the ratio of RNA encoding two isoforms of the insulin receptor between control and NIDDM Patients. The RNA variant without exon 11 predominates in both groups. *Diabetes*. 1993;42(5):675–681.

Noskov SY, Roux B. Control of ion selectivity in LeuT: two Na+ binding sites with two different mechanisms. *J Mol Biol*. 2008;377(3):804–818.

Novosyadlyy R, Le Roith D. Insulin–like growth factors and insulin: at the crossroad between tumor development and longevity. *J Gerontol A Bio Sci Med Sci.* 2012;67(6):640–651.

O'Connor KG, Tobin JD, Harman SM, Plato CC, Roy TA, Sherman SS, Blackman MR. Serum levels of insulin–like growth factor–I are related to age and not to body composition in healthy women and man. *J Gerontol Med Sci*. 1988;53A(3):M176–M182.

Ogawa O, Becroft DM, Morison IM, Eccles MR, Skeen JE, Mauger DC, Reeve AE. Constitutional relaxation of insulin–like growth factor II gene imprinting associated with Wilms' tumour and gigantism. *Nat Genet*. 1993;5(4):408–412.

O'Gorman DB, Weiss J, Hettiaratchi A, Firth SM, Scott CD. Insulin–like growth factor–II/mannose 6–phosphate receptor overexpression reduces growth of choriocarcinoma cells in vitro and in vivo. *Endocrinology*. 2002;143(11):4287–4294.

Ohtsubo K, Marth JD. Glycosylation in cellular mechanisms of health and disease. *Cell*. 2006;126(5):855–867.

Olivella M, Deupi X, Govaerts C, Pardo L. Influence of the environment in the conformation of alpha-helices studied by protein database search and molecular dynamics simulations. *Biophys J*. 2002;82(6):3207-3213.

Olson LJ, Castonguay AC, Lasanajak Y, Peterson FC, Cummings RD, Smith DF, Dahms NM. Identification of a fourth mannose 6–phosphate binding site in the cation–independent mannose 6–phosphate receptor. *Glycobiology*. 2014;25(6):591–606.

Omote H, Hiasa M, Matsumoto T, Otsuka M, Moriyama Y. The MATE proteins as fundamental transporters of metabolic and xenobiotic organic cations. *Trends Pharmacol Sci*. 2006;27(11):587–593.

Ong K, Kratzsch J, Kiess W, Costello M, Scott C, Dunger D. Size at birth and cord blood levels of insulin, insulin–like growth factor I (IGF–I), IGF–II, IGF–binding protein–1 (IGFBP–1), IGFBP–3, and the soluble IGF–II/mannose–6–phosphate receptor in term human infants. The ALSPAC Study Team. Avon Longitudinal Study of Pregnancy and Childhood. *J Clin Endocrinol Metab*. 2000;85(11):4266–4269.

Orelle C, Mathieu K, Jault JM. Multidrug ABC transporters in bacteria. *Res Microbiol*. 2019;170(8):381–391.

Orme SM, McNally RJ, Cartwright RA, Belchetz PE. Mortality and cancer incidence in acromegaly: A retrospective cohort study. United Kingdom Acromegaly Study Group. *J Clin Endocrinol Metab*. 1998;83(8):2730–2734.

Östlund C, Folker ES, Choi JC, Gomes ER, Gundersen GG, Worman HJ. Dynamics and molecular interactions of linker of nucleoskeleton and cytoskeleton (LINC) complex proteins. *J Cell Sci*. 2009;122(Pt 22):4099–4108.

Otsuka M, Matsumoto T, Morimoto R, Arioka S, Omote H, Moriyama Y. A human transporter protein that mediates the final excretion step for toxic organic cations. *Proc Natl Acad Sci U S A*. 2005;102(50):17923–17928.

Otsuka M, Yasuda M, Morita Y, Otsuka C, Tsuchiya T, Omote H, Moriyama Y. Identification of essential amino acid residues of the NorM Na^+/multidrug antiporter in *Vibrio parahaemolyticus*. *J Bacteriol*. 2005;187(5):1552–1558.

Ottolia M, John S, Xie Y, Ren X, Philipson KD. Shedding light on the Na^+/Ca^{2+} exchanger. *Ann N Y Acad Sci*. 2007;1099:78–85.

Padan E. Functional and structural dynamics of NhaA, a prototype for Na^+ and H^+ antiporters, which are responsible for Na^+ and H^+ homeostasis in cells. *Biochimica et Biophysica Acta – Bioenergetics*. 2014;1837(7):1047–1062.

Pang A, Arinaminpathy Y, Sansom MSP, Biggin PC. Interdomain dynamics and ligand binding: molecular dynamics simulations of glutamine binding protein. *FEBS Lett*. 2003;550(1-3):168-174.

Pantazopoulou A, Diallinas G. Fungal nucleobase transporters. *FEMS Microbiol Rev*. 2007;31(6):657-675.

Park E, Rapoport TA. Mechanisms of Sec61/SecY-mediated protein translocation across membranes. *Annu Rev Biophys*. 2012;41:21–40.

Patching SG. Synthesis of highly pure ^{14}C-labelled *DL*-allantoin and ^{13}C NMR analysis of labelling integrity. *J Labelled Comp Radiopharm*. 2009;52(9):401–404.

Patching SG. Efficient syntheses of ^{13}C- and ^{14}C-labelled 5-benzyl and 5-indolylmethyl *L*-hydantoins. *J Labelled Comp Radiopharm*. 2011;54(2):110-114.

Patching SG. Synthesis, NMR analysis and applications of isotope-labelled hydantoins. *Journal of Diagnostic Imaging in Therapy*. 2017;4(1):3-26.

Patching SG. Recent developments in Nucleobase Cation Symporter-1 (NCS1) family transport proteins from bacteria, archaea, fungi and plants. *J Biosci*. 2018;43(4):797-815.

Patel S, Mackerell AD Jr, Brooks CL 3rd. CHARMM fluctuating charge force field for proteins: II protein/solvent properties from molecular dynamics simulations using a nonadditive electrostatic model. *J Comput Chem*. 2004;25(12):1504–1514.

Pathmaperuma AN, Mana P, Cheung SN, Kugathas K, Josiah A, Koina ME, Broomfield A, et al. Fatty acids alter glycerolipid metabolism and induce lipid droplet formation, syncytialisation and cytokine production in human trophoblasts with minimal glucose effect or interaction. *Placenta*. 2010;31(3):230–239.

Paulin-Levasseur M, Blake DL, Julien M, Rouleau L. The MAN antigens are non-lamin constituents of the nuclear lamina in vertebrate cells. *Chromosoma*. 1996;104(5):367–379.

Peng HY, Xue M, Xia AB. Study on changes of IGF–I and leptin levels in serum and placental tissue of preeclampsia patients and their associativity. *Xi Bao Yu Fen Zi Mian Yi Xue Za Zhi*. 2011;27(2):192–194.

Perez C, Faust B, Mehdipour AR, Francesconi KA, Forrest LR, Ziegler C. Substrate-bound outward-open state of the betaine transporter BetP provides insights into Na^+ coupling. *Nat Commun*. 2014;5:4231.

Perez C, Koshy C, Yildiz O, Ziegler C. Alternating access mechanism in conformationally asymmetric trimers of the betaine transporter BetP. *Nature*. 2012;490:126–130.

Perkins E, Murphy SK, Murtha AP, Schildkraut J, Jirtle RL, Demark–Wahnefried W, Forman MR, et al. Insulin–like growth factor 2/H19 methylation at birth and risk of overweight and obesity in children. *J Pediatr*. 2012;161(1):31–39.

Perozo E, Cortes DM, Sompornpisut P, Kloda A, Martinac B. Open channel structure of MscL and the gating mechanism of mechanosensitive channels. *Nature*. 2002;418(6901):942-948.

Perozo E, Rees DC. Structure and mechanism in prokaryotic mechanosensitive channels. *Curr Opin Struct Biol*. 2003;1(4):432-442.

Petrache HI, Zuckerman DM, Sachs JN, Killian JA, Koeppe RE, Woolf TB. Hydrophobic matching mechanism investigated by molecular dynamics simulations. *Langmuir*. 2002;18(4):1340–1351.

Pfau JD, Taylor RK. Mutations in toxR and toxS that separate transcriptional activation from DNA binding at the cholera toxin gene promoter. *J Bacteriol*. 1998;180(17):4724–4733.

Phillips JC, Braun R, Wang W, Gumbart J, Tajkhorshid E, Villa E, Chipot C, Skeel RD, Kal´e L, Schulten K. Scalable molecular dynamics with NAMD. *J Comput Chem*. 2005;26(16):1781–1802.

Phiske MM. An approach to acanthosis nigricans. *Indian Dermatol Online J*. 2014;5(3):239–249.

Phongphanphanee S, Yoshida N, Hirata F. (2008) On the proton exclusion of aquaporins: A statistical mechanics study. *J Am Chem Soc*. 2008;130(5):1540-1541.

Pollak M. The insulin receptor/insulin–like growth factor receptor family as a therapeutic target in oncology. *Clin Cancer Res*. 2012;18(1):40–50.

Pomero F, Di Minno MND, Fenoglio L, Gianni M, Ageno W, Dentali F. Is diabetes a hypercoagulable state? A critical appraisal. *Acta Diabetol*. 2015;52(6):1007–1016.

Popot JL. Amphipols, nanodiscs, and fluorinated surfactants: three nonconventional approaches to studying membrane proteins in aqueous solutions. *Annu Rev Biochem*. 2010;79:737–775.

Porzio O, Federici M, Hribal ML, Lauro D, Accili D, Lauro R, Borboni P, Sesti G. The Gly^{972}→Arg amino acid polymorphism in IRS–1 impairs insulin secretion in pancreatic β cells. *J Clin Invest*. 1999;104(3):357–364.

Postis V, Rawson S, Mitchell JK, Lee SC, Parslow RA, Dafforn TR, Baldwin SA, Muench SP. The use of SMALPs as a novel membrane protein scaffold for structure study by negative stain electron microscopy. *Biochim Biophys Acta*. 2015;1848(2):496–501.

Postma PW, Lengeler JW, Jacobson G. Phosphoenolpyruvate:carbohydrate phosphotransferase systems of bacteria. *Microbiol Rev*. 1993;57(3):543–594.

Powell L, Burke B. Internuclear exchange of an inner nuclear membrane protein (p55) in heterokaryons: *In vivo* evidence for the interaction of p55 with the nuclear lamina. *J Cell Biol*. 1990;111(6 Pt 1):2225–2234.

Provenzano D, Klose KE. Altered expression of the ToxR-regulated porins OmpU and OmpT diminishes *Vibrio cholerae* bile resistance, virulence factor expression, and intestinal colonization. *Proc Natl Acad Sci U S A*. 2000;97(18):10220–10224.

Pshezhetsky AV, Ashmarina LI. Desialylation of surface receptors as a new dimension in cell signaling. *Biochemistry (Moscow)*. 2013;78(7):736–745.

Putman M, Koole LA, van Veen HW, Konings WN. The secondary multidrug transporter LmrP contains multiple drug interaction sites. *Biochemistry*. 1999;38(42):13900–13905.

Qazi SJS, Chew R, Bay DC, Turner RJ. Structural and functional comparison of hexahistidine tagged and untagged forms of small multidrug resistance protein, EmrE. *Biochem Biophys Rep*. 2015;1:22–32.

Qi F, Turnbough Jr CL. Regulation of codBA operon expression in *Escherichia coli* by UTP-dependent reiterative transcription and UTP-sensitive transcriptional start site switching. *J Mol Biol*. 1995;254(4):552-565.

Quistgaard EM, Löw C, Guettou F, Nordlund P. Understanding transport by the major facilitator superfamily (MFS): structures pave the way. *Nat Rev Mol Cell Biol*. 2016;17(2):123–132.

Rabson SM, Mendenhall EN. Familial hypertrophy of pineal body, hyperplasia of adrenal cortex and diabetes mellitus. *Am J Clin Pathol*. 1956;26(3):283–290.

Radaelli T, Varastehpour A, Catalano P, Hauguel–de–Mouzon S. Gestational diabetes induces placental genes for chronic stress and inflammatory pathways. *Diabetes*. 2003;52(12):2951–2958.

Radchenko M, Symersky J, Nie R, Lu M. Structural basis for the blockade of MATE multidrug efflux pumps. *Nat Commun*. 2015;6:7995.

Radestock S, Forrest LR. The alternating-access mechanism of MFS transporters arises from inverted-topology repeats. *J Mol Biol*. 2011;407(5):698–715.

Randriamboavonjy V, Fleming I. Insulin, insulin resistance, and platelet signaling in diabetes. *Diabetes Care*. 2009;32(4):528–530.

Rapaport DC. *The Art of Molecular Dynamics Simulation*. Cambridge University Press, Cambridge, UK, 2004.

Rapoport TA, Goder V, Heinrich SU, Matlack KE. Membrane-protein integration and the role of the translocation channel. *Trends Cell Biol*. 2004;14(10):568–575.

Rapp M, Schein J, Hunt KA, Nalam V, Mourad GS, Schultes NP. The solute specificity profiles of nucleobase cation symporter 1 (NCS1) from Zea mays and Setaria viridis illustrate functional flexibility. *Protoplasma*. 2016;253(2):611-623.

Rath A, Deber CM. Correction factors for membrane protein molecular weight readouts on sodium dodecyl sulfate-polyacrylamide gel electrophoresis. *Anal Biochem*. 2013;434(1):67-72.

Rath A, Glibowicka M, Nadeau VG, Chen G, Deber CM. Detergent binding explains anomalous SDS-PAGE migration of membrane proteins. *Proc Natl Acad Sci U S A*. 2009;106(6):1760–1765.

Reddy T, Shorthouse D, Parton DL, Jefferys E, Fowler PW, Chavent M, Baaden M, Sansom MSP. Nothing to sneeze at: A dynamic and integrative computational model of an influenza A virion. *Structure*. 2015;23(3):584–597.

Reichelt R, Holzenburg A, Buhle EL Jr, Jarnik M, Engel A, Aebi U. Correlation between structure and mass distribution of the nuclear pore complex and of distinct pore complex components. *J Cell Biol*. 1990;110(4):883–894.

Reidl J, Klose KE. *Vibrio cholerae* and cholera: out of the water and into the host. *FEMS Microbiol Rev*. 2002;26(2):125–139.

Remko M, Šoralová S. Effect of water coordination on competition between π and non-π cation binding sites in aromatic amino acids: L-phenylalanine, L-tyrosine, and L-tryptophan Li^+, Na^+, and K^+ complexes. *J Biol Inorg Chem*. 2012;17(4):621–630.

Renehan AG, Zwahlen M, Minder C, O'Dwyer ST, Shalet SM, Egger M. Insulin–like growth factor (IGF)–I, IGF binding protein–3, and cancer risk: Systematic review and meta–regression analysis. *Lancet*. 2004;363(9418):1346–1453.

Ressl S, Terwisscha van Scheltinga AC, Vonrhein C, Ott V, Ziegler C. Molecular basis of transport and regulation in the Na^+/betaine symporter BetP. *Nature*. 2009;458(7234):47–52.

Reuter S, Gupta SC, Chaturvedi MM, Aggarwal BB. Oxidative stress, inflammation, and cancer: How are they linked? *Free Radic Biol Med*. 2010;49(11):1603–1616.

Rexach MF. A sorting importin on Sec61. *Nat Struct Mol Biol*. 2006;13(6):476–478.

Reyes N, Ginter C, Boudker O. Transport mechanism of a bacterial homologue of glutamate transporters. *Nature*. 2009;462(7275):880–885.

Ribatti D. Endogenous inhibitors of angiogenesis: a historical review. *Leuk Res*. 2009;33(5):638–644.

Ribatti D. A revisited concept: Contact inhibition of growth. From cell biology to malignancy. *Exp Cell Res*. 2017a;359(1):17–19.

Ribatti D. The concept of immune surveillance against tumors. The first theories. *Oncotarget*. 2017b;8(4):7175–7180.

Rinderknecht E, Humbel RE. The amino acid sequence of human insulin–like growth factor I and its structural homology with proinsulin. *J Biol Chem*. 1978;253(8):2769–2776.

Robajac D, Križáková M, Masnikosa R, Miljuš G, Šunderić M, Nedić O, Katrlík J. Sensitive glycoprofiling of insulin–like growth factor receptors isolated from colon tissue of patients with colorectal carcinoma using lectin-based protein microarray. *Int J Biol Macromol*. 2020;144:932–937.

Robajac D, Masnikosa R, Filimonović D, Miković Ž, Nedić O. N–glycosylation pattern of human placental insulin–like growth factor and insulin receptors in well–controlled pregestational diabetes mellitus. *J Med Biochem*. 2012;31(3):205–210.

Robajac D, Masnikosa R, Miković Ž, Mandić V, Nedić O. Oxidation of placental insulin and insulin–like growth factor receptors in mothers with diabetes mellitus or preeclampsia complicated with intrauterine growth restriction. *Free Radic Res*. 2015;49(8):984–989.

Robajac D, Masnikosa R, Miković Ž, Nedić O. Gestation–associated changes in the glycosylation of placental insulin and insulin–like growth factor receptors. *Placenta*. 2016a ;39:70–76.

Robajac D, Masnikosa R, Vanhooren V, Libert C, Miković Ž, Nedić O. The N–glycan profile of placental membrane glycoproteins alters during gestation and ageing. *Mech Ageing Dev*. 2014;138:1–9.

Robajac D, Vanhooren V, Masnikosa R, Miković Ž, Mandić V, Libert C, Nedić O. Preeclampsia transforms membrane N–glycome in human placenta. *Exp Mol Pathol*. 2016b;100(1):26–30.

Robajac D, Zámorová M, Katrlík J, Miković Ž, Nedić O. Screening for the best detergent for the isolation of placental membrane proteins. *Int J Biol Macromol*. 2017;102:431–437.

Rogers J, Wiltrout L, Nanu L, Fant ME. Developmentally regulated expression of IGF binding protein–3 (IGFBP–3) in human placental fibroblasts: Effect of exogenous IGFBP3 on IGF–1 action. *Regul Pept*. 1996;61(3):189–195.

Rolfe DF, Brown GC. Cellular energy utilization and molecular origin of standard metabolic rate in mammals. *Physiol Rev*. 1997;77(3):731–758.

Rolls MM, Stein PA, Taylor SS, Ha E, McKeon F, Rapoport TA. A visual screen of a GFP-fusion library identifies a new type of nuclear envelope membrane protein. *J Cell Biol*. 1999;146(1):29–44.

Romano G. The complex biology of the receptor for the insulin–like growth factor–1. *Drug News Perspect*. 2003;16(8):525–531.

Roos S, Lagerlof O, Wennergren M, Powell TL, Jansson T. Regulation of amino acid transporters by glucose and growth factors in cultured primary human trophoblast cells is mediated by mTOR signaling. *Am J Physiol Cell Physiol*. 2009;297(3):C723–C731.

Roy NK. A new semi-explicit atomistic molecular dynamics simulation method for membrane proteins. *J Comput Methods Sci Eng*. 2019;19(1):259-286.

Ruiz–Palacios M, Prieto–Sánchez M, Ruiz–Alcaraz A, Blanco–Carnero J, Sanchez–Campillo M, Parrilla J, Larqué E. Insulin treatment may enhance fatty acid

carriers in placentas from gestational diabetes subjects. *Int J Mol Sci*. 2017b;18(6). pii: E1203.

Ruiz–Palacios M, Ruiz–Alcaraz AJ, Sanchez–Campillo M, Larqué E. Role of insulin in placental transport of nutrients in gestational diabetes mellitus. *Ann Nutr Metab*. 2017;70(1):16–25.

Russo VC, Bach LA, Fosang AJ, Baker NL, Werther GA. Insulin like growth factor binding protein–2 binds to cell surface proteoglycans in the rat brain olfactory bulb. *Endocrinology*. 1997;138(11):4858–4856.

Ryan PD, Goss PE. The emerging role of the insulin–like growth factor pathway as a therapeutic target in cancer. *Oncologist*. 2008;13:16–24.

Rzepiela AJ, Schafer LV, Goga N, Risselada HJ, de Vries AH, Marrink SJ. Reconstruction of atomistic details from coarse-grained structures. *J Comput Chem.* 2010;31(6):1333–1343.

Sack DA, Sack RB, Nair GB, Siddique AK. Cholera. *Lancet*. 2004;363(9404):223–233.

Saidijam M, Azizpour S, Patching SG. Comprehensive analysis of the numbers, lengths and amino acid compositions of transmembrane helices in prokaryotic, eukaryotic and viral integral membrane proteins of high-resolution structure. *J Biomol Struct Dyn*. 2018;36(2):443-464.

Saidijam M, Bettaney KE, Szakonyi G, Psakis G, Shibayama K, Suzuki S, Clough JL, Blessie V, Abu-Bakr A, Baumberg S, Meuller J, Hoyle CK, Palmer SL, Butaye P, Walravens K, Patching SG, O'reilly J, Rutherford NG, Bill RM, Roper DI, Phillips-Jones MK, Henderson PJ. Active membrane transport and receptor proteins from bacteria. *Biochem Soc Trans*. 2005;33(Pt 4):867-872.

Saidijam M, Psakis G, Clough JL, Meuller J, Suzuki S, Hoyle CJ, Palmer SL, Morrison SM, Pos MK, Essenberg RC, Maiden MC, Abu-bakr A, Baumberg SG, Neyfakh AA, Griffith JK, Stark MJ, Ward A, O'Reilly J, Rutherford NG, Phillips-Jones MK, Henderson PJ. Collection and characterisation of bacterial membrane proteins. *FEBS Lett*. 2003;555(1):170-175.

Saier MH Jr, Yen MR, Noto K, Tamang DG, Elkan C. The Transporter Classification Database: Recent advances. *Nucleic Acids Res*. 2009;37(Database issue):D274-D278.

Saier MH Jr, Paulsen IT. Phylogeny of multidrug transporters. *Semin Cell Dev Biol*. 2001;12(3):205–213.

Saito–Hakoda A, Nishii A, Uchida T, Kikuchi A, Kanno J, Fujiwara I, Kure S. A follow–up during puberty in a Japanese girl with type A insulin resistance due to a novel mutation in *INSR*. *Clin Pediatr Endocrinol*. 2018;27(1):53–57.

Sakai K, Lowman HB, Clemmons DR. Increases in free, unbound insulin–like growth factor I enhance insulin responsiveness in human hepatoma G2 cells in culture. *J Biol Chem*. 2002;277(16):13620–13627.

Samani AA, Yakar S, LeRoith D, Brodt P. The role of the IGF system in cancer growth and metastasis: Overview and recent insights. *Endocr Rev*. 2007;28(1):20–47.

Sandberg AC, Engberg C, Lake M, von Holst H, Sara VR. The expression of insulin–like growth factor I and insulin–like growth factor II genes in the human fetal and adult brain and in glioma. *Neurosci Lett*. 1988;93(1):114–119.

Sanders CR, Prosser RS. Bicelles: A model membrane system for all seasons? *Structure*. 1998;6(10):1227–1234.

Sandovici I, Hoelle K, Angiolini E, Constância M. Placental adaptations to the maternal–fetal environment: Implications for fetal growth and developmental programming. *Reprod Biomed Online*. 2012;25(1):68–89.

Santoni V, Molloy M, Rabilloud T. Membrane proteins and proteomics: un amour impossible? *Electrophoresis*. 2000;21(6):1054–1070.

Sar N, McCarter L, Simon M, Silverman M. Chemotactic control of the two flagellar systems of *Vibrio parahaemolyticus*. *J Bacteriol*. 1990;172(1):334-341.

Sarfstein R, Pasmanik–Chor M, Yeheskel A, Edry L, Shomron N, Warman N, Wertheimer E, Maor S, Shochat L, Werner H. Insulin–like growth factor–I receptor (IGF–IR) translocates to nucleus and autoregulates IGF–IR gene expression in breast cancer cells. *J Biol Chem*. 2012;287(4):2766–2776.

Sasaoka T, Ishiki M, Wada T, Hori H, Hirai H, Haruta T, Ishihara H, Kobayashi M. Tyrosine phosphorylation–dependent and –independent role of Shc in the regulation of IGF–1–induced mitogenesis and glycogen synthesis. *Endocrinology*. 2001;142(12):5226–5235.

Saul-McBeth J, Matson JS. A periplasmic antimicrobial peptide-binding protein is required for stress survival in *Vibrio cholerae*. *Front Microbiol*. 2019;10:161.

Saurabh S, Vidyarthi AS, Prasad D. RNA interference: concept to reality in crop improvement. *Planta*. 2014;239(3):543–564.

Sayer RA, Lancaster JM, Pittman J, Gray J, Whitaker R, Marks JR, Berchuck A. High insulin–like growth factor–2 (IGF–2) gene expression is an independent predictor of poor survival for patients with advanced stage serous epithelial ovarian cancer. *Gynecol Oncol*. 2005;96(2):355–361.

Sazanov LA. A giant molecular proton pump: structure and mechanism of respiratory complex I. *Nat Rev Mol Cell Biol*. 2015;16(6):375–388.

Sbraccia P, D'Adamo M, Leonetti F, Caiola S, Iozzo P, Giaccari A, Buongiorno A, Tamburrano G. Chronic primary hyperinsulinaemia is associated with altered

insulin receptor mRNA splicing in muscle of patients with insulinoma. *Diabetologia*. 1996;39(2):220–225.

Schaffner W, Weissmann C. A rapid, sensitive, and specific method for the determination of protein in dilute solution. *Anal Biochem*. 1973;56(2):502-514.

Schein JR, Hunt KA, Minton JA, Schultes NP, Mourad GS. The nucleobase cation symporter 1 of *Chlamydomonas reinhardtii* and that of the evolutionarily distant *Arabidopsis thaliana* display parallel function and establish a plant-specific solute transport profile. *Plant Physiol Biochem*. 2013;70:52-60.

Schirmer EC, Gerace L. The nuclear membrane proteome: extending the envelope. *Trends Biochem Sci*. 2005;30(10):551–558.

Schlegel S, Hjelm A, Baumgarten T, Vikström D, de Gier JW. Bacterial-based membrane protein production. *Biochim Biophys Acta*. 2014;1843(8):1739–1749.

Schlegel S, Löfblom J, Lee C, Hjelm A, Klepsch M, Strous M, Drew D, Slotboom DJ, de Gier JW. Optimizing membrane protein overexpression in the *Escherichia coli* strain Lemo21(DE3). *J Mol Biol*. 2012;423(4):648–659.

Schnell SJ, Ma J, Yang W. Three-dimensional mapping of mRNA export through the nuclear pore complex. *Genes (Basel)*. 2014;5(4):1032–1049.

Schuldiner S. Competition as a way of life for H(+)-coupled antiporters. *J Mol Biol*. 2014;426(14):2539–2546.

Schulz GE. The structure of bacterial outer membrane proteins. *Biochim Biophys acta - Biomembranes*. 2002;1565(2):308-317.

Schulze S, Köster S, Geldmacher U, Terwisscha van Scheltinga AC, Kühlbrandt W. Structural basis of Na(+)-independent and cooperative substrate/product antiport in CaiT. *Nature*. 2010;467(7312):233–236.

Schushan M, Rimon A, Haliloglu T, Forrest LR, Padan E, and Ben-Tal N. A model-structure of a periplasm-facing state of the NhaA antiporter suggests the molecular underpinnings of pH-induced conformational changes. *J Biol Chem*. 2012;287(22):18249–18261.

Schwacke R, Schneider A, van der Graaff E, Fischer K, Catoni E, Desimone M, Frommer WB, Flügge UI, Kunze R. ARAMEMNON, a novel database for Arabidopsis integral membrane proteins. *Plant Physiol*. 2003;131(1):16-26.

Schwartz SD, Schramm VL. Enzymatic transition states and dynamic motion in barrier crossing. *Nat Chem Biol*. 2009;5(8):551–558.

Schweikhard ES, Ziegler CM. Amino acid secondary transporters: toward a common transport mechanism. Chapter 1 in Co-Transport Systems, edited by Bevensee MO, 2012;70:1–28. *Curr Top Membranes*. Elsevier Inc.

Scott CD, Firth SM. The role of the M6P/IGF–II receptor in cancer: Tumor suppression or garbage disposal? *Horm. Metab. Res*. 2004;36(5):261–271.

Seino S, Bell GI. Alternative splicing of human insulin receptor messenger RNA. *Biochem Biophys Res Commun*. 1989;159(1):312–316.

Selvam B, Mittal S, Shukla D. Free energy landscape of the complete transport cycle in a key bacterial transporter. *ACS Cent Sci*. 2018;4(9):1146–1154.

Senior A, Gerace L. Integral membrane proteins specific to the inner nuclear membrane and associated with the nuclear lamina. *J Cell Biol*. 1988;107(6 Pt 1):2029–2036.

Serebryannyy LA, Ball DA, Karpova TS, Misteli T. Single molecule analysis of lamin dynamics. *Methods*. 2019;157:56–65.

Sesti G, D'Alfonso R, Punti MDV, Frittitta L, Trischitta V, Liu YY, Borboni P, Longhi R, Montemurro A, Lauro R. Peptide–based radioimmunoassay for the two isoforms of the human insulin receptor. *Diabetologia*. 1995;38(4):445–453.

Sesti G, Federici M, Lauro D, Sbraccia P, Lauro R. Molecular mechanism of insulin resistance in type 2 diabetes mellitus: Role of the insulin receptor variant forms. *Diabetes Metab Res Rev*. 2001;17(5):363–373.

Sesti G, Marini MA, Tullio AN, Montemurro A, Borboni P, Fusco A, Accili D, Renato Lauro R. Altered expression of the two naturally occurring human insulin receptor variants in isolated adipocytes of non–insulin–dependent diabetes mellitus patients. *Biochem Biophys Res Commun*. 1991;181(3):1419–1424.

Sever R, Brugge JS. Signal transduction in cancer. *Cold Spring Harb Perspect Med*. 2015;5(4):pii:a006098.

Seyfried TN, Huysentruyt LC. On the origin of cancer metastasis. *Crit Rev Oncog*. 2013;18(1-2):43–73.

Sferruzzi–Perri AN, Sandovici I, Constancia M, Fowden AL. Placental phenotype and the insulin–like growth factors: resource allocation to fetal growth. *J Physiol*. 2017;595(15):5057–5093.

Shaw DE, Maragakis P, Lindorff-Larsen K, Piana S, Dror RO, Eastwood MP, Bank JA, et al. Atomic-level characterization of the structural dynamics of proteins. *Science*. 2020;330(6002):341-346.

Shelley JC, Shelley MY, Reeder RC, Bandyopadhyay S, Klein ML. A coarse grain model for phospholipid simulations. *J Phys Chem B.* 2001;105(40):4464–4470.

Shi Y. Common folds and transport mechanisms of secondary active transporters. *Ann Rev Biophys*. 2013;42(1):51–72.

Shimamura T, Weyand S, Beckstein O, Rutherford NG, Hadden JM, Sharples D, Sansom MSP, Iwata I, Henderson PJF, Cameron AD. Molecular basis of alternating access membrane transport by the sodium-hydantoin transporter Mhp1. *Science*. 2010;328(5977):470–473.

Shimi T, Koujin T, Segura-Totten M, Wilson KL, Haraguchi T, Hiraoka Y. Dynamic interaction between BAF and emerin revealed by FRAP, FLIP, and FRET analyses in living HeLa cells. *J Struct Biol*. 2004;147(1):31–41.

Shinoda W, DeVane R, Klein ML. Zwitterionic lipid assemblies: Molecular dynamics studies of monolayers, bilayers, and vesicles using a new coarse grain force field. *J Phys Chem B*. 2010;114(20):6836–6849.

Shiratsuchi I, Akagi Y, Kawahara A, Kinugasa T, Romeo K, Yoshida T, Ryu Y, Gotanda Y, Kage M, Shirouzu K. Expression of IGF–1 and IGF–1R and their relation to clinicopathological factors in colorectal cancer. *Anticancer Res*. 2011;31(7):2541–2545.

Shukla S, Abel B, Chufan EE, Ambudkar SV. Effects of a detergent micelle environment on P-glycoprotein (ABCB1)-ligand interactions. *J Biol Chem*. 2017;292(17):7066–7076.

Sibley CP, Turner MA, Cetin I, Ayuk P, Boyd CA, D'Souza SW, Glazier JD, Greenwood SL, Jansson T, Powell T. Placental phenotypes of intrauterine growth. *Pediatr Res*. 2005;58(5):827–832.

Sievers F, Wilm A, Dineen D, Gibson TJ, Karplus K, Li W, Lopez R, McWilliam H, Remmert M, Söding J, Thompson JD, Higgins DG. Fast, scalable generation of high-quality protein multiple sequence alignments using Clustal Omega. *Mol Syst Biol*. 2011;7:539.

Sigal N, Fluman N, Siemion S, Bibi E. The secondary multidrug/proton antiporter MdfA tolerates displacements of an essential negatively charged side chain. *J Biol Chem.* 2009;284(11):6966–6971.

Sigel SP, Payne SM. Effect of iron limitation on growth, siderophore production, and expression of outer membrane proteins of *Vibrio cholerae*. J *Bacteriol*. 1982;150(1):148–155.

Sikora CW, Turner RJ. Investigation of ligand binding to the multidrug resistance protein EmrE by isothermal titration calorimetry. *Biophys J*. 2005;88(1):475–482.

Silhavy TJ, Kahne D, Walker S. The bacterial cell envelope. *Cold Spring Harb Perspect Biol*. 2010;2(5):a000414.

Silva AJ, Benitez JA. *Vibrio cholerae* biofilms and cholera pathogenesis. *PLoS Negl Trop Dis*. 2016;10(2):e0004330.

Simmons KJ, Jackson SM, Brueckner F, Patching SG, Beckstein O, Ivanova E, Geng T, Weyand S, Drew D, Lanigan J, Sharples DJ, Sansom MS, Iwata S, Fishwick CW, Johnson AP, Cameron AD, Henderson PJ. Molecular mechanism of ligand recognition by membrane transport protein, Mhp1. *EMBO J*. 2014;33(16):1831-1844.

Sinclair D, Abba K, Zaman K, Qadri F, Graves PM. Oral vaccines for preventing cholera. *Cochrane Database Syst Rev*. 2011;(3):CD008603.

Sioupouli G, Lambrinidis G, Mikros E, Amillis S, Diallinas G. Cryptic purine transporters in *Aspergillus nidulans* reveal the role of specific residues in the evolution of specificity in the NCS1 family. *Mol Microbiol*. 2017;103(2):319-332.

Sjögren K, Wallenius K, Liu J, Bohlooly M, Pacini G, Svensson L, Törnell J, et al. Liver–derived IGF–I is of importance for normal carbohydrate and lipid metabolism. *Diabetes*. 2001;50(7):1539–1545.

Sklar MM, Thomas CL, Municchi G, Roberts CT Jr, LeRoith D, Kiess W, Nissley P. Developmental expression of rat insulin–like growth factor II/mannose 6–phosphate receptor messenger ribonucleic acid. *Endocrinology*. 1992;130(6):3484–3491.

Skyler JS, Bakris GL, Bonifacio E, Darsow T, Eckel RH, Groop L, Groo PH, et al. Differentiation of diabetes by pathophysiology, natural history, and prognosis. *Diabetes*. 2017;66(2):241–255.

Slotboom DJ. Structural and mechanistic insights into prokaryotic energycoupling factor transporters. *Nat Rev Microbiol*. 2014;12(2):79–87.

Smart OS, Neduvelil JG, Wang X, Wallace BA, Sansom MSP. HOLE: A program for the analysis of the pore dimensions of ion channel structural models. *J Mol Graph*. 1996;14:354–360.

Smirnova I, Kasho V, Kaback HR. Engineered occluded apointermediate of LacY. *Proc Natl Acad Sci USA*. 2018;115(50):12716–12721.

Smith KP, Kumar S, Varela MF. Identification, cloning, and functional characterization of EmrD-3, a putative multidrug efflux pump of the major facilitator superfamily from *Vibrio cholerae O395*. *Arch Microbiol*. 2009;191(12):903–911.

So AI, Levitt RJ, Eigl B, Fazli L, Muramaki M, Leung S, Cheang MC, Nielsen TO, Gleave M, Pollak M. Insulin–like growth factor binding protein–2 is a novel therapeutic target associated with breast cancer. *Clin Cancer Res*. 2008;14(21):6944–6954.

Solomon AL, Siddals KW, Baker PN, Gibson JM, Aplin JD, Westwood M. Placental alkaline phosphatase de–phosphorylates insulin–like growth factor (IGF)–binding protein–1. *Placenta*. 2014;35(7):520–522.

Soltysiak D, Kaniuga Z. The effect of triton X-100 on the respiratory chain enzymes of a heart-muscle preparation. *Eur J Biochem*. 1970;14(1):70–74.

Soullam B, Worman HJ. The amino-terminal domain of the lamin B receptor is a nuclear envelope targeting signal. *J Cell Biol*. 1993;120(5):1093–1100.

Soullam B, Worman. Signals and structural features involved in integral membrane protein targeting to the inner nuclear membrane. *J Cell Biol*. 1995;130(1):15–27.

Soussi T, Wiman KG2. TP53: An oncogene in disguise. *Cell Death Differ*. 2015;22(8):1239–49.

Souza RF, Wang S, Thakar M, Smolinski KN, Yin J, Zou TT, Kong D, Abraham JM, Toretsky JA, Meltzer SJ. Expression of the wild–type insulin–like growth factor II receptor gene suppresses growth and causes death in colorectal carcinoma cells. *Oncogene*. 1999;18(28):4063–4068.

Spampinato D, Pandini G, Iuppa A, Trischitta V, Vigneri R, Frittitta L. Insulin/insulin–like growth factor I hybrid receptors overexpression is not an early defect in insulin–resistant subjects. *J Clin Endocrinol Metab*. 2000;85(11):4219–4223.

Sparrow LG, Lawrence MC, Gorman JJ, Strike PM, Robinson CP, McKern NM, Ward CW. N–linked glycans of the human insulin receptor and their distribution over the crystal structure. *Proteins*. 2008;71(1):426–439.

Sprague BL, McNally JG. FRAP analysis of binding: proper and fitting. *Trends Cell Biol*. 2005;15(2):84–91.

Sprague BL, Pego RL, Stavreva DA, McNally JG. Analysis of binding reactions by fluorescence recovery after photobleaching. *Biophys J*. 2004;86(6):3473-3495.

Stanley HE. *Introduction of Phase Transitions and Critical Phenomena*. Oxford University Press, New York, 1971.

Stansfeld PJ, Goose JE, Caffrey M, Carpenter EP, Parker JL, Newstead S, Sansom MS. MemProtMD: Automated insertion of membrane protein structures into explicit lipid membranes. *Structure*. 2015;23(7):1350–1361.

Stansfeld PJ, Jefferys E, Sansom, MSP. Multiscale simulations reveal conserved patterns of lipid interactions with aquaporins. *Structure*. 2013;21(5):810–819.

Stansfeld PJ, Sansom MSP. Molecular simulation approaches to membrane proteins. *Structure*. 2011;19:1562–1572.

Stark MJ. Multicopy expression vectors carrying the lac repressor gene for regulated high-level expression of genes in *Escherichia coli*. *Gene*. 1987;51(2-3):255-267.

Stelzl LS, Fowler PW, Sansom MSP, Beckstein O. Flexible gates generate occluded intermediates in the transport cycle of LacY. *J Mol Biol*. 2014;426:735–751.

Stenham DR, Campbell JD, Sansom MS, Higgins CF, Kerr ID, Linton KJ. An atomic detail model for the human ATP binding cassette transporter P-glycoprotein derived from disulfide cross-linking and homology modeling. *FASEB J*. 2003;17(15):2287-2289.

Stockner T, Ash WL, MacCallum JL, Tieleman DP. Direct simulation of transmembrane helix association: Role of asparagines. *Biophys J*. 2004;87(3):1650–1656.

Stoop JM, Mooibroek H. Cloning and characterization of NADP-mannitol dehydrogenase cDNA from the button mushroom, *Agaricus bisporus*, and its expression in response to NaCl stress. *Appl Environ Microbiol*. 1998;64(12):4689–4696.

Succurro E, Andreozzi F, Marini MA, Lauro R, Hribal ML, Perticone F, Sesti G. Low plasma insulin–like growth factor–1 levels are associated with reduced insulin sensitivity and increased insulin secretion in nondiabetic subjects. *Nutr Metab Cardiovasc Dis*. 2009;19(10):713–719.

Sudarsanam S, Johnson DE. Functional consequences of mTOR inhibition. *Curr Opin Drug Discov Devel*. 2010;13(1):31–40.

Šunderić M, Đukanović B, Malenković V, Nedić O. Molecular forms of the insulin–like growth factor–binding protein–2 in patients with colorectal cancer. *Exp Mol Pathol*. 2014;96(1):48–53.

Šunderić M, Križakova M, Malenković V, Ćujić D, Katrlik J, Nedić O. Changes due to ageing in the glycan structure of alpha–2–macroglobulin and its reactivity with ligands. *Prot J*. 2019;38(1):23–29.

Suzuki S, Henderson PJF. The hydantoin transport protein from *Microbacterium liquefaciens*. *J Bacteriol*. 2006;188(9):3329–3336.

Szakonyi G, Leng D, Ma P, Bettaney KE, Saidijam M, Ward A, Zibaei S, Gardiner AT, Cogdell RJ, Butaye P, Kolsto AB, O'reilly J, Hope RJ, Rutherford NG, Hoyle CJ, Henderson PJ. A genomic strategy for cloning, expressing and purifying efflux proteins of the major facilitator superfamily. *J Antimicrob Chemother*. 2007;59(6):1265-1270.

Tamm LK, Abildgaard F, Arora A, Blad H, Bushweller JH. Structure, dynamics and function of the outer membrane protein A (OmpA) and influenza hemagglutinin fusion domain in detergent micelles by solutions NMR, *FEBS Lett*. 2003;555(1):139-143.

Tan EK, Tan EL. Alterations in physiology and anatomy during pregnancy. *Best Pract Res Clin Obstet Gynaecol*. 2013;27(6):791–802.

Tanaka Y, Hipolito CJ, Maturana AD, Ito K, Kuroda T, Higuchi T, Katoh T, et al. Structural basis for the drug extrusion mechanism by a MATE multidrug transporter. *Nature*. 2013;496(7444):247–251.

Tanaka Y, Iwaki S, Tsukazaki T. Crystal structure of a plant multidrug and toxic compound extrusion family protein. *Structure*. 2017;25(9):1455–1460.e2.

Tanford C. Translocation pathway in the catalysis of active transport. *Proc Natl Acad Sci USA*. 1983;80(12):3701–3705.

Tang L, Bai L, Wang WH, Jiang T. Crystal structure of the carnitine transporter and insights into the antiport mechanism. *Nat Struct Mol Biol*. 2010;17(4):492–496.

Tani K, Mitsuma T, Hiroaki Y, Kamegawa A, Nishikawa K, Tanimura Y, Fujiyoshi Y. Mechanism of aquaporin-4's fast and highly selective water conduction and proton exclusion. *J Mol Biol*. 2009;389(4):694-706.

Tapley EC, Ly N, Starr DA. Multiple mechanisms actively target the SUN protein UNC-84 to the inner nuclear membrane. *Mol Biol Cell*. 2011;22(10):1739–1752.

Taylor DL, Bina XR, Bina JE. *Vibrio cholerae* VexH encodes a multiple drug efflux pump that contributes to the production of cholera toxin and the toxin co-regulated pilus. *PLoS One*. 2012;7(5):e38208.

Taylor SI, Cama A, Accili D, Barbetti F, Quon MJ, de la Luz Sierra M, Suzuki Y, et al. Mutations in the insulin receptor gene. *Endocr Rev*. 1992;13(3):566–595.

Teppala S, Shankar A. Association between serum IGF–1 and diabetes among US adults. *Diabetes Care*. 2010;33(10):2257–2259.

Tepper OM, Capla JM, Galiano RD, Ceradini DJ, Callaghan MJ, Kleinman ME, Gurtner GC. Adult vasculogenesis occurs through in situ recruitment, proliferation, and tubulization of circulating bone marrow–derived cells. *Blood*. 2005;105(3):1068–1077.

Terpe K. Overview of tag protein fusions: from molecular and biochemical fundamentals to commercial systems. *Appl Microbiol Biotechnol*. 2003;60(5):523–533.

Teschler JK, Zamorano-Sánchez D, Utada AS, Warner CJ, Wong GC, Linington RG, Yildiz FH. Living in the matrix: assembly and control of *Vibrio cholerae* biofilms. *Nat Rev Microbiol*. 2015;13(5):255–268.

Thomas JR, Gedeon PC, Grant BJ, Madura JD. LeuT conformational sampling utilizing accelerated molecular dynamics and principal component analysis. *Biophys J*. 2012;103(1):L1-L3.

Tieleman DP, Sansom MSP. Molecular dynamics simulations of antimicrobial peptides: From membrane binding to trans-membrane channels. *Int J Quantum Chem*. 2001;83(3-4):166–179.

Tirosh O, Sigal N, Gelman A, Sahar N, Fluman N, Siemion S, Bibi E. Manipulating the drug/proton antiport stoichiometry of the secondary multidrug transporter MdfA. *Proc Natl Acad Sci U S A*. 2012;109(31):12473–12478.

Tischler AD, Camilli A. Cyclic diguanylate regulates *Vibrio cholerae* virulence gene expression. *Infect Immun*. 2005;73(9):5873–5882.

Tokunaga M, Imamoto N, Sakata-Sogawa K. Highly inclined thin illumination enables clear single-molecule imaging in cells. *Nat Methods*. 2008;5(2):159–161.

Treptow W, Marrink SJ, Tarek M. Gating motions in voltage-gated potassium channels revealed by coarse-grained molecular dynamics simulations. *J Phys Chem*. 2008;B112(11):3277-3282.

Tripodi A, Branchi A, Chantarangkul V, Clerici M, Merati G, Artoni A, Mannucci PM. Hypercoagulability in patients with type 2 diabetes mellitus detected by a thrombin generation assay. *J Thromb Thrombolysis*. 2011;31(2):165–172.

Tsirigos KD, Govindarajan S, Bassot C, Västermark Å, Lamb J, Shu N, Elofsson A. Topology of membrane proteins-predictions, limitations and variations. *Curr Opin Struct Biol*. 2018;50:9–17.

Tsirigos KD, Hennerdal A, Käll L, Elofsson A. A guideline to proteome-wide α-helical membrane protein topology predictions. *Proteomics*. 2012;12(14):2282–2294.

Tsirigos KD, Peters C, Shu N, Käll L, Elofsson A. The TOPCONS web server for consensus prediction of membrane protein topology and signal peptides. *Nucleic Acids Res*. 2015;43(W1):W401-W407.

Tulumello DV, Deber CM. Efficiency of detergents at maintaining membrane protein structures in their biologically relevant forms. *Biochim Biophys Acta*. 2012;1818(5):1351–1358.

Turgay Y, Ungricht R, Rothballer A, Kiss A, Csucs G, Horvath P, Kutay U. A classical NLS and the SUN domain contribute to the targeting of SUN2 to the inner nuclear membrane. *EMBO J*. 2010;29(14):2262–2275.

Turner RJ, Weiner JH. Evaluation of transmembrane helix prediction methods using the recently defined NMR structures of the coat proteins from bacteriophages M13 and Pf1. *Biochim Biophys Acta*. 1993;1202(1):161–168.

Uhles S, Moede T, Leibiger B, Berggren PO, Leibiger IB. Isoform–specific insulin receptor signaling involves different plasma membrane domains. *J Cell Biol*. 2003;163(6):1327–1237.

Ulitzur S. *Vibrio parahaemolyticus* and *Vibrio alginolyticus*: Short generation-time marine bacteria. *Microb Ecol*. 1974;1(1):127-135.

Ullrich A, Gray A, Tam AW, Yang–Feng T, Tsubokawa M, Collins C, Henzel W, et al. Insulin–like growth factor 1 receptor primary structure: comparison with insulin receptor suggests structural determinants that define functional specificity. *EMBO J*. 1986;5(10):2503–2512.

Ungricht R, Kutay U. Establishment of NE asymmetry—targeting of membrane proteins to the inner nuclear membrane. *Curr Opin Cell Biol*. 2015;34:135–141.

Uzoh CC, Holly JM, Biernacka KM, Persad RA, Bahl A, Gillatt D, Perks CM. Insulin–like growth factor–binding protein–2 promotes prostate cancer cell growth via IGF–dependent or –independent mechanisms and reduces the efficacy of docetaxel. *Br J Cancer*. 2011;104(10):1587–1593.

Valadie H, Lacapcre JJ, Sanejouand YH, Etchebest C. Dynamical properties of the MscL of *Escherichia coli*: A normal mode analysis. *J. Mol. Biol*. 2003;332(3):657-674.

Valensise H, Liu YY, Federici M, Lauro D, Dell'anna D, Romanini C, Sesti G. Increased expression of low–affinity insulin receptor isoform and insulin/insulin–like growth factor–I hybrid receptors in term placenta from insulin–resistant women with gestational hypertension. *Diabetologia*. 1996;39(8):952–960.

Vandenberg RJ., Huang S, Ryan RM. Slips, leaks and channels in glutamate transporters. *Channels*. 2008;2(1):51–58.

Vander Heiden MG, Cantley LC, Thompson CB. Understanding the Warburg effect: The metabolic requirements of cell proliferation. *Science*. 2009;324(5930):1029–1033.

Van der Ploeg P, Berendsen HJC. Molecular-dynamics of a bilayer-membrane. *Mol Phys*. 1983;49(1):233–248.

van Geest M, Lolkema JS. Membrane topology and insertion of membrane proteins: Search for topogenic signals. *Microbiol Mol Biol Rev*. 2000;64(1):13–33.

Vardy E, Arkin IT, Gottschalk KE, Kaback HR, Schuldiner S. Structural conservation in the major facilitator superfamily as revealed by comparative modeling. *Protein Sci*. 2004;13(7):1832-1840.

Västermark Å, Wollwage S, Houle ME, Rio R, Saier Jr MH. Expansion of the APC superfamily of secondary carriers. *Proteins*. 2014;82(10):2797–2811.

Vazzana N, Ranalli P, Cuccurullo C, Davì G. Diabetes mellitus and thrombosis. *Thromb Res*. 2012;129(3):371–377.

Vella V, Malaguarnera R. The emerging role of insulin receptor isoforms in thyroid cancer: clinical implications and new perspectives. *Int J Mol Sci*. 2018;19(12):3814.

Varela MF. *Antimicrobial Efflux Pumps*. In Antibiotic Drug Resistance, John Wiley & Sons, Ltd., 2019, Chapter 8, pp167-179.

Varela MF, Andersen JL, Ranjana KC, Kumar S, Sanford LM, Hernandez AJ. *Bacterial Resistance Mechanisms and Inhibitors of Multidrug Efflux Pumps Belonging to the Major Facilitator Superfamily of Solute Transport Systems*, 2017. https://ebooks.benthamscience.com/book/9781681082912/chapter/152013/

Vergara-Jaque A, Fenollar-Ferrer C, Kaufmann D, Forrest LR. Repeat-swap homology modeling of secondary active transporters: updated protocol and prediction of elevator-type mechanisms. *Front Pharmacol*. 2015;6:183.

Vesel M, Rapp J, Feller D, Kiss E, Jaromi L, Meggyes M, Miskei G, et al. ABCB1 and ABCG2 drug transporters are differentially expressed in non–small cell lung cancers (NSCLC) and expression is modified by cisplatin treatment via altered Wnt signaling. *Respir Res*. 2017;18(1):52.

Viklund H, Elofsson A. Best alpha-helical transmembrane protein topology predictions are achieved using hidden Markov models and evolutionary information. *Protein Sci*. 2004;13(7):1908–1917.

von Appen A, Beck M. Structure determination of the nuclear pore complex with three-dimensional cryo electron microscopy. *J Mol Biol*. 2016;428(10 Pt A):2001–2010.

von Heijne G. Membrane protein structure prediction. Hydrophobicity analysis and the positive-inside rule. *J Mol Biol*. 1992;225(2):487–494.

von Heijne G. A day in the life of Dr K. or how I learned to stop worrying and love lysozyme: A tragedy in six acts. *J Mol Biol*. 1999;293(2):367–379.

von Heijne G, Rees D. Membranes: reading between the lines. *Curr Opin Struct Biol*. 2008;18(4):403–405.

Wagner N, Krohne G. LEM-Domain proteins: New insights into lamin-interacting proteins. *Int Rev Cytol*. 2007;261:1–46.

Wakeling EL, Brioude F, Lokulo–Sodipe O, O'Connell SM, Salem J, Bliek J, Canton AP, et al. Diagnosis and management of Silver–Russell syndrome: First international consensus statement. *Nat Rev Endocrinol*. 2017;13(2):105–24.

Walenkamp MJ, van der Kamp HJ, Pereira AM, Kant SG, van Duyvenvoorde HA, Kruithof MF, Breuning MH, Romijn JA, Karperien M, Wit JM. A variable degree of intrauterine and postnatal growth retardation in a family with a missense mutation in the insulin–like growth factor I receptor. *J Clin Endocrinol Metab*. 2006;91(8):3062–3070.

Wallborn T, Wüller S, Klammt J, Kruis T, Kratzsch J, Schmidt G, Schlicke M, et al. A heterozygous mutation of the insulin–like growth factor–I receptor causes retention of the nascent protein in the endoplasmic reticulum and results in intrauterine and postnatal growth retardation. *J Clin Endocrinol Metab*. 2010;95(5):2316–2324.

Walsh CT, Garneau–Tsodikova S, Gatto GJ Jr. Protein posttranslational modifications: The chemistry of proteome diversifications. *Angew Chem Int Ed Engl*. 2005;44(45):7342–7372.

Walsh JH, Karnes WE, Cuttitta F, Walker A. Autocrine growth factors and solid tumor malignancy. *West J Med*. 1991;155(2):152–163.

Wang T, Ge G, Ding Y, Zhou X, Huang Z, Zhu W, Shu Y, Liu P. MiR–503 regulates cisplatin resistance of human gastric cancer cell lines by targeting IGF1R and BCL2. *Chin Med J (Engl)*. 2014;127(12):2357–2362.

Wang Y, Harrison C, Schulten K, McCammon JA. Implementation of accelerated molecular dynamics in NAMD. *Comput Sci Discov*. 2011;4(1):015002.

Wang Q, Millet YA, Chao MC, Sasabe J, Davis BM, Waldor MK. A genome-wide screen reveals that the *Vibrio cholerae* phosphoenolpyruvate phosphotransferase system modulates virulence gene expression. *Infect Immun*. 2015;83(9):3381–3395.

Wang A, Rana S, Karumanchi SA. Preeclampsia: The role of angiogenic factors in its pathogenesis. *Physiology (Bethesda)*. 2009;24:147–158.

Wang W, Shi Z, Jiao S, Chen C, Wang H, Liu G, Wang Q. Structural insights into SUN-KASH complexes across the nuclear envelope. *Cell Res*. 2012;22(10):1440–1452.

Wang HY, Yan MY, Zhao YW, Kan B. Transcriptional repressor gene--mtlR of mannitol PTS operon in *Vibrio cholerae*. *Wei Sheng Wu Xue Bao*. 2007;47(3):522–525.

Warburg O. On respiratory impairment in cancer cells. *Science*. 1956;124(3215):269–270.

Ward A, O'Reilly J, Rutherford NG, Ferguson SM, Hoyle CK, Palmer SL, Clough JL, Venter H, Xie H, Litherland GJ, Martin GE, Wood JM, Roberts PE, Groves MA, Liang WJ, Steel A, McKeown BJ, Henderson PJ. Expression of prokaryotic membrane transport proteins in Escherichia coli. *Biochem Soc Trans*. 1999;27(6):893-899.

Ward A, Sanderson NM, O'Reilly J, Rutherford NG, Poolman B, Henderson PJF. The amplified expression, identification, purification, assay and properties of hexahistidine tagged bacterial membrane transport proteins. In Baldwin SA (Ed) Membrane transport – a Practical Approach, 2000;141–166. Oxford: Blackwell.

Ward GM, Walters JM, Barton J, Alford FP, Boston RC. Physiologic modeling of the intravenous glucose tolerance test in type 2 diabetes: A new approach to the insulin compartment. *Metabolism*. 2001;50(5):512–519.

Warshel A. Molecular dynamics simulations of biological reactions. *Acc Chem Res*. 2002;35(6):385-395.

Washburn MP, Wolters D, Yates JR 3rd. Large-scale analysis of the yeast proteome by multidimensional protein identification technology. *Nat Biotechnol*. 2001;19(3):242–247.

Watnick PI, Kolter R. Steps in the development of a *Vibrio cholerae* El Tor biofilm. *Mol Microbiol*. 1999;34(3):586–595.

Weiss B, Davidkova G, Zhou LW. Antisense RNA gene therapy for studying and modulating biological processes. *Cell Mol Life Sci*. 1999;55(3):334–358.

Werner H, Le Roith D. New concepts in regulation and function of the insulin–like growth factors: Implications for understanding normal growth and neoplasia. *Cell Mol Life Sci*. 2000;57(6):932–942.

West RC, Bouma GJ, Winger QA. Shifting perspectives from "oncogenic" to oncofetal proteins; how these factors drive placental development. *Reprod Biol Endocrinol*. 2018;16(1):101.

West CKG, Klein SL, Lovell CR. High frequency of virulence factor genes tdh, trh, and tlh in *Vibrio parahaemolyticus* strains isolated from a pristine estuary. *Appl Environ Microbiol*. 2013;79(7):2247-2252.

Westwood M, Gibson JM, Davies AJ, Young RJ, White A. The phosphorylation pattern of insulin–like growth factor binding protein–1 in normal plasma is different from that in amniotic fluid and changes during pregnancy. *J Clin Endocrinol Metab*. 1994;79(6):1735–1741.

Weyand S, Ma P, Saidijam M, Baldwin J, Beckstein O, Jackson S, Suzuki S, Patching SG, Shimamura T, Sansom MS, Iwata S, Cameron AD, Baldwin SA, Henderson PJ. 2010. The Nucleobase-Cation-Symport-1 family of membrane transport proteins. 11. In Handbook of Metalloproteins, John Wiley and Sons. DOI: 10.1002/0470028637.met268

Weyand S, Shimamura T, Beckstein O, Sansom MSP, Iwata S, Henderson PJF, Cameron AD. The alternating access mechanism of transport as observed in the sodium-hydantoin transporter Mhp1. *J Synchrotron Rad*. 2011;18(1):20–23.

Weyand S, Shimamura T, Yajima S, Suzuki S, Mirza O, Krusong K, Carpenter EP, Rutherford NG, Hadden JM, O'Reilly J, Ma P, Saidijam M, Patching SG, Hope RJ, Norbertczak HT, Roach PCJ, Iwata S, Henderson PJF, Cameron AD. Structure and molecular mechanism of a nucleobase-cation-symport-1 family transporter. *Science*. 2008;322(5902):709–713.

White SH. The messy process of guiding proteins into membranes. *Elife*. 2015;4. pii: e12100.

White SH, Wimley WC. Membrane protein folding and stability: Physical principles. *Annu Rev Biophys Biomol Struct*. 1999;28:319–365.

Willegems K, Efremov RG. Influence of lipid mimetics on gating of ryanodine receptor. *Structure*. 2018;26(10):1303–1313.e4.

Winstone TL, Duncalf KA, Turner RJ. Optimization of expression and the purification by organic extraction of the integral membrane protein EmrE. *Protein Expr Purif*. 2002;26(1):111–121.

WHO. Cholera outbreak: Assessing the outbreak response and improving preparedness. WHO. 2004. https://www.who.int/cholera/publications/OutbreakAssessment/en/.

WHO (World Health Organization), Health topics, Cancer [updated 2019]. Available from: (www.who.int/cancer/en/)

Witholt B, Boekhout M, Brock M, Kingma J, Heerikhuizen HV, Leij LD. An efficient and reproducible procedure for the formation of spheroplasts from variously grown *Escherichia coli*. *Anal Biochem*. 1976;74(1):160-170.

Witz S, Panwar P, Schober M, Deppe J, Pasha FA, Lemieux MJ, Möhlmann T. Structure-function relationship of a plant NCS1 member-homology modeling and mutagenesis identified residues critical for substrate specificity of PLUTO, a nucleobase transporter from Arabidopsis. *PLoS One*. 2014;9(3):e91343.

Wong TC. Membrane structure of the human immunodeficiency virus gp41 fusion peptide by molecular dynamics simulation II. The glycine mutants. *Biochim Biophys Acta – Biomembranes*. 2003;1609(1):45–54.

Woolley RC, Vediyappan G, Anderson M, Lackey M, Ramasubramanian B, Jiangping B, Borisova T, et al. Characterization of the *Vibrio cholerae* vceCAB multiple-

drug resistance efflux operon in *Escherichia coli*. *J Bacteriol*. 2005;187(15):5500–5503.

World Cancer Research Fund/American Institute for Cancer Research, Colorectal cancer statistsics, [updated 2019]. Available from: (https://www.wcrf.org/dietandcancer/cancer–trends/colorectal–cancer–statistics)

Worman HJ, Evans CD, Blobel G. The lamin B receptor of the nuclear envelope inner membrane: a polytopic protein with eight potential transmembrane domains. *J Cell Biol*. 1990;111(4):1535–1542.

Worman HJ, Yuan J, Blobel G, Georgatos SD. A lamin B receptor in the nuclear envelope. *Proc Natl Acad Sci U S A*. 1988;85(22):8531-8534.

Wu W, Lin F, Worman HJ. Intracellular trafficking of MAN1, an integral protein of the nuclear envelope inner membrane. *J Cell Sci*. 2002;115(Pt 7):1361–1371.

Wu HH, Symersky J, Lu M. Structure of an engineered multidrug transporter MdfA reveals the molecular basis for substrate recognition. *Commun Biol*. 2019;2(1):210.

Wyckoff EE, Stoebner JA, Reed KE, Payne SM. Cloning of a *Vibrio cholerae* vibriobactin gene cluster: identification of genes required for early steps in siderophore biosynthesis. *J Bacteriol*. 1997;179(22):7055–7062.

Xue Y, Davis AV, Balakrishnan G, Stasser JP, Staehlin BM, Focia P, Spiro TG, Penner-Hahn JE, O'Halloran TV. Cu(I) recognition via cation-pi and methionine interactions in CusF. *Nat Chem Biol*. 2008;4(2):107–109.

Yamashita A, Singh SK, Kawate T, Jin Y, Gouaux E. Crystal structure of a bacterial homologue of Na^+/Cl^--dependent neurotransmitter transporters. *Nature*. 2005;437(7056):215–223.

Yan N. Structural advances for the major facilitator superfamily (MFS) transporters. *Trends Biochem Sci*. 2013;38(3):151–159.

Yan N. A glimpse of membrane transport through structures-advances in the structural biology of the GLUT glucose transporters. *J Mol Biol*. 2017;429(17):2710–2725.

Yang W. Distinct, but not completely separate spatial transport routes in the nuclear pore complex. *Nucleus*. 2013;4(3):166–175.

Yang JW, Fu JX, Li J, Cheng XL, Li F, Dong JF, Liu ZL, Zhuang CX. A novel co-immunoprecipitation protocol based on protoplast transient gene expression for studying protein–protein interactions in rice. *Plant Mol Biol Rep*. 2014;32(1):153–161.

Yang Z, Wang C, Zhou Q, An J, Hildebrandt E, Aleksandrov LA, Kappes JC Membrane protein stability can be compromised by detergent interactions with the extramembranous soluble domains. *Protein Sci*. 2014;23(6):769–789.

Yardeni EH, Zomot E, Bibi E. The fascinating but mysterious mechanistic aspects of multidrug transport by MdfA from *Escherichia coli*. *Res Microbiol*. 2018;169(7–8):455–460.

Ye Q, Worman HJ. Primary structure analysis and lamin B and DNA binding of human LBR, an integral protein of the nuclear envelope inner membrane. *J Biol Chem*. 1994;269(15):11306–11311.

Ye Q, Worman HJ. Interaction between an integral protein of the nuclear envelope inner membrane and human chromodomain proteins homologous to Drosophila HP1. *J Biol Chem*. 1996;271(25):14653–14656.

Yin Y, He X, Szewczyk P, Nguyen T, Chang G. Structure of the multidrug transporter EmrD from *Escherichia coli*. *Science*. 2006;312(5774):741–744.

Youssef A, Han VK. Low oxygen tension modulates the insulin–like growth factor–1 or –2 signaling via both insulin–like growth factor–1 receptor and insulin receptor to maintain stem cell identity in placental mesenchymal stem cells. *Endocrinology*. 2016;157(3):1163–1174.

Youssef A, Iosef C, Han VK. Low–oxygen tension and IGF–I promote proliferation and multipotency of placental mesenchymal stem cells (PMSCs) from different gestations via distinct signaling pathways. *Endocrinology*. 2014;155(4):1386–1397.

Yu CH, Cukierman S, Pomes R. Theoretical study of the structure and dynamic fluctuations of dioxolane-linked gramicidin channels. *Biophys J*. 2003;84(2 Pt 1), 816-831.

Yu CH, Pomes R. Functional dynamics of ion channels: Modulation of proton movement by conformational switches. *J Am Chem Soc*. 2003;125(45):13890-13894.

Yu H, Rohan T. Role of the insulin–like growth factor family in cancer development and progression. *J Natl Cancer Inst*. 2000;92(18):1472–1489.

Yu M, Yuan C, Wang H, Liu J, Qin H, Liu S, Yan Q. FUT8 drives the proliferation and invasion of trophoblastic cells via IGF–1/IGF–1R signaling pathway. *Placenta*. 2019;75:45–53.

Yuan TL, Cantley LC. PI3K pathway alterations in cancer: Variations on a theme. *Oncogene*. 2008;27(41):5497–5510.

Yung HW, Cox M, Tissot van Patot M, Burton GJ. Evidence of endoplasmic reticulum stress and protein synthesis inhibition in the placenta of non–native women at high altitude. *FASEB J*. 2012:26(5):1970–1981.

Zacharias N, Dougherty DA. Cation-pi interactions in ligand recognition and catalysis. *Trends Pharmacol Sci*. 2002;23(6):281–287.

Zakrzewska S, Mehdipour AR, Malviya VN, Nonaka T, Koepke J, Muenke C, Hausner W, Hummer G, Safarian S, Michel H. Inward-facing conformation of a

multidrug resistance MATE family transporter. *Proc Natl Acad Sci U S A*. 2019;116(25):12275–12284.

Zarrilli R, Pignata S, Romano M, Gravina A, Casola S, Bruni CB, Acquaviva AM. Expression of insulin–like growth factor (IGF)–II and IGF–I receptor during proliferation and differentiation of CaCo–2 human colon carcinoma cells. *Cell Growth Differ*. 1994;5(10):1085–1091.

Zawacka–Pankau J, Selivanova G. Pharmacological reactivation of p53 as a strategy to treat cancer. *J Intern Med*. 2015;277(2):248–259.

Zelzer E, Levy Y, Kahana C, Shilo BZ, Rubinstein M, Cohen B. Insulin induces transcription of target genes through the hypoxia–inducible factor HIF–1alpha/ARNT. *EMBO J*. 1998;17(17):5085–5094.

Zeng L, Perks CM, Holly JM. IGFBP–2/PTEN: A critical interaction for tumours and for general physiology? *Growth Horm IGF Res*. 2015;25(3):103–107.

Zhang YK, Wang YJ, Gupta P, Chen ZS. Multidrug resistance proteins (MRPs) and cancer therapy. *AAPS J*. 2015;17(4):802–812.

Zhao G, London E. An amino acid "transmembrane tendency" scale that approaches the theoretical limit to accuracy for prediction of transmembrane helices: Relationship to biological hydrophobicity. *Protein Sci*. 2006;15(8):1987–2001.

Zheng J. *Spectroscopy-Based Quantitative Fluorescence Resonance Energy Transfer Analysis*. In Ion Channels, Springer, 2006, pp65–77.

Zhou Y, Bushweller JH. Solution structure and elevator mechanism of the membrane electron transporter CcdA. *Nat Struct Mol Biol*. 2018;25(2):163–169.

Zhou R, Diehl D, Hoeflich A, Lahm H, Wolf E. IGF–binding protein–4: Biochemical characteristics and functional consequences. *J Endocrinol*. 2003;178(2):177–193.

Zhou P, Ten S, Sinha S, Ramchandani N, Vogiatzi M, Maclaren N. Insulin receptor autoimmunity and insulin resistance. *J Pediatr Endocrinol Metab*. 2008;21(4):369–375.

Zhu FQ, Tajkhorshid E, Schulten K. Molecular dynamics study of aquaporin-1 water channel in a lipid bilayer. *FEBS Lett*. 2001;504(3):212-218.

Zhu FQ, Tajkhorshid E, Schulten K. Theory and simulation of water permeation in aquaporin-1. *Biophys J*. 2004;86(1 Pt 1):50-57.

Zomot E, Yardeni EH, Vargiu AV, Tam HK, Malloci G, Ramaswamy VK, Perach M, Ruggerone P, Pos KM, Bibi E. A new critical conformational determinant of multidrug efflux by an MFS transporter. *J Mol Biol*. 2018;430(9):1368–1385.

Zuckerman DM. Physical lens on the cell. 2019 online. https://www.physicallensonthecell.org/.

Zuleger N, Kelly DA, Richardson AC, Kerr AR, Goldberg MW, Goryachev AB, Schirmer EC. System analysis shows distinct mechanisms and common principles of nuclear envelope protein dynamics. *J Cell Biol*. 2011;193(1):109–123.

Zuleger N, Korfali N, Schirmer EC. Inner nuclear membrane protein transport is mediated by multiple mechanisms. *Biochem Soc Trans*. 2008;36(Pt 6):1373–1377.